Characterization of Volatile Organic Compound Emissions from Anthropogenic and Emerging Biogenic Sources

Sam Rossabi

B.S., University of North Carolina Asheville, 2014

A thesis submitted to the

Faculty of the Graduate School of the

University of Colorado in partial fulfillment

of the requirement for the degree of

Doctor of Philosophy

Department of Chemistry

2018

This thesis entitled:

Characterization of Volatile Organic Compound Emissions from Anthropogenic and Emerging

Biogenic Sources

written by Sam Rossabi

has been approved for the Department of Chemistry

_____

Dr. Detlev Helmig

_____

Dr. Steven Brown

_____

Dr. Joost De Gouw

_____

Dr. Gordana Dukovic

_____

Dr. Alan Fried

Rossabi, Sam (Ph.D., Department of Chemistry, Institute of Arctic and Alpine Research, Cooperative Institute for Research in Environmental Sciences)

Characterization of Volatile Organic Compound Emissions from Anthropogenic and Emerging Biogenic Sources

Thesis directed by Fellow and Associate Research Professor of INSTAAR Detlev Helmig and Adjoint Professor Steven Brown.

Volatile organic compounds are emitted by myriad sources. This thesis investigates trends in emissions on global, regional, and local scales. Globally, an increasing trend in ethane and propane emissions was observed, mainly as a result of oil and natural gas (O&NG) development. Regionally, air composition varied as a result of the efficacy of emission controls from mobile and industrial sources, and unconventional O&NG development. Unconventional O&NG development has also had a demonstrated effect of Colorado's Northern Front Range. An elevation gradient was observed that suggests emissions from metropolitan and O&NG development centers in this area influence air composition in the adjacent foothills. A spatial gradient of O&NG tracers was also observed; mixing ratios increased as distance to an area of concentrated O&NG development decreased. Given the ever increasing proximity of O&NG emissions to population centers, concerned citizens desire a method to assess air quality in and around their homes, schools, and offices. An affordable method for measuring C_3-C_5 alkanes was developed utilizing passive adsorbent sampling cartridges, though further experimentation is needed to determine the absolute accuracy of these devices. Finally, VOC emissions from soil and bacteria are characterized. Soil VOC emissions mirrored the "Birch Effect", and spiked

following a wetting event. Bacterial VOC emission profiles displayed strong taxonomic and

phylogenetic signals, and suggest VOC play a role in finer-scale patterns of ecological diversity.

Dedication

This thesis is dedicated to my partner, Erin Cox, for your unwavering support throughout my studies, for encouraging me on my worst days, celebrating with me on my best days, and for joining me on countless adventures. This thesis is also dedicated to my parents, Joe and Terry, and my sister, Jessie, for supporting me and guiding my development as a human and instilling the importance of work ethic, respect, and grit. Thank you being the best family I could ever hope for, and for teaching me to be humble, thankful, and to stay low. I would also like to thank the numerous friends that reminded me of the joys of life, and the importance of preserving our planet and areas in which we recreate.

Acknowledgements

I would like to thank Dr. Detlev Helmig, Dr. Noah Fierer, and the University of Colorado Boulder's Chemistry Department for providing funding for my thesis work, for guiding and informing the research I conducted, and for fostering my growth as a scientist. I would also like to thank Dr. Steve Brown for being my chemistry department adviser, for sitting on my competency committee and my defense committee, for reviewing my thesis, and for guiding me through my graduate studies. Thanks to Dr. Veronica Vaida for being a part of my competency committee and for assuring that I connect my research to the fundamentals of chemistry. Thanks to Dr. Gordana Dukovic for being a part of my competency and defense committees, and for reviewing my thesis. I would like to thank Dr. Joost De Gouw, and Dr. Alan Fried for sitting on my defense committee and for reviewing and contributing to the development of my thesis. Thanks to Dr. Bert Holmes for introducing me to research, being a great example of a scientist and a person, and for encouraging me to pursue my doctorate.

Contents

Figures

Chapter 1

Introduction

1. Pre-Industrial Air Pollution

Air pollution has negatively affected human health since at least the Paleolithic era. Mummified black lung tissue has been found at archaeological sites around the world [*Colbeck*, 2007; *McNeill*, 2001]. This anthracosis was likely caused by fires in enclosed shelters that were necessary for cooking and warding off cold and insects. Domestic cooking and heating fires are still used by ~3 billion people [*WHO*, 2018]. The World Health Organization estimates that 3.3 million deaths in 2012 were related to indoor air pollution [*WHO*, 2014].

As population density increased, outdoor air pollution concerns arose in addition to smoke from domestic fires. Preindustrial manufacturing processes and equipment, such as ceramic firing furnaces and metal smelting, caused noticeably dark and smoky skies in ancient Rome [*Mosley*, 2014]. Lead production reached 80,000 tons per year during the Greco-Roman period [*Mosley*, 2014]. Particulate emitted from smelting furnaces was transported and polluted much of the Northern Hemisphere. Arctic ice core studies reveal that lead in the environment increased by an order of magnitude due to Roman smelting [*Nriagu and Norton*, 1983]. Further, more copper was deposited in the Northern Hemisphere prior to the Industrial Revolution than after it due to inefficient smelting practices [*Hong et al.*, 1996]. Acute exposure to lead was estimated to have caused the deaths of hundreds of thousands of lead miners and smelters [*Hong et al.*, 1994; *Nriagu and Norton*, 1983]. The total atmospheric lead fallout as a result of the Greek and Roman Empires was 15% of that emitted due to the use of lead alkyl gasoline from

the 1930s until 1995 [*Hong et al.*, 1994], which caused lead concentrations in North Pole ice sheets to eclipse 0.2 µg Pb kg^{-1} ice [*Murozumi et al.*, 1969].

Growing population density again resulted in air pollution concerns as harvesting wood for fuel from local forests became unsustainable. Coal and fossil fuels were increasingly used to meet the demands of city residents. British royalty objected to use of 'sea-coal', a particularly smoky variety, as early as the 1300s [*Mosley*, 2014], but these objections were not enforced strongly enough to have any real effect on air quality.

2. Industrial Revolution

Coal and fossil fuel use exploded during the Industrial Revolution, increasing from 10 million tons in 1800 to 780 million tons in 1900. This massive increase in production was a result of increasing population. The number of cities in the world with 500,000 residents increased from 6 to 43 in the same time period [*Nye*, 1998; *Sieferle*, 2001; *Smil*, 1994]. Despite the need for cheap energy, coal burning's deleterious effects were recognized by this time as well. The primary pollutants associated with coal burning are smoke, sulfur dioxide, nitrogen oxides, and carbon dioxide. Smoke is a collection of carbon-based gases, and solid and liquid particulate matter.

The term smog was coined in the early 20th century and is a portmanteau of smoke and fog. Smog events were the most noticeable negative effects related to coal burning. Smog events disrupted the rhythm of city life by reducing visibility to a few meters, coal residue was apparent on buildings and vegetation, and smoke pollution was linked to psychological problems such as irritability and morbid emotions [*Luckin*, 2003; *Mosley*, 2008; *Tarr*, 1996]. Inhalation of smoke irritates the victim's respiratory tract, and noxious compounds such as carbon monoxide and

hydrogen cyanide poison victims. Sulfur dioxide is a toxic gas and a precursor to acid rain and particulate. Nitrogen oxides decrease lung function and can cause acute illnesses such as bronchitis. Bronchitis was the biggest killer in Britain's factory towns [*Stradling*, 1999; *Stradling and Thorsheim*, 1999]. Nitrogen oxides also lead to the formation of ozone, particulate, and acid rain. The pH of rain water was as low as 3.5 during this period.

In response to the negative effects of coal burning, various attempts at regulation were made via anti-smoke groups, campaigns, and regulations. The Taylor Committee on Steam Engines and Furnaces (1819-1820), the Mackinnon Committees on Smoke Prevention (1843 and 1845), the Select Committee on Smoke Nuisance Abatement (1887), the Newton Committee on Smoke and Noxious Vapors (1914 and 1920-1921) were all formed to combat the smoke problem. Smoke abatement committees in London encouraged citizens to use more fuel-efficient appliances [*Ranlett*, 1981]. The 1875 Public Health Act outlined the day's health issues and included "any chimney sending forth black smoke in such quantity as to be a nuisance shall be deemed a nuisance." The Act further required that fireplaces and chimneys "consume their own smoke", though only between working hours. The International Smoke Abatement Exhibition was held in London in 1912 and hosted delegates from the United States. The first smoke ordinances in the U.S. were passed in the 1880s [*Stradling*, 1999; *Stradling and Thorsheim*, 1999]. These early anti-smoke laws contained exemptions, and a 'best practicable means' clause that only required industrialists to utilize abatement strategies that came at a reasonable cost. When offenders were found in violation of policy, they were assigned insignificant fines [*Ashby and Anderson*, 1976; 1977a; b]. As a result, these efforts had limited success regulating emissions.

3. Automobiles, oil, natural gas

Coal accounted for 70% of American energy production in 1920, but lost favor to oil and natural gas, which made up 41 and 26% of energy production in 1955 [*Nye*, 1998; *Tarr*, 1996]. Despite being a cleaner energy source than coal, oil and natural gas combustion still results in smoke, NOx, SOx, and CO_2. Automobiles became more readily available during this time period. There were less than 1 million registered vehicles in the U.S. in 1912. By 1968, 100 million vehicles were registered, and by 1995 this number doubled [*FHA*, 2000]. The resulting emissions increase associated with increasing traffic volume became the next major air quality concern.

Los Angeles was planned with the private automobile in mind and had the highest per capita car registration in the world in 1910 [*McShane*, 1999], and by 1950, Los Angeles' photochemical smog problems were evident [*Haagen-Smit*, 1952; *Renzetti*, 1956]. In addition to Los Angeles' high population and traffic density, mountains to the north and east trap emissions in the basin, which leads to highly polluted air. In the 1960s and prior to regulations, maximum 1-hour average mixing ratios reached nearly 700 ppb in the LA Basin [*Fujita et al.*, 2013]. Regulations of NO_X and VOC have improved air quality; ozone 8-hour maximum mixing ratios in the LA basin have decreased from 0.315 ppm in 1973 to 0.136 ppm in 2017 [*CARB*, 2018]. However, ozone formation is a complex and nonlinear process, and decreasing emissions of precursors does not guarantee a reduction in ozone formation [*Stockwell et al.*, 2012; *Whitten et al.*, 1980]. An example of this nonlinearity is the "weekend effect". The weekend effect has been observed in several urban areas and describes the observation of elevated mixing ratios of ozone on weekends, despite lower emissions of VOC and NOX on these days [*Blanchard and Tanenbaum*, 2003; *Chinkin et al.*, 2003; *Elkus and Wilson*, 1977; *Fujita et al.*, 2003a; *Fujita et*

al., 2003b; *Yarwood et al.*, 2003]. Another confounding factor is the effect of climate on ozone levels. *Rasmussen et al*. [2012] predicts a 3-6 ppb rise in ozone per K increase in temperature. This ozone/temperature relationship is fairly consistent with other studies that have suggested a ~ 2 ppb increase in ozone $°C^{-1}$ [*Bloomer et al.*, 2009], a 2-15 ppb K^{-1} increase in ozone mixing ratios [*Kleeman*, 2008], and an additional 22- 30 days $year^{-1}$ in California where ozone exceeds 90 ppb as a result of increasing temperatures [*Mahmud et al.*, 2008]. Higher temperatures decrease sequestration of NO_X and HO_X by peroxyactylnitrates, and thus increase availability of these ozone precursors [*Cardelino and Chameides*, 1990; *Sillman and Samson*, 1995]. Higher temperatures are also associated with stagnant air masses that allow abundances of locally emitted ozone precursors to build up [*Leibensperger et al.*, 2008; *Olszyna et al.*, 1997]. Anthropogenic and biogenic emissions of NOx can increase as temperature increases [*Bruhl and Crutzen*, 1988; *Logan*, 1983; *Yienger and Levy*, 1995]. Natural emissions of isoprene, another potent ozone precursor, also rise with temperature [*Guenther et al.*, 1993; *Lamb et al.*, 1987; *Meleux et al.*, 2007].

Emission control strategies for NO_X are broadly categorized as combustion controls and post-combustion controls. Combustion controls alter combustion conditions to mitigate NO_X production. For example, combustion is modified to occur at lower temperature, in a fuel rich conditions, or with less opportunity for oxidation [*EPA*, 1978]. These controls can reduce NO_X production by 40 – 60% compared to conventional methods. Post-combustion controls reduce NO_X emissions by converting NO_X to nitrogen (N_2). Catalytic converters are an example of a post-combustion control, and became mandatory components of vehicles in the U.S. in the 1970s. In addition to reducing NO_X to N_2, catalytic converters also oxidize carbon monoxide and unburned hydrocarbons to CO_2. One shortcoming of the catalytic converter is the ~5 minute

warm up time during which most of the total pollution of the engine is emitted from the vehicle. Some vehicles are equipped with a heater to bring the catalyst up to temperature more quickly, and reduce emissions. Other vehicles have a "pre-cat" – a smaller catalytic converter that warms up more quickly than the main catalyst and reduces emissions while the main catalytic converter warms up.

VOC emissions from vehicles come from three main sources, tailpipe, gasoline vapor, and liquid gasoline emissions. Gasoline vapor emissions are a result of headspace vapors in enclosed gas tanks being emitted during refueling and during storage and transport. Liquid gasoline emissions are a result of liquid leaks and spillage during refueling. Evaporative emissions are controlled by features such as sealed fuel systems, charcoal traps for fugitive emissions, and vacuum fuel caps.

VOC emission reduction can also be achieved by lowering a fuel's Reid Vapor Pressure (RVP) [*EIA*, 1998]. RVP is a measure of gasoline volatility and varies as a result of the unique blend of compounds that make up the gasoline. Special blends of gasoline with reduced RVP are often developed in response to air quality standards in a particular region or time of year. Winter formulations of gasoline can include higher concentrations of more volatile components without violating regulations [*Wells*, 2005]. For example, *n*-butane is present in higher concentrations in wintertime gasoline [*Goldstein et al.*, 1995] because of its high octane rating (94), but its high vapor pressure prevents it from being used in high concentrations in summertime gasoline. In California, a reformulated gasoline blend was estimated to have a 25-29% lower fraction of VOC compared to conventional gasoline used before 1995.

Ozone production in urban environments is complex and highly dependent on relative emission rates of NOx and VOC [*Ehhalt*, 1999; *Monks et al.*, 2015]. The presence of NOx is

necessary for the primary production mechanism of tropospheric ozone, but ozone production can be halted by high relative emissions of VOCs, which lead to the production of HOx, and later, the destruction of ozone [*Lightfoot et al.*, 1992]. Similarly, a lack of VOCs can lead to an NO dominated regime that also destroys ozone [*Zhou et al.*, 2014]. However, an ideal ratio of VOCs and NOx (~10 mg C_{VOC} m^{-2} hr^{-1} to 1 mg N_{NOX} m^{-2} hr^{-1}) to can lead to rapid production of ozone, which in turn results in areas of non-attainment [*Monks et al.*, 2015]. A 2017 study suggested that VOC emissions from O&NG can contribute up to 30 ppb of ozone in Colorado's Northern Front Range, though this process is likely facilitated by NO_X emitted from vehicle, industrial, and petroleum related sources [*Cheadle et al.*, 2017].

3.1 Regulations

Ever increasing energy demands resulted in higher emissions than ever before and caused catastrophic acute exposure events. These incidents occurred in the Meuse River Valley, Belgium in 1930, Donora, PA, USA in 1948, London, UK in 1952, 1956, and 1962, and New York City, NY, USA in 1963. In each of these events, a persistent fog settled over the area for at least a few days. Deaths that could be attributed to pollution from these incidents ranged from 20 to 4000 in each event. These events inspired the passing of air quality laws with clout. Britain's Clean Air Act of 1956 regulated domestic and industial emissions sources, and America's Clean Air Act of 1970 set national air quality standards for the first time [*Davis*, 2002; *Morag-Levine*, 2003; *Stradling and Thorsheim*, 1999; *Thorsheim*, 2004].

The Trail smelter dispute between Canada and the U.S. established that the polluter pays for damages even if the damages occurred across the border [*Wirth*, 2000]. This precedent evolved with better understanding of transport. Originally it applied to an easily identifiable source near a border. Scandinavian scientists determined British sulfur emissions were acidifying

lakes and rivers in Norway and Sweden and causing forest decline [*Lundgren*, 1998; *Osborn*, 2004]. As this involved transport over several hundred miles, it was a new situation. Ultimately, it is much more difficult to be certain of the origin of pollution that travels such a great distance, but the United Nations Conference on the Human Environment in 1972 developed language that made pollution emitters responsible for damages outside their jurisdiction [*UNEP*, 1972]. The Convention on Long-Range Transboundary Pollution was held in 1979 and included 34 governments. The original convention worked to reduce sulfur dioxide emissions and establish monitoring programs. Plans of the original have been extended to nitrogen oxides, volatile organic compounds, heavy metals, and tropospheric ozone [*UNEC*, 2004]. The 1990 Clean Air Act Amendments in the United States evaluated an emissions trading system to reduce SO_2 emissions [*Brimblecombe*, 2008]. Despite the formation of the Acid Precipitation Monitoring Network in East Asia, acid rain remains a major issue in this part of the world. China's coal use is a major emitter of SO_2 [*EANET*, 2013].

Though America and Britain have improved smoke pollution, the developing world still lags behind. China's coal consumption peaked at 4.2 billion tons in 2013 [*Qi et al.*, 2016] but remained at ~ 3.8 billion tons in 2017 [*Qi and Jiaqui*, 2018]. India's population continues to grow and is among the top five nations for coal production. Energy usage across the world continues to rise, and though coal's relative contribution is declining, 5.4 billion tons of coal were consumed in 2016 [*IEA*, 2017].

3.2 Invisible threats

The clean air acts in developed nations were successful in reducing smoke emissions, but were less effective at limiting emissions of less visible pollutants such as sulfur dioxide, nitrogen

oxides, tropospheric ozone, chlorofluorocarbons (CFCs), volatile organic compounds (VOCs), and tropospheric ozone. Photochemical, rather than smoke derived, smog became the dominant urban air quality challenge.

3.2.1 Sulfur Dioxide

Sulfur dioxide (SO_2) is mostly produced by processes that burn fossil fuels with high sulfur content such as coal. SO_2 leads to the formation of other sulfur oxides ($SO_X = SO_2 + SO_3 + SO_4$) which are a particulate matter source. These particles are harmful if inhaled and reduce visibility.

SO_2 has decreased by about 90% since 1980 [*EPA*, 2017b]. SO_2 is oxidized by OH and forms sulfuric acid and sulfate aerosol. SO_2 dissolves in water droplets in the atmosphere [*Berglen et al.*, 2004]. In addition to health effects from acute exposure, long term exposure to sulfur dioxide and particulate matter has been correlated with increased deaths from bronchitis, though the correlation with particulate matter was less consistent than with sulfur dioxide [*Katsouyanni et al.*, 1997; *Samet et al.*, 2000].

3.2.2 Nitrogen Oxides

Sources of nitrogen oxides ($NO_X = NO + NO_2$) are fossil fuel combustion, lightning flashes, nitrogen fixing by plants and microorganisms [*Galloway et al.*, 2004; *Levine et al.*, 1984]. NO_X leads to the formation of ozone, particulate, and acid rain [*Logan*, 1985; *Pankow*, 1987; *Schwartz*, 1989]. Exposure to NO_X can decrease lung function, and increase the likelihood of respiratory ailments [*Bascom et al.*, 1996]. Catalytic converters effectively reduced NO_X

emissions from mobile sources, but Los Angeles remains in nonattainment for NO_X, likely due to high traffic volume and changing environmental conditions.

3.2.3 Chlorofluorocarbons

CFCs were invented in the early 20th century by DuPont to be used as refrigerants, and propellants. Production of these compounds was relatively low until DuPont's patents expired. New companies produced cheap refrigerators and air conditioning units using CFCs and production increased by a factor of ~40 between 1950 and the 1970s [*Stutz et al.*, 2002]. In 1979, Sherry Rowland recognized the destruction to the stratospheric ozone layer caused by CFCs [*Molina and Rowland*, 1974]. The increased UV radiation reaching Earth's surface as a result of the ozone holes caused skin cancer and eye disorders in humans, disrupted photosynthesis, and impaired fish and phytoplankton reproduction [*McKenzie et al.*, 2011]. The Montreal Protocol in 1987 was developed to phase out the most harmful CFCs in developed nations. This was the first universally ratified treaty and 95% of ozone depleting substances have been phased out. Hydrofluorocarbons (HFCs) were developed as a less harmful alternative to CFCs and were phased in almost immediately [*Solomon et al.*, 1992]. More recently it has been shown that the recovery of the ozone layer seems to have stalled possible as a result of depletion by chlorinated-very short-lived substances emitted from industrial sources in East Asia [*Oram et al.*, 2017].

3.2.4 Volatile Organic Compounds

Volatile organic compounds (VOCs) are emitted from numerous anthropogenic and biogenic sources [*Abeleira et al.*, 2017; *Karl et al.*, 2001; *Kim et al.*, 2011; *Von Schneidemesser et al.*, 2011]. Biogenic sources are responsible for ~90% of global VOC emissions, and include

emissions from vegetation, biomass burning, livestock, and volcanic activity [*Calfapietra et al.*, 2013; *Helmig et al.*, 1999; *Yuan et al.*, 2017]. Anthropogenic sources include fossil fuel production and use, industrial activity, and consumer products such as adhesives, and coatings [*Borbon et al.*, 2013; *Honrath et al.*, 2004; *Lamarque et al.*, 2005; *McDonald et al.*, 2018; *Vinciguerra et al.*, 2015; *Warneke et al.*, 2007]. VOCs are tropospheric ozone and particulate matter precursors [*Chameides et al.*, 1992].

3.2.5 Tropospheric Ozone

Ozone is a critical part of tropospheric chemistry and plays a role in numerous processes. Ozone is a greenhouse gas, a tropospheric oxidant, the main source of the hydroxyl radical, and its formation is a result of photochemistry, NO_X cycling, and VOC degradation. Ozone has been linked to premature human and plant mortality [*Bell et al.*, 2005; *Fiscus et al.*, 2005; *Gryparis et al.*, 2004; *Reich and Amundson*, 1985]. Ozone is responsible for 5-20% of air pollution related deaths, which is equivalent to 350,000 to 1,400,000 deaths each year [*Anenberg et al.*, 2009; *Brauer et al.*, 2012; *Lim et al.*, 2012b; *Silva et al.*, 2013]. Figure 1 shows areas in nonattainment for the 8-hr ozone standard.

The first ozone standard was introduced in 1971; total photochemical oxidants were not to exceed a 1-hour average of 80 ppb for more than one hour per year [*EPA*, 2015b]. In 1979, this was revised to a 1-hour average of 120 ppb of ozone, and attainment was redefined as not exceeding the standard on more than 1 day per year. The city of Houston challenged this revision on the grounds that background ozone abundances and physical features of the area made it impossible to meet this standard. However, The U.S. Court of Appeals ruled that Houston's claims were irrelevant [*Costle*, 1981]. Research conducted in the 1980s and 90s warned of the

negative health and welfare effects related to elevated levels of ozone, and catalyzed a review of the 1979 standard [*Bascom et al.*, 1996; *Devlin et al.*, 1991; *Molfino et al.*, 1991; *Reich*, 1987]. In 1997, the ozone standard became an 8-hour average of 80 ppb, and attainment was defined not exceeding the standard with the fourth-highest daily maximum 8-hour average mixing ratio in a 3 year period. This new standard was challenged by the American Trucking Association, with the central argument being that the tropospheric ozone would shield the public from ultraviolet radiation [*EPA*, 1999]. Additionally, a proposal to lower the standard to 70 ppb was rejected because no standard less than 80 ppb had been set and there was lack of scientific evidence to support further lowering the standard. In 2000, the EPA began the ozone standard review process again and completed the review in 2003 in order to satisfy the terms of a lawsuit brought about by several national environmental and public health organizations [*EPA*, 2015b]. By 2008, the standard was lowered to an 8-hour average of 75 ppb in 2008. The EPA was immediately challenged by representative of state, public health, environmental, and industrial organizations. Epidemiologic studies continued to be published that related negative health effects to exposure to ozone less than 80 ppb [*Anenberg et al.*, 2009; *Brauer et al.*, 2012; *Lim et al.*, 2012b; *Silva et al.*, 2013]. The EPA also solicited public opinion and received testimonies from 500 individuals and ~430000 written comments. As a result, the ozone standard was lowered again to 70 ppb in 2015 [*EPA*, 2015c]. Figure 1 shows areas in nonattainment for the 2015 ozone standard as of September 30, 2018 [*EPA*, 2018].

8-Hour Ozone Nonattainment Areas (2015 Standard)

09/30/2018

8-hour Ozone Classification
- Extreme
- Severe-17
- Severe-15
- Serious
- Moderate
- Marginal
- Marginal (Rural Transport)

Nonattainment areas are indicated by color.
When only a portion of a county is shown in color,
it indicates that only that part of the county is within
a nonattainment area boundary.
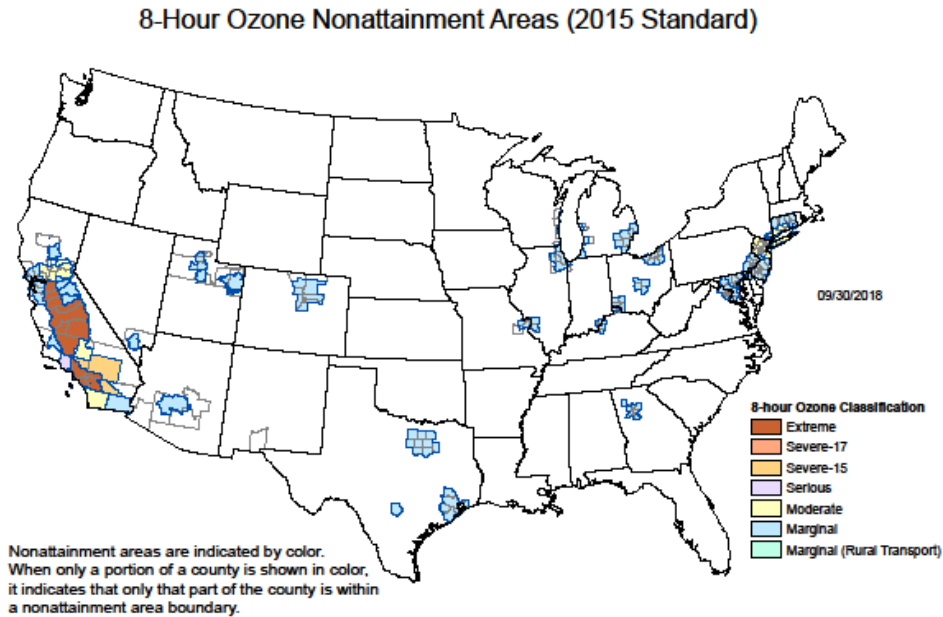
Figure 1. As of September 30, 2018, areas of nonattainment of the 2015 8-hr ozone standard. An area is found to be in nonattainment of this standard if the 4th highest daily 8-hour maximum ozone mixing ratio in a 3 year period exceeds 70 ppb. Definition for mixing ratios of ozone for each ozone classification are as follows: Extreme, $O_3 \geq 0.163$ ppm; Severe-17, 0.111 ppm $\geq O_3 > 0.163$ ppm; Severe-15, 0.105 ppm $\geq O_3 > 0.111$ ppm; Serious, 0.093 ppm $\geq O_3 > 0.105$ ppm; Moderate, 0.081 ppm $\geq O_3 > 0.093$ ppm; Marginal, 0.071 ppm $\geq O_3 > 0.081$ ppm; Marginal (Rural Transport) areas are defined as an ozone nonattainment area that does not include, and is not adjacent to any part of a Metropolitan Statistical Area.

4. Inventories vs. Monitoring

Emission inventories are a method of determining the amount of pollutants released into the atmosphere. Inventories may be built for a class of emitters, such as automobiles or power plants, or for a class of compounds, such as greenhouse gases or ozone precursors. Emissions are typically calculated using the activity rate of a source (i.e. gallons of fuel used by automobiles), the emission factor (i.e. mass of compounds emitted per mile driven), and factors that apply to abatement option usage, source types, and species (i.e. usage of catalytic converters). Inventories may determine emissions on regional or global scales [*Monks et al.*, 2009].

In some cases, such as for power plant emissions, inventories can be very representative of emissions [*Chen et al.*, 2014]. However, there are examples of disagreements between ambient measurements and inventories. *Magliano et al.* [1999] found emissions of non-methane hydrocarbons were underestimated by inventories compared to ambient measurements in the San Joaquin Valley. VOC emissions relative to NOX were underestimated by a factor of ~2 in a 2009 inventory of emissions in the South Coast Air Basin [*Fujita et al.*, 2013]. Building emission inventories for fossil fuel combustion is particularly challenging. The automobile fleet on the road is constantly changing and emission factors may not be representative of this fleet. For example, the California Air Resources Board estimates that modern vehicles emit 99% less than 30 year old vehicles [*CARB*, 2011]. Given the magnitude of this difference, relatively small inaccuracies in the age of the on road vehicle fleet can lead to significant over- or underestimations of emissions. Further, unregistered vehicles are not accounted for and may make up a significant portion of emissions. The emergence of understudied emission sources can also undermine the accuracy of models. For example, OH reactivity was underestimated in the LA Basin, prior to the addition of the contribution of volatile chemical products (VCP) [*Griffith et al.*, 2016; *McDonald et al.*, 2018]. Evidence has also been found that suggests European emission inventories should also be updated to include the contribution of emissions from VCPs [*Niedojadlo et al.*, 2007; *von Schneidemesser et al.*, 2016].

In addition to the uncertainties associated with estimating emissions from one of many VOC sources (vehicles), the fate of VOCs in the atmosphere is also difficult to forecast. Many VOCs have the potential to undergo 10^5-10^6 reactions during their degradation, further complicating the determination of their relative contribution to ozone or particulate matter [*Pinho et al.*, 2007; *Pinho et al.*, 2005; *Wang et al.*, 2000]. The degradation of many VOCs has

not been studied experimentally, and thus their degradation is inferred from similar species and structure-activity relationships [*Aumont et al.*, 2005; *Jenkin et al.*, 2003; *Jenkin et al.*, 2015; *Saunders et al.*, 2003]. Urban areas in developed and undeveloped nations may have very different emissions profiles. Positive matrix factorization has been developed to calculate emission inventories using speciated ambient data [*Brown et al.*, 2007; *Xie and Berkowitz*, 2006].

5. Overview of Present Dissertation

Given the difficulties associated with forecasting VOC emissions and the resulting ozone formation, it is essential to monitor atmospheric VOC composition with high spatial and temporal resolution. It is also important to consider new sources of VOCs as emissions from dominant sectors are reigned in. **My dissertation: 1) examines anthropogenic VOC emissions, primarily from oil and natural gas development, on global, regional, and local scales (Chapters 2-4). 2) Develops a cost effective method for analyzing light hydrocarbons, the compounds most emitted by oil and natural gas development (Chapter 5). 3) Investigates the potential contribution of soil and bacteria to VOC emissions (Chapter 6-7).**

Chapter 2 analyzes ten years of ethane and propane mixing ratio data from ~40 sites in a global network. Ethane mixing ratios declined steadily from a peak 1970s, but this decline halted between 2005 and 2010 in the Northern Hemisphere, and a 0.42 Tg yr^{-1} increase was observed between mid-2009 and mid-2014. The largest increases in ethane mixing ratios were observed at sites in the central and eastern United States, and north Atlantic. Propane's shorter atmospheric lifetime makes it a better indicator of the emission source region. Propane mixing ratios were most elevated at sites in the central and eastern U.S. These compounds are primarily produced by anthropogenic sources, and their increase coincides with an increase in unconventional oil and

gas production. It is estimated that oil and gas related non-methane hydrocarbon emissions increased 1.2 Tg yr^{-1} during this period, and would result in surface ozone enhancements of several nmol mol^{-1} in areas immediately downwind of oil and gas development [*Helmig et al.*, 2016]. Methane/ethane ratios observed from several shale oil plays in the United States were used to estimate a 4.4 Tg yr^{-1} increase in methane emissions as a function of the observed ethane enhancement. This implies a doubling of O&NG related methane emissions in the U.S., which is not consistent with surface and aircraft observations of methane stable isotopes [*Schaefer et al.*, 2016].

Mixing ratio trends of i-butane, n-butane, i-pentane, and n-pentane, and (i/n) isomeric ratios from sites across the continental United States from 2001-2015 were analyzed in the next chapter. Data from Photochemical Assessment Monitoring Stations (PAMS) and the Global Greenhouse Gas Reference Network (GGGRN) were analyzed. PAMS stations were mandated by the U.S. Environmental Protection Agency in ozone nonattainment areas. These sites are downwind of major urban areas. Many of the GGGRN sites are background sites, and are intended to be removed from urban emissions. Negative slopes were observed for individual isomer time series at 81% of sites. This is likely a result of better emission controls and fuel economy of mobile sources, and a decrease in the abundance of the heaviest emitters in the on road automotive fleet. Negative slopes for the (i/n) butane and pentane ratios were found for 78% of the sites over the ~15 year period. Trends of the individual isomers varied by site, so the factors responsible for the changing isomeric ratio are also likely to vary by site. However, because the butane and pentane isomers are largely emitted as a result of fossil fuel production and use, the most likely causes of the shifting isomeric ratios are changes in relative abundances of these compounds in gasoline sector emissions, and increasing influence of oil and natural gas

industry emissions. A key factor in this suggestion is the (i/n) pentane ratio trending toward a ratios characteristic of unconventional oil and gas production (~1) and away from typical urban emission ratios (~3) [*Gilman et al.*, 2013].

Volatile organic compounds (VOCs) were monitored at two networks of sites near Boulder, Colorado to study the spatial distribution of these compounds. One site network extended along an elevation gradient from the city of Boulder (elevation 1600 m) to the Mountain Research Station (2900 m). Longer lived compounds ethane and propane decreased with increasing elevation, suggesting that the city was the origin of these anthropogenic compounds. Diurnal cycles of these compounds were also studied, and a few high daytime mixing ratio events were observed, which were likely the result of a nearby emissions source. This conclusion was reached because the expected diurnal cycle would feature a relative minimum during the day as a result of oxidation by the hydroxyl radical (OH) and boundary layer dynamics. The other site network was in eastern Boulder County approaching a region of oil and gas development. VOCs were monitored at five sites increasingly close to oil and natural gas (O&NG) development. O&NG related VOCs increased as the distance to O&NG producing region decreased. Further, the variability of mixing ratios increased as distance to the region decreased. This behavior is typical of measurements taken from near an emissions source.

Human health impacts have been demonstrated in proximity to oil and natural gas (O&NG) operations and are cause for increased interest in monitoring exposure to emissions [*Halliday et al.*, 2016; *McKenzie et al.*, 2018; *McKenzie et al.*, 2015; *McKenzie et al.*, 2014; *McKenzie et al.*, 2012]. Adsorbent sampling cartridges offer an attractive sampling approach for evaluating exposure to O&NG hydrocarbons as they are inexpensive, and can be deployed with little training in a variety of environments. The goal of this project is to expand passive adsorbent

sampling to selective O&NG tracer compounds, C2-6 hydrocarbons, which previously had not been sampled by this method. Stronger adsorbent materials are required to sample these highly volatile compounds, so the carbon based adsorbents Carboxen 1000 and 1016 were evaluated in laboratory and field monitoring settings. A thermal desorption Gas Chromatograph/Flame Ionization Detector/Mass Spectrometer (GC/FID/MS) was used for analysis. Challenges inherent to the increased affinity of these adsorbent materials are the relatively high uptake rates of atmospheric water vapor and the high blank signal that often dictates the limit of detection. This challenge was overcome by selecting the adsorbent with the best signal to noise ratio for the target compounds, optimizing conditioning parameters to reduce blank signals, and reducing the adsorbent mass loaded in the cartridge, which reduced blank signals by a factor of 4 without sacrificing sampling performance. This strategy reduced blanks sufficiently (to equivalent ambient air mole fractions of < 50 pmol mol-1) to sample target compounds at levels > 0.5 nmol mol^{-1} (ppbv). Linear uptake by cartridges was observed in a simulated environment devoid of humidity, though uptake rates declined over the course of a week of sampling. Water uptake was as high as 0.65 gH2O g-1adsorbent in environments above ~75% RH, and reduced the target analyte uptake by up to 88%. Average uptake rates in a humidified test atmosphere were 34% of those in the dry simulated environment. Despite this, representative sampling was achieved for C3-5 alkanes during three field studies, where cartridges were deployed alongside sampling canisters for whole air collection with subsequent GC/FID/MS analysis. Agreement varied by compound; ethane and alkene mixing ratios correlated poorly ($R2 < 0.40$), but propane, n-butane, i-pentane, and n-pentane correlated well ($R2 > 0.75$) and support the use of passive adsorbent sampling for assessing a community's exposure to O&NG emissions.

Dynamics of carbon dioxide (CO_2) emissions following the wetting of dry soil have been widely studied in field and laboratory settings. Non-methane volatile organic compounds (VOCs) are also emitted from soil following a rain event, and are evident from the characteristic smell of wet soil. Few studies have documented VOC emissions before and after soil rewetting. Soil emissions were studied using a dynamic flux chamber system purged with VOC-free air, with identification and quantification of emissions performed by gas chromatography/mass spectrometry. The use of VOC-free air neglects the possibility of VOC uptake by soil, however, our goal was to characterize and quantify emissions from soil samples rather than simulate natural conditions. More discussion on this is available in Chapter 6. All soils exhibited a rewetting-induced pulse of VOC emissions, with VOC emissions 14 times higher (on average) in the few hours after rewetting compared to moist soils 2 days after rewetting. This VOC rewetting pulse mirrored the CO_2 rewetting pulse (the so-called "Birch Effect") but was shorter in duration [*Birch*, 1958; *Fierer and Schimel*, 2002; 2003; *Gray et al.*, 2010; *Leff and Fierer*, 2008; *Ramirez et al.*, 2010]. Average VOC emissions were $5.0 \pm 2.0\%$ of CO_2 emissions (molar C equivalent), and increased with increasing soil organic matter content ($\rho=0.40$, $\rho=0.99$ with one soil excluded). The amounts and types of VOCs varied with time since rewetting and across the five studied soil types, though acetone and small hydrocarbons were the dominant compounds emitted from all soils. Some of the VOCs emitted are likely important mediators of microbial activities and relevant to atmospheric chemical dynamics. Soil VOC emissions, similar to CO_2 emissions, are strongly affected by rewetting events, and it is important to consider these rewetting dynamics when modeling soil and ecosystem VOC emissions and understand their relevance to terrestrial ecosystem functioning and atmospheric processes.

Soil microbes emit numerous volatile organic compounds (VOCs), which play a role in a variety of microbe-microbe interactions, and can have an effect on the structure and function of microbial communities. However, the field of microbial volatiles is largely unexplored. We used gas chromatography/mass spectrometry (GC/MS) to study the VOCs emitted by 48 Actinobacteria isolated from soil and airborne dust. We detected 126 distinct VOCs and structurally identified approximately 20% of these compounds. Most of the identified species were < C5 alcohols, ketones, esters, nitrogen-, and sulfur-containing compounds. Each Actinobacterial strain produced a unique VOC profile composed of largely strain-specific VOC. Some VOCs were present in the emission profiles of several strains; these compounds are likely byproducts of primary metabolism. The diversity of observed VOC profiles suggests their role in finer-scale patterns of ecological diversity. We also studied the effect of VOCs on growth rates of both pathogenic and non-pathogenic pseudomonad strains, and observed sets of VOCs that correlated with growth inhibition and stimulation. Further investigation of these relationships may allow for the development of microbial VOC-based pathogen control strategies.

Chapter 2

Reversal of global atmospheric ethane and propane trends largely due to US oil and natural gas production

Detlev Helmig[1]*, Samuel Rossabi[1]**, Jacques Hueber[1], Pieter Tans[2], Stephen A. Montzka[2], Ken Masarie[2], Kirk Thoning[2], Christian Plass-Duelmer[3], Anja Claude[3], Lucy J. Carpenter[4], Alastair C. Lewis[5], Shalini Punjabi[4], Stefan Reimann[6], Martin K. Vollmer[6], Rainer Steinbrecher[7], James W. Hannigan[8], Louisa K. Emmons[8], Emmanuel Mahieu[9], Bruno Franco[9], Dan Smale[10] and Andrea Pozzer[11]

[1]Institute of Arctic and Alpine Research, University of Colorado, Boulder, Colorado 80305, USA.
[2]Earth Systems Research Laboratory, National Oceanic and Atmospheric Administration, Boulder, Colorado 80305, USA.
[3]Deutscher Wetterdienst, 82383 Hohenpeissenberg, Germany.
[4]Wolfson Atmospheric Chemistry Laboratories, University of York, York YO10 5DD, UK.
[5]National Centre for Atmospheric Science, University of York, York YO10 5DD, UK.
[6]Laboratory for Air Pollution and Environmental Technology, Empa, Swiss Federal Laboratories for Materials Science and Technology, 8600 Duebendorf, Switzerland.
[7]Karlsruhe Institute for Technology, Campus Alpine, 82467 Garmisch-Partenkirchen, Germany.
[8]National Center for Atmospheric Research, Boulder, Colorado 80301, USA.
[9]Institute of Astrophysics and Geophysics, University of Liège, 4000 Liège, Belgium.
[10]National Institute of Water and Atmospheric Research, Lauder 9352, New Zealand.
[11]Max Planck Institute for Chemistry, 55128 Mainz, Germany.

*Corresponding author: Detlev Helmig (detlev.helmig@colorado.edu)
**SR's Contribution to this manuscript: data processing, preparation of graphs, manuscript preparation.

Abstract

Non-methane hydrocarbons such as ethane are important precursors to tropospheric ozone and aerosols. Using data from a global surface network and atmospheric column observations we show that the steady decline in the ethane mole fraction that began in the 1970s [*Aydin et al.*, 2011; *Helmig et al.*, 2014; *Worton et al.*, 2012] halted between 2005 and 2010 in

most of the Northern Hemisphere and has since reversed. We calculate a yearly increase in ethane emissions in the Northern Hemisphere of 0.42 (0.19) Tg yr^{-1} between mid-2009 and mid-2014. The largest increases in ethane and the shorter-lived propane are seen over the central and eastern USA, with a spatial distribution that suggests North American oil and natural gas development as the primary source of increasing emissions. By including other co-emitted oil and natural gas non-methane hydrocarbons, we estimate a Northern Hemisphere total non-methane hydrocarbon yearly emission increase of 1.2 (0.8) Tg yr^{-1}. Atmospheric chemical transport modelling suggests that these emissions could augment summertime mean surface ozone by several nanomoles per mole near oil and natural gas production regions. Methane/ethane oil and natural gas emission ratios could suggest a significant increase in associated methane emissions; however, this increase is inconsistent with observed leak rates in production regions and changes in methane's global isotopic ratio.

1. Introduction

Oxidation of atmospheric non-methane hydrocarbons (NMHCs) contributes to production of surface ozone and secondary aerosol, both of which impact air quality and climate. NMHCs are emitted into the atmosphere from a variety of biogenic and anthropogenic sources. Ethane is the longest-lived and most abundant NMHC, found typically at 0.4–2.5 nmol mol^{-1} (ppb) in the background atmosphere. It is released from seepage of fossil carbon deposits, volcanoes, fires, and from human activities, with fossil fuel extraction, distribution leakage, and industrial use being the main sources. Pre-industrial ethane atmospheric mole fractions measured in polar ice cores were ~400 pmol mol^{-1} in the Northern Hemisphere (NH) and 100 pmol mol-1 in the Southern Hemisphere (SH), that is between 1/4–1/2 of current levels [*Nicewonger et al.*, 2016].

Firn air records [*Aydin et al.*, 2011; *Helmig et al.*, 2014; *Worton et al.*, 2012] show that in the early part of the twentieth century NMHCs increased steadily in the global atmosphere. Light alkane NMHCs (C2–C5) reached a maximum that was 50% above 1950 levels during 1970–1985. Global atmospheric ethane peaked around 1970. NMHCs have since been steadily declining to mole fractions that are closer to the earliest data in the Greenland firn record (Fig. 1a).These trends are primarily due to stricter air quality emission controls that were first implemented some 50 years ago with the goal to reduce human exposure to NMHCs and surface ozone. The regulations resulted in reduced emissions from sources such as the oil and natural gas (O&NG) industries and automobiles, and a gradual decline of atmospheric NMHCs in urban air in many developed countries and also in the background atmosphere [*Simpson et al.*, 2012; *Von Schneidemesser et al.*, 2010; *Warneke et al.*, 2012].
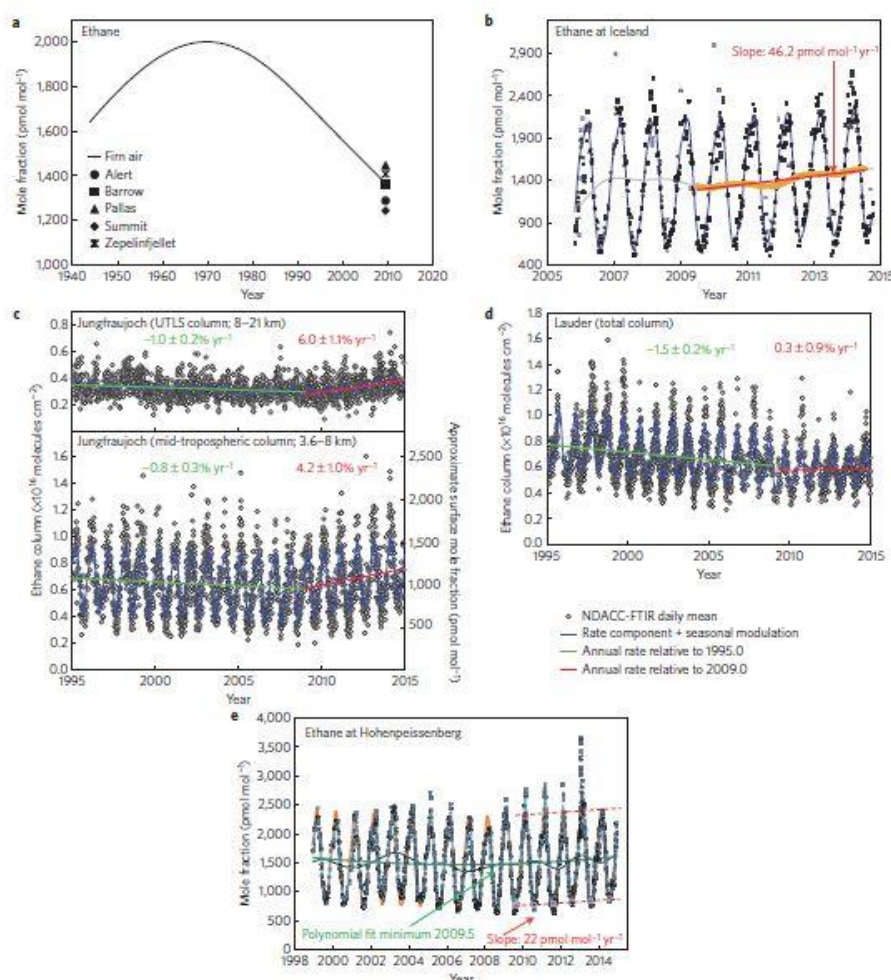
Figure 1. Histories of atmospheric ethane. a, Reconstructed 1950–2010 ethane history from firn air sampling at NEEM in Greenland3 with 2009.5 mean seasonally detrended atmospheric values at five Arctic sites for comparison. Data from [*Helmig et al.*, 2014]. b, Ten years of NMHC flask network data in south Iceland. Individual flask data, identified outliers (smaller blue points), a smoothed fit, the trend results after removal of harmonic components, and the linear regression fit are shown, with a 46.2 pmol mol−1 yr−1 increase from 2009.5 to 2014.5. c,d, Ethane upper troposphere and lower stratosphere (UTLS), and mid troposphere FTIR columns showing a trend reversal and increasing rate of change after 2009 at Jungfraujoch, Switzerland (c), in contrast to Lauder, New Zealand (d). e, Monthly running median data from the daily in situ record at Hohenpeissenberg, with smoothed, function, and trend fits. A polynomial fit shows a minimum in the second half of 2009; the linear regression to the post 2009.5 trend curves and seasonal maxima and minima show increases of 22–23 pmol mol^{-1} yr^{-1}.

Ethane and methane are co-emitted from O&NG sources. Ethane observations have been used to attribute anthropogenic methane emission changes [*Simpson et al.*, 2012]. Having the longest NMHC lifetime, of the order of 2 (summer) to 6 (winter) months, ethane is the NMHC

observed with the least spatial and short-term variability in background air, making it the best candidate species for studying hemispheric gradients and long-term changes.

2. Discussion

We analyzed ten years of NMHC data collected at 44 remote global sampling sites from the National Oceanic and Atmospheric Administration (NOAA) Global Greenhouse Gas Reference Network (GGGRN). We also include data from in situ monitoring at Summit, Greenland [*Kramer et al.*, 2015], at Hohenpeissenberg (HPB) in Southern Germany [*Plass-Duelmer et al.*, 2002], Jungfraujoch (JFJ) and Rigi, Switzerland, and Cape Verde in the Mid-Atlantic [*Read et al.*, 2009]. For propane, we further included results from eight sites within NOAA's GGGRN (Methods).

Atmospheric NMHCs exhibit a dynamic seasonal and latitudinal behavior. Maxima are seen in late winter, and minima in the summer (Fig.1b–e). Sources of light NMHCs do not vary much seasonally [*Leuchner et al.*, 2015]; seasonal cycles are primarily driven by photochemical loss. Consequently, seasonal cycles exhibit the largest amplitude near the poles, are small near the Equator (Fig.2), and are shifted by 6 months in the SH owing to the opposite season. There is also a strong latitudinal gradient of absolute values, with highest abundances observed in the Arctic, steeply declining levels at mid- latitudes, and lower abundance in the SH. These gradients are caused by sources that are dominated by anthropogenic emissions, which are highest in the industrialized mid-northern latitudes, and the slower transport across the equatorial zone compared with intrahemisphere mixing. Gases with shorter lifetimes, that is, propane, iso-butane, and n-butane, exhibit more pronounced seasonal and latitudinal gradients (Fig.2).
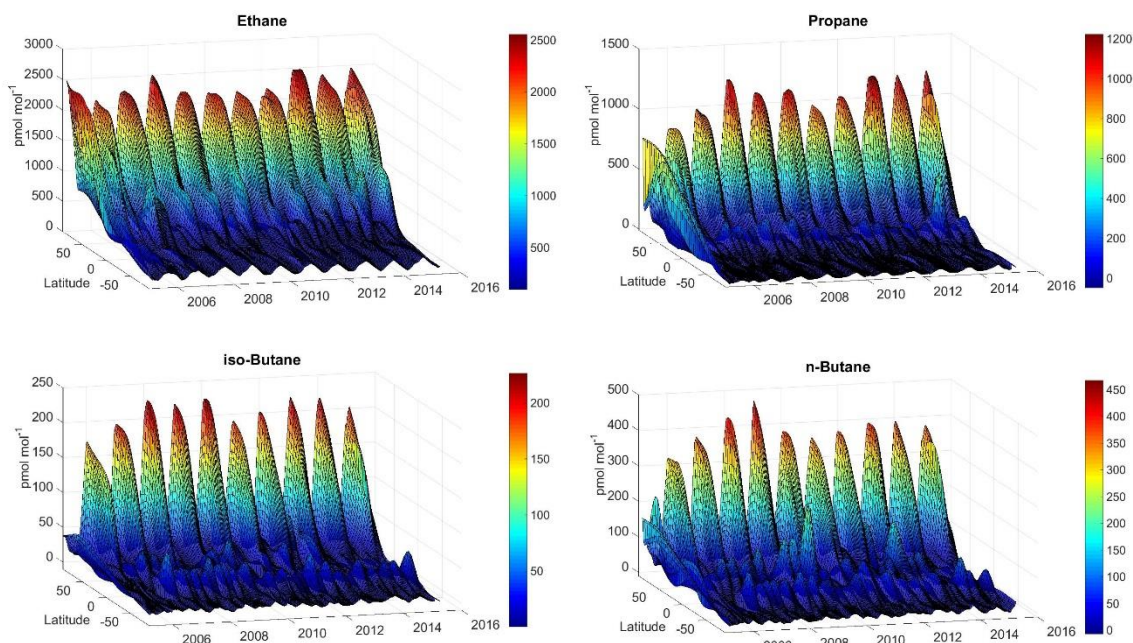
Figure 2. Latitudinal distribution of ethane, propane, iso-butane, and n-butane. These representations of surface mole fractions were generated using weekly data from 37 to 39 global background monitoring sites, altogether some 30,000 data points for each graph. Note that these plots are a representation of latitudinal averages of atmospheric mole fractions; therefore, they do not capture differences between continents at the same latitude. Procedures for data filtering and processing are discussed in the Methods.

Individual site data reveal that for many NH locations the downward trend reported in earlier work has halted and reversed to increasing NMHC levels. As the flask network programme started in 2006, data for most sites do not go back far enough for deciphering the exact time of the trend reversal. The second-order polynomial fit through the longest, and most highly time-resolved in situ record from HPB has its minimum in 2009 (Fig.1e), in agreement with the JFJ Fourier transform infrared (FTIR) column observations (Fig.1c). Focusing on the most recent five years (2009.5–2014.5) we find variable results in the observed rate of change; however, a consistent picture emerges that shows the largest increases at NH sites (Fig.3). Of 32 NH sites, 9 exhibit ethane growth rates >50 pmol mol^{-1} yr^{-1}, and 13 sites exhibit growth rates between 25 and 50 pmol mol^{-1} yr^{-1} (Supplementary Table 1). Depending on grouping of sites and averaging across regions and calculation method, a mean NH ethane increase rate of 2.9–

4.7% yr^{-1} is calculated (Methods). These rates of change in atmospheric ethane have not been

seen at SH sites; most SH sites show only small changes, with poorer regression results.

Applying a second-order polynomial fit to the NH trend curves yields positive quadratic

coefficients in 22 out of 32 cases, showing that for most cases, ethane trend curves are becoming

steeper; that is, rates of change in atmospheric abundance have been increasing at most of the

sites during this time window.
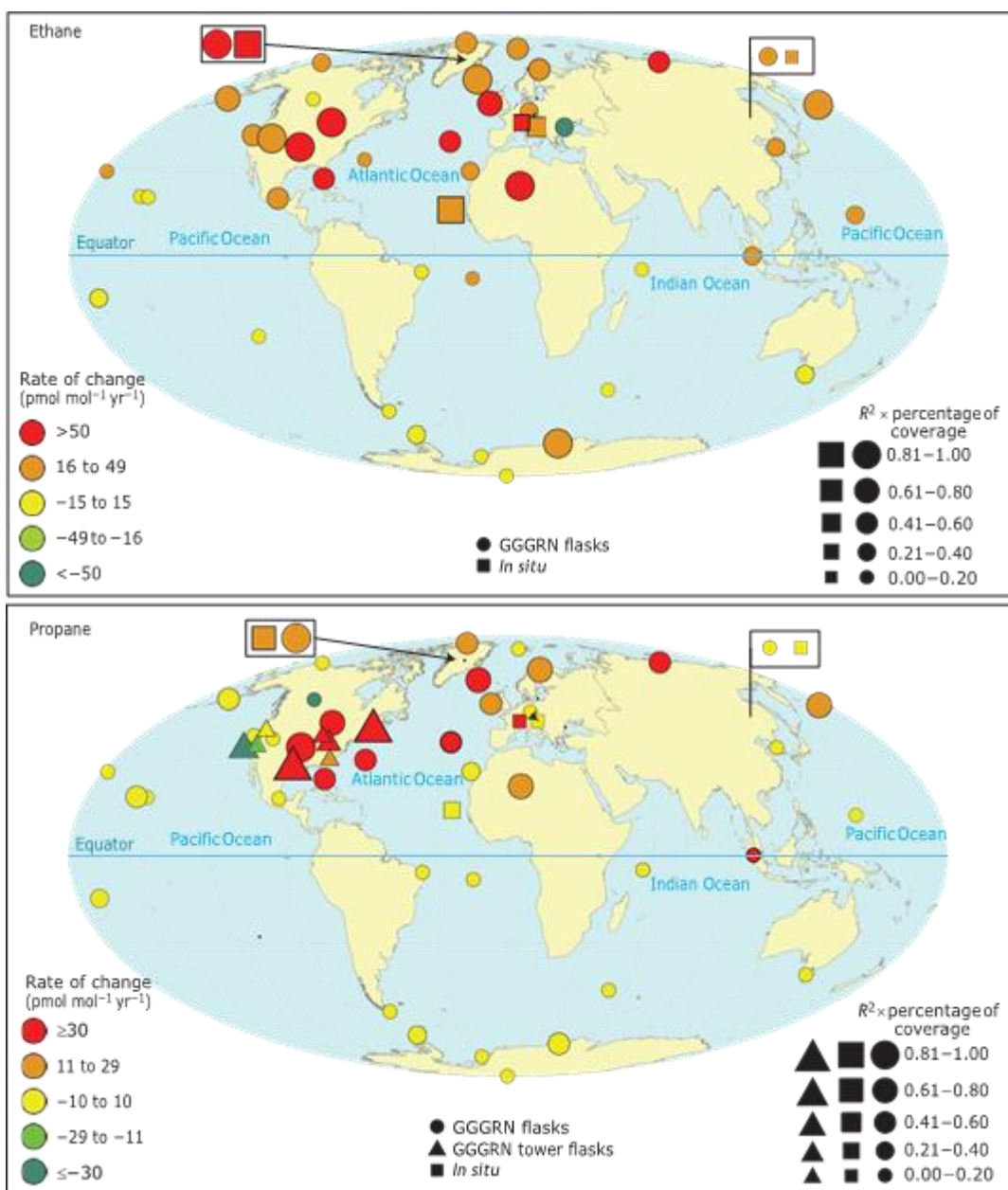
Figure 3. Ethane and propane trends at global monitoring sites. Mole fraction changes are indicated by the colour scale with marker size corresponding to the R2 of the fit multiplied by the fraction of available site data. Results from overlapping GGGRN flask and in situ measurements are shown in black rectangles for Summit and Hohenpeissenberg. a, Increasing ethane is observed throughout the NH, with the strongest signal in North America, the North Atlantic, and neighbouring continents. There is no or very little change in ethane at SH sites. b, Propane shows a more pronounced region of increasing mole fractions in the eastern USA and at nearby downwind sites. Again, these changes are not seen at the SH sites.

This hemispheric difference in ethane trends is further supported by two contrasting

records of ethane column observations (that is, the number of molecules integrated between the

ground and the top of the atmosphere), one from JFJ (Fig.1c) [*Franco et al.*, 2015], and the other

one from Lauder, New Zealand (Fig.1d). At the 3,580 m elevation of JFJ, these data are a good

representation of free tropospheric ethane, reflecting the continental background and long range

transport. Whereas there was a slight downward trend in the data for the first 15 years of the

record, in agreement with the trends inferred from the firn and HPB data, a reversal is evident

after 2009, with a post-2009 rate of increase in the mid-troposphere of $4.2 \pm 1.0\%$ yr^{-1}. The

upward trend is evident in both the mid-troposphere and upper troposphere/lower stratosphere

partial columns, indicative of the hemispheric nature of the ethane increase. The ethane trend

reversal is absent in the SH FTIR column data (Fig.1d). The difference in trends in the

hemispheres is consistent with an increasing NH source.

Notably, ethane rates of change are highest at the central and eastern USA and nearby

downwind sites, suggesting that the ethane increase is driven to a large part by emissions from

North America. The regional hotspot of increasing NMHC levels can be pinpointed more

narrowly from propane observations. Propane, with a lifetime 1/4 of ethane, is a more sensitive

indicator for local/regional emissions. Propane data show the greatest increases in the central and

eastern USA, and in the downwind North Atlantic region (Fig.3). In contrast, propane levels

have been relatively stable in central Europe, the Pacific region, and the SH. Also, measurements

in the western USA do not show propane increases. With the primary synoptic transport

direction being west and southwest to east, the spatial analyses of ethane and propane increases

point to the central to eastern parts of the USA as the regions where most of the emission

increases have occurred.

The O&NG sector is a major source of light NMHC emissions. A surge in O&NG

production has occurred in recent years, particularly in the USA, where unconventional oil and

natural gas drilling has resulted in estimated 10–20-fold increases in shale O&NG production between 2000 and 2015 (www.eia.gov), making the USA the fastest growing and a leading O&NG producing nation. Ground and airborne observations have consistently shown elevated levels of methane and NMHC as a result of venting, flaring, and leakage. NMHC ambient mole fractions measured in O&NG basins can far exceed (up to >100 times) the regional background and those in urban and other industrial regions, and top-down emission estimates are well above inventory estimates [*Helmig. et al.*, 2014b; *Karion et al.*, 2013; *Pétron et al.*, 2012; *Swarthout. et al.*, 2015; *Thompson. et al.*, 2014]. Resulting ozone production from these emissions has led to air quality standard exceedances in the Uintah Basin, Utah, and Upper Green River Basin, Wyoming, O&NG regions [*Oltmans et al.*, 2014; *Schnell et al.*, 2009]. Two other regional studies have previously noted upwards trends in ambient NMHC and associated these changes with upwind O&NG activities. An increase from 7% to 13% of the total observed non-methane organic carbon abundance during 2010–2013, and increasing ethane mole fractions were measured in Baltimore, Maryland, downwind of the Marcellus Shale [*Vinciguerra et al.*, 2015]. Similarly, data from southern Texas showed steeply increasing ethane levels associated with transport from the Eagle Ford Shale [*Schade and Roest*, 2015].

Applying the JFJ FTIR mid-troposphere column trend value of 4.2% yr^{-1} to the NH annual ethane emission estimate of 9.9 Tg yr^{-1} (Methods) yields an estimate for an ethane annual emission increase of 0.42 ± 0.19 Tg yr^{-1} (see Methods for all uncertainty range calculations), resulting in an overall 2.1 ± 1.0 Tg yr^{-1} emission increase during 2009.5–2014.5. This additional emission is 1.5 times the North America inventory estimate of 1.6 Tg yr^{-1} for 2007. Considering estimates of co-emitted NMHC yields an estimate for a yearly total NMHC

emissions increase of 1.2 ± 0.8 Tg yr^{-1} (5.9 ± 4.0 Tg yr^{-1} overall emissions increase during 2009.5–2014.5).

There is no evidence for major non-O&NG NMHC emissions increases. From the spatial overlap of USA O&NG regions with identified areas of largest NMHC increases it seems likely that the NMHC increase is largely driven by USA O&NG production. This added NMHC emission is expected to fuel additional surface ozone production in source and downwind regions. Figure 4 illustrates modelling results from a first order of magnitude sensitivity study, where the 4.2% yr^{-1} increase in the C2–C5 NMHC flux was at- tributed to USA O&NG emissions over five years at constant emissions of nitrogen oxides (NOx). This added emission causes changes in surface ozone in regions with O&NG development and downwind, reaching up to 0.5 nmol mol^{-1} yr^{-1} average ozone increases for June–August, corresponding to 2.5 nmol mol^{-1} increases overall over the five year period simulated with the model. The sensitivity is particularly high in the western USA, mostly driven by higher NOx in that region. Consequently, these NMHC emission changes can potentially offset emission controls that have been implemented for curbing photochemical ozone production, and therefore can be a concern for attaining the ozone air quality standard.
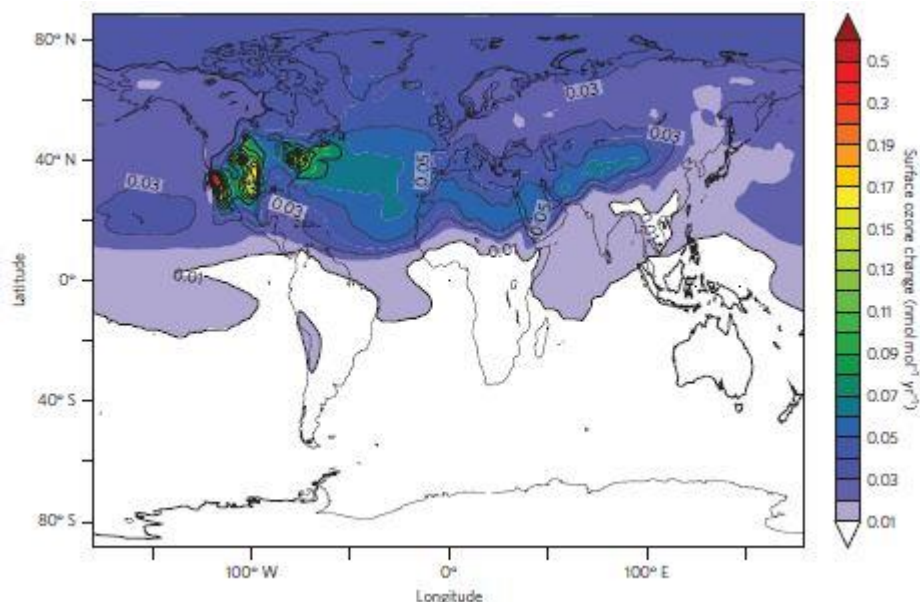
Figure 4. Ozone sensitivity study. Estimate for the average annual 2009.5–2014.5 June–August change in surface ozone from a 4.2% yr−1 NH increase in ethane, and inferred emission increases in propane, butane and pentane isomers from USA O&NG sources. The modelling did not consider increases in methane and NMHC >C5 emissions, and assumed constant emissions of nitrogen oxides and volatile organic compounds from other emission sectors. Increases in surface ozone are predicted over extended areas of the USA and downwind.

Atmospheric methane has been increasing since ~2007, after ~8 year period of stable levels. Continental emission changes of O&NG-related methane USA inventory emissions [*EPA*, 2016] and a 6.2% total increase between 2009.5 and 2014.5 of the 330 Tg yr^{-1} [*Kirschke et al.*, 2013] global anthropogenic methane emission. Although other recent studies [*Franco et al.*, 2015; *Franco et al.*, 2016b; *Hausmann et al.*, 2016; *Turner et al.*, 2016] have derived similar estimates for methane emission increases and associated those with increased North American O&NG emissions, most also rely on the extrapolation of NMHC results to infer methane emission changes. We note that surface and aircraft observations of methane stable isotopes from the GGGRN are inconsistent with such a large North American methane flux increase from O&NG sources [*Schaefer et al.*, 2016]. Furthermore, the methane emission implied by this analysis of NMHC data as a fraction of O&NG production is a substantially higher percentage

than what has been observed in O&NG fields in North America [*Karion et al.*, 2015; *Karion et al.*, 2013; *Peischl et al.*, 2015b; *Pétron et al.*, 2012; *Petron et al.*, 2014]. This suggests yet unidentified increasing sources for NMHC emissions independent of methane or with lower methane/ethane emission ratios, or potential emission increases outside North America that cannot be well defined at present owing to the sparsity of observations in those regions (for instance, in the Middle East, Africa, and Asia).

3. Methods

3.1 Global VOC network

Since 2004 the NOAA GMD and INSTAAR in Boulder, Colorado, have been operating a global volatile organic compound (VOC) monitoring program that is building on the NOAA Global Greenhouse Gas Reference Network (GGGRN). VOCs are quantified in whole air sampled in pairs of glass flasks that are collected weekly to bi-weekly at 44 global background monitoring sites, with a total sample number of 3,000 per year. At present, ethane, acetylene, propane, iso-butane, n-butane, iso-pentane, n-pentane, isoprene, benzene, and toluene are analysed in the sample remaining in the flasks after completion of analyses of greenhouse gases, and of CO_2 and methane stable isotopic ratios. The gas chromatography (GC) with flame ionization detection method [*Pollmann et al.*, 2008b] is calibrated by a series of gravimetrically prepared synthetic and whole air standards. The programme operates under the umbrella of the World Meteorological Organization Global Atmospheric Watch (WMO-GAW) and is collaborating with international partners on exchange of calibration standards and comparison of calibration scales [*Helmig et al.*, 2009]. The INSTAAR laboratory was audited by the World Calibration Center (WCC) for VOC [*WCC-VOC*, 2016] in 2008 and 2011. Five unknown

standards were analysed and results reported to the WCC. Mean results of five repeated measurements of the provided standards deviated <1.5% ethane, and <0.8% for propane from the certified values. These deviations are well below the deviation criteria set by GAW [*WMO/GAW*, 2006] . Uncertainties in the NMHC data are estimated to be 5% for results >100 pmol mol^{-1} , and 5 pmol mol^{-1} for results <100 pmol mol^{-1}. More analytical and programme details are provided by [*Pollmann et al.*, 2008b; *Pollmann et al.*, 2006; *Program*, 2016]. VOC in situ monitoring at Summit (SUM), Greenland. Year-round VOC monitoring at Summit (72.6 ∘ N, 38.5 ∘ W; 3,216 m asl) was performed from 26 June 2008 to 22 July 2010, totaling 756 days (just over 2 years)37 , and resumed in May 2012 and is ongoing. The GC is calibrated several times per week using standards that are cross-referenced against the global flask network laboratory scale. Uncertainties in the NMHC data are estimated to be ≤5% for results >100 pmol mol^{-1} , and ≤5 pmol mol^{-1} for results <100 pmol mol^{-1} .

3.2 VOC in situ monitoring at Hohenpeissenberg (HPB)

Continuous VOC monitoring at HPB (47.8° N, 11.8° E, 980 m asl) has been conducted since 1998 as part of the WMO-GAW [*Plass-Duelmer et al.*, 2002]. Calibrations rely on a series of gravimetric and whole air standards referenced to the WCC. VOC sampling is conducted daily at noontime. Uncertainties (95% confidence interval) are generally ± (1.9 pmol mol^{-1} + 2.9%) in the ethane mole fraction, and ± (1.3 pmol mol^{-1} + 2.9%) for propane, except for isolated periods of degraded chromatography or other instrumental issues that result in higher uncertainties. Detection limits are at 3 and 2 pmol mol^{-1} for ethane and propane, respectively.

3.3 VOC in situ monitoring at Jungfraujoch (JFJ)

At JFJ, a high-elevation site in the central Swiss Alps (46.5° N, 7.6° E, 3,580 m asl),

VOCs are measured using a Medusa GC/mass spectrometer (MS) [*Miller et al.*, 2008] hourly

with each pair of measurements bracketed by standard measurements. Ethane and propane

measurements started in 2008 and are ongoing. Measurement precisions are 0.3% for ethane and

0.8% for propane (1σ). Calibration is provided by referencing standards against primary

reference gases of the National Physical Laboratories (UK) and thus is linked to the WMO-VOC

scale. Uncertainties are ∼10% for ethane and 3% for propane.

3.4 VOC in situ monitoring at Cape Verde (CVO)

The Cape Verde Atmospheric Observatory Humberto Duarte Fonseca (16.8° N, 24.9° W,

10 m asl) is positioned upwind of Calhau on the northeastern side of São Vicente, Cape Verdes.

Hourly VOC measurements are made from a height of 20 m asl; analytical details are provided

by *Read et al.* [2009]. Uncertainties in the NMHC data are estimated to be 5% for results >100

pmol mol^{-1}, and 5 pmol mol^{-1} for results <100 pmol mol^{-1} .Detection limits are 2.6 and 1.6

pmol mol^{-1} for ethane and propane, respectively. Calibrations are linked to the WMO-VOC

scale.

3.5 VOC measurements from North American tower sites

Glass flasks are also collected with automated samplers at tower sites across North

America as part of the NOAA GGGRN. These samples are collected at a higher sampling

frequency (daily) and are analysed at NOAA by GC/MS [*Pétron et al.*, 2012]. Reported mole

fractions for propane are based on a suite of gravimetric standards prepared at NOAA;

calibration consistency is maintained independently from INSTAAR. The resulting NOAA

calibration scale for propane has been assessed in an international round-robin exercise and was found to be consistent within 5% to other internationally recognized and well-established scales [*Rhoderick et al.*, 2014].

3.6 Data processing

At the time of the data processing final data from all considered sites until June 2014 (2014.5) were available, which was used as the cutoff of the analyses. The criterion for individual sites data to be included was that data were available for at least 50% of the sampling days for 2009.5–2014.5. Two flask network and three tower site data sets were excluded because they did not meet this criterion. Similarly, in situ data from remote monitoring sites were only included if data were available for at least 50% of the 2009.5–2014.5 sampling dates. NMHC data were first filtered for outliers; values that deviated more than 2σ from a running median were excluded from trend analyses. Filtered data were then uploaded to the NOAA server for filtering and trend determination using the method of [*Thoning et al.*, 1989] and described at http://www.esrl.noaa.gov/gmd/ccgg/mbl/crvfit/crvfit.html. The first step is to fit a function, consisting of the sum of a polynomial and four harmonics (amplitude and phase of 1 through 4 cycles per year). The residuals of the function fit are smoothed by two low-pass filters, one for the trend (1.1 year full-width at half-maximum), and one for anomalies of the seasonal cycle (full-width at half-maximum 50 days). The function and filtered data are then combined to generate a smoothed data curve, trend curve, a detrended seasonal cycle, seasonal amplitude, a polynomial fit, and the long-term growth rate. The smoothed data curve is a combination of the function and the short-term filter of the residuals. The trend curve is the polynomial part of the function plus the long-term filtered residuals, and represents the growth or decline of the data

with the seasonal oscillations removed. The detrended seasonal cycle is complementary to the trend curve; it is the interannually varying cycle with the trend removed. The seasonal amplitude is the amplitude of the detrended seasonal cycle, and the growth rate is the rate of increase or decrease of the trend, found by taking the first derivative of the trend. Results of a trends statistical significance test are included in Supplementary Tables 1 and 2. To avoid a bias from oversampling of the trend curve, its output was sampled only at times when retained flask data were available. These data were then subjected to the Mann–Kendall test [*Yue et al.*, 2002] using a significance value of α 0.01. Results (calculated p values) are presented in column 12 of Supplementary Tables 1 and 2. Values <0.01 reflect the rejection of the null-hypothesis that there is no trend. In these cases, the trend is found to be true at 99% confidence. Incidences where trends were found to be not statistically significant are listed in italic font and in brackets. Results show that of 34 NH ethane trend series (flask and in situ), 32 show a positive trend. All positive trends are statistically significant. Lac La Biche, Alberta (LLB), shows a slight, nonsignificant negative trend. The LLB series has a reduced data coverage (73%), a high number of outlier points, and an R^2 0 result, all of which reduce the robustness of the LLB trend result. The other site showing a negative trend is Black Sea, Constanta (BSC). Similar to LLB, this site suffers from reduced data coverage (50%), and a high number of outlier points. Furthermore, this site seems to be severely impacted by nearby pollution sources. Despite these two sites showing rather noisy records and poor regression results, they were retained in the presentation of our results, as we did not want to use arbitrary filtering criteria. The data used in the maps (Fig.3) were generated by applying a linear least-squares fit of the trend data from each site for the period 2009.5–2014.5. The slope of the fit determined the colour of the marker. The R^2 value times the coverage of the fit determined the size of the marker. Most of the data are from

NOAA/INSTAAR network flask sites. Furthermore, in situ monitored sites were included, as well as propane data from the tower sites.

Easter Island (EIC) propane data were excluded because they showed influence from a local source. Propane network data from BSC, and propane tower flask data from Mount Wilson Observatory (MWO) were excluded because a representative fit could not be drawn. A summary of trend results from all surface network and tower flask, and in situ observations is provided in Supplementary Table 1 for ethane, and in Supplementary Table 2 for propane.

3.7 Network flask–in situ trend results evaluation

There is overlap of flask and in situ VOC monitoring at two sites, that is, SUM and HPB. The parallel observations at these two sites were used to evaluate the quality of the trend fit results from the weekly network flask measurements against the higher time resolution in-situ measurements. Details of these comparison studies will be presented in a forthcoming publication. In summary, these investigations showed that the less frequent flask records provide a good representation of the in situ records, yielding trend results of the same magnitude (Fig.3).

3.8 Average ethane trend calculations

There are 45 sites that met the requirements (>50% data coverage for 2009.5–2014.5) for inclusion in the trend analyses, with 32 of these sites in the NH. As can be seen in Supplementary Tables 1 and 2, data coverage, quality of the correlation analyses, and trend results vary widely. We explored a number of methods for deriving an average NH ethane trend from these data. First, data from all sites, regardless of data coverage and quality of the regression fit, were treated equal. For sites with flask and in situ data, the mean of both trend

38

values was used (SUM and HPB). Sites were grouped by latitude zone, NH longitude, and continental/oceanic region, and average and median ethane trends were calculated from all sites within each region (Supplementary Table 3). Please note the uneven representation of regions, as some of them have fewer sites than others, making results for regions with low representation less certain. Depending on the grouping and averaging, ethane trend results range from 3.5 to 4.3% yr^{-1} for the mean values, and 2.9–4.2% yr^{-1} for the median results across all sub-regions. The lower mean values are largely due to the negative trend (7.6% yr^{-1}) at BSC, a site that suffers from reduced data coverage (50%), and a high number of outliers, and seems to be severely impacted by nearby pollution sources (see above). Nonetheless, we kept the BSC result in the calculations for treating all sites equally for the NH mean trend calculations. Rates of increases are relatively high at Tiksi (TIK). Monitoring at TIK began in autumn 2011; therefore, the Tiksi record misses the first two years of the 2009.5–2014.5 window. The data coverage is just slightly above the 50% cutoff value (Supplementary Tables 1 and 2). TIK is the site with the second lowest coverage of all sites that were included. Given the short record the uncertainty is much higher than for other sites.

Second, a mean NH ethane trend was calculated by weighting each individual trend result (Supplementary Table 1) by the percentage of coverage of the data, and the R2 of the linear regression fit. For the two sites with flask and in situ measurements the mean value of both trends, a 100% coverage value, and the sum of both R^2 values was used, to reflect the higher certainty from having two parallel results. The result of this analysis was a NH ethane increase rate of 4.7% yr^{-1}. This value is relatively strongly influenced by the two highest individual results from two sites in the central USA, that is, Southern Great Plains (SGP) with a rate of change of 10.7% yr^{-1}, and Park Falls (LEF), Wisconsin, with a value of 7.9% yr^{-1}, also because

both sites have full data coverage, and relatively high R^2 results. Removing these two sites reduces the mean NH ethane rate of change to 4.2% yr^{-1}. It is notable, though, that sites that are far distant from local influences, by horizontal separation, elevation, or by both, and located in the Atlantic region, downwind of North America, showed the cleanest records, that is, the highest correlation coefficient and on average relatively high rate of change values. Sites that fall into these categories (with their rate of change and R^2 results) are SUM (63.9 pmol mol^{-1} yr^{-1}, 4.7% yr^{-1}, R2 0.97 for flask results and 67.2 pmol mol^{-1} yr^{-1}, 5.4% yr^{-1}, R^2 0.96 for in situ), Iceland (ICE) (46.2 pmol mol^{-1} yr^{-1}, 3.4% yr^{-1}, R^2 0.86), Mace Head (MHD) (53.1 pmol mol^{-1} yr^{-1}, 4.3% yr^{-1}, R^2 0.65), Azores (AZR) (86.7 pmol mol^{-1} yr^{-1}, 7.7% yr^{-1}, R^2 0.57), Assekrem (ASK) (72.9 pmol mol^{-1} yr^{-1}, 7.4% yr^{-1}, R^2 0.95), Tenerife (IZO) (30.0 pmol mol^{-1} yr^{-1}, 3.5% yr^{-1}, R^2 0.32) and CVO (44.7 pmol mol^{-1} yr^{-1}, 5.6% yr^{-1}, R^2 0.96). The mean weighted ethane rate of change from these North Atlantic sites accounts to 5.3% yr^{-1}. These comparisons point towards highest rates of ethane increase in the central to eastern USA, followed by the North Atlantic region.

The overall hemispheric ethane trend result of 4.7% yr^{-1} from the latter method using R2 coverage as a weighting factor is 0.4–1.8% yr^{-1} higher than the regional results presented in Supplementary Table 3. This possibly reflects a bias in the calculation as it places lower weight on sites with flat trends and corresponding low R^2 results.
The uncertainty (0.9%) of the best estimate of the ethane NH rate of change was determined as 1/2 of the range of the lowest (2.9%) to the highest value (4.7%) of the different types of regional and hemispheric trend determination.

3.9 NMHC surfaces

Graphs in Fig. 2 were derived using weekly data from the GGGRN sites. To reduce noise in the latitudinal distribution due to synoptic-scale atmospheric variability, records were fitted with a smooth curve [*Thoning et al.*, 1989]. We then used a data extension methodology [*Masarie and Tans*, 1995] with important revisions [*GLOBALVIEW-CO2*, 2011] to produce a set of smoothed records, which are synchronized in time and have no temporal gaps. For each synchronized weekly time step, a latitude distribution (mole fraction versus sine of latitude) was constructed. Each value in the weekly distribution was assigned a relative weight using a strategy that assigns greater significance to sites with high signal-to-noise and consistent sampling. A curve was then fitted to each weekly weighted latitudinal distribution [*Tans et al.*, 1989]. Finally, values were extracted from each weekly latitudinal fit at intervals of 0.05 sine of latitude from 90° S to 90° N and joined together to create the two-dimensional matrix (time versus latitude) of mole fractions.

3.10 FTIR column observations

FTIR total and partial column data were derived from ongoing Network for the Detection of Atmospheric Composition Change (NDACC,www.ndacc.org) observations from solar viewing FTIR instruments. The network instruments are calibrated to common standards to ensure consistent optical performance across the network and over time. High-resolution mid-infrared solar radiation is recorded on a near daily basis. Analyses of the JFJ ethane retrieval and time series are presented in [*Franco et al.*, 2015]. An improved retrieval approach delivers enhanced information content and sensitivity up to 20 km altitude, providing two independent partial column time series, for the 3.58–8 and 8–21 km altitude. The ethane retrieval used for the Lauder spectra is presented in [*Rinsland et al.*, 2002]. Initial analyses of Lauder time series are

described in [*Zeng et al.*, 2012], where SH decreasing trends are given up to 2009. The statistical

bootstrap resampling tool used for the trend calculations is presented in [*Gardiner et al.*, 2008].

It determines a linear trend and corresponding uncertainties, and accounts for the seasonal/intra-

annual variability of the data. Determination of the uncertainty in the ethane column trend of the

JFJ time series is explained in [*Franco et al.*, 2015]. Several settings were tried (that is, adjusting

the step and integration interval) for the running mean calculations at JFJ and other NH FTIR

sites (for example, Toronto), always coming up with an ethane trend reversal date close to late

2008–early 2009.

3.11 Emissions inventory

The ethane emissions inventory is a best estimate based on three different resources that

build on other previous inventories and publications. On the basis of reconstructed ambient air

histories,a year 2000 global ethane emission was estimated at 8–10 Tg yr^{-1} [*Aydin et al.*, 2011].

These authors do not differentiate between NH and SH emissions. Approximately 85% of ethane

is estimated to be emitted in the NH (see (2) and (3) below). Based on that the global estimate

translates to 7–9 Tg yr^{-1} of NH ethane emissions. Second, we evaluated the inventory developed

for the Hemispheric Transport of Air Pollutants, Phase II (HTAP2), which is a composite of

regional inventories harmonized to represent 2008 and 2010 emissions [*Janssens-Maenhout et

al.*, 2015]. Additional ethane emissions included in these simulations are biogenic emissions

from the MEGAN2.1 [*Guenther et al.*, 2012], and fire emissions from FINNv1.5 [*Wiedinmyer et

al.*, 2011]. Simulations with CAM-chem indicated that the anthropogenic emissions needed to be

doubled to match the pre-2009 NMHC FTIR observations at JFJ. A summary of these adjusted

emissions by region and sources is given in Supplementary Table 4 for 2007. Year 2009.5 NH

ethane emissions are estimated as 15 Tg yr^{-1} from the 'Globe—all' minus the SH emissions. For

a third resource, we used the RCP85 database (Representative Concentration Pathway 8.5)

[*Pozzer et al.*, 2015; *Riahi et al.*, 2007]. It includes total emissions of ethane of 12.9 Tg yr^{-1}, of

which 0.53, 2.3 and 10 Tg yr^{-1} are emitted from biogenic, biomass burning, and anthropogenic

sources, respectively. Of the total 12.9 Tg yr^{-1}, 9.9 Tg yr^{-1} are emitted in the NH.

We used 9.9 Tg yr^{-1} , which is the middle value of these three estimates for the ethane,

NMHC, and methane emission increase, and ozone sensitivity modelling, and 1/2 of the

minimum (7 Tg yr^{-1}) to maximum (15 Tg yr^{-1}) range as the uncertainty interval (4 Tg yr^{-1}).

3.11.1 Scaling of methane to ethane

The methane/ethane emission ratio was determined as the median of available data from

analyses of both compounds in USA O&NG regions (Supplementary Table 5). We used 1/2 of

the difference between the minimum and maximum value in the data as the uncertainty interval

(5.6). The methane emission estimation uncertainty interval was calculated by error propagation

including uncertainties in the ethane growth rate, the ethane inventory emission, and the

methane/ethane ratio.

3.12 Scaling of total NMHC to ethane calculation

There are few publications that report speciated NMHCs, and there are even fewer that

include ethane, from O&NG source regions. Furthermore, some of the available literature studies

suffer from measurements being influenced to a variable degree by other contributing sources.

We compiled published speciated NMHC/ethane emission ratios from O&NG development areas

in Supplementary Table 6. Ambient air measurements were converted to relative mass emission

ratios scaled to ethane. The contribution of missing NMHC to the total NMHC emission >C2

was estimated by adding up the relative fractions of missing species reported in the [*Swarthout. et al.*, 2013] study and pro-rating the contribution of the missing species. There is a considerable amount of variability in these data, probably caused by the different NMHC emission ratios in different shale regions.

Among these data sets results from the Uintah Basin are likely to be of a relatively high representativeness for several reasons. First, despite the Uintah Basin having a low population density, atmospheric VOCs have been found to be highly elevated, dominated by emission from O&NG operations. In 2013 the basin had an estimated 4,300 oil- and 6,900 gas-producing wells; therefore, emissions reflect a combination of both types of wells. Second, this data set is the average over two campaigns from two subsequent years. Third, measurements represent an overall high number of samples. Fourth, data are from surface and tethered balloon measurements from January to February, when relatively shallow boundary layer conditions prevailed, which fostered accumulation of nearby emissions [*Helmig. et al.*, 2014b].
The mean and median values for $\Sigma E_{NMHC>C2}/E_{ethane}$ (NMHC/ethane emission ratios) from these studies were calculated as 2.47 and 1.85, respectively, with the Uintah Basin result being the medium value. For the reasons detailed above, we chose a Uintah median $\Sigma E_{NMHC>C2}/E_{ethane}$ value as scaling factor. The uncertainty of 1.4 was determined as 0.5 times the range of minimum to maximum scaling factors from individual studies. Uncertainty of the scaled total NMHC emission was calculated by error propagation.

3.13 Ozone modelling

EMAC (ECHAM5/MESSy for atmospheric chemistry version 2.50 [*Jöckel et al.*, 2010]) was used to develop a first order of magnitude estimation of the impact of the emissions increase

of simple NMHC on ozone formation. Although most of the added ethane flux is probably from the USA, other global regions may potentially have contributed to the flux increase. To reflect this uncertainty, we applied lower estimates for several of the applied variables. We did not consider an increase in methane emissions on ozone production. We considered only estimated associated emissions of C2–C5, excluding NMHC > C5, which constitute 10% of the total O&NG NMHC emission (Supplementary Table 6), and on average have higher reactivity and ozone production potential than the lighter NMHC. Furthermore, the scaling value applied here is below the mean of available observations (Supplementary Table 6). The applied ethane NH inventory flux of 9.9 Tg yr^{-1} is a significantly lower value compared with the most recent estimate (15 Tg yr^{-1} , as explained above and in [*Franco et al.*, 2016b]). The model set-up was the same as in [*Pozzer et al.*, 2010], with the only exception of an augmented chemical scheme, which includes oxidation chemistry of simple C4–C5 hydrocarbons (that is, n- and iso-butane, and n- and iso-pentane). The model simulations adopted emissions from the RCP85 database (Representative Concentration Pathway 8.5) [*Pozzer et al.*, 2015; *Riahi et al.*, 2007] . Two simulations were performed for 2009.5–2014.5: one with constant NMHC emissions, named CONST, and the other with increasing NMHC, named TREND. To disentangle the impact of increased NMHC emissions, all other tracer emissions were kept constant. We applied a trend of 4.2% yr−1 for the NH emissions of ethane over five years based on the JFJ FTIR mid-troposphere column trend value. In the model NH emissions of ethane are 9.9 Tg yr^{-1}, of which 0.17, 0.9, and 8.8 Tg yr^{-1} are emitted from biogenic, biomass burning and anthropogenic sources, respectively. Therefore, the ethane growth rate accounts to an increase in ethane emission O&NG sources of 0.41 Tg yr^{-1}. Based on observed ambient air relative ratios of NMHC in source regions, see Supplementary Table 6, 0.30, 0.11, 0.08, 0.05 and 0.06 Tg yr^{-1}

increases were prescribed to propane, n-butane, iso-butane, n-pentane, and iso-pentane, every

year for five years, so that after five years the total emission increase was five times these listed

emissions. Uncertainties in all scaling ratios propagate into the calculated ozone changes. The

emissions map was based on shale O&NG wells distribution, availableathttp://frack.skytruth.org.

Information used for generating this map is based on 'voluntary disclosure reports submitted by

oil and gas drilling operators' and relies on locations of more than 15,000 wells. We assumed

that all wells emit the same amounts of NMHC, neglecting difference in wells size and leakage

rate. Finally, the distributed map of the wells was aggregated in a 0.5 0.5∘ regular map, and

emissions were scaled on the basis of the well number density in each grid cell. The resulting

emissions map (see Supplementary Fig. 1) identifies regions that have experienced recent growth

of O&NG development, with regions of large emission increases in the central and northeastern

USA.

Modelling results in Fig.4 show the differences in the ozone molar fraction between

model results from the simulation CONST and TREND. Note that these results are based on

constant emissions of other precursors, including those of nitrogen oxides (NOx). Decreasing

trends of NOx over the USA and of VOCs in urban areas have led to a general decrease of ozone

in many urban regions. Omission of these effects will cause a high bias of the ozone changes that

were calculated here. Consequently, these model results should be considered as preliminary

results, providing an indication of the direction of ozone effects from added O&NG emissions,

and taken as motivation for more in-depth modelling of the net effect resulting from these

emission changes.

3.14 Data availability

The NMHC surface data used for this research are available at

http://www.esrl.noaa.gov/gmd/dv/dataandhttp://ds.data.jma.go.jp/gmd/wdcgg. The FTIR column

observations can be retrieved from ftp://ftp.cpc.ncep.noaa.gov/ndacc/station.

Chapter 3

Changes in Atmospheric Butanes and Pentanes and their Isomeric Ratios in the Continental United States

Sam Rossabi[1], and Detlev Helmig[1,*]

[1]Institute of Arctic and Alpine Research, University of Colorado, Boulder, Colorado, 80303, USA

*Corresponding author: Detlev Helmig (Detlev.Helmig@colorado.edu)

Abstract

Non-methane hydrocarbons (NMHCs) have been used as tracers in research on emissions and atmospheric oxidation chemistry. This research investigates source region mixing ratio trends of the NMHCs *i*-butane, *n*-butane, *i*-pentane, and *n*-pentane, and the (*i/n*) isomeric ratios of these compounds between 2001 and 2015. Data collected at Photochemical Assessment Monitoring Stations (PAMS), mandated by the U.S. Environmental Protection Agency (EPA) in ozone nonattainment areas, and data collected at Global Greenhouse Gas Reference Network (GGGRN) sites within the National Oceanic and Atmospheric Administration (NOAA) network, and analyzed at the Institute of Arctic and Alpine Research (INSTAAR), were examined. Among all considered species, regression analyses on concentration time series had negative slopes at 81% of sites, indicating predominantly declining butane and pentane atmospheric concentrations. Mostly negative slopes (78% of sites) were found for the (*i/n*) butane and pentane isomeric

ratios, including all six and seven statistically significant (i/n) butane and pentane trends, respectively. Over the ~15 year investigation period and averaged over all sites, total relative changes were ~30 and 45% for the (i/n) ratios of butanes and pentanes, respectively, with a relative in- crease in the prominence of the *n*-isomers. Most likely causes include changing isomeric ratios in gasoline sector emissions, and increasing influence of oil and natural gas industry emissions.

Changes in concentrations and isomeric ratios depend on proximity of contributing emission sources to measurement sites.

1. Introduction

Atmospheric hydrocarbons, excluding methane, are commonly referred to as Non-Methane Hydrocarbons (NMHCs). NMHCs play a significant role in atmospheric oxidation chemistry. This work investigates atmospheric mixing ratios and (i/n) isomer ratios of the NMHCs butane and pentane.

1.1 NMHC Sources

NMHCs have numerous anthropogenic and biogenic sources. Anthropogenic sources are responsible for ~100 Tg NMHC carbon (C) emissions yr^{-1} [*Atkinson and Arey*, 2003b]. At 40-45%, alkanes constitute the largest fraction of atmospheric anthropogenic volatile organic compounds (VOCs) in urban environments [*Fujita et al.*, 1992]. Despite contributing less than 10% to total global VOC emissions, anthropogenic sources generally dominate air quality in urban areas. The majority of urban alkane emissions are from transportation sector emissions, i.e. gasoline and diesel distribution and automobiles. Atmospheric NMHCs increased from the early 1900s until regulations, such as the Clean Air Act of 1963 and its amendments in 1970,

mandated emissions reductions from automobiles, oil and natural gas (O&NG) production, and industrial processes, and led to decreasing trends in urban NMHC mixing ratios [*Von Schneidemesser et al.*, 2010; *Warneke et al.*, 2012]. Declining NMHC trends have also been found in records from background monitoring sites and firn air [*Aydin et al.*, 2011; *Helmig et al.*, 2014; *Worton et al.*, 2012]. At the peak of mixing ratios in the 1970s, automobile emissions were responsible for 75-93% of the NMHC composition in urban air in Los Angeles [*Mayrsohn and Crabtree*, 1976]. *i*- and *n*-butane are emitted from a variety of sources, such as biomass burning, petroleum production and use, and natural gas emissions. *i*- and *n*-pentane have similar sources, but have a relatively larger contribution from liquid fuels [*Singh and Zimmerman*, 1992]. In an urban study, *i*-butane, *i*-pentane, and *n*-pentane were each shown to correlate well with *n*-butane, suggesting they have similar sources in urban environments [*Goldan et al.*, 1995]. In the same study, these alkanes had a weaker correlation with aromatic VOC. Aromatics are predominately a result of vehicle tailpipe emissions; this suggests other significant urban sources of these NMHC alkanes. Later studies showed butane and pentane isomers were present in petroleum refinery emissions, vehicle running and tailpipe emissions, and gasoline vapor [*Pierson et al.*, 1999; *Scheff et al.*, 1996].

1.2 NMHC Sinks

NMHCs significantly influence tropospheric chemistry, especially concentrations of the hydroxyl radical, [OH], by consumption, and of ozone [O3] by contributing to its production [*Isaksen et al.*, 1985; *Kasting and Singh*, 1986; *Liu et al.*, 1987; *Trainer et al.*, 1987]. Oxidation by OH is the predominant sink of atmospheric alkanes [*Atkinson*, 1997]. The rate of removal by OH depends on the OH production rate, and as such on atmospheric O3 and water vapor and the

solar flux, and consequently exhibits diurnal and seasonal cycles [*Jobson et al.*, 1994a; *Rudolph and Ehhalt*, 1981]. NMHCs are also oxidized by nitrate (NO3) and halogen radicals, albeit to a much smaller extent [*Atkinson*, 2000]. NMHCs are not appreciably photolyzed by wavelengths present in the troposphere. Light alkanes do not react appreciably with O3, but contribute to tropospheric O3 production during their atmospheric oxidation [*Atkinson and Arey*, 2003a; *Atkinson and Carter*, 1984]. Neither wet nor dry deposition are significant sinks of light alkanes.

1.3 Use of NMHC in Atmospheric Research

Atmospheric chemistry research has extensively employed NMHCs. Longer-lived NMHCs and ratios of NMHC pairs are usually less variable and more consistent than absolute concentrations [*Pollmann et al.*, 2016]. They have been used to test the accuracy of tropospheric NMHC measurements, with deviations from expected relationships between compounds indicating sampling and instrument problems [*Parrish et al.*, 1998]. NMHC ratios have been used as tracers in many emission source and atmospheric oxidation studies. Emission sources have been studied by examining relative compositions of NMHCs [*Mayrsohn and Crabtree*, 1976]. Ratios of NMHCs have been used to estimate rural and urban [OH] [*Blake et al.*, 1993; *Calvert*, 1976; *Roberts et al.*, 1984]. The ratios of acetylene and benzene to NMHC and pentane isomers can be indicators of biomass burning, even after many days of transport [*Andreae and Merlet*, 2001; *de Gouw et al.*, 2004; *Helmig et al.*, 2008]. *Lewis et al.* [2013] used NMHC to carbon monoxide (CO) ratios to identify biomass burning emissions. Biomass burning, in general, is a larger fractional contributor to atmospheric NMHCs in the southern hemisphere atmosphere, where the largest emissions sources are extratropical forest fires and biofuel burning [*Andreae and Merlet*, 2001; *Borner and Wunder*, 2012]. In many places, biomass burning is the

largest contributor to benzene, toluene, ethene, and propene concentrations. Further, *n*-butane

and *n*-pentane correlate well with both biomass burning and anthropogenic emissions. Emission

factors for NMHCs vary considerably depending on the fuel source and fire type (flaming,

smoldering, etc.) [*Andreae and Merlet*, 2001; *Borner and Wunder*, 2012]

Halogen chemistry can influence isomeric hydrocarbon ratios, specifically (*i/n*) isomer

ratios [*Gilman et al.*, 2013; *Hornbrook et al.*, 2016; *Jobson et al.*, 1994a]. Increased (*i/n*) ratios

can indicate chlorine radical chemistry because the *n*-isomers of butane and pentane react faster

with chlorine than the *i*-isomers, while having similar rate constants for oxidation by OH

[*Swarthout. et al.*, 2013]. NMHC ratios such as the isomeric butane ratio were used to infer

chlorine radical concentrations during the eruption of the Icelandic volcano Eyjafjallajokull

[*Baker et al.*, 2011]. *Gilman et al.* [2013] also examined propane/*i*-butane ratios. These

compounds have similar chlorine rate coefficients, but *i*-butane has a faster OH rate coefficient

than propane. An increase in this ratio indicated an increasing influence of oxidation by OH.

Nitrate (NO_3) radical chemistry can also play a role in the removal of hydrocarbons from the

atmosphere [*Penkett et al.*, 1993]. Branched alkanes (*i*-isomers) have faster rate constants for

reaction with NO_3 than non-branched alkanes. However, rate constants for reaction with NO_3 are

4-5 orders of magnitude lower than with OH, and thus degradation via NO_3 is rarely competitive

with OH oxidation. NO_3 mixing ratios can be high enough to be competitive with OH chemistry,

particularly in the winter season at higher latitudes, however this is typically only the case for

alkenes [*Atkinson et al.*, 1986; *Penkett et al.*, 1993; *Platt et al.*, 1980; *Wayne et al.*, 1991].

The dispersion and mixing of emissions from distinct sources is relatively fast compared

to butane and pentane photochemical lifetimes, which are on the order of days. Isomeric ratios of

these compounds are assumed to be representative of the air mass sampled. The OH reaction rate

constants of the butane isomers are within 10% [*Atkinson and Arey*, 2003a], yielding consistent (*i/n*) isomeric ratios during transport dominated by OH oxidation chemistry from source to downwind regions. *Mayrsohn and Crabtree* [1976] found an (*i/n*) butane isomeric ratio of ~0.5 with σ=18% despite measuring at four sites with unique conditions in the Los Angeles area. The collection of sites presented by *Parrish et al.* [1998] showed (*i/n*) butane isomeric ratios varying from 0.37 to 0.57. Ratios in this range were found in other studies as well, both in proximity of source regions [*Goldstein et al.*, 1995; *Jobson et al.*, 1994b] and far downwind [*Helmig et al.*, 2008]. Jobson et al [2004] found average (*i/n*) butane isomeric ratios of 0.18-0.19 in samples dominated by vehicle exhaust, and 1.03 at a site heavily influenced by industrial emissions emanating from the Houston Ship Channel. Further, there are no notable systematic seasonal changes in the (*i/n*) butane isomeric ratio [*Helmig et al.*, 2008]. Jobson et al [2004] found average (*i/n*) pentane ratios of 2-97-3.36 in Houston at sites influenced by vehicular and industrial emissions.

A wider range of values is generally observed for the (*i/n*) pentane isomeric ratio compared to the butane isomeric ratio. Use of the (*i/n*) pentane isomeric ratio as an emission tracer was recently demonstrated by *Gilman et al.* [2013]. A ratio of 0.86 indicated O&NG activity, while a ratio of ~2.5 characterized urban emissions. *Jobson et al.* [2004] found (*i/n*) pentane ratios of ~3.3 in Houston at sites influenced by vehicular and industrial emissions. Building on this, *Thompson et al.* [2014] observed the (*i/n*) pentane isomeric ratio in ambient air to determine if increased VOC loading was related to vehicle tailpipe emissions or O&NG development. *Helmig et al.* [2008] argued that the drop in the (*i/n*) pentane isomeric ratio during summer transport events to the Azores, Portugal, was caused by occurrences of biomass burning transport events.

Non-isomeric NHMC ratios, such as ln([propane]/[ethane]) and ln([n-butane]/[ethane]), have been used to study photochemical processing during transport; these ratios have been labeled as 'photochemical clocks'. *Parrish et al.* [1992] found that light alkane ratios differed when air masses had different trajectories, and that photochemical aging was consistent with a given trajectory. *McKeen and Liu [1993]* showed that photochemical aging and transport determine hydrocarbon ratios. *Honrath et al.* [2008] used these ratios to estimate the age of air parcels transported across the mid-North Atlantic. This work found that it is possible to determine the age of an air parcel making assumptions about source region hydrocarbon emission ratios and mean [OH]. The ln([propane]/[ethane]) ratio has also been used to investigate O_3 production as a function of transport and the seasonal photochemical processing [*Helmig et al.*, 2015; *Helmig et al.*, 2008; *Honrath et al.*, 2008].

In summary, a myriad of atmospheric research has focused on light NMHCs and their ratios. Much of this research relies on the assumption of temporarily and regionally consistent NMHC ratios in source regions. This condition is preemptive to identify sampling inconsistencies, studies on the aging of an air mass, and emission sources as discussed above. Changes in technologies, fuel types, and relative contributions from different emissions sources question if and how these isomers and ratios have changed over time. This is evaluated here, utilizing ambient NMHC source region observations from ten urban monitoring sites in the United States. We also considered data from six mostly background sites for contrasting with the urban data. To our knowledge, the analyses and results presented here are the most comprehensive investigation of isomeric ratios of butanes and pentanes in the continental United States to date.

2. Methods

Considered data are from the U.S. Environmental Protection Agency (EPA) Photochemical Assessment Monitoring Station (PAMS) network, and the U.S. National Oceanic and Atmospheric Administration (NOAA) Global Greenhouse Gas Reference Network (GGGRN) [*EPA*, 2016]. Panel (a) in Figure 1 shows the site locations; site coordinates are summarized in Table 1.
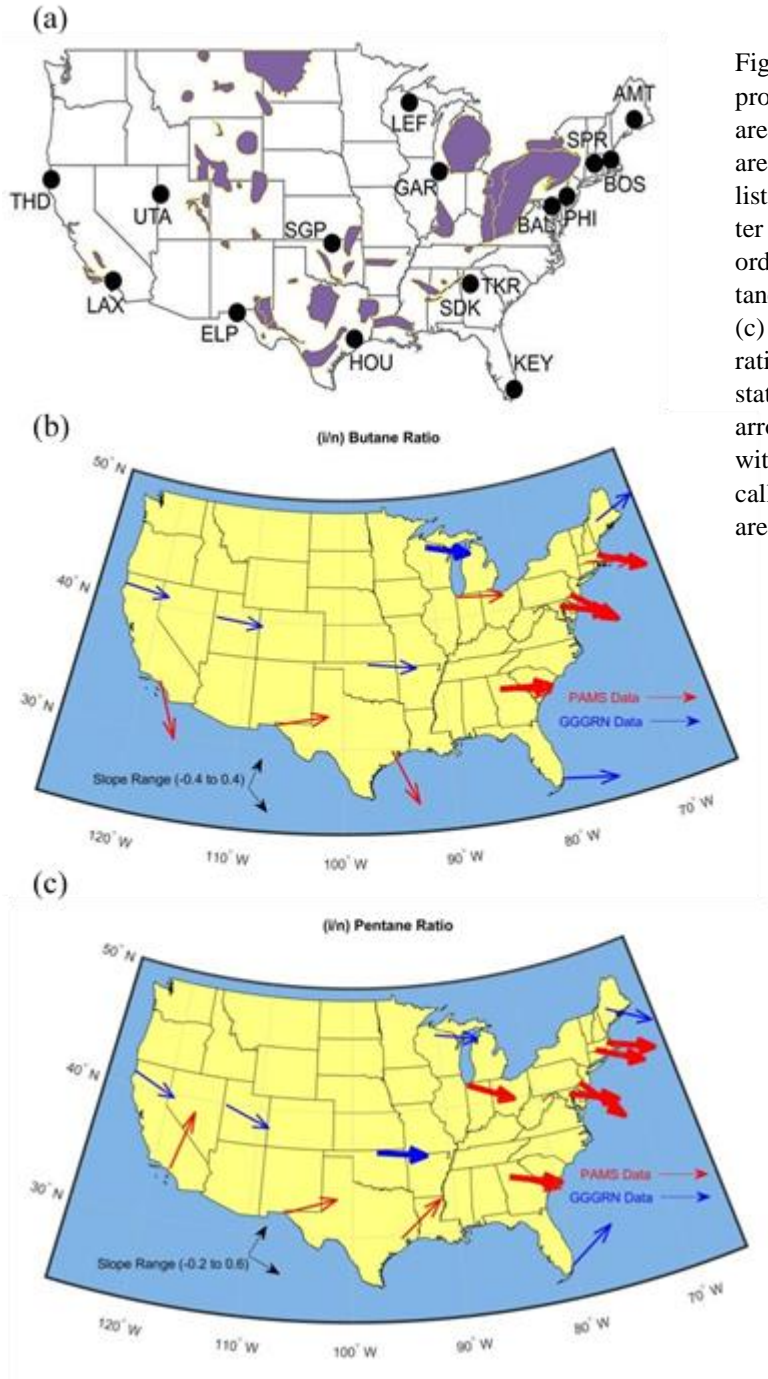
Figure 1. (a) Site locations and their proximity to shale plays. Shale plays are shown in purple, monitoring sites are indicated as black dots. Table 1 lists full site names with the three letter codes used in the map and site coordinates. Graph (b) shows (*i/n*) butane isomeric ratio trends, and graph (c) shows the (*i/n*) pentane isomeric ratio trends. Solid arrows indicate a statistically significant trend; dotted arrows indicate the rate of change, without this change being a statistically significant trend. PAMS data are in red. GGGRN data are in blue.

2.1 PAMS Data

The main objective of PAMS is to maintain an air quality database to evaluate progress toward meeting the ozone National Ambient Air Quality Standard (NAAQS). PAMS were

established in urban areas that were in ozone nonattainment in 1997. Sites are classified by their position relative to the urban area and typical morning wind direction. For example, some locations are <u>background</u> sites upwind of the urban area (type 1); others are maximum <u>ozone concentration</u> sites (type 3), which are about 10 to 30 miles downwind of the urban area. In total, there are 78 PAMS sites. All data in this paper are from type 2 sites, which are maximum <u>ozone precursor</u> sites. These sites are directly downwind of the urban area's central business district. We chose those sites because we sought the most representative source region data while minimizing the degree of oxidation of these compounds. Data from ten PAMS sites (Table 1) were used. Sampling occurred between 2000 and 2015, although temporal data coverage varied by site. According to the PAMS protocol, 24-hour integrated samples were collected every sixth day. Samples were collected in canisters and analyzed by gas chromatography with flame ionization detection (GC/FID) using a DB-1 column [*EPA*, 1998] at a series of contracted laboratories. Two calibration standards were used, a propane and benzene mixture as a primary calibration standard, and a standard composed of all target VOC at varying concentrations as a retention time standard.

While the same type of sampler is used across the PAMS network, and instruments are calibrated with the same type of standard, site audits have shown that sites averaged an 11.3% deviation error for a variety of compounds against a reference standard analysis [*EPA*, 1997].

Table 1. Site names, three letter code, location information, and trend analysis results for the (*i/n*) butane and (*i/n*) pentane isomeric ratio. Statistical significant results are indicated by italics font.

	Agency	Lat.	Long.	(i/n) Butane				(i/n) Pentane			
				Median	Slope (yr^{-1})	Slope (% yr^{-1})	P-Value	Median	Slope (yr^{-1})	Slope (% yr^{-1})	P-Value
Atlanta, GA (SDK)	PAMS	33.8	-84.4	0.68	*-0.003*	*-0.43*	*0.037*	1.9	*-0.043*	*-2.2*	*0.004*
Atlanta, GA (TKR)	PAMS	33.8	-84.4	0.35	-0.006	-1.7	0.45	2.2	-0.060	-2.7	0.26
Baltimore, MD (BAL)	PAMS	39.3	-76.6	0.48	*-0.009*	*-1.9*	*0.021*	1.6	*-0.050*	*-3.1*	*0.003*
Boston, MA (BOS)	PAMS	42.4	-71.1	0.57	*-0.012*	*-2.2*	*0.000*	1.9	*-0.055*	*-2.9*	*0.000*
El Paso, TX (ELP)	PAMS	31.8	-106.4	0.43	0.005	1.1	0.39	2.1	0.042	2.0	0.54
Gary, IN (GAR)	PAMS	41.6	-87.3	0.42	-0.003	-0.59	0.38	1.7	*-0.058*	*-3.3*	*0.000*
Houston, TX (HOU)	PAMS	29.8	-95.4	0.67	*-0.058*	*-8.7*	*0.027*	2.7	0.12	4.5	0.22
Los Angeles, CA (LAX)	PAMS	34.1	-118.3	0.56	-0.056	-10	1.0	2.5	0.55	22	0.46
Philadelphia, PA (PHI)	PAMS	40.0	-75.2	0.57	*-0.021*	*-3.7*	*0.000*	2.5	*-0.17*	*-6.7*	*0.009*
Springfield, MA (SPR)	PAMS	42.1	-72.5	0.60	-0.006	-0.99	0.13	1.8	*-0.069*	*-3.9*	*0.001*
Argyle, ME (AMT)	GGGRN	45.0	-68.7	0.57	0.007	1.2	1.0	1.6	-0.076	-4.7	1.0
Key Biscayne, FL (KEY)	GGGRN	25.7	-80.2	0.50	-0.006	-1.1	0.55	1.3	0.10	7.7	0.23
Park Falls, WI (LEF)	GGGRN	45.9	-90.3	0.45	*-0.006*	*-1.2*	*0.005*	1.3	-0.024	-1.9	0.28
So. Grt. Plns., OK (SGP)	GGGRN	36.6	-97.5	0.40	-0.003	-0.70	0.12	0.98	*-0.015*	*-1.5*	*0.002*
Trinidad Head, CA (THD)	GGGRN	41.1	-124.2	0.56	-0.002	-0.35	0.24	1.5	-0.048	-3.3	0.19
Wendover, UT (UTA)	GGGRN	39.9	-113.7	0.54	-0.002	-0.34	0.53	1.4	-0.050	-3.7	0.27

PAMS data were downloaded from the PAMS database (AirNow – DART - https://www.airnowtech.org/dart/dartstatus.cfm, downloaded January 2016) and underwent a filtering routine. First, the median and standard deviation of the datasets were determined for the whole record. Data points three standard deviations above or below the median value were excluded. Next, data were run through a Hampel filter [*Davies and Gather*, 1993; *Pearson et al.*, 2015]. This filter considers a data point and the three points before and after the central point. If the central data point is three standard deviations away from the median of the seven points, it is replaced with the median value. This procedure removes extreme values and improves the data for the purpose of trend analyses because averaged data are considered instead of events. Finally, data were subjected to a running monthly median. An example of a data set before and after applying the filtering routines is shown in Supplement Figure S1. Supplement Figure S2 shows time series data after the filtering routine has been performed.

2.2 NOAA/INSTAAR Data

GGGRN Flask data were downloaded from the NOAA Earth System Research Laboratories/Global Monitoring Division (ESRL/GMD) database (March 2016) (ftp://aftp.cmdl.noaa.gov/data/trace_gases/voc/). These data are also publicly available from the World Data Center for Greenhouse Gases (WDCGG) (http://ds.data.jma.go.jp/gmd/wdcgg/). There are 46 sites worldwide; data from the six sites in the continental United States were considered here. These samples were collected approximately weekly. NMHC measurements are made by the Atmospheric Research Laboratory at the Institute of Arctic and Alpine Research (INSTAAR) at the University of Colorado, Boulder, USA, by preconcentrating NMHC onto a micro-adsorbent trap, followed by thermal desorption and GC/FID [*Pollmann et al.*, 2008a]. A

reference gas calibrated against gravimetrically prepared NMHC standards was used to calibrate the system daily. All GGGRN samples have been analyzed on the same instrument, in the same laboratory, and following the same analytical protocol since the beginning of the program [*Pollmann et al.*, 2008a], which is advantageous for achieving good comparability between sites. Two audits conducted by the World Calibration Centre for VOC (http://www.imk-ifu.kit.edu/wcc-voc/) yielded analysis result deviations of <5% for butane and pentane isomers against a series of reference standards. The GGGRN data were first filtered using a NOAA filtering routine [*Thoning et al.*, 1989], and then by the same filtering routine applied to the PAMS data (Supplement Figure S1). Filtered Data are available in Supplement Figure S2.

2.3 Data Analyses

Isomeric ratio data were determined by dividing the *i*-isomer mixing ratio value by the *n*-isomer value in a given sample. Samples without a matching measurement result for the other isomer were excluded. Filtering removed outliers and reduced the range of data. This yielded a more reliable representation of the behavior of the whole data set. Once filtered, a variety of analyses were conducted:

2.3.1 Seasonal Cycles

Data at each site were sorted by collection month. A box-whisker plot was constructed for each month's data to investigate the average seasonal cycle. In all box plots dis- played in this work and the supplement (Supplement Figure S3), the center, red line is the median of the data considered for the box, the top of the box indicates the data's upper quartile (75th percentile), the bottom of the box the lower quartile (25th percentile), and whiskers the

60

maximum and minimum of the data. Relative seasonal amplitudes were calculated by subtracting the lowest monthly median from the highest monthly median and dividing by each site's overall median mixing ratio.

2.3.2 Multi-Year Changes

Box-whisker plots for each year of data were plotted against the observation year (Supplement Figure S4). Relative yearly ranges were calculated by calculating the median mixing ratio for each calendar year, and subtracting the lowest annual median from the highest annual median, and then dividing by the site's overall median across all years of available data. This quantifies the variability observed over each site's available data.

2.4 Trend Analyses

Statistical trend analyses were conducted by calculating the median for each calendar year at each site, and subjecting the time series of medians to a Mann-Kendall Test [*Hirsch et al.*, 1991; *Kendall*, 1975; *Mann*, 1945] to determine the presence of a trend over the entirety of the site's data record. Trends were tested at the 95% confidence level. Trend values were calculated using a Theil-Sen robust linear regression [*Sen*, 1968; *Theil*, 1950]. The Theil-Sen method is a robust nonparametric technique for quantifying a linear trend because it is resistant to outliers.

Relative trends for each site were found by dividing the Theil-Sen slope result by each site's overall median mixing ratio. Some of the sites, i.e. Los Angeles, Argyle, and Key Biscayne had less than a 10-year record. These shorter records result in reduced statistical power [*Hatch*, 2003], which could result in an acceptance of the null hypothesis despite the absence of a trend. For more discussion on statistical power, please refer to Supplement Text STx1.

3. Results

Time series plots for all four isomers at all sites are available in Figure S2a-o of the Supplement. The tables below summarize the mean mole fraction and trend analysis results. Table 1 lists p-values, trend slopes, slope percentiles, and trend significance results for each of the (i/n) butane and pentane isomer ratios. A p-value less than 0.05 indicates a statistically significant trend at 95% confidence. Table 2 shows these results for each of the butane and pentane isomers. Tables 3 and 4 show relative seasonal amplitudes and relative yearly ranges of mixing ratios for each isomer and ratio.

3.1 Absolute Mole Fractions

We chose Trinidad Head (THD) as a reference to compare and contrast with the urban PAMS data. THD is located on the Northern California Pacific coast, largely free from nearby anthropogenic influence. With prevailing winds coming from the Pacific Ocean, most air sampled at THD reflects the marine Pacific background atmosphere. The upper panel of Figure 2 shows seasonal cycles and isomeric ratios at THD. For comparison, seasonal cycles for the same compounds and isomer ratios for the inner city PAMS Atlanta – SDK (SDK) site are shown in the lower panel. Please note the different mole fraction scales (y-axis) of the two sets of plots, indicating the on average ~100 times higher butane and pentane mole fractions in the Atlanta urban atmosphere compared to THD. Of the considered PAMS sites, SDK falls into about the middle range of observed butane and pentane mixing ratios (Table 2), making it a representative ex- ample for illustrating the influence of urban anthropogenic emissions. The corresponding plots for all other sites are presented in Supplement Figure S3a-p.
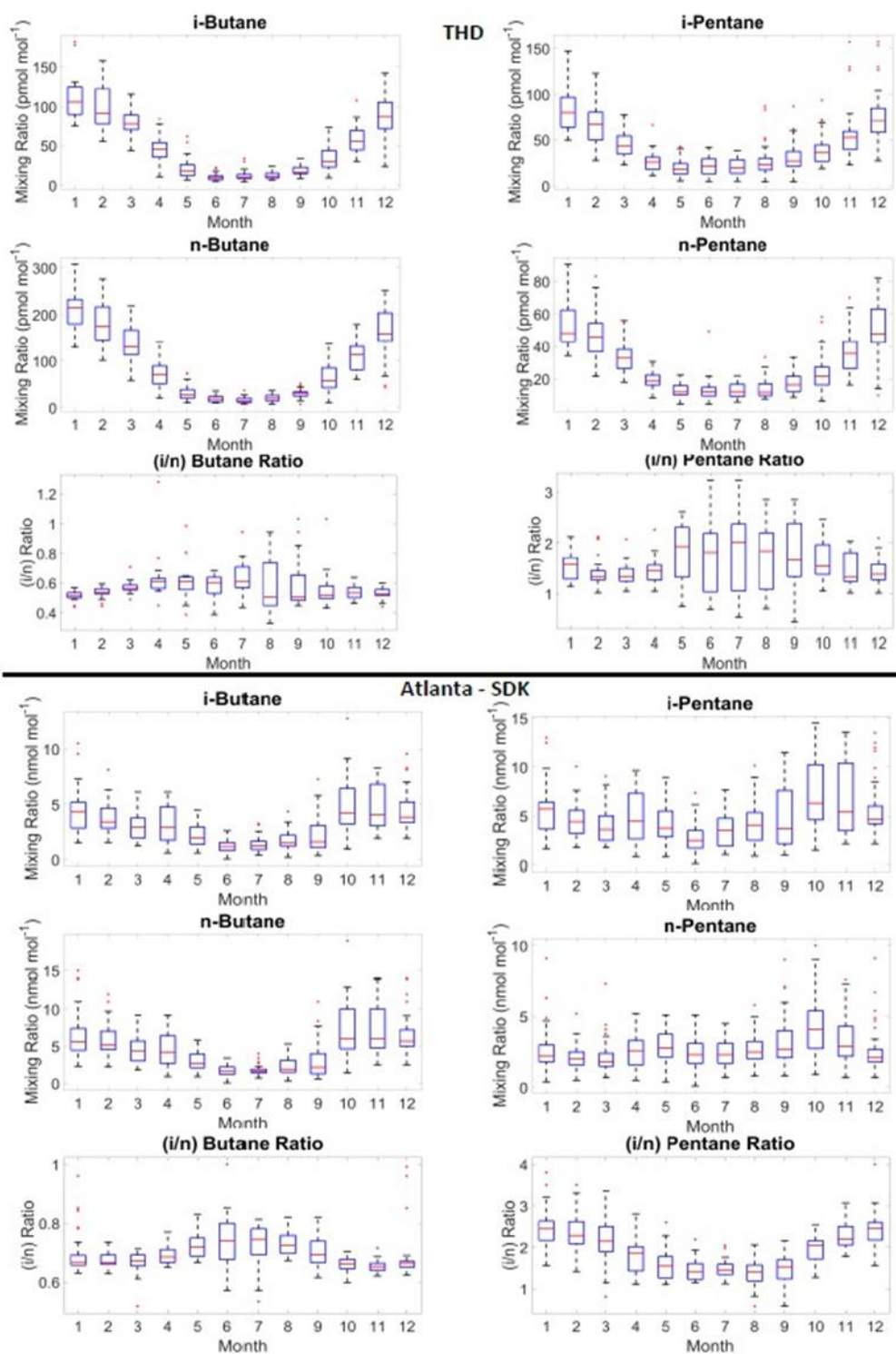
Figure 2. Box-whisker plots with statistical analysis results of monthly butane and pentane isomer and ratio data at THD (top) and Atlanta - SDK (bottom). Note that different scales and units are used for the y-axis in both the top and bottom panels.

Mixing ratios of individual isomers at PAMS sites were highest for i-pentane, followed by n-butane, n-pentane, and i-butane. At GGGRN sites, mixing ratios were highest for n-butane followed by i-butane, i-pentane, n-pentane. This was determined by finding the median of all sites' mixing ratios for each isomer. Median mixing ratios at PAMS sites were 2-3 orders of magnitude larger than GGGRN sites, with the exception of SGP, which had mixing ratios ~10 times higher than other GGGRN sites for all isomers. The highest mixing ratios for all isomerswere observed at the Houston (HOU) site; these ranged from 6.13-16.8 nmol mol^{-1}. The lowest mixing ratios for three of the four isomers were observed at Key Biscayne (KEY), and ranged from 0.030-0.061 nmol mol^{-1}. THD displayed lowest mixing ratios for n-pentane (0.022 nmol mol^{-1}). Mixing ratios for all isomers at all sites are available in Table 2.

Table 2. *i*-Butane, *n*-butane, *i*-pentane, and *n*-pentane median mixing ratios, trend slopes, and p-values. Statistical significant results are indicated by italics font.

	i-Butane				n-Butane				i-Pentane				n-Pentane			
	Median (nmol mol^{-1})	Slope (nmol mol^{-1} yr^{-1})	Slope (% yr^{-1})	P-Value	Median (nmol mol^{-1})	Slope (nmol mol^{-1} yr^{-1})	Slope (% yr^{-1})	P-Value	Median (nmol mol^{-1})	Slope (nmol mol^{-1} yr^{-1})	Slope (% yr^{-1})	P-Value	Median (nmol mol^{-1})	Slope (nmol mol^{-1} yr^{-1})	Slope (% yr^{-1})	P-Value
Atlanta (SDK)	2.75	*-0.150*	*-5.45*	*0.000*	*4.00*	*-0.200*	*-5.00*	*0.001*	4.35	*-0.239*	*-5.49*	*0.003*	2.40	*-0.150*	*-6.25*	*0.002*
Atlanta (TKR)	1.90	-0.070	-3.68	0.573	5.40	-0.320	-5.93	0.060	6.70	0.000	0.00	1.000	2.90	0.100	3.45	0.452
Baltimore	1.80	*-0.086*	*-4.76*	*0.004*	3.61	-0.113	-3.14	0.080	4.52	*-0.251*	*-5.55*	0.006	2.54	-0.030	-1.18	0.250
Boston	1.15	*-0.050*	*-4.35*	*0.049*	1.80	-0.054	-2.98	0.063	2.00	*-0.167*	*-8.33*	*0.002*	1.05	*-0.029*	*-2.80*	*0.001*
El Paso	3.56	-0.197	-5.52	0.174	6.72	-0.128	-1.90	0.266	8.45	*-0.946*	*-11.2*	*0.009*	3.90	*-0.431*	*-11.1*	*0.026*
Gary	1.40	-0.040	-2.86	0.208	3.34	-0.049	-1.47	0.208	2.73	*-0.167*	*-6.12*	*0.012*	1.50	-0.038	-2.56	0.125
Houston	11.72	*-1.80*	*-15.4*	*0.027*	16.8	-2.26	-13.5	0.220	16.4	1.6	9.76	0.806	6.13	-0.625	-10.2	0.462
Los Angeles	2.99	-0.025	-0.84	1.000	4.72	0.085	1.80	0.806	9.51	2.22	23.4	0.296	3.53	-0.080	-2.27	1.000
Philadelphia	3.80	*-0.349*	*-9.20*	*0.002*	5.93	*-0.426*	*-7.18*	*0.009*	10.8	*-1.03*	*-9.55*	*0.014*	3.90	*-0.142*	*-3.63*	*0.019*
Springfield	1.20	-0.026	-2.20	0.217	1.85	-0.015	-0.84	0.337	2.10	*-0.092*	*-4.39*	*0.034*	1.10	0.000	0.00	1.000
Argyle	0.083	-0.012	-14.0	1.000	0.139	-0.016	-11.6	1.000	0.102	-0.025	-24.3	1.000	0.064	-0.006	-9.92	1.000
Key Biscayne	0.033	-0.002	-5.38	0.230	0.061	-0.000	-0.70	0.548	0.030	-0.001	-2.20	0.368	0.024	-0.002	-9.07	0.133
Park Falls	0.078	*-0.004*	*-5.52*	*0.029*	0.168	-0.007	-3.86	0.161	0.078	*-0.003*	*-4.30*	*0.005*	0.056	-0.002	-2.69	0.161
So. Grt. Plns.	0.407	*0.032*	*7.75*	*0.005*	1.02	*0.095*	*9.39*	*0.000*	0.345	0.019	5.54	0.086	0.325	*0.028*	*8.49*	*0.000*
Trinidad Head	0.044	0.001	2.22	0.304	0.070	0.003	4.33	0.086	0.035	-0.002	-3.38	0.304	0.022	-0.000	-1.52	0.537
Wendover	0.041	-0.002	-5.90	0.062	0.069	*-0.003*	*-4.61*	*0.029*	0.037	*-0.004*	*-11.5*	0.003	0.027	*-0.002*	*-6.00*	*0.029*

Butane (*i/n*) ratio values ranged from 0.352 at Atlanta-TKR (TKR) to 0.677 at SDK. Pentane (*i/n*) ratio values ranged from 0.980 at SGP to 2.70 at HOU. Butane ratios were similar at PAMS and GGGRN sites, but pentane ratios were, on average, higher at PAMS sites than at GGGRN sites. Butane and pentane ratios observed at all sites are available in Table 1.

3.2 Yearly Ranges

The year-to-year differences in median mixing ratios, here termed 'yearly ranges' were studied to determine the interannual variability. Yearly ranges can identify changes in emissions profiles that don't necessarily result in a consistent trend from year to year. Yearly range data for butanes and pentanes for selected sites are summarized in Tables 3 and 4, and seasonal amplitude and yearly range plots in Supplement Figures S3a-p and Figures S4a-p, respectively. The largest yearly ranges for *i*-butane, *n*-butane, and *n*-pentane were observed at SGP; the largest *i*-pentane yearly range was at Gary (GAR). TKR exhibited the smallest yearly ranges for the butane isomers. The smallest yearly ranges for *i*- and *n*-pentane were observed at Key Biscayne and Argyle, respectively.

Table 3. Relative seasonal amplitudes and relative yearly ranges of butane isomers and butane ratio at all sites.

Site	i-Butane (nmol mol^{-1})		n-Butane (nmol mol^{-1})		Butane Ratio	
	Seasonal Amp.	Yearly Range	Seasonal Amp.	Yearly Range	Seasonal Amp.	Yearly Range
Atlanta, GA (SDK)	0.89	0.87	1.00	0.75	-0.11	0.10
Atlanta, GA (TKR)	0.74	0.32	0.94	0.37	-0.24	0.19
Baltimore, MD	0.74	0.79	1.11	0.68	-0.27	0.45
Boston, MA	0.70	0.93	0.97	0.74	-0.16	0.34
El Paso, TX	1.06	2.45	1.29	0.89	-0.26	0.37
Gary, IN	0.80	1.36	1.08	1.71	-0.31	0.47
Houston, TX	0.12	0.98	0.60	1.35	-0.41	1.11
Los Angeles, CA	0.70	0.61	1.41	0.48	-0.33	0.48
Philadelphia, PA	0.91	1.32	0.99	1.10	-0.24	0.74
Springfield, MA	1.08	1.54	1.27	0.89	-0.15	0.42
Argyle, ME	1.87	0.46	1.98	1.62	-0.08	0.28
Key Biscayne, FL	1.24	0.63	1.32	0.63	-0.26	0.53
Park Falls, WI	2.10	0.69	1.70	0.62	0.32	0.14
SGP, OK	0.85	2.46	0.89	2.38	0.06	0.10
Trinidad Head, CA	2.04	1.28	2.33	1.38	-0.13	0.22
Wendover, UT	1.42	1.12	1.68	1.50	0.10	0.32

Table 4. Relative seasonal amplitudes and relative yearly ranges of pentane isomers and pentane ratio at all sites.

Site	i-Pentane (nmol mol^{-1})		n-Pentane (nmol mol^{-1})		Pentane Ratio	
	Seasonal Amp.	Yearly Range	Seasonal Amp.	Yearly Range	Seasonal Amp.	Yearly Range
Atlanta, GA (SDK)	0.43	0.90	-0.08	1.04	0.51	0.44
Atlanta, GA (TKR)	-0.05	0.57	0.00	0.67	-0.10	0.15
Baltimore, MD	0.09	1.37	0.19	0.47	-0.17	0.59
Boston, MA	-0.38	1.51	-0.10	1.10	-0.29	0.42
El Paso, TX	0.40	0.94	0.65	1.53	-0.20	0.38
Gary, IN	0.17	2.13	0.47	1.80	-0.19	0.55
Houston, TX	-0.14	0.71	-0.01	1.14	-0.13	0.48
Los Angeles, CA	0.89	1.50	0.32	0.62	0.15	2.04
Philadelphia, PA	0.66	1.58	-0.02	1.32	0.78	1.20
Springfield, MA	0.14	1.02	0.45	0.86	-0.19	0.44
Argyle, ME	0.96	0.49	0.85	0.43	-0.17	0.29
Key Biscayne, FL	0.60	0.40	0.70	1.13	0.12	1.02
Park Falls, WI	1.23	0.69	1.28	0.62	-0.23	0.42
SGP, OK	0.93	1.63	0.73	1.99	0.04	0.29
Trinidad Head, CA	1.47	0.78	1.63	0.82	-0.29	0.61
Wendover, UT	0.83	1.56	0.69	1.02	0.11	0.65

Butane and pentane ratio yearly ranges were generally smaller than for individual isomers. The lowest butane ratio yearly ranges were observed at SDK and SGP; the largest was in Houston. The lowest pentane ratio yearly range was observed at TKR, and the largest value was in Los Angeles (LAX). Yearly ranges of these ratios for all sites are in Tables 3 and 4.

3.3 Seasonal Amplitudes

Seasonal amplitude data from THD, as seen in the upper panel of Figure 2, show a good example of how the butane and pentane isomers behave in the background atmosphere. Note that mixing ratios are less variable within a given month at THD than at SDK, and one to two orders of magnitude lower. Seasonal amplitude and yearly range plots for butanes and pentanes at all other sites are available in Supplement Figures S3a-p and S4a-p. Seasonal cycles for the individual isomers at the PAMS SDK site are not as pronounced as at THD (Figure 2). The smaller relative seasonal amplitudes at SDK show the strong influence of local emissions. A graphical site comparison of the relative amplitudes of the seasonal cycle as a function of median mixing ratios, and the relative seasonal cycle of isomeric ratios as a function of the median isomeric ratio, illustrated in Figure 3, shows that relative seasonal amplitudes are lower and median mixing ratios are higher for the individual isomers at PAMS sites in comparison to GGGRN sites, but there are no clear trends within the site types. These results show that near the sources (PAMS sites) ambient levels are more dependent on emissions than on photochemical processing (GGGRN sites). All seasonal amplitudes were positive for *i*- and *n*-butane, indicating that mixing ratios were higher in winter than summer at all sites. Negative seasonal amplitudes (maxima observed in summer, minima observed in winter) were observed at three and four sites for *i*- and *n*-pentane; all of these sites were PAMS sites. The most negative amplitudes for both

69

isomers were observed in Boston (BOS). The largest seasonal amplitudes were observed at THD for three of the four isomers; the largest seasonal amplitude for *i*-butane was at KEY. The smallest seasonal amplitudes for *i*- and *n*-butane were in HOU. Seasonal amplitudes for all isomers at all sites are in Tables 3 and 4.
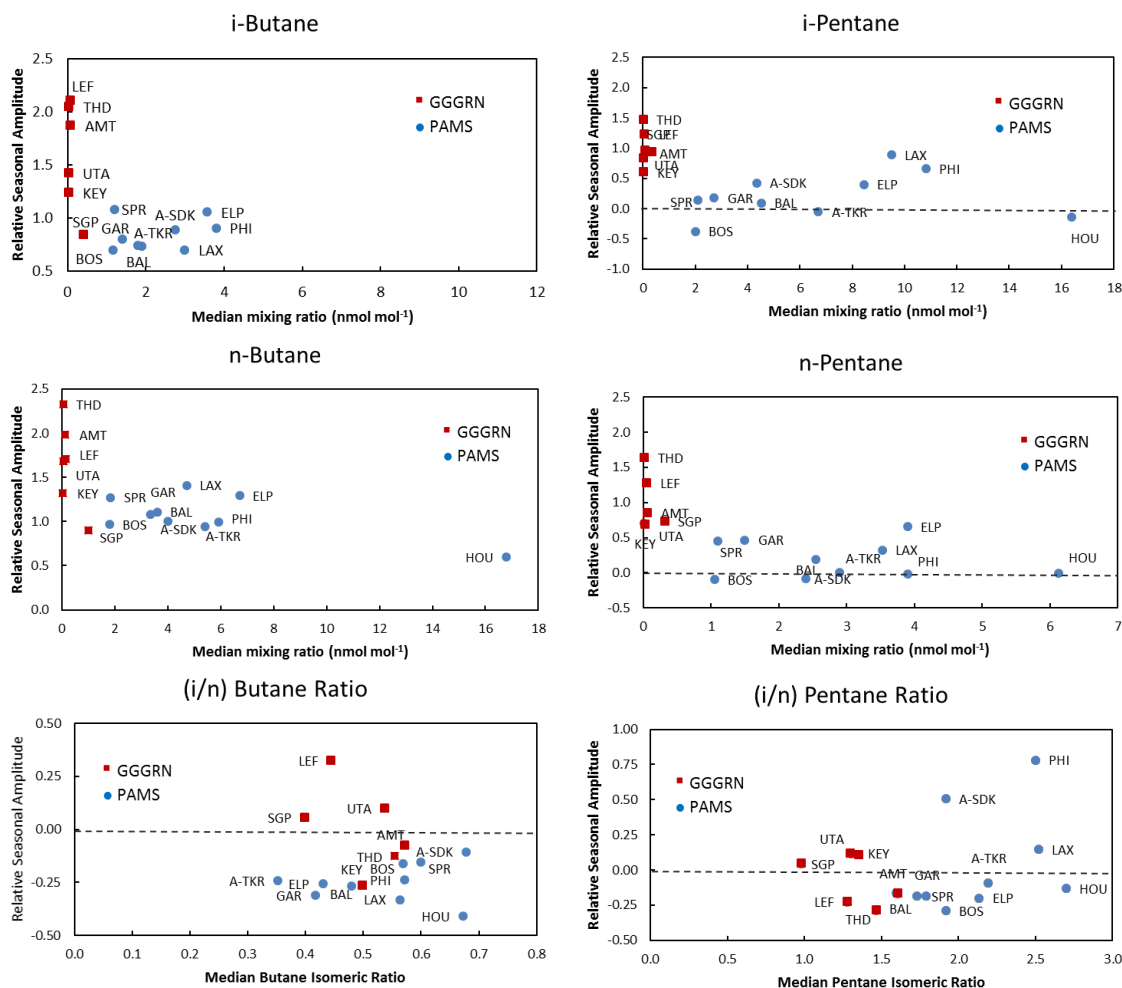
Figure 3. Seasonal amplitudes of butane isomers, pentane isomer, and their isomeric ratio as a function of the annual median mixing ratios. GGGRN sites data are in red, PAMS data are in blue. Axes ranges vary by plot.

All (*i/n*) butane ratio seasonal amplitudes at PAMS sites were negative. Seven of ten (*i/n*)

pentane ratio seasonal amplitudes at PAMS sites were negative. Half of the amplitudes of both

butane and pentane ratios were negative at GGGRN sites. Seasonal amplitudes of the butane

ratio ranged from -0.41 at HOU to 0.32 at Park Falls (LEF). Seasonal amplitudes of the pentane

ratio ranged from -0.29 at BOS and THD to 0.78 at Philadelphia (PHI). All butane and pentane

ratio seasonal amplitudes are available in Tables 3 and 4.

3.4 Changes over Time in Absolute Levels and Isomeric Ratios

Theil-Sen linear regression of annual median data was used to investigate changes over

time in absolute values and isomeric ratios, with regression slope values used as indicators of the

rate of change. These analyses yielded some similarities between sites, although no two sites

were identical with respect to statistically significant trends. Tables 1 and 2 summarize results

for all sites and compounds, italicized results indicate statistically significant trends. Supplement

Table 1 (STb1) shows the confidence intervals for the trend slopes shown in Tables 1 and 2.

Figures 4a and 4b display results graphically for sites with statistically significant (*i/n*) alkane

iso- meric ratio trends along with THD. Results for other sites are shown in Supplement Figure

S4a-p. Figure 5 presents a summary of slope results for all isomers and (*i/n*) isomeric ratios at all

sites, with squares representing statistically significant trend slopes.
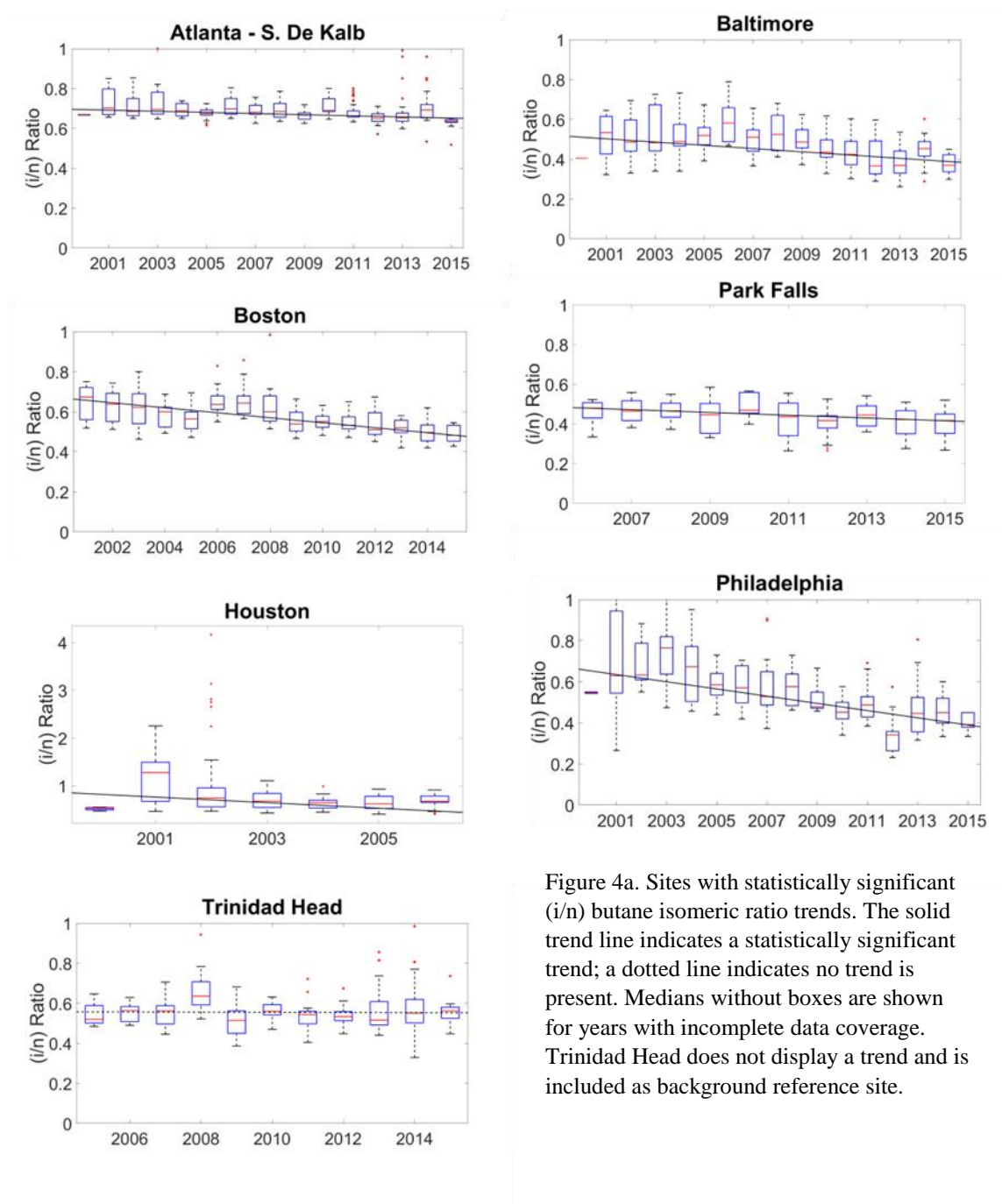
Figure 4a. Sites with statistically significant (i/n) butane isomeric ratio trends. The solid trend line indicates a statistically significant trend; a dotted line indicates no trend is present. Medians without boxes are shown for years with incomplete data coverage. Trinidad Head does not display a trend and is included as background reference site.
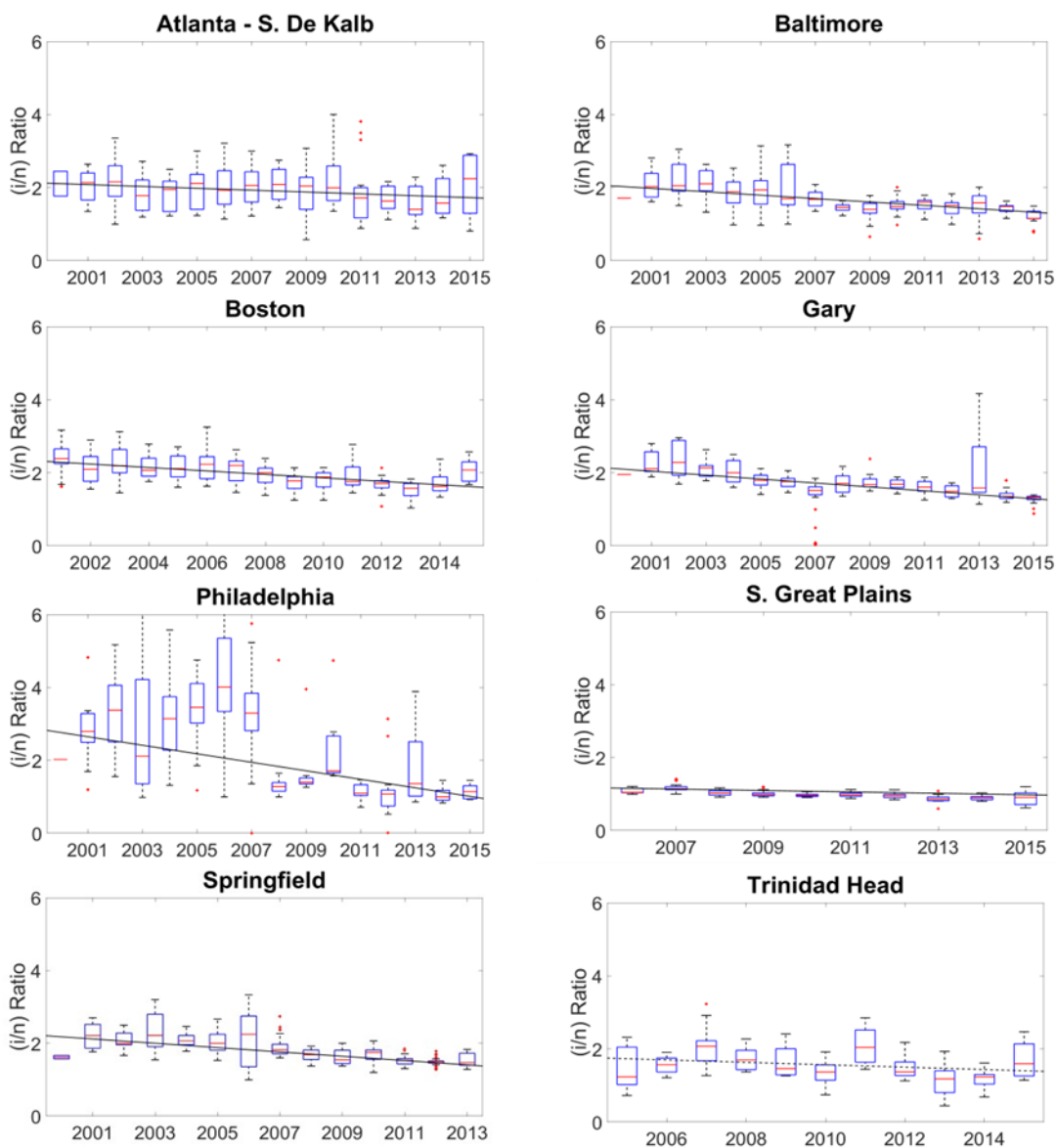
Figure 4b. Sites with statistically significant (i/n) pentane isomeric ratio trends. Solid lines indicate a statistically significant trend. Medians without boxes are shown for years with incomplete data cover- age. Trinidad Head does not show a statistically significant trend and is included as a background reference site.

Mixing ratios of the butane and pentane isomers have been decreasing at most of the sites, i.e. 81%, considered in this study. The magnitude of these changes varies widely across the U.S., i.e. -15% yr^{-1} to 7.8% yr^{-1} for i-butane, -14% yr^{-1} to 9.4% yr^{-1} for n-butane, -24% yr^{-1} to

23% yr^{-1} for *i*-pentane, and -11% yr^{-1} to 8.5% yr^{-1} for *n*-pentane. Similarly, large ranges were

ob- served in changes of the (*i/n*) butane and pentane isomeric ratio (-10% yr^{-1} to 1.2% yr^{-1}, and

- 6.7% yr^{-1} to 22 % yr^{-1}, respectively). Among the isomers, the only positive, statistically

significant rates of change were observed at SGP. The most negative, statistically significant

rates of change were observed at PHI for all isomers except *n*-pentane; El Paso's (ELP) n-

pentane rate of change was the most negative. The only PAMS site with positive rates of change

for any isomer was LAX, with positive slopes for *n*-butane and *i*-pentane, which is not consistent

with *Warneke et al.* [2012]. However, the slopes for LAX were far from statistically significant

(P-value = 0.806 and 0.296, for *n*-butane and *i*-pentane) and is positive as a result of higher

medians observed in 2014 and 2015; these years were not included in the *Warneke et al.* [2012]

analyses. Further, the LAX PAMS record included only five years of data, giving the 2014 and

2015 data a high influence over the slope result.

All statistically significant rates of change for the isomer ratios were negative. Six sites

had statistically significant negative trends for the (*i/n*) butane isomeric ratio. Four of these are

East Coast cities (Atlanta, Baltimore, Boston, and Philadelphia). The most negative was at HOU.

The pentane isomeric ratio had statistically significant negative trends at seven sites (Figure 4b),

with six of these sites located east of the Mississippi River (SDK, Baltimore (BAL), BOS, GAR

PHI, Springfield (SPR)).
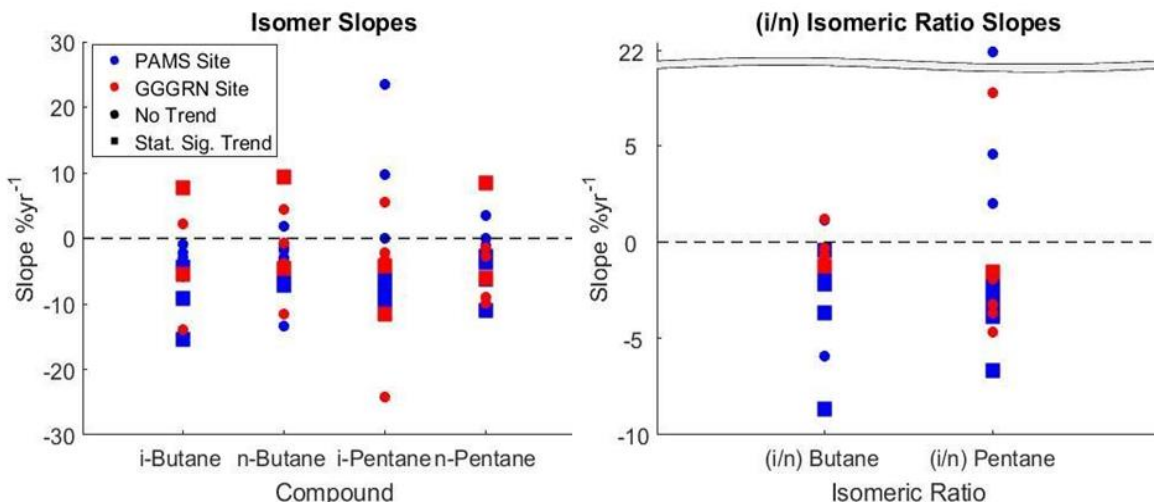
Figure 5. Summary plots of (a) butane and pentane isomers and (b) (i/n) isomeric ratio linear regression slopes observed at all sites. PAMS sites are in red, GGGRN sites are in blue. Square points indicate a statistically significant trend at 95% confidence. Circular points indicate rate of change results, without the value being a statistically significant trend. The legend in (a) applies to (b) as well.

4. Discussion

Results for individual compounds and sites vary rather widely. It is likely that a fraction of the observed spread and variability in results from different sites, in particular from the PAMS network, may arise from a relatively lower measurement precision (larger measurement uncertainty), as different instruments and laboratories were used for the measurements (see Methods section). A common feature in the data are the mostly declining atmospheric mole fractions across sites within both networks. Average (PAMS + GGGRN) atmospheric mole fraction declines for the 2000-2015 time window were (overall median of slope values among sites with 1σ standard deviation) -5.1 ± 5.3, -3.1 ± 5.4, -4.9 ± 10.1, -2.7 ± 5.0 % yr^{-1} for *i*-, *n*-butane, and *i*-, *n*-pentane respectively. This finding is in agreement with other previous work that has shown declining light NMHCs in U.S. urban atmospheres [*Bishop and Stedman*, 2008; *Warneke et al.*, 2012]. This general behavior is also in accord with observations outside of the U.S., mainly in Europe, where urban NMHCs have been steadily declining since ~1990 [*Derwent et al.*, 2017; *Monks et al.*, 2009; *Von Schneidemesser et al.*, 2010]. As mentioned

earlier, a recent study of C2- C8 hydrocarbons in the United Kingdom using 1993 to 2012 data found declining concentrations of most $\geq$ C4 VOC, whereas ethane and propane concentrations have remained near 1993 values [*Derwent et al.*, 2017].

The observed seasonal amplitudes in the data are expected to be the net effect of chemistry, boundary layer dynamics, and emissions. With reaction by OH being the primary removal of these NMHCs, lower mixing ratios are naturally expected during the summer, when the removal rate is higher due to the higher summertime [OH]. Diurnal and seasonal boundary layer height (BLH) dynamics are another variable exerting an influence on the NMHC seasonality at the surface. BLH determines the rate of dilution of surface based emissions. BLH depends on multiple variables, including surface type, topography, and vegetation land cover [*Stull*, 1988]. Daytime maxima BLH can be as high as 5 km over low latitude deserts, and as low as 0.5 km over the ocean [*Garratt*, 1992]. Further, BLH varies by season, typically being higher in summer [*Seidel et al.*, 2012]. Coastal sites, such as THD, have on average lower BLH and less seasonal variation of BLH than inland sites. This would be expected to result in a weaker dilution of surface emissions, and a lower seasonal influence by BLH dynamics exerted on seasonal NMHC cycles. However, the amplitude of the seasonal cycle at THD is among the largest relative seasonal amplitudes observed in this work. This large signal is likely predominantly driven by the seasonal cycle of oxidation chemistry. From the BLH consideration, larger seasonal amplitude signals would be expected at the inland sites from stronger dilution during the summer (deeper BLH). This generally is not observed in the data: The urban sites on average display the smallest relative seasonal amplitude. This behavior can be taken as an indication that proximity to and strength of emissions exert an overall stronger influence than the seasonal BLH and oxidation chemistry cycles at these locations.

The (*i/n*) butane isomeric ratio displayed a seasonal cycle, peaking in the summer at all

sites except LEF, SGP, and Wendover (Figure 3). The (*i/n*) pentane isomeric ratio peaked in the

summer at 7 PAMS sites and 3 GGGRN sites. The summer peak in this ratio is expected from

considerations. The *n*-isomers have the slightly faster OH reaction rate constants of the isomeric

pairs, resulting in a relatively faster removal of the *n*-isomer at the higher summertime [OH], and

higher (*i/n*) isomeric ratios. Further, the relative differences of the reaction rate constants of these

isomers with OH increase during the summer from their OH reaction rate temperature

dependences (Supplement Figure S6) [*Atkinson*, 2003; *Wilson et al.*, 2006]. If emissions were

constant, one could expect a ~5% and 7% seasonal variation of isomeric ratios of butanes and

pentanes, respectively, from the reaction rate constant temperature dependency alone

(Supplement Figure S6). Combined, these two effects result in an overall relatively faster

removal rate of the *n*-isomer, and higher (*i/n*) isomeric ratios in the summer.

Previously published (*i/n*) butane isomeric ratios ranged from ~0.4–0.6 [*Goldstein et al.*,

1995; *Jobson et al.*, 1994a; *Parrish et al.*, 1998]. The median (*i/n*) butane isomeric ratios

observed in the data considered in this study mostly fall within this range. The center of the

distribution is similar, but the results across PAMS and GGGRN sites suggest a larger range of

values than previous work that mostly focused on individual site observations.

Over the 15-year study period declining (*i/n*) isomeric ratio trends were observed at the

majority of sites. The median rates of change (overall (all sites) median of determined slope

values with 1σ standard deviation) were -1.0 ± 3.1 % yr^{-1} for the (*i/n*) butane, and -2.8 ± 6.9 %

yr^{-1} for the (*i/n*) isomeric pentane ratio. If only statistical significant cases are considered, then

median results are -2.0 ± 3.0 % yr^{-1} for the (*i/n*) butane, and -3.1 ± 1.6 % yr^{-1} for the (*i/n*)

isomeric pentane ratio. Over the ~15 years investigation period these values account to total

changes of ~30 and 45% for these isomeric ratios.

The relative ratio of isomeric pentane emissions varies widely among emission categories and study region [*Andreae and Merlet*, 2001; *Gilman et al.*, 2013; *Helmig. et al.*, 2014b; *Jobson et al.*, 2004; *LaFranchi et al.*, 2013; *Peischl et al.*, 2013; *Petron et al.*, 2012; *Swarthout. et al.*, 2013; *Swarthout. et al.*, 2015], (Supplement Table STb2). The observed changes seen in the data considered here could be due to changes in sources, sinks, or a combination of both. Likely, the relative influence of these processes will vary between urban, semi-urban, semi-rural, and rural locations. In the following we will discuss a series of probable causes.

Since transportation sector/mobile source-related emissions are a major source of atmospheric butane and pentane isomers, it is likely that these results reflect a series of obvious changes in gasoline composition, consumption, tailpipe emissions, and evaporative losses. In 2004, at least 45 different blends of gasoline were produced in the United States. This myriad of blends developed because as of 2005, the EPA could not deny a special blend of gasoline com-pliant with the Clean Air Act (1963) and its amendments (1970) [*Wells*, 2005]. VOC emission reduction is primarily achieved by lowering a fuel's Reid Vapor Pressure [*EIA*, 1998]. There has been a notable reduction of the VOC fraction in gasoline formulations used in U.S. cities. In California, a reformulated gasoline blend was estimated to have a 25-29% lower fraction of VOCs compared to conventional gasoline used before 1995. Similarly, during 1995-2006, volatiles in gasoline declined by 26.6-30.2% in Boston, Chicago, Gary, Philadelphia, Baltimore, Springfield, and Houston [*EPA*, 2006a; b; c; d; e; f] in comparison to conventional formulations of gasoline used before 1995. Tailpipe emissions of hydrocarbons from light duty gasoline vehicles were reduced by a factor of 100 from 1968 to 2004 [*Faiz et al.*, 1996] from technical improvements, such as catalytic converters, evaporative emissions control systems, computer

controlled fuel injection, and engine efficiency [*McDonald et al.*, 2013]. These VOC reformulations and emission reductions from the transportation sector are likely explanations for the decreasing mixing ratios of butane and pentane isomers in urban areas. Obviously, these reductions have superseded expected emission increases from the steady growth of the automobile fleet across the nation.

Changes in gasoline formulations could also play a role in seasonal changes in butane and pentane isomers and their ratios. Special blends of gasoline are often developed in response to air quality standards in a particular region or time of year [*EPA*, 2017a]. Winter formulations of gasoline can include higher concentrations of butane and pentane isomers without violating regulations [*Wells*, 2005]. *n*-butane is present in higher concentrations in wintertime gasoline [*Goldstein et al.*, 1995] because of its high octane rating (94), but its high vapor pressure prevents it from being used in high concentrations in summertime gasoline.

The volume of the shale gas production in the United States increased by a factor of 4 from 2009 to 2014 [*EIA*, 2017b]. O&NG development is a common source of atmospheric alkanes, and recent studies have shown increasing influence and dominance of O&NG emissions on observed atmospheric NMHCs within and downwind of O&NG basins [*Gilman et al.*, 2013; *Helmig. et al.*, 2014b; *Schade and Roest*, 2015; *Swarthout. et al.*, 2013; *Thompson et al.*, 2014].

SGP provides a case study example for investigating the influence and changes in O&NG emissions on the alkane isomers. SGP is a rural site within the Woodford shale play, which produced some 403 billion cubic feet of shale gas in 2010 [*EIA*, 2017a]. There are greater than 60 active oil wells within a ten-mile radius of the SGP monitoring station; a map showing well locations surrounding SGP is shown in Supplement Figure S5. The strong influence from O&NG production is apparent in the data shown in Figures 3 and 4b. SGP had highest absolute NMHC

levels among GGGRN sites. SGP was also the only site where mixing ratios of all isomers have been increasing. Trends for all isomers were at least 5.5% yr^{-1}, and *n*-butane displayed a slope of 9.4% yr^{-1}. The relative seasonal amplitudes and interannual variability at SGP are the lowest of all sites (PAMS+GGGRN). The (*i/n*) pentane isomeric value (dropping from 1.0 in 2006 to 0.9 in 2015) at the end of the record matches the natural gas pentane isomeric ratio in *Gilman et al.* [2013]. As already noted further above, SGP was one of three sites (including LEF and Wendover) where the seasonal cycle of the isomeric butane ratio deviated from what would be expected from the seasonality of OH oxidation. A likely explanation is that at these locations the emission influence overwhelms the signal from seasonal OH chemistry seen at the other sites. Collectively, these data features indicate a dominant emission source with constant isomeric ratios, a dominance of emission over photochemical processing, and increasing emissions from nearby O&NG sources.

Across all sites, the pentane isomeric ratio shows a wider range, and is a more selective tracer for source attribution than the butane isomeric ratio. While in urban environments an (*i/n*) pentane ratio in the range of 2-3 is characteristic, the (*i/n*) ratio in O&NG-dominated atmosphere is ~1, as demonstrated for SGP in the preceding paragraph. This difference offers a sensitive tool for deciphering the relative influence of these two (urban versus O&NG) emission categories on atmospheric NMHCs. *Gilman et al.* [2013] and *Thompson et al.* [2014] demonstrated a temporal shift in the isomeric pentane ratio from increasing O&NG emissions. As seen in Figure 4, at the beginning of the time period studied here, every PAMS site that exhibits a statistically significant (*i/n*) pentane isomeric ratio trend had an (*i/n*) pentane isomeric ratio of at least 2, as typical for an urban environment. By the end of the study period, the (*i/n*) pentane ratio had dropped to values below 2 throughout the network, indicating possible increasing influence from O&NG sources at

these sites.

Panels (b) and (c) in Figure 1 show the trend slope values for the butane and pentane isomeric ratios, and panel (a) the spatial relation of monitoring sites to shale oil and gas plays. There are seven sites directly east of, and within ~200 miles of a shale play that have a statistically significant decreasing (i/n) pentane isomeric ratio trend: SDK, BAL, BOS, GAR, PHI, SGP, and SPR. With pentane isomeric ratio values of 1.3, LEF gave the second lowest result (after SGP), approaching the signature O&NG isomeric ratio. In a recent survey of ethane and pro- pane trends at ~40 monitoring stations worldwide, LEF had the second highest increasing ethane trend, and fourth highest increasing propane trend among all sites considered [*Helmig et al.*, 2016]. Consequently, our results presented here confirm the signature of the previously noted ap- parent increasing O&NG emissions at LEF, despite major O&NG shales being more than 200 km away from the site (Bakken to the West and Antrim to the East).

Two of the fastest growing O&NG basins are the Marcellus shale and the New Albany shale. The Marcellus shale has accounted for 85% of US shale production growth since 2012 [*Krohn and Nulle*, 2015]. This shale play is located primarily in Pennsylvania and West Virginia. The data from the sites studied in this work located in Indiana, Maryland, Massachusetts, and Pennsylvania possibly reflect emission changes from the Illinois Basin and the Marcellus Shale. Regional differences in natural gas composition must also be considered in evaluating possible oil and natural gas signatures on observed NMHC. For instance, methane composition of gas produced across Pennsylvania ranges from <75% methane to >90% methane [*Burruss and Ryder*, 2014; *Colon-Roman and Ruppert*, 2014]. Produced gas from the Marcellus Shale in central and northeast Pennsylvania is considered "dry gas"; it is >85% methane with negligible liquid petroleum constituents, making its emissions signature difficult to source using NMHC

tracers. Natural gas from Alleghany county in southwestern Pennsylvania, which produced 34 million Mcf of gas from 2000-2010 [*D.E.P.*, 2017], typically has a lower methane composition ("wet gas") and higher concentrations of heavier NMHCs [*Demirbas*, 2010; *Lacey et al.*, 1934]. During west to east air transport, variable emissions contributions with different NMHC signatures from both of these O&NG regions would be expected to be sampled at the downwind monitoring locations listed above. All five of the sites in the states mentioned above displayed statistically significant decreasing trends for the (i/n) pentane isomeric ratio, which would be consistent with an increasing emissions influence from these basins.

Another possible influence might be exerted by biomass burning emissions. Most types of biomass burning emissions exhibit relatively higher fractions of the *n*-isomers of butane and pentane, and have (i/n) isomeric ratios that are smaller (Supplement Table STb2) [*Akagi et al.*, 2011; *Andreae and Merlet*, 2001] than the average values calculated in our study. The frequency and the area burnt by U.S. wildfires rose from 1984-2011 [*Dennison et al.*, 2014]. Wildfires are a seasonal emissions source, occurring mostly in the summer, with a trend of increasing seasonal variability from 1995-2001 [*Zhang et al.*, 2014]. This increase in biomass burning emissions would be expected to result in an increased NMHC source that would drive (i/n) isomer ratios to lower values. Seven of ten urban sites had lower (i/n) pentane isomer ratios in winter months (Table 4). This seasonal signature in the data is the opposite of what would be expected if wildfire emissions exerted a strong summer influence. Therefore, it seems unlikely that increasing biomass burning emissions are exhibiting a determining signature on the data from the urban areas that were considered in this study.

5. Summary and Conclusions

NMHC atmospheric mole fractions, butanes and pentanes isomeric ratios, and trends showed a wide range and high variability among sites. A common feature was that average mixing ratios of the butane and pentane isomers have been decreasing at most, i.e. 81% of the sites, considered in this study. The exception was SGP, where all four isomers have been increasing (three have a statistically significant trend), most certainly due to increasing O&NG emissions. Similar to individual species, a large range was observed for changes of the (i/n) butane and pentane isomeric ratio, however, all six statistically significant (i/n) butane trends, and all seven statistically significant (i/n) pentane trends were negative, indicating a relative increase in the prominence of the *n*-isomers.

The most obvious explanation for the observed declines in concentrations and in the (i/n) isomeric ratio are changes in emission strength and relative contribution from different emission sectors. In the last century, motor vehicle sources have dominated urban emissions of VOC [*Parrish et al.*, 2009; *Von Schneidemesser et al.*, 2010]. Clearly, regulations of emission sources have brought mixing ratios of VOC down from their highest levels in the 1970s. Data from our analyses support this previous research, as levels appear to be continuing their decline at most sites evaluated in this work.

The abundance of decreasing (i/n) pentane ratios, both at urban sites and in the GGGRN, suggests influences on pentane emissions on wide geographical scales. There is a potential contribution from a changing isomeric ratio in gasoline pentanes, but the quantitative contribution from changes in this emission sector cannot be conclusively resolved with the data sets analyzed here. Another possible influence is an increase of the relative contribution of biomass burning emissions. Thirdly, it is notable that decreasing (i/n) pentane isomeric ratio trends were consistently observed at a site that is heavily influenced, and at sites within relatively close proximity,

i.e. ~200 miles, of O&NG development regions. Recent research has shown regionally elevated hydrocarbon concentrations in the United States as a result of O&NG development [*Franco et al.*, 2016a; *Helmig et al.*, 2016; *Kort et al.*, 2016; *Schade and Roest*, 2015; *Vinciguerra et al.*, 2015], with pentane isomers constituting on the order of 10% of the total NMHC mass [*Helmig. et al.*, 2014b]. The fact that (i/n) pentane isomeric ratio trends agree with the expected signature of increasing O&NG influence, and the geographic distribution of sites with statistically significant trends of the (i/n) pentane isomeric ratio and shale plays (Figure 1) suggest an increasing influence of O&NG emissions, regionally and nationwide. This conclusion is in agreement with findings from other recent studies that have shown that O&NG NMHC emissions are constituting an increasing fraction of the urban and rural VOC mix [*Schade and Roest*, 2015; *Vinciguerra et al.*, 2015] in the U.S. Similar observations were reported for the United Kingdom: While most C2-C8 hydrocarbons steadily declined from 1993 to 2012, ethane and propane, which are mostly associated to NG emissions, have remained near their 1993 values [*Derwent et al.*, 2017].

Given the relatively wide spread in results it is difficult to conclude at what exact rate these compounds and their isomeric ratios have changed in the U.S. as a whole. It is very obvious that multiple sources, exhibiting regionally diverse and different trends, are influencing atmospheric concentrations and isomeric ratios to a variable degree at the considered monitoring sites. Care should be taken utilizing these observations for evaluating emissions inventories, as the representativeness of the considered site locations is uncertain. Clearly, there is a need for consideration and comparison of spatially and temporally resolved data for deriving representative estimates on a national scale.

Acknowledgements

Chapter 4

Volatile Organic Compounds in the Northern Colorado Front Range

Samuel Rossabi[1], Jacques Hueber[1], Reed Terrell[1], Katie Smith[1], Wei Wang[1], and Detlev Helmig[1,*]

[1]Institute of Arctic and Alpine Research, University of Colorado, Boulder, CO 80309, USA

*Corresponding author: Detlev Helmig (detlev.helmig@colorado.edu)

Abstract

Volatile organic compounds (VOCs) were monitored within two networks near Boulder, Colorado, to investigate the spatial distribution and sources of these compounds. One site network extended along an elevation gradient from the city of Boulder (elevation 1600 m) to the Mountain Research Station (2900 m) on the eastern slopes of the Rocky Mountains. The longer-lived VOCs ethane and propane decreased with increasing elevation, suggesting that the city and surrounding plains were a source of these anthropogenic compounds. VOC diurnal cycles showed a few daytime events with elevated mixing ratios which were likely the result of a nearby emissions source. Within the other site network extending into eastern Boulder County, VOCs were monitored at five sites increasingly close to oil and natural gas (O&NG) development. Mixing ratios and variability of O&G-associated VOCs (ethane, propane, butane isomers) increased by a factor of ~2.4 - 5.2 as the distance to O&NG producing region decreased.

1. Introduction

Volatile organic compounds (VOCs) are major contributors to the organic carbon loadings in Earth's atmosphere. VOC emissions, excluding methane, from biogenic sources are estimated to be 29 MT of carbon (C) yr^{-1} in the US and 1150 MT(C) yr^{-1} globally [*Guenther et al.*, 1995]. Anthropogenic sources contribute 20 MT(C) yr^{-1} in the US and 60 – 140 MT(C) yr^{-1} globally [*EPA*, 2014; *Piccot et al.*, 1992]. Anthropogenic emissions arise from sources such as combustion in fossil-fuel powered engines, fuel storage, solvent usage or spillage, industrial sites, oil and natural gas (O&NG) operations and waste facilities. Tracer compounds and characteristic ratios of compounds are often utilized to determine the origin of a plume or the dominant emission sources in an area. Acetylene, aromatic compounds, and are mostly associated with urban emissions [*Gilman et al.*, 2013; *Ho et al.*, 2009; *Warneke et al.*, 2007]. O&NG emissions are marked by light, saturated hydrocarbons and (i/n) isomeric pentane ratios of ~1 [*Gilman et al.*, 2013].

The city of Boulder, CO is located in the foothills of the Front Range of the Rocky Mountains. Local wind patterns expose Boulder to air plumes from many directions. Relatively clean air reaches Boulder from over the mountains to the west. This downslope flow occurs mostly at night when cooler air from the mountains descends and moves east [*Johnson and Toth*, 1982]. Upslope and east to west flow is thermally driven by insolation and is especially dominant in summer. Boulder is ~50 km northwest of Denver and is subjected to urban and industrial emissions when winds are from the southeast. Agricultural emissions dominate air composition to the east. Weld County is ~50 km northeast of Boulder, and is home to O&NG development and exploration. From 2008-2015, the number of active wells in Weld County almost doubled. Annual oil production quadrupled (21 to 81 million barrels) from 2010-2014, and annual gas

production nearly doubled (219 to 392 billion cubic feet) [*COGCC*, 2014; 2016]. Vehicle traffic in the city of Boulder is also a major contributor to air emissions. The sum of 2016 annual average daily traffic figures from the six most heavily trafficked access points to Boulder is ~160,000 AADT (annual average daily traffic, total number of vehicles on a road for a year divided by 365) [*Colorado-DOT*, 2016].

Exposure to emissions related to O&NG development has had a demonstrated negative effect on human health. A positive relation has been observed between maternal residence within 10 miles of O&NG wells and congenital heart defects in their children [*McKenzie et al.*, 2014]. Other studies have demonstrated that health risks, such as birth defects, low birth weight, preterm birth, and cancer are increasingly likely when exposed to air near O&NG sites [*Ballester et al.*, 2010; *Bowen et al.*, 2009; *Brauer*, 2008; *Dadvand et al.*, 2013; *Ghosh et al.*, 2012; *Llop et al.*, 2010; *Lupo et al.*, 2011; *McKenzie et al.*, 2018; *McKenzie et al.*, 2015; *Wennborg et al.*, 2005]. Enhanced levels of VOCs have been observed in ground level air around O&NG wells, including the carcinogens benzene and toluene [*Huff*, 2007; *Macey et al.*, 2014; *Sovacool*, 2014; *Verma et al.*, 2000]. Further, VOCs contribute to the photochemical formation of ozone and secondary aerosols [*Bowman and Seinfeld*, 1994; *Chameides et al.*, 1992], which are health concerns for those exposed to them [*Colborn et al.*, 2011; *Colborn et al.*, 2014; *McKenzie et al.*, 2018; *McKenzie et al.*, 2012].

Air quality as a result of O&NG emissions in Colorado's Front Range has been the subject of several studies [*Brown et al.*, 2013; *Gilman et al.*, 2013; *Pétron et al.*, 2012; *Petron et al.*, 2014; *Swarthout. et al.*, 2013; *Thompson et al.*, 2014]. This study seeks to add to that body of work by observing spatial relations of VOC in the area around Boulder, CO.

2. Methods

VOC and methane data were collected at two networks of sites near Boulder, CO. The elevation gradient network included five sites that increased in elevation from Boulder (~1600 m) to the Mountain Research Station (~2900 m) near Ward, CO. The other network included five sites in the eastern portion of Boulder County. All VOC sampling systems employed selective ozone removal from the sampling stream by directing the air flow through sodium-thiosulfate coated glass fiber inlet filters [*Pollmann et al.*, 2006].   Calibrations were based on a series of gravimetric synthetic and whole air standards referenced against the World Meteorological Organization Global Atmospheric Watch Ozone scale (described in [*Helmig et al.*, 2016]). These data and their discussion are presented in *Sterling et al.* [2018].

2.1 Elevation Gradient Measurements

Information on the sites in the elevation gradient network is available in Table 1; locations are shown in yellow in Figure 1. Canisters and Programmable Flask Packages (PFPs) (Atmospheric Observing Systems, INC., Boulder, Co, USA) were deployed in parallel on 8 days in July and August 2014. The PFPs were used to investigate the diurnal cycle of VOCs by sampling once every 2 hours Summa canisters were sampled at a rate of ~2 ml min^{-1} over the course of the entire day.

2.2 East Boulder Measurements

Samples were collected from multiple monitoring sites in Eastern Boulder County to investigate the influence of the nearby O&NG drilling region on atmospheric VOCs and

methane. The five sampling sites and their distances from the Weld County border are listed in Table 1. Figure 1 shows these sites and their locations with respect to active O&NG wells. A map of all sites is available in Figure 1; East Boulder sites are marked by green text. More information on these sites is available in Table 1.
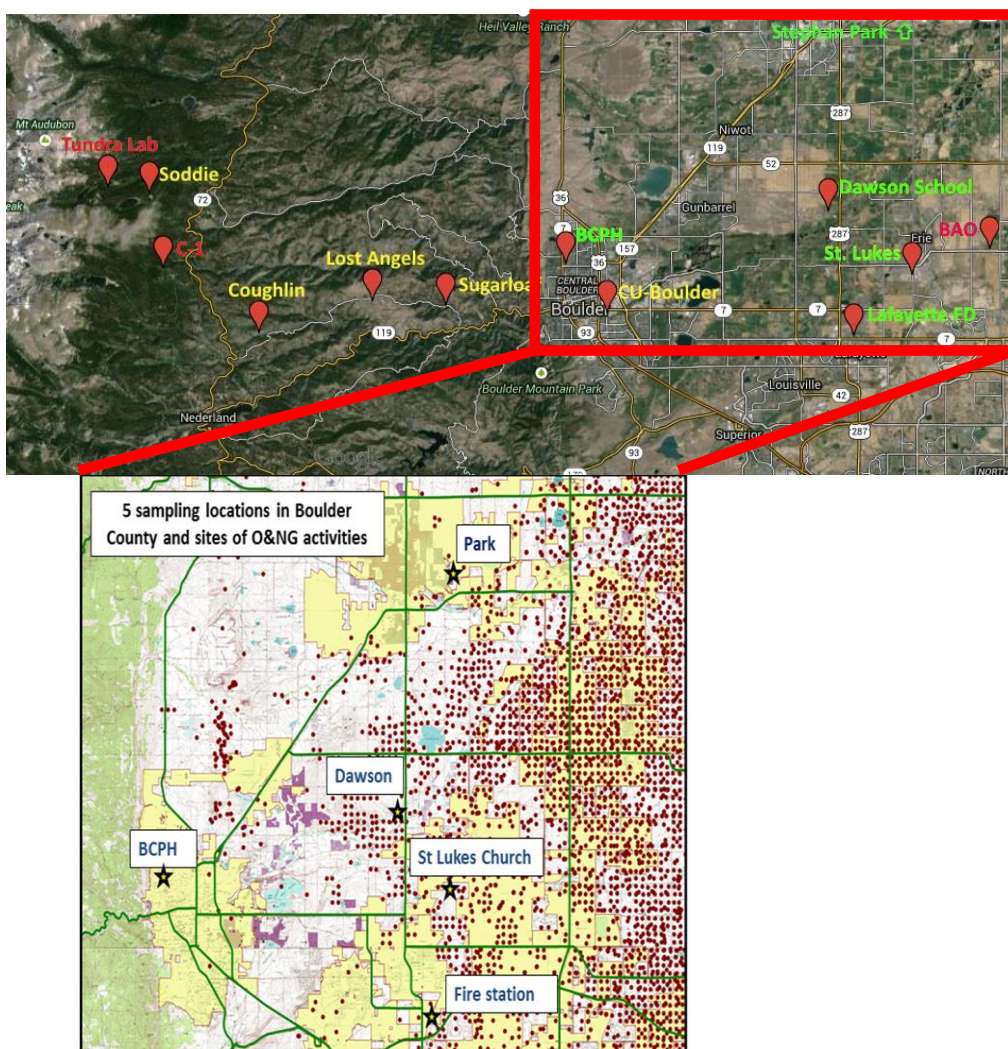
Figure 1. Map displaying sites where VOC and methane measurements were taken. PFPs were used at sites indicted by yellow markers. Canisters and cartridges were used at green sites. O3, and weather data were collected at red sites. (inset) The five sites in the Boulder County Health Study. Red dots are O&NG wells.

Table 1. Monitoring sites with site name abbreviation, location, elevation, and sampling methods used at the site. MRS stands for University of Colorado's Mountain Research Station. Distances to the O&NG producing region are included for East Boulder county sites.

Site Name	Site Abbr.	Lat.	Lon.	Elevation (m)	Sampling Methods Employed	Distance to O&NG Region
Tundra Lab (MRS)	Tundra	40° 3' 17" N	105° 35' 21" W	3528	PFP	-
Soddie Lab (MRS)	SO	40° 2' 52" N	105° 34' 15" W	3345	PFP	-
C-1 Site (MRS)	C-1	40° 2' 9" N	105° 32' 9" W	3021	PFP	-
Coughlin	CO	40° 0' 13" N	105° 28' 43" W	2523	PFP	-
Lost Angels Road	LA	40° 1' 8" N	105° 24' 18" W	2392	PFP	-
Sugarloaf Road	SL	40° 1' 1" N	105° 21' 28" W	1978	PFP	-
INSTAAR, CU-Boulder	BO	40° 0' 48"	105° 15' 11" W	1607	Canisters, Cartridges	-
Stephen Day Park	SDP	40° 10' 57"	105° 3' 49" W	1522	Canisters, Cartridges, OG Pods	30
Lafayette Fire Department	LFD	40° 0' 6" N	105° 5' 40" W	1600	Canisters, Cartridges, OG Pods	44
Boulder County Public Health	BCPH	40° 2' 14" N	105° 16' 53" W	1569	Canisters, Cartridges, OG Pods	48
Dawson School	DAW	40° 3' 50" N	105° 6' 37" W	1562	Canisters, Cartridges, OG Pods, Ozone Monitor	39
St. Luke's Church	SLC	40° 1' 56" N	105° 3' 24" W	1550	Canisters, Cartridges, OG Pods	38

The Boulder County Public Health (BCPH) building was chosen as the 'urban reference' site among the sites in eastern Boulder County. As the BCPH site is located in the city of Boulder, and is subjected to typical urban emission profiles emanating from mobile and industrial sources. It is the furthest of the five sites from Boulder County's border with Weld County (~25 km), which marks the southwest corner of the region of concentrated O&NG operations.

Samples were collected in Summa stainless steel canisters (Restek #27420, Bellefonte, PA) and by passive sampling collection on solid adsorbent cartridges (Chapter 5 of this dissertation). These sampling apparatus were deployed on 14 occasions for 3-day periods from mid-May to late August 2014 (sampling schedule in Figure S1; example of the sampling set up in Figure S2).

Whole air samples were collected at a constant flow rate of ~1 ml min^{-1} using commercial constant flow sampling devices (Restek #24232, Bellefonte, PA) (Figure S2b). These time integrated air samples were analyzed for methane and C_2-C_8 VOC in the C2-C8 (including benzene, toluene, ethylbenzene, xylenes (BTEX compounds)) using GC-FID/MS (section 2.4).

A second set of samples was collected by passive sampling onto cartridges packed with carbon-based adsorbents Carboxen 1000 and Carboxen 1016. (Supplemental Figure 2a). (Chapter 5 of this dissertation). Adsorbent cartridges were deployed in pairs to investigate the reproducibility of the measurement. In total, 62 canister and 71 adsorbent tube samples were collected and analyzed (400 days total of integrated sample collection).

2.3 Continuous GC Data

VOCs were analyzed by an in-situ GC/FID continuously at 2-hour time resolution with an on the days that PFPs and canisters sampled along the elevation gradient at the Rose Litman Laboratory 1 (RL1) on University of Colorado's east campus (Figure 1). Air was sampled from an inlet outside a second story window. The analytical system was very similar in its configuration as described in *Tanner et al*. [2006].

2.4 Analysis

Canister and PFP samples were analyzed by GC/FID-MS (Agilent Technologies #8500-5890 & G2578A, Santa Clara, CA). The GC was fitted with a GasPro PLOT column (Agilent Technologies #113-4362, Santa Clara, CA). Methane data were also collected with a Picarro cavity ring-down methane analyzer and OG-Pod methane sensors.

3. Results and Discussion

3.1 Elevation Gradient Data

Figure 2 shows average box plots of ethane mixing ratios along the elevation gradient averaged across the summer. There is a clear gradient from high elevation to low elevation and west to east indicating the source of the ethane is near Boulder and some of these emissions make their way into the foothills. A small portion of Boulder's ethane emissions reach the highest elevation and farthest west SO site; ethane measurements at this site rarely exceed 2.5 ppb. For all sites but SO, the mean is at least 2 ppb higher than the median, suggesting that the majority of measurements are relatively low, but means are biased upward by events of high mixing ratios of ethane. The CO site is dominated by clean air from the west, evidenced by the similarity of its median observation to SO, but there is clearly a non-negligible influence from Boulder as measurements of 7 ppb are within the 75th percentile of measurements.
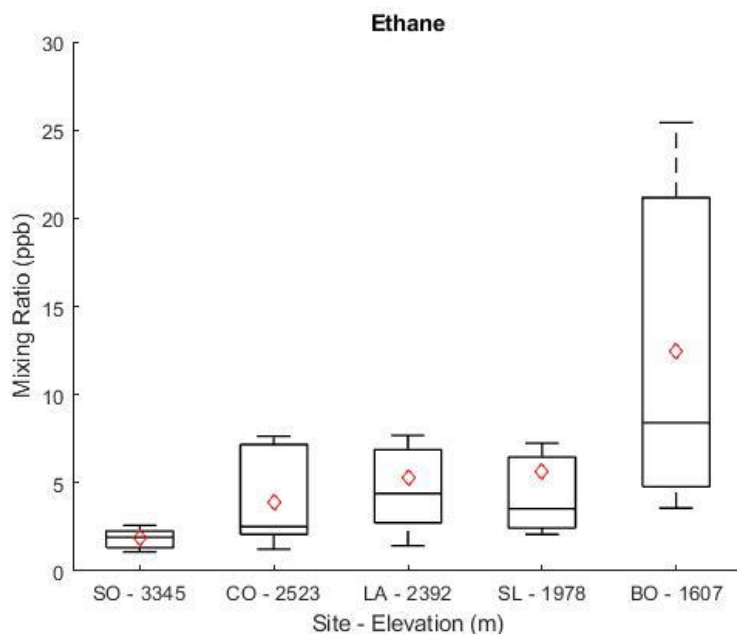
Figure 2. Ethane mixing ratios along elevation gradient. Sites on x-axis are in order of decreasing elevation. Boxes show the range of 25th to 75th percentile data. The middle line represents the median. The diamond represents the mean. Whiskers show 10th and 90th percentile ranges. Mixing ratios are highest and most variable in Boulder and steadily decrease and become less variable as the elevation increases.

There were several days where this general elevation gradient deviated (see Figure S3 for six sampling days in July and August 2014). In those cases, VOC concentrations were highest 1000 m above the city of Boulder. On these days, mixing ratios for all compounds were low at the highest elevation site, peaked at the CO site (mixing ratios > 50 ppb were observed on August 10 for propane, n-butane, i-pentane, and n-pentane) and were then again significantly lower at the LA, SL, and BO sites (Figure S3). This may be due to the prevailing daytime upslope winds that transport emissions from Boulder and the surrounding areas. However, we also suspect that a local natural gas source near the CO site may have contributed to this behavior. Mountain homes in the area are primarily fueled by propane gas storage tanks on

premises. This amounts to a high number of potential point sources within the area and may explain the high mixing ratios observed on August 10.

3.2 Eastern Boulder County Monitoring

The statistical distribution of VOC mixing ratio results from the sites in eastern Boulder County are shown in Figure 3. Sites are ordered by decreasing distance from Weld County, (distances available in Table 1). The box plots in Figure 3 show a clear spatial gradient that increases as the distance to the O&NG region decreases for the C_2-C_5 alkanes, which are the VOC most abundantly emitted from O&NG operations [*Helmig. et al.*, 2014b; *Pétron et al.*, 2012; *Petron et al.*, 2014; *Thompson. et al.*, 2014]. Ethane and propane mixing ratios increase by > 10 ppb going from BCPH to Stephen Day Park (SDP). This is rather remarkable given that BCPH, centrally located in the city of Boulder, is the most urban location of this series of sites. While very few O&NG wells are in close proximity to BCPH, vehicle emissions influence air composition at this site. The high traffic density has a relatively small influence on atmospheric ethane levels because ethane appears to be more strongly tied to the proximity of oil and gas operations. This association underscores the dominant role that O&NG sources play in the regional ethane emissions, and demonstrates how selective ethane is as an O&NG emissions tracer.

The BTEX compounds show similar distribution across sites. Absolute mole fractions and variations in mole fractions increase towards the eastern sites, but a trend is less evident than for the <C_6 alkanes. This suggests multiple sources are responsible for BTEX emissions in this region, and is consistent with previous studies [*Pétron et al.*, 2012; *Petron et al.*, 2014; *Swarthout. et al.*, 2013; *Thompson. et al.*, 2014]. These studies have shown that oil and gas

operations are a significant, but not dominant source of BTEX compounds in the Colorado Front Range [*Derwent et al.*, 2000; *Ho et al.*, 2009].

The variability of the observed mixing ratios, shown by the height of the boxes in Figure 3, increased with decreasing distance to Weld County. High variability has indicated proximity to a source in other work [*Russo et al.*, 2011; *Sharma et al.*, 2016; *Zheng et al.*, 2017]. Variability can indicate of proximity to a source because direction of transport influences observed mixing ratios at a given site. This is exacerbated at sites closer to a source because a larger range of transport direction will influence air at the site, and emissions plumes will have had less time to mix into surrounding air. A high degree of variability indicates emissions have not yet been well mixed into the surrounding area and are therefore very high indicating the emissions source is not constant or the wind direction is not constant.

The bottom right panel of Figure 3 shows the (*i/n*) pentane isomeric ratios observed at each of these sites. Similar isomeric ratios are observed at all sites and are closer to the characteristic ratio of O&NG gas emissions (~1) than the typical urban ratio (~3) [*Gilman et al.*, 2013]. The highest (*i/n*) pentane ratio were observed at BCPH, but a clear spatial gradient is not present in these data. (*i/n*) pentane ratios of ~1 are observed at all sites. *Gilman et al.* [2013] investigated the range of values and distribution of this isomeric ratio in different urban and O&G influenced settings. The defined an overall range of ~ 0.9 – 3, with the lower end values being characteristic of O&G emissions, and the higher end values being typical urban signatures. Values seen in the BC data clearly are on low end side of this spectrum, which indicates that emissions from O&NG development have a dominant influence on the VOC air composition at these sites and throughout the region. There is a slight gradient towards lower values at the eastern sites, indicative of the increasing O&NG influence along this transect, with BCPH being

the location most heavily effected by urban, i.e. automobile emissions. Other VOC, e.g. hexane,

alkenes and aromatic compounds, show similar mixing ratios across all sites.
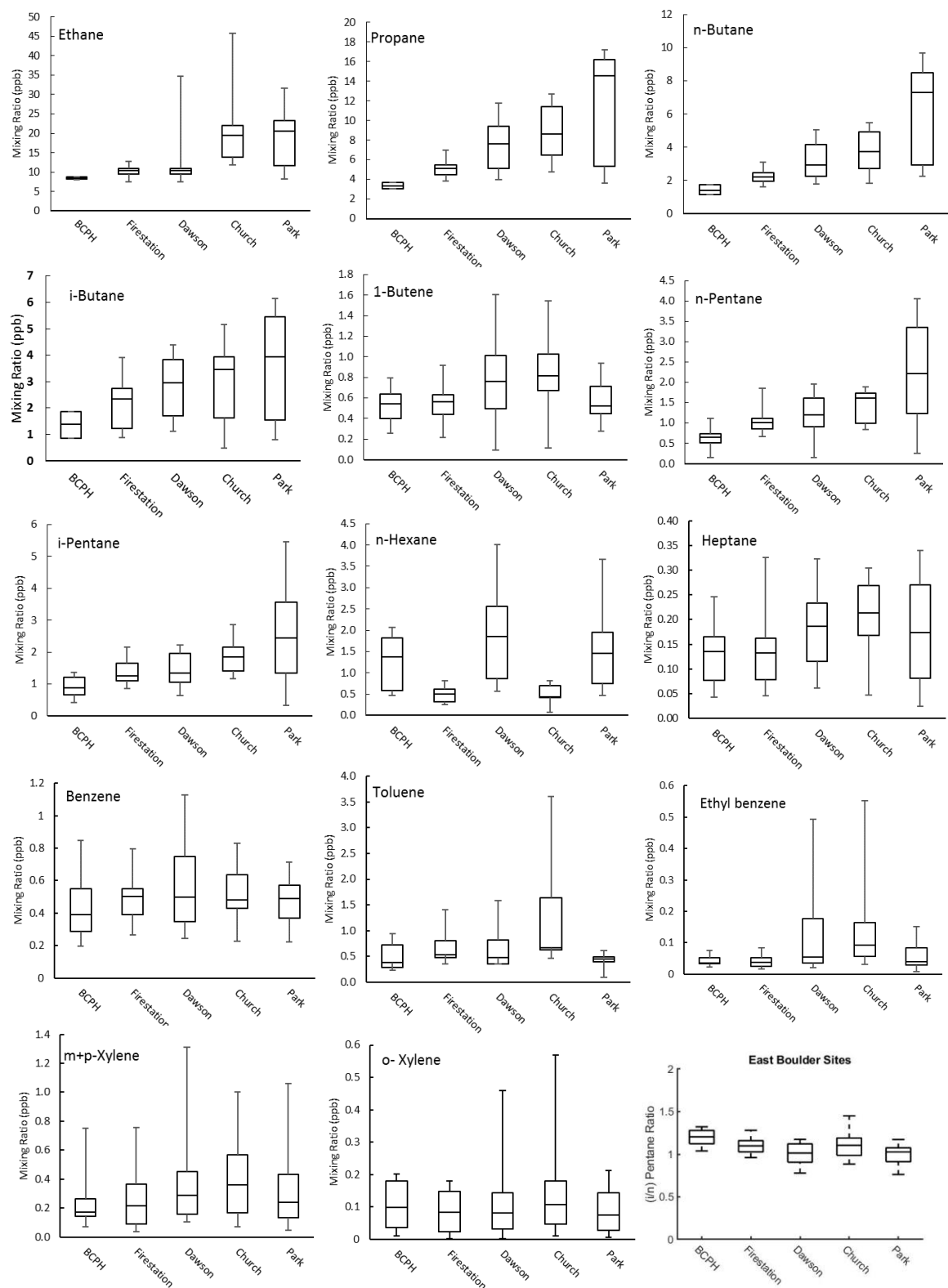
Figure 3. Box and whisker plots of VOCs captured by canisters at Eastern Boulder County sites. The bottom right panel shows (i/n) pentane ratios.

3.2.1 Methane

Figure 4 shows box plots of methane values at sites in the East Boulder County network. The atmospheric background during the summer of 2014 was approximately 1.87 ppm (value derived from NOAA measurements conducted at Niwot Ridge), shown as a red horizontal line in the figure. There was a significant degree of variability in the methane data between measurement days, which likely is mostly driven by variable atmospheric transport conditions on particular sampling days. Methane was lowest at the BCPH site. Methane increased towards the east of the county; highest levels were observed at Stephen Day Park (SDP) in Longmont. The methane enhancement (values above background) at SDP was approximately twice that seen in Boulder. There was a noticeable increase in variability with increasing absolute levels, indicated by the wider spread of the data at the eastern monitoring sites. These two features (higher absolute levels as well as higher variability) are a clear indication of higher abundance and stronger strength of methane sources in the eastern part of the county, respectively toward the eastern county boundaries.
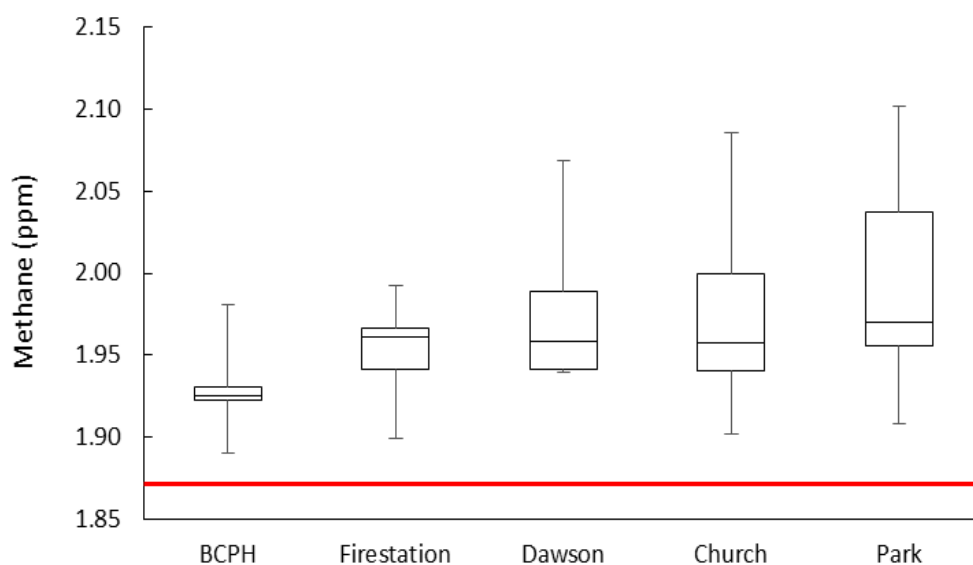
Figure 4. Spatial gradient of methane. in 3-day integrated canister samples collected at the five study sites. Each box was derived from 9-11 individual measurements. The upper and lower borders of the boxes show the 25 and 75 percentile of the data, the horizontal line in the center the median, and the whiskers depict the minima and maxima. The red line shows the approximate background level of methane (1.87 ppm) during summer 2014.
Sites on x-axis are ordered by decreasing distance to Weld County. Methane was measured by methane analyzer on OG pod. Red line indicates Northern Hemisphere background methane mixing ratios.

Methane is emitted from a variety of sources, but co-emission with tracers of particular sources can aid in determining the source of the methane (Figure 5). The lack of correlation with propene, 1-butene, and 1-pentene (R^2 = -0.03 to 0.31) suggests the methane is not from a biogenic source, at least not a plant source, methane is frequently emitted by livestock. Poor correlations with BTEX compounds (R^2 = -0.31 to 0.15), especially toluene and ethylbenzene suggest this methane was not emitted by mobile sources. The best correlations are observed for the light alkanes and methane. Ethane and propane show the highest correlations (R^2 = 0.75 and 0.54, respectively). The butane and pentane isomers have correlations with methane that range from R^2 = 0.37 to 0.46. This behavior suggests that methane and the light n-alkanes (especially ethane and propane) in the Northern Front Range share common sources. This is supported by the increasing methane mixing ratios as the distance to Weld County decreases (Figure 4). Other

VOC sources are likely more diverse, and also shows a spatial gradient with highest mixing ratios closest to Weld County. This suggests this methane originated from oil and gas activity in Weld County.
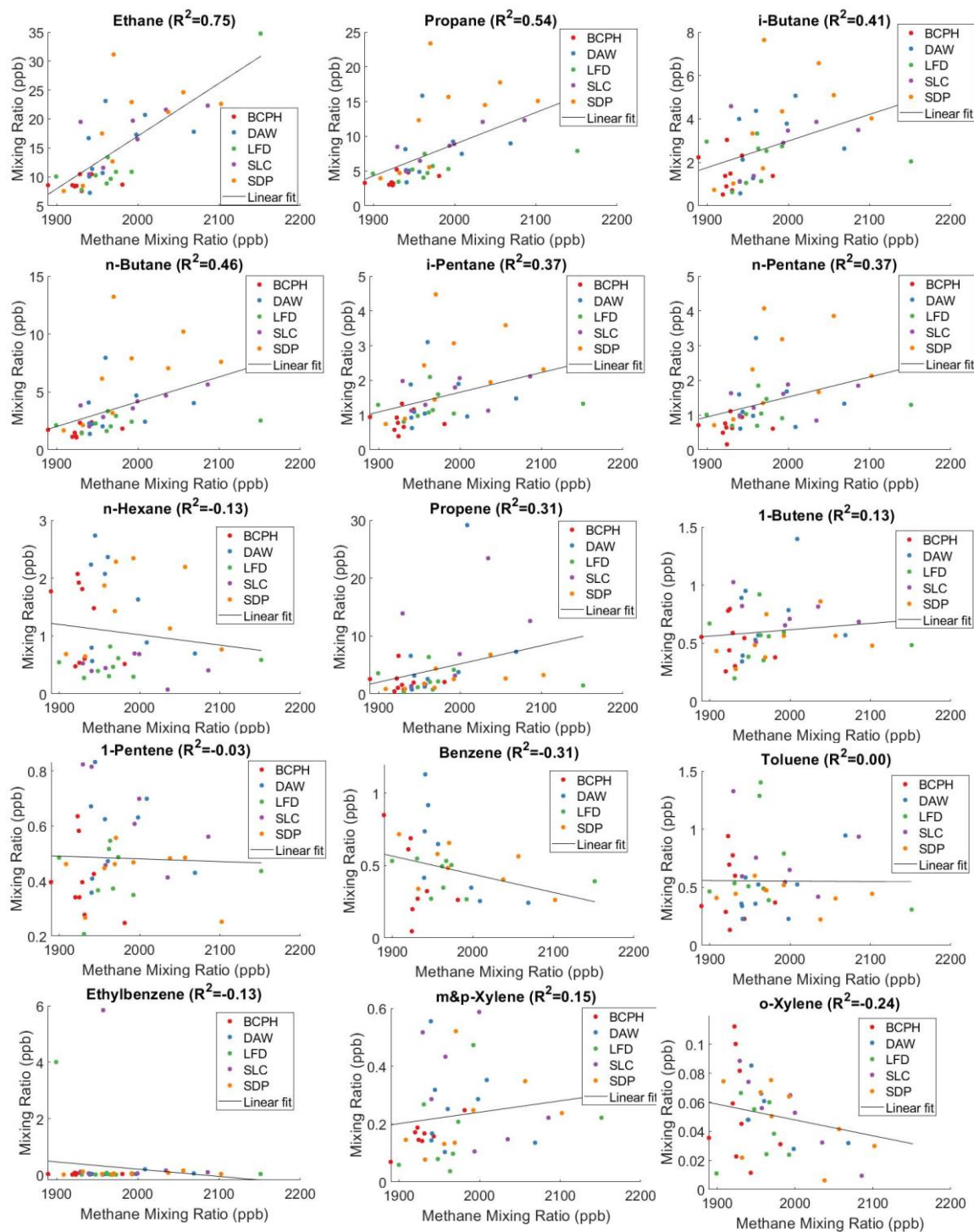
Figure 5. Comparison of VOC and methane mixing ratios at East Boulder sites. Colored markers indicate site at which measurement was taken. Note that y-axes vary between plots.

3.3 Diurnal Cycle of VOC

Figure 6 shows six diurnal cycles of VOC measured by the in-situ GC at INSTAAR in Boulder (other dates available in Figure S4). Three of the dates have daytime spikes in VOC mixing ratios. *n*-Butane and *i*-pentane are among the most elevated compounds in all three spikes. *i*-Butane is also present in all three, but is relatively small. Propane is highly elevated on July 26 and 31. On all three occasions, most compounds return to lower mixing ratios within 10 hours. The other three dates do not have daytime spikes, but are similar in that propane and n-butane mixing ratios are elevated for the majority of the day. On July 22, mixing ratios of *i*-pentane and *i*-butane exhibit varying degrees of matching the temporal dynamics of mixing ratios of propane and *n*-butane. Similarities in temporal dynamics can indicate the compounds involved originate from the same source. Near emission sources, higher mixing ratios are often observed at night when the low boundary layer and low levels of oxidant allow for higher mixing ratios of VOCs [*Halliday et al.*, 2016]. Night time removal mechanisms are slower than day time mechanisms, resulting in longer residence times [*Atkinson*, 2000]. The primary daytime removal mechanism of most of the compounds from the atmosphere is through oxidation by OH, and ozone to a lesser extent. Both of these compounds are generated through photochemistry and are higher during the day [*Finlayson-Pitts and Pitts*, 2000]. Further, the boundary layer collapses at night [*Menut et al.*, 1999] and tropospheric mixing is limited [*Deardorff*, 1972], which results in higher mixing ratios.

The highly variable behavior seen in these data suggests that these light alkane VOC likely arise from nearby emission sources that could be variable in their strength and/or that transport regimes vary so that polluted air from theses source is only transported to the site at certain particular air flow conditions. Propane, and isomers of butane and pentane are more often the elevated compounds, and are commonly associated with O&NG emissions.
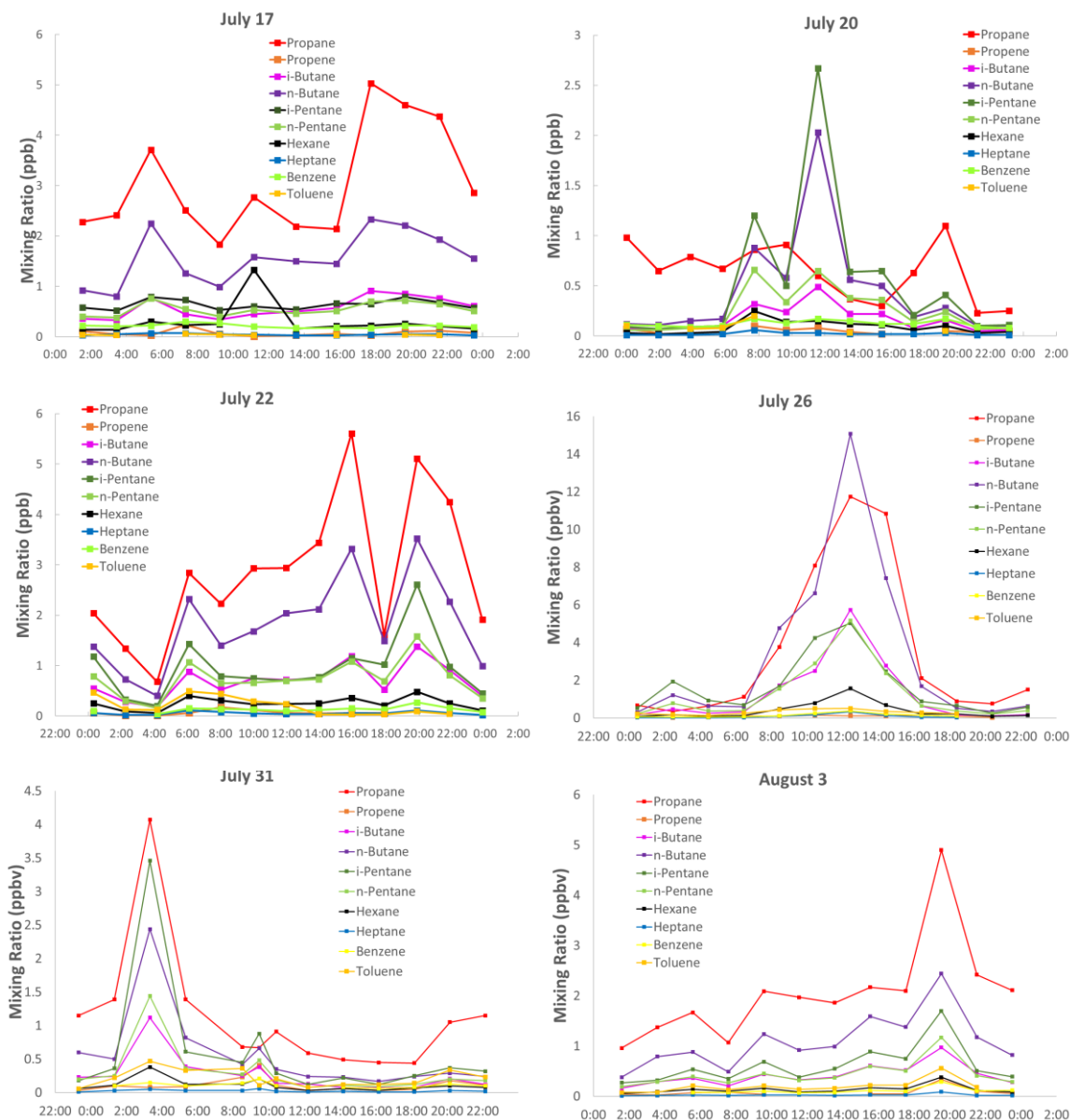
Figure 6. VOC event measured by in-situ GC/MS at INSTAAR on July 26. The opposite of the expected diurnal VOC cycle is observed. The x-axis displays the time in 24 hour format.

4. Conclusions

In this study, two networks of monitoring sites were employed to survey the species and abundances of VOCs present in the air in Boulder, CO. Elevated mixing ratios of <C6 alkanes

and BTEX compounds were present as a result of the variety of anthropogenic sources present in this region.

Anthropogenic influence was observed along elevation gradient as longer lived compounds were present at higher mixing ratios at higher elevations. Finally, several daytime spikes of anthropogenic VOCs, which are opposite the expected diurnal cycle, provide more evidence of a nearby emission source. These and future studies of VOCs in this region will yield a better understanding of the environmental impacts of O&NG operations, and enable policy makers to make better decisions regarding air quality regulations necessary to maintain the health of Boulder County residents.

At the east Boulder network, mixing ratios of O&NG related compounds increased as distance to the O&NG producing region decreased. Measurement variability also increased as distance decreased. Spatial trends for VOCs more associated with mobile source emissions, such as BTEX, were not observed. The evidence for ozone precursor emissions being dominated by O&NG sources is further supported by (i/n) pentane ratios characteristic of O&NG observed at East Boulder sites. This is particularly interesting in the Front Range, a metropolitan area that is more influenced by oil and gas than other metropolitan areas [*Abeleira et al.*, 2017].

The influence of O&NG development has been observed in Colorado's Front Range in many studies [*Abeleira et al.*, 2017; *Gilman et al.*, 2013; *Pétron et al.*, 2012; *Petron et al.*, 2014; *Swarthout. et al.*, 2013]. VOCs, ozone, and particulate have all been shown to be elevated as a result of O&NG emissions [*Dingle et al.*, 2016; *Vu et al.*, 2016]. These compounds have been observed at elevated levels (i.e. > 100 ppb of ethane) in other O&NG development regions such as the Uintah Basin in Utah, and the Green River Basin in Wyoming [*Helmig. et al.*, 2014b; *Oltmans et al.*, 2014].

Ozone production and destruction in an urban setting are highly dependent on the relative emission ratios of NOx and VOCs [*Ehhalt*, 1999; *Monks*, 2005]. The presence of NOx is necessary for the primary production mechanism of tropospheric ozone, but this process can be halted by high relative emissions of VOCs, which lead to the production of HOx, and later, the destruction of ozone [*Lightfoot et al.*, 1992]. Similarly, a lack of VOCs can lead to an NO dominated regime that also destroys ozone [*Zhou et al.*, 2014]. However, an ideal ratio of VOCs and NOx (~10 mg C_{VOC} m^{-2} hr^{-1} to 1 mg N_{NOX} m^{-2} hr^{-1}) to can lead to rapid production of ozone, which in turn results in areas of non-attainment [*Monks et al.*, 2015]. In Cheadle suggests that O&NG emissions can contribute up to 30 ppb of ozone in Colorado's Northern Front Range [*Cheadle et al.*, 2017].

In addition to O&NG, urban, industrial, and agricultural sources contribute to ozone precursor emissions in the region. Feedlots have been shown to be heavy emitters of ozone precursors and solar occultation flux instrument has suggested that emissions may be underestimated by a factor of 2 − 10 [*Kille et al.*, 2017].

While many studies have investigated emissions and sources of anthropogenic pollutants in Colorado's Front Range, efforts have been made to understand how physical and meteorological features affect air quality in this region. The Denver Cyclone deposits plumes from the Northern Front Range in the Denver Metropolitan area. Mass concentrations of organic aerosol, nitrate, and sulfate are elevated in Denver when the cyclone is active [*Vu et al.*, 2016]. Visibility and air quality is negatively affected as a result of this transport. O&NG can produce as much as 38% of the secondary organic aerosol in the Northern Front Range, and plumes originating in oil and gas regions were shown to have higher aerosol mass concentrations than urban plumes [*Bahreini et al.*, 2018]. Thermal flow drives emissions from urban and agricultural

areas up into the foothills. This has been shown to affect air quality at high altitude sites in the Front Range and up to the Continental Divide [*Pfister et al.*, 2017; *Sullivan et al.*, 2016]. Sullivan employed ozone sondes, aircraft, and surface measurements to track a high ozone plume into the foothills. Pfsiter saw elevated levels of hydrocarbons and ozone up to the continental divide. This behavior is supported by the elevation gradient of ethane seen in this study. . Ozone mixing ratios as a result of atmospheric boundary layer conditions and diurnal entrainment have been studied [*Kaser et al.*, 2017].

Chapter 5

A Preliminary Examination of Passive Cartridge Samplers for Measurements of Atmospheric Oil and Natural Gas Hydrocarbons

Samuel Rossabi[1], Joshua Fuchs[1,2], Kate R. Smith[1,3], Jens Fangmeyer[1,2], Jacques Hueber[1], Detlev Helmig[1,*]

[1]Institute of Arctic and Alpine Research, University of Colorado-Boulder, Boulder, CO, 80303, USA
[2]Institute of Inorganic and Analytical Chemistry, University of Muenster, Muenster, DE
[3]Department of Chemistry, University of York, Heslington, York, UK

*Corresponding Author: Detlev Helmig (detlev.helmig@colorado.edu)

Abstract

Human health impacts have been demonstrated in proximity to oil and natural gas (O&NG) operations and are cause for increased interest in monitoring exposure to O&NG atmospheric emissions. Passive adsorbent sampling cartridges offer an attractive sampling approach for evaluating exposure to O&NG volatile organic compound (VOC) emissions as they are inexpensive, and can be used with little training in a variety of environments. Further, because they rely on diffusive uptake for sampling, rather than a pump, they do not require electrical power for deployment. The goal of this project was to expand passive adsorbent sampling to selective O&NG tracer compounds, i.e. C_{2-6} hydrocarbons, which previously have rarely been sampled by this method. Stronger adsorbent materials are required to sample these highly volatile compounds, so the carbon based adsorbents Carboxen 1000 and 1016 were evaluated in laboratory and field monitoring settings. A thermal desorption Gas Chromatograph/Flame Ionization Detector/Mass Spectrometer (GC/FID/MS) instrument was used for analysis. Challenges inherent to the increased affinity of these adsorbent materials are

the relatively high uptake rates for atmospheric water vapor and the high blank signal that often dictates the limit of detection. This challenge was overcome by selecting the adsorbent (Carboxen 1000), which exhibited the best signal to noise ratio for the target compounds, optimizing conditioning parameters to reduce blank signals, and reducing the adsorbent mass loaded in the cartridge. This strategy reduced blanks sufficiently (to equivalent ambient air mole fractions of < 50 pmol mol^{-1}, pptv) to sample the O&NG tracers at levels $\geq$ 0.5-1 ppbv. Linear VOC uptake by cartridges was observed in a simulated environment devoid of humidity, though uptake rates varied over the course of a week of sampling. Water uptake was as high as 0.65 g_{H2O} $g^{-1}_{adsorbent}$ in environments with RHs above ~75%, and reduced average target analyte uptake rates to 34% of those in the dry simulated environment. This potentially causes mixing ratios to be biased low when cartridges are deployed overnight, due to nighttime RHs elevated over daytime levels. However, higher nighttime VOC mixing ratios as a result of the compressed boundary layer may counter this effect. Despite the potential for analytical bias, representative sampling results were obtained for C_3-C_5 alkanes during three field studies, where cartridges were deployed alongside sampling canisters for whole air collection with subsequent GC/FID/MS analysis. Agreement varied by compound; ethane and alkene mixing ratios correlated poorly (linear regression R^2 value < 0.40), but propane, *n*-butane, *i*-pentane, and *n*-pentane correlated well (R^2 > 0.75). These results support the use of this passive adsorbent sampling for assessing exposure to O&NG emissions.

1. Introduction

The United States was the world's top producer of petroleum and natural gas hydrocarbons from 2012 to 2016 [*EIA*, 2017c]. Horizontal drilling techniques made this

production increase possible, and led to drilling in areas previously unexplored by oil and natural gas operations (O&NG). In 2010, there were over one million producing oil and gas wells in the United States [*EIA*, 2012; 2017b]. The large number of wells, along with a continued interest in drilling new wells, has led to O&NG operations increasingly approaching populated areas. Concern regarding nearing O&NG operations led Colorado legislators in 2012 to mandate O&NG operations not to take place within 500 feet of residences, and 1000 feet of high-occupancy buildings such as schools or day care facilities [*COGCC*, 2012]. Despite this legislation, conflicts abound between homeowners and O&NG companies over proximity of operations to residential areas [*CPR*, 2017; *Ray*, 2017; *Urbina*, 2011].

Much of the controversy is centered on the association of negative health effects with nearby O&NG wells. A relation between pregnant mothers living within 10 miles of O&NG wells and congenital heart defects in their children has been observed [*McKenzie et al.*, 2014]. Exposure to air near O&NG sites has been shown to increase the likelihood of health risks such as birth defects, low birth weight, preterm birth, and cancer [*Ballester et al.*, 2010; *Bowen et al.*, 2009; *Brauer*, 2008; *Dadvand et al.*, 2013; *Ghosh et al.*, 2012; *Llop et al.*, 2010; *Lupo et al.*, 2011; *McKenzie et al.*, 2018; *McKenzie et al.*, 2015; *Wennborg et al.*, 2005]. Ground level air around O&NG operations has been shown to have elevated concentrations of volatile organic compounds (VOCs), including hazardous air pollutants such as benzene and toluene [*Macey et al.*, 2014; *Sovacool*, 2014], both of which are known carcinogens [*Huff*, 2007; *Verma et al.*, 2000]. Further, VOCs contribute to the photochemical formation of ozone and secondary aerosols [*Bowman and Seinfeld*, 1994; *Chameides et al.*, 1992], which are health concerns for those exposed to them [*Colborn et al.*, 2011; *Colborn et al.*, 2014; *McKenzie et al.*, 2018; *McKenzie et al.*, 2012].

Increasing interest in the possibility of exposure to O&NG emissions begs a highly spatially and temporally resolved monitoring strategy that is robust, cheap, and easily deployed in myriad environments. Passive sampling devices have been used to monitor workplace exposure to gaseous compounds [*Brown*, 2000; *Palmes and Gunnison*, 1973]. They are small and durable enough to be deployed in industrial environments, or worn on one's person in such environments, and typically cost less than US$100 each. Additionally, these devices can be deployed without supervision, power, or other equipment, and can sample several target compounds simultaneously. Samples are integrated over the time for which samplers are deployed. This presents a more characteristic measurement than grab samples that collect a snapshot measurement of air quality. Multiple passive sampling devices can be deployed to the same location sequentially to increase temporal resolution, or to neighboring locations to investigate the spatial distribution of exposure. These devices have been used in the form of badge-type samplers with a surface of adsorbent, diffusion tube-filter adsorbent surface, cartridges loaded with adsorbent, diffusion denuders, lead sulfation candles, and sulfation plates [*Krupa and Legge*, 2000; *Lodge*, 1999]. Solid adsorbent sampling cartridges were used in this work because they have been shown to sample volatiles with high sensitivity [*Brown*, 1995], and have shown good agreement with continuous monitoring methods [*ISO*, 1999]. Furthermore, automated thermal desorption instruments are available that allow for automated and highly sensitive analysis of cartridges in sequence.

This sampling method relies on diffusion to collect compounds of interest on the adsorbent bed. As diffusion can be affected by environmental conditions, care must be taken to ensure a representative sample is collected. Temperature and air flow have been shown to affect sample collection [*Brown*, 2000; *Koutrakis et al.*, 1993; *Seethapathy et al.*, 2008]. Changes in

wind speed and direction relative to the sampler can vary effective diffusion path length, thereby impacting sampling performance [*Brown*, 2000; *Tompkins and Goldsmith*, 1977; *Underhill and Feigley*, 1991]. Diffusive uptake is directly affected by temperature, theoretically by 0.2 - 0.4% K^{-1} [*Brown*, 2000].

Adsorbents such as Carbotrap, Carbosieve, and Tenax used in previous passive sampling [*Bates et al.*, 1997; *Mowrer et al.*, 1996; *WMO*, 1997] are mostly suited to measuring hydrocarbons > C_6, including BTEX (benzene, toluene, ethylbenzene, xylenes) compounds, which are associated with O&NG emissions [*Allen*, 2014; *Helmig. et al.*, 2014b; *Howarth et al.*, 2011; *Pétron et al.*, 2012; *Zavala-Araiza et al.*, 2014]. The adsorbents Carbograph 4, Carbopack-X, and Carbopack-Z were shown to be suitable for diffusively sampling *i*-pentane, *n*-pentane, and larger compounds, but were unable to sample *i*-butane and *n*-butane [*Martin et al.*, 2010; *Verriele et al.*, 2015].

Adsorbent cartridges are employed in the EPA Method 325 A/B (also known as: fence line monitoring) [*EPA*, 2015a; *Thoma et al.*, 2011] for passive sampling from the property boundary of a suspected source of VOCs. This method was used in a campaign that deployed cartridges around the perimeter of a petroleum refinery to measure benzene emissions over two week periods. A model predicted concentrations around the refinery of 0.2 ppbv or less, but downwind mixing ratios were up to 2.3 ppbv, and exceeded upwind measurements by 1.7 ppbv. Cartridge measurements correlated with nearby GC measurements (R^2=0.86); duplicate cartridges agreed with an R^2=0.97 [*Thoma et al.*, 2011].

This work seeks to expand passive sampling techniques to VOCs most heavily emitted by and most indicative of O&NG operations, i.e. C_2 - C_6 hydrocarbons [*Franco et al.*, 2016b; *Gilman et al.*, 2013; *Helmig et al.*, 2016; *Howarth et al.*, 2011; *Karion et al.*, 2013; *Pétron et al.*,

2012; *Petron et al.*, 2014]. Stronger adsorbents must be employed to sample $< C_6$ hydrocarbons.

The adsorbent strength typically scales with the adsorbent surface area. This study investigated

Carboxen 1000 (Sigma Aldrich, United States, 11052-U Supleco) and Carboxen 1016 (Sigma

Aldrich, United States, 11021-U Supleco, now known as Graphsphere 2016). These carbon-

based adsorbents have surface areas of 1200 m^2 g^{-1} and 75 m^2 g^{-1}, respectively, while Tenax has a

surface area of ~35 m^2 g^{-1}.

An analytical challenge of using carbon based adsorbents is that thermal cycling (i.e.

processes such as conditioning and desorption) can produce benzene [*Helmig*, 1996], a target

compound in O&NG monitoring. Another challenge inherent to using such strong adsorbents is

the potential to co-sample H_2O and CO_2 [*Pollmann et al.*, 2006]. As atmospheric H_2O and CO_2

are 4-6 orders of magnitude more abundant than hydrocarbons $< C_7$, they compete with target

compounds for adsorbent sites during sample collection. Elevated humidity levels can limit the

adsorbent bed's ability to collect target compounds [*Helmig and Vierling*, 1995]. During

analysis, H_2O can displace carrier gas, change chromatography, co-elute with some target

compounds, interfere with the detector, and can freeze out and clog GC capillary columns during

sub-ambient oven cooling [*Ciccioli et al.*, 1992; *Fabbri et al.*, 1987; *Helmig et al.*, 1990; *Helmig

and Vierling*, 1995; *Sturges and Elkins*, 1993; *Wood*, 1987]. Furthermore, H_2O can obscure

chromatograms so that results are difficult to interpret, deteriorate the stationary phase of GC

columns, and damage the Mass Spectrometer (MS) ion source [*Helmig and Vierling*, 1995; *Ras

et al.*, 2009].

2. Overview of Experiments

Laboratory and field experiments took place over two years. A series of lab experiments were performed using both passive and active sampling. Active sampling entails using a pump to force air through the adsorbent bed, whereas passive sampling relies on diffusion of air into the cartridge. While the intention was always to use the cartridges passively, active sampling experiments were performed to calibrate the mass response of the analytical system by loading defined masses of standard components on to the cartridges. A dynamic dilution system consisting of two mass flow controllers (Tylan, Coastal Instruments, Inc., Burgaw, NC), one metering a multi-component standard (standard components and mole fraction listed in Supplemental Tables 1-4), the other metering zero air, was used to generate defined VOC standard mixing ratios. The adsorbents Tenax-GR, Carboxen 1000, Carboxen 1016, and cartridges filled with a combination of Carboxen 1000 and 1016 were evaluated for their ability to collect $< C_6$ and BTEX hydrocarbons in active sampling mass loading experiments, laboratory passive sampling uptake experiments, water uptake experiments, blank experiments, and field campaigns. Cartridges were deployed to the field in parallel with sampling canisters to determine their field sampling efficacy.

2.1 Cartridge Assembly

Unfilled, stainless-steel cartridges were purchased from Perkin-Elmer (Part # L4270123, Richmond, CA, USA) (89 mm long x 6.4 mm outer diameter, 4.8 mm inner diameter). Cartridges are open on each end, and have a unique identification number. The cartridge's sampling inlet or front opening is identified by two grooves 1.5 cm from the opening. A cartridge schematic is shown in Figure 1.

All cartridges, internal components (not including adsorbents), and tools were rinsed with deionized water, sonicated in methanol, and dried at 125°C. Cleaned cartridges and components were stored in rinsed and sonicated jars and handled wearing latex gloves. Assembly of sampling cartridges began by positioning metal gauze 1.5 cm from the front opening. The following components were then added in order behind the gauze: silanized glass fiber filter disks (Tissueglass 2500A0; Pallftex, Putnam, CT, USA), pre-weighed adsorbent, a second glass fiber filter disk, metal gauze, and a spring to immobilize components. Cartridges loaded with multiple adsorbents employed an extra glass fiber filter disk between adsorbents. Larger springs were used in cartridges packed with smaller adsorbent quantities. A cross section of a filled tube is shown in Figure 1. Cartridges were conditioned immediately after assembly by flowing purified nitrogen at 25 mL min^{-1} through the filled cartridge in a 300°C oven for 30 min (cartridges were conditioned again before use, the conditioning parameters were optimized experimentally, see section 4.2). Once cool enough to handle, cartridges were capped with ¼ " brass Swagelok tube fittings and caps using PTFE ferrules.
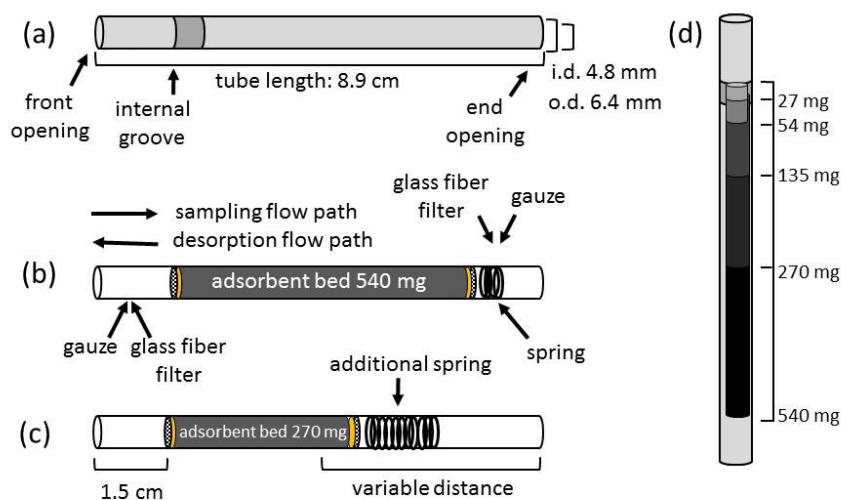
Figure 1. Schematic of adsorbent cartridges used. (a) Adsorbent cartridge dimension shown with front opening on the left. (b) Schematic of internal components of a cartridge loaded with 540 mg of adsorbent. The glass fiber filter disk, adsorbent, glass fiber filter disk, gauze, and spring (overlapping circles) follow from left. (c) Identical to (b), but with half the mass of adsorbent (270 mg) and a larger spring. Regardless of the adsorbent bed mass, the distance from the front opening to the adsorbent bed is 1.5 cm. The distance from the end opening to the adsorbent bed varies based on the mass and packing of the adsorbent bed (see section 4.1.2.1 for more discussion on distance from the adsorbent to the end opening). (d) Shows the relative volume of the cartridge occupied by 27, 54, 135, 270, and 540 mg of adsorbent.

2.2 Analysis of Cartridges

An automated adsorbent cartridge thermal desorption instrument (Perkin Elmer ATD400, Part # M041-3331, Richmond, CA, USA) was used for cartridge analysis. Following purging, analytes were desorbed from the cartridge and refocused onto a cooled micro-adsorbent trap. The micro-trap contained 25 mg of Carboxen 1016, and 220 mg of Carboxen 1000. Standard analysis parameters were set to a primary desorption time of 20 min at a temperature of 300°C, 50 mL min^{-1} of desorption gas flow (helium), -10°C cold trap temperature, and 300°C trap injection temperature. After sample transfer, the cold trap was heated rapidly to 300°C to inject the sample onto the GC column. A 50 m, 0.53 mm i.d., 15 micron Al_2O_3 PLOT column was used with a

Flame Ionization Detector (GC-FID) (Agilent 5890, Agilent Technologies, Boulder, CO, USA). The GC temperature program consisted of an initial oven temperature of 40°C for 2 min, a ramp of 10°C min^{-1} up to 200°C, and a final hold at 200°C for 15 min. Chromatograms were evaluated with the software program *PeakSimple* (SRI International, Menlo Park, CA, USA). VOC standards obtained from NIST and Apel-Riemer Environmental Inc. (components and concentrations available in the supplement to this manuscript, Table ST1), were used to determine analyte carbon response factors.

3. Initial Field Studies

Adsorbent cartridges and whole air sampling canisters were deployed to the field side by side to assess cartridge sampling capabilities, using the canister results as reference. Cartridges and canisters were sampled during the same time interval, with the canister sampling relying on a passive constant flow device (see below). Pearson correlation coefficients (PCC), which are a measure of the strength of a linear association of two variables, were used to quantify the correlation of mean cartridge versus canister data for specific VOCs. The statistical significance (p-values) of these correlations was determined from the PCCs (Table 1).

Cartridges deployed in the 2014 field studies contained 220 mg each of the adsorbents Carboxen 1016 and Carboxen 1000, separated by a glass wool plug or glass fiber filter. The weaker adsorbent (Carboxen 1016) was positioned closer to the front opening.

The cartridges were deployed in an inverted, lidless coffee can with a clip that held them vertically with the inlet pointing down. On the front opening side, the storage cap was replaced with a diffusion cap (Perkin Elmer Standard Diffusion Caps, Part # L4070207, Richmond, CA,

USA), to protect the cartridges from precipitation, direct sunlight, and minimize turbulent transport within the cartridge. A photo of the deployment setup is available in Supplement Figure S1. The diffusion cap was replaced with a metal cap and Teflon ferrule after the three day sampling period, placed in an air tight Mason jar, and stored at 3-4°C until analysis.

6-L Summa canisters (part #27405, Restek, Bellefonte, PA, USA) were conditioned prior to deployment by repeated filling with humidified zero air and evacuation three times, with a final pressure of ~1 to 2 in Hg following the third evacuation. Canister sampling was controlled using Veriflo passive flow devices (part #24232, Restek) that maintained a constant flow of ~1 mL min^{-1} over the 3-day sampling period. These devices ensured that cartridge and canister samples were collected over identical time intervals. In the field, canisters were placed in ~ 45 L cooler boxes with ~ 6 L of water in bottles to minimize temperature variations. A stainless steel sampling tube with an ozone scrubber inlet (glass fiber filter soaked in sodium thiosulfate solution, preparation details available in [*Helmig*, 1997]), was fed through a hole in the cooler to sample ambient air. Following sampling to a final pressure of ~19 in Hg, canisters were capped and transported to the lab for analysis. Sample volumes of 500 mL were withdrawn from the canister, scrubbed of water with a cryogenic trap, pre-concentrated on a Peltier-cooled micro-adsorbent trap, and injected into a GC-FID/MS with a 60 m, 0.32 mm i.d. GAS-PRO column, with the column flow split between an FID and a MS. The GC oven temperature began at 50°C for 2 min, was ramped at a rate of 8°C min^{-1}, and held at 225°C for 15 min before cooling to 50°C. Calibration standards used are listed in Table ST1.

Cartridges and canisters were deployed twice in 2014: for 3 days each week from June-August 2014 at five sites around Boulder County, and over three weeks in November/December 2014 outside of INSTAAR on the University of Colorado's East Campus (site locations are

provided in Table ST2). Temperature and relative humidity information for these campaigns are given in Table ST3. The summer 2014 deployment was a part of the Front Range Air Pollution and Photochemistry Experiment (FRAPPE, https://www2.acom.ucar.edu/frappe) and a Boulder County Public Health project, which had a particular emphasis on assessing concentrations of light hydrocarbons and BTEX compounds from O&NG development. Cartridges were deployed in pairs at each site. Due to a limited number of available canisters, only one canister was deployed to each site. Therefore, the reproducibility of canister sampling during the summer 2014 study is not available, but reproducibility of canister data was available during the winter 2014 study, as we discuss below.

The winter 2014 study site is located less than 100 m from the intersection of 30th Street and Arapahoe Ave, one of the busiest intersections in Boulder. The sampling was repeated ten times, resulting in twenty samples for each method. The repeatability of canister measurements was compared to that of the cartridges by calculating the relative standard deviation (RSD) of cartridge and canister results (available in Table 1). RSDs were calculated by finding the mean and standard deviation of paired samples collected using the same method (i.e. cartridge and canister samples are considered separately), and dividing the standard deviation by the mean. Relative Standard Deviations Ratios (RSDRs) are the RSDs of the cartridge sample pairs divided by the RSDs of the canister sample pairs. RSDs and RSDRs were calculated for each sampling date and compound, and the median values for all dates were determined and are shown in Table 1. The RSDs and RSDRs compare the variances of these methods, but do not address the agreement. The agreement of the cartridge and canister sampling techniques is developed and discussed in section 6.1. Due to the proximity to O&NG development, mixing ratios in samples from the FRAPPE study sites were generally higher than mixing ratios during the winter 2014

119

campaign. The absolute humidity was also higher during the summer 2014 campaign than during the winter 2014 campaign (Table ST3).

Table 1. Pearson correlation coefficients and p-values of cartridge and canister sampling during the summer and winter 2014 field campaigns. Canister and cartridge median relative standard deviations (RSDs), and median relative standard deviation ratios (RSDRs; cartridge/cans) from the Winter 2014 (n = 10) campaign are shown.

| Compound | Summer 2014 | | Winter 2014 | | | | |
	Pearson Correlation	P-Value	Pearson Correlation	P-Value	Canister RSD	Cartridge RSD	RSDR
Ethane	0.212	0.117	-0.380	0.278	0.011	0.413	42
Propane	0.855	0.000	0.925	0.000	0.011	0.043	5.2
Propene	0.450	0.001	0.245	0.495	0.054	0.383	3.8
i-Butane	0.672	0.000	0.884	0.001	0.013	0.062	4.5
n-Butane	0.931	0.000	0.925	0.000	0.009	0.089	14
1-Butene	-0.062	0.652	0.561	0.092	0.057	0.312	5.5
i-Pentane	0.909	0.000	0.865	0.001	0.014	0.088	9.0
n-Pentane	0.740	0.000	0.879	0.001	0.008	0.099	18
1-Pentene	0.463	0.000	0.521	0.123	0.107	0.240	3.3
n-Hexane	0.280	0.042	0.215	0.550	0.029	0.055	3.7
n-Heptane			0.879	0.001	0.097	0.301	3.1
Isoprene			0.069	0.849	0.053	0.415	2.7
Benzene	0.241	0.085	-0.308	0.386	0.020	0.153	7.8
Toluene	0.477	0.007	0.832	0.003	0.030	0.185	6.2
Ethylbenzene	0.136	0.333	0.071	0.846	0.025	0.134	12
o-Xylene	0.302	0.026	0.809	0.005	0.029	0.124	4.3

Precision errors and correlation results vary largely by compounds. RSDs for the cartridge analyses are generally higher (by a factor of 3-5 for most compounds) than for canister samples. RSDs for C_3-C_5 alkanes from the cartridge sampling in the winter 2014 campaign were below 10%; BTEX compounds fall within 10-20%. Pearson Correlation Coefficients (PCCs) were used as a first approximation for the agreement of the canister and cartridge sampling methods. A more rigorous assessment of the agreement of these methods is developed in section 6.1. PCCs for these compounds between canister and cartridge samples ranged from 0.67-0.93 in the summer 2014 campaign, and 0.87-0.93 in the winter 2014 campaign. PCCs for the BTEX

compounds were highly variable, ranging from -0.31 to 0.83 in these campaigns. These unsatisfactory results prompted a re-evaluation of the adsorbent cartridges with a particular emphasis on improving results for these aromatics.

4. Cartridge Optimization

The adsorbent, or combination of adsorbents, cartridge conditioning method, and adsorbent bed mass were further investigated for optimizing sampling of $< C_6$ alkanes, while also allowing representative sampling of BTEX compounds. The signal in blank runs of passive adsorbent cartridges typically determines the limit of detection, so it is essential to minimize the background and its variability when sampling ambient concentrations. Experiments to minimize the background signal of light alkanes and BTEX compounds are described below.

4.1 Adsorbent Selection

Cartridges containing the adsorbents Carboxen 1000, Carboxen 1016, Tenax GR, and an ~ equal combination of Carboxen 1000 and 1016 were evaluated (Table 2) using fully loaded cartridges only (the last four rows of Table 2). Cartridges were analyzed five consecutive times on the ATD400. Repeated thermal desorption yielded progressively lower backgrounds until the fifth desorption, when peak areas stopped decreasing significantly. The adsorbents were compared using the peak areas of ethane, propane, *n*-butane, *n*-propane, *n*-hexane, benzene, toluene, ethylbenzene, *m*-, *p*- and *o*-xylene, and the total VOC signal. The fifth run of each cartridge was considered for its blank VOC profile.

Table 2. Adsorbent cartridge types tested. Multiple cartridges of each unique adsorbent type and mass were assembled.

Adsorbent Type	Mass Adsorbent (mg)	Approximate % of Tube Occupied by Adsorbent
Carboxen 1000	27	5
Carboxen 1000	54	10
Carboxen 1000	135	25
Carboxen 1000	270	50
Carboxen 1000	540	100
Carboxen 1016	520	100
Tenax GR	320	100
Carboxen 1000/1016	285/255	50/50

4.1.1 Cartridge Blanks

Examples of blank chromatograms of the 5th run of each adsorbent are shown in Figure 2. Table 3 gives the corresponding peak areas for compounds of interest for each of the adsorbents. The chromatogram of Carboxen 1000 shows fewer and smaller peaks than for other adsorbents analyzed. Carboxen 1016 displayed the highest background, exceeding Carboxen 1000's total alkane response by a factor of 10, and the total BTEX response by a factor of 43. Tenax GR's total alkane and total BTEX peak areas were factors of 3 and 4 higher, respectively, than Carboxen 1000. The total peak area observed for the Carboxen 1000 and 1016 combination cartridge was 70% of the Carboxen 1016 only cartridge, and a factor of ~ 30 higher than Carboxen 1000 alone.
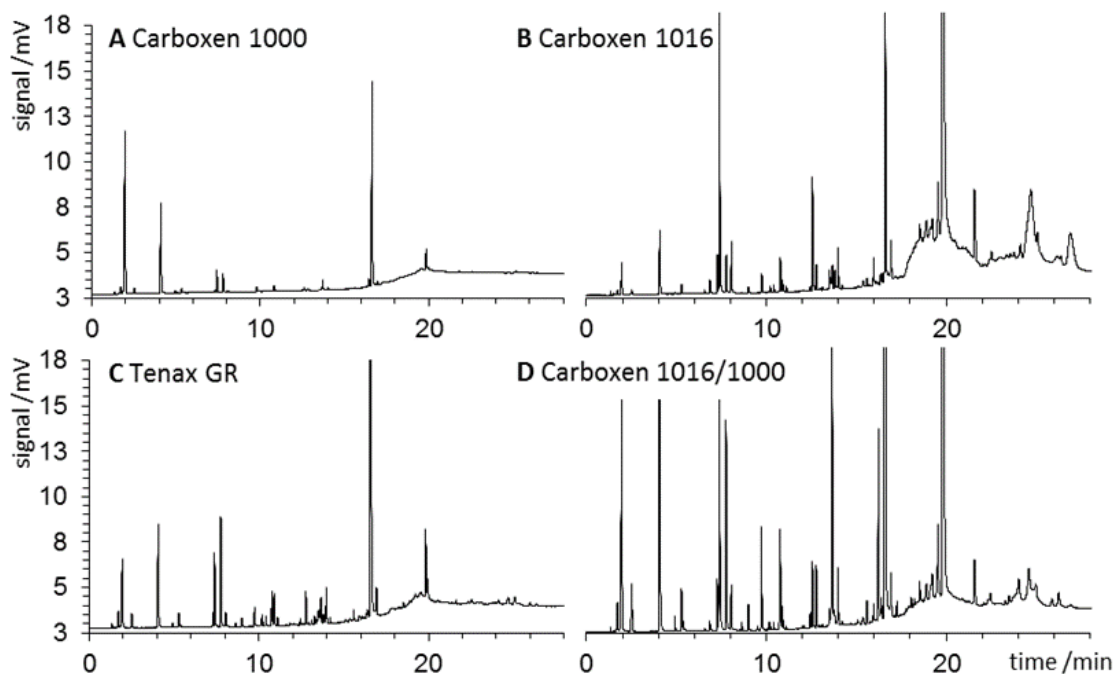
Figure 2. Blank chromatograms from cartridges loaded with (A) Carboxen 1000, (B) Carboxen 1016, (C) Tenax GR, and (D) a combination of Carboxen 1000 and 1016. Masses vary among adsorbents, 6.75 cm of each cartridge was occupied with adsorbent. The y-axis scale is identical for all panels.

Table 3. Peak areas (mV min) for several n-alkane and BTEX compounds from integrated blank chromatograms of each adsorbent type (n=5).

Compound	Peak area (mV min) by Adsorbent			
	Carboxen 1000	Carboxen 1016	Tenax GR	Carboxen 1016/1000
Ethane	1.97	1.27	4.90	7.61
Propane	1.70	1.52	4.44	12.9
n-Butane	0.893	18.1	2.60	6.59
n-Pentane	0.309	1.26	1.85	4.68
n-Hexane	0.199	31.7	0.337	19.2
n-Alkane Total	5.07	53.8	14.1	51.0
Benzene	57.7	96.7	255	418
Toluene	4.71	2590	14.2	1480
Ethylbenzene	0.316	14.1	1.20	7.99
(m + p)-Xylenes	0.539	22.9	15.5	19.2
o-Xylene	0.216	51.1	1.75	4.18
BTEX Total	63.5	2770	288	1930
All Compound Total	68.6	2830	302	1980

123

4.1.2 Adsorbent Evaluation

Carboxen 1016/1000 cartridges and Tenax-GR cartridges were actively loaded using a

custom automated sampler (diagram in [*Helmig et al.*, 2004]) with 1 L of the Apel-Riemer multi-

component standard (Table ST1). In a separate experiment, 2 L of an *n*-alkane and BTEX

standard were actively loaded on cartridges containing only Carboxen 1000 adsorbent. To

compare the performance of the different adsorbents, an Analytical System Response (ASR) was

calculated. The ASR is similar to a carbon response factor in that these values were calculated by

dividing the peak area for a compound by the mole fraction of the compound in the standard

(ppbC) and volume of sample (L). It is a measure of the collection and desorption efficiencies of

the adsorbent bed in the cartridge, the adsorbent microtrap in the ATD-400, the injection

efficiency into the GC/MS/FID, and the FID response. The average ASRs and their relative

standard deviations (RSDs) are listed in Table 4. The Carboxen based cartridges had larger

average response factors for the C_{3-5} alkanes, and lower relative standard deviations than the

Tenax-GR cartridges, but ASRs became progressively lower for heavier BTEX compounds.

Table 4. Comparison of Carboxen 1000, Carboxen 1016/1000 multi-stage adsorbent cartridges, and Tenax-GR cartridges. Analytical System Responses (ASRs) are the instrument response divided by the mixing ratio of the standard (ppbC) and the sample volume with relative standard deviations (RSD) for n = 5.

	Carboxen 1000		Carboxen 1016/1000		Tenax	
Compound	ASR	RSD	ASR	RSD	ASR	RSD
Ethane	2.13	1.4%	0.388	39%	0.069	35%
Propane	6.61	0.24%	6.79	12%	0.194	41%
Propene			13.3	4.1%	2.38	46%
i-Butane			6.05	4.3%	0.197	14%
n-Butane	6.57	0.26%	6.15	3.0%	0.329	13%
trans-2-Butene			14.1	11%	0.543	7.8%
1-Butene			10.1	9.2%	1.06	47%
iso-Butene			4.50	1.1%	0.833	30%
iso-Pentane			5.98	3.8%	0.791	2.0%

n-Pentane	6.24	0.35%	5.63	3.6%	1.47	2.4%
1-Pentene			4.90	3.2%	1.64	0.8%
Methylcyclopentane			18.6	4.5%	3.76	3.4%
2-Methylpentane			6.14	7.4%	2.03	39%
3-Methylpentane			6.07	5.1%	2.50	3.5%
Hexane	5.73	0.41%	5.88	2.1%	4.98	2.0%
Isoprene			6.45	2.7%	2.05	7.7%
trans-2-Hexene			2.90	0.1%	5.11	10%
cis-2-Hexene			5.22	3.0%	4.69	8.5%
n-Heptane			5.91	1.4%	5.93	1.1%
Benzene	5.99	1.1%	12.6	19%	18.3	12%
Octane			5.71	1.0%	5.89	1.1%
Toluene	5.41	0.94%	7.77	21%	7.02	7.3%
Ethylbenzene	2.87	5.9%	6.73	3.2%	6.53	3.1%
o-xylene	3.26	4.2%	6.32	1.3%	6.46	6.0%

4.1.2.1 Sampling onto dual-bed adsorbent cartridges

The sampling efficiency of Carboxen 1016 and Carboxen 1000 were tested and compared using the duel-bed adsorbent cartridges. All cartridges were prepared with the weaker adsorbent (Carboxen 1016) closer to the inlet (1016/1000 cartridges) (Figure 1). Twenty cartridges were used in the conventional sampling direction, and twenty were used in reverse, i.e. with sampling from the stronger adsorbent (Carboxen 1000) side ("1000/1016" cartridges). Because they were prepared with respect to the typical front opening, the distance to the adsorbent bed in the reversed sampling configuration varied more than for the 1016/1000 cartridges. Furthermore, the distance from the cartridge end to the adsorbent bed in the "1000/1016" cartridges was generally longer than for the 1016/1000 cartridges, because the inner components of the cartridge were packed down from the rear opening and held in place with a spring. All cartridges were placed inside a bag with a glass beaker containing deionized for humidifying the sample. A small humidity sensor thumb drive was used to monitor %RH inside the bag (Extech Instruments, RHT10, Nashua, NH, USA). The Apel-Riemer multicomponent standard was flowed into the

bag at 200 mL min^{-1}. 1016/1000 and "1000/1016" cartridges were placed in the bag with their respective "front" ends open to passively sample the standard atmosphere in the bag. Two cartridges of each configuration were removed at regular intervals over the course of a 10-day period and analyzed.

Table 5 lists the uptake rates (slopes of linear regression analysis of collected mass on the adsorbent cartridge versus sampling time), PCCs, and p-values for the 1016/1000 and "1000/1016" cartridges. Figure 3 shows peak areas of selected compounds versus sampling time. Slopes for the "1000/1016" cartridges are larger than for the 1016/1000 cartridges for all alkanes, toluene, and ethylbenzene, indicating that the "1000/1016" cartridges collected these compounds more efficiently. Both cartridge types had negative correlations for benzene collection. Despite having higher slopes, PCCs were lower in general for the "1000/1016" cartridges, which suggests that the sampling/analysis was less consistent and then for the 1016/1000 cartridges.

Following Fick's Law of Diffusion, the mass of analytes collected onto the adsorbent should be inversely proportional to the diffusion path length (the distance between the cartridge's opening and the adsorbent bed; Figure S2), which, besides the uptake on the adsorbent, likely explains some of the differences in the results between the 1016/1000 and "1000/1016" cartridges(Figure 1). The groove in the cartridge made the diffusion path length consistent and shorter for the 1016/1000 cartridges than for the "1000/1016" cartridges. In addition to the metal gauze and filter disk at both ends of the cartridge, a spring was present in the diffusion path for the "1000/1016" cartridges. Both of these factors should result in more efficient uptake by the 1016/1000 cartridges, however, this was not observed. While we assume both adsorbents are a perfect sink, the stronger adsorbent Carboxen 1000 may trap these compounds more effectively than Carboxen 1016. Having this adsorbent closer to the inlet would reduce the diffusion path

length, and therefore increase the mass of analyte collected. This may explain the higher slopes observed for the "1000/1016" cartridges. The distance to the cartridge opening was less consistent for the "1000/1016" cartridges because they were constructed with the intention of being sampled from the other opening. When constructing cartridges, all internal components are loaded through the rear opening and pushed down until they reach an internal groove 1.5 cm from the front opening. This variable diffusion path length may be responsible for the more variable sampling by the "1000/1016", which is reflected by the lower PCCs for these cartridges.

Table 5. Linear regression results for analyte peak area (mV min) versus sampling time. Slope values represent analyte uptake rates. Other regression results are Pearson Correlation Coefficients (PCCs), and P-Values for collection of a standard mixture onto 1016/1000 and '1000/1016' cartridges in a test atmosphere.

Compound	1016/1000			'1000/1016'		
	Slope (x 10^{-3})	PCC	P-Value	Slope (x 10^{-3})	PCC	P-Value
Ethane	0.04	0.15	0.48	0.1	0.18	0.46
Propane	1. 5	0.85	0.00	4.3	0.51	0.02
Propene	1.0	0.41	0.04	1.2	0.19	0.41
i-Butane	2.5	0.97	0.00	8.2	0.97	0.00
n-Butane	7.1	0.96	0.00	19	0.97	0.00
i-Butene	3.4	0.91	0.00	10	0.96	0.00
i-Pentane	8.9	0.97	0.00	14	0.95	0.00
n-Pentane	9.6	0.96	0.00	14	0.95	0.00
1-Pentene	0.2	0.44	0.03	0.2	0.25	0.29
Hexane	2.3	0.94	0.00	3.0	0.90	0.00
Heptane	0.2	0.49	0.01	0.2	0.39	0.09
Benzene	-0.3	-0.06	0.79	-3.6	-0.18	0.46
Toluene	-0.4	-0.05	0.83	1.8	0.49	0.03
Ethylbenzene	0.2	0.27	0.19	0.3	0.22	0.36
o-Xylene	0.2	0.47	0.02	0.1	0.21	0.38
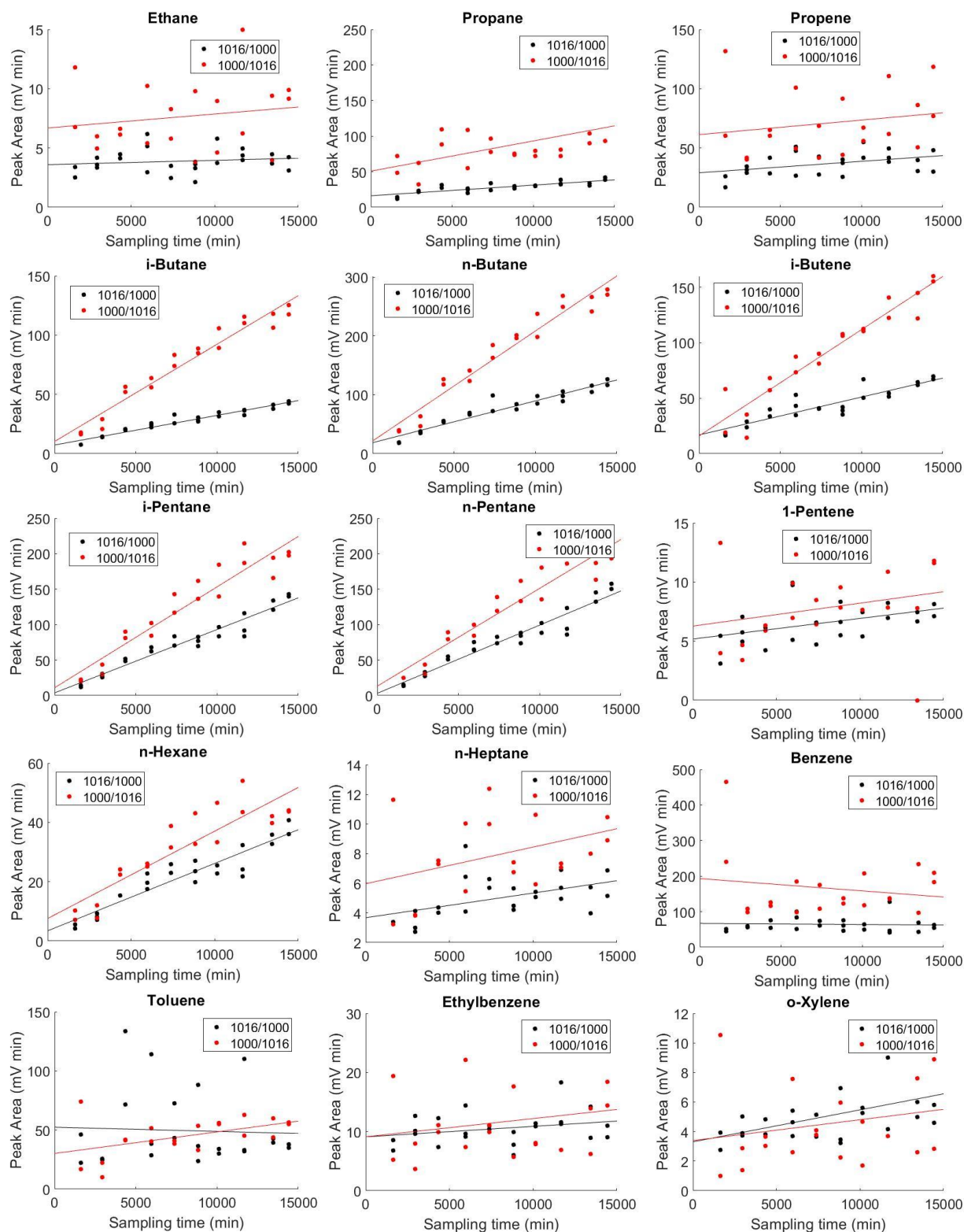
Figure 3. Comparison of diffusive uptake on multi-stage cartridges for passive sampling of a standard gas mixture. Black data correspond to "1000/1016" cartridges (see 2.4.2). Red data are 1016/1000 cartridges. Note differences in y-axis ranges.

4.2 Adsorbent Conditioning

Proper storage and conditioning of adsorbent cartridges are critical for achieving low detection limits [*Cao and Hewitt*, 1994; *Helmig*, 1996]. After determining the Carboxen 1000 adsorbent had the lowest blanks among tested adsorbent types, conditioning parameters were investigated with the goal to further reduce blank values, particularly for benzene. Cartridges were conditioned on a manifold placed inside a GC oven while being purged with N_2. Conditioning temperature, duration, and purge flow rate were evaluated by comparing BTEX blank levels from six sets of three cartridges loaded with 540 mg Carboxen 1000. Conditioning parameters are listed in Table 6.

Table 6. Details of conditions of Conditioning Optimization experiment.

Conditioning Trial #	Oven Temp (∘C)	Time (min)	N_2 Flow (mL min^{-1})
1	250	60	25
2	300	60	25
3	300	10	100
4	300	60	100
5	300	1200	25
6	350	1200	25

Figure 4 shows BTEX total peak area using various conditioning parameters. The blank response decreased > 50% when conditioning at 300°C compared to < 300 °C (trials 1 and 2), and by ~80% when conditioning at 350°C instead of 300°C (trials 5 and 6). Increasing the nitrogen gas flow from 25 mL min^{-1} to 100 mL min^{-1} resulted in a 40% decrease in blank signals (trials 2 and 4). Increasing conditioning time from 10 minutes to 1 hour resulted in a 25% decrease in the blank response (trials 3 and 4). A further 70% decrease in response was observed when increasing conditioning time from 1 hour to 20 hours (trials 2 and 5, Figure 4).
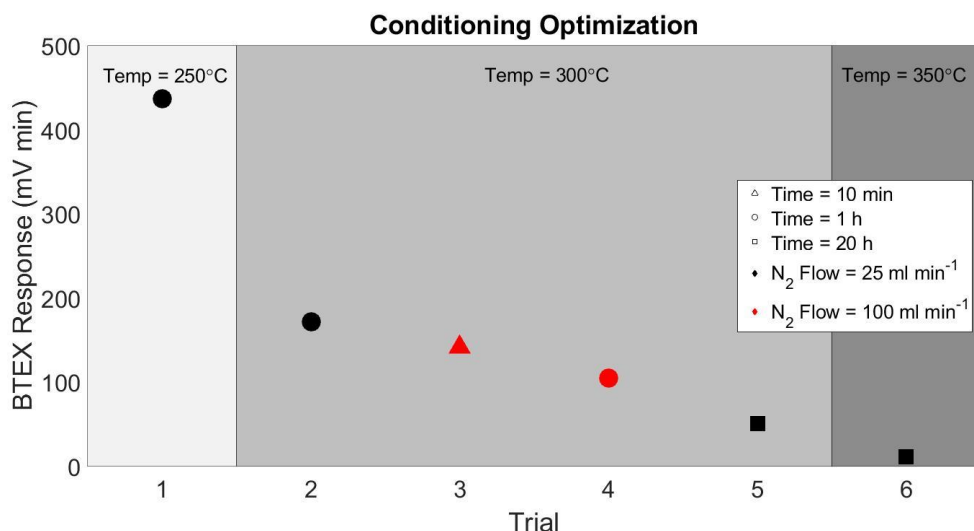
Figure 4. Total BTEX peak area from three cartridges conditioned under different conditions for Carboxen 1000 adsorbent Symbol shape indicates conditioning time, symbol color indicates nitrogen flow through the cartridge during conditioning, and region of the graph indicates conditioning temperature.

4.3 Adsorbent Bed Mass

Thermal cycling and breakdown of the carbon-based Carboxen adsorbent material has been noted as one source for contaminant peaks [*Cao and Hewitt*, 1994; *Helmig*, 1996]. Therefore, it appeared likely that the adsorbent bed mass in a cartridge scales with the cartridge's blank signal. Experiments were performed to investigate if reduction of the adsorbent bed mass would result in lowered blanks, while still providing sufficient trapping efficacy. Carboxen 1000 cartridges were prepared with adsorbent bed masses of 27, 54, 135, 270, and 540 mg. Three cartridges of each adsorbent bed mass were conditioned at 350°C for 20 h with a nitrogen purge flow rate of 25 mL min^{-1} and analyzed Blank peak areas of benzene clearly showed that the benzene blank increased with the mass of the cartridge's adsorbent bed (Table 7); blank levels in the cartridge loaded with 27 mg of adsorbent were ~ 25% of 540 mg cartridge blanks.

Next, active sampling was employed to test if the cartridges with reduced Carboxen 1000 adsorbent bed masses were capable of adsorbing as much sample as the fully loaded tubes   Three cartridges of each mass were loaded for 10 min at a flow of 200 mL min^{-1}, with the *n*-alkane/BTEX standard gas mixture listed in Table ST1. One tube of each mass was reserved as a blank.

Table 7. Benzene peak area (mean of three runs) versus mass of Carboxen 1000 adsorbent bed.

Adsorbent Mass (mg)	% of Full Cartridge	Benzene Peak Area (mV min)
27	5	3.6
54	10	5.3
135	25	6.7
270	50	9.6
540	100	16

Figure 5 shows peak areas for the collection of selected compounds from cartridges containing 27 mg, 135 mg, 270 mg, and 540 mg of adsorbent. All *n*-alkanes, except ethane, have RSDs of less than 2% across all adsorbent bed masses (Table ST4). Toluene and ethylbenzene display variation of a similar magnitude. The RSDs of benzene and all xylene isomers were 6% and ~4%. While the reduced adsorbent bed lowered blank signals (Table 7), they did not noticeably sacrifice the trapping efficiency. Therefore, the lower adsorbent mass cartridges will have improved the signal to noise ratio, and lower detection limits. Furthermore, reducing the adsorbent bed mass from 540 mg to 27 mg reduces the cost for the adsorbent material per cartridge by ~$20.

The minimum benzene peak area that we were able to achieve in the blanks (3.6 mV min) was comparable to 4% of the signal from an actively loaded 2 L 1 ppb VOC/BTEX standard (Figure 5, Table ST4), which is equivalent to the mass of benzene that would be loaded at a mixing ratio of 0.018 ppbv over three days of passive sampling at a temperature of 20°C at an diffusive uptake rate of 2.7 ng ppm^{-1}min^{-1}, (see below).
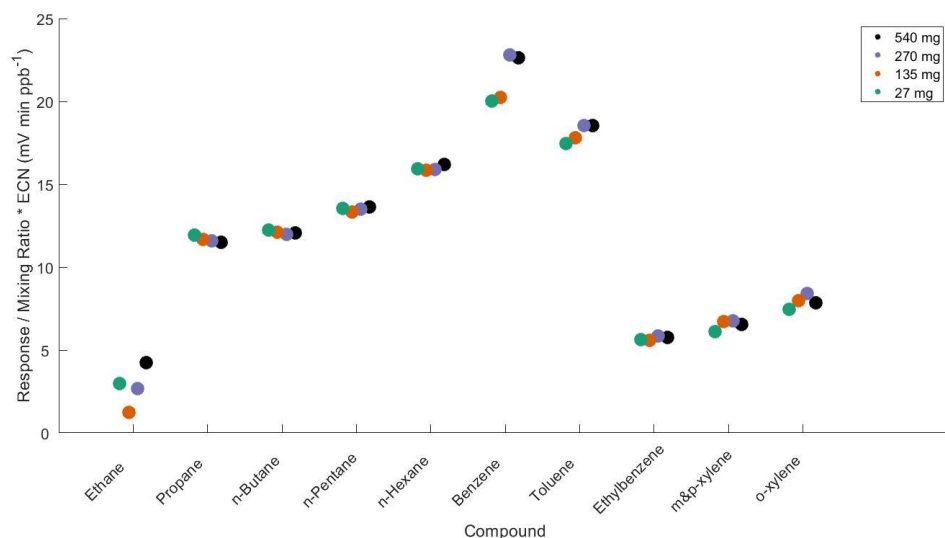
Figure 5. Sampling performance of cartridges with increasing masses of Carboxen 1000. All cartridges were actively loaded by pulling identical quantities of a multi-component VOC standard through the adsorbent bed. Peak areas were normalized by the analyte mixing ratio in the standard (ppbv) and the effective carbon number (ECN).

This experiment was repeated with a 12x higher analyte loading (2 L of a 12 ppbv standard gas mixture, or the theoretical equivalent to the mass captured from diffusively sampling a 1 ppbv atmosphere for ~16.5 days). Similar to the lower concentration standard, the obtained instrument response from the 27 mg cartridge was within 10% of the response of the 540 mg (fully loaded) cartridge (Figure S1) for the C$_{3-6}$ alkanes, benzene, and toluene; the response from the 27 mg cartridge was 20% lower for ethylbenzene and (*m&p*)-xylene and 40% lower for *o*-xylene than the 540 mg cartridge.

132

5. Passive Sampling Experiments

The uptake rate of VOCs over time must be constant for diffusive sampling to yield a truly average value over the sampling interval. This also dictates that the sampling ends before the adsorbent bed become saturated. An artificial, constant concentration atmosphere was created to test diffusive sampling to conditions. Cartridges were placed in a 20 L PTFE-bag that was purged continuously with a stream of VOC standard that included light *n*-alkanes, alkenes, and BTEX compounds (Table ST1). The VOC standard was diluted dynamically with zero air. Both the standard and zero air flows were controlled by mass flow controllers (MFCs). Experiments were performed in both dry and humidified test atmospheres. The relative humidity in the dry experiment was $4.6 \pm 0.7\%$ RH (temperature = $19.6 \pm 0.9°C$). An RH of $96.5 \pm 4.0\%$ (temperature = $20.2 \pm 1.1°C$) was maintained during the humidified experiment by flowing zero air flow through a Nafion membrane submerged in a small reservoir of water [*Boylan et al.*, 2014]. A small fan circulated air inside the bag. The bag was flushed at a rate of 200 mL min^{-1} for at least 12 h before placing the cartridges inside the bag. Cartridges loaded with 27 mg, 54 mg, 135 mg, 270 mg, and 540 mg of Carboxen 1000 adsorbent were tested. An extra 540 mg cartridge was placed inside the bag with storage caps on throughout the experiment as a reference blank. A cartridge of each unique mass of adsorbent was removed after 0.5, 1, 2, 3, 5 and 7 days. Upon removal from the bag, cartridges were capped and stored at -10°C until analysis. Temperature and moisture inside the bag were recorded for the duration of the experiment. Ambient pressure data were obtained from the nearby Boulder Municipal Airport. Uptake rates (URs) were calculated as differences between two sampling time points using the formula

$$UR = \frac{\Delta m}{c * \Delta t} \quad ,$$

where Δm is the difference in the analyte mass found on the cartridges between two sampling

points, Δt is the corresponding sampling interval, and c is the analyte concentration in the bag.

URs were calculated for each compound, and adsorbent bed mass, and for each segment of the

sampling period using results from cartridges removed consecutively. Occasionally, this resulted

in a negative uptake rate. We do not believe that compounds were desorbing during the sampling

period; rather these results stem from the precision error of the successive determinations.

5.1 Uptake in Dry Air

In the dry test atmosphere, propane, butane, pentane, hexane, benzene, and toluene showed a

steady increase in VOC mass loading throughout the seven-day period for all adsorbent bed

masses (Figure 6). Correlation coefficients (R^2) for the linear regression analysis of the collected

analyte mass versus the sampling time range from 0.993 to 0.999. Uptake behavior was similar

across all adsorbent bed masses, supporting the finding of the actively loaded experiment that

lower mass adsorbent cartridges were sufficient for achieving quantitative sampling. Ethane

uptake was nonlinear throughout the sampling, except for cartridges loaded with 540 mg of

adsorbent. The uptake rates of the heavier aromatic compounds, ethylbenzene and all xylene

isomers, slowed towards the end of the sampling period for all masses of adsorbent. Cartridges

loaded with 540 mg of adsorbent showed more variable uptake rates for ethylbenzene and (*m&*

p)-xylene.
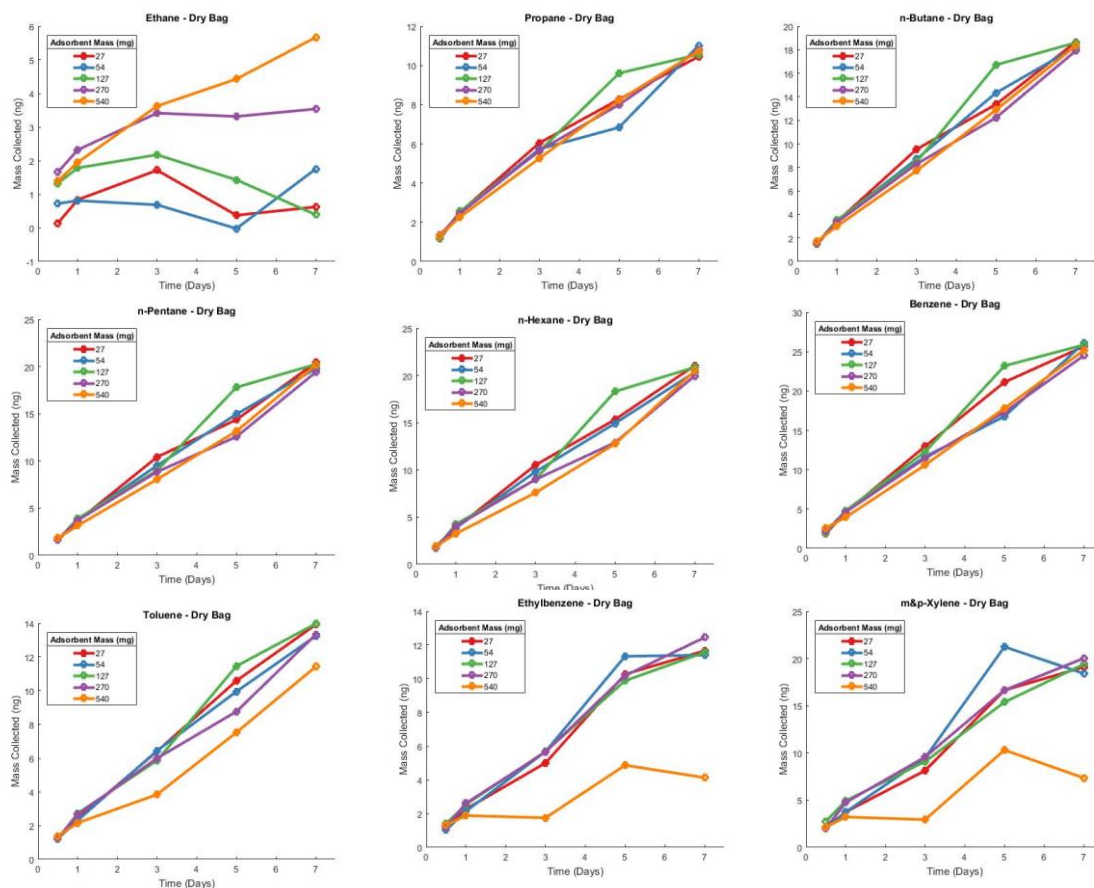
Figure 6. Mass of analytes collected from a dry test atmosphere on cartridges with increasing amounts of adsorbent over 7 days. Multiple cartridges of each adsorbent bed mass were placed in the bag at the beginning of the experiment. One cartridge of each adsorbent bed mass was removed after 0.5, 1, 3, 5, and 7 days and analyzed.

5.2 Uptake in Humidified Air

The uptake experiment was repeated with the standard mixture humidified to 95% RH. The humidity compromised the uptake of all compounds (Figure 7). Sampling of propane and ethane was nonlinear and near the limit of detection. For the larger *n*-alkanes and BTEX compounds, masses collected were 30-80% lower than in the dry test atmosphere. For *n*-butane, only 12% of the mass collected in the dry test atmosphere was collected. Recoveries of toluene, ethylbenzene, and the xylenes were less than 40%. Benzene uptake was the least affected by the

humidity with 80% recovery. Uptake was most linear for the BTEX compounds in cartridges

loaded with 135 and 270 mg of adsorbent.
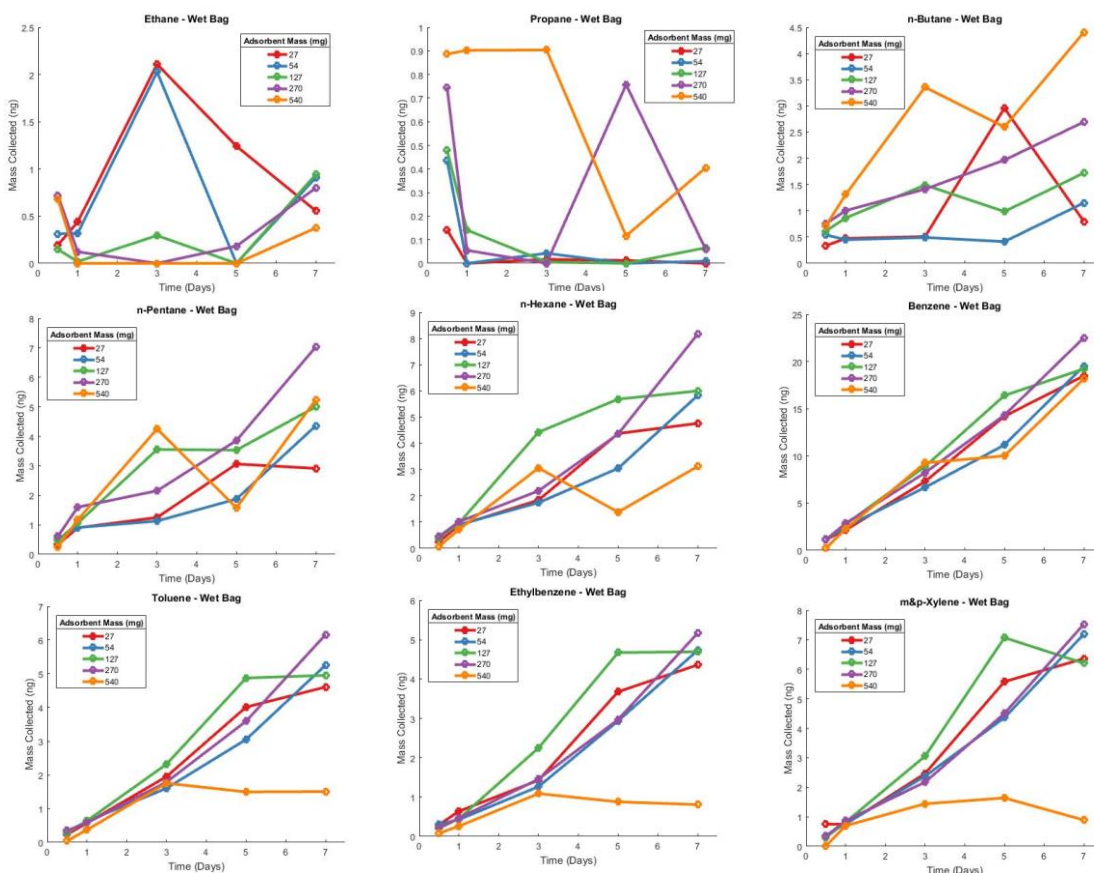
Figure 7. Mass of VOCs collected on cartridges from a humidified test atmosphere on adsorbent beds of varying masses over 7 days. Note that the y-axis scales are smaller in these graphs than in Figure 6.

5.2.1 Water Uptake

To investigate causes of the reduced VOC update rates and water uptake to the adsorbent

in the humidified air, 200 mL min^{-1} of humidified air with levels of < 5, 27, 57, 75 and 92% RH

were actively pumped through the cartridges with adsorbent beds of 540, 135, and 27 mg of

Carboxen 1000. The cartridges were weighed at increasing intervals to determine the mass of

water that had been collected. Sampling was halted after cartridges did no longer show a weight

gain. A cartridge with no adsorbent bed was weighed alongside loaded cartridges to correct for

drifts of the balance. The volumes of air pumped and masses of H_2O loaded are shown in Table 8.

Table 8. Summary of H_2O loading experiment. A 200 mL min-1 stream of zero air humidified to different RH % were sampled over three different adsorbent bed masses until the weight gain leveled off. The volume of humidified air and the mass of H_2O loaded are shown for each adsorbent bed mass and RH %.

| H₂O Loading | | | | | | | | |
| 540 mg Carboxen 1000 | | | 135 mg Carboxen 1000 | | | 27 mg Carboxen 1000 | | |
RH (%)	Sampled volume (mL)	Mass of H_2O taken up (g)	RH (%)	Sampled volume (mL)	Mass of H_2O taken up (g)	RH (%)	Sampled volume (mL)	Mass of H_2O taken up (g)
5	100	0.0002	5	100	0.0001	5	100	0.0008
25	500	0.0021	25	500	0.0002	25	500	0.0006
57	2400	0.0042	57	300	0.0009	57	1200	0.0008
75	47200	0.12	75	18200	0.030	75	11200	0.017
92	29000	0.12	92	8200	0.030	92	6200	0.018

Figure 8 clearly illustrates that water uptake was not linear, but increased steeply at higher humidity. Water uptake was minimal for all cartridges at RH ≤ 57%, but increased by a factor of 20 at RH > 75%. The amount of water collected on the adsorbent was 0.01 g (water) g^{-1} (adsorbent) for the 135 mg and 540 mg cartridges, and 0.04 g g^{-1} for the 27 mg cartridge at the lower %RH levels (< 57%). In the moister test atmospheres the water uptake was significantly higher, up to a rate of 0.63 g g^{-1} for the 27 mg cartridge. Similar non-linear water uptake dependencies on carbon-based adsorbents have previously been reported by Helmig and Vierling [1995]. Their study showed that the adsorbents Carboxen 569 and Carbosieve SIII collected < 20 mg H_2O g^{-1} at RH ≤ 40%, but 60 - 400 mg H_2O g^{-1} at RH ≥ 60% and temperatures ≥ 20°C. Our results add to this previous literature, demonstrating that stronger adsorbents tend to be more hydrophilic, which increases their affinity to collection of atmospheric water vapor. This in turn reduces their capacity for uptake of VOCs, and limits the collection efficiency, precision, and applicability of these type of adsorbents in humid and variable humidity environments .

In real world applications, adsorbent cartridges will be exposed to a variable RH conditions as atmospheric moisture fluctuates throughout as well as from day to day. For example, the frequency distribution of ambient relative humidity for a site near Boulder over a 15 year period (Figure S3) shows that RH was ≤ 57% in 72% of measurements, and only 14% of the time RH was >75% RH. Consequently, the interference and potential reduction in the passive sampling rate will fluctuate with the change in humidity conditions.
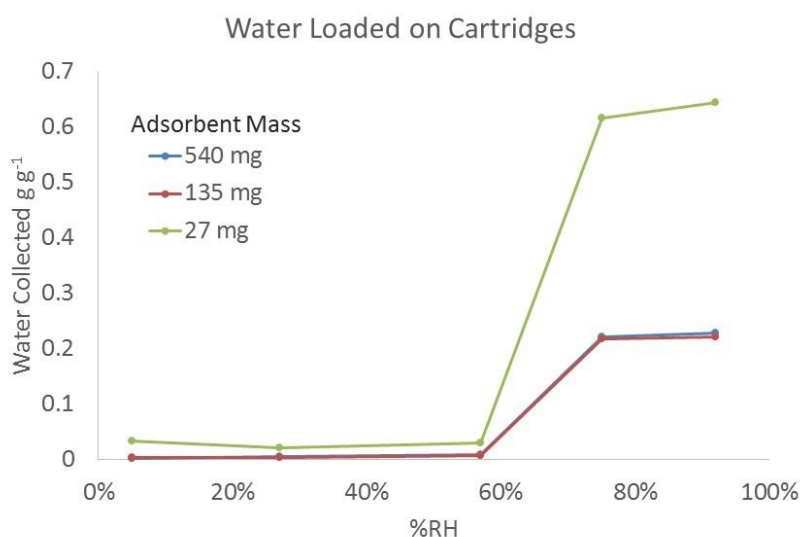
Figure 8. Normalized water uptake on cartridges with varying masses of Carboxen 1000 adsorbent as a function of relative humidity after up to 49 L of humidified zero air was pumped through the cartridges. H_2O loading was stopped when the mass loaded stopped increasing.

When considering the effect of factors influenced by diurnal cycles, two competing processes are relevant to the collection of VOC by the cartridges. In areas near emission sources, VOC concentrations are typically higher at night due to shallow boundary layer heights and weaker convective mixing. For instance, at a site near O&NG operations near Platteville, CO, most of the highest benzene occurrences were at night, and nighttime mean median ratios were approximately three times higher than during the day [*Halliday et al., 2016*]. However, generally lower nighttime temperatures cause the RH to be higher at night. It is unclear what effect these

processes have on cartridge sampling because higher nighttime mixing ratios of VOCs should increase the collection of these compounds by the cartridges, but increased RH should decrease the collection efficiency of the cartridges. An open question is the real world effectiveness of this sampling strategy as mixing ratio and RH conditions vary back and forth. Our experiments demonstrated that uptake rates typically drop under higher RH conditions; but these findings to not (yet) answer the question if and to what degree URs rebound under subsequent lower RH conditions.

5.3 Uptake Rates

URs are valuable metrics that have been used to calculate mixing ratios of VOCs in the atmosphere during passive adsorbent sampling using [*Perkin-Elmer*, 1991] based on solely theoretical considerations, without need for a calibration setup as used in our study:

$$\text{Concentration (mg m}^{-3}) = \frac{Mass\ of\ compound\ on\ tube}{UR * Sampling\ time}$$

Figures 9a and 9b show all calculated UR, organized by the mass of adsorbent in the cartridge in ng ppm^{-1} min^{-1}. Median URs (excluding ethane) in the dry test atmosphere were 1.4-5.1 times higher than in the humidified test atmosphere. UR of benzene were least affected by humidity, propane UR were most affected, and in general, URs of alkanes decreased more in the humidified test atmosphere than URs of aromatics. Table 9 shows that under both dry and humid conditions, the RSDs of URs from segments of a week of sampling are highly variable despite standard concentration and flow, temperature, and humidity conditions held constant.

RSDS of URs in the dry test atmosphere ranged from 66-144%, and from 93–364% in the

humidified test atmosphere.

Table 9. Median uptake rates (n= 30) of cartridges loaded with 27, 54, 135, 270, and 540 mg of Carboxen 1000 adsorbent in dry and humidified simulated environments over the course of 0.5–7 days.

Alkanes				Aromatics			
Compound	RH (%)	Median UR (ng ppm^{-1} min^{-1})	Rel. Std. Dev. (%)	Compound	RH (%)	Median UR (ng ppm^{-1} min^{-1})	Rel. Std. Dev. (%)
Ethane	5	0.16	651	Benzene	5	2.71	93
	95	0.45	104		95	1.95	132
Propane	5	1.09	114	Toluene	5	2.41	66
	95	0.21	364		95	0.76	158
n-Butane	5	2.38	84	Ethylbenzene	5	1.76	144
	95	0.49	141		95	0.51	140
n-Pentane	5	2.57	87	m&p-Xylene	5	1.62	111
	95	0.99	93		95	0.57	117
n-Hexane	5	2.63	87	o-Xylene	5	1.74	112
	95	0.74	147		95	0.47	209

Despite the potential for environmental conditions to affect URs (commonly converted

and reported in units of mL min to eliminate a mixing ratio dependency and reflect an equivalent

sample volume flow rate) [*Brown*, 2000; *Koutrakis et al.*, 1993; *Seethapathy et al.*, 2008], both

experimentally and theoretically derived URs from available literature are relatively consistent

for the BTEX compounds (Table 10). One similarity between these studies URs represent an

average value over the sampling period. Importantly, these studies all build on the same type of

adsorbent cartridge, i.e. the Perkin-Elmer type cartridges, which have a groove 1.5 cm from the

front opening that the metal gauze is pushed against, which fixes the diffusion path length to a

consistent distance.

Table 10. Comparison of passive sampling uptake rates (in units of mL min^{-1}) for BTEX compounds reported in the literature and results from this study. An 'x' in the diffusion cap (Diff. cap) column indicates a diffusion cap was used.

Study	Adsorbent Material	Cartridge Type	Diff. cap	Sampling Duration	Relative Humidity (%)	Temp (°C)	Benzene	Toluene	Ethylbenzene	m&p-Xylene	o-Xylene
						Uptake Rates (ml min^{-1})					
Jia et al. 2017 (Ideal)							0.73	0.65	0.60	0.60	0.60
Mowrer et al. 1996	Tenax-TA	Perkin-Elmer	x	7 d	N/A	-5 - 5	0.41	0.45	0.55	0.55	0.55
Markes International	Tenax-TA	Markes International		8 h	N/A	N/A	0.41	0.44	0.46	0.42	0.42
Walgraeve et al. 2011	Tenax-TA	Markes International	x	7 d	5 - 80	18 - 24	0.27	0.32	0.35	0.36	0.34
Civan et al. 2012	Chromosorb 106	Gradko International		12 h	50 - 86	-1 - 20	0.39	0.44	0.39	0.40	0.35
Martin et al. 2010	Tenax-TA	Perkin-Elmer	x	14 d	0	20	0.57	0.53			0.52
Martin et al. 2010	Tenax-TA	Perkin-Elmer	x	14 d	80	20	0.54	0.48			0.47
Roche et al. 1999	Tenax-TA	Perkin-Elmer	x	0.5 - 24 h	5 - 10	25	0.57	0.51	0.45	0.43	0.43
Hellen et al. 2002	Carbopack-B	Perkin-Elmer		14 d	N/A	-8 - 20	0.68	0.62	0.55	0.55	0.53
ISO/DIS 16017-2	Tenax-TA	Perkin-Elmer		8 h			0.63	0.56	0.50	0.47	0.47
Oury et al. 2006	Tenax-TA	Perkin-Elmer		1 d	50	20	0.40	0.45		0.45	
Oury et al. 2006	Tenax-TA	Perkin-Elmer		3 d	50	20	0.32	0.40		0.43	
Oury et al. 2006	Tenax-TA	Perkin-Elmer		6 d	50	20	0.27	0.37		0.42	
Oury et al. 2006	Tenax-TA	Perkin-Elmer		14 d	50	20	0.20	0.30		0.37	
Tolnai et al. 2001	Carbopack-B and Tenax-TA	Perkin-Elmer		7 d	n/a	-16	0.57 to 0.61	0.42 to 0.47	0.51 to 0.54	0.41 to 0.58	0.41 to 0.48
						Mean	0.46	0.47	0.48	0.45	0.47
						Rel. Std. Dev. (%)	36	22	18	17	18
This Study	Carboxen 1000	Perkin-Elmer		0.5 - 7 d	5	23	1.02	0.77	0.49	0.45	0.48
This Study	Carboxen 1000	Perkin-Elmer		0.5 - 7 d	95	23	0.73	0.24	0.14	0.16	0.13

[*Civan et al.*, 2012; *Hellen et al.*, 2002; *Jia and Fu*, 2017; *Martin et al.*, 2010; *Mowrer et al.*, 1996; *Oury et al.*, 2006; *Roche et al.*, 1999; *Tolnai et al.*, 2001; *Walgraeve et al.*, 2011]

Our data included in Table 10 are the median URs from adsorbent bed masses of 27, 54, 135, 270, and 540 mg, as there was relatively good agreement seen in both the active and passive standard loading experiments among those cartridges (Figures 5-7), with results being differentiated for the dry and humidified test atmospheres. Despite the relatively high RSDs, the

median UR results from our sampling compare reasonably well with URs in other studies. Notably, the agreement is better for the low RH experiments, where our URs are within 10% of the median literature data for the C_2-aromatics, and within a factor of two for benzene and toluene.
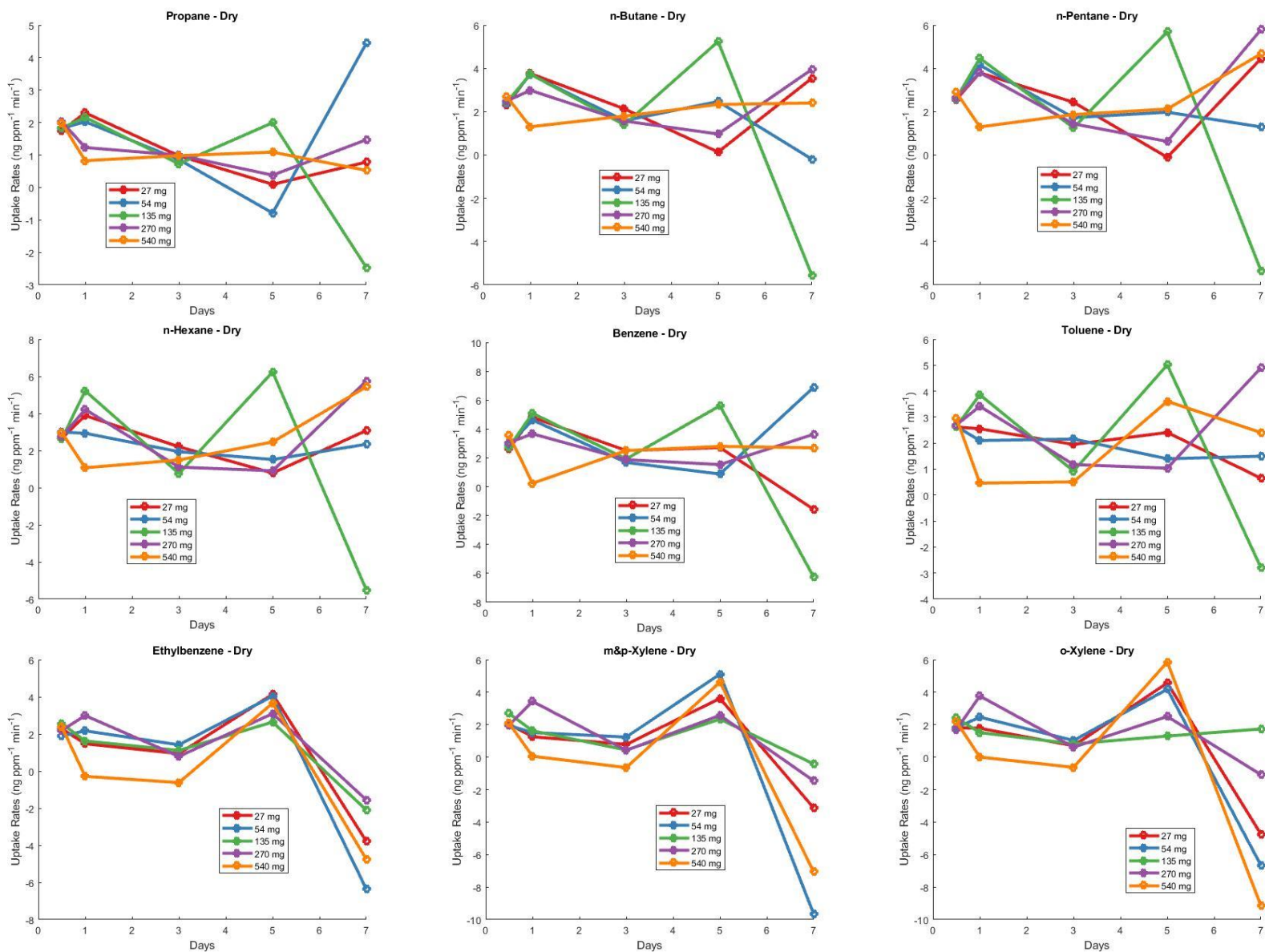
Figure 9a. UR for n-alkanes and aromatics for the simulated dry environment. UR were calculated for each interval of sampling and plotted at the time of the end of the interval. For example, the UR at day 3 is the UR from day 1 to day 3.
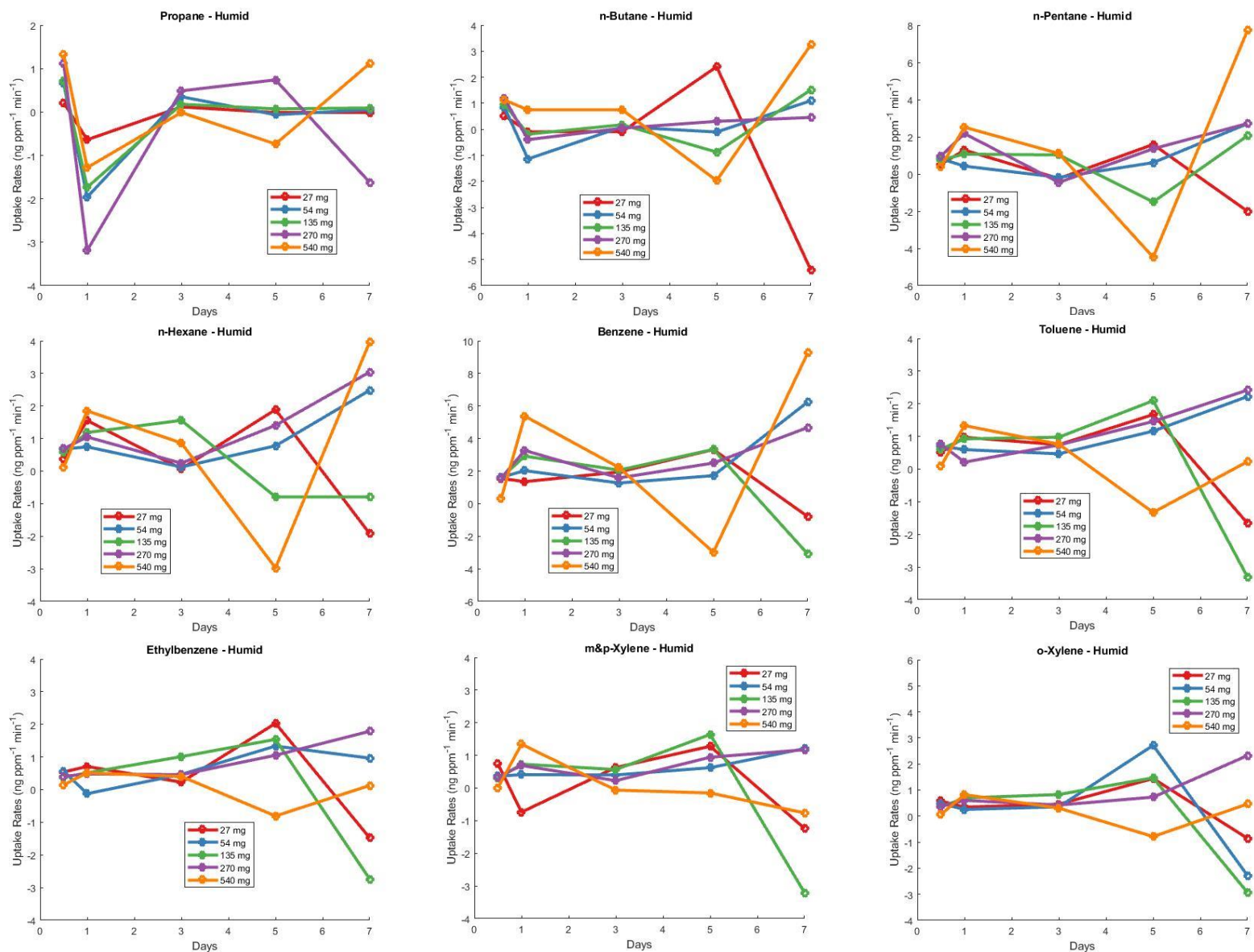
Figure 9b. Same as Figure 9a, but with URs for n-alkanes and aromatics in humid air (95% RH).

144

6. Field Results using the Optimized Cartridges

Cartridges were again deployed alongside canisters in October and November 2016 on the roof of the SEEC building on the University of Colorado Boulder's East Campus. This site is ~100 m from Foothills Parkway, a major thoroughfare for commuters moving north or south through Boulder. Cartridges and canisters were deployed for 3 day periods on 10 occasions. The deployed cartridges contained 27 mg of Carboxen 1000 adsorbent, and were conditioned for 20 hours at 350°C with 25 mL min^{-1} N$_2$ flow. Linear correlation results for cartridge with canister data comparisons (PCCs, and p-values; median RSDs, and median RSDRs) are summarized in Table 11, and PCCs are visualized in Figure 10. An assessment of agreement between canister and cartridge sampling in all field campaigns is in section 6.1.

In Figure 10, results from the 2016 campaign are placed side by side with the earlier (2014) field study. Relatively poor cartridge-canister correlations of ethane and alkenes across all sampling periods were found. Significantly better results, with PCC > 0.75 were obtained for the primary O&NG emission tracer compounds, i.e. propane, *n*-butane, *i*-pentane, *n*-pentane in all three field campaigns. PCCs improved in the 2016 campaign for ethane, propane, and *n*-butane. PCCs in the 2016 campaign were within 0.1 units of the 2014 campaigns for *i*-butane, *i*-pentane, and *n*-pentane. Ambient mixing ratios during the 2016 campaign were lower than the 2014 campaigns (Figure 11), which indicates that the cartridges used in 2016 performed similarly to the 2014 campaign despite the lower mixing ratios in most of the samples, which overall most likely represents an improvement of the method.

Table 11. Canister and cartridge Pearson correlation coefficients and p-values during the 2016 campaign. Canister and cartridge median relative standard deviations (RSDs), and median relative standard deviation ratios (RSDRs) of the cartridge RSD/canister RSD.

	2016

Compound	Pearson Correlation	P-Value	Canister RSD	Cartridge RSD	RSDR
Ethane	0.68	0.015	0.031	0.08	4.1
Propane	0.97	0.000	0.024	0.12	8.8
Propene	-0.67	0.018	0.50	0.14	0.39
i-Butane	0.56	0.058	0.11	0.12	1.4
n-Butane	0.96	0.000	0.011	0.097	8.3
i-Pentane	0.86	0.000	0.018	0.16	8.7
n-Pentane	0.79	0.002	0.03	0.22	7.7
n-Hexane	0.12	0.71	0.046	0.32	6.9
Benzene	-0.38	0.25	0.060	0.37	5.3
Toluene	0.79	0.011	0.040	0.34	6.2
o-Xylene	-0.73	0.025	0.11	0.88	6.2

6.1 Assessment of field sampling performance
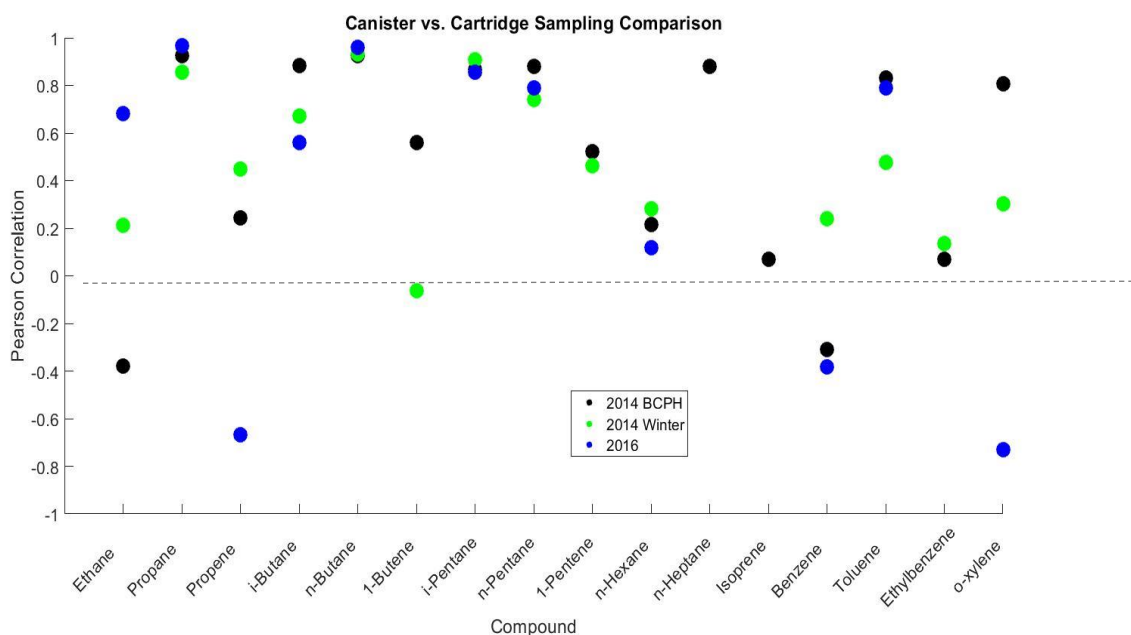
Figure 10. Pearson Correlation of canister and cartridge data during the 2014 BCPH field campaign (Carboxen 1016/1000), the winter 2014 comparison study (Carboxen 1016/1000), and the 2016 comparison study (Carboxen 1000). Data for some compounds are not available for each campaign. P-Values and RSDRs are available in Table 1 and 12.

Determining the absolute accuracy of the cartridge samplers is difficult due to the nature

of the sample collection. Because cartridge sampling is not a whole air sampling method,

converting the response of the analytical system to mixing ratios of target compounds cannot be

done as it is done for canister samples. Uptake rates have been used to convert instrument response to mixing rates. However, the demonstrated variability in uptake rates dissuades us from using this method. Ideally, cartridges would be deployed in an environment with where mixing ratios of target compounds are known, consistent for 3 day periods, and can be manipulated to develop a calibration curve that allows the response of the cartridge analytical system to be converted to mixing ratios. While it would be possible to conduct this type of experiment using the simulated environment discussed in section 5, this experiment has not yet been conducted, and would have differences from real deployments such as a lack of diurnal temperature, RH, and mixing ratio variation.

In lieu of such an experiment, we developed a first order assessment of the agreement of cartridge and canister sampling by finding the linear regression of cartridge versus canister samples from all field campaigns, and determining the relative distance of the cartridge samples from the expected linear regression response. This assessment assumes the canister samples are the "gold standard" and that linear agreement of cartridge samples with canister samples indicates the validity of the cartridge sampling method. The linear regressions used to determine the relative residuals are shown in Figure 11. Data points in Figure 11 are colored according to the ambient temperature range at the time of sampling. A confounding factor that cannot be addressed within this dataset is the higher mixing ratios that were observed during the summer 2014 campaign (median mixing ratios during each campaign are available in Table ST3). Further experiments should be conducted to disentangle the effects of temperature and magnitude of ambient mixing ratios on sampling performance.
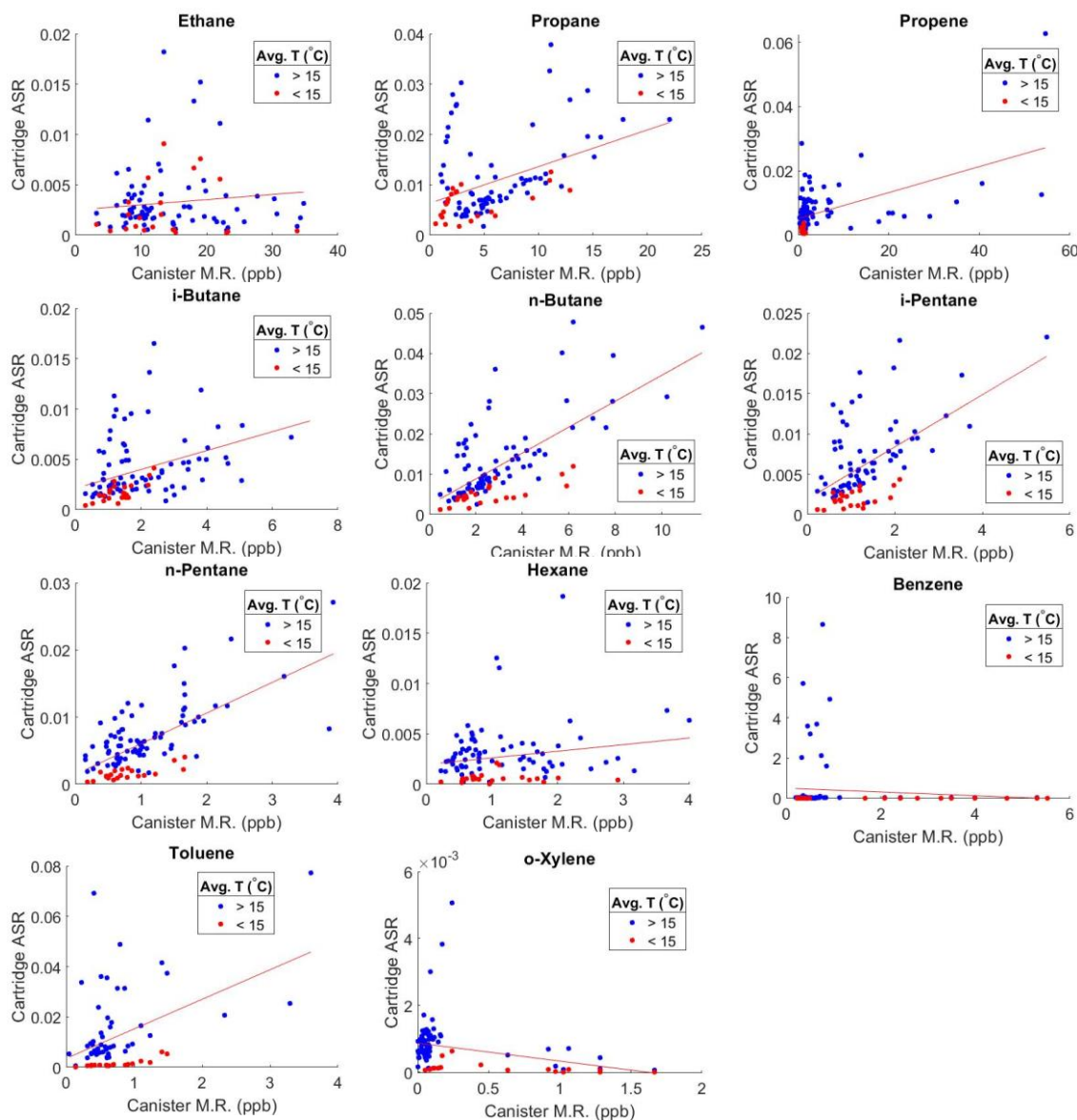
Figure 11. Linear regressions of cartridge ASR versus canister mixing ratios. Blue points indicate the average temperature during sampling was > 15 °C, red points were < 15 °C.

Relative residuals were found by finding the vertical distance of each canister sample analytical system response from the expected linear regression response. This value was divided by the linear regression response to find a relative residual. The relative residuals were assigned to bins with widths of 0.1. These data are available in Figure 12.
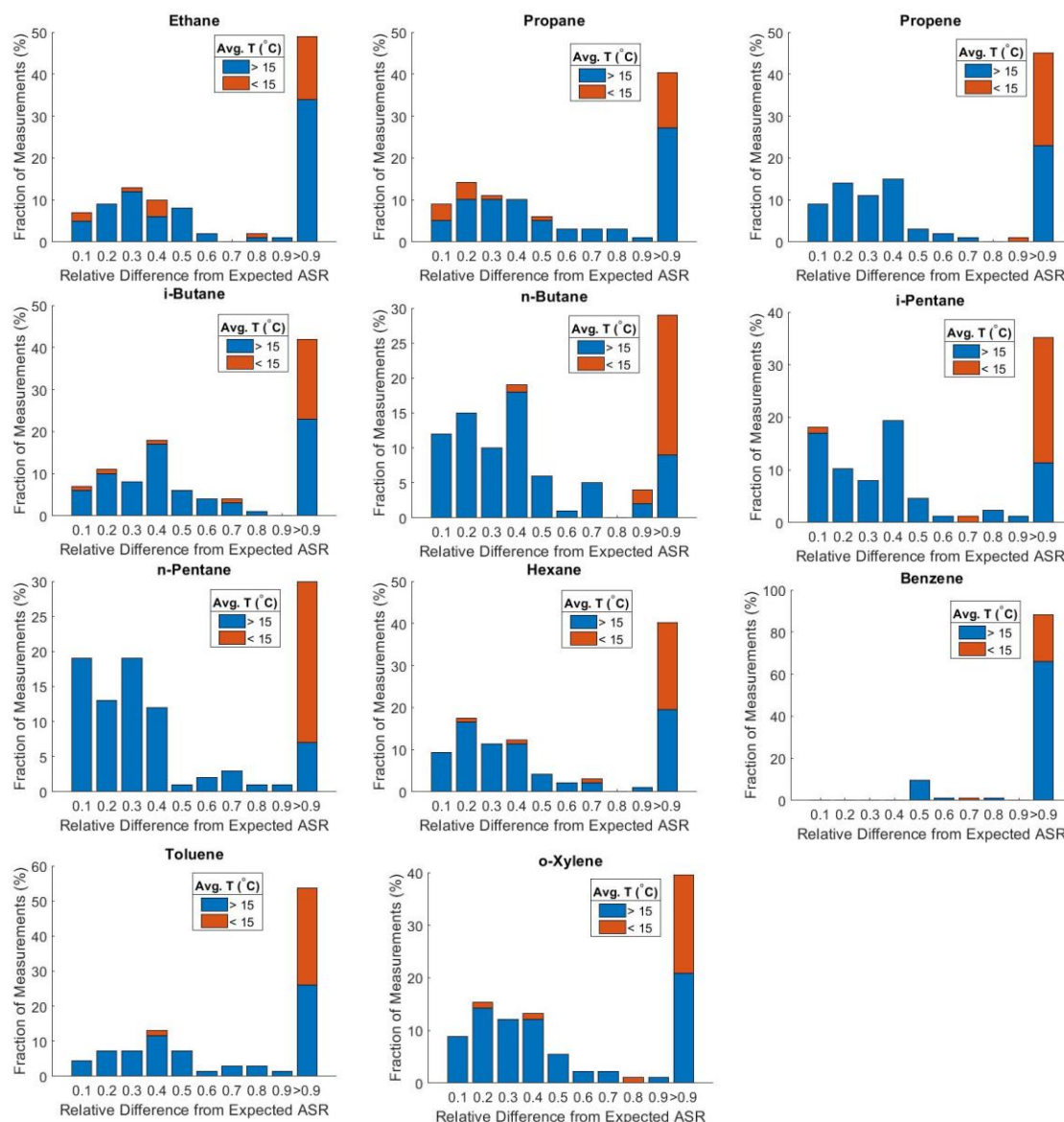
Figure 12. Stacked histograms of the fraction of measurements within a relative difference from the expected linear regression response (given by the x-axis). Values on the x-axis state the upper end of the bin's range (i.e. 0.2 displays the fraction of measurements < 0.2, but > 0.1. The >1 bin includes all values greater than 0.9)

We use the relative distance of cartridge ASRs from expected response determined using linear regression analysis to assess the agreement of cartridge samples with canister samples. Figure 12 uses stacked histograms to show the fraction of cartridge measurements within relative distance bins of width 0.1. For all compounds, the > 0.9 bin contains the largest fraction of data

points. This indicates that the distance of the largest fraction of cartridge ASR from the linear regression response is greater than the magnitude of the linear regression response. This suggests that cartridge measurements are variable with respect to the canister measurements, and are not yet a viable sampling technique. However, the results for n-butane, i-pentane, and n-pentane indicate that further optimization of this sampling technique could result in representative sampling. For these compounds, 27-33% of measurements are within 20% of the linear regression response. Further, less than 20% of measurements collected at average temperatures > 15 °C are greater than 90% different than the linear regression response. Again, mixing ratios were higher during the warmer weather sampling period. Regardless of the factor that contributes to improved agreement with the gold standard, these data indicate that continued investigation of this sampling technique could result in representative sampling.

The repeatability error (RSD) of the canister methods from the paired sampling (Table 1, Table 2) was <11% for all compounds, except propene, in both deployments. RSDs of the cartridges analyses are generally larger, but cartridge RSDs for C_3-C_6 alkanes in the winter 2014 campaign were all <10%. C_3-C_6 alkane RSDs from cartridge samples in the 2016 campaign were in many cases twice what they were in 2014, but the relative standard deviation ratio (RSDR) for cartridge results/canister results is lower for many compounds in 2016, indicating a relative improvement in the cartridges sampling. This also suggests that the larger RSDs observed in 2016 is likely due to lower mixing ratios or variable conditions during that campaign, rather than inconsistent sampling. Importantly, average VOCs mixing ratios during the 2014 field campaigns were 4 times higher than the 2016 campaign (Table ST5). An analysis of the dependency of RSD on absolute mixing ratio (Figure 13) shows that for propane RSDs drop below 10% at mixing ratios > 4 ppbv. RSDs for propane, *i*-butane, *n*-butane, *i*-pentane, and *n*-

pentane are below 20% at mixing ratios > 2 ppbv. The repeatability of the benzene

determination is difficult to evaluate given the much different range of ambient levels observed

in these deployments. RSDs for the toluene determination drop to <50% at levels > 0.5 ppbv.

These analyses demonstrate that for n-alkanes and BTEX compounds the cartridge

method RSDs drop with increasing missing ratios. RSDs also vary by compound. Depending on

the VOC, under conditions encountered in our studies RSD's <25% could be achieved at mixing

ratios of > 0.5 – 4 ppb.   This approximately defines the lower limit of mixing ratios where this

passive sampling method is applicable.   This sensitivity would be insufficient for determining

these VOCs in the background atmosphere and most residential and urban settings. An array of

recent studies has found significantly enhanced levels of VOCs, in particular of the light n-

alkanes, in the vicinity and downwind of oil and gas operations. Light alkanes have been

reported at levels 1-2 order of magnitudes higher than in urban air, approaching and at times

exceeding the 100 ppb threshold [*Gilman et al.*, 2013; *Halliday et al.*, 2016; *Helmig. et al.*,

2014b; *Petron et al.*, 2014; *Schade and Roest*, 2015; *Thompson et al.*, 2014]. Consequently, the

sensitivity of this passive cartridge sampling for propane, the butane, and the pentane isomers, is

well sufficient for a semi-quantitative assessment of the exposure levels to these compounds

under those conditions.   BTEX compounds make up a smaller percentage of O&NG emissions.

For most studies, the range of ambient air BTEX VOC mixing ratios reported stretches from 0.1

– 10s of ppb. [*Halliday et al.*, 2016; *Helmig. et al.*, 2014b; *Pétron et al.*, 2012; *Petron et al.*,

2014; *Rappenglueck et al.*, 2014; *Thompson. et al.*, 2014]. While RSDs for BTEX compounds

were somewhat higher, passive sampling is suitable for providing a first assessment of exposure
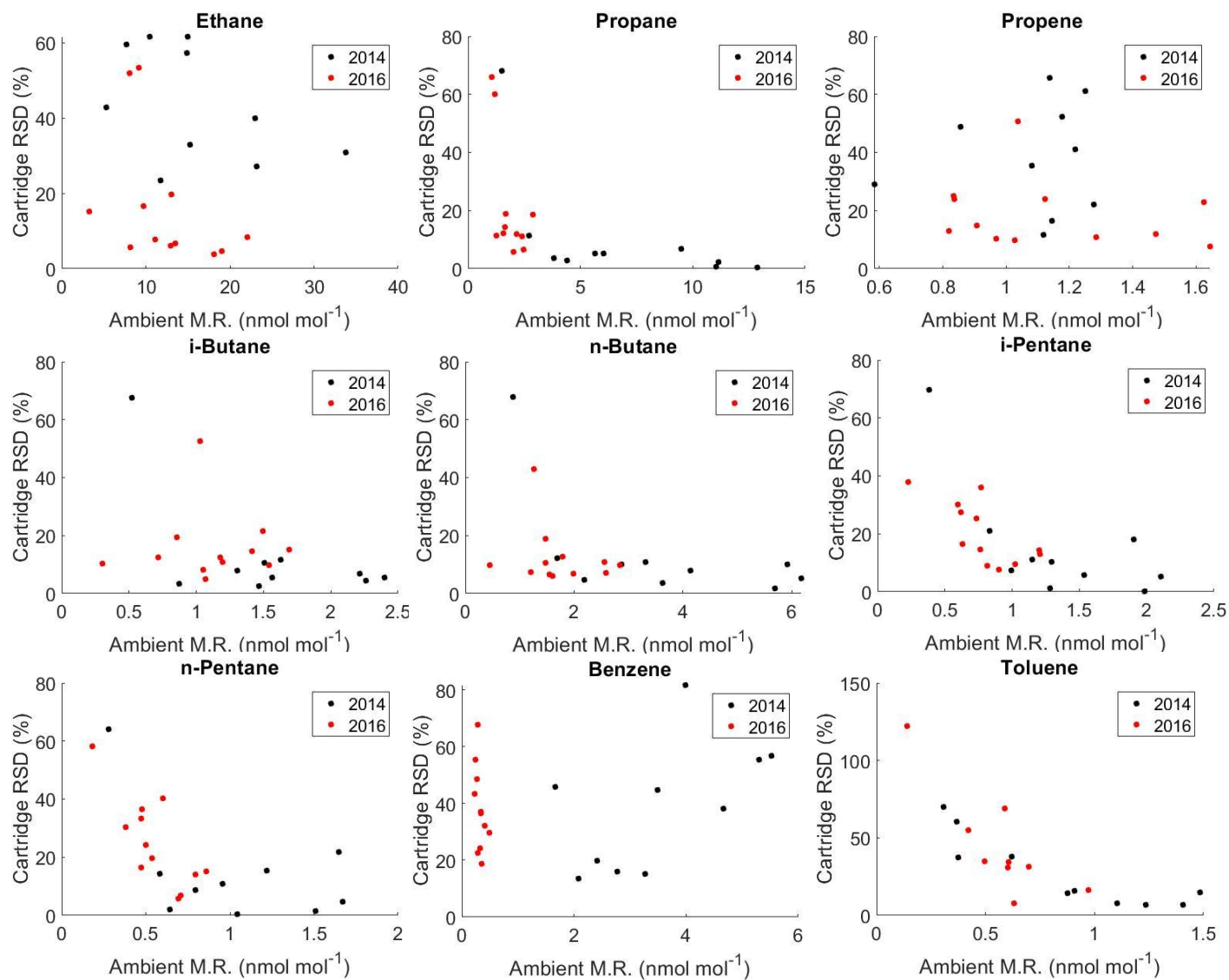
levels for these compounds.

Figure 13. RSDs of paired passive VOC sampling adsorbent cartridges versus ambient mixing ratios (from the canister sampling) during the 2014 and 2016 field deployments. Please note the different sampling strategies deployed during the two campaigns (see text).

152

7. Summary and Conclusions

Carboxen 1000 was found to be the most suitable adsorbent (compared to Tenax-GR, Carboxen 1016, and a combination of Carboxen 1000 and 1016) for passive sampling of C_3-C_5 petrochemical hydrocarbons, yielding highest trapping efficiency, lowest blanks, and the lowest RSDs in experiments conducted in the laboratory. Reducing the blank signals was a key factor in improving the sensitivity of the samplers, and was achieved with more stringent cartridge conditioning procedures, and decreased adsorbent bed masses in each cartridge. Quantitative sampling was achieved via active loading on cartridges loaded with ~5% (27 mg) of adsorbent (compared to possible maximum capacity), without sacrificing sampling performance. With these improvements, linear passive uptake on Carboxen 1000 was observed in a simulated environment with constant 1 ppbv mixing ratios of a standard mixture. This level of performance in the field would be sufficient for assessing both light n-alkane VOC and BTEX exposure from/near O&NG emissions influenced sites.

Laboratory experiments also demonstrated the effect of humidity on the cartridge samplers. Elevated RH reduced VOC URs significantly; median URs of C_3-C_6 alkanes and BTEX compounds in a humidified test atmosphere were, on average, only 27-39% of those in the dry test atmosphere. This dependency infers that VOCs are collected at a slower rate during high RH conditions, such as during wet/rainy weather and at night, when RH typically is higher. However, ambient VOC levels are often higher at night near O&G emissions sources due to suppressed boundary layer mixing. As a result, it is unclear what effect these competing factors may have on passive uptake during a field deployment.

Despite the impact of humidity on uptake, there is a remarkably good agreement in published URs of BTEX compounds across studies that used adsorbent cartridges with the same

physical dimensions. Our average URs observed in the 7 day experiment in simulated

environments for ethylbenzene and the xylenes in the dry air, and benzene in the humidified air

were within the standard deviation of literature values. However, URs calculated for 24-48 hr

periods within the 7 day experiment varied with a RSDs > 66% in a simulated atmosphere with

constant mixing ratios and 5% RH. Further study will be needed to understand the factors

influencing the inconsistency of UR rates observed in the controlled environment

Carboxen 1000 cartridges were deployed alongside sampling canisters during three field

campaigns under ambient conditions. Linear regressions of cartridge ASRs versus canister

measurements for light alkanes and BTEX compounds were used to assess the correlation and

agreement of the two sampling methods. Canister measurements are considered the "gold

standard" in these analyses. Correlations with R^2 >0.70 for propane, *n*-butane, *i*-pentane, and *n*-

pentane were observed. The equations of the linear regressions were assumed to give the

expected cartridge ASR at a given mixing ratio (as measured by the canisters), and were used to

develop relative residuals of cartridge ASRs, which are used here to assess the agreement of the

two sampling methods. The majority of measurements for all compounds had residuals with

magnitudes larger than the expected analytical system response. This suggests that the cartridge

sampling is not a representative sampling technique at the moment, though a few compounds (n-

butane, i-pentane, n-pentane) show some promise, particularly at higher temperatures. Higher

mixing ratios were also present during the warmer field campaign, so the effect of these two

variables on sampling performance cannot be disentangled with this dataset. However, the

precision of ASRs from paired cartridge samples as a function of ambient mixing ratios suggests

this factor influences sampling performance. During field deployments where ambient mixing

ratios were above 1-4 ppbv, C_3-C_5 hydrocarbons were collected with RSDs of 10-20%. This

sensitivity is sufficient for applications in studies that target the assessment of elevated VOC in proximity to O&NG operations. While extensive work remains to optimize and better understand the capabilities and limitations of this sampling technique, passive adsorbent cartridge samplers have demonstrated potential to be a representative sampling technique for assessing exposure to O&NG emissions in a wide range of conditions and applications, and can also be deployed with little preparation time, relatively low cost, and without electrical power.

Acknowledgments

<center>Chapter 6</center>

<center>**Volatile organic compound emissions from soil following wetting events**</center>

Sam Rossabi[1,2], Mallory Choudoir[1], Detlev Helmig[2], Jacques Hueber[2], Noah Fierer[1,3*]

[1]Cooperative Institute for Research in Environmental Sciences, University of Colorado- Boulder, Boulder, CO, 80309, USA
[2]Institute of Arctic and Alpine Research, University of Colorado-Boulder, Boulder, CO, 80303, USA
[3]Department of Ecology and Evolutionary Biology, University of Colorado-Boulder, Boulder, CO 80309

*Corresponding Author: Noah Fierer (noah.fierer@colorado.edu)

Abstract

Dynamics of carbon dioxide (CO_2) emissions following the wetting of dry soil have been widely studied in field and laboratory settings. Non-methane volatile organic compounds (VOCs) are also emitted from soil following a rain event, and are evident from the characteristic smell of wet soil. Few studies have documented VOC emissions before and after soil rewetting. Soil emissions were studied using a dynamic flux chamber system purged with VOC-free air, with identification and quantification of emissions performed by gas chromatography/mass spectrometry. All soils exhibited a rewetting-induced pulse of VOC emissions, with VOC emissions 14 times higher (on average) in the few hours after rewetting compared to moist soils 2 days after rewetting. This VOC rewetting pulse mirrored the CO_2 rewetting pulse (the so-called "Birch Effect") but was shorter in duration. Average VOC emissions were $5.0 \pm 2.0\%$ of CO_2 emissions (molar C equivalent) and increased with increasing soil organic matter content ($\rho=0.40$, $\rho=0.99$ with one soil excluded). The amounts and types of VOCs varied with time since

rewetting and across the five studied soil types, though acetone and small hydrocarbons were the dominant compounds emitted from all soils. Some of the VOCs emitted are likely important mediators of microbial activities and relevant to atmospheric chemical dynamics. Soil VOC emissions, similar to CO_2 emissions, are strongly affected by rewetting events, and it is important to consider these rewetting dynamics when modeling soil and ecosystem VOC emissions and understand their relevance to terrestrial ecosystem functioning and atmospheric processes.

1. Introduction

A rapid increase in microbial CO_2 production is widely observed when a dry soil is rewet [*Birch*, 1958; *Bloem et al.*, 1992; *Cui and Caldwell*, 1997; *Fierer and Schimel*, 2002; *Franzluebbers et al.*, 2000]. This phenomenon, termed the "Birch Effect", has been documented both in the field (e.g. [*Cui and Caldwell*, 1997]) and in the laboratory (e.g. [*Franzluebbers et al.*, 2000]). The magnitude and duration of the Birch Effect varies depending on soil type [*Huxman et al.*, 2004; *Waring and Powers*, 2016], temperature [*Borken et al.*, 2003], and moisture conditions [*Lado-Monserrat et al.*, 2014; *Sponseller*, 2007; *Xiang et al.*, 2008]. The rewetting pulse in microbial CO_2 emissions has been attributed to a rewetting-induced release of labile soil organic carbon pools, rapid catabolism of microbial osmoregulants by intact cells, or microbial cell lysis resulting from osmotic shock [*Adu and Oades*, 1978; *Appel*, 1998; *Bottner*, 1985; *Jenerette and Chatterjee*, 2012; *Lundquist et al.*, 1999; *Moyano et al.*, 2013; *Unger et al.*, 2010; *Vangestel et al.*, 1992]. These rewetting-associated pulses of CO_2 can be important to consider when quantifying and predicting soil CO_2 emissions, particularly in areas subject to frequent drying and rewetting events [*Huxman et al.*, 2004; *Schimel et al.*, 1999]. CO_2 emissions typically

peak within 24– 48 h after a rewetting event, with CO_2 emissions subsequently declining by 50–95% even if soil moisture levels remain elevated [*Schimel et al.*, 2007; *Wang et al.*, 2015; *Waring and Powers*, 2016]. For example, integrated CO_2 emissions following precipitation events in the Sonoran Desert ranged from 2.5–19.3 g carbon-CO_2 (C_{CO2}) m-2 depending on the amount and frequency of the rain. Emissions returned to background rates (0.03–0.13 g C_{CO2} m-2 h-1) 48 hr after the event [*Sponseller*, 2007]. Likewise, in a laboratory-based incubation, soil CO_2 emissions 24 h after rewetting were 3 times higher than emission rates 72 h after the rewetting event, even though soil moisture levels remained elevated [*Fierer and Schimel*, 2003]. CO_2 is not the only gaseous form of carbon (C) emitted by soil microbes, as microbes can also generate a chemically diverse range of volatile organic compounds (VOCs). These soil VOC emissions can have important impacts on soil nutrient cycling, soil microbial activities, and atmospheric chemistry. For example, VOCs mediate bacterial-fungal, bacterial-bacterial, and fungal-fungal interactions in soil, often through effects on quorum sensing and gene expression [*Wheatley*, 2002]. These soil VOCs can also influence the growth, colonization, and metabolic activity of soil microorganisms [*Schmidt et al.*, 2015].

Likewise, VOCs can influence rates of specific microbial processes in soil, including nitrogen (N)-cycling (e.g. nitrification and N mineralization rates) [*Bending and Lincoln*, 2000; *Paavolainen et al.*, 1998; *White*, 1988]. VOCs can also stimulate or inhibit growth of certain microbial species or act as signaling molecules for inter- and intra-species communication [*Baldwin and Preston*, 1999; *Effmert et al.*, 2012; *Falik et al.*, 2011; *Frost et al.*, 2007; *Kai et al.*, 2009; *Pichersky and Gershenzon*, 2002; *Wenke et al.*, 2010]. The ecosystem-level consequences of soil VOC emissions extend beyond microbial processes, as some soil-derived VOCs are

highly reactive compounds that modulate key chemical reactions in the atmosphere, including

ozone and secondary organic aerosol production [*Bowman and Seinfeld*, 1994].

While these low molecular weight organic compounds (typically <250 AMU) can be produced

by abiotic processes, such as hydrolysis, oxidation, and photochemistry [*Bruggemann et al.*,

2017; *Gray et al.*, 2010], microbial processes are likely responsible for the majority of soil VOC

emissions [*Leff and Fierer*, 2008; *Monson and Holland*, 2001]. Compounds that have been

reported in emissions from microbial metabolism include alcohols, aldehydes, alkenes, esters,

hydrocarbons, ketones, and terpenoids, with distinct soils typically emitting distinct VOC

profiles [*Isidorov and Jdanova*, 2002; *Jelen and Wasowicz*, 1998; *Larsen and Frisvad*, 1995; *Leff

and Fierer*, 2008; *Smolander et al.*, 2006; *Stahl and Parkin*, 1996; *Wilkins and Larsen*, 1995].

    Few studies have characterized soil VOC emissions and their dynamics upon rewetting of

soil. There is evidence that certain VOCs, including methanol, acetone, formaldehyde,

acetaldehyde, and terpenes, are released upon soil rewetting [*Asensio et al.*, 2007; *Schade and

Goldstein*, 2001; *Veres et al.*, 2014]. The amounts and types of VOCs emitted from soil can also

vary as a function of soil moisture dynamics, soil temperature, solar irradiance, and carbon

availability [*Asensio et al.*, 2007; *Bachy et al.*, 2018; *Schade and Custer*, 2004; *Waring and

Powers*, 2016]. While plants are generally the main sources of non-methane VOC emissions in

most terrestrial ecosystems [*Fehsenfeld et al.*, 1992; *Fuentes et al.*, 2000; *Penuelas et al.*, 2014],

soil VOC emissions can represent 10–50% of the net forest canopy VOC flux depending on the

ecosystem type and environmental conditions [*Aaltonen et al.*, 2013; *Janson*, 1993; *Schade and

Goldstein*, 2001]. In other words, microbial VOC emissions from soil could be relevant to

atmospheric chemistry given that soil and litter emissions of specific VOCs can be similar in

magnitude those from aboveground vegetation [*Potard et al.*, 2017; *Schade and Goldstein*, 2001].

In this study, we investigated the chemical diversity and temporal dynamics of soil VOCs across distinct soil types following a rewetting event, information that is critical for understanding soil VOC emissions in ecosystems that experience frequent drying-rewetting [*Fierer and Schimel*, 2002; *Leff and Fierer*, 2008]. Specifically, we asked if VOC emissions parallel the burst in CO_2 following rewetting as characterized by the Birch Effect. In addition, we asked if the types of VOCs emitted from soil vary before and after a rewetting event and how these emissions differ across distinct soil types. To address these questions, we designed a laboratory-based soil microcosm experiment to simulate a precipitation event that rapidly increased moisture levels in air-dried soils. We simultaneously measured CO_2 and speciated VOC emissions before and after the rewetting event, tracking these emissions over time to determine if VOC emissions follow the canonical Birch Effect observed for CO2 emissions.

2. Materials and Methods

2.1 Sample Collection and Characterization

Five soils (S1-S5) were collected in early May 2017 from sites across Boulder County, Colorado, USA. Soils were chosen to represent a range of edaphic characteristics, with samples collected from tilled agricultural soils (S1 and S2), a semi-arid grassland (S3), and sub-alpine forest soils (S4 and S5) (Table 1). At each sampling location, the litter layer was removed and surface soil (0–6 cm depth) was collected. Soils were sieved to 2.0 mm and stored field moist at 4˚C for <2 months prior to the start of the experiment.

Field gravimetric water content was determined from sieved soil before and after drying at 80°C for 48 h. Soils were saturated with deionized water and allowed to drain for 1 h to determine maximum water holding capacity (WHC). Physical and chemical soil characteristics (Table 1) were measured at the Colorado State University's Soil, Water, and Plant Testing Laboratory (Fort Collins, CO, USA) using standard methods.

Table 1. Source and physical properties for soils studied. Soils are referred to by their number (i.e. S1- S5). Abbreviated column headings are organic matter (OM), nitrate content (NO3 (N)), electrical conductivity (EC), phosphorus content (P), and potassium content (K).

Soil	Site	pH	OM %	NO_3 (N) (ppm)	EC (mmhos/cm)	P (ppm)	K (ppm)	Texture
S1	Tilled Agricultural	7.2	6.4	21.9	0.7	124	698	sandy loam
S2	Tilled Agricultural	7.6	6.8	7.8	0.6	169	864	sandy loam
S3	Semi-Arid Grassland	7.6	3.6	11.9	0.4	4.60	236	sandy clay loam
S4	Sub-alpine, North facing	4.7	21.2	85.0	0.8	58.5	244	sandy loam
S5	Sub-alpine, South facing	6.3	15.6	80.9	0.7	19.4	203	sandy loam

2.2 Wetting Experiments, Flux chamber design, Custom Inlet System, and Instrument

Experiments were conducted using a dynamic flux chamber system. Soil sub-samples of approximately 30 cm3 were allocated into 100 mL uncovered glass jars that were then placed inside a 475 mL glass jar with a steel lid, plastisol liner, and silicone rubber seal containing approximately 50 mL of water to maintain soil moisture throughout the experiment (Figure S1). A custom sampling manifold and inlet system was built to manipulate soils and to sample the purge air flow through the dynamic flux chambers containing the soil sample (plumbing diagram of the dynamic flux chamber system is available in Figure S2, and plumbing diagram of sampling inlet system is available in S3). All tubing and fittings used in the system were stainless steel. The combination of the standing water and humidified zero air flow (140 ml/min, residence

time 3.5 min) maintained 25–29 parts per thousand H_2O in the jars at a temperature of 23°C. The zero air flow was humidified with a stone bubbler in a water-filled polycarbonate tube with a polypropylene cap. To generate zero air, ambient air was compressed and flowed through a custom zero air generator that catalytically oxidized hydrocarbons present in the air to CO_2. To determine baseline ambient CO_2 levels, air from the room was analyzed for 24 h leading up to soil experiments. The median of CO_2 measurements taken each minute during that period was used as the baseline CO_2 level. The sampling manifold, inlet system, and instrument were set up in a laboratory kept at 23°C. Room lights other than the emergency light were kept off during most of the experiment. Further, jars had opaque lids and sat in a wooden housing that blocked most light from reaching the soil samples (Figure S1).

Jars, and the samples contained within them, were subject to a 140 ml/min purge flow of zero air throughout the experiment. Removing VOCs from the air to which the soil is exposed does not allow the possibility of flux into the soil and forces VOCs from the soil. This setup does not necessarily mimic natural conditions, but allowed us to study emissions from a variety of soil types under controlled conditions. Purge air was split and analyzed on a LI-COR LI-840a (LI-COR Environmental, Lincoln, NE, USA) to measure CO_2 and water vapor, with the instrument calibrated with dry zero air, humidified air, and CO_2 standards (Airgas, Radnor, PA, USA, calibrated against 423.0 ± 0.1 ppm CO_2 AmeriFlux standard, Berkeley, CA, USA) directed through a LI-COR LI-7000.

For the VOC sampling, a fraction of the purge flow from the jar was collected at a rate of 50 mL min-1 for 40 min, which resulted in a 2 L sample. Sampling flow from individual flux chambers was selected using an automated Valco gas switching valve (Valco Instruments Co. Inc., Part# EUTA-2SD10MWE, Houston, TX, USA). This setup allowed for the continuous and

sequential sampling of up to 10 chambers, plus an empty chamber that served as a blank reference. Samples were drawn through a Peltier-cooled (-45°C) water trap for removal of water vapor, and then collected on a microadsorbent trap cooled to -30°C that contained 25 mg of Carboxen 1016 and 220 mg Carboxen 1000 (Sigma Aldrich, St. Louis, MO, USA, Part # 11052-U and 11021-U Supleco) [*Tanner et al.*, 2006]. The adsorbent trap was rapidly heated to 290°C to inject samples onto the gas chromatography (GC) column (details below). Following sampling, carrier gas (helium) was purged through the trap as it was heated to 325°C to clean and condition the trap for the next sample (bakeout). The water trap was also cleaned and conditioned following sampling by heating and pulling zero air through it. The saturation vapor saturation pressures of the VOC of interest at -45°C correspond to mixing ratios in the ppm range. Given that VOC mixing ratios in the sample air were several orders of magnitude lower, they are not expected to condense, respectively freeze out in the water trap. A Hewlett Packard 5890 Gas Chromatograph/Flame Ionization Detector/Agilent 5971 Mass Spectrometer (GC/FID/MS) instrument (Agilent Technologies, Santa Clara, CA, USA) with a 60 m DB-624 (Agilent Technologies, Santa Clara, CA, USA, Part # 123-1364) column was used to separate compounds, the FID to quantify VOCs, and the MS for compound identification. It should be noted that the applied analytical method has limitations for detecting multifunctional and highly polar compounds.

2.3 VOC Identification and Quantification

VOCs were identified based on comparison of peak retention time and mass spectra with components in four multicomponent standards and with reference data. Table 2 characterizes compounds based on their identification. The standards used were an oxygenated VOC standard,

and a multicomponent reference standard, both obtained from Apel-Riemer Environmental, Inc.

(Broomfield, CO, USA), a National Physical Laboratory (NPL) (London, UK) primary reference

gas mixture, and a National Institute of Standards and Technology (NIST) (Gaithersburg, MD,

USA) certified monoterpene standard. Standard compositions and analyte mole fractions are

available in Supplemental Table ST1. Emitted compounds that were not present in the standards

were identified by comparing their spectra to the NIST Spectral Library. Chromatograms and

spectra were analyzed using the Agilent Chemstation F.01.03.2357 software. Mass spectra were

found by averaging 3-5 scans at the peak maximum, subtracting background signals, and

searching for matching spectra using the NIST mass spectral search program (Version 2.2, June

10, 2014). These mass spectra, and the top three matches from the NIST mass spectral search

program are available in Table ST2.

Table 2. Table of retention times (RT) and identifications for compounds in soil samples. The right four columns indicate how the compound was identified and the confidence in the identification. Compounds with an "X" in the "Standard" column were present in one of the multicomponent standards. "X's" in the MS (Mass Spectrometer) and Elution Ref. (elution order reference) indicates that the compound was identified by its mass spectra and a reference for the elution order of that compound are available. "X's" in the tentative column indicate that a compound was identified solely by the mass spectrometer and NIST spectral library and is therefore a tentative identification. See Table ST2 for mass spectra and library match identification. Elution order references are available in Table ST3 and compared to our elution order in Figure S4.

Compound	RT (min)	Soil	Standard	MS	Elution Ref.	Tentative
Ethylene oxide	19.5	1--5		x		x
2-Butene	19.9	1--5	x			
Acetone	22.1	1--5	x		x	
Isopropyl Alcohol	22.4	4		x		x
Pentane	23.1	1--5	x		x	
Dimethyl Sulfide	23.4	1--5		x	x	
Methylene chloride	23.7	4,5		x	x	
Nitromethane	24.1	1--5		x		x
Carbon Disulfide	24.2	1--5		x	x	
Trimethylsilanol	25.0	1--5		x		x
2-Butanone	25.7	1--5		x	x	

2-Methyl-1-pentene	26.1	2--5	x	x
2-Methyl-3-buten-2-ol	26.4	4,5	x	x
2-Azido-2,3,3-trimethyl-butane	26.5	1--5	x	x
Tetrahydrofuran	27.1	1--5	x	x
2-Methyl-3-pentanol	27.5	1,3,4	x	x
3-Methyl-2-butanone	28.0	2--5	x	x
3,3-Dimethyl-2-butanone	29.7	1,2,3,5	x	x
Hexanal	32.3	1--5	x	x
1,3-Octadiene	33.4	4,5	x	x
2,2,4,6,6-Pentamethyl-3-heptene	38.5	1--5	x	x

Elution orders were compared against other records that utilized the DB-624 column, i.e. the Agilent elution order reference [Agilent, 2014], the elution order from the Nitrogen, Aerosol Composition, and Halogens on a Tall Tower (NACHTT) campaign [*Brown et al.*, 2013], and an instrument calibrated to measure air toxics [*Apel et al.*, 1998]. Figure S4 shows the correlations between reference elution orders and the identifications proposed by this work. Correlations were fit with a 2nd order polynomial, and all R2 values were > 0.95. Table ST3 lists identified compounds supported by elution order data. Identified compounds not supported by reference elution order should be regarded as tentative because they were selected solely based on the best available library match. Quantitation proceeded under the assumption that these identifications were correct, but we have limited confidence in these tentative identifications.

To mimic sampling conditions, standard mixtures were purged through the dynamic flux chamber system and collected by the sampling system. Compared with direct sampling from the tank, instrument response was within 10%. A dynamic dilution system consisting of zero air regulated by a mass flow controller (MFC) (Tylan Coastal Instruments, INC. Burgaw, NC, USA) and an additional MFC to meter the standard flow was used to calibrate the instrument response in the 1–5 ppb range.

Blank samples were collected between soil samples by capturing a fraction of the purge air flow through an empty jar with 50 mL of water. Dichlorodifluoromethane, styrene, toluene, and ethylbenzene were present in blank samples. These peaks were occasionally present in soil samples but, because of their presence in blank samples, were not reported as soil emissions.

The FID was used to quantify VOC mixing ratios. Total C emitted as VOC (C_{VOC}) flux was calculated by summing all chromatogram peaks minus peaks present in blank runs. C fluxes were determined for identified compounds present in one of the standards (Table ST1) by integrating their peak areas in the chromatogram and converting peak areas to mixing ratios using response factors calculated from standards. Response factors for individual components of the standard were also used to develop a calibration curve to estimate response factors for compounds not present in standards, based on their retention times. A second order polynomial was fit to response factors of standard components, and the resulting formula was used to calculate response factors for compounds not present in standards. The standard components used to build the calibration curve are listed in Table ST4. The calibration curve is shown in Figure S5. Response factors were calculated per ppb C using effective carbon numbers as described in Scanion and Willis [1985]. All standard components with peaks that could be separated and integrated were included initially. After fitting with a second order polynomial, compounds with residuals greater than 3 standard deviations from the curve were excluded and the curve was recalculated. This curve was used to determine the response factor for compounds based on their retention time. All compounds considered and the final response factor curve are shown in Figure S5. This factor was multiplied by the theoretical effective carbon number of each identified compound to convert FID response to the mixing ratio (in ppb) of the compound, and the mixing ratio of carbon by dividing through the number of carbon atoms in the molecule

(ppb C). FID responses of unidentified compounds were converted to ppb C using the response factor curve (Figure S5) based on the peak retention time. Purge flow rates through the jars were used to convert mixing ratios to VOC masses emitted from the soil. Masses of dry soils and sampling time were used to calculate soil VOC fluxes. For unknown compounds, a C mass calibration curve (as a function of retention time, Figure S6) was used to convert mixing ratios to VOC fluxes. This curve is a 2nd order polynomial fit of the C mass present in standard components versus their retention times. Fluxes of unknown VOCs were summed. The proportional contributions of individual VOCs to total VOC emissions were calculated by dividing the compound's flux by the total VOC flux. Flux rates of both VOCs and CO_2 were integrated over the sampling time to determine the total mass of C emitted per unit soil throughout the incubation period.

2.4 Rewetting Experiment

Three samples of each soil type were evaluated. For each soil sample, approximately 30 cm3 of field moist soil from the refrigerator was air-dried at room temperature in open glass jars for 5–10 days. Samples were not subject to purge air flows while drying. Samples were then placed in a sampling jar on the manifold and subjected to purge air flow for ~20 min before sampling began. Two data points from the purge air flowed over air-dried soils were collected prior to the rewetting event (T0). To simulate a moderate precipitation event, soils were brought to 50% of their maximum water holding capacity (WHC) with deionized water. Ten minutes after rewetting, 2 L air from the purge air flow was collected (40 min purge air collection per air sample). Sample collections continued once every ~2 hrs for a total of 48 hrs after the rewetting event. After the initial rewetting at T0, additional water (never more than 2.2 mL) was added to

each soil sample as needed approximately every 12 h to maintain the soils at 50% of maximum WHC. This was done by removing the small jars containing the soil from the dynamic flux chamber, weighing the small jar and soil, and adding enough water to bring the soil back to 50% WHC. Emission experiments from three samples of each soil type were conducted. Emission experiments were discrete and sequential; the 52 hr emissions collection process was completed for each sample before analyzing the next sample.

2.5 Statistical Analyses

We used non-parametric multivariate statistics to determine if VOC profiles changed temporally over the experiment and if VOC profiles were different across soil samples. For this, the experiment was divided into three temporal segments based on sampling time. "Pre- pulse" refers to the two purge air samples collected prior to the T0 rewetting event. "Pulse" refers to the 5 h window immediately following the T0 rewetting event, and "post-pulse" refers to all sampling points post 5 h through the end of the 48 hrs incubation. The permutational multivariate analysis of variance (PERMANOVA) [*Anderson*, 2001] was used to test the null hypothesis that the arithmetic mean (centroid) and the variability (statistical dispersion) of VOC speciation and relative abundances are equivalent among these temporal segments. For each soil replicate (i.e. triplicates of S1-S5), C_{VOC} flux was averaged for each unique VOC across all sample points within each temporal segment. We used the R package 'vegan' [*Oksanen et al.*, 2017] to perform PERMANOVA on Bray-Curtis dissimilarities of VOC profiles, and statistical significance was evaluated from 999 permutations. Further, we constructed a Non-Metric Multidimensional Scaling (NMDS) ordination plot to illustrate the dissimilarities of VOC speciation and relative abundances.

3. Results

3.1 Total CO2 and VOC Emissions

We observed a pulse in CO_2 emissions immediately after rewetting. Within an hour of the rewetting event, CO_2 emissions were on average 20 times higher than emissions from the dry soil. Emission rates of CO_2 dropped exponentially over the next 3–6 h post-rewetting, and on average 48 h after the rewetting event (with soils maintained at 50% WHC for the entire 48 h period) were 3 times greater than the CO_2 emission rates from the dry soils (Figure 1). Soils were only exposed to the air flow present in the sampling manifold for 20 minutes prior to the pre-rewetting samples. A 'dry' experiment was conducted to examine the effect of the initial exposure to air flow on emissions from the dried soils. Dried garden soils (soil S1 soil) were put on the sampling manifold under normal flow conditions and sampled repeatedly. Total VOCs emissions from the dry soils decreased to 70% of initial emissions after being exposed to manifold flow conditions for 7 h (Figure S7) and decreased to ~20% of the initial response after 72 h. Emissions remained constant over the next 28 h, for a total of 100 h of exposure to purge air flow.

Table 3 shows mean CO_2 and VOC emissions integrated across the 48 h sampling period for each soil type, averaged across replicate samples. Table 3 also shows the standard deviation across samples as a measure of the repeatability and/or variability of emissions within soil type. The relative standard deviation of the CO_2 emissions within soil samples of each soil type were $\leq$ 10% for S1, S2, and S5, 12% for S4, and 36% for S3. Relative standard deviations of total VOC emissions between samples within soil types were < 10% of for S1– 2, 20% for S3, and 69 and 84% for S4 and S5, respectively (Table 3).

Table 3. VOC and CO_2 emissions integrated over the 48 hr sampling period and averaged across three replicate samples of each soil type. Standard deviations are included as a measure of the repeatability of the experiment. One S3 VOC sample was excluded due to lost chromatogram runs.

Soil	C_{VOC} Emissions (ng g^{-1}$_{soil}$)	C_{VOC} STD	C_{CO2} Emissions (ng g^{-1}$_{soil}$)	C_{CO2} STD	C_{VOC}/C_{CO2} (%)	C_{VOC}/C_{CO2} STD
1	771	67	13600	1400	5.75	1.03
2	520	46	8590	604	6.10	1.00
3	462	92	7650	2780	7.40	2.14
4	700	480	30000	3530	3.16	0.72
5	636	533	31700	2300	2.73	1.39

Total VOC emissions immediately after rewetting were an average of 6 times greater than from dry soil before the rewetting event, and an average of 14 times greater than VOC emissions from moist soils 2 days after rewetting. Assuming the results of the dried soil purge air experiment described above are representative of all soils, had emissions from dried soils been allowed to equilibrate, total VOC emissions immediately after rewetting would have been an average of 30 times greater than emissions from dried soils. The pulse in total VOC emissions typically lasted for 1–5 h (Figure 1). Peak total VOC flux rates, averaged across samples within a soil type, varied from 25 ng C g^{-1}$_{soil}$ hr^{-1} in S3, to 190 ng C g^{-1}$_{soil}$ hr^{-1} in S5 during the pulse event.
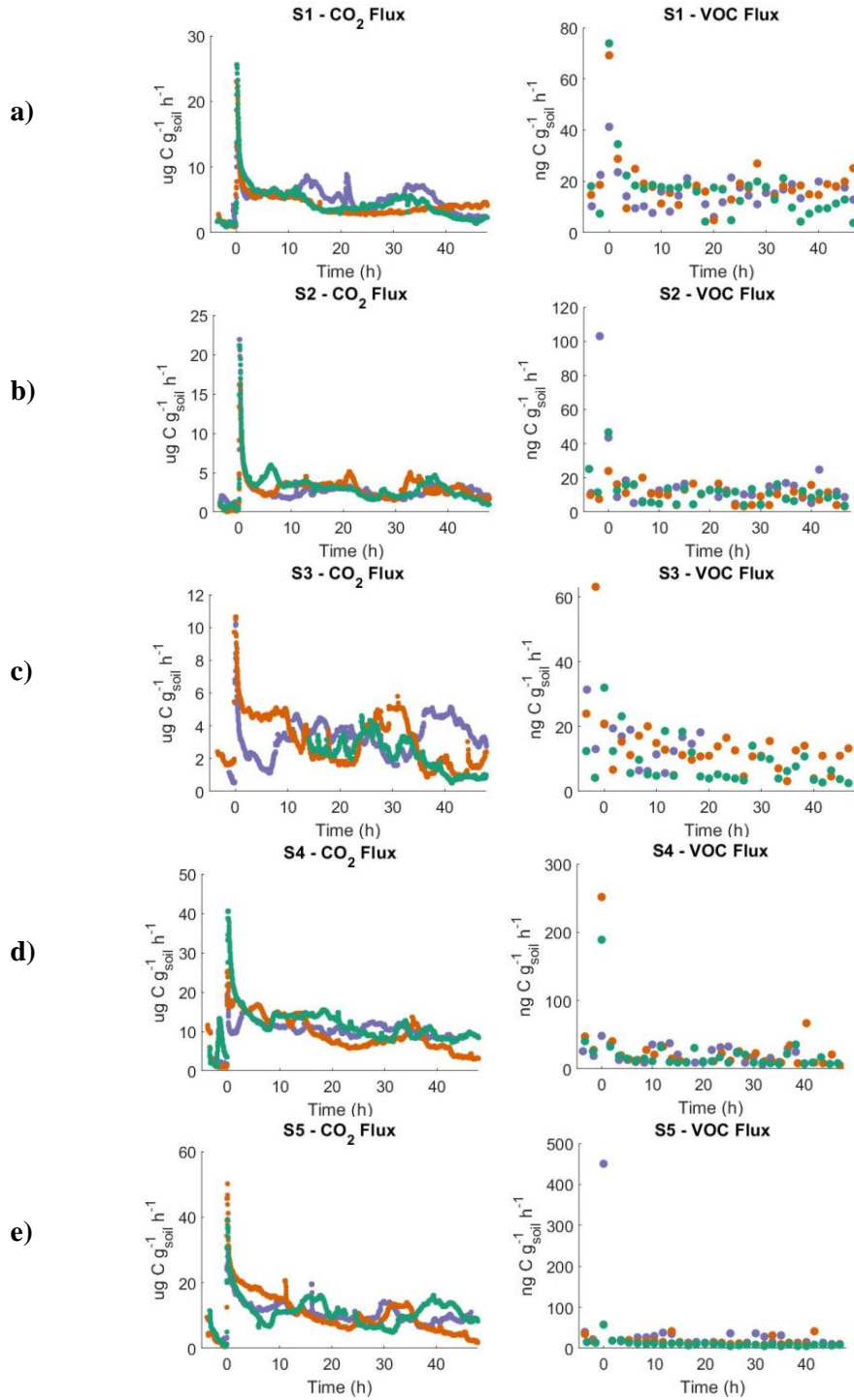
Figure 1. C_{VOC} and C_{CO_2} flux rates over the duration of the 48 h experiment. The y-axis shows the C_{CO_2} (left column of graphs) or C_{VOC} (right column of graphs) flux rates. Note the difference in units between CO_2 and VOC fluxes. Soils were rewet at time zero to 50% maximum WHC. Panels a-e correspond to soils S1-S5. Triplicate samples are shown for each soil. The legend in panel (a) shows the color assigned to each replicate, which is consist throughout all panels. Median ambient CO_2 levels between sampling periods were subtracted from CO_2 measurements.

Across all soils, CO_2 was the dominant form of C emitted. Normalized to carbon (C), total carbon from VOC, C_{VOC}, was $5.03 \pm 2.01\%$ (mean $\pm$ S.D.) of the total carbon from CO_2 (C_{CO2}) emissions (Figure 1). This mean was calculated by averaging the ratio of C_{VOC} to C_{CO2} for each replicate of each soil type (available in Table 3) and then averaging across soil types. C_{VOC} emissions correlated with C_{CO2} emissions (Figure 2, linear regression results from all soil experiments combined were: slope $= 0.0256$, $\rho = 0.83$, $P < 0.001$) across soil samples integrated over the first 12 h of the experiment. The other 12 h segments of the sampling period did not have statistically significant correlations (Figure 2, $\rho < 0.50$, $P > 0.05$), but there was a correlation over the entire 48 h experiment (Figure S8, $\rho = 0.59$, $P = 0.03$). When we compare total C_{CO2} and C_{VOC} emissions for the entire incubation period to each soil's organic matter content (Figure S9), C_{CO2} emissions were higher in soils with higher soil organic matter concentrations (Spearman's $\rho = 0.93$ for total C_{CO2} emissions, $P = 0.13$). C_{VOC} emissions also tended to be higher in soils with higher soil organic matter concentrations (Spearman's $\rho = 0.40$ for total C_{VOC} emissions, $P = 0.52$). Though the correlation is not statistically significant in either case, the correlation between C_{VOC} emissions and soil organic matter concentrations was stronger when S1 (residual $= 3.6\sigma$) was removed ($\rho = 0.99$, $P = 0.08$) (Figure S9).
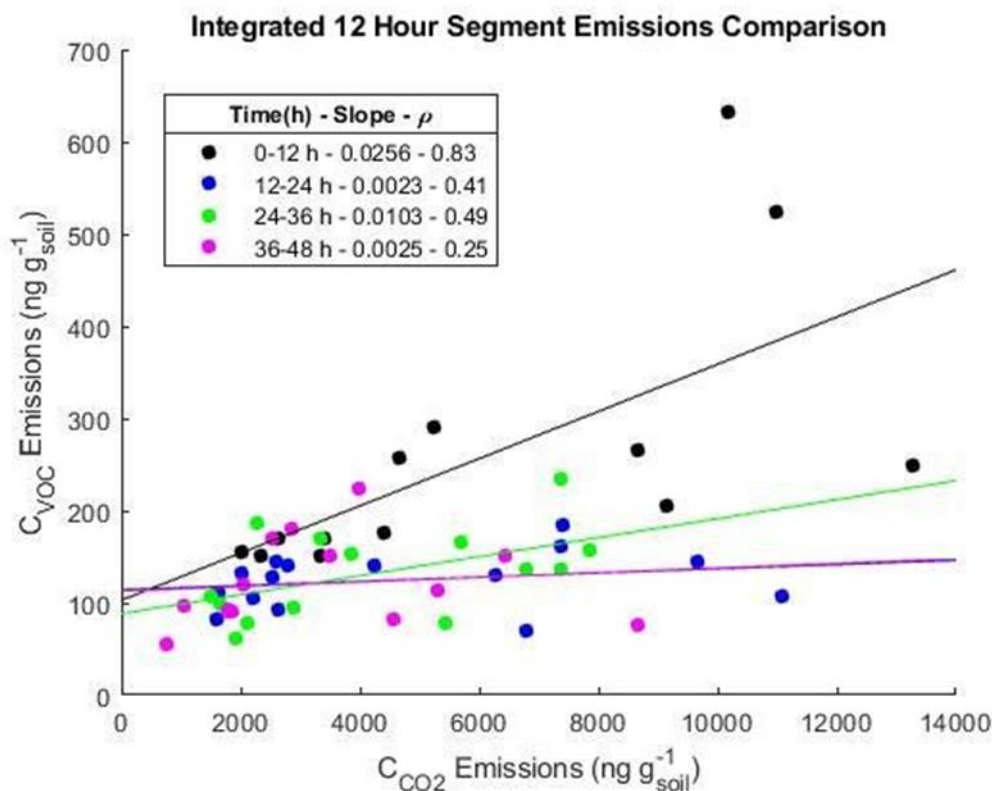
Figure 2. Integrated normalized C_{VOC} emissions y-axis) versus integrated C_{CO2} emissions (x- axis) divided into 12 h segments. Time segments with interruptions in sampling were excluded. Linear regressions show the correlation between CO_2 and VOC emissions, and Spearman's ρ values and regression line slopes are reported in the legend. Colors correspond to different sampling times (see legend). P-values are < 0.001 for all time segments except 36-48 h, where P = 0.02.

3.2 VOC profiles by soil type

While rewetting drives most of the variation in the chemical diversity and quantities of VOCs across the entire experiment, VOCs varied by soil type, with 4.9% of the variation in VOC profiles being due to the soil type (PERMANOVA; R2 = 0.049, P = 0.035) (Figure 3). Compound identifications, by elution order and characterization method are shown in Table 2. Table 3 contains compounds identified by mass spectra not present in the multicomponent standard, as well as their top five mass fragments, library match percentage, and other possible matches. 2,2,4,6,6-Pentamethyl-3-heptene (PMH), dimethyl sulfide (DMS), acetone, ethylene oxide, 2-butanone, hexanal, nitromethane, and 2-butene were present in post-pulse emissions of

173

all soils but their relative abundances varied. The identifications of PMH, ethylene oxide, nitromethane, and 2-butene should be regarded as tentative because they are not supported by reference elution order data, nor were they present in standards. DMS made up 3.6% of C_{VOC} emissions in S1 but <2% of S2, S4, and S5 emissions. Following T0, 0.3 to 1.1% of C_{VOC} emitted was in the form of tetrahydrofuran. Acetone made up 4.6% of S5 CVOC emissions, but < 2% of S1 C_{VOC} emissions. Trimethylsilanol made 0.5% of S1 pulse C_{VOC} emissions but less than 0.1% of S3–5 pulse emissions. 1,3-Octadiene was responsible for 0.8% of pulse C_{VOC} emissions in S4, but was not present in S2 and S3.
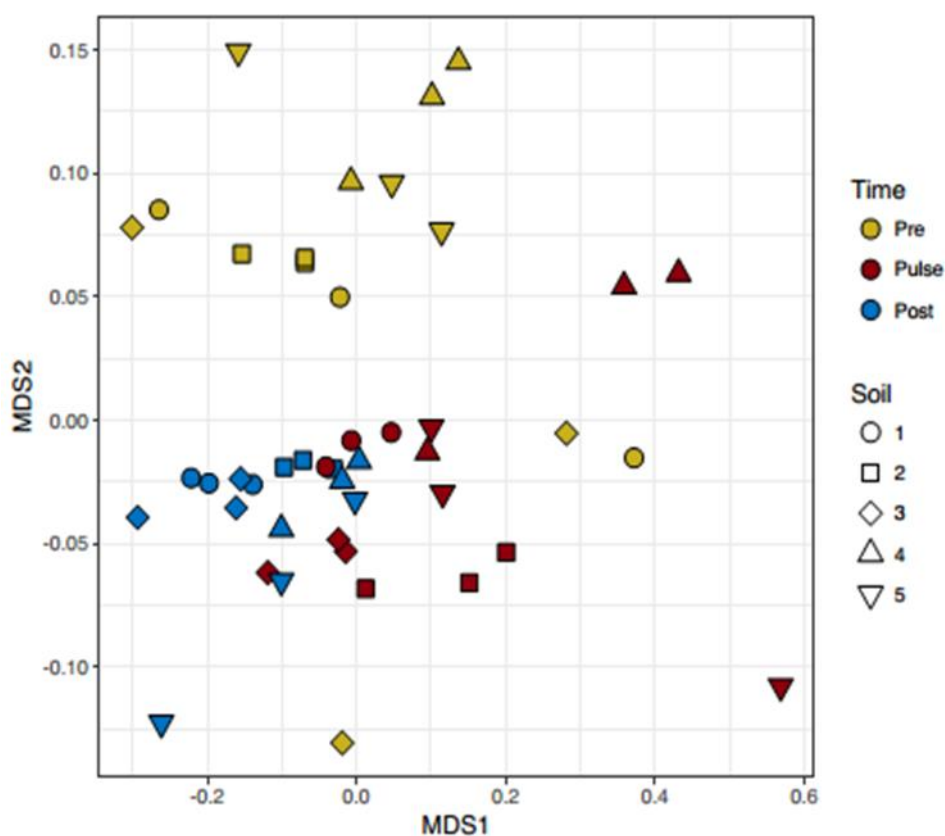
Figure 3. Nonmetric multidimensional scaling (NMDS) ordination plot. Each point represents the VOC speciation and relative abundances from soils S1-S5 (different shapes) averaged across various time sections of the rewetting experiment (colors). "Pre-pulse" reflects dry soils sampled prior to wetting. "Pulse" represents VOCs identified during the first 5 h following rewetting soils to 50% WHC. "Post-pulse" represents VOCs identified during the remainder of the experiment between 5-48 h following rewetting. VOC profiles vary across time segments (PERMANOVA; R2 = 0.28, P = 0.001) as well as across soil types (PERMANOVA; R2 = 0.049, P = 0.035).

3.3 Temporal Variation in VOC profiles

The types and amounts of VOCs emitted varied temporally across the experiment as well as between soil types (Figure 3). More of this variation (28%) was driven by the rewetting event than by soil type. VOC emission profiles from dry soils prior to rewetting ("pre-pulse"), moist soils immediately following the rewetting ("pulse", 1-5 h), and moist soils during late stages of the experiment ("post-pulse", 5-48 h) were significantly distinct (PERMANOVA; R2 = 0.28, P = 0.001) (see Materials and Methods) (Figure 3).

Figure 4 highlights the temporal changes in emissions of the most abundant VOCs detected in all soil types. A maximum number of compounds was observed in the first sample after rewetting for all soils; these chromatograms featured 40–70 peaks, while 20 or fewer peaks were observed at T48. The most abundant VOCs included ethylene oxide, acetone, DMS, 2-butanone, 2-methyl-1-pentene (2MP), tetrahydrofuran (THF), and PMH. Ethylene oxide and acetone made up 6.5–34% of pre-pulse CVOC emissions for all soils. The most abundant VOCs represented 17–35% of the total VOCs emitted from the moist soils approximately 10 h after the wetting event through the end of the 48 h experiment. However, during the rewetting pulse (T0–5 h), these VOCs accounted for a slightly lower portion (i.e.13–22% of the total VOC flux). Further, acetone, DMS, and PMH were responsible for 8.6– 18% of C_{VOC} emissions from all soils from 0–5 h and for 15–30% of emissions from all soils from 10–48 h. 2-butanone was responsible for 0.6–1% of the post-pulse C_{VOC} emissions from all soils. Emissions from S5 immediately after rewetting were dominated by unidentifiable compounds (67%), and the chemical diversity of VOCs emitted peaked at this time (Figure 4).

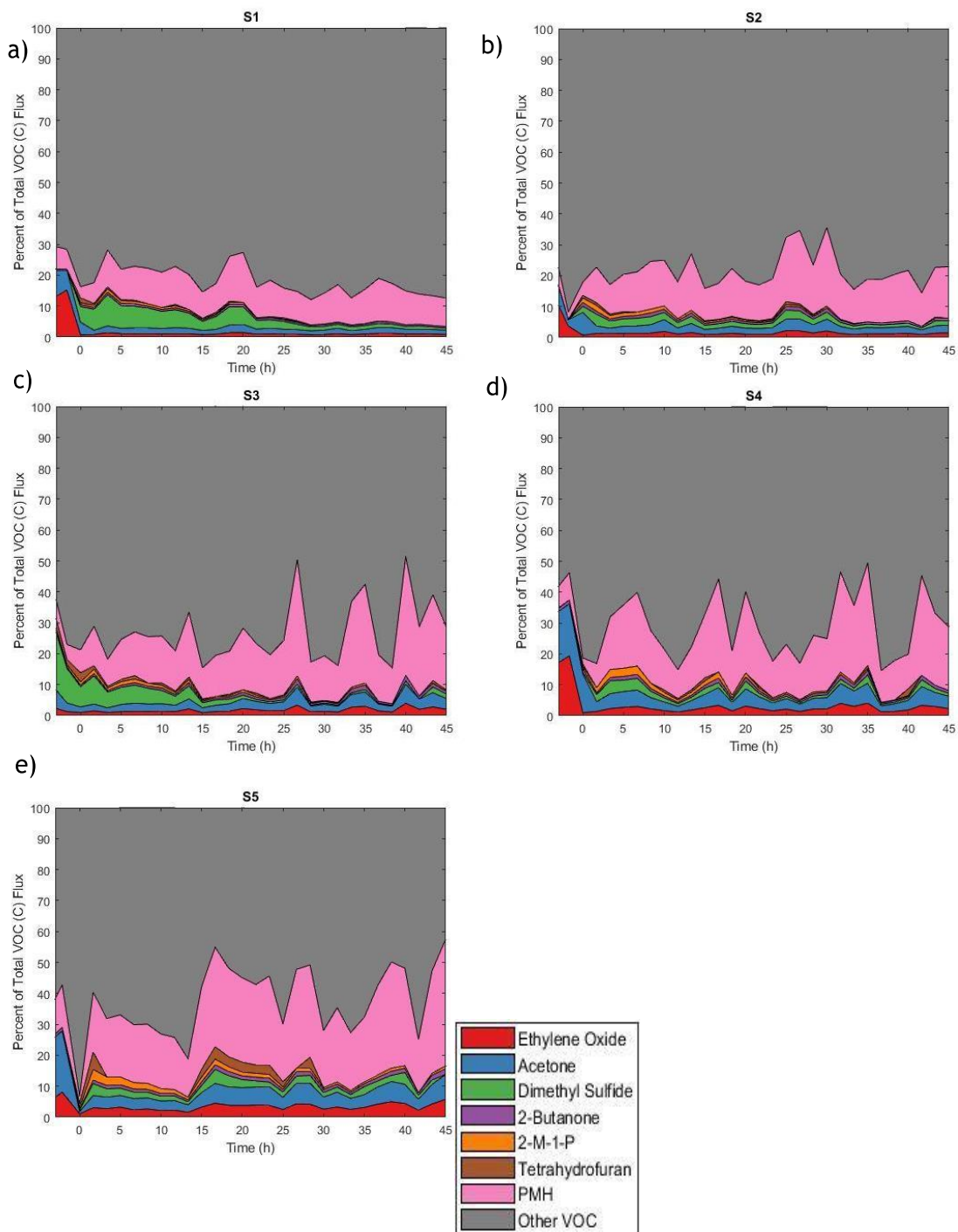Figure 4. Individual C_{VOC} flux relative to total C_{VOC} flux (averaged across 3 replicates) of the dominant VOC for soils S1-S5. Rewetting of soil to 50% WHC occurred at time zero. Colors correspond to VOC identity (see legend), with "Other VOC" consisting of the sum of all less abundant and unidentified VOCs. 2-M-1 P is 2-methyl-1-pentene. PMH is 2,2,4,6,6-pentamethyl-3-heptene.

4. Discussion

4.1 Temporal Dynamics

In all soils, the magnitude and duration of the rewetting CO_2 pulse was equivalent to what has been observed in previous laboratory-based soil rewetting experiments [*Fierer and Schimel*, 2003; *Franzluebbers et al.*, 2000]. The temporal dynamics of total VOC emissions upon rewetting were qualitatively similar to those observed for the soil CO_2 emissions (Figure 1). VOC emissions peaked in the first sample taken after rewetting (sample air collection began 10 min after rewetting and continued for 40 min) and remained elevated for approximately 5 h compared to dried soil emissions. If the soil had been given more time to come to equilibrium with the purge flow prior to the wetting (Figure S7), lower emission rates would have been expected before the wetting, which probably then would have resulted in a longer period of elevated VOC emissions (Figure S7). Our observed pulse in total VOC emissions immediately following rewetting was similar to that described in Veres et al. [*Veres et al.*, 2014], where in a laboratory experiment including agricultural and rainforest soils, it was also observed that the majority of gaseous organic carbon was released within the first 2 h following a rewetting event. Likewise, a pulse in VOC emissions was detected above a ponderosa pine plantation following a rain event, and acetone fluxes were 3–4 times higher the morning after a rain event than during dry periods with similar soil temperatures [*Schade and Goldstein*, 2001].

Besides rewetting triggering CO_2 and VOC fluxes, it is also well established that emissions of NOx from soil are elevated following a wetting event [*Hudman et al.*, 2012; *Yienger and Levy*, 1995] and are mostly due to microbial community activity in the soil [*Conrad*, 1996]. NO fluxes following the rewetting of dried soil increased by up to five orders of magnitude with an average of ~1000% in the field and ~2000% in the lab [*Kim et al.*, 2012].

4.2 Comparison of CO₂ and VOC Emissions

The ratio of VOC to CO_2 production in this experiment averaged 5.0±2.0% across all samples included in this study. This ratio is lower than the ratio of C_{VOC} to C_{CO2} emitted by leaf litter, where microbial activity was also recognized as the primary driver of emissions [Gray et al., 2010]. Leaf litter C_{VOC} emissions from Eucalyptus sp. and Populus tremuloides made up 88 and 80%, respectively, of C_{CO2} emissions [*Gray*, 2014]. Though the VOC emissions were smaller than CO_2 emissions from the soils studied here, VOCs are important mediators of microbial interactions as they can play vital roles in bacterial quorum sensing, motility, gene expression, and antibiotic resistance [*Schmidt et al.*, 2015]. For example, lactones, a class of volatile cyclic esters, prevented quorum sensing among a variety of Gram- positive and Gram-negative bacteria [*Schulz et al.*, 2010]. As another example, certain bacteria can produce caryophyllene, a sesquiterpene, which inhibits virulence gene expression in the pathogenic fungi Fusarium oxysporum [*Minerdi et al.*, 2008].

Total C_{CO2} and C_{VOC} emissions were generally higher for those soils with higher soil organic matter concentrations (Figure S9). This was expected given that soil organic matter levels often correspond to overall enhanced microbial activity [*Barton et al.*, 2016; *Schimel et al.*, 1994; *Seewald et al.*, 2010].

4.3 VOC Emission Profiles

Our findings are in line with previous work showing that different soils have distinct VOC emission profiles [*Mancuso et al.*, 2015; *Veres et al.*, 2014]. Some specific compounds identified in both Veres et al. [2014] and this study are acetone, DMS, and 2-butanone.

Hexanal emissions from soil were observed by Mancuso [2015]. Studies have also reported that methanol emissions from soil can be high [*Gray et al.*, 2010; *Stacheter et al.*, 2013].

However, we were unable to measure methanol and other highly polar compounds with the analytical methods used here. Several compounds observed in this study are commonly found in soil, such as acetone and 2-butanone. Other observed compounds are found in materials that are introduced into soil from other sources. Still other compounds observed here have been shown to be products of microbial metabolism. Acetone is produced by a variety of bacteria including Escherichia coli and Clostridium acetobutylicum [*Maddula et al.*, 2009]. Bacterial catabolism can produce DMS from dimethylsulfidepropionate (DMSP) [*Todd et al.*, 2007]. This is most common in marine bacteria, but DMS has been shown to be produced by soil bacteria reducing DMSO [*Omori et al.*, 1995]. Carbon disulfide is a product of metabolism of microbial soil communities, and as much as 80% of emissions are from natural sources [*Canada*, 1999]. Some of the VOCs emitted from the soils can also be relevant to atmospheric chemistry. For example, hydrocarbon and DMS oxidation by OH leads to atmospheric aerosol formation [*Ayers and Cainey*, 2007; *Bowman and Seinfeld*, 1994]. Acetone is oxidized by OH as well, but the majority of acetone is degraded through photolysis, which can lead to the production of PAN [*Singh et al.*, 1994] that can transport nitrogen oxides great distances and leads to formation of tropospheric ozone far down wind [*Singh and Hanst*, 1981].

VOC profiles varied as a result of the time with respect to rewetting (Figure 3). Bunge et al. [2008] found that emitted VOCs changed with respect to the growth stage of a microbial consortium. This is a likely explanation for the observed temporal diversity in VOC profiles. From the PERMANOVA analysis, we also found a significant dependence of VOC emission profiles on soil type, though the variation in emission profiles across soil types was less than the

temporal variation. Another study found varying VOC profiles from different soil types [*Mancuso et al.*, 2015]. The distinct VOC profiles emitted from the different soil types may be a product of differences in soil microbial communities, the amounts and types of carbon metabolized, and soil nutrient levels [*Larsen and Frisvad*, 1995; *Stahl and Parkin*, 1996; *Stotzky and Schenck*, 1976; *Wheatley et al.*, 1997].

We cannot confirm the fraction of emissions that result from abiotic or microbial processes. Abiotic processes can be important contributors to VOC emissions [*de Gouw et al.*, 1999; *Warneke et al.*, 1999]. However, previous research suggests that biotic emissions of VOCs from soil or litter are 5–10 times higher than abiotic VOC emissions [*Gray et al.*, 2010; *Leff and Fierer*, 2008]. Thus, given the observed temporal dynamics in VOC emissions (Figure 1) and their correlation to CO_2 emissions (Figure 2 and S2), we predict that microbial activities are responsible for the majority of the VOC emissions measured here. Together, these results highlight that a short-lived pulse in total VOC emissions occurs following the rewetting of dry soils, and most of these VOCs are likely a product of microbial metabolism.

4.4 Relevance of soil VOC emissions to atmospheric chemistry

Our results demonstrate that soil VOC emission rates can change rapidly in response to rewetting events, with VOC emission dynamics being similar to those observed for CO_2 emissions. While the flux rates measured here are likely to differ from those measured in the field, the general phenomenon characterized in these experiments may have implications for modeling terrestrial sources of atmospheric VOCs.

Soil emissions of nitrogen oxide (NO), and their increase from soil wetting, have long been recognized and included in models. Over the African Sahel NO emissions pulses after rain

events contribute 21–44% of soil NOx emissions [*Zörner et al.*, 2016]. Soil NOx emissions following the wetting of dry soil have been shown to contribute up to 22% of annual emissions in a Venezuelan savanna [*Davidson*, 1992]. Therefore, NO emissions from soil, including their increases during and after precipitation events, have been included in atmospheric chemistry and transport models, such as the Community Land Model, Version 4 (CLM4) and the Goddard Earth Observing System Model, Version 5 (GEOS-5) that factor in weather conditions such as temperature and precipitation to correctly forecast soil NOx emissions [*Lawrence et al.*, 2011; *Lin*, 2012].

Atmospheric models include components that consider biogenic VOC emission from terrestrial sources; vegetative and oceanic emissions are the dominant components [*Guenther et al.*, 1995; *Guenther et al.*, 2012; *Lamarque et al.*, 2012]. Soil VOC emissions have been included in models in varying forms. The Goddard chemistry climate model (GEOSCCM) includes isoprene and other VOC emissions from soil that are adjusted according to meteorological conditions; the ECHAM/MESSy Atmospheric Chemistry (EMAC) model has fixed VOC soil emissions scaled to meet annual net emissions [*Jockel et al.*, 2006; *Lamarque et al.*, 2013]. As we have shown, soils can emit an abundance of VOCs, this behavior was consistent among five types of soils, and emissions were elevated after soil wetting. Based on the degree to which emissions were elevated following wetting, soil moisture, and changes in soil moisture levels should be considered when incorporating soil VOC emissions into models. While our experimental approach did not allow extrapolation of the laboratory results to environmental surface fluxes, these observations nonetheless argue for further research, and that consideration of soil fluxes and their parameterization in models may improve regional to global estimates of VOC fluxes and their role in atmospheric chemistry.

Acknowledgements

Chapter 7

A phylogenetic and functional perspective on volatile organic compound production by Actinobacteria

Mallory Choudoir[1], Sam Rossabi[1,2], Matthew Gebert[1], Detlev Helmig[2], and Noah Fierer*[1,3]

[1]Cooperative Institute for Research in Environmental Sciences, University of Colorado-Boulder, Boulder, CO, USA; [2]Institute of Arctic and Alpine Research, University of Colorado-Boulder, Boulder, CO, USA; [3]Department of Ecology and Evolutionary Biology, University of Colorado-Boulder, Boulder, CO USA

***Corresponding Author: Noah Fierer Noah.Fierer@colorado.edu

Abstract

Soil microbes produce an immense diversity of metabolites, including volatile organic compounds (VOCs), which can shape the structure and function of microbial communities. VOCs mediate a multitude of microbe-microbe interactions, including antagonism. Despite their importance, the diversity and functional relevance of most microbial volatiles remains uncharacterized. We assembled a taxonomically diverse collection of 48 Actinobacteria isolated from soil and airborne dust and surveyed the VOCs produced by these strains on two different media types *in vitro* using gas chromatography/mass spectrometry (GC/MS). We detected 126 distinct VOCs and structurally identified approximately 20% of these compounds, which were predominately C_1-C_5 hetero-VOCs, including (oxygenated) alcohols, ketones, esters, nitrogen-, and sulfur-containing compounds. Each strain produced a unique VOC profile. While the most common VOCs were likely byproducts of primary metabolism, most of the VOCs were strain-specific. We observed a strong taxonomic and phylogenetic signal for VOC profiles, suggesting their role in finer-scale patterns of ecological diversity. Finally, we investigated the functional

potential of these VOCs by assessing their effects on growth rates of both pathogenic and non-pathogenic pseudomonad strains. We identified sets of VOCs that correlated with growth inhibition and stimulation, information that may facilitate the development of microbial VOC-based pathogen control strategies.

1. Introduction

Microbial metabolism yields an extensive assortment of primary and secondary metabolites. While many of these metabolites are non-volatile, including many therapeutic antibiotics, microbes can also produce volatile organic compounds (microbial VOCs, or mVOCs). VOCs are relatively small organic molecules ($<C_{20}$) with low molecular mass (<300 Da) that are readily volatilized at ambient temperatures due to their high vapor pressures and low boiling points.

Many mVOCs are byproducts of primary metabolism generated via aerobic heterotrophy, fermentation, amino acid catabolism, terpenoid biosynthesis, and sulfur reduction [*Penuelas et al.*, 2014], while other mVOCs are produced via specialized secondary metabolic pathways [*Tyc et al.*, 2017]. Some of the most commonly observed mVOCs are fatty acid derivatives (including alcohols, alkanes, and alkenes), aromatic compounds, nitrogen and sulfur-containing compounds, and terpenoids [*Schmidt et al.*, 2015; *Schulz and Dickschat*, 2007]. To date, the chemical structures of approximately 2000 VOCs from 1000 bacterial and fungal species have been cataloged [*Lemfack et al.*, 2018; *Lemfack et al.*, 2014]. However, patterns of VOC production between closely related strains can vary considerably [*Scholler et al.*, 2002; *Shestivska et al.*,

2012], and many mVOCs remain uncharacterized, highlighting the vast potential for discovery and exploration of microbial volatiles.

Soil microbes are a particularly rich source of VOCs [*Insam and Seewald*, 2010; *Penuelas et al.*, 2014; *Stahl and Parkin*, 1996], and soil VOCs can impact both above and belowground processes. Although plants are often the dominant source of VOCs in terrestrial ecosystems [*Fehsenfeld et al.*, 1992], mVOC emissions from soils can be considerable [*Leff and Fierer*, 2008; *Rossabi et al.*, 2018], and biogenic VOC fluxes can exert a strong influence on oxidative chemistry within the troposphere [*Monson and Holland*, 2001]. Microbial volatiles can also influence rates of microbial activities associated with nitrogen and carbon transformations [*Bending and Lincoln*, 2000; *Paavolainen et al.*, 1998; *Smolander et al.*, 2006] and mediate biotic interactions between bacteria, fungi, plants, arthropods, insects, and animals [*Penuelas et al.*, 2014; *Schulz-Bohm et al.*, 2017]. In the unsaturated conditions typical of most soils, VOCs can readily diffuse through air-filled pore spaces in the soil matrix [*Minnich*, 1993], thus serving as potentially important short and long-distance signaling molecules.

mVOCs mediate microbe-microbe interactions in two major ways: by serving as infochemicals that influence morphology, physiology, gene expression, and population dynamics, and by serving as agents of chemical warfare, competition, and antagonism, which can, in turn, shape the structure and function of soil communities [*Schmidt et al.*, 2015]. For example, differentiation of *Streptomyces* 'explorer' cells are triggered by VOCs in response to signals driven by nutrient limitation and changes in pH [*Jones and Elliot*, 2017; *Jones et al.*, 2017]. Volatiles can also influence bacterial motility behavior and stress responses [*Kim et al.*, 2013; *Schmidt et al.*, 2016], and rhizosphere-associated bacterial VOCs have been shown to quench quorum-sensing activities of other bacterial populations [*Chernin et al.*, 2011]. Previous

work has also demonstrated that a broad collection of microbial volatiles can have both inhibitory and stimulatory growth effects on diverse pathogenic fungi [*Briard et al.*, 2016; *Bruce et al.*, 2003; *Kai et al.*, 2007; *Wheatley*, 2002; *Zou et al.*, 2007]. Despite their potential importance, the activities and functional relevance of most mVOCs remain unknown [*Lemfack et al.*, 2018; *Piechulla et al.*, 2017].

Soil-dwelling actinobacteria are an ideal group for studying mVOC production. Members of the phylum Actinobacteria are ubiquitous and abundant in soil habitats, and many genera are well-studied and well-represented in culture collections [*Janssen*, 2006]. Actinobacteria are known to produce a wide range of secondary metabolites, including volatiles, and actinomycetes are the predominant source of microbial-derived therapeutic antibiotics, antifungals, and other bioactive compounds [*Berdy*, 2005; *Hopwood*, 2007]. The distribution of secondary metabolites between closely related actinomycetes reveals a strong correlation with phylogeny, suggesting that these compounds represent cohesive ecological traits [*Doroghazi et al.*, 2014; *Jensen et al.*, 2007; *Ziemert et al.*, 2014]. However, it remains unclear if the types and amounts of mVOCs produced by actinobacteria are predictable from actinobacterial phylogeny. Resolving this knowledge gap is important for building a comprehensive understanding of mVOC production and for ultimately identifying how distinct lineages of bacteria differ with respect to their capacity to produce distinct VOCs.

Here, we assembled a culture collection of taxonomically diverse soil and airborne dust-associated actinobacteria. We surveyed the diversity of VOCs produced by each of these strains *in vitro*. We then asked if more closely related strains had similar VOC emission profiles. Finally, we explored the functional potential of these VOCs by determining the effect of the actinobacterial VOCs on growth rates of both pathogenic and non-pathogenic pseudomonad test

strains. Together, these results expand our understanding of actinobacterial VOC diversity and strengthen our knowledge of how microbial interactions can be mediated by mVOC production, information that could ultimately inform the development of strategies to control soil-borne pathogens.

2. Methods and Materials

2.1 Actinobacterial strain isolation

The actinobacterial strains used in this study were obtained from various culture collections (see Table S1). *Streptomyces* sp. ms115, *Streptomyces* sp. or3, *Streptomyces* sp. t99, and *Streptomyces* sp. wa1063 were isolated from grassland soils across the United States as previously described [*Andam et al.*, 2016; *Choudoir et al.*, 2016]. Type strains *Streptomyces anulatus* B2000, *S. atratus* B16727, *S. aureus* B2808, *S. bikiniensis* B2690, and *S. grisues* B2682 were obtained from the Agricultural Research Service (NRRL) culture collection (https://nrrl.ncaur.usda.gov/). The remaining strains were isolated at the University of Colorado, Boulder between 2016–2017. Briefly, soil and airborne dust samples were plated onto solid media and incubated at 25 ˚C for approximately 3 weeks. Actinobacterial colonies were transferred from the enrichment plates into Axygen® 2 mL 96-deep well plates (Corning Life Sciences, Tewksbury, MA, USA) containing liquid media and incubated at 25 ˚C for 6–9 weeks. Strains were streaked for final isolation on solid media (see Table S1 for additional isolation information and Table S2 for media recipes). Prior to the experiment, strain purity was verified through multiple rounds of streaking for isolation on ISP2 agar.

2.2 16S rRNA gene sequencing and phylogenetic analyses

Full length 16S rRNA gene sequences were obtained from public sequence databases when available. For all remaining strains, SSU rRNA gene sequences were amplified with primers 27F (GTGCTGCAGAGAGTTTGATCCTGGCTCAG) and 1492R (CACGGATCCTACGGGTACCTTGTTACGACTT) [*Munson et al.*, 2004] with the following 24 µl PCR reaction: 12.5 µl GoTaq® Hot Start Master Mix (Promega, Madison, WI, USA), 10.5 µl H$_2$O, 0.5 µl forward primer from 10 mM stock, 0.5 µl reverse primer from 10 mM stock, and direct-from-colony template. The following thermocycler conditions were used: 98 ˚C for 10 min, 35 cycles of 94 ˚C for 1 min, 55 ˚C for 1 min, 72 ˚C for 2 min, and 72 ˚C for 10 min followed by a short-term hold at 4 ˚C. Genewiz (South Plainfield, NJ, USA) generated Sanger sequences from the amplicon using sequencing primer 27F. Automatic base calling and quality control of trace files was performed using Phred [*Ewing and Green*, 1998]. Taxonomy was determined using the Ribosomal Database Project classifier [*Ewing and Green*, 1998; *Wang et al.*, 2007] trained on Greengenes 13_8 16S rRNA database [*McDonald et al.*, 2012]. See Supplementary Data for the actinobacterial 16S rRNA gene sequences.

Phylogenetic relationships were determined from partial 16S rRNA gene sequences. 16S rRNA sequences were aligned using MAFFT [*Katoh and Standley*, 2013], and poorly aligned regions were removed with trimAL [*Capella-Gutierrez et al.*, 2009], resulting in an aligned nucleotide fragment of 682 bp. A maximum likelihood (ML) tree was constructed using the generalized time reversible nucleotide substitution model [*Tavare*, 1986] with gamma distributed rate heterogeneity among sites (GTRGAMMA) in RAxML v7.3.0 [*Stamatakis*, 2006]. Bootstrap support was determined from 100 inferences using the RAxML rapid bootstrapping algorithm

[*Stamatakis et al.*, 2008]. The tree was rooted with *Bifidobacterium bifidium* JCM 1255 and *Bifidobacterium breve* KSS01.

2.3 Volatile organic compound (VOC) collection and sampling

VOCs produced by the actinobacterial strains were characterized using a dynamic flux chamber system with a custom sampling manifold and VOC preconcentration inlet system [*Rossabi et al.*, 2018]. As previous studies have shown that media type influences the types of VOCs produced by microbes *in vitro* [*Kuntzel et al.*, 2016; *Tait et al.*, 2014], we evaluated VOC emission profiles on two different media types: a complex rich media (ISP2) and a minimal sporulation media (glycerol arginine, GA) (Table S2). More strains were able to grow on ISP2 than on GA (46 and 30 strains, respectively), and VOC profiles were only quantified for strains that grew readily on a given media type (Fig. S1, Table S3). Strains were plated onto triplicate 60 mm petri plates with both ISP2 and GA agar media types and incubated at 30 ˚C for 12–13 d, which resulted in a heavy lawn of growth coating the entire plate. Triplicate plates were placed in 475 mL glass jars and maintained at 23 ˚C throughout the VOC sampling as described below.

For VOC analyses, the jars containing the culture plates were connected to a dynamic flow-through through system with zero air flowed through the jars at 140 mL min^{-1}. Zero air was generated by passing compressed air through a custom zero air generator, which oxidizes hydrocarbons to CO_2. Samples were collected after culture plates had been exposed to the zero air flow for between 10 min and 8 hours. Of note, there may be a dependency of the intensity of VOC emission peaks on the flushing time. Because of this uncertainty, results are presented in a solely qualitative manner. For VOC analyses, a fraction of the exhaust purge flow was collected

at a rate of 50 mL min^{-1} for 40 min, resulting in a 2 L sample volume. Samples were first drawn

through a Peltier-cooled (-20 $°$C) trap to remove water vapor by freezeout from the sample

stream. Next, VOCs were collected on a cooled (-30 $°$C) micro-adsorbent trap that contained 25

mg of Carboxen 1016 and 220 mg Carboxen 1000 solid adsorbent (Sigma Aldrich, St. Louis,

MO, USA). After sample collection, VOCs were mobilized by rapidly heating the trap to 290 $°$C

for injection onto the gas chromatography (GC) column. A Hewlett Packard 5890 Gas

Chromatograph/Flame Ionization Detector/Agilent 5971 Mass Spectrometer (GC/FID/MS)

instrument (Agilent Technologies, Boulder, CO, USA) was used. Separation was achieved with a

0.32 mm ID x 60 m length, 5 $\Box$m film thickness DB-624 (Agilent Technologies, Boulder, CO,

USA) capillary column. The GC oven temperature program had the following steps: 40 $^°$C for 10

min, 8 $^°$C min^{-1} to 250 $^°$C, followed by 250 $^°$C for 15 min. The column flow was split to direct

approximately 1.5 mL min^{-1} of the column flow to the MS for compound identification and the

remainder to the FID for compound quantification. Additional details on the instrument setup

and sample collection are provided in Rossabi *et al*. [2018].

2.4 Volatile organic compound (VOC) identification

VOCs were identified using retention index data and by comparing their spectra to the

National Institute of Standards and Technology (NIST) spectral library (version 2.2; June 10,

2014; Gaithersburg, MD, USA) using Agilent Chemstation software version F.01.03.2357.

Linear programmed retention indices [*van Den Dool and Dec. Kratz*, 1963] were calculated

based on retention times of n-alkanes that were observed in standard runs. Mass spectra were

found by averaging approximately five scans at the peak maximum, subtracting an averaged

background signal, and searching for matching spectra in the library. Based on compounds

present in the NPL standard, a VOC had to be present at mixing ratios of approximately 100 ppt to give a large enough signal within the 2 L samples for structural peak identification. Because of the approximately seven times greater sensitivity of the FID detector compared to the MS, more VOCs are reported for the profile analyses (see below) that are based on the FID detection than what could be structurally identified by the MS analyses. Two identified compounds co-eluted at the same retention time of 31.1 min, 3-methyl-2-pentanone and dimethyldisulfide. For the quantitative VOC profile analyses (see below), these were treated as a single compound but were treated as distinct compounds for qualitative descriptions.

2.5 Volatile organic compound (VOC) profile analyses

All actinobacterial VOC profile analyses were performed using presence/absence criterion. Only compounds with retention times between 18.7–40 min and FID peak areas of >5000 mVs were included. This peak area threshold corresponds to VOC mixing ratios of approximately 15 ppt. A compound was considered distinct based on its retention time, rounded to the nearest tenth decimal place. Finally, we removed VOCs that were consistently emitted by sterile media samples (i.e. 'media blanks,' or VOCs released from the media by abiotic processes), which included acetaldehyde, acetone, 2-methylpropanal, 2-butanone, 3-methylbutanal, and 2-methylbutanal. To note, we detected a number of compounds in the ISP2 media blanks that were not detected the GA media blanks (including acetonitrile), and while these compounds were included in the GA media VOC profile analyses, we acknowledge that these could represent sterile media emissions (see Table S3).

Differences in VOC emission profiles between strains were visualized using nonmetric multidimensional scaling (NMDS) of Jaccard dissimilarities. Strains that did not produce any detectable VOCs were removed to minimize distance in the matrix. We used permutational analysis of variance (ANOVA) implemented with the R package 'vegan' [*Oksanen et al.*, 2017] to test for differences in VOC profiles between strains and growth conditions, and statistical significance was evaluated following 999 permutations. We used the R package 'ade4' [*Dray and Dufour*, 2007] to perform Mantel tests to determine the relationship between pairwise 16S rRNA gene sequence distances and VOC profile Jaccard dissimilarities, with statistical significance evaluated following 999 permutations.

2.6 Pseudomonad growth assay

We investigated the ecological relevance and functional potential of these mVOCs by evaluating differences in growth rates of two test pseudomonad strains in the presence of actinobacterial VOCs. These pseudomonads were chosen as they are plant colonizing rhizobacteria that are considered either plant growth-promoting (*Pseudomonas fluorescens* SBW25, [*Naseby et al.*, 2001]) or phytopathogenic (*Pseudomonas syringae* pv. tomato DC3000, [*Preston*, 2000]). We randomly subsampled actinobacterial strains for this assay and further restricted our analyses to those strains that grew readily on ISP2, and these 24 actinobacterial strains (see Table S1) were plated onto ISP2 agar and incubated at 30 ˚C for 12–14 d. Cells were harvested by washing plates with 0.1% TWEEN® 20 (Sigma Aldrich, St. Louis, MO, USA), centrifuging at 12 000 g for 5 min, and suspending cell pellets in 1 mL 0.1X PBS. 20 µl of cell suspension were transferred into the wells of a Nunc™ MicroWell™ 96-well microplate (Thermo Fisher Scientific, Waltham, MA, USA) containing 300 µL of ISP2 agar (32 replicate

wells; A1–A8, C1–C8, E1–E8, and G1–G8). Culture plates were incubated at 30 ˚C for 5 d to ensure VOC production.

Pseudomonad strains were grown overnight at 30 ˚C with shaking (180 rpm) in King's B media (Table S2). Overnight cultures were diluted into fresh media to an optical density (OD 600 nm) of 0.05, and 250 µl of diluted pseudomonad cultures were transferred to the culture plate containing the actinobacterial cultures (8 replicate wells per strain; B1–B8 for *P. fluorescens* SBW25 and D1–D8 for *P. syringae* pv. tomato DC3000). Thus, the pseudomonad cultures were exposed to actinobacterial volatiles that diffused across the shared headspace of the culture plate throughout the growth assay. Growth rates of pseudomonad test strains were measured using a Synergy HT microplate reader (BioTek, Winnoski, VT, USA) at 24 ˚C with slow, continuous shaking. Absorbance at 630 nm was measured every 20 min for a total of 980 min. The absorbance values of sterile King's B media (i.e. 'media blanks') were subtracted from each measurement.

Growth rates were determined using the R package 'Growthcurver' [*Sprouffske and Wagner*, 2016]. We asked whether the mean growth rate of pseudomonad strains (averaged across the eight replicates per growth curve) exposed to the volatiles from each actinobacterial strain differed from the mean growth rate of pseudomonad test strains in the presence of sterile ISP2 media blanks (t-test without p-value adjustment). For each growth curve, we excluded replicates with poor fit to the logistic curve and also excluded outliers with sigma values ≤0.08 (see Growthcurver documentation), which resulted in removing strain FLCC682 from *P. fluorescens* SBW25 analyses. Mean pseudomonad control growth rates (i.e. ISP2 media blanks) were averaged across independent growth curve experiments, and growth rates were equivalent across biological replicates (t-test, $P > 0.05$). We randomly choose two actinobacterial strains

(FLCC45 and FLCC517) for independent validation of this method, and mean pseudomonad growth rates across biological replicates were equivalent (t-test, $P > 0.05$). Finally, we used the R package 'UpSetR' [*Conway et al.*, 2017] to identify and visualize collections of VOCs correlated with inhibition or stimulation of pseudomonad growth.

3. Results

3.1 Actinobacterial volatile organic compound (VOC) emission profiles

We assembled a set of 48 phylogenetically diverse soil and airborne dust-associated actinobacterial strains that represented 14 taxonomic families within the Actinobacteria phylum (Fig. 1, Table S1). We used the GC/MS method to survey the chemical diversity of VOCs produced by these strains grown on different media types, glycerol arginine (GA) agar – a minimal sporulation media – and ISP2 agar – a complex rich media (Table S2). Not all strains grew well on both media types, so we measured VOC production for 46 strains on ISP2 and for 34 strains on GA.
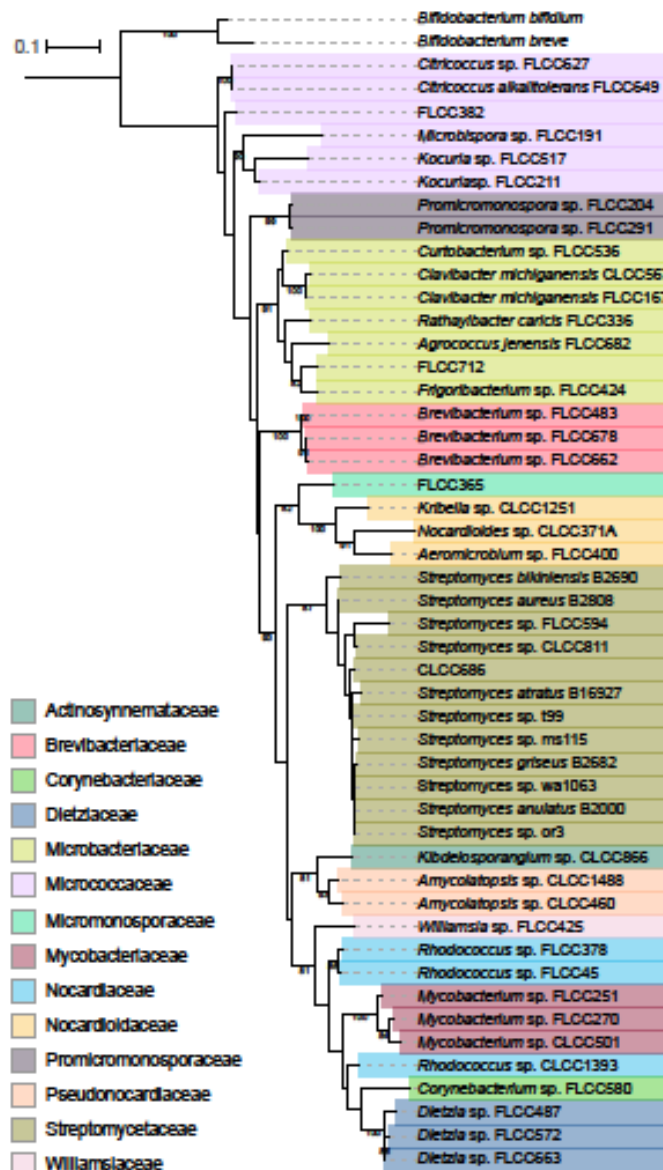
Figure 1. We surveyed VOCs produced by 48 soil and air-borne dust associated actinobacterial strains, and the tree depicts the phylogenetic relationships of all strains included in this study. The phylogeny was constructed from nucleotide alignments of partial 16S rRNA gene sequences using maximum likelihood and a GTRGAMMA model of evolution. Scale bar indicates nucleotide substitutions per site. Nodes with bootstrap support values ≥70 are labeled. The tree was rooted with *Bifidobacterium* strains *Bifidobacterium bifidium* JCM 1255 and *Bifidobacterium breve* KSS01. Strain names reflect their isolation conditions and culture collection of origin (Table S1). Strains are colored by their taxonomic assignment at the family level according to the legend, and taxonomic assignments at the genus and species level are included when available. The family Nocardiaceae is not monophyletic.

We detected a total of 126 distinct VOCs across all samples (Fig. 2a), with 92 compounds detected on GA media and 108 compounds detected on ISP2 media (Fig. 2b). 74 compounds were detected on both media types, while 34 VOCs were ISP2-specific and 18 VOCs were GA-specific (Fig. 2b). Of these, we were able to verify the chemical structure of 28 compounds based on their mass spectra (see Materials and Methods) (Fig. 2a, Table S4). 31% of these compounds were alcohols, 31% were ketones, and the remaining VOCs were esters or nitrogen- or sulfur-containing compounds (Table 1). We identified over 90% of the most abundant VOCs (i.e. VOCs detected in $\geq$24 samples), and these included 3-methyl-1-butanol (n=33 samples), 2-methyl-2-propanol (n=32 samples), 2-methyl-1-butanol (n=30 samples), 2-methyl-1-propanol and 2-pentanone (n=29 samples), and 3-methyl-2-pentanone/dimethyldisulfide (n=28 samples) (Fig. 2a). Conversely, over 77% of volatile compounds detected could not be identified, mostly because of the low signal intensity in their mass spectra, and many of these unidentified compounds were detected in few samples and produced by only a subset of the actinobacterial strains (Fig. 2). Importantly, our ability to detect and identify the VOCs are limited by the specific analytical methods used here. The methods were not able to detect all types of VOCs such as methane or highly polar VOCs with multi-functional groups. Thus, the detected VOCs likely represented an undetermined fraction of the total VOCs emitted from these samples.
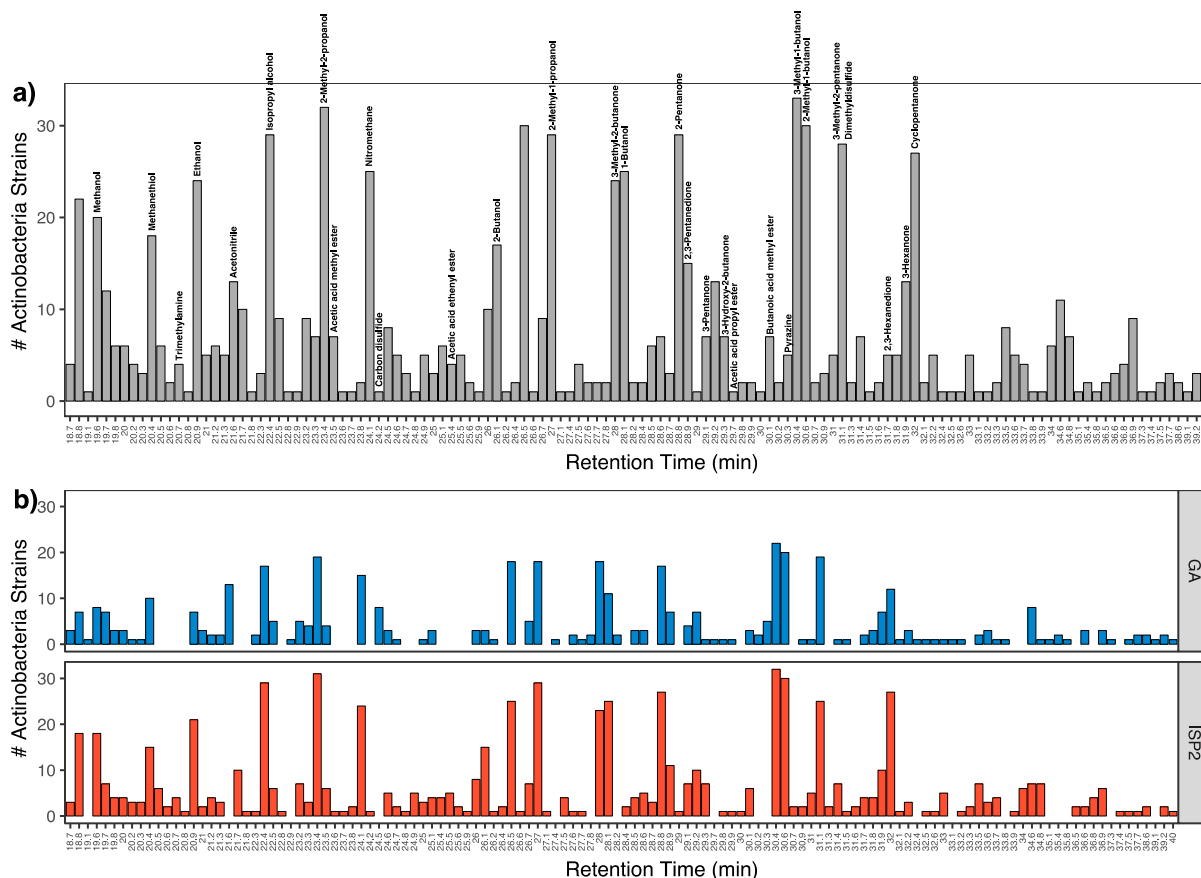
Figure 2. We identified a total of 126 VOCs (Table S3) produced by 48 actinobacterial strains. Distinct volatiles are ordered by their retention times and approximately by increasing molecule size. Bars show the total number of actinobacterial strains that produced each VOC (2a) and the total number of strains that produced each VOC on glycerol arginine (GA) media and on ISP2 media (2b). The 28 compounds identified from their mass spectra are labeled with text (2a) (see Materials and Methods, Table S4). To note, two identified compounds co-eluted at the same retention time of 31.1 min, 3-methyl-2-pentanone and dimethyldisulfide.

The number and types of VOCs emitted varied between strains. We detected 0–36 total distinct VOCs per strain, and in general, the number of VOCs produced differed between media types (Fig. S1, Table S3). Two strains, FLCC378 and FLCC662, produced no VOCs above our level of detection or what was emitted from the sterile media blanks. Most VOCs were produced by very few strains such that 24.6% of total VOCs were strain-specific and only 11 VOCs were produced by more than 50% of strains (Fig. S2a). This right-skewed frequency distribution was consistently observed for VOCs produced on GA and ISP2 media (Fig. S2b). Each

197

actinobacterial strain produced a unique combination of VOCs (Table S3). Actinobacterial VOC profiles differed between ISP2 and GA media samples (PERMANOVA; $R^2 = 0.025$, $P = 0.04$) (Fig. S3a), indicating that strains produced different VOCs when grown on different media types. Despite this effect of media type on VOC profiles, strain-level differences explained far more of the variation in VOC profiles (PERMANOVA; $R^2 = 0.82$, $P = 0.001$) (Fig. S3b). Namely, the strain-level variation in VOC profiles exceeded the variation in VOC profiles observed across the two media types.

3.2 Taxonomic and phylogenetic signal of volatile organic compound (VOC) production

Next, we determined if the strain-level variation in actinobacterial VOC emissions were predictable from taxonomic or phylogenetic differences between the strains. Indeed, we found that more closely related strains shared similar patterns of VOC production (Fig. 3). First, we asked if the number of distinct VOCs varied between strains and across taxonomic groups. We observed a taxonomic signal in the number of unique VOCs produced, and the number of total VOCs per strain varied across the taxonomic families (ANOVA; $F_{13,34}=5.7$, $P < 0.001$). For example, strains within the family Streptomycetaceae produced more distinct VOCs per strain than the families Brevibacteriaceae, Dietziaceae, Micrococcaceae, Mycobacteriaceae, and Nocardiaceae (post-hoc Tukey's test, $P < 0.01$).
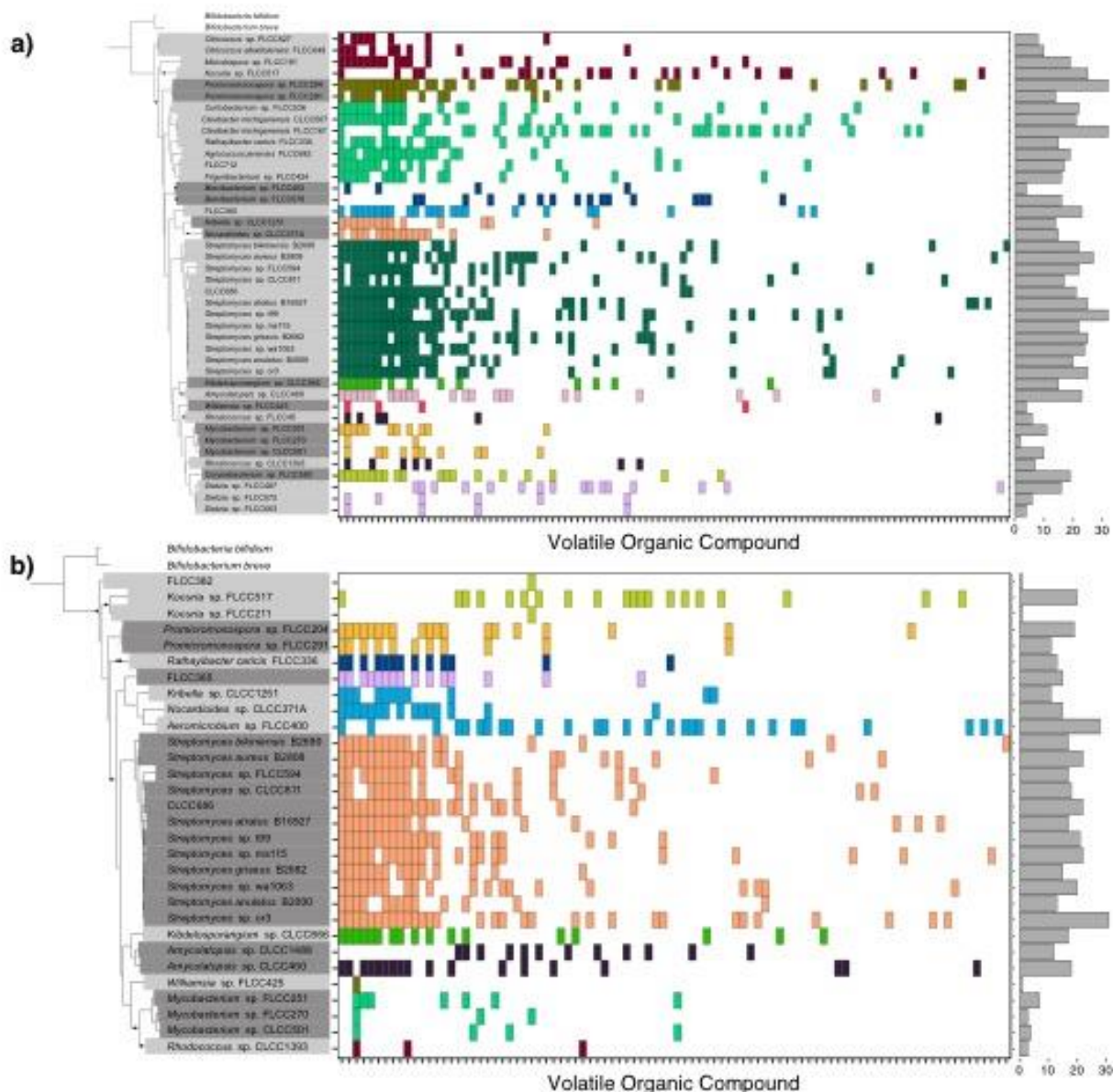
Figure 3. Closely related actinobacterial strains produced similar VOC profiles. In the left panel, trees reflect the phylogenetic relationships of 16S rRNA gene sequences between actinobacterial strains (see Fig. 1). The 6 and 18 strains that did not grow or produced no detectable mVOCs on ISP2 and glycerol arginine (GA) media, respectively, were trimmed from the phylogeny. Deleted leaves and nodes in the resulting tree are indicated by black circles. In the center panel, the colored boxes along the x-axis depict distinct volatiles produced by strains grown on ISP2 (3a) and GA media (3b). Volatiles are ordered by the number of strains that produced each compound. Boxes of the same color are VOCs produced by strains sharing the same taxonomic assignment at the family level. In the right panel, bars show the total number of VOCs produced by each strain on each media type.

199

Next, we asked if VOC emission profiles varied depending on the taxonomic identity of the strains or their phylogenetic relationships. In other words, did more closely related strains emit more similar types of VOCs? Strain-level VOC profiles varied depending on taxonomy at the family-level classification (PERMANOVA; $R^2 = 0.34$, $P = 0.001$), and this variation was consistently observed for strains grown on GA media (PERMANOVA; $R^2 = 0.52$, $P = 0.001$) and on ISP2 media (PERMANOVA; $R^2 = 0.43$, $P = 0.002$) (Fig. S3b-d). For example, the two strains within the family Promicromonosporaceae consistently emitted an unknown VOC (retention time 32.5 min) across both media types, and this VOC was not emitted from other actinobacterial strains outside this family. Hence, there were specific VOCs that were emitted exclusively across strains within the same taxonomic group (Fig. 3). We also observed a phylogenetic signal in VOC production such that strains which were more closely related (estimated from their 16S rRNA gene sequences) also had more similar VOC profiles on both ISP2 (Mantel r = 0.22, $P = 0.005$) and GA (Mantel r = 0.37, $P = 0.001$) media (Fig. S4).

Despite an overall strong taxonomic and phylogenetic signal, an appreciable number of VOCs were produced by distantly related strains. All taxonomic families shared at least one VOC with strains from a different family (Fig. 3). For example, while the family Streptomycetaceae had the largest collection of family-specific VOCs (21 unique VOCs on ISP and 24 unique VOCs on GA), strains within this family also shared 19 VOCs across taxonomic groups on ISP2 media and 38 VOCs across taxonomic groups on GA media (Fig. 3).

3.3 Effect of volatiles on pseudomonad growth

Finally, we asked if volatiles produced by actinobacteria influenced the growth of pseudomonad test strains *P. fluorescens* SBW25 and *P. syringae* pv. tomato DC3000. To answer this question, we designed an assay that exposed pseudomonad test strains throughout the course of a growth curve to the volatiles emitted by 24 actinobacterial strains and measured differences in growth rates as compared to growth rates of the pseudomonads exposed to sterile media blanks (see Materials and Methods and Fig. S5).

Actinobacterial volatiles correlated with both stimulatory and inhibitory effects on pseudomonad growth rates. For *P. fluorescens* SBW25, nine strains were associated with a significant decrease in growth rate, while three strains were associated with a significant increase in growth rate (Fig. 4). For *P. syringae* pv. tomato DC3000, two strains were associated with a significant decrease in growth rate, while eight strains were associated with a significant increase in growth rate (Fig. 4). In some cases, the magnitude of growth effects was quite large. For example, exposure to the volatiles of strain FLCC712 correlated with a 52% reduction in growth of *P. fluorescens* SBW25 compared to that of the media blank. Conversely, exposure to the VOCs of strain FLCC291 correlated in a growth rate for *P. syringae* pv. tomato DC3000 that was 135% greater than that of the media blank.
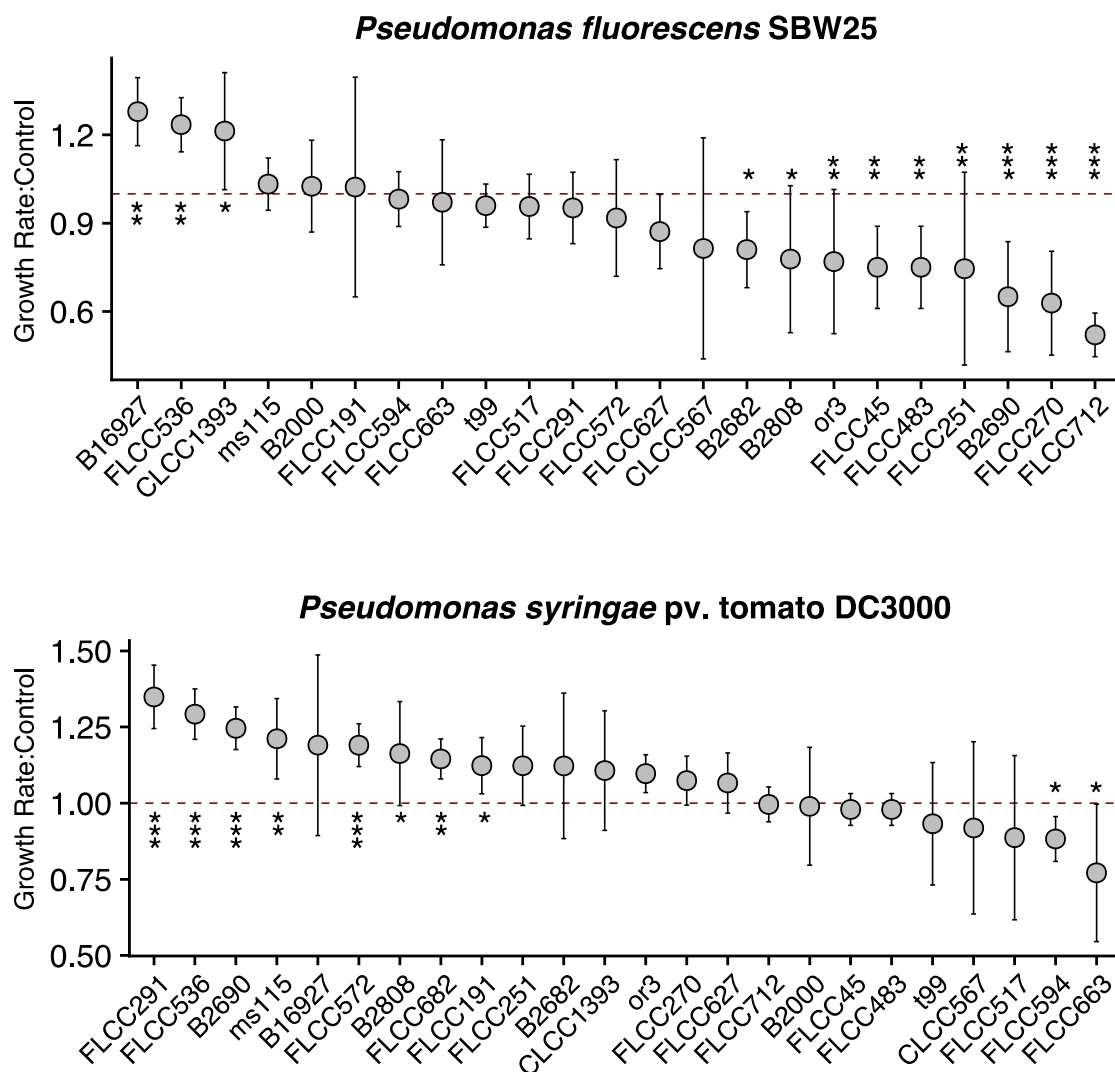
Figure 4. Actinobacterial VOCs correlate with effects on growth rates of pseudomonad test strains. Non-pathogenic *Pseudomonas fluorescens* SBW25 (top) and pathogenic *Pseudomonas syringae* pv. tomato DC3000 (bottom) were exposed to actinobacterial VOCs throughout exponential growth (see Materials and Methods, Fig. S5). Circles show the mean ratio of pseudomonad growth rates in the presence of actinobacterial VOCs (strain names are included on x-axis) to pseudomonad growth rates in the presence of sterile media blanks (i.e. control), and error bars show the standard deviations. If the growth rate ratio to control, or 'Growth Rate:Control' equals one (i.e. dashed red line), this indicates no difference in growth rate to that of the control, values greater than one indicate growth stimulation, and values less than one indicate growth inhibition. Pseudomonad growth rates that were significantly different from controls are marked with asterisks (t-test without p-value adjustment, P < 0.05*, 0.01**, 0.001***).

We were able to identify discrete actinobacterial VOCs that were associated with inhibitory or stimulatory growth effects of pseudomonads (Fig. 5). 56 and 39 compounds

comprised the total collection of VOCs produced by actinobacterial strains that associated with inhibited or stimulated, respectively, growth of *P. fluorescens* SB525. 26 and 54 compounds comprised the total collection of VOCs that associated with inhibited or stimulated, respectively, growth of *P. syringae* pv. tomato DC3000 (Fig. 5). There were nine and five discrete VOCs that were exclusively correlated with growth rate inhibition of *P. fluorescens* SB525 and *P. syringae* pv. tomato DC3000, respectively (Fig. 5). For instance, butanoic acid methyl ester was associated with inhibition of *P. syringae* pv. tomato DC3000. There were four and three discrete VOCs that were exclusively correlated with growth rate stimulation of *P. fluorescens* SB525 and *P. syringae* pv. tomato DC3000, respectively, and a shared set of seven discrete VOCs that correlated to stimulated growth of both pseudomonads, including 3-hydroxy-2-butanone (Fig. 5). However, besides the two VOCs mentioned above, the chemical identities of most these compounds could not be determined.
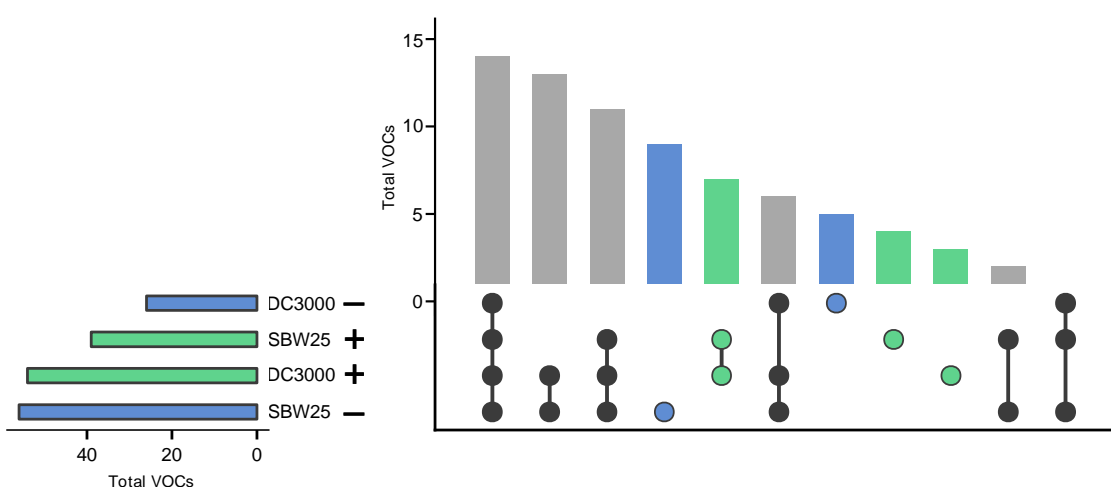

Figure 5. Sets of actinobacterial VOCs were associated with effects on growth rates of pseudomonad test strains. The left panel shows the total number of distinct VOCs from all actinobacterial strains associated with growth inhibition (blue, –) or stimulation (green, +) of non-pathogenic *Pseudomonas fluorescens* SBW25 (SBW25) and

pathogenic *Pseudomonas syringae* pv. tomato DC3000 (DC3000). The right panel bars and matrix show the collection of discrete VOCs that were unique to pseudomonad strain-specific growth stimulation or inhibition. Blue circles depict collections of VOCs that were exclusive to growth inhibition, and green circles depict collections of VOCs that were exclusive to growth stimulation. Black circles depict collections of VOCs that were associated with both growth stimulation and inhibition.

4. Discussion

Soil microbes are a rich source of metabolites, including some that are VOCs. These microbially-produced VOCs – or mVOCs – have long been of interest given their potential to serve as carbon and nutrient sources [*Owen et al.*, 2007; *Ramirez et al.*, 2010] or to act as signaling molecules that mediate a multitude of biotic interactions [*Penuelas et al.*, 2014; *Schulz-Bohm et al.*, 2017]. Despite a large catalogue of mVOCs [*Lemfack et al.*, 2018; *Lemfack et al.*, 2014], the majority of mVOCs remain uncharacterized in terms of both their chemical structure and activity. Furthermore, we lack a comprehensive understanding of the evolutionary and ecological processes that generate and maintain this vast mVOC diversity in soil ecosystems.

Given these knowledge gaps, we sought to understand the diversity of VOCs produced by bacteria within the phylum Actinobacteria viewed through a phylogenetic and functional lens. We used GS/MS to survey the volatile compounds produced by 48 actinobacterial strains isolated from soil and airborne dust (Fig. 2, Table S1). The assembled actinobacterial culture collection included strains from 14 different families (Fig. 1) and well represents the overall taxonomic diversity within the phylum Actinobacteria [*Ludwig et al.*, 2015]. We further investigated the role of theses volatiles in microbe-microbe interactions by looking at the effect of actinobacterial VOCs on pseudomonad growth (Fig. 4).

From these 48 strains, we detected a total of 126 distinct compounds which ranged in carbon content from about C_3–C_{10} and with each strain producing 0–36 VOCs (Fig. 2, Fig. S1).

We were able to structurally identify approximately 22% of these compounds, which spanned broad chemical classes including alcohols, esters, ketones, and nitrogen- or sulfur-containing compounds (Table 1, Table S4). Previous studies have also detected diverse collections of microbially-produced VOCs, and in particular, the types of volatiles detected here are routinely identified in mVOC surveys of microbial soil communities and of soil-derived microbial isolates (see [*Insam and Seewald*, 2010; *Penuelas et al.*, 2014] and references therein). Similar to our study, previous studies of microbial volatiles surveyed using GC/MS approaches also reported a high percentage of unknown mVOCs [*Kai et al.*, 2007; *Leff and Fierer*, 2008; *Stahl and Parkin*, 1996], suggesting a need for improved VOC analytical capabilities for identification of polar and multi-functional volatiles.

Many of the abundant compounds identified here are likely the byproducts of primary metabolic pathways, which are generally conserved at the phylum level. For example, alcohols 3-methyl-1-butanol, 2-methyl-1-butanol, 2-methyl-1-propanol, and 1-butanol were some of the most abundant VOCs detected here (Fig. 2, Table 1), and these were also among the most abundant compounds detected in other actinomycetes [*Scholler et al.*, 2002]. Alcohols are often generated through amino acid metabolism [*Schmidt et al.*, 2015], and 3-methyl-1-butanol is a known by-product of leucine catabolism [*Filipiak et al.*, 2012]. We also identified a number of branched ketones, including 3-methyl-2-butanone, 3-pentanone, and 3-methyl-2-pentanone, and cyco-pentanone (Fig. 2, Table 1), which are characteristic of actinomycetes [*Wilkins*, 1996]. In addition, dimethyl disulfide (DMDS) is commonly produced by diverse actinobacterial species (Fig. 2, Table 1) [*Scholler et al.*, 2002; *Wilkins*, 1996], and DMDS has been shown to display antimicrobial and pesticidal properties [*Tyc et al.*, 2017] and to also inhibit quorum-sensing [*Chernin et al.*, 2011].

205

Table 1. Of the 126 distinct volatile organic compounds (VOCs) detected, we were able to identify the chemical structures of 28 compounds which can be categorized into five broad chemical classes. Asterisks indicate compounds detected in the ISP2 media blanks but not the GA media blanks.

Class

Alcohol	Ester	Ketone	Nitrogen-containing	Sulfur-containing
Methanol	Acetic acid methyl ester	3-Methyl-2-butanone	Trimethylamine	Methanethiol
Ethanol	Acetic acid ethenyl ester	2-Pentanone	Nitromethane	Carbon disulfide
Isopropyl alcohol	Acetic acid propyl ester	3-Pentanone	Pyrazine*	Dimethyl-disulfide
2-Methyl-2-propanol	Butanoic acid methyl ester	2,3-Pentanedione	Acetonitrile*	
2-Methyl-1-propanol		3-Methyl-2-pentanone		
1-Butanol		3-Hydroxy-2-butanone		
2-Butanol		2,3-Hexanedione		
3-Methyl-1-butanol		3-Hexanone		
2-Methyl-1-butanol		Cyclo-pentanone		

Each strain produced a unique combination of VOCs (Fig. 3, Table S3). While strain-level variation explains most of the variation in VOC profiles, we also observed a media effect (Fig. S1, Fig. S3), and this is consistent with previous studies that have also shown that differences in growth media can influence the types of VOCs produced by individual strains *in vitro* [*Kuntzel et al.*, 2016; *Tait et al.*, 2014]. Indeed, there are various factors that may influence the types and amounts of VOCs produced, including, but not limited to, nutrient conditions, underlying genomic variation, microbial growth phase and cell morphology, and proximity to other species. For instance, the metabolite profiles of *Streptomyces coelicolor* differ between co-cultures with other actinomycetes [*Traxler et al.*, 2013]. Thus, the VOCs identified here likely represent a fraction of a broader chemical potential of these isolates, and we would expect to detect different VOCs under varying abiotic as well as biotic conditions. These 'cryptic' metabolites highlight a major challenge in the world of microbial natural product discovery [*Baltz*, 2008; *Lim et al.*, 2012a; *Ochi and Hosaka*, 2013]. However, recent advances in computational methods that enable 'genome mining' of cryptic metabolites have created a paradigm shift in microbial natural product discovery pipelines [*Medema and Fischbach*, 2015; *Weber et al.*, 2015].

We observed a taxonomic and phylogenetic signal for mVOCs such that more closely related actinobacterial strains had more similar VOC emission profiles (Fig. 3, Fig. S3, Fig. S4). As discussed previously, many of the abundant mVOCs detected are likely associated with central metabolism and thus represent evolutionary cohesive traits conserved across broader taxonomic classifications. However, most of the VOCs were strain-specific (Fig. S2), a pattern that was also observed for mVOCs [*Kai et al.*, 2007] and for secondary metabolite gene clusters [*Choudoir et al.*, 2018]. Of note, *Streptomyces* produce, on average, the greatest number of

207

distinct VOCs per strain (22–34 VOCs) (Fig. 3), and this aligns with other studies that identified 14–42 VOCs emitted per streptomycete [*Scholler et al.*, 2002]. Within the phylum Actinobacteria, the genus *Streptomyces* are known for their prolific production of secondary metabolites and natural products [*Watve et al.*, 2001], and correspondingly, it is unsurprising that *Streptomyces* also produced the most unique VOC profiles here. These results suggest that mVOCs can act as dynamic agents of evolutionary and ecological processes shaping finer scales of diversity [*Doroghazi et al.*, 2014; *Jensen et al.*, 2007; *Ziemert et al.*, 2014]. Indeed, variation in mVOC production is a promising diagnostic tool for strain-level microbial identification [*Bos et al.*, 2013; *Filipiak et al.*, 2012].

Given the chemical diversity of mVOCs detected in our survey, we proposed that these compounds also possessed a broad functional diversity. In particular, there is some evidence that actinobacterial mVOCs may be responsible for pathogen control in disease suppressive soils [*Cordovez et al.*, 2015; *van der Voort et al.*, 2016]. Along these lines, we tested the influence of these mVOCs on the growth of two pseudomonad test strains – *Pseudomonas fluorescens* SBW25, a plant growth-promoting symbiont [*Naseby et al.*, 2001], and *Pseudomonas syringae* pv. tomato DC300, the causative agent of bacterial speck of tomato [*Preston*, 2000]. We found that actinobacterial VOCs correlated with both stimulatory and inhibitory effects on the growth rates of pseudomonad test strains, and in some instances, these effects were quite large (Fig. 4). While we focused on maximum growth rate, it is also possible that actinobacterial volatiles could impact additional pseudomonad growth characteristics, such as increased lag time to exponential phase. From these assays, we were able to identify a collection of nine and five mVOCs that were exclusively associated with growth inhibition of *P. fluorescens* SBW25 and *P. syringae* pv. tomato DC300, respectively (Fig. 5). Of particular interest, butanoic acid methyl ester correlated

with growth inhibition of the phytopathogenic pseudomonad, and this compound has been shown to exhibit antimicrobial activity against other microbial pathogens [*Huang et al.*, 2011; *Namkung et al.*, 2011]. Future work should focus on confirming the specific activity and identity of these actinobacterial VOCs demonstrated to correlate with altered pseudomonad growth rates. In addition, future work could aim to determine whether VOC-mediated differences in pseudomonad growth are the result of the synergistic effects of exposure to a combination of volatiles as opposed to exposure to individual compounds.

We surveyed the chemical VOC diversity of a collection of taxonomically diverse soil and airborne dust-associated actinobacterial strains. While we identified common VOCs that are likely byproducts of central metabolic pathways presumably shared by most Actinobacteria, we also observed a strong taxonomic and phylogenetic signal. A majority of the mVOCs in our collection were detected at low frequency and were of unknown identities. These data highlight the importance of viewing chemical diversity within a phylogenetic framework and emphasize that actinobacteria can produce a vast repertoire of uncharacterized microbial natural products. Finally, these VOCs impacted microbe-microbe interactions, and in particular, some VOCs were associated with growth inhibition of pseudomonad strains that have previously been shown to be important to plant health. This work may provide useful information for the future development of microbial-based solutions to pathogen control in agricultural ecosystems.

Funding

Acknowledgments

Chapter 8

Overall Conclusions from this Dissertation

O&NG production in the U.S. has surged since the turn of the century. Unconventional oil and natural gas drilling resulted in ~10–20-fold increases in shale O&NG production between 2000 and 2015 (www.eia.gov). Ground and airborne observations have consistently shown elevated levels of light NMHC as a result of venting, flaring, and leakage. Observed NMHC ambient mole fractions measured in O&NG basins exceed bottom-up estimates; background levels can be 100 times greater than the regional background [Helmig. et al., 2014; Karion et al., 2013; Pétron et al., 2012; Swarthout. et al., 2015; Thompson. et al., 2014]. These emissions have led to ozone nonattainment in the Uintah Basin, Utah, and Upper Green River Basin, Wyoming, O&NG regions [Oltmans et al., 2014; Schnell et al., 2009]. Increasing ethane mole fractions were measured in Baltimore, Maryland, downwind of the Marcellus Shale [Vinciguerra et al., 2015], and in southern Texas as a result of transport from the Eagle Ford Shale [Schade and Roest, 2015].

Chapter 2 shows ethane rates of change are highest at the central and eastern USA and nearby downwind sites, suggesting that the ethane increase is driven to a large part by emissions from North America. The regional hotspot of increasing NMHC levels can be pinpointed more narrowly from propane observations. Propane, with a lifetime 1/4 of ethane, is a more sensitive indicator for local/regional emissions. Propane data show the greatest increases in the central and eastern USA, and in the downwind North Atlantic region (Fig.3). In contrast, propane levels have been relatively stable in central Europe, the Pacific region, and the SH. Also, measurements

in the western USA do not show propane increases. With the primary synoptic transport direction being west and southwest to east, the spatial analyses of ethane and propane increases point to the central to eastern parts of the USA as the regions where most of the emission increases have occurred.

We estimate for an ethane annual emission increase of 0.42 ± 0.19 Tg yr^{-1}, resulting in an overall 2.1 ± 1.0 Tg yr^{-1} emission increase during 2009.5–2014.5. This additional emission is 1.5 times the North America inventory estimate of 1.6 Tg yr^{-1} for 2007. Considering estimates of co-emitted NMHC yields an estimate for a yearly total NMHC emissions increase of 1.2 ± 0.8 Tg yr−1 (5.9 ± 4.0 Tg yr−1 overall emissions increase during 2009.5–2014.5). This added NMHC emission is expected to fuel additional surface ozone production in source and downwind regions, and potentially offset emission controls that have been implemented for curbing photochemical ozone production, and therefore can be a concern for attaining the ozone air quality standard.

While enhanced ethane emissions were observed as a result of O&NG development, it is unclear what effect O&NG emissions are having on isomeric ratios of butanes and pentanes, especially in urban areas in the U.S. Butane and pentane isomeric ratios can be affected by several processes and emission sources, including changing gasoline formulations, increasing oil and gas emissions, decreasing emissions in general from mobile sources.

Trends in atmospheric mole fractions of butanes and pentanes, and their (i/n) isomeric ratios were highly variability among sites. A common feature was that average mixing ratios of the butane and pentane isomers have been decreasing at most, i.e. 81% of the sites, considered in this study. The exception was SGP, where all four isomers have been increasing (three have a statistically significant trend), most certainly due to increasing O&NG emissions. Similar to

individual species, a large range was observed for changes of the (i/n) butane and pentane isomeric ratio, however, all six statistically significant (i/n) butane trends, and all seven statistically significant (i/n) pentane trends were negative, indicating a relative increase in the prominence of the n-isomers.

The most obvious explanation for the observed declines in concentrations and in the (i/n) isomeric ratio are changes in emission strength and relative contribution from different emission sectors. In the last century, motor vehicle sources have dominated urban emissions of VOC [Parrish et al., 2009; Von Schneidemesser et al., 2010]. Studies of firn air in Greenland have demonstrated that regulations of emission sources have brought mixing ratios of VOC down from their highest levels in the 1970s [*Aydin et al.*, 2011; *Helmig. et al.*, 2014a; *Worton et al.*, 2012]. Data from our analyses support this previous research, as levels appear to be continuing their decline at most sites evaluated in this work.

The abundance of decreasing (i/n) pentane ratios, both at urban sites and in the GGGRN, suggests influences on pentane emissions on wide geographical scales. There is a potential contribution from a changing isomeric ratio in gasoline pentanes, but the quantitative contribution from changes in this emission sector cannot be conclusively resolved with the data sets analyzed here. Another possible influence is an increase of the relative contribution of biomass burning emissions. Thirdly, it is notable that decreasing (i/n) pentane isomeric ratio trends were consistently observed at a site that is heavily influenced, and at sites within relatively close proximity, i.e. ~200 miles, of O&NG development regions. Recent research has shown regionally elevated hydrocarbon concentrations in the United States as a result of O&NG development [Franco et al., 2016a; Helmig et al., 2016; Kort et al., 2016; Schade and Roest, 2015; Vinciguerra et al., 2015], with pentane isomers constituting on the order of 10% of the

total NMHC mass [Helmig. et al., 2014]. The fact that (i/n) pentane isomeric ratio trends agree with the expected signature of increasing O&NG influence, and the geographic distribution of sites with statistically significant trends of the (i/n) pentane isomeric ratio and shale plays (Figure 1) suggest an increasing influence of O&NG emissions, regionally and nationwide. This conclusion is in agreement with findings from other recent studies that have shown that O&NG NMHC emissions are constituting an increasing fraction of the urban and rural VOC mix [Schade and Roest, 2015; Vinciguerra et al., 2015] in the U.S. Similar observations were reported for the United Kingdom: While most C2-C8 hydrocarbons steadily declined from 1993 to 2012, ethane and propane, which are mostly associated to NG emissions, have remained near their 1993 values [Derwent et al., 2017].

Despite the uncertainty in the factor influencing isomeric ratios in many cities in the U.S., air quality in Boulder, Co is certainly influenced by nearby oil and gas development. This has been shown by numerous studies and has implications for continuing ozone nonattainment in the region. We found spatial gradients of O&NG related compounds that increased as distance to the O&NG producing region decreased. Measurement variability also increased as distance decreased. This behavior also suggests Weld County is the source region because levels observed at nearby monitoring sites will be more sensitive to changes in emission rates and transport conditions. We also saw an elevation gradient that suggests emissions from the Front Range can influence air quality up to the continental divide. Further, regular diurnal cycles of ozone precursors are frequently interrupted by emission events.

Our analysis of global, regional, and local datasets demonstrates that air quality is dynamic system and varies according to local emission sources, and physical and meteorological factors. As a result, monitoring with high spatial and temporal resolution is essential for

determining what conditions individuals are exposed to in any given area. Because of the deleterious health effects that can be caused by compounds discussed in this manuscript such as ozone and BTEX, there is public interest in local air quality. To help address the concerns of citizens, we have developed a monitoring tool that is an order of magnitude cheaper than other monitoring strategies. Passive adsorbent sampling cartridges can be deployed to an area of interest with minimal accompanying equipment, and by individuals with minimal training.

These cartridges could potentially measure C3-C5 hydrocarbons quantitatively under field conditions. Mixing ratios of C3-C5 alkanes collected by cartridges and canisters deployed side by side correlated with R2 > 0.70. Cartridges sampled with acceptable precision (10-20% RSD) at mixing ratios above 1-4 ppbv, depending on the compound. However, analysis of the relative residuals of the cartridge ASRs, which were calculated from a linear regression of cartridge measurements versus canister measurements, suggests that cartridge ASRs are not in good agreement with the "gold standard," canister measurements. Further work is needed to determine the viability of passive sampling by adsorbent cartridges as an analytical method.

Optimizing cartridge preparation was critical and lowered background levels enough to achieve representative sampling at low mixing ratios. The adsorbent was selected because of its low background and affinity for the target compounds. A conditioning method was developed that reduced background levels of BTEX compounds by ~ an order of magnitude. Finally, the adsorbent bed mass was reduced to 5% of the original mass used. As a result, mixing ratios of benzene that average > 0.018 ppb for three days can be detected. Further, the reduction in adsorbent material saves about $20 per cartridge in assembly costs.

Analysis of literature yielded surprisingly consistent uptake rates (URs) of BTEX compounds. We found URs of 24 – 48 hr periods within a 7 day period to vary by 80% in a

simulated atmosphere. The uniform diameter and distance to the adsorbent bed cartridges is likely what allows for the consistency observed between studies sampling with a variety of conditions and time periods.

As emission sources change, we must be aware of contributions from previously not considered sources. Few studies have been conducted on emissions of VOCs from soil and leaf litter. CO2 emissions from soil have been studied extensively and the "Birch Effect" – highly elevated emissions of CO2 in the ~24 hours following a soil wetting event – is well documented. We found a spike in VOC emissions following a wetting event in a variety of soils. The compounds emitted were mostly oxygenated VOCs, and the carbon emitted as VOC was equivalent to $5.0 \pm 2.0\%$ of the carbon emitted as CO_2. Emissions varied between soils (PERMANOVA; R^2=0.049. P=0.035 of the variation could be explain by soil type), but the time with respect to the wetting event was more associated with the differences in emissions than the soil type (PERMANOVA; R^2=0.28. P=0.001). C_{VOC} emissions generally scaled with soil organic matter content. Soil VOC emissions have been shown to be competitive with other VOC sources in a forest [*Schade and Goldstein*, 2001]. Soil VOC emissions are considered in the Goddard chemistry climate model (GEOSCCM), which adjust emissions according to meteorological conditions, and the ECHAM/MESSy Atmospheric Chemistry (EMAC) model, which scales soil emissions to meet annual net emissions. Due to variability we observed in emissions, we recommend that soil organic matter content, and changes in soil moisture levels be considered in these models.

We also surveyed the VOC emission profiles from a variety of soil and airborne dust-associated actinobacterial strains. VOCs that are likely byproducts of central metabolic pathways were emitted by most of the Actinobacterial strains surveyed. However, emission profiles varied enough to suggest taxonomic and phylogenetic charateristics influence the speciation of emissions. A majority of the

mVOCs observed were detected infrequently and at levels too low to allow for identification. Further, microbe-microbe interactions were affected by the VOC emissions, for example, the growth of some pseudomonad strains was inhibited in the presence of some VOCs. As these pseudomonad strains have been associated with plant health, studies of this nature may result in the development of microbial-based solutions to pathogen control in agricultural ecosystems.

The overall conclusion of this dissertation is that VOCs emissions are highly variable spatially and temporally, and are sensitive to changes in energy production and usage, regulations, and changes in relative contributions from a variety of sources. The atmosphere is a dynamic system; continued and improved understanding of this system relies on learning the intricacies of known emission sources, assessing emerging and understudied sources, evaluating atmospheric composition from both top-down and bottom up perspectives, and resolving the findings from these perspectives [*Vaughn et al.*, 2018]. Further, the effect of the changing climate cannot be ignored. The ozone - climate penalty refers to the increase in ozone as a result of increasing global temperature [*Bloomer et al.*, 2009; *Jacob and Winner*, 2009; *Rasmussen et al.*, 2013; *Wu et al.*, 2008]. Ozone mixing ratios are forecasted to increase $2 - 5$ ppb by 2050 [*Wu et al.*, 2008], and $1 - 8$ ppb by 2100 [*Jacob and Winner*, 2009], though increases are dependent on chemical and meteorological factors unique to the area being considered [*Kleeman*, 2008; *Mahmud et al.*, 2008; *Millstein and Harley*, 2009]. The factors that seem to best explain the ozone $-$ temperature relationship are the accumulation of ozone precursors in stagnant air masses that are associated with higher temperatures [*Jacob et al.*, 1993], changes in chemical reaction rates [*Sillman and Samson*, 1995], and increased biogenic emissions of ozone precursors [*Guenther et al.*, 1993; *Harley et al.*, 1998].

Los Angeles is an example of the interaction of changing and emerging emissions sources, and changing climate. Despite the country's most stringent air quality laws, Los Angeles

remains in ozone nonattainment, and recently broke its own record for number of consecutive days above the 8-hr ozone standard [*Barboza*, 2018]. It is likely that a variety of factors related to climate change and rising temperatures contributed to this record, including: increased emission of VOCs from biogenic sources [*Constable et al.*, 1999; *Fuentes et al.*, 2000; *Sanderson et al.*, 2003], increased atmospheric stagnation [*Leung and Gustafson*, 2005], and the combination of an abundance of NO emissions with increasing mixing layer depth, which stimulates ozone formation [*Kleeman*, 2008]. Further, emissions from volatile chemical products (VCPs), or products containing organic solvents and capable of emitting VOCs, have been increasing in Los Angeles [*Harley et al.*, 1992; *McDonald et al.*, 2018; *Warneke et al.*, 2012]. Emission factors from VCPs that are an order of magnitude higher than those from mobile sources explain the observed shift in relative contribution to VOC emissions [*McDonald et al.*, 2018], and adding the contribution of VCP emissions to a model that underestimated OH reactivity in the L.A. Basin by a factor of ~2 brought the model to within ~25% of observed OH reactivity [*Griffith et al.*, 2016; *McDonald et al.*, 2018].

Understanding changes in sources of energy, energy use, and climate change are central to predicting air quality trends; VCPs, unconventional O&NG development, modern agriculture, and biomass burning are a few of the most critical emission sources [*Baylon et al.*, 2017; *Koss et al.*, 2017; *Lack et al.*, 2012; *Yuan et al.*, 2017]. Both this dissertation, and the body of research conducted on Los Angeles' air composition demonstrate that it is essential to continue to monitor air in order to understand what must be done to improve air quality, and therefore, the health and welfare of those breathing it.

References:

Gasoline Reid Vapor Pressure, edited, US Environmental Protection Agency, Gasoline Standards.

Aaltonen, H., J. Aalto, P. Kolari, M. Pihlatie, J. Pumpanen, M. Kulmala, E. Nikinmaa, T. Vesala, and J. Back (2013), Continuous VOC flux measurements on boreal forest floor, *Plant Soil*, *369*(1-2), 241-256.

Abeleira, A., I. B. Pollack, B. Sive, Y. Zhou, E. V. Fischer, and D. K. Farmer (2017), Source characterization of volatile organic compounds in the Colorado Northern Front Range Metropolitan Area during spring and summer 2015, *J. Geophys. Res.-Atmos.*, *122*(6), 3595-3613.

Adu, J. K., and J. M. Oades (1978), Physical factors influencing decomposition of organic materials in soil aggregates *Soil Biol. Biochem.*, *10*(2), 109-115.

Agilent (2014), GC Column Solvent Retention Table, edited, pp. 1-6, Agilent Technologies, United Kingdom.

Akagi, S. K., R. J. Yokelson, C. Wiedinmyer, M. J. Alvarado, J. S. Reid, T. Karl, J. D. Crounse, and P. O. Wennberg (2011), Emission factors for open and domestic biomass burning for use in atmospheric models, *Atmos. Chem. Phys.*, *11*(9), 4039-4072.

Allen, D. T. (2014), Methane emissions from natural gas production and use: reconciling bottom-up and top-down measurements, *Curr. Opin. Chem. Eng.*, *5*, 78-83.

Andam, C. P., J. R. Doroghazi, A. N. Campbell, P. J. Kelly, M. J. Choudoir, and D. H. Buckley (2016), A Latitudinal Diversity Gradient in Terrestrial Bacteria of the Genus Streptomyces, *mBio*, *7*(2).

Anderson, M. J. (2001), A new method for non-parametric multivariate analysis of variance, *Austral Ecol.*, *26*(1), 32-46.

Andreae, M. O., and P. Merlet (2001), Emission of trace gases and aerosols from biomass burning, *Glob. Biogeochem. Cycle*, *15*(4), 955-966.

Anenberg, S. C., J. J. West, A. M. Fiore, D. A. Jaffe, M. J. Prather, D. Bergmann, K. Cuvelier, F. J. Dentener, B. N. Duncan, M. Gauss, P. Hess, J. E. Jonson, A. Lupu, I. A. MacKenzie, E. Marmer, R. J. Park, M. G. Sanderson, M. Schultz, D. T. Shindell, S. Szopa, M. G. Vivanco, O. Wild, and G. Zang (2009), Intercontinental Impacts of Ozone Pollution on Human Mortality, *Environ. Sci. Technol.*, *43*(17), 6482-6487.

Apel, E. C., J. G. Calvert, J. P. Greenberg, D. Riemer, R. Zika, T. E. Kleindienst, W. A. Lonneman, K. Fung, and E. Fujita (1998), Generation and validation of oxygenated volatile organic carbon standards for the 1995 Southern Oxidants Study Nashville Intensive, *J. Geophys. Res.-Atmos.*, *103*(D17), 22281-22294.

Appel, T. (1998), Non-biomass soil organic N - the substrate for N mineralization flushes following soil drying-rewetting and for organic N rendered CaCl2-extractable upon soil drying, *Soil Biol. Biochem.*, *30*(10-11), 1445-1456.

Asensio, D., J. Penuelas, I. Filella, and J. Llusia (2007), On-line screening of soil VOCs exchange responses to moisture, temperature and root presence, *Plant Soil*, *291*(1-2), 249-261.

Ashby, and M. Anderson (1976), Studies in politics of environmental protection - historical roots of British Clean Air Act 1956, 1. Awakening of public opinion over industrial smoke, 1843-1853 *Interdiscip. Sci. Rev.*, *1*(4), 279-290.

Ashby, and M. Anderson (1977a), Studies in politics of environmental protection - historical roots of British Clean Air Act 1956, 2. Appeal to public opinion over domestic smoke, 1880-1892 *Interdiscip. Sci. Rev.*, *2*(1), 9-26.

Ashby, and M. Anderson (1977b), Studies in politics of environmental protection - historical roots of British Clean Air Act 1956, 3. Ripening of public opinion 1898-1952, *Interdiscip. Sci. Rev.*, *2*(3), 190-206.

Atkinson, R. (2000), Atmospheric chemistry of VOCs and NOx, *Atmospheric Environment*, *34*(12–14), 2063-2101.

Atkinson, R. (1997), Gas-phase tropospheric chemistry of volatile organic compounds .1. Alkanes and alkenes, *J. Phys. Chem. Ref. Data*, *26*(2), 215-290.

Atkinson, R. (2003), Kinetics of the gas-phase reactions of OH radicals with alkanes and cycloalkanes, *Atmos. Chem. Phys.*, *3*, 2233-2307.

Atkinson, R., and J. Arey (2003a), Atmospheric degradation of volatile organic compounds, *Chem. Rev.*, *103*(12), 4605-4638.

Atkinson, R., and J. Arey (2003b), Gas-phase tropospheric chemistry of biogenic volatile organic compounds: a review, *Atmospheric Environment*, *37*, S197-S219.

Atkinson, R., and W. P. L. Carter (1984), Kinetics and Mechanisms of the Gas-Phase Reactions of Ozone with Organic-Compounds Under Atmospheric Conditions, *Chem. Rev.*, *84*(5), 437-470.

Atkinson, R., A. M. Winer, and J. N. Pitts (1986), Estimation of Nighttime N2O5 concentrations from Ambient NO2 and NO3 Radical concentrations and the Role of N2O5 in Nighttime Chemistry, *Atmospheric Environment*, *20*(2), 331-339.

Aumont, B., S. Szopa, and S. Madronich (2005), Modelling the evolution of organic carbon during its gas-phase tropospheric oxidation: development of an explicit model based on a self generating approach, *Atmos. Chem. Phys.*, *5*, 2497-2517.

Aydin, M., K. R. Verhulst, E. S. Saltzman, M. O. Battle, S. A. Montzka, D. R. Blake, Q. Tang, and M. J. Prather (2011), Recent decreases in fossil-fuel emissions of ethane and methane derived from firn air, *Nature*, *476*(7359), 198-201.

Ayers, G. P., and J. M. Cainey (2007), The CLAW hypothesis: a review of the major developments, *Environ. Chem.*, *4*(6), 366-374.

Bachy, A., M. Aubinet, C. Amelynck, N. Schoon, B. Bodson, C. Moureaux, P. Delaplace, A. De Ligne, and B. Heinesch (2018), Methanol exchange dynamics between a temperate cropland soil and the atmosphere, *Atmospheric Environment*, *176*, 229-239.

Bahreini, R., R. Ahmadov, S. A. McKeen, K. T. Vu, J. H. Dingle, E. C. Apel, D. R. Blake, N. Blake, T. L. Campos, C. Cantrell, F. Flocke, A. Fried, J. B. Gilman, A. J. Hills, R. S. Hornbrook, G. Huey, L. Kaser, B. M. Lerner, R. L. Mauldin, S. Meinardi, D. D. Montzka, D. Richter, J. R. Schroeder, M. Stell, D. Tanner, J. Walega, P. Weibring, and A. Weinheimer (2018), Sources and characteristics of summertime organic aerosol in the Colorado Front Range: perspective from measurements and WRF-Chem modeling, *Atmos. Chem. Phys.*, *18*(11), 8293-8312.

Baker, A. K., A. Rauthe-Schoch, T. J. Schuck, C. A. M. Brenninkmeijer, P. F. J. van Velthoven, A. Wisher, and D. E. Oram (2011), Investigation of chlorine radical chemistry in the Eyjafjallajokull volcanic plume using observed depletions in non-methane hydrocarbons, *Geophys. Res. Lett.*, *38*.

Baldwin, I. T., and C. A. Preston (1999), The eco-physiological complexity of plant responses to insect herbivores, *Planta*, *208*(2), 137-145.

Ballester, F., M. Estarlich, C. Iniguez, S. Llop, R. Ramon, A. Esplugues, M. Lacasana, and M. Rebagliato (2010), Air pollution exposure during pregnancy and reduced birth size: a prospective birth cohort study in Valencia, Spain, *Environ. Health*, *9*.

Baltz, R. H. (2008), Renaissance in antibacterial discovery from actinomycetes, *Curr. Opin. Pharmacol.*, *8*(5), 557-563.

Barboza, T. (2018), 87 days of smog: Southern California just saw its longest streak of bad air in decades, in *Los Angeles Times*, edited, http://www.latimes.com/local/lanow/la-me-smog-streak-20180921-story.html#nws=mcnewsletter.

Barton, L., F. C. Hoyle, K. T. Stefanova, and D. V. Murphy (2016), Incorporating organic matter alters soil greenhouse gas emissions and increases grain yield in a semi-arid climate, *Agriculture, Ecosystems & Environment*, *231*, 320-330.

Bascom, R., P. A. Bromberg, D. A. Costa, R. Devlin, D. W. Dockery, M. W. Frampton, W. Lambert, J. M. Samet, F. E. Speizer, and M. Utell (1996), Health effects of outdoor air pollution, *Am. J. Respir. Crit. Care Med.*, *153*(1), 3-50.

Baylon, P., D. A. Jaffe, J. de Gouw, and C. Warneke (2017), Influence of Long-Range Transport of Siberian Biomass Burning at the Mt. Bachelor Observatory during the Spring of 2015, *Aerosol Air Qual. Res.*, *17*(11), 2751-2761.

Bell, M. L., F. Dominici, and J. M. Samet (2005), Meta-analysis of ozone and mortality, *Epidemiology*, *16*(5), S35-S35.

Bending, G. D., and S. D. Lincoln (2000), Inhibition of soil nitrifying bacteria communities and their activities by glucosinolate hydrolysis products, *Soil Biol. Biochem.*, *32*(8-9), 1261-1269.

Berdy, J. (2005), Bioactive microbial metabolites - A personal view, *J. Antibiot.*, *58*(1), 1-26.

Berglen, T. F., T. K. Berntsen, I. S. A. Isaksen, and J. K. Sundet (2004), A global model of the coupled sulfur/oxidant chemistry in the troposphere: The sulfur cycle, *J. Geophys. Res.-Atmos.*, *109*(D19).

Birch, H. F. (1958), The effect of soil drying on humus decomposition and nitrogen availability, *Plant Soil*, *10*, 9-31.

Bishop, G., and D. H. Stedman (2008), A decade of on-road emissions measurements, *Environ. Sci. Technol.*, *45*, 1651-1656.

Blake, N. J., S. A. Penkett, K. C. Clemitshaw, P. Anwyl, P. Lightman, A. R. W. Marsh, and G. Butcher (1993), Estimates of Atmospheric Hydroxyl Radical Concentrations from the Observed Decay of Many Reactive Hydrocarbons in Well-Defined Urban Plumes, *J. Geophys. Res.-Atmos.*, *98*(D2), 2851-2864.

Blanchard, C. L., and S. J. Tanenbaum (2003), Differences between weekday and weekend air pollutant levels in southern California, *J. Air Waste Manage. Assoc.*, *53*(7), 816-828.

Bloem, J., P. C. Deruiter, G. J. Koopman, G. Lebbink, and L. Brussaard (1992), Microbial numbers and activity in dried and rewetted arable soil under integrated and conventional management *Soil Biol. Biochem.*, *24*(7), 655-665.

Bloomer, B. J., J. W. Stehr, C. A. Piety, R. J. Salawitch, and R. R. Dickerson (2009), Observed relationships of ozone air pollution with temperature and emissions, *Geophys. Res. Lett.*, *36*.

Borbon, A., J. B. Gilman, W. C. Kuster, N. Grand, S. Chevaillier, A. Colomb, C. Dolgorouky, V. Gros, M. Lopez, R. Sarda-Esteve, J. Holloway, J. Stutz, H. Petetin, S. McKeen, M. Beekmann, C. Warneke, D. D. Parrish, and J. A. de Gouw (2013), Emission ratios of anthropogenic volatile organic compounds in northern mid-latitude megacities: Observations versus emission inventories in Los Angeles and Paris, *Journal of Geophysical Research: Atmospheres*, *118*(4), 2041-2057.

Borken, W., E. A. Davidson, K. Savage, J. Gaudinski, and S. E. Trumbore (2003), Drying and wetting effects on carbon dioxide release from organic horizons, *Soil Sci. Soc. Am. J.*, *67*(6), 1888-1896.

Borner, J., and S. Wunder (2012), The Scope for Reducing Emissions from Forestry and Agriculture in the Brazilian Amazon, *Forests*, *3*(3), 546-572.

Bos, L. D. J., P. J. Sterk, and M. J. Schultz (2013), Volatile Metabolites of Pathogens: A Systematic Review, *PLoS Pathog.*, *9*(5).

Bottner, P. (1985), Response of microbial biomass to alternate moist and dry conditions in a soil incubated with C-14 labeled and N-15 labeled plant material *Soil Biol. Biochem.*, *17*(3), 329-337.

Bowen, S. E., S. Irtenkauf, J. H. Hannigan, and A. L. Stefanski (2009), Alterations in rat fetal morphology following abuse patterns of toluene exposure, *Reprod. Toxicol.*, *27*(2), 161-169.

Bowman, F. M., and J. H. Seinfeld (1994), Ozone productivity of atmospheric organics, *J. Geophys. Res.-Atmos.*, *99*(D3), 5309-5324.

Boylan, P., D. Helmig, and J. H. Park (2014), Characterization and mitigation of water vapor effects in the measurement of ozone by chemiluminescence with nitric oxide, *Atmos. Meas. Tech.*, *7*(5), 1231-1244.

Brauer, M. (2008), A cohort study of traffic related air-pollution impacts on birth outcomes (vol 116, pg 680, 2008), *Environ. Health Perspect.*, *116*(12), A519-A519.

Brauer, M., M. Amann, R. T. Burnett, A. Cohen, F. Dentener, M. Ezzati, S. B. Henderson, M. Krzyzanowski, R. V. Martin, R. Van Dingenen, A. van Donkelaar, and G. D. Thurston (2012), Exposure Assessment for Estimation of the Global Burden of Disease Attributable to Outdoor Air Pollution, *Environ. Sci. Technol.*, *46*(2), 652-660.

Briard, B., C. Heddergott, and J. P. Latge (2016), Volatile Compounds Emitted by Pseudomonas aeruginosa Stimulate Growth of the Fungal Pathogen Aspergillus fumigatus, *mBio*, *7*(2).

Brimblecombe, P. (2008), Air pollution history, in *Sohki RS (ed) World Atlas of atmospheric pollution*, edited, pp. 7-18, Anthem Press, London.

Brown, R. H. (2000), Monitoring the ambient environment with diffusive samplers: theory and practical considerations, *J. Environ. Monit.*, *2*(1), 1-9.

Brown, R. H. (1995), The use of diffusive samplers to assess local air-pollution problems *Pure Appl. Chem.*, *67*(8-9), 1423-1425.

Brown, S. G., A. Frankel, and H. R. Hafner (2007), Source apportionment of VOCs in the Los Angeles area using positive matrix factorization, *Atmospheric Environment*, *41*(2), 227-237.

Brown, S. S., J. A. Thornton, W. C. Keene, A. A. P. Pszenny, B. C. Sive, W. P. Dube, N. L. Wagner, C. J. Young, T. P. Riedel, J. M. Roberts, T. C. VandenBoer, R. Bahreini, F. Ozturk, A. M. Middlebrook, S. Kim, G. Hubler, and D. E. Wolfe (2013), Nitrogen, Aerosol Composition, and Halogens on a Tall Tower (NACHTT): Overview of a wintertime air chemistry field study in the front range urban corridor of Colorado, *J. Geophys. Res.-Atmos.*, *118*(14), 8067-8085.

Bruce, A., D. Stewart, S. Verrall, and R. E. Wheatley (2003), Effect of volatiles from bacteria and yeast on the growth and pigmentation of sapstain fungi, *Int. Biodeterior. Biodegrad.*, *51*(2), 101-108.

Bruggemann, M., N. Hayeck, C. Bonnineau, S. Pesce, P. A. Alpert, S. Perrier, C. Zuth, T. Hoffmann, J. M. Chen, and C. George (2017), Interfacial photochemistry of biogenic surfactants: a major source of abiotic volatile organic compounds, *Faraday Discuss.*, *200*, 59-74.

Bruhl, C., and P. J. Crutzen (1988), Scenarios of possible changes in atmospheric temperatures and ozone concentrations due to man's activities, estimated with a one-dimensional coupled photochemical climate model, *Clim. Dyn.*, *2*(3), 173-203.

Bunge, M., N. Araghipour, T. Mikoviny, J. Dunkl, R. Schnitzhofer, A. Hansel, F. Schinner, A. Wisthaler, R. Margesin, and T. D. Mark (2008), On-line monitoring of microbial volatile metabolites by proton transfer reaction-mass spectrometry, *Appl. Environ. Microbiol.*, *74*(7), 2179-2186.

Burruss, R. C., and R. T. Ryder (2014), Composition of natural gas and crude oil produced from 14 wells in the Lower Silurian "Clinton" Sandstone and Medina Group Sandstones, northeastern Ohio and Northwestern Pennsylvania., *U.S. Geological Survey Professional Paper 1708,* , 38 p.

Calfapietra, C., S. Fares, F. Manes, A. Morani, G. Sgrigna, and F. Loreto (2013), Role of Biogenic Volatile Organic Compounds (BVOC) emitted by urban trees on ozone concentration in cities: A review, *Environ. Pollut.*, *183*, 71-80.

Calvert, J. G. (1976), Hydrocarbon Involvement in Photochemical Smog Formation in Los Angeles Atmosphere, *Environ. Sci. Technol.*, *10*(3), 256-262.

Canada, E. (1999), Canadian Environmental Protection Act— Priority Substances List — Supporting document for the environmental assessment of carbon disulfide, edited by E. Canada, Commercial Chemicals Evaluation Branch, Hull, Quebec.

Cao, X. L., and C. N. Hewitt (1994), Buildup of artifacts on adsorbents during storage and its effect on passive sampling and gas chromatography-flame ionization detection of low concentrations of volatile organic compounds in air *J. Chromatogr. A*, *688*(1-2), 368-374.

Capella-Gutierrez, S., J. M. Silla-Martinez, and T. Gabaldon (2009), trimAl: a tool for automated alignment trimming in large-scale phylogenetic analyses, *Bioinformatics*, *25*(15), 1972-1973.

CARB (2018), Air Quality Data Statistics, edited by C. A. R. Board, California Environmental Protection Agency, https://www.arb.ca.gov/adam/trends/trends1.php.

CARB (2011), EMFAC 2011, edited by C. A. R. Board, California Environmental Protection Agency.

Cardelino, C. A., and W. L. Chameides (1990), Natural hydrocarbons, urbanization, and urban ozone *J. Geophys. Res.-Atmos.*, *95*(D9), 13971-13979.

Chameides, W. L., F. Fehsenfeld, M. O. Rodgers, C. Cardelino, J. Martinez, D. Parrish, W. Lonneman, D. R. Lawson, R. A. Rasmussen, P. Zimmerman, J. Greenberg, P. Middleton, and T. Wang (1992), Ozone precursor relationships in the ambient atmosphere, *J. Geophys. Res.-Atmos.*, *97*(D5), 6037-6055.

Cheadle, L. C., S. J. Oltmans, G. Petron, R. C. Schnell, E. J. Mattson, S. C. Herndon, A. M. Thompson, D. R. Blake, and A. McClure-Begley (2017), Surface ozone in the Colorado northern Front Range and the influence of oil and gas development during FRAPPE/DISCOVER-AQ in summer 2014, *Elementa-Sci. Anthrop.*, *5*.

Chen, L., Y. Sun, X. Wu, Y. Zhang, C. Zheng, X. Gao, and K. Cen (2014), Unit-based emission inventory and uncertainty assessment of coal-fired power plants, *Atmospheric Environment*, *99*, 527-535.

Chernin, L., N. Toklikishvili, M. Ovadis, S. Kim, J. Ben-Ari, I. Khmel, and A. Vainstein (2011), Quorum-sensing quenching by rhizobacterial volatiles, *Environ. Microbiol. Rep.*, *3*(6), 698-704.

Chinkin, L. R., D. L. Coe, T. H. Funk, H. R. Hafner, P. T. Roberts, P. A. Ryan, and D. R. Lawson (2003), Weekday versus weekend activity patterns for ozone precursor emissions in California's South Coast Air Basin, *J. Air Waste Manage. Assoc.*, *53*(7), 829-843.

Choudoir, M. J., J. R. Doroghazi, and D. H. Buckley (2016), Latitude delineates patterns of biogeography in terrestrial Streptomyces, *Environ. Microbiol.*, *18*(12), 4931-4945.

Choudoir, M. J., C. Pepe-Ranney, and D. H. Buckley (2018), Diversification of Secondary Metabolite Biosynthetic Gene Clusters Coincides with Lineage Divergence in Streptomyces, *Antibiotics-Basel*, *7*(1).

Ciccioli, P., A. Cecinato, E. Brancaleoni, M. Frattoni, and A. Liberti (1992), Use of carbon adsorption traps combined with high-resolution gas-chromatograpy-mass-spectrometry for the analysis of polar and nonpolar C4-C14 hydrocarbons involved in photochemical smog formation *HRC-J. High Resolut. Chromatogr.*, *15*(2), 75-84.

Civan, M. Y., S. Yurdakul, and G. Tuncel (2012), Improvement of uptake rate equations depending on meteorological conditions for 25 volatile organic compounds, *Talanta*, *99*, 720-729.

COGCC (2014), County level production data

available in the "Data: COGIS DataBase" section

[dataset], edited by C. O. a. G. C. Comission, http://cogcc.state.co.us/.

COGCC (2016), Oil and natural gas wells data available in the "Downloads" section, edited by C. O. a. G. C. Comission, http://cogcc.state.co.us/data2.html-/downloads.

COGCC (2012), Statement of Basis, Specific Statutory Authority, and Purpose. New Rules and Amendments to Current Rules of the Colorado Oil and Gas Conservation Commission, 2 CCR 404-1, edited by C. O. a. G. C. Comission, http://cogcc.state.co.us/documents/reg/Rules/2012/setback/Final_SetbackRules-StatementOfBasisAndPurpose.pdf.

Colbeck, I. (2007), *Air pollution: history of actions and effectiveness of change*, Sage, London.

Colborn, T., C. Kwiatkowski, K. Schultz, and M. Bachran (2011), Natural gas operations from a public health perspective, *Human and Ecological Risk Assessment: An International Journal*, *17*(5), 1039-1056.

Colborn, T., K. Schultz, L. Herrick, and C. Kwiatkowski (2014), An exploratory study of air quality near natural gas operations, *Human and Ecological Risk Assessment: An International Journal*, *20*(1), 86-105.

Colon-Roman, Y. A., and L. F. Ruppert (2014), Central Appalachian basin natural gas database–Distribution, composition, and origin of natural gases., *U.S. Geological Survey Open-File Report 2014–1207*, 13 p.

Colorado-DOT (2016), Online Transportation Information System, edited, Colorado Department of Transportation, http://dtdapps.coloradodot.info/otis/TrafficData#ui/0/0/0/criteria/7850//true/true/.

Conrad, R. (1996), Soil microorganisms as controllers of atmospheric trace gases (H-2, CO, CH4, OCS, N2O, and NO), *Microbiol. Rev.*, *60*(4), 609-+.

Constable, J. V. H., A. B. Guenther, D. S. Schimel, and R. K. Monson (1999), Modelling changes in VOC emission in response to climate change in the continental United States, *Glob. Change Biol.*, *5*(7), 791-806.

Conway, J. R., A. Lex, and N. Gehlenborg (2017), UpSetR: an R package for the visualization of intersecting sets and their properties, *Bioinformatics*, *33*(18), 2938-2940.

Cordovez, V., V. J. Carrion, D. W. Etalo, R. Mumm, H. Zhu, G. P. van Wezel, and J. M. Raaijmakers (2015), Diversity and functions of volatile organic compounds produced by Streptomyces from a disease-suppressive soil, *Front. Microbiol.*, *6*.

Costle, A. v. (1981), API v. Costle, in *665 F.2d 1176*, edited by D. C. Cir., pp. 1184-1186.

CPR (2017), Is The Broomfield Recall Effort A Proxy Fight For Colorado's Oil And Gas Conflicts?, edited by C. P. Radio, http://www.cpr.org/news/story/is-the-broomfield-recall-effort-a-proxy-fight-for-colorado-s-oil-and-gas-conflicts.

Cui, M. Y., and M. M. Caldwell (1997), A large ephemeral release of nitrogen upon wetting of dry soil and corresponding root responses in the field, *Plant Soil*, *191*(2), 291-299.

D.E.P., P. D. o. E. P. (2017), Oil and Gas Well Production, edited by P. D. o. E. Protection, Pennsylvania Department of Environmental Protection, http://www.depreportingservices.state.pa.us/ReportServer/Pages/ReportViewer.aspx?%2fOil_Gas%2fOil_Gas_Well_Production.

Dadvand, P., J. Parker, M. L. Bell, M. Bonzini, M. Brauer, L. A. Darrow, U. Gehring, S. V. Glinianaia, N. Gouveia, E. H. Ha, J. H. Leem, E. H. van den Hooven, B. Jalaludin, B. M. Jesdale, J. Lepeule, R. Morello-Frosch, G. G. Morgan, A. C. Pesatori, F. H. Pierik, T. Pless-Mulloli, D. Q. Rich, S. Sathyanarayana, J. Seo, R. Slama, M. Strickland, L. Tamburic, D.

Wartenberg, M. J. Nieuwenhuijsen, and T. J. Woodruff (2013), Maternal exposure to particulate air pollution and term birth weight: A multi-country evaluation of effect and heterogeneity, *Environ. Health Perspect.*, *121*(3), 367-373.

Davidson, E. A. (1992), Pulses of Nitric Oxide and Nitrous Oxide Flux following Wetting of Dry Soil: An Assessment of Probable Sources and Importance Relative to Annual Fluxes, *Ecological Bulletins*(42), 149-155.

Davies, L., and U. Gather (1993), The Identification of Multiple Outliers, *J. Am. Stat. Assoc.*, *88*(423), 782-792.

Davis, D. (2002), *When smoke ran like water: tales of environmental deception and the battle against pollution*, Perseus Press, Oxford.

de Gouw, J. A., O. R. Cooper, C. Warneke, P. K. Hudson, F. C. Fehsenfeld, J. S. Holloway, G. Hubler, D. K. Nicks, J. B. Nowak, D. D. Parrish, T. B. Ryerson, E. L. Atlas, S. G. Donnelly, S. M. Schauffler, V. Stroud, K. Johnson, G. R. Carmichael, and D. G. Streets (2004), Chemical composition of air masses transported from Asia to the U. S. West Coast during ITCT 2K2: Fossil fuel combustion versus biomass-burning signatures, *J. Geophys. Res.-Atmos.*, *109*(D23), 15.

de Gouw, J. A., C. J. Howard, T. G. Custer, and R. Fall (1999), Emissions of volatile organic compounds from cut grass and clover are enhanced during the drying process, *Geophys. Res. Lett.*, *26*(7), 811-814.

Deardorff, J. W. (1972), Parameterization of Planetary Boundary-Layer for use in general circulation models *Mon. Weather Rev.*, *100*(2), 93-+.

Demirbas, A. (2010), Methane Gas Hydrate, in *Methane Gas Hydrate*, edited, pp. 1-186, Springer, New York.

Dennison, P. E., S. C. Brewer, J. D. Arnold, and M. A. Moritz (2014), Large wildfire trends in the western United States, 1984-2011, *Geophys. Res. Lett.*, *41*(8), 2928-2933.

Derwent, R. G., T. J. Davies, M. Delaney, G. J. Dollard, R. A. Field, P. Dumitrean, P. D. Nason, B. M. R. Jones, and S. A. Pepler (2000), Analysis and interpretation of the continuous hourly monitoring data for 26 C-2-C-8 hydrocarbons at 12 United Kingdom sites during 1996, *Atmospheric Environment*, *34*(2), 297-312.

Derwent, R. G., R. A. Field, P. Dumitrean, T. P. Murrells, and S. P. Telling (2017), Origins and trends in ethane and propane in the United Kingdom from 1993 to 2012, *Atmospheric Environment*, *156*, 15-23.

Devlin, R. B., W. F. McDonnell, R. Mann, S. Becker, D. E. House, D. Schreinemachers, and H. S. Koren (1991), Exposure of humans to ambient levels of ozone for 6.6 hours causes cellular and biochemical changes in the lung, *Am. J. Respir. Cell Mol. Biol.*, *4*(1), 72-81.

Dingle, J. H., K. Vu, R. Bahreini, E. C. Apel, T. L. Campos, F. Flocke, A. Fried, S. Herndon, A. J. Hills, R. S. Hornbrook, G. Huey, L. Kaser, D. D. Montzka, J. B. Nowak, M. Reeves, D. Richter, J. R. Roscioli, S. Shertz, M. Stell, D. Tanner, G. Tyndall, J. Walega, P. Weibring, and A. Weinheimer (2016), Aerosol optical extinction during the Front Range Air Pollution and Photochemistry Experiment (FRAPPE) 2014 summertime field campaign, Colorado, USA, *Atmos. Chem. Phys.*, *16*(17).

Doroghazi, J. R., J. C. Albright, A. W. Goering, K. S. Ju, R. R. Haines, K. A. Tchalukov, D. P. Labeda, N. L. Kelleher, and W. W. Metcalf (2014), A roadmap for natural product discovery based on large-scale genomics and metabolomics, *Nat. Chem. Biol.*, *10*(11), 963-968.

Dray, S., and A. B. Dufour (2007), The ade4 package: Implementing the duality diagram for ecologists, *J. Stat. Softw.*, *22*(4), 1-20.

EANET (2013), EANET Science Bulletin, edited by A. D. M. N. i. E. Asia, Asia Center for Air Pollution Research, Niigata, Japan.

Effmert, U., J. Kalderas, R. Warnke, and B. Piechulla (2012), Volatile Mediated Interactions Between Bacteria and Fungi in the Soil, *J. Chem. Ecol.*, *38*(6), 665-703.

Ehhalt, D. H. (1999), Photooxidation of trace gases in the troposphere, *Phys. Chem. Chem. Phys.*, *1*(24), 5401-5408.

EIA (2012), Annual Energy Review, in *Total Energy*, edited by U. S. E. I. Administration, https://www.eia.gov/totalenergy/data/annual/showtext.php?t=ptb0502.

EIA (2017a), Drilling Productivity Report, in *Petroleum & Other Liquids*, edited by U. S. E. I. Administration, https://www.eia.gov/petroleum/drilling/#tabs-summary-3.

EIA (2017b), Number of Producing Gas Wells, edited by U. S. E. I. Administration, https://www.eia.gov/dnav/ng/ng_prod_wells_s1_a.htm.

EIA (1998), Refiners Switch to Reformulated

Gasoline Complex Model, edited by D. o. Energy, United State Energy Information Administration.

EIA (2017c), United States remains the world's top producer of petroleum and natural gas hydrocarbons, in *Today in Energy*, edited by U. S. E. I. Administration, https://www.eia.gov/todayinenergy/detail.php?id=31532#.

Elkus, B., and K. R. Wilson (1977), Photochemical air pollution - Weekend weekday differences, *Atmospheric Environment*, *11*(6), 509-515.

EPA (2018), 8-Hour Ozone Nonattainment Areas (2015 Standard), edited, Environmental Protection Agency, https://www3.epa.gov/airquality/greenbook/map8hr_2015.html.

EPA (1978), Control techniques for nitrogen oxides emissions from stationary sources - second edition, edited by E. P. Agency, Office of Air and Waste Management, Research Triangle Park, North Carolina.

EPA (2015a), EPA Method 325 - Volatile Organic Compounds from Fugitive and Area Sources, edited by EPA, National Air Toxics Monitoring and Data Analysis Workshop.

EPA (2017a), Gasoline Reid Vapor Pressure.

EPA (2015b), National Ambient Air Quality Standards for Ozone, edited by E. P. Agency, pp. 65292-65468.

EPA (2015c), Ozone (O3) Standards - Table of Historical Ozone NAAQS, edited by U. S. E. P. Agency, National Ambient Air Quality Standards.

EPA (1997), Photochemical Assessment Monitoring Stations (PAMS) Performance Evaluation Program, edited by E. P. Agency, Office of Air Quality Planning and Standards, Morrisville, NC.

EPA (2014), Report on the Environment (ROE): Volatile Organic Compound Emissions, edited by E. P. Agency, (http://www3.epa.gov/ttn/chief/eiinformation.html).

EPA (2006a), RFG Property and Performance Averages for Baltimore, MD, edited, United States Environmental Protection Agency.

EPA (2006b), RFG Property and Performance Averages for Boston-Worchester, MA, in *Fuels and Fuel Additives*, edited, United States Environmental Protection Agency

EPA (2006c), RFG Property and Performance Averages for Chicago-Lake Co., IL, Gary, IN, in *Fuels and Fuel Additives*, edited, United States Environmental Protection Agency.

EPA (2006d), RFG Property and Performance Averages for Houston-Galveston, TX, in *Fuels and Fuel Additives*, edited, United States Environmental Protection Agency.

EPA (2006e), RFG Property and Performance Averages for Phila.-Wilm, DE-Trenton, NJ, in *Fuels and Fuel Additives*, edited, United States Environmental Protection Agency.

EPA (2006f), RFG Property and Performance Averages for Springfield, MA, in *Fuels and Fuel Additives*, edited, United States Environmental Protection Agency.

EPA (2017b), Sulfur Dioxide Trends, edited, Environmental Protection Agency, https://www.epa.gov/air-trends/sulfur-dioxide-trends.

EPA (1998), Technical Assistance Document (TAD) for Sampling and Analysis of Ozone Precursors, edited, EPA.

EPA (2016), US Greenhouse Gas Inventory, *https://www3.epa.gov/climatechange/ghgemissions/index.html*.

EPA, A. v. (1999), American Trucking Assoc. v. EPA, in *175 F.3d 1027*, edited by D. C. Cir., D.C. Cir.

Ewing, B., and P. Green (1998), Base-calling of automated sequencer traces using phred. II. Error probabilities, *Genome Res.*, *8*(3), 186-194.

Fabbri, A., G. Crescentini, F. Mangani, A. R. Mastrogiacomo, and F. Bruner (1987), Advances in the determination of volatile organic solvents and other organic pollutants by gas chromatograph with thermal desorption sampling and injection *Chromatographia*, *23*(11), 856-860.

Faiz, A., C. S. Weaver, and M. P. Walsh (1996), Air Pollution from Motor Vehicles, edited by T. I. Bank, Library of Congress Cataloging-in-Publication Data, Reconstruction and Development/ The World Bank.

Falik, O., Y. Mordoch, L. Quansah, A. Fait, and A. Novoplansky (2011), Rumor Has It ... : Relay Communication of Stress Cues in Plants, *PLoS One*, *6*(11).

Fehsenfeld, F., J. Calvert, R. Fall, P. Goldan, A. B. Guenther, C. N. Hewitt, B. Lamb, S. Liu, and M. Trainer (1992), Emissions of volatile organic compounds from vegetation and the implications for atmospheric chemistry, *Glob. Biogeochem. Cycle*, *6*(4), 389-430.

FHA, U. S. (2000), Motor Vehicle Registrations, edited by U. S. F. H. Administration, http://www.fhwa.dot.gov/ohim/ohimstat.htm.

Field, R. A., J. Soltis, M. C. McCarthy, S. Murphy, and D. C. Montague (2015), Influence of oil and gas field operations on spatial and temporal distributions of atmospheric non-methane hydrocarbons and their effect on ozone formation in winter, *Atmos. Chem. Phys.*, *15*(6), 3527-3542.

Fierer, N., and J. P. Schimel (2002), Effects of drying-rewetting frequency on soil carbon and nitrogen transformations, *Soil Biol. Biochem.*, *34*(6), 777-787.

Fierer, N., and J. P. Schimel (2003), A proposed mechanism for the pulse in carbon dioxide production commonly observed following the rapid rewetting of a dry soil, *Soil Sci. Soc. Am. J.*, *67*(3), 798-805.

Filipiak, W., A. Sponring, M. M. Baur, A. Filipiak, C. Ager, H. Wiesenhofer, M. Nagl, J. Troppmair, and A. Amann (2012), Molecular analysis of volatile metabolites released specifically by staphylococcus aureus and pseudomonas aeruginosa, *BMC Microbiol.*, *12*.

Finlayson-Pitts, B. J., and J. N. Pitts (2000), *Chemistry of the Upper and Lower Atmosphere*, Academic Press, San Diego.

Fiscus, E. L., F. L. Booker, and K. O. Burkey (2005), Crop responses to ozone: uptake, modes of action, carbon assimilation and partitioning, *Plant Cell Environ.*, *28*(8), 997-1011.

Franco, B., W. Bader, G. C. Toon, C. Bray, A. Perrin, E. V. Fischer, K. Sudo, C. D. Boone, B. Bovy, B. Lejeune, C. Servais, and E. Mahieu (2015), Retrieval of ethane from ground-based FTIR solar spectra using improved spectroscopy: Recent burden increase above Jungfraujoch, *Journal of Quantitative Spectroscopy & Radiative Transfer*, *160*, 36-49.

Franco, B., E. Mahieu, L. K. Emmons, Z. A. Tzompa-Sosa, E. V. Fischer, K. Sudo, B. Bovy, S. Conway, D. Griffin, J. W. Hannigan, K. Strong, and K. A. Walker (2016a), Evaluating ethane and methane emissions associated with the development of oil and natural gas extraction in North America, *Environ. Res. Lett.*, *11*(4).

Franco, B., E. Mahieu, L. K. Emmons, Z. A. Tzompa-Sosa, E. V. Fisher, K. Sudo, B. Bovy, S. Conway, D. Griffin, J. Hannigan, K. Strong, and K. A. Walker (2016b), Evaluating ethane and methane emissions associated with the development of oil and natural gas extraction in North America, *Environ. Res. Lett.*, *11*(4).

Franzluebbers, A. J., R. L. Haney, C. W. Honeycutt, H. H. Schomberg, and F. M. Hons (2000), Flush of carbon dioxide following rewetting of dried soil relates to active organic pools, *Soil Sci. Soc. Am. J.*, *64*(2), 613-623.

Frost, C. J., M. Appel, J. E. Carlson, C. M. De Moraes, M. C. Mescher, and J. C. Schultz (2007), Within-plant signalling via volatiles overcomes vascular constraints on systemic signalling and primes responses against herbivores, *Ecol. Lett.*, *10*(6), 490-498.

Fuentes, J. D., M. Lerdau, R. Atkinson, D. Baldocchi, J. W. Bottenheim, P. Ciccioli, B. Lamb, C. Geron, L. Gu, A. Guenther, T. D. Sharkey, and W. Stockwell (2000), Biogenic hydrocarbons in the atmospheric boundary layer: A review, *Bulletin of the American Meteorological Society*, *81*(7), 1537-1575.

Fujita, E. M., D. E. Campbell, W. R. Stockwell, and D. R. Lawson (2013), Past and future ozone trends in California's South Coast Air Basin: Reconciliation of ambient measurements with past and projected emission inventories, *J. Air Waste Manage. Assoc.*, *63*(1), 54-69.

Fujita, E. M., D. E. Campbell, B. Zielinska, J. C. Sagebiel, J. L. Bowen, W. S. Goliff, W. R. Stockwell, and D. R. Lawson (2003a), Diurnal and weekday variations in the source contributions of ozone precursors in California's South Coast Air Basin, *J. Air Waste Manage. Assoc.*, *53*(7), 844-863.

Fujita, E. M., B. E. Croes, C. L. Bennett, D. R. Lawson, F. W. Lurmann, and H. H. Main (1992), Comparison of emission inventory and ambient concentration ratios of CO NMOG, and NOx in California South Coast Air Basin *J. Air Waste Manage. Assoc.*, *42*(3), 264-276.

Fujita, E. M., W. R. Stockwell, D. E. Campbell, R. E. Keislar, and D. R. Lawson (2003b), Evolution of the magnitude and spatial extent of the weekend ozone effect in California's South Coast Air Basin, 1981-2000, *J. Air Waste Manage. Assoc.*, *53*(7), 802-815.

Galloway, J. N., F. J. Dentener, D. G. Capone, E. W. Boyer, R. W. Howarth, S. P. Seitzinger, G. P. Asner, C. C. Cleveland, P. A. Green, E. A. Holland, D. M. Karl, A. F. Michaels, J. H. Porter,

A. R. Townsend, and C. J. Vorosmarty (2004), Nitrogen cycles: past, present, and future, *Biogeochemistry*, *70*(2), 153-226.

Gardiner, T., A. Forbes, M. de Maziere, C. Vigouroux, E. Mahieu, P. Demoulin, V. Velazco, J. Notholt, T. Blumenstock, F. Hase, I. Kramer, R. Sussmann, W. Stremme, J. Mellqvist, A. Strandberg, K. Ellingsen, and M. Gauss (2008), Trend analysis of greenhouse gases over Europe measured by a network of ground-based remote FTIR instruments, *Atmos. Chem. Phys.*, *8*(22), 6719-6727.

Garratt, J. R. (1992), *The atmospheric boundary layer / J. R. Garratt*, Cambridge University Press, Cambridge ; New York.

Ghosh, J. K. C., M. Wilhelm, J. Su, D. Goldberg, M. Cockburn, M. Jerrett, and B. Ritz (2012), Assessing the influence of traffic-related air pollution on risk of term low birth weight on the basis of land-use-based regression models and measures of air toxics, *Am. J. Epidemiol.*, *175*(12), 1262-1274.

Gilman, J. B., B. M. Lerner, W. C. Kuster, and J. A. de Gouw (2013), Source signature of volatile organic compounds from oil and natural gas operations in northeastern Colorado, *Environ. Sci. Technol.*, *47*(3), 1297-1305.

GLOBALVIEW-CO2 (2011), Cooperative Atmospheric Data Integration Project - Carbon Dioxide. CD-ROM, NOAA ESRL, Boulder, Colorado *ftp.cmdl.noaa.gov, Path: ccg/co2/GLOBALVIEW*.

Goldan, P. D., W. C. Kuster, F. C. Fehsenfeld, and S. A. Montzka (1995), Hydrocarbon measurements in the southeastern United States: The Rural Oxidants in the Southern Environment (ROSE) program 1990, *J. Geophys. Res.-Atmos.*, *100*(D12), 25945-25963.

Goldstein, A. H., S. C. Wofsy, and C. M. Spivakovsky (1995), Seasonal variations of nonmethane hydrocarbons in rural New England: Constraints on OH concentrations in northern midlatitudes (vol 100, pg 21023, 1995), *J. Geophys. Res.-Atmos.*, *100*(D12), 26273-26274.

Gray, C. M. (2014), The Production and Consumption of Volatile Organic Compounds in Soil and Decomposing Litter, 86 pp, University of Colorado-Boulder, Ecology & Evolutionary Biology Graduate Theses & Dissertations.

Gray, C. M., R. K. Monson, and N. Fierer (2010), Emissions of volatile organic compounds during the decomposition of plant litter, *J. Geophys. Res.-Biogeosci.*, *115*.

Griffith, S. M., R. F. Hansen, S. Dusanter, V. Michoud, J. B. Gilman, W. C. Kuster, P. R. Veres, M. Graus, J. A. de Gouw, J. Roberts, C. Young, R. Washenfelder, S. S. Brown, R. Thalman, E. Waxman, R. Volkamer, C. Tsai, J. Stutz, J. H. Flynn, N. Grossberg, B. Lefer, S. L. Alvarez, B. Rappenglueck, L. H. Mielke, H. D. Osthoff, and P. S. Stevens (2016), Measurements of hydroxyl and hydroperoxy radicals during CalNex-LA: Model comparisons and radical budgets, *J. Geophys. Res.-Atmos.*, *121*(8), 4211-4232.

Gryparis, A., B. Forsberg, K. Katsouyanni, A. Analitis, G. Touloumi, J. Schwartz, E. Samoli, S. Medina, H. R. Anderson, E. M. Niciu, H. E. Wichmann, B. Kriz, M. Kosnik, J. Skorkovsky, J. M. Vonk, and Z. Dortbudak (2004), Acute effects of ozone on mortality from the "Air pollution and health: A European approach" project, *Am. J. Respir. Crit. Care Med.*, *170*(10), 1080-1087.

Guenther, A., C. N. Hewitt, D. Erickson, R. Fall, C. Geron, T. Graedel, P. Harley, L. Klinger, M. Lerdau, W. A. McKay, T. Pierce, B. Scholes, R. Steinbrecher, R. Tallamraju, J. Taylor, and P. Zimmerman (1995), A global model of natural volatile organic compound emissions, *Journal of Geophysical Research: Atmospheres*, *100*(D5), 8873-8892.

Guenther, A., X. Jiang, C. L. Heald, T. Sakulyanontvittaya, T. Duhl, L. K. Emmons, and X. Wang (2012), The Model of Emissions of Gases and Aerosols from Nature version 2.1 (MEGAN2.1): an extended and updated framework for modeling biogenic emissions, *Geoscientific Model Development*, *5*(6), 1471-1492.

Guenther, A. B., P. R. Zimmerman, P. C. Harley, R. K. Monson, and R. Fall (1993), Isoprene and monoterpene emission rate variability - Model evaluations and sensitivity analyses, *J. Geophys. Res.-Atmos.*, *98*(D7), 12609-12617.

Haagen-Smit, A. J. (1952), Chemistry and physiology of Los Angeles smog, *Industrial and Engineering Chemistry*, *44*(6), 1342-1346.

Halliday, H. S., A. M. Thompson, A. Wisthaler, D. R. Blake, R. S. Hornbrook, T. Mikoviny, M. Muller, P. Eichler, E. C. Apel, and A. J. Hills (2016), Atmospheric benzene observations from oil and gas production in the Denver-Julesburg Basin in July and August 2014, *J. Geophys. Res.-Atmos.*, *121*(18), 11055-11074.

Harley, P., V. Fridd-Stroud, J. Greenberg, A. Guenther, and P. Vasconcellos (1998), Emission of 2-methyl-3-buten-2-ol by pines: A potentially large natural source of reactive carbon to the atmosphere, *J. Geophys. Res.-Atmos.*, *103*(D19), 25479-25486.

Harley, R. A., M. P. Hannigan, and G. R. Cass (1992), Respeciation of organic gas emissions and the detection of excess unburned gasoline in the atmosphere, *Environ. Sci. Technol.*, *26*(12), 2395-2408.

Hatch, S. A. (2003), Statistical power for detecting trends with applications to seabird monitoring, *Biological Conservation*, *111*(3), 317-329.

Hausmann, P., R. Sussmann, and D. Smale (2016), Contribution of oil and natural gas production to renewed increase of atmospheric methane (2007–2014): top-down estimate from ethane and methane column observations, *Atmos. Chem. Phys.*, *16*, 3227-3244.

Hellen, H., H. Hakola, T. Laurila, V. Hiltunen, and T. Koskentalo (2002), Aromatic hydrocarbon and methyl tert-butyl, ether measurements in ambient air of Helsinki (Finland) using diffusive samplers, *Sci. Total Environ.*, *298*(1-3), 55-64.

Helmig, D. (1996), Artifact-free preparation, storage and analysis of solid adsorbent sampling cartridges used in the analysis of volatile organic compounds in air, *J. Chromatogr. A*, *732*(2), 414-417.

Helmig, D. (1997), Ozone removal techniques in the sampling of atmospheric volatile organic trace gases, *Atmospheric Environment*, *31*(21), 3635-3651.

Helmig, D., F. Bocquet, J. Pollmann, and T. Revermann (2004), Analytical techniques for sesquiterpene emission rate studies in vegetation enclosure experiments, *Atmospheric Environment*, *38*(4), 557-572.

Helmig, D., J. Bottenheim, I. E. Galbally, A. Lewis, M. J. T. Milton, S. Penkett, C. Plass-Duelmer, S. Reimann , P. Tans, and S. Theil (2009), Volatile Organic Compounds in the Global Atmosphere, *Eos Trans. AGU*, *90*(52).

Helmig, D., L. F. Klinger, A. Guenther, L. Vierling, C. Geron, and P. Zimmerman (1999), Biogenic volatile organic compound emissions (BVOCs) I. Identifications from three continental sites in the US, *Chemosphere*, *38*(9), 2163-2187.

Helmig, D., M. Munoz, J. Hueber, C. Mazzoleni, L. Mazzoleni, R. C. Owen, M. Val-Martin, P. Fialho, C. Plass-Duelmer, P. I. Palmer, A. C. Lewis, and G. Pfister (2015), Climatology and atmospheric chemistry of the non-methane hydrocarbons ethane and propane over the North Atlantic, *Elementa-Sci. Anthrop.*, *3*, 1-16.

Helmig, D., V. Petrenko, P. Martinerie, E. Witrant, T. Rockmann, A. Zuiderweg, R. Holzinger, J. Hueber, C. Thompson, J. W. C. White, W. Sturges, A. Baker, T. Blunier, D. Etheridge, M. Rubino, and P. Tans (2014), Reconstruction of Northern Hemisphere 1950-2010 atmospheric non-methane hydrocarbons, *Atmos. Chem. Phys.*, *14*(3), 1463-1483.

Helmig, D., S. Rossabi, J. Hueber, P. Tans, S. Montzka, K. Masarie, K. Thoning, C. Plass-Duelmer, A. Claude, L. Carpenter, A. C. Lewis, S. Punjabi, S. Reimann, M. Vollmer, R. Steinbrecher, J. Hannigan, L. Emmons, E. Mahieu, B. Franco, D. Smale, and A. Pozzer (2016), Reversal of global atmospheric ethane and propane trends largely due to US Oil and natural gas production. Nature Geoscience, *Nat. Geosci.*, *9*, 490–495.

Helmig, D., N. Schwarzer, and J. Steinhanses (1990), Flame control accessory for GC-FID operation with autosampler injection, *HRC-J. High Resolut. Chromatogr.*, *13*(12), 849-851.

Helmig, D., D. M. Tanner, R. E. Honrath, R. C. Owen, and D. D. Parrish (2008), Nonmethane hydrocarbons at Pico Mountain, Azores: 1. Oxidation chemistry in the North Atlantic region, *J. Geophys. Res.-Atmos.*, *113*(D20).

Helmig, D., and L. Vierling (1995), Water-adsorption capacity of the solid adsorbents Tenax-TA, Tenax-GR, Carbotrap, Carbotrap-C, Carbosieve-SIII, and Carboxen-569 and water management techniques for the atmospheric sampling of volatile organic trace gases, *Anal. Chem.*, *67*(23), 4380-4386.

Helmig., C. R. Stephens, J. Caramore, and J. Hueber (2014a), Seasonal behavior of non-methane hydrocarbons in the firn air at Summit, Greenland, *Atmospheric Environment*, *85*, 234-246.

Helmig., C. R. Thompson, J. Evans, P. Boylan, J. Hueber, and J. H. Park (2014b), Highly elevated atmospheric levels of volatile organic compounds in the Uintah Basin, Utah, *Environ. Sci. Technol.*, *48*(9), 4707-4715.

Hirsch, R. M., R. B. Alexander, and R. A. Smith (1991), Selection of Methods for the Detection and Estimation of Trends in Water-Quality, *Water Resour. Res.*, *27*(5), 803-813.

Ho, K. F., S. C. Lee, W. K. Ho, D. R. Blake, Y. Cheng, Y. S. Li, S. S. H. Ho, K. Fung, P. K. K. Louie, and D. Park (2009), Vehicular emission of volatile organic compounds (VOCs) from a tunnel study in Hong Kong, *Atmos. Chem. Phys.*, *9*(19), 7491-7504.

Hong, S. M., J. P. Candelone, C. C. Patterson, and C. F. Boutron (1994), Greenland ice evidence of hemispheric lead pollution 2 millennia ago by Greek and Roman civilizations, *Science*, *265*(5180), 1841-1843.

Hong, S. M., J. P. Candelone, C. C. Patterson, and C. F. Boutron (1996), History of ancient copper smelting pollution during Roman and medieval times recorded in Greenland ice, *Science*, *272*(5259), 246-249.

Honrath, R. E., D. Helmig, R. C. Owen, D. D. Parrish, and D. M. Tanner (2008), Nonmethane hydrocarbons at Pico Mountain, Azores: 2. Event-specific analyses of the impacts of mixing and photochemistry on hydrocarbon ratios, *J. Geophys. Res.-Atmos.*, *113*(D20).

Honrath, R. E., R. C. Owen, M. Val-Martin, J. S. Reid, K. Lapina, P. Fialho, M. P. Dziobak, J. Kleissl, and D. L. Westphal (2004), Regional and hemispheric impacts of anthropogenic and biomass burning emissions on summertime CO and O3 in the North Atlantic lower free troposphere, *J. Geophys. Res.-Atmos.*, *109*(D24).

Hopwood, D. A. (2007), *Streptomyces in Nature and Medicine: The Antibiotic Makers*, Oxford University Press, Oxford.

Hornbrook, R. S., A. J. Hills, D. D. Riemer, A. Abdelhamid, F. M. Flocke, S. R. Hall, L. G. Huey, D. J. Knapp, J. Liao, R. L. Mauldin, D. D. Montzka, J. J. Orlando, P. B. Shepson, B. Sive, R. M. Staebler, D. J. Tanner, C. R. Thompson, A. Turnipseed, K. Ullmann, A. J. Weinheimer, and E. C. Apel (2016), Arctic springtime observations of volatile organic compounds during the OASIS-2009 campaign, *J. Geophys. Res.-Atmos.*, *121*(16), 9789-9813.

Howarth, R. W., R. Santoro, and A. Ingraffea (2011), Methane and the greenhouse-gas footprint of natural gas from shale formations, *Clim. Change*, *106*(4), 679-690.

Huang, C. B., Y. Alimova, T. M. Myers, and J. L. Ebersole (2011), Short- and medium-chain fatty acids exhibit antimicrobial activity for oral microorganisms, *Arch. Oral Biol.*, *56*(7), 650-654.

Hudman, R. C., N. E. Moore, A. K. Mebust, R. V. Martin, A. R. Russell, L. C. Valin, and R. C. Cohen (2012), Steps towards a mechanistic model of global soil nitric oxide emissions: implementation and space based-constraints, *Atmos. Chem. Phys.*, *12*(16), 7779-7795.

Huff, J. (2007), Benzene-induced cancers: Abridged history and occupational health impact, *Int. J. Occup. Environ. Health*, *13*(2), 213-221.

Huxman, T. E., K. A. Snyder, D. Tissue, A. J. Leffler, K. Ogle, W. T. Pockman, D. R. Sandquist, D. L. Potts, and S. Schwinning (2004), Precipitation pulses and carbon fluxes in semiarid and arid ecosystems, *Oecologia*, *141*(2), 254-268.

IEA (2017), Coal 2017*Rep.*, International Energy Agency, https://www.iea.org/coal2017/.

Insam, H., and M. S. A. Seewald (2010), Volatile organic compounds (VOCs) in soils, *Biol. Fertil. Soils*, *46*(3), 199-213.

Isaksen, I. S. A., O. Hov, S. A. Penkett, and A. Semb (1985), Model analysis of the measured concentration of organic gases in the Norwegian Arctic *J. Atmos. Chem.*, *3*(1), 3-27.

Isidorov, V., and M. Jdanova (2002), Volatile organic compounds from leaves litter, *Chemosphere*, *48*(9), 975-979.

ISO, I. S. O. (1999), Ambient, Indoor and Workplace Air ± Determination of Concentrations of Volatile Organic Compounds in Air, Thermal Desorption Method ± Part 2: Diffusive Sampling Method, *ISO/DIS*, *16017-2*(ISO, Geneva).

Jacob, D. J., J. A. Logan, R. M. Yevich, G. M. Gardner, C. M. Spivakovsky, S. C. Wofsy, J. W. Munger, S. Sillman, M. J. Prather, M. O. Rodgers, H. Westberg, and P. R. Zimmerman (1993), Simulation of summertime ozone over North America, *J. Geophys. Res.-Atmos.*, *98*(D8), 14797-14816.

Jacob, D. J., and D. A. Winner (2009), Effect of climate change on air quality, *Atmospheric Environment*, *43*(1), 51-63.

Janson, R. W. (1993), Monoterpene emissions from Scots Pine and Norwegian Spruce *J. Geophys. Res.-Atmos.*, *98*(D2), 2839-2850.

Janssen, P. H. (2006), Identifying the dominant soil bacterial taxa in libraries of 16S rRNA and 16S rRNA genes, *Appl. Environ. Microbiol.*, *72*(3), 1719-1728.

Janssens-Maenhout, G., M. Crippa, D. Guizzardi, F. Dentener, M. Muntean, G. Pouliot, T. Keating, Q. Zhang, J. Kurokawa, R. Wankmüller, H. Denier van der Gon, Z. Klimont, G. Frost, S. Darras, and B. Koffi (2015), HTAP_v2: a mosaic of regional and global emission gridmaps for 2008 and 2010 to study hemispheric transport of air pollution., *Atmos. Chem. Phys.*, *15*(doi:10.5194/acpd-15-12867-2015), 12867-12909.

Jelen, H., and E. Wasowicz (1998), Volatile fungal metabolites and their relation to the spoilage of agricultural commodities, *Food Rev. Int.*, *14*(4), 391-426.

Jenerette, G. D., and A. Chatterjee (2012), Soil metabolic pulses: water, substrate, and biological regulation, *Ecology*, *93*(5), 959-966.

Jenkin, M. E., S. M. Saunders, V. Wagner, and M. J. Pilling (2003), Protocol for the development of the Master Chemical Mechanism, MCM v3 (Part B): tropospheric degradation of aromatic volatile organic compounds, *Atmos. Chem. Phys.*, *3*, 181-193.

Jenkin, M. E., J. C. Young, and A. R. Rickard (2015), The MCM v3.3.1 degradation scheme for isoprene, *Atmos. Chem. Phys.*, *15*(20), 11433-11459.

Jensen, P. R., P. G. Williams, D. C. Oh, L. Zeigler, and W. Fenical (2007), Species-specific secondary metabolite production in marine actinomycetes of the genus Salinispora, *Appl. Environ. Microbiol.*, *73*(4), 1146-1152.

Jia, C. R., and X. Q. Fu (2017), Diffusive uptake rates of volatile organic compounds on standard ATD tubes for environmental and workplace applications, *Environments*, *4*(4).

Jobson, B. T., C. M. Berkowitz, W. C. Kuster, P. D. Goldan, E. J. Williams, F. C. Fesenfeld, E. C. Apel, T. Karl, W. A. Lonneman, and D. Riemer (2004), Hydrocarbon source signatures in Houston, Texas: Influence of the petrochemical industry, *J. Geophys. Res.-Atmos.*, *109*(D24).

Jobson, B. T., H. Niki, Y. Yokouchi, J. Bottenheim, F. Hopper, and R. Leaitch (1994a), Measurements of C-2-C-6 hydrocarbons during the polar sunrise 1992 experiment - evidence of Cl atom and Br atom chemistry, *J. Geophys. Res.-Atmos.*, *99*(D12), 25355-25368.

Jobson, B. T., Z. Wu, H. Niki, and L. A. Barrie (1994b), Seasonal trends of isoprene, C-2-C-5 alkanes, and acetylene at a remote boreal site in Canada, *J. Geophys. Res.-Atmos.*, *99*(D1), 1589-1599.

Jöckel, P., A. Kerkweg, A. Pozzer, R. Sander, H. Tost, H. Riede, A. Baumgaertner, S. Gromov, and B. Kern (2010), Development cycle 2 of the Modular Earth Submodel System (MESSy2), *Geosci. Model Dev.*, *3*(2), 717-752.

Jockel, P., H. Tost, A. Pozzer, C. Bruhl, J. Buchholz, L. Ganzeveld, P. Hoor, A. Kerkweg, M. G. Lawrence, R. Sander, B. Steil, G. Stiller, M. Tanarhte, D. Taraborrelli, J. Van Aardenne, and J. Lelieveld (2006), The atmospheric chemistry general circulation model ECHAM5/MESSy1: consistent simulation of ozone from the surface to the mesosphere, *Atmos. Chem. Phys.*, *6*, 5067-5104.

Johnson, R., and J. J. Toth (1982), A climatology of the July 1981 surface flow over northeast Colorado, *Department of Atmospheric Science, Colorado State University*, *Paper No. 342*.

Jones, S. E., and M. A. Elliot (2017), Streptomyces Exploration: Competition, Volatile Communication and New Bacterial Behaviours, *Trends Microbiol.*, *25*(7), 523-532.

Jones, S. E., L. Ho, C. A. Rees, J. E. Hill, J. R. Nodwell, and M. A. Elliot (2017), Streptomyces exploration is triggered by fungal interactions and volatile signals, *eLife*, *6*.

Kai, M., U. Effmert, G. Berg, and B. Piechulla (2007), Volatiles of bacterial antagonists inhibit mycelial growth of the plant pathogen Rhizoctonia solani, *Arch. Microbiol.*, *187*(5), 351-360.

Kai, M., M. Haustein, F. Molina, A. Petri, B. Scholz, and B. Piechulla (2009), Bacterial volatiles and their action potential, *Appl. Microbiol. Biotechnol.*, *81*(6), 1001-1012.

Kang, M., C. M. Kanno, M. C. Reid, X. Zhang, D. L. Mauzerall, M. A. Celia, Y. Chen, and T. C. Onstott (2014), Direct measurements of methane emissions from abandoned oil and gas wells in Pennsylvania, *Proceedings of the National Academy of Sciences*, *111*(51), 18173-18177.

Karion, A., C. Sweeney, E. A. Kort, P. B. Shepson, A. Brewer, M. Cambaliza, S. A. Conley, K. Davis, A. Deng, M. Hardesty, S. C. Herndon, T. Lauvaux, T. Lavoie, D. Lyon, T. Newberger, G. Petron, C. Rella, M. Smith, S. Wolter, T. I. Yacovitch, and P. Tans (2015), Aircraft-Based Estimate of Total Methane Emissions from the Barnett Shale Region, *Environ. Sci. Technol.*, *49*(13), 8124-8131.

Karion, A., C. Sweeney, G. Petron, G. Frost, M. Hardesty, J. Kofler, B. R. Miller, T. Newberger, S. Wolter, R. Banta, A. Brewer, E. J. Dlugkencky, P. Lang, S. A. Montzka, R. C. Schnell, P. Tans, M. Trainer, R. Zomora, and S. Conley (2013), Methane emissions estimate from airborne measurements over a western United States natural gas field, *Geophys. Res. Lett.*, *40*, 1-5.

Karl, T., R. Fall, P. J. Crutzen, A. Jordan, and W. Lindinger (2001), High concentrations of reactive biogenic VOCs at a high altitude site in late autumn, *Geophys. Res. Lett.*, *28*(3), 507-510.

Kaser, L., E. G. Patton, G. G. Pfister, A. J. Weinheimer, D. D. Montzka, F. Flocke, A. M. Thompson, R. M. Stauffer, and H. S. Halliday (2017), The effect of entrainment through atmospheric boundary layer growth on observed and modeled surface ozone in the Colorado Front Range, *J. Geophys. Res.-Atmos.*, *122*(11), 6075-6093.

Kasting, J. F., and H. B. Singh (1986), Nonmethane hydrocarbons in the troposphere - Impact on the odd hydrogen and odd nitrogen chemistry *J. Geophys. Res.-Atmos.*, *91*(D12), 3239-3256.

Katoh, K., and D. M. Standley (2013), MAFFT Multiple Sequence Alignment Software Version 7: Improvements in Performance and Usability, *Mol. Biol. Evol.*, *30*(4), 772-780.

Katsouyanni, K., G. Touloumi, C. Spix, J. Schwartz, F. Balducci, S. Medina, G. Rossi, B. Wojtyniak, J. Sunyer, L. Bacharova, J. P. Schouten, A. Ponka, and H. R. Anderson (1997), Short term effects of ambient sulphur dioxide and particulate matter on mortality in 12 European cities: Results from time series data from the APHEA project, *BMJ-British Medical Journal*, *314*(7095), 1658-1663.

Katzenstein, A. S., L. A. Doezema, I. J. Simpson, D. R. Balke, and F. S. Rowland (2003), Extensive regional atmospheric hydrocarbon pollution in the southwestern United States, *Proc. Natl. Acad. Sci. U. S. A.*, *100*(21), 11975-11979.

Kendall, M. G. (1975), *Rank Correlation Methods*, 4th ed., Charles Griffin, London.

Kille, N., S. Baidar, P. Handley, I. Ortega, R. Sinreich, O. R. Cooper, F. Hase, J. W. Hannigan, G. Pfister, and R. Volkamer (2017), The CU mobile Solar Occultation Flux instrument: structure functions and emission rates of NH3, NO2 and C2H6, *Atmos. Meas. Tech.*, *10*(1), 373-392.

Kim, D. G., R. Vargas, B. Bond-Lamberty, and M. R. Turetsky (2012), Effects of soil rewetting and thawing on soil gas fluxes: a review of current literature and suggestions for future research, *Biogeosciences*, *9*(7), 2459-2483.

Kim, K. S., S. Lee, and C. M. Ryu (2013), Interspecific bacterial sensing through airborne signals modulates locomotion and drug resistance, *Nat. Commun.*, *4*.

Kim, S., A. Guenther, T. Karl, and J. Greenberg (2011), Contributions of primary and secondary biogenic VOC tototal OH reactivity during the CABINEX (Community Atmosphere-Biosphere INteractions Experiments)-09 field campaign, *Atmos. Chem. Phys.*, *11*(16), 8613-8623.

Kirschke, S., P. Bousquet, P. Ciais, M. Saunois, J. G. Canadell, E. J. Dlugokencky, P. Bergamaschi, D. Bergmann, D. R. Blake, L. Bruhwiler, P. Cameron-Smith, S. Castaldi, F. Chevallier, L. Feng, A. Fraser, M. Heimann, E. L. Hodson, S. Houweling, B. Josse, P. J. Fraser, P. B. Krummel, J.-F. Lamarque, R. L. Langenfelds, C. Le Quere, V. Naik, S. O'Doherty, P. I. Palmer, I. Pison, D. Plummer, B. Poulter, R. G. Prinn, M. Rigby, B. Ringeval, M. Santini, M. Schmidt, D. T. Shindell, I. J. Simpson, R. Spahni, L. P. Steele, S. A. Strode, K. Sudo, S. Szopa, G. R. van der Werf, A. Voulgarakis, M. van Weele, R. F. Weiss, J. E. Williams, and G. Zeng (2013), Three decades of global methane sources and sinks, *Nat. Geosci.*, *6*(10), 813-823.

Kleeman, M. J. (2008), A preliminary assessment of the sensitivity of air quality in California to global change, *Clim. Change*, *87*, S273-S292.

Kort, E. A., M. L. Smith, L. T. Murray, A. Gvakharia, A. R. Brandt, J. Peischl, T. B. Ryerson, C. Sweeney, and K. Travis (2016), Fugitive emissions from the Bakken shale illustrate role of shale production in global ethane shift, *Geophys. Res. Lett.*, *43*(9), 4617-4623.

Koss, A., B. Yuan, C. Warneke, J. B. Gilman, B. M. Lerner, P. R. Veres, J. Peischl, S. Eilerman, R. Wild, S. S. Brown, C. R. Thompson, T. Ryerson, T. Hanisco, G. M. Wolfe, J. M. S. Clair, M. Thayer, F. N. Keutsch, S. Murphy, and J. de Gouw (2017), Observations of VOC emissions and photochemical products over US oil- and gas-producing regions using high-resolution H3O+ CIMS (PTR-ToF-MS), *Atmos. Meas. Tech.*, *10*(8), 2941-2968.

Koutrakis, P., J. M. Wolfson, A. Bunyaviroch, S. E. Froehlich, K. Hirano, and J. D. Mulik (1993), Measurement of ambient ozone using a nitrite-coated filter *Anal. Chem.*, *65*(3), 209-214.

Kramer, L. J., D. Helmig, J. F. Burkhart, A. Stohl, S. Oltmans, and R. E. Honrath (2015), Seasonal variability of atmospheric nitrogen oxides and non-methane hydrocarbons at the GEOSummit station, Greenland, *Atmos. Chem. Phys.*, *15*(12), 6827-6849.

Krohn, J., and G. Nulle (2015), Utica Provides 85% of U.S. Shale Gas Production Growth Since Start of 2012, edited, U.S. Energy Information Administration.

Krupa, S. V., and A. H. Legge (2000), Passive sampling of ambient, gaseous air pollutants: an assessment from an ecological perspective, *Environ. Pollut.*, *107*(1), 31-45.

Kuntzel, A., S. Fischer, A. Bergmann, P. Oertel, M. Steffens, P. Trefz, W. Miekisch, J. K. Schubert, P. Reinhold, and H. Kohler (2016), Effects of biological and methodological factors on volatile organic compound patterns during cultural growth of Mycobacterium avium ssp paratuberculosis, *J. Breath Res.*, *10*(3).

Lacey, W. N., B. H. Sage, and C. E. Kircher (1934), Phase equilibria in hydrocarbon systems III Solubility of a dry natural gas in crude oil, *Industrial and Engineering Chemistry*, *26*, 652-654.

Lack, D. A., J. M. Langridge, R. Bahreini, C. D. Cappa, A. M. Middlebrook, and J. P. Schwarz (2012), Brown carbon and internal mixing in biomass burning particles, *Proc. Natl. Acad. Sci. U. S. A.*, *109*(37), 14802-14807.

Lado-Monserrat, L., C. Lull, I. Bautista, A. Lidon, and R. Herrera (2014), Soil moisture increment as a controlling variable of the "Birch effect". Interactions with the pre-wetting soil moisture and litter addition, *Plant Soil*, *379*(1-2), 21-34.

LaFranchi, B. W., G. Petron, J. B. Miller, S. J. Lehman, A. E. Andrews, E. J. Dlugokencky, B. Hall, B. R. Miller, S. A. Montzka, W. Neff, P. C. Novelli, C. Sweeney, J. C. Turnbull, D. E. Wolfe, P. P. Tans, K. R. Gurney, and T. P. Guilderson (2013), Constraints on emissions of carbon monoxide, methane, and a suite of hydrocarbons in the Colorado Front Range using observations of (CO2)-C-14, *Atmos. Chem. Phys.*, *13*(21), 11101-11120.

Lamarque, J. F., L. K. Emmons, P. G. Hess, D. E. Kinnison, S. Tilmes, F. Vitt, C. L. Heald, E. A. Holland, P. H. Lauritzen, J. Neu, J. J. Orlando, P. J. Rasch, and G. K. Tyndall (2012), CAM-chem: description and evaluation of interactive atmospheric chemistry in the Community Earth System Model, *Geosci. Model Dev.*, *5*(2), 369-411.

Lamarque, J. F., P. Hess, L. Emmons, L. Buja, W. Washington, and C. Granier (2005), Tropospheric ozone evolution between 1890 and 1990, *J. Geophys. Res.-Atmos.*, *110*(D8).

Lamarque, J. F., D. T. Shindell, B. Josse, P. J. Young, I. Cionni, V. Eyring, D. Bergmann, P. Cameron-Smith, W. J. Collins, R. Doherty, S. Dalsoren, G. Faluvegi, G. Folberth, S. J. Ghan, L. W. Horowitz, Y. H. Lee, I. A. MacKenzie, T. Nagashima, V. Naik, D. Plummer, M. Righi, S. T. Rumbold, M. Schulz, R. B. Skeie, D. S. Stevenson, S. Strode, K. Sudo, S. Szopa, A. Voulgarakis, and G. Zeng (2013), The Atmospheric Chemistry and Climate Model Intercomparison Project (ACCMIP): overview and description of models, simulations and climate diagnostics, *Geoscientific Model Development*, *6*(1), 179-206.

Lamb, B., A. Guenther, D. Gay, and H. Westberg (1987), A national inventory of biogenic hydrocarbon emissions *Atmospheric Environment*, *21*(8), 1695-1705.

Larsen, T. O., and J. C. Frisvad (1995), Characterization of Volatile Metabolites from 47 Penicillum-Taxa, *Mycol. Res.*, *99*, 1153-1166.

Lawrence, D. M., K. W. Oleson, M. G. Flanner, P. E. Thornton, S. C. Swenson, P. J. Lawrence, X. B. Zeng, Z. L. Yang, S. Levis, K. Sakaguchi, G. B. Bonan, and A. G. Slater (2011), Parameterization Improvements and Functional and Structural Advances in Version 4 of the Community Land Model, *J. Adv. Model. Earth Syst.*, *3*.

Leff, J. W., and N. Fierer (2008), Volatile organic compound (VOC) emissions from soil and litter samples, *Soil Biol. Biochem.*, *40*(7), 1629-1636.

Leibensperger, E. M., L. J. Mickley, and D. J. Jacob (2008), Sensitivity of US air quality to mid-latitude cyclone frequency and implications of 1980-2006 climate change, *Atmos. Chem. Phys.*, *8*(23), 7075-7086.

Lemfack, M. C., B. O. Gohlke, S. M. T. Toguem, S. Preissner, B. Piechulla, and R. Preissner (2018), mVOC 2.0: a database of microbial volatiles, *Nucleic Acids Res.*, *46*(D1), D1261-D1265.

Lemfack, M. C., J. Nickel, M. Dunkel, R. Preissner, and B. Piechulla (2014), mVOC: a database of microbial volatiles, *Nucleic Acids Res.*, *42*(D1), D744-D748.

Leuchner, M., S. Gubo, C. Schunk, C. Wastl, M. Kirchner, A. Menzel, and C. Plass-Dülmer (2015), Can positive matrix factorization help to understand patterns of organic trace gases at the continental Global Atmosphere Watch site Hohenpeissenberg?, *Atmos. Chem. Phys.*, *15*, 1221-1236.

Leung, L. R., and W. I. Gustafson (2005), Potential regional climate change and implications to US air quality, *Geophys. Res. Lett.*, *32*(16).

Levine, J. S., T. R. Augustsson, I. C. Anderson, J. M. Hoell, and D. A. Brewer (1984), Tropospheric sources of NOx - Lightning and biology *Atmospheric Environment*, *18*(9), 1797-1804.

Lewis, A. C., M. J. Evans, J. R. Hopkins, S. Punjabi, K. A. Read, R. M. Purvis, S. J. Andrews, S. J. Moller, L. J. Carpenter, J. D. Lee, A. R. Rickard, P. I. Palmer, and M. Parrington (2013), The influence of biomass burning on the global distribution of selected non-methane organic compounds, *Atmos. Chem. Phys.*, *13*(2), 851-867.

Lightfoot, P. D., R. A. Cox, J. N. Crowley, M. Destriau, G. D. Hayman, M. E. Jenkin, G. K. Moortgat, and F. Zabel (1992), Organic peroxy radicals - Kinetics, spectroscopy, and tropospheric chemistry *Atmospheric Environment Part a-General Topics*, *26*(10), 1805-1961.

Lim, F. Y., J. F. Sanchez, C. C. C. Wang, and N. P. Keller (2012a), Toward Awakening Cryptic Secondary Metabolite Gene Clusters in Filamentous Fungi, in *Natural Product Biosynthesis by Microorganisms and Plants, Pt C*, edited by D. A. Hopwood, pp. 303-324, Elsevier Academic Press Inc, San Diego.

Lim, S. S., T. Vos, A. D. Flaxman, G. Danaei, K. Shibuya, H. Adair-Rohani, M. Amann, H. R. Anderson, K. G. Andrews, M. Aryee, C. Atkinson, L. J. Bacchus, A. N. Bahalim, K. Balakrishnan, J. Balmes, S. Barker-Collo, A. Baxter, M. L. Bell, J. D. Blore, F. Blyth, C. Bonner, G. Borges, R. Bourne, M. Boussinesq, M. Brauer, P. Brooks, N. G. Bruce, B.

Brunekreef, C. Bryan-Hancock, C. Bucello, R. Buchbinder, F. Bull, R. T. Burnett, T. E. Byers, B. Calabria, J. Carapetis, E. Carnahan, Z. Chafe, F. Charlson, H. L. Chen, J. S. Chen, A. T. A. Cheng, J. C. Child, A. Cohen, K. E. Colson, B. C. Cowie, S. Darby, S. Darling, A. Davis, L. Degenhardt, F. Dentener, D. C. Des Jarlais, K. Devries, M. Dherani, E. L. Ding, E. R. Dorsey, T. Driscoll, K. Edmond, S. E. Ali, R. E. Engell, P. J. Erwin, S. Fahimi, G. Falder, F. Farzadfar, A. Ferrari, M. M. Finucane, S. Flaxman, F. G. R. Fowkes, G. Freedman, M. K. Freeman, E. Gakidou, S. Ghosh, E. Giovannucci, G. Gmel, K. Graham, R. Grainger, B. Grant, D. Gunnell, H. R. Gutierrez, W. Hall, H. W. Hoek, A. Hogan, H. D. Hosgood, D. Hoy, H. Hu, B. J. Hubbell, S. J. Hutchings, S. E. Ibeanusi, G. L. Jacklyn, R. Jasrasaria, J. B. Jonas, H. D. Kan, J. A. Kanis, N. Kassebaum, N. Kawakami, Y. H. Khang, S. Khatibzadeh, J. P. Khoo, C. Kok, F. Laden, R. Lalloo, Q. Lan, T. Lathlean, J. L. Leasher, J. Leigh, Y. Li, J. K. Lin, S. E. Lipshultz, S. London, R. Lozano, Y. Lu, J. Mak, R. Malekzadeh, L. Mallinger, W. Marcenes, L. March, R. Marks, R. Martin, P. McGale, J. McGrath, S. Mehta, G. A. Mensah, T. R. Merriman, R. Micha, C. Michaud, V. Mishra, K. M. Hanafiah, A. A. Mokdad, L. Morawska, D. Mozaffarian, T. Murphy, M. Naghavi, B. Neal, P. K. Nelson, J. M. Nolla, R. Norman, C. Olives, S. B. Omer, J. Orchard, R. Osborne, B. Ostro, A. Page, K. D. Pandey, C. D. H. Parry, E. Passmore, J. Patra, N. Pearce, P. M. Pelizzari, M. Petzold, M. R. Phillips, D. Pope, C. A. Pope, J. Powles, M. Rao, H. Razavi, E. A. Rehfuess, J. T. Rehm, B. Ritz, F. P. Rivara, T. Roberts, C. Robinson, J. A. Rodriguez-Portales, I. Romieu, R. Room, L. C. Rosenfeld, A. Roy, L. Rushton, J. A. Salomon, U. Sampson, L. Sanchez-Riera, E. Sanman, A. Sapkota, S. Seedat, P. L. Shi, K. Shield, R. Shivakoti, G. M. Singh, D. A. Sleet, E. Smith, K. R. Smith, N. J. C. Stapelberg, K. Steenland, H. Stockl, L. J. Stovner, K. Straif, L. Straney, G. D. Thurston, J. H. Tran, R. Van Dingenen, A. van Donkelaar, J. L. Veerman, L. Vijayakumar, R. Weintraub, M. M. Weissman, R. A. White, H. Whiteford, S. T. Wiersma, J. D. Wilkinson, H. C. Williams, W. Williams, N. Wilson, A. D. Woolf, P. Yip, J. M. Zielinski, A. D. Lopez, C. J. L. Murray, and M. Ezzati (2012b), A comparative risk assessment of burden of disease and injury attributable to 67 risk factors and risk factor clusters in 21 regions, 1990-2010: a systematic analysis for the Global Burden of Disease Study 2010, *Lancet*, *380*(9859), 2224-2260.

Lin, J. T. (2012), Satellite constraint for emissions of nitrogen oxides from anthropogenic, lightning and soil sources over East China on a high-resolution grid, *Atmos. Chem. Phys.*, *12*(6), 2881-2898.

Liu, S. C., M. Trainer, F. C. Fehsenfeld, D. D. Parrish, E. J. Williams, D. W. Fahey, G. Hubler, and P. C. Murphy (1987), Ozone production in the rural troposphere and the implications for regional and global ozone distributions *J. Geophys. Res.-Atmos.*, *92*(D4), 4191-4207.

Llop, S., F. Ballester, M. Estarlich, A. Esplugues, M. Rebagliato, and C. Iniguez (2010), Preterm birth and exposure to air pollutants during pregnancy, *Environ. Res.*, *110*(8), 778-785.

Lodge, J. P. (1999), *Methods of Air Sampling and Analysis, 4th ed.*, CRC Press, Boca Raton, FL.

Logan, J. A. (1983), Nitrogen oxides in the troposphere - global and regional budgets, *Journal of Geophysical Research-Oceans and Atmospheres*, *88*(NC15), 785-807.

Logan, J. A. (1985), Tropospheric ozone - Seasonal behavior, trends, and anthropogenic influence *J. Geophys. Res.-Atmos.*, *90*(ND6), 10463-10482.

Luckin, B. (2003), 'The heart and home of horror': The great London fogs of the late nineteenth century, *Soc. Hist.*, *28*(1), 31-48.

Ludwig, W., J. Euzeby, and P. Schumann (2015), Road map of the phylum Actinobacteria, in *Bergey's Manual of Systematics of Archaea and Bacteria*, edited.

Lundgren, L. (1998), *Acid rain on the agenda: a picture of a chain of events in Sweden, 1966-1968*, Lund University Press, Lund.

Lundquist, E. J., L. E. Jackson, and K. M. Scow (1999), Wet-dry cycles affect dissolved organic carbon in two California agricultural soils, *Soil Biol. Biochem.*, *31*(7), 1031-1038.

Lupo, P. J., E. Symanski, D. K. Waller, W. Y. Chan, P. H. Langlois, M. A. Canfield, and L. E. Mitchell (2011), Maternal exposure to ambient levels of benzene and neural tube defects among offspring: Texas, 1999-2004, *Environ. Health Perspect.*, *119*(3), 397-402.

Macey, G. P., R. Breech, M. Chernaik, C. Cox, D. Larson, D. Thomas, and D. O. Carpenter (2014), Air concentrations of volatile compounds near oil and gas production: a community-based exploratory study, *Environ. Health*, *13*.

Maddula, S., L. M. Blank, A. Schmid, and J. I. Baumbach (2009), Detection of volatile metabolites of Escherichia coli by multi capillary column coupled ion mobility spectrometry, *Analytical and Bioanalytical Chemistry*, *394*(3), 791-800.

Magliano, K. L., V. M. Hughes, L. R. Chinkin, D. L. Coe, T. L. Haste, N. Kumar, and F. W. Lurmann (1999), Spatial and temporal variations in PM10 and PM2.5 source contributions and comparison to emissions during the 1995 integrated monitoring study, *Atmospheric Environment*, *33*(29), 4757-4773.

Mahmud, A., M. Tyree, D. Cayan, N. Motallebi, and M. J. Kleeman (2008), Statistical downscaling of climate change impacts on ozone concentrations in California, *J. Geophys. Res.-Atmos.*, *113*(D21).

Mancuso, S., C. Taiti, N. Bazihizina, C. Costa, P. Menesatti, L. Giagnoni, M. Arenella, P. Nannipieri, and G. Renella (2015), Soil volatile analysis by proton transfer reaction-time of flight mass spectrometry (PTR-TOF-MS), *Appl. Soil Ecol.*, *86*, 182-191.

Mann, H. B. (1945), Nonparametric Tests Against Trend, *Econometrica*, *13*(3), 245-259.

Martin, N. A., E. J. Leming, M. H. Henderson, R. P. Lipscombe, J. K. Black, and S. D. Jarvis (2010), Verification of diffusive and pumped samplers for volatile organic compounds using a controlled atmosphere test facility, *Atmospheric Environment*, *44*(28), 3378-3385.

Masarie, K. A., and P. P. Tans (1995), Extension and integration of atmospheric carbon-dioxide data into a globally consistent measurement record, *J. Geophys. Res.-Atmos.*, *100*(D6), 11593-11610.

Mayrsohn, H., and J. H. Crabtree (1976), Source reconciliation of atmospheric hydrocarbons, *Atmospheric Environment*, *10*(2), 137-143.

McDonald, B. C., J. A. de Gouw, J. B. Gilman, S. H. Jathar, A. Akherati, C. D. Cappa, J. L. Jimenez, J. Lee-Taylor, P. L. Hayes, S. A. McKeen, Y. Y. Cui, S. W. Kim, D. R. Gentner, G. Isaacman-VanWertz, A. H. Goldstein, R. A. Harley, G. J. Frost, J. M. Roberts, T. B. Ryerson, and M. Trainer (2018), Volatile chemical products emerging as largest petrochemical source of urban organic emissions, *Science*, *359*(6377), 760-764.

McDonald, B. C., D. R. Gentner, A. H. Goldstein, and R. A. Harley (2013), Long-Term Trends in Motor Vehicle Emissions in US Urban Areas, *Environ. Sci. Technol.*, *47*(17), 10022-10031.

McDonald, D., M. N. Price, J. Goodrich, E. P. Nawrocki, T. Z. DeSantis, A. Probst, G. L. Andersen, R. Knight, and P. Hugenholtz (2012), An improved Greengenes taxonomy with explicit ranks for ecological and evolutionary analyses of bacteria and archaea, *Isme J.*, *6*(3), 610-618.

McKeen, S. A., and S. C. Liu (1993), Hydrocarbon ratios and photochemical histories of air masses, *Geophys. Res. Lett.*, *20*(21), 2363-2366.

McKenzie, L. M., B. Blair, J. Hughes, W. B. Allshouse, N. J. Blake, D. Helmig, P. Milmoe, H. Halliday, D. R. Blake, and J. L. Adgate (2018), Ambient nonmethane hydrocarbon levels along Colorado's Northern Front Range: Acute and chronic health risks, *Environ. Sci. Technol.*, *52*(8), 4514-4525.

McKenzie, L. M., R. Guo, R. Z. Witter, D. A. Savitz, L. S. Newman, and J. L. Adgate (2015), Birth outcomes and maternal residential proximity to natural lgas development in rural Colorado, *Environ. Health Perspect.*, *http://dx.doi.org/10.1289/ehp.1306722*.

McKenzie, L. M., R. Guo, R. Z. Witter, D. A. Savitz, L. S. Newman, and J. L. Adgate (2014), Birth outcomes and natural gas development: McKenzie et al. respond, *Environ. Health Perspect.*, *122*(9), A232-A233.

McKenzie, L. M., R. Z. Witter, L. S. Newman, and J. L. Adgate (2012), Human health risk assessment of air emissions from development of unconventional natural gas resources, *Sci. Total Environ.*, *424*, 79-87.

McKenzie, R. L., P. J. Aucamp, A. F. Bais, L. O. Bjorn, M. Ilyas, and S. Madronich (2011), Ozone depletion and climate change: impacts on UV radiation, *Photochem. Photobiol. Sci.*, *10*(2), 182-198.

McNeill, J. R. (2001), *Something new under the Sun. An environmental history of the 20th century world*, W.W. Norton Company, New York.

McShane, C. (1999), The origins and globalization of traffic control signals, *J. Urban Hist.*, *25*(3), 379-404.

Medema, M. H., and M. A. Fischbach (2015), Computational approaches to natural product discovery, *Nat. Chem. Biol.*, *11*(9), 639-648.

Meleux, F., F. Solmon, and F. Giorgi (2007), Increase in summer European ozone amounts due to climate change, *Atmospheric Environment*, *41*(35), 7577-7587.

Menut, L., C. Flamant, J. Pelon, and P. H. Flamant (1999), Urban boundary-layer height determination from lidar measurements over the Paris area, *Appl. Optics*, *38*(6), 945-954.

Miller, B. R., R. F. Weiss, P. K. Salameh, T. Tanhua, B. R. Greally, J. Muhle, and P. G. Simmonds (2008), Medusa: A sample preconcentration and GC/MS detector system for in situ measurements of atmospheric trace halocarbons, hydrocarbons, and sulfur compounds, *Anal. Chem.*, *80*(5), 1536-1545.

Millstein, D. E., and R. A. Harley (2009), Impact of climate change on photochemical air pollution in Southern California, *Atmos. Chem. Phys.*, *9*(11), 3745-3754.

Minerdi, D., M. Moretti, G. Gilardi, C. Barberio, M. L. Gullino, and A. Garibaldi (2008), Bacterial ectosymbionts and virulence silencing in a Fusarium oxysporum strain, *Environ. Microbiol.*, *10*(7), 1725-1741.

Minnich, M. (1993), *Behavior and determination of volatile organic compounds in soil: A literature review*.

Molfino, N. A., S. C. Wright, I. Katz, S. Tarlo, F. Silverman, P. A. McClean, J. P. Szalai, M. Raizenne, A. S. Slutsky, and N. Zamel (1991), Effect of low concentrations of ozone on inhalded allergen responses in asthmatic subjects *Lancet*, *338*(8761), 199-203.

Molina, M. J., and F. S. Rowland (1974), Stratospheric sink for chlorofluoromethanes - chlorine atomic - catalyzed destruction of ozone *Nature*, *249*(5460), 810-812.

Monks, P. S. (2005), Gas-phase radical chemistry in the troposphere, *Chem. Soc. Rev.*, *34*(5), 376-395.

Monks, P. S., A. T. Archibald, A. Colette, O. Cooper, M. Coyle, R. Derwent, D. Fowler, C. Granier, K. S. Law, G. E. Mills, D. S. Stevenson, O. Tarasova, V. Thouret, E. von Schneidemesser, R. Sommariva, O. Wild, and M. L. Williams (2015), Tropospheric ozone and its precursors from the urban to the global scale from air quality to short-lived climate forcer, *Atmos. Chem. Phys.*, *15*(15), 8889-8973.

Monks, P. S., C. Granier, S. Fuzzi, A. Stohl, M. L. Williams, H. Akimoto, M. Amann, A. Baklanov, U. Baltensperger, I. Bey, N. Blake, R. S. Blake, K. Carslaw, O. R. Cooper, F. Dentener, D. Fowler, E. Fragkou, G. J. Frost, S. Generoso, P. Ginoux, V. Grewe, A. Guenther, H. C. Hansson, S. Henne, J. Hjorth, A. Hofzumahaus, H. Huntrieser, I. S. A. Isaksen, M. E. Jenkin, J. Kaiser, M. Kanakidou, Z. Klimont, M. Kulmala, P. Laj, M. G. Lawrence, J. D. Lee, C. Liousse, M. Maione, G. McFiggans, A. Metzger, A. Mieville, N. Moussiopoulos, J. J. Orlando, C. D. O'Dowd, P. I. Palmer, D. D. Parrish, A. Petzold, U. Platt, U. Poschl, A. S. H. Prevot, C. E. Reeves, S. Reimann, Y. Rudich, K. Sellegri, R. Steinbrecher, D. Simpson, H. ten Brink, J.

Theloke, G. R. van der Werf, R. Vautard, V. Vestreng, C. Vlachokostas, and R. von Glasow (2009), Atmospheric composition change - global and regional air quality, *Atmospheric Environment*, *43*(33), 5268-5350.

Monson, R. K., and E. A. Holland (2001), Biospheric trace gas fluxes and their control over tropospheric chemistry, *Annu. Rev. Ecol. Syst.*, *32*, 547-+.

Morag-Levine, N. (2003), *Chasing the wind: regulating air pollution in the common law state*, Perseus Press, Princeton.

Mosley, S. (2008), *The chimney of the world: a history of smoke pollution in Victorian and Edwardian Manchester*, Routledge, London.

Mosley, S. (2014), Environmental History of Air Pollution and Protection, in *The Basic Environmental History*, edited by M. Agnoletti and S. Neri Serneri, pp. 143-169, Springer International Publishing, Cham.

Mowrer, J., P.-A. Svanberg, A. Potter, and A. Lindskog (1996), Diffusive monitoring of C6-C9 hydrocarbons in urban air in Sweden, *Analyst*, *121*, 1295-1300.

Moyano, F. E., S. Manzoni, and C. Chenu (2013), Responses of soil heterotrophic respiration to moisture availability: An exploration of processes and models, *Soil Biol. Biochem.*, *59*, 72-85.

Munson, M. A., A. Banerjee, T. F. Watson, and W. G. Wade (2004), Molecular analysis of the microflora associated with dental caries, *J. Clin. Microbiol.*, *42*(7), 3023-3029.

Murozumi, M., T. J. Chow, and C. Patterson (1969), Chemical concentrations of pollutant lead aerosols, terrestrial dusts and sea salts in Greenland and Antarctic snow strata *Geochim. Cosmochim. Acta*, *33*(10), 1247-+.

Namkung, H., H. Yu, J. Gong, and S. Leeson (2011), Antimicrobial activity of butyrate glycerides toward Salmonella Typhimurium and Clostridium perfringens, *Poult. Sci.*, *90*(10), 2217-2222.

Naseby, D. C., J. A. Way, N. J. Bainton, and J. M. Lynch (2001), Biocontrol of Pythium in the pea rhizosphere by antifungal metabolite producing and non-producing Pseudomonas strains, *J. Appl. Microbiol.*, *90*(3), 421-429.

Nicewonger, M. R., K. R. Verhulst, M. Aydin, and E. S. Saltzman (2016), Preindustrial atmospheric ethane levels inferred from polar ice cores: A constraint on the geologic sources of atmospheric ethane and methane, *Geophys. Res. Lett.*, *43*(1), 214-221.

Niedojadlo, A., K. H. Becker, R. Kurtenbach, and P. Wiesen (2007), The contribution of traffic and solvent use to the total NMVOC emission in a German city derived from measurements and CMB modelling, *Atmospheric Environment*, *41*(33), 7108-7126.

Nriagu, J., and S. Norton (1983), Lead and lead poisoning in antiquity, *N. Engl. J. Med.*, *309*(14), 864-864.

Nye, D. E. (1998), *Consuming power: A social history of American energies*, MIT Press, Cambridge, MA.

Ochi, K., and T. Hosaka (2013), New strategies for drug discovery: activation of silent or weakly expressed microbial gene clusters, *Appl. Microbiol. Biotechnol.*, *97*(1), 87-98.

Oksanen, J., F. G. Blanchet, R. Kindt, P. Legendre, P. Minchin, R. B. O'Hara, G. Simpson, P. Solymos, M. H. H. Stevens, and H. Wagner (2017), *Vegan: community ecology package. R package version 2.4-3 https://CRAN.R-project.org/package=vegan*.

Olszyna, K. J., M. Luria, and J. F. Meagher (1997), The correlation of temperature and rural ozone levels in southeastern USA, *Atmospheric Environment*, *31*(18), 3011-3022.

Oltmans, S., R. C. Schnell, B. Johnson, G. Petron, T. Mefford, and R. N. I. Neely (2014), Anatomy of wintertime ozone associated with oil and natural gas extraction activity in Wyoming and Utah, *Elementa*, *2*, doi: 10.12952/journal.elementa.000024.

Omori, T., Y. Saiki, K. Kasuga, and T. Kodama (1995), Desulfurization of alkyl and aromatic sulfides and sulfonates by dibenzothiophene-desulfurizing rhodococcus sp strain SY1 *Biosci. Biotechnol. Biochem.*, *59*(7), 1195-1198.

Oram, D. E., M. J. Ashfold, J. C. Laube, L. J. Gooch, S. Humphrey, W. T. Sturges, E. Leedham-Elvidge, G. L. Forster, N. R. P. Harris, M. I. Mead, A. Abu Samah, S. M. Phang, C. F. Ou-Yang, N. H. Lin, J. L. Wang, A. K. Baker, C. A. M. Brenninkmeijer, and D. Sherry (2017), A growing threat to the ozone layer from short-lived anthropogenic chlorocarbons, *Atmos. Chem. Phys.*, *17*(19), 11929-11941.

Osborn, M. (2004), *Uplands downwind: acidity and ecological change in the Southeast Lancashire*

Moorlands. In: Dupuis EM (ed) Smoke and mirrors: the politics and culture of air pollution, New York University Press, New York.

Oury, B., F. Lhuillier, J. C. Protois, and Y. Morele (2006), Behavior of the GABIE, 3M 3500, PerkinElmer Tenax TA, and RADIELLO 145 diffusive samplers exposed over a long time to a low concentration of VOCs, *J. Occup. Environ. Hyg.*, *3*(10), 547-557.

Owen, S. M., S. Clark, M. Pompe, and K. T. Semple (2007), Biogenic volatile organic compounds as potential carbon sources for microbial communities in soil from the rhizosphere of Populus tremula, *FEMS Microbiol. Lett.*, *268*(1), 34-39.

Paavolainen, L., V. Kitunen, and A. Smolander (1998), Inhibition of nitrification in forest soil by monoterpenes, *Plant Soil*, *205*(2), 147-154.

Palmes, E. D., and A. F. Gunnison (1973), Personal monitoring device for gaseous contaminants, *Am. Ind. Hyg. Assoc. J.*, *34*(2), 78-81.

Pankow, J. F. (1987), Review and comparitive analysis of the theories on partitioning between the gas and aersol particulate phases in the atmosphere, *Atmospheric Environment*, *21*(11), 2275-2283.

Parrish, D. D., C. J. Hahn, E. J. Williams, R. B. Norton, F. C. Fehsenfeld, H. B. Singh, J. D. Shetter, B. W. Gandrud, and B. A. Ridley (1992), Indications of photochemical histories of Pacific air masses from measurements of atmospheric trace species at Point Arena, California, *J. Geophys. Res.-Atmos.*, *97*(D14), 15883-15901.

Parrish, D. D., W. C. Kuster, M. Shao, Y. Yokouchi, Y. Kondo, P. D. Goldan, J. A. de Gouw, M. Koike, and T. Shirai (2009), Comparison of air pollutant emissions among mega-cities, *Atmospheric Environment*, *43*(40), 6435-6441.

Parrish, D. D., M. Trainer, V. Young, P. D. Goldan, W. C. Kuster, B. T. Jobson, F. C. Fehsenfeld, W. A. Lonneman, R. D. Zika, C. T. Farmer, D. D. Riemer, and M. O. Rodgers (1998), Internal consistency tests for evaluation of measurements of anthropogenic hydrocarbons in the troposphere, *J. Geophys. Res.-Atmos.*, *103*(D17), 22339-22359.

Pearson, R. K., Y. Neuvo, J. Astola, M. Gabbouj, and Ieee (2015), The Class of Generalized Hampel Filters, in *2015 23rd European Signal Processing Conference*, edited, pp. 2501-2505, Ieee, New York.

Peischl, J., K. Aikin, S. Eilerman, J. Gilman, J. De Gouw, S. Herndon, B. Lerner, A. Neuman, T. Tokarek, M. Trainer, C. Warneke, and T. Ryerson (2015a), Quantification of methane emissions from oil and natural gas extraction regions in the Central/Western U.S. and comparison to previous studies, *AGU Fall Meeting*, *Abstract A24F-02*.

Peischl, J., T. B. Ryerson, K. C. Aikin, J. A. de Gouw, J. B. Gilman, J. S. Holloway, B. M. Lerner, R. Nadkarni, J. A. Neuman, J. B. Nowak, M. Trainer, C. Warneke, and D. D. Parrish (2015b), Quantifying atmospheric methane emissions from the Haynesville, Fayetteville, and northeastern Marcellus shale gas production regions, *J. Geophys. Res.-Atmos.*, *120*(5), 2119-2139.

Peischl, J., T. B. Ryerson, J. Brioude, K. C. Aikin, A. E. Andrews, E. Atlas, D. Blake, B. C. Daube, J. A. de Gouw, E. Dlugokencky, G. J. Frost, D. R. Gentner, J. B. Gilman, A. H. Goldstein, R. A. Harley, J. S. Holloway, J. Kofler, W. C. Kuster, P. M. Lang, P. C. Novelli, G. W. Santoni, M. Trainer, S. C. Wofsy, and D. D. Parrish (2013), Quantifying sources of methane using light alkanes in the Los Angeles basin, California, *J. Geophys. Res.-Atmos.*, *118*(10), 4974-4990.

Penkett, S. A., N. J. Blake, P. Lightman, A. R. W. Marsh, P. Anwyl, and G. Butcher (1993), The Seasonal-Variation of Nonmethane Hydrocarbons in the Free Troposphere over the North-Atlantic Ocean - Possible Evidence for Extensive Reaction of Hydrocarbons with the Nitrate Radical, *J. Geophys. Res.-Atmos.*, *98*(D2), 2865-2885.

Penuelas, J., D. Asensio, D. Tholl, K. Wenke, M. Rosenkranz, B. Piechulla, and J. P. Schnitzler (2014), Biogenic volatile emissions from the soil, *Plant Cell Environ.*, *37*(8), 1866-1891.

Perkin-Elmer (1991), ATD 400 User's Manual, Uptake Rates, edited by Perkin-Elmer, Beaconsfield.

Petron, G., G. Frost, B. R. Miller, A. I. Hirsch, S. A. Montzka, A. Karion, M. Trainer, C. Sweeney, A. E. Andrews, L. Miller, J. Kofler, A. Bar-Ilan, E. J. Dlugokencky, L. Patrick, C. T. Moore, T. B. Ryerson, C. Siso, W. Kolodzey, P. M. Lang, T. Conway, P. Novelli, K. Masarie, B. Hall, D. Guenther, D. Kitzis, J. Miller, D. Welsh, D. Wolfe, W. Neff, and P. Tans (2012), Hydrocarbon emissions characterization in the Colorado Front Range: A pilot study, *J. Geophys. Res.-Atmos.*, *117*.

Pétron, G., G. Frost, B. R. Miller, A. I. Hirsch, S. A. Montzka, A. Karion, M. Trainer, C. Sweeney, A. E. Andrews, L. Miller, J. Kofler, A. Bar-Ilan, E. J. Dlugokencky, L. Patrick, C. T. Moore, T. B. Ryerson, C. Siso, W. Kolodzey, P. M. Lang, T. Conway, P. Novelli, K. Masarie, B. Hall, D. Guenther, D. Kitzis, J. Miller, D. Welsh, D. Wolfe, W. Neff, and P. Tans (2012), Hydrocarbon emissions characterization in the Colorado Front Range: A pilot study, *J. Geophys. Res.-Atmos.*, *117*, 1-19.

Petron, G., A. Karion, C. Sweeney, B. R. Miller, S. A. Montzka, G. J. Frost, M. Trainer, P. Tans, A. Andrews, J. Kofler, D. Helmig, D. Guenther, E. Dlugokencky, P. Lang, T. Newberger, S. Wolter, B. Hall, P. Novelli, A. Brewer, S. Conley, M. Hardesty, R. Banta, A. White, D. Noone, D. Wolfe, and R. Schnell (2014), A new look at methane and nonmethane hydrocarbon emissions from oil and natural gas operations in the Colorado Denver-Julesburg Basin, *J. Geophys. Res.-Atmos.*, *119*(11), 6836-6852.

Pfister, G. G., P. J. Reddy, M. C. Barth, F. F. Flocke, A. Fried, S. C. Herndon, B. C. Sive, J. T. Sullivan, A. M. Thompson, T. I. Yacovitch, A. J. Weinheimer, and A. Wisthaler (2017), Using Observations and Source-Specific Model Tracers to Characterize Pollutant Transport During FRAPPE and DISCOVER-AQ, *J. Geophys. Res.-Atmos.*, *122*(19), 10474-10502.

Piccot, S. D., J. J. Watson, and J. W. Jones (1992), A global inventory of volatile organic compound emissions from anthropogenic sources *J. Geophys. Res.-Atmos.*, *97*(D9), 9897-9912.

Pichersky, E., and J. Gershenzon (2002), The formation and function of plant volatiles: perfumes for pollinator attraction and defense, *Curr. Opin. Plant Biol.*, *5*(3), 237-243.

Piechulla, B., M. C. Lemfack, and M. Kai (2017), Effects of discrete bioactive microbial volatiles on plants and fungi, *Plant Cell Environ.*, *40*(10), 2042-2067.

Pierson, W. R., D. E. Schorran, E. M. Fujita, J. C. Sagebiel, D. R. Lawson, and R. L. Tanner (1999), Assessment of nontailpipe hydrocarbon emissions from motor vehicles, *J. Air Waste Manage. Assoc.*, *49*(5), 498-519.

Pinho, P. G., C. A. Pio, W. P. L. Carter, and M. E. Jenkin (2007), Evaluation of alpha- and beta-pinene degradation in the detailed tropospheric chemistry mechanism, MCM v3.1, using environmental chamber data, *J. Atmos. Chem.*, *57*(2), 171-202.

Pinho, P. G., C. A. Pio, and M. E. Jenkin (2005), Evaluation of isoprene degradation in the detailed tropospheric chemical mechanism, MCM v3, using environmental chamber data, *Atmospheric Environment*, *39*(7), 1303-1322.

Plass-Duelmer, C., K. Michl, R. Ruf, and H. Berresheim (2002), C-2-C-8 hydrocarbon measurement and quality control procedures at the Global Atmosphere Watch Observatory Hohenpeissenberg, *J. Chromatogr. A*, *953*(1-2), 175-197.

Platt, U., D. Perner, A. M. Winer, G. W. Harris, and J. N. Pitts (1980), Detection of NO3 in the Polluted Troposphere by Differential Optical Absorption, *Geophys. Res. Lett.*, *7*(1), 89-92.

Pollmann, J., D. Helmig, J. Hueber, C. Plass-Dulmer, and P. Tans (2008a), Sampling, storage, and analysis of C-2-C-7 non-methane hydrocarbons from the US National Oceanic and Atmospheric Administration Cooperative Air Sampling Network glass flasks, *J. Chromatogr. A*, *1188*(2), 75-87.

Pollmann, J., D. Helmig, J. Hueber, C. Plass-Dülmer, and P. Tans (2008b), Sampling, storage, and analysis of C2-C7 non-methane hydrocarbons from the US National Oceanic and Atmospheric Administration Cooperative Air Sampling Network glass flasks, *J. Chromatogr. A*, *1188*(2), 75-87.

Pollmann, J., D. Helmig, J. Hueber, D. Tanner, and P. P. Tans (2006), Evaluation of solid adsorbent materials for cryogen-free trapping - gas chromatographic analysis of atmospheric C2-C6 non-methane hydrocarbons, *J. Chromatogr. A*, *1134*(1-2), 1-15.

Pollmann, J., D. Helmig, D. Liptzin, C. R. Thompson, J. Hueber, and P. Tans (2016), Variability analyses, site characterization, and regional [OH] estimates using trace gas measurements from NOAA Global Greenhouse Gas Reference Network, *Elementa*, *4*(128).

Potard, K., C. Monard, J. L. Le Garrec, J. P. Caudal, N. Le Bris, and F. Binet (2017), Organic amendment practices as possible drivers of biogenic Volatile Organic Compounds emitted by soils in agrosystems, *Agric. Ecosyst. Environ.*, *250*, 25-36.

Pozzer, A., A. de Meij, J. Yoon, H. Tost, A. K. Georgoulias, and M. Astitha (2015), AOD trends during 2001–2010 from observations and model simulations, *Atmos. Chem. Phys.*, *15*(10), 5521-5535.

Pozzer, A., J. Pollmann, D. Taraborrelli, P. Jöckel, D. Helmig, P. Tans, J. Hueber, and J. Lelieveld (2010), Observed and simulated global distribution and budget of atmospheric C2-C5 alkanes, *Atmos. Chem. Phys.*, *10*(9), 4403-4422.

Preston, G. M. (2000), Pseudomonas syringae pv. tomato: the right pathogen, of the right plant, at the right time, *Mol. Plant Pathol.*, *1*(5), 263-275.

Program, G. A. V. M. (2016), *http://instaar.colorado.edu/arl/Global_VOC.html*.

Qi, Y., and L. Jiaqui (2018), China's Coal consumption has peaked, *Brookings*.

Qi, Y., N. Stern, T. Wu, J. Lu, and F. Green (2016), China's post-coal growth, *Nat. Geosci.*, *9*, 564.

Ramirez, K. S., C. L. Lauber, and N. Fierer (2010), Microbial consumption and production of volatile organic compounds at the soil-litter interface, *Biogeochemistry*, *99*(1-3), 97-107.

Ranlett, J. (1981), The smoke abatement exhibition of 1881, *Hist. Today*, *31*(NOV), 10-13.

Rappenglueck, B., L. Ackermann, S. Alvarez, J. Golovko, M. Buhr, R. A. Field, J. Soltis, D. C. Montague, B. Hauze, S. Adamson, D. Risch, G. Wilkerson, D. Bush, T. Stoeckenius, and C. Keslar (2014), Strong wintertime ozone events in the Upper Green River basin, Wyoming, *Atmos. Chem. Phys.*, *14*(10), 4909-4934.

Ras, M. R., F. Borrull, and R. M. Marce (2009), Sampling and preconcentration techniques for determination of volatile organic compounds in air samples, *Trac-Trends Anal. Chem.*, *28*(3), 347-361.

Rasmussen, D. J., A. M. Fiore, V. Naik, L. W. Horowitz, S. J. McGinnis, and M. G. Schultz (2012), Surface ozone-temperature relationships in the eastern US: A monthly climatology for evaluating chemistry-climate models, *Atmospheric Environment*, *47*, 142-153.

Rasmussen, D. J., J. L. Hu, A. Mahmud, and M. J. Kleeman (2013), The Ozone-Climate Penalty: Past, Present, and Future, *Environ. Sci. Technol.*, *47*(24), 14258-14266.

Ray, K. (2017), Rising global oil prices portend increased conflict over residential drilling in Colorado, in *Colorado Independent*, edited, http://www.coloradoindependent.com/164728/rising-oil-prices-colorado-drilling.

Read, K. A., J. D. Lee, A. C. Lewis, S. J. Moller, L. Mendes, and L. J. Carpenter (2009), Intra-annual cycles of NMVOC in the tropical marine boundary layer and their use for interpreting seasonal variability in CO, *J. Geophys. Res.-Atmos.*, *114*.

Reich, P. B. (1987), Quantifying plant response to ozone: a unifying theory, *Tree Physiol.*, *3*(1), 63-91.

Reich, P. B., and R. G. Amundson (1985), Ambient levels of ozone reduce net photosynthesis in tree and crop species *Science*, *230*(4725), 566-570.

Renzetti, N. A. (1956), Ozone in the Los Angeles atmosphere, *J. Chem. Phys.*, *24*(4), 909-909.

Rhoderick, G. C., D. L. Duewer, E. Apel, A. Baldan, B. Hall, A. Harling, D. Helmig, G. S. Heo, J. Hueber, M. E. Kim, Y. D. Kim, B. Miller, S. Montzka, and D. Riemer (2014), International comparison of a hydrocarbon gas standard at the picomol per mol level, *Anal. Chem.*, *86*(5), 2580-2589.

Riahi, K., A. Grübler, and N. Nakicenovic (2007), Scenarios of long-term socio-economic and environmental development under climate stabilization, *Technological Forecasting and Social Change*, *74*(7), 887-935.

Rinsland, C. P., N. B. Jones, B. J. Connor, S. W. Wood, A. Goldman, T. M. Stephen, F. J. Murcray, L. S. Chiou, R. Zander, and E. Mahieu (2002), Multiyear infrared solar spectroscopic measurements of HCN, CO, C2H6, and C2H2 tropospheric columns above Lauder, New Zealand (45°S latitude), *Journal of Geophysical Research: Atmospheres*, *107*(D14), ACH 1-1-ACH 1-12.

Roberts, J. M., F. C. Fehsenfeld, S. C. Liu, M. J. Bollinger, C. Hahn, D. L. Albritton, and R. E. Sievers (1984), Measurements of Aromatic Hydrocarbon Ratios and NOx Concentrations in the Rural Troposphere - Observation of Air-Mass Photochemical Aging and NOx Removal, *Atmospheric Environment*, *18*(11), 2421-2432.

Roche, A., R. Thevenet, V. Jacob, P. Kaluzny, C. Ferrari, P. Baussand, and P. Foster (1999), Performance of a thermally desorbable type-tube diffusive sampler for very low air concentrations monitoring, *Atmospheric Environment*, *33*(12), 1905-1912.

Rossabi, S., M. Choudoir, D. Helmig, J. Hueber, and N. Fierer (2018), Volatile Organic Compound Emissions From Soil Following Wetting Events, *J. Geophys. Res.-Biogeosci.*, *123*(6), 1988-2001.

Rudolph, J., and D. H. Ehhalt (1981), Measurements of C2-C5 Hydrocarbons over the North Atlantic, *Journal of Geophysical Research-Oceans and Atmospheres*, *86*(NC12), 1959-1964.

Russo, R. S., M. L. White, Y. Zhou, K. B. Haase, J. L. Ambrose, L. Conway, E. Mentis, R. Talbot, and B. Sive (2011), Spatial Variation, Sources, and Emission Rates of Volatile Organic Compounds over the Northeastern U.S., in *Air Quality-Models and Applications*, edited by N. Mazzeo, Climate Change Research Center, Institute for the Study of Earth, Oceans, and Space, University of New Hampshire, Durham, NH.

Samet, J. M., F. Dominici, F. C. Curriero, I. Coursac, and S. L. Zeger (2000), Fine particulate air pollution and mortality in 20 US Cities, 1987-1994, *N. Engl. J. Med.*, *343*(24), 1742-1749.

Sanderson, M. G., C. D. Jones, W. J. Collins, C. E. Johnson, and R. G. Derwent (2003), Effect of climate change on isoprene emissions and surface ozone levels, *Geophys. Res. Lett.*, *30*(18).

Saunders, S. M., M. E. Jenkin, R. G. Derwent, and M. J. Pilling (2003), Protocol for the development of the Master Chemical Mechanism, MCM v3 (Part A): tropospheric degradation of non-aromatic volatile organic compounds, *Atmos. Chem. Phys.*, *3*, 161-180.

Scanion, J. T., and D. E. Willis (1985), Calculation of flame ionization detector relative response factors using the effective carbon number concept *J. Chromatogr. Sci.*, *23*(8), 333-340.

Schade, G. W., and T. G. Custer (2004), OVOC emissions from agricultural soil in northern Germany during the 2003 European heat wave, *Atmospheric Environment*, *38*(36), 6105-6114.

Schade, G. W., and A. H. Goldstein (2001), Fluxes of oxygenated volatile organic compounds from a ponderosa pine plantation, *J. Geophys. Res.-Atmos.*, *106*(D3), 3111-3123.

Schade, G. W., and G. S. Roest (2015), Is the shale boom reversing progress in curbing ozone pollution?, *EOS 96*, doi:10.1029/2015EO028279.

Schaefer, H., S. E. Mikaloff Fletcher, C. Veidt, K. R. Lassey, G. Brailsford, T. M. Bromley, E. J. Dlugokencky, S. E. Michel, J. B. Miller, I. Levin, D. C. Lowe, R. J. Martin, B. H. Vaughn, and J. W. C. Whilte (2016), A 21st century shift from fossil-fuel to biogenic methane emissions indicated by 13CH4, *Science*, *10.1126/science.aad2705*.

Scheff, P. A., R. A. Wadden, D. M. Kenski, J. Chung, and G. Wolff (1996), Receptor model evaluation of the southeast Michigan ozone study ambient NMOC measurements, *J. Air Waste Manage. Assoc.*, *46*(11), 1048-1057.

Schimel, D. S., B. H. Braswell, E. A. Holland, R. McKeown, D. S. Ojima, T. H. Painter, W. J. Parton, and A. R. Townsend (1994), Climatic, edaphic, and biotic controls over storage and turnover of carbon in soils *Glob. Biogeochem. Cycle*, *8*(3), 279-293.

Schimel, J. P., T. C. Balser, and M. Wallenstein (2007), Microbial stress-response physiology and its implications for ecosystem function, *Ecology*, *88*(6), 1386-1394.

Schimel, J. P., J. M. Gulledge, J. S. Clein-Curley, J. E. Lindstrom, and J. F. Braddock (1999), Moisture effects on microbial activity and community structure in decomposing birch litter in the Alaskan taiga, *Soil Biol. Biochem.*, *31*(6), 831-838.

Schmidt, R., V. Cordovez, W. de Boer, J. Raaijmakers, and P. Garbeva (2015), Volatile affairs in microbial interactions, *Isme J.*, *9*(11), 2329-2335.

Schmidt, R., D. W. Etalo, V. de Jager, S. Gerards, H. Zweers, W. de Boer, and P. Garbeva (2016), Microbial Small Talk: Volatiles in Fungal-Bacterial Interactions, *Front. Microbiol.*, *6*.

Schnell, R. C., S. J. Oltmans, R. R. Neely, M. S. Endres, J. V. Molenar, and A. B. White (2009), Rapid photochemical production of ozone at high concentrations in a rural site during winter, *Nat. Geosci.*, *2*(2), 120-122.

Scholler, C. E. G., H. Gurtler, R. Pedersen, S. Molin, and K. Wilkins (2002), Volatile metabolites from actinomycetes, *J. Agric. Food Chem.*, *50*(9), 2615-2621.

Schulz-Bohm, K., L. Martin-Sanchez, and P. Garbeva (2017), Microbial Volatiles: Small Molecules with an Important Role in Infra- and Inter-Kingdom Interactions, *Front. Microbiol.*, *8*.

Schulz, S., and J. S. Dickschat (2007), Bacterial volatiles: the smell of small organisms, *Nat. Prod. Rep.*, *24*(4), 814-842.

Schulz, S., J. S. Dickschat, B. Kunze, I. Wagner-Dobler, R. Diestel, and F. Sasse (2010), Biological Activity of Volatiles from Marine and Terrestrial Bacteria, *Mar. Drugs*, *8*(12), 2976-2987.

Schwartz, S. E. (1989), Acid deposition - unraveling a regional phenomenon, *Science*, *243*(4892), 753-763.

Seethapathy, S., T. Gorecki, and X. J. Li (2008), Passive sampling in environmental analysis, *J. Chromatogr. A*, *1184*(1-2), 234-253.

Seewald, M. S. A., W. Singer, B. A. Knapp, I. H. Franke-Whittle, A. Hansel, and H. Insam (2010), Substrate-induced volatile organic compound emissions from compost-amended soils, *Biol. Fertil. Soils*, *46*(4), 371-382.

Seidel, D. J., Y. Zhang, A. Beljaars, J.-C. Golaz, A. R. Jacobson, and B. Medeiros (2012), Climatology of the planetary boundary layer over the continental United States and Europe, *Journal of Geophysical Research: Atmospheres*, *117*(D17), n/a-n/a.

Sen, P. K. (1968), Estimates of Regression Coefficient based on Kendall's Tau, *J. Am. Stat. Assoc.*, *63*(324), 1379-&.

Sharma, S., B. Giri, and K. S. Patel (2016), Ambient volatile organic compounds in the atmosphere of industrial central India, *J. Atmos. Chem.*, *73*(4), 381-395.

Shestivska, V., P. Spanel, K. Dryahina, K. Sovova, D. Smith, M. Musilek, and A. Nemec (2012), Variability in the concentrations of volatile metabolites emitted by genotypically different strains of Pseudomonas aeruginosa, *J. Appl. Microbiol.*, *113*(3), 701-713.

Sieferle, R. P. (2001), *The subterranean forest: Energy systems and the industrial revolution*, The White Horse Press, Cambridge.

Sillman, S., and F. J. Samson (1995), Impact of temperature on oxidant photochemistry in urban, polluted rural, and remote environments, *J. Geophys. Res.-Atmos.*, *100*(D6), 11497-11508.

Silva, R. A., J. J. West, Y. Q. Zhang, S. C. Anenberg, J. F. Lamarque, D. T. Shindell, W. J. Collins, S. Dalsoren, G. Faluvegi, G. Folberth, L. W. Horowitz, T. Nagashima, V. Naik, S. Rumbold, R. Skeie, K. Sudo, T. Takemura, D. Bergmann, P. Cameron-Smith, I. Cionni, R. M. Doherty, V. Eyring, B. Josse, I. A. MacKenzie, D. Plummer, M. Righi, D. S. Stevenson, S. Strode, S. Szopa, and G. Zeng (2013), Global premature mortality due to anthropogenic outdoor air pollution and the contribution of past climate change, *Environ. Res. Lett.*, *8*(3).

Simpson, I. J., M. P. S. Andersen, S. Meinardi, L. Bruhwiler, N. J. Blake, D. Helmig, F. S. Rowland, and D. R. Blake (2012), Long-term decline of global atmospheric ethane concentrations and implications for methane, *Nature*, *488*(7412), 490-494.

Singh, H. B., and P. L. Hanst (1981), Peroxyacetyl nitrate (PAN) in the unpolluted atmosphere - an important reservoir for nitrogen oxides *Geophys. Res. Lett.*, *8*(8), 941-944.

Singh, H. B., D. Ohara, D. Herlth, W. Sachse, D. R. Blake, J. D. Bradshaw, M. Kanakidou, and P. J. Crutzen (1994), Acetone in the atmosphere - distribution, sources, and sinks *J. Geophys. Res.-Atmos.*, *99*(D1), 1805-1819.

Singh, H. B., and P. B. Zimmerman (1992), Atmospheric distribution and sources of nonmethane hydrocarbons, *Adv. Environ. Sci. Technol.*, *24*, 177-235.

Smil, V. (1994), *Energy in World History*, Westview Press, Boulder.

Smith, M. L., E. A. Kort, A. Karion, C. Sweeney, S. C. Herndon, and T. I. Yacovitch (2015), Airborne Ethane Observations in the Barnett Shale: Quantification of Ethane Flux and Attribution of Methane Emissions, *Environ. Sci. Technol.*, *49*(13), 8158-8166.

Smolander, A., R. A. Ketola, T. Kotiaho, S. Kanerva, K. Suominen, and V. Kitunen (2006), Volatile monoterpenes in soil atmosphere under birch and conifers: Effects on soil N transformations, *Soil Biol. Biochem.*, *38*(12), 3436-3442.

Solomon, S., M. Mills, L. E. Heidt, W. H. Pollock, and A. F. Tuck (1992), On the evaluation of ozone depletion potentials, *J. Geophys. Res.-Atmos.*, *97*(D1), 825-842.

Sovacool, B. K. (2014), Cornucopia or curse? Reviewing the costs and benefits of shale gas hydraulic fracturing (fracking), *Renew. Sust. Energ. Rev.*, *37*, 249-264.

Sponseller, R. A. (2007), Precipitation pulses and soil CO2 flux in a Sonoran Desert ecosystem, *Glob. Change Biol.*, *13*(2), 426-436.

Sprouffske, K., and A. Wagner (2016), Growthcurver: an R package for obtaining interpretable metrics from microbial growth curves, *BMC Bioinformatics*, *17*.

Stacheter, A., M. Noll, C. K. Lee, M. Selzer, B. Glowik, L. Ebertsch, R. Mertel, D. Schulz, N. Lampert, H. L. Drake, and S. Kolb (2013), Methanol oxidation by temperate soils and environmental determinants of associated methylotrophs, *Isme J.*, *7*(5), 1051-1064.

Stahl, P. D., and T. B. Parkin (1996), Microbial production of volatile organic compounds in soil microcosms, *Soil Sci. Soc. Am. J.*, *60*(3), 821-828.

Stamatakis, A. (2006), RAxML-VI-HPC: Maximum likelihood-based phylogenetic analyses with thousands of taxa and mixed models, *Bioinformatics*, *22*(21), 2688-2690.

Stamatakis, A., P. Hoover, and J. Rougemont (2008), A Rapid Bootstrap Algorithm for the RAxML Web Servers, *Syst. Biol.*, *57*(5), 758-771.

Sterling, C. W., B. J. Johnson, S. J. Oltmans, H. G. J. Smit, A. F. Jordan, P. D. Cullis, E. G. Hall, A. M. Thompson, and J. C. Witte (2018), Homogenizing and estimating the uncertainty in NOAA's long-term vertical ozone profile records measured with the electrochemical concentration cell ozonesonde, *Atmos. Meas. Tech.*, *11*(6), 3661-3687.

Stockwell, W. R., C. V. Lawson, E. Saunders, and W. S. Goliff (2012), A Review of Tropospheric Atmospheric Chemistry and Gas-Phase Chemical Mechanisms for Air Quality Modeling, *Atmosphere*, *3*(1), 1-32.

Stotzky, G., and S. Schenck (1976), Observations on organic volatiles from germinating seeds and seedlings *Am. J. Bot.*, *63*(6), 798-805.

Stradling, D. (1999), *Smokestacks and progressives: environmentalists, enigineers, and air quality in America, 1881 - 1951*, John Hopkins University Press, Baltimore.

Stradling, D., and P. Thorsheim (1999), The smoke of great cities - British and American efforts to control air pollution, 1860-1914, *Environ. Hist.*, *4*(1), 6-31.

Stull, R. B. (1988), *An Intoduction to Boundary Layer Meteorology*, 1 ed., 670 pp., Springer Netherlands.

Sturges, W. T., and J. W. Elkins (1993), Use of adsorbents to collect selected halocarbons and hydrohalocarbons of environmental interest from large air volumes, *Journal of Chromatography*, *642*(1-2), 123-134.

Stutz, J., R. Ackermann, J. D. Fast, and L. Barrie (2002), Atmospheric reactive chlorine and bromine at the Great Salt Lake, Utah, *Geophys. Res. Lett.*, *29*(10).

Sullivan, J. T., T. J. McGee, A. O. Langford, R. J. Alvarez, C. J. Senff, P. J. Reddy, A. M. Thompson, L. W. Twigg, G. K. Sumnicht, P. Lee, A. Weinheimer, C. Knote, R. W. Long, and R. M. Hoff (2016), Quantifying the contribution of thermally driven recirculation to a high-ozone event along the Colorado Front Range using lidar, *J. Geophys. Res.-Atmos.*, *121*(17), 10377-10390.

Swarthout., R. S. Russo, Y. Zhou, A. H. Hart, and B. C. Sive (2013), Volatile organic compound distributions during the NACHTT campaign at the Boulder Atmospheric Observatory: Influence of urban and natural gas sources, *J. Geophys. Res.-Atmos.*, *118*(18), 10614-10637.

Swarthout., R. S. Russo, Y. Zhou, B. M. Miller, B. Mitchell, E. Horsman, E. Lipsky, D. C. McCabe, E. Baum, and B. C. Sive (2015), Impact of Marcellus Shale Natural Gas Development in Southwest Pennsylvania on Volatile Organic Compound Emissions and Regional Air Quality, *Environ. Sci. Technol.*, *49*(5), 3175-3184.

Tait, E., J. D. Perry, S. P. Stanforth, and J. R. Dean (2014), Identification of Volatile Organic Compounds Produced by Bacteria Using HS-SPME-GC-MS, *J. Chromatogr. Sci.*, *52*(4), 363-373.

Tanner, D., D. Helmig, J. Hueber, and P. Goldan (2006), Gas chromatography system for the automated, unattended, and cryogen-free monitoring of C2 to C6 non-methane hydrocarbons in the remote troposphere, *J. Chromatogr. A*, *1111*(1), 76-88.

Tans, P. P., T. J. Conway, and T. Nakazawa (1989), Latitudinal distribution of the sources and sinks of atmospheric carbon-dioxide derived from surface observations and an atmospheric transport model, *J. Geophys. Res.-Atmos.*, *94*(D4), 5151-5172.

Tarr, J. A. (1996), *The search for the ultimate sink: urban pollution in historical perspective*, Akron University Press, Akron.

Tavare, S. (1986), Some Probabilistic and Statistical Problems in the Analysis of DNA Sequences, *Lectures on Mathematics in the Life Sciences*, *17*.

Theil, H. (1950), A rank invariant method of linear and polynomial regression analysis, *Nederl. Akad. Wetensch.*, *Proc. 53*(I, II, III), 386-392,521-525.1397-1412.

Thoma, E. D., M. C. Miller, K. C. Chung, N. L. Parsons, and B. C. Shine (2011), Facility fence-line monitoring using passive samplers, *J. Air Waste Manage. Assoc.*, *61*(8), 834-842.

Thompson, C. R., J. Hueber, and D. Helmig (2014), Influence of oil and gas emissions on ambient atmospheric non-methane hydrocarbons in residential areas of Northeastern Colorado, *Elementa*, *2*(000035).

Thompson., J. Hueber, and D. Helmig (2014), Influence of oil and gas emissions on ambient atmospheric non-methane hydrocarbons in residential areas of Northeastern Colorado, *Elementa: Science of the Anthropocene*, *2*, 000035.

Thoning, K. W., P. P. Tans, and W. D. Komhyr (1989), Atmospheric carbon-dioxide at Mauna Loa observatory .2. analysis of the NOAA GMCC data, 1974-1985, *J. Geophys. Res.-Atmos.*, *94*(D6), 8549-8565.

Thorsheim, P. (2004), *Interpreting the London fog disaster of 1952. In: Dupuis EM (ed) Smoke and*

mirrors: the politics and culture of air pollution, New York University Press, New York.

Todd, J. D., R. Rogers, Y. G. Li, M. Wexler, P. L. Bond, L. Sun, A. R. J. Curson, G. Malin, M. Steinke, and A. W. B. Johnston (2007), Structural and regulatory genes required to make the gas dimethyl sulfide in bacteria, *Science*, *315*(5812), 666-669.

Tolnai, B., A. Gelencser, and J. Hlavay (2001), Theoretical approach to non-constant uptake rates for tube-type diffusive samplers, *Talanta*, *54*(4), 703-713.

Tompkins, F. C., and R. L. Goldsmith (1977), New personal dosimeter for monitoring of industrial pollutants, *Am. Ind. Hyg. Assoc. J.*, *38*(8), 371-377.

Trainer, M., E. Y. Hsie, S. A. McKeen, R. Tallamraju, D. D. Parrish, F. C. Fehsenfeld, and S. C. Liu (1987), Impact of natural hydrocarbons on hydroxy and peroxy-radicals at a remote site *J. Geophys. Res.-Atmos.*, *92*(D10), 11879-11894.

Traxler, M. F., J. D. Watrous, T. Alexandrov, P. C. Dorrestein, and R. Kolter (2013), Interspecies Interactions Stimulate Diversification of the Streptomyces coelicolor Secreted Metabolome, *mBio*, *4*(4).

Turner, A. J., D. J. Jacob, J. Benmergui, S. C. Wofsy, J. D. Maasakkers, A. Butz, O. Hasenkamp, S. C. Biraud, and E. Dlugokencky (2016), A large increase in US methane emissions over the past decade inferred from satellite data and surface observations, *Geophys. Res. Let.*, *in press.*

Tyc, O., C. X. Song, J. S. Dickschat, M. Vos, and P. Garbeva (2017), The Ecological Role of Volatile and Soluble Secondary Metabolites Produced by Soil Bacteria, *Trends Microbiol.*, *25*(4), 280-292.

Underhill, D. W., and C. E. Feigley (1991), Boundary-layer effect in diffusive monitoring, *Anal. Chem.*, *63*(10), 1011-1013.

UNEC (2004), Handbook for the 1979 convention on

long-range transboundary pollution*Rep.*, United Nations Economic Comission for Europe, New York and Geneva.

UNEP (1972), Report of the United Nations Conference on the Human Environment*Rep.*, United Nations Environmental Programme, Stockholm.

Unger, S., C. Maguas, J. S. Pereira, T. S. David, and C. Werner (2010), The influence of precipitation pulses on soil respiration - Assessing the "Birch effect" by stable carbon isotopes, *Soil Biol. Biochem.*, *42*(10), 1800-1810.

Urbina, I. (2011), Rush to Drill for Natural Gas Creates Conflicts With Mortgages, in *New York Times*, edited, http://www.nytimes.com/2011/10/20/us/rush-to-drill-for-gas-creates-mortgage-conflicts.html?mcubz=0.

van Den Dool, H., and P. Dec. Kratz (1963), A generalization of the retention index system including linear temperature programmed gas—liquid partition chromatography, *J. Chromatogr. A*, *11*, 463-471.

van der Voort, M., M. Kempenaar, M. van Driel, J. M. Raaijmakers, and R. Mendes (2016), Impact of soil heat on reassembly of bacterial communities in the rhizosphere microbiome and plant disease suppression, *Ecol. Lett.*, *19*(4), 375-382.

Vangestel, M., J. N. Ladd, and M. Amato (1992), Microbial biomass responses to seasonal change and imposed drying regimes at increasing depths of undisturbed topsoil profiles *Soil Biol. Biochem.*, *24*(2), 103-111.

Vaughn, T. L., C. S. Bell, C. K. Pickering, S. Schwietzke, G. A. Heath, G. Pétron, D. J. Zimmerle, R. C. Schnell, and D. Nummedal (2018), Temporal variability largely explains top-down/bottom-up difference in methane emission estimates from a natural gas production region, *Proceedings of the National Academy of Sciences*.

Veres, P. R., T. Behrendt, A. Klapthor, F. X. Meixner, and J. Williams (2014), Volatile Organic Compound emissions from soil: using Proton-Transfer-Reaction Time-of-Flight Mass Spectrometry (PTR-TOF-MS) for the real time observation of microbial processes, *Biogeosciences Discuss.*, *2014*, 12009-12038.

Verma, D. K., D. M. Johnson, and J. D. McLean (2000), Benzene and total hydrocarbon exposures in the upstream petroleum oil and gas industry, *Am. Ind. Hyg. Assoc. J.*, *61*(2), 255-263.

Verriele, M., N. Allam, L. Depelchin, L. Le Coq, and N. Locoge (2015), Improvement in 8h-sampling rate assessment considering meteorological parameters variability for biogas VOC passive measurements in the surroundings of a French landfill, *Talanta*, *144*, 294-302.

Vinciguerra, T., S. Yao, J. Dadzie, A. Chittams, T. Deskins, S. Ehrman, and R. R. Dickerson (2015), Regional air quality impacts of hydraulic fracturing and shale natural gas activity: Evidence from ambient VOC observations, *Atmospheric Environment*, *110*, 144-150.

von Schneidemesser, E., J. Coates, H. van der Gon, A. J. H. Visschedijk, and T. M. Butler (2016), Variation of the NMVOC speciation in the solvent sector and the sensitivity of modelled tropospheric ozone, *Atmospheric Environment*, *135*, 59-72.

Von Schneidemesser, E., P. S. Monks, V. Gros, J. Gauduin, and O. Sanchez (2011), How important is biogenic isoprene in an urban environment? A study in London and Paris, *Geophys. Res. Lett.*, *38*.

Von Schneidemesser, E., P. S. Monks, and C. Plass-Duelmer (2010), Global comparison of VOC and CO observations in urban areas, *Atmospheric Environment*, *44*(39), 5053-5064.

Vu, K. T., J. H. Dingle, R. Bahreini, P. J. Reddy, E. C. Apel, T. L. Campos, J. P. DiGangi, G. S. Diskin, A. Fried, S. C. Herndon, A. J. Hills, R. S. Hornbrook, G. Huey, L. Kaser, D. D. Montzka, J. B. Nowak, S. E. Pusede, D. Richter, J. R. Roscioli, G. W. Sachse, S. Shertz, M. Stell, D. Tanner, G. S. Tyndall, J. Walega, P. Weibring, A. J. Weinheimer, G. Pfister, and F. Flocke (2016), Impacts of the Denver Cyclone on regional air quality and aerosol formation in the Colorado Front Range during FRAPPE 2014, *Atmos. Chem. Phys.*, *16*(18), 12039-12058.

Walgraeve, C., K. Demeestere, J. Dewulf, K. Van Huffel, and H. Van Langenhove (2011), Uptake rate behavior of tube-type passive samplers for volatile organic compounds under controlled atmospheric conditions, *Atmospheric Environment*, *45*(32), 5872-5879.

Wang, L. H., J. B. Milford, and W. P. L. Carter (2000), Reactivity estimates for aromatic compounds. Part 1. Uncertainty in chamber-derived parameters, *Atmospheric Environment*, *34*(25), 4337-4348.

Wang, L. X., S. Manzoni, S. Ravi, D. Riveros-Iregui, and K. Caylor (2015), Dynamic interactions of ecohydrological and biogeochemical processes in water-limited systems, *Ecosphere*, *6*(8).

Wang, Q., G. M. Garrity, J. M. Tiedje, and J. R. Cole (2007), Naive Bayesian classifier for rapid assignment of rRNA sequences into the new bacterial taxonomy, *Appl. Environ. Microbiol.*, *73*(16), 5261-5267.

Waring, B. G., and J. S. Powers (2016), Unraveling the mechanisms underlying pulse dynamics of soil respiration in tropical dry forests, *Environ. Res. Lett.*, *11*(10).

Warneke, C., J. A. de Gouw, J. S. Holloway, J. Peischl, T. B. Ryerson, E. Atlas, D. Blake, M. Trainer, and D. D. Parrish (2012), Multiyear trends in volatile organic compounds in Los Angeles, California: Five decades of decreasing emissions, *J. Geophys. Res.-Atmos.*, *117*.

Warneke, C., T. Karl, H. Judmaier, A. Hansel, A. Jordan, W. Lindinger, and P. J. Crutzen (1999), Acetone, methanol, and other partially oxidized volatile organic emissions from dead

plant matter by abiological processes: Significance for atmospheric HOx chemistry, *Glob. Biogeochem. Cycle*, *13*(1), 9-17.

Warneke, C., S. A. McKeen, J. A. de Gouw, P. D. Goldan, W. C. Kuster, J. S. Holloway, E. J. Williams, B. M. Lerner, D. D. Parrish, M. Trainer, F. C. Fehsenfeld, S. Kato, E. L. Atlas, A. Baker, and D. R. Blake (2007), Determination of urban volatile organic compound emission ratios and comparison with an emissions database, *J. Geophys. Res.-Atmos.*, *112*(D10).

Watve, M. G., R. Tickoo, M. M. Jog, and B. D. Bhole (2001), How many antibiotics are produced by the genus Streptomyces?, *Arch. Microbiol.*, *176*(5), 386-390.

Wayne, R. P., I. Barnes, P. Biggs, J. P. Burrows, C. E. Canosamas, J. Hjorth, G. Lebras, G. K. Moortgat, D. Perner, G. Poulet, G. Restelli, and H. Sidebottom (1991), The Nitrate Radical - Physics, Chemistry, and the Atmosphere, *Atmospheric Environment Part a-General Topics*, *25*(1), 1-203.

WCC-VOC (2016), Karlsruhe Institute of Technology, *http://www.imk-ifu.kit.edu/wcc-voc/*, *2016*(World Calibration Centre for Volatile Organic Comounds), Accessed February 2016.

Weber, T., K. Blin, S. Duddela, D. Krug, H. U. Kim, R. Bruccoleri, S. Y. Lee, M. A. Fischbach, R. Muller, W. Wohlleben, R. Breitling, E. Takano, and M. H. Medema (2015), antiSMASH 3.0-a comprehensive resource for the genome mining of biosynthetic gene clusters, *Nucleic Acids Res.*, *43*(W1), W237-W243.

Wells, J. (2005), Special Gasoline Blends Reduce Emissions and Improve Air Quality, but Complicate Supply and Contribute to Higher Prices, *Government Accountability Office*, *05*(421), 1-47.

Wenke, K., M. Kai, and B. Piechulla (2010), Belowground volatiles facilitate interactions between plant roots and soil organisms, *Planta*, *231*(3), 499-506.

Wennborg, H., L. L. Magnusson, J. P. Bonde, and J. Olsen (2005), Congenital malformations related to maternal exposure to specific agents in biomedical research laboratories, *J. Occup. Environ. Med.*, *47*(1), 11-19.

Wheatley (2002), The consequences of volatile organic compound mediated bacterial and fungal interactions, *Antonie Van Leeuwenhoek*, *81*(1-4), 357-364.

Wheatley, R., C. Hackett, A. Bruce, and A. Kundzewicz (1997), Effect of substrate composition on production of volatile organic compounds from Trichoderma spp. inhibitory to wood decay fungi, *Int. Biodeterior. Biodegrad.*, *39*(2-3), 199-205.

White, C. S. (1988), Nitrification inhibition by monoterpenoids - Theoretical-mode of action based on molecular-structures, *Ecology*, *69*(5), 1631-1633.

Whitten, G. Z., H. Hogo, and J. P. Killus (1980), The carbon-bond mechanism - A condensed kinetic mechanism for photochemical smog *Environ. Sci. Technol.*, *14*(6), 690-700.

WHO (2014), 7 million premature deaths annually linked to air pollution, in *News release*, edited, World Health Organization, https://www.who.int/mediacentre/news/releases/2014/air-pollution/en/.

WHO (2018), Household air pollution from cooking, heating, and lighting.

Wiedinmyer, C., S. K. Akagi, R. J. Yokelson, L. K. Emmons, J. A. Al-Saadi, J. J. Orlando, and A. J. Soja (2011), The Fire INventory from NCAR (FINN): a high resolution global model to estimate the emissions from open burning, *Geoscientific Model Development*, *4*(3), 625-641.

Wilkins, K. (1996), Volatile metabolites from actinomycetes, *Chemosphere*, *32*(7), 1427-1434.

Wilkins, K., and K. Larsen (1995), Variation of Volatile Organic-Compound Patterns of Mold Species From Damp Buildings, *Chemosphere*, *31*(5), 3225-3236.

Wilson, E. W., W. A. Hamilton, H. R. Kennington, B. Evans, N. W. Scott, and W. B. DeMore (2006), Measurement and estimation of rate constants for the reactions of hydroxyl radical with several alkanes and cycloalkanes, *J. Phys. Chem. A*, *110*(10), 3593-3604.

Wirth, J. (2000), *Smelter smoke in North America: the politics of transborder pollution*, University Press of Kansas, Lawrence, KS.

WMO/GAW (2006), A WMO/GAW Expert Workshop on Global Long-Term Measurements of Volatile Organic Compounds (VOCs), paper presented at WMO GAW Report No. 171, World Meteorological Organization, Geneva, Switzerland, January 30 - February 1, 2006.

Wood, G. O. (1987), A model for adsorption capacities of charcoal beds. 1. Relative humidity effects *Am. Ind. Hyg. Assoc. J.*, *48*(7), 622-625.

Worton, D. R., W. T. Sturges, R. C.E., M. J. Newland, S. A. Penkett, E. Atlas, V. Stroud, K. Johnson, N. Schmidbauer, S. Solberg, J. Schwander, and J.-M. Barnola (2012), Evidence from firn air for recent decreases in non-methane hydrocarbons and a 20th century increase in nitrogen oxides in the northern hemisphere, *Atmospheric Environment*, *54*, 592-602.

Wu, S. L., L. J. Mickley, D. J. Jacob, D. Rind, and D. G. Streets (2008), Effects of 2000-2050 changes in climate and emissions on global tropospheric ozone and the policy-relevant background surface ozone in the United States, *J. Geophys. Res.-Atmos.*, *113*(D18).

Xiang, S. R., A. Doyle, P. A. Holden, and J. P. Schimel (2008), Drying and rewetting effects on C and N mineralization and microbial activity in surface and subsurface California grassland soils, *Soil Biol. Biochem.*, *40*(9), 2281-2289.

Xie, Y. L., and C. M. Berkowitz (2006), The use of positive matrix factorization with conditional probability functions in air quality studies: An application to hydrocarbon emissions in Houston, Texas, *Atmospheric Environment*, *40*(17), 3070-3091.

Yarwood, G., T. E. Stoeckenius, J. G. Heiken, and A. M. Dunker (2003), Modeling weekday/weekend Los Angeles region for 1997, *J. Air Waste Manage. Assoc.*, *53*(7), 864-875.

Yienger, J. J., and H. Levy (1995), Empirical-model of global soil-biogenic NOx emissions, *J. Geophys. Res.-Atmos.*, *100*(D6), 11447-11464.

Yuan, B., M. M. Coggon, A. R. Koss, C. Warneke, S. Eilerman, J. Peischl, K. C. Aikin, T. B. Ryerson, and J. A. de Gouw (2017), Emissions of volatile organic compounds (VOCs) from concentrated animal feeding operations (CAFOs): chemical compositions and separation of sources, *Atmos. Chem. Phys.*, *17*(8), 4945-4956.

Yue, S., P. Pilon, and G. Cavadias (2002), Power of the Mann-Kendall and Spearman's rho tests for detecting monotonic trends in hydrological series, *Journal of Hydrology*, *259*(1-4), 254-271.

Zavala-Araiza, D., D. W. Sullivan, and D. T. Allen (2014), Atmospheric hydrocarbon emissions and concentrations in the Barnett Shale natural gas production region, *Environ. Sci. Technol.*, *48*(9), 5314-5321.

Zeng, G., S. W. Wood, O. Morgenstern, N. B. Jones, J. Robinson, and D. Smale (2012), Trends and variations in CO, C2H6, and HCN in the Southern Hemisphere point to the declining anthropogenic emissions of CO and C2H6, *Atmos. Chem. Phys.*, *12*(16), 7543-7555.

Zhang, B., R. C. Owen, J. A. Perlinger, A. Kumar, S. Wu, M. V. Martin, L. Kramer, D. Helmig, and R. E. Honrath (2014), A semi-Lagrangian view of ozone production tendency in North American outflow in the summers of 2009 and 2010, *Atmos. Chem. Phys.*, *14*(5), 2267-2287.

Zheng, C. H., J. L. Shen, Y. X. Zhang, W. W. Huang, X. B. Zhu, X. C. Wu, L. H. Chen, X. Gao, and K. F. Cen (2017), Quantitative assessment of industrial VOC emissions in China: Historical trend, spatial distribution, uncertainties, and projection, *Atmospheric Environment*, *150*, 116-125.

Zhou, W., D. S. Cohan, and B. H. Henderson (2014), Slower ozone production in Houston, Texas following emission reductions: evidence from Texas Air Quality Studies in 2000 and 2006, *Atmos. Chem. Phys.*, *14*(6), 2777-2788.

Ziemert, N., A. Lechner, M. Wietz, N. Millan-Aguinaga, K. L. Chavarria, and P. R. Jensen (2014), Diversity and evolution of secondary metabolism in the marine actinomycete genus Salinispora, *Proc. Natl. Acad. Sci. U. S. A.*, *111*(12), E1130-E1139.

Zörner, J., M. Penning de Vries, S. Beirle, H. Sihler, P. R. Veres, J. Williams, and T. Wagner (2016), Multi-satellite sensor study on precipitation-induced emission pulses of NOx from soils in semi-arid ecosystems, *Atmos. Chem. Phys.*, *16*(14), 9457-9487.

Zou, C. S., M. H. Mo, Y. Q. Gu, J. P. Zhou, and K. Q. Zhang (2007), Possible contributions of volatile-producing bacteria to soil fungistasis, *Soil Biol. Biochem.*, *39*(9), 2371-2379.

Appendix:

Supplemental Material:

Chapter 2

Reversal of global atmospheric ethane and propane trends largely due to US oil and

natural gas production

Detlev Helmig[1]*, Samuel Rossabi[1], Jacques Hueber[1], Pieter Tans[2], Stephen A. Montzka[2], Ken Masarie[2], Kirk Thoning[2], Christian Plass-Duelmer[3], Anja Claude[3], Lucy J. Carpenter[4], Alastair C. Lewis[5], Shalini Punjabi[4], Stefan Reimann[6], Martin K. Vollmer[6], Rainer Steinbrecher[7], James W. Hannigan[8], Louisa K. Emmons[8], Emmanuel Mahieu[9], Bruno Franco[9], Dan Smale[10] and Andrea Pozzer[11]

[1]Institute of Arctic and Alpine Research, University of Colorado, Boulder, Colorado 80305, USA.
[2]Earth Systems Research Laboratory, National Oceanic and Atmospheric Administration, Boulder, Colorado 80305, USA.
[3]Deutscher Wetterdienst, 82383 Hohenpeissenberg, Germany.
[4]Wolfson Atmospheric Chemistry Laboratories, University of York, York YO10 5DD, UK.
[5]National Centre for Atmospheric Science, University of York, York YO10 5DD, UK.
[6]Laboratory for Air Pollution and Environmental Technology, Empa, Swiss Federal Laboratories for Materials Science and Technology, 8600 Duebendorf, Switzerland.
[7]Karlsruhe Institute for Technology, Campus Alpine, 82467 Garmisch-Partenkirchen, Germany.
[8]National Center for Atmospheric Research, Boulder, Colorado 80301, USA.
[9]Institute of Astrophysics and Geophysics, University of Liège, 4000 Liège, Belgium.
[10]National Institute of Water and Atmospheric Research, Lauder 9352, New Zealand.
[11]Max Planck Institute for Chemistry, 55128 Mainz, Germany.

*Corresponding Author: Detlev Helmig (detlev.helmig@colorado.edu)

Table S1. Site information, ethane data statistics, number of considered sampling days after removal of outliers, and rate of change results.

Ethane

Site Three Letter Code	Name, State	Country	Lat	Long	End of 2011 Mixing Ratio (pmol mol^{-1})	Trend (pmol mol^{-1} year^{-1})	Trend (%)	R^2	2009.5-2014.5 Coverage	Total points	R2 * Coverage	Comments
Network Flasks												
ALT	Alert, Nunavut	Canada	82.5	-62.5	1350	39.9	3.0	0.59	100%	262	0.59	
ZEP	Ny-Alesund, Svalbard	Norway	78.9	11.9	1390	37.4	2.7	0.52	100%	262	0.52	
SUM	Summit	Greenland	72.6	-38.5	1360	63.9	4.7	0.97	100%	263	0.97	
TIK	Tiksi	Russia	71.6	128.9	1520	137	9.0	0.87	58%	152	0.51	
BRW	Barrow, Alaska	United States	71.3	-156.6	1340	21.1	1.6	0.37	100%	262	0.37	
PAL	Pallas-Sammaltunturi	Finland	68.0	24.1	1450	40.7	2.8	0.48	100%	263	0.48	
ICE	Storhofdi, Vestmannaeyjar	Iceland	63.3	-20.3	1354	46.2	3.4	0.86	100%	263	0.86	
BAL	Baltic Sea	Poland	55.4	17.2		23.8		0.18	40%	104	0.07	1
CBA	Cold Bay, Alaska	United States	55.2	-162.7	1350	28.8	2.1	0.61	100%	262	0.61	
LLB	Lac La Biche, Alberta	Canada	55.0	-112.5	2240	-13.5	-0.6	0.00	73%	192	0.00	
MHD	Mace Head, County Galway	Ireland	53.3	-9.9	1230	53.1	4.3	0.65	100%	263	0.65	
SHM	Shemya Island, Alaska	United States	52.7	174.1	1407	34.5	2.5	0.84	100%	263	0.84	
OXK	Ochsenkopf	Germany	50.0	11.8	1290	37.7	2.9	0.21	100%	263	0.21	
HPB	Hohenpeissenberg	Germany	47.8	11.0	1450	21.2	1.5	0.28	100%	262	0.28	

264

LEF	Park Falls, Wisconsin	United States	45.9	-90.3	1730	136	7.9	0.89	100%	262	0.89	
BSC	Black Sea, Constanta	Romania	44.2	28.7	2760	-210	-7.6	0.78	50%	131	0.39	
THD	Trinidad Head, California	United States	41.1	-124.2	1220	20.6	1.7	0.43	100%	262	0.43	
UTA	Wendover, Utah	United States	39.9	-113.7	1130	33.5	3.0	0.81	100%	263	0.81	
AZR	Terceira Island, Azores	Portugal	38.8	-27.4	1130	86.7	7.7	0.57	100%	262	0.57	
SGP	Southern Great Plains, Oklahoma	United States	36.8	-97.5	7590	814	10.7	0.84	100%	262	0.84	
TAP	Tae-ahn Peninsula	Korea	36.7	126.1	2010	24.7	1.2	0.24	100%	263	0.24	
BMW	Tudor Hill	Bermuda	32.3	-64.9	1150	21.0	1.8	0.15	82%	216	0.13	
IZO	Tenerife, Canary Islands	Spain	28.3	-16.5	864	30.0	3.5	0.32	100%	262	0.32	
MID	Sand Island, Midway	United States	28.2	-177.4	920	15.7	1.7	0.18	100%	263	0.18	
KEY	Key Biscayne, Florida	United States	25.7	-80.2	1200	99.9	8.3	0.59	100%	262	0.59	
ASK	Assekrem	Algeria	23.2	5.4	990	72.9	7.4	0.95	100%	262	0.95	
KUM	Cape Kumakahi, Hawaii	United States	19.5	-154.8	760	6.34	0.8	0.13	100%	263	0.13	
MLO	Mauna Loa, Hawaii	United States	19.5	-155.6	597	5.85	1.0	0.05	100%	262	0.05	
MEX	High Altitude Global Climate Observation Center	Mexico	19.0	-97.3	761	36.6	4.8	0.47	100%	263	0.47	
GMI	Mariana Islands	Guam	13.4	144.8	502	17.0	3.4	0.23	100%	263	0.23	
MKN	Mount Kenya	Kenya	-0.1	37.3		106		0.95	40%	104	0.38	1
BKT	Bukit Kototabang	Indonesia	-0.2	100.3	453	46.1	10.2	0.23	100%	262	0.23	
SEY	Mahe Island	Seychelles	-4.7	55.2	408	10.2	2.5	0.13	100%	263	0.13	
NAT	Maxaranguape	Brazil	-5.5	-35.3	273	-6.01	-2.2	0.05	76%	199	0.04	
ASC	Ascension Island	United Kingdom	-7.9	-14.4	621	24.9	4.0	0.07	100%	263	0.07	

SMO	Tutulia	Samoa	-14.2	-170.6	212	2.28	1.1	0.28	100%	262	0.28
EIC	Easter Island	Chile	-27.2	-109.5	209	3.58	1.7	0.07	100%	263	0.07
CGO	Cape Grim, Tasmania	Australia	-40.7	144.7	202	7.62	3.8	0.38	100%	262	0.38
CRZ	Crozet Island	France	-46.5	51.9	204	2.95	1.5	0.16	94%	245	0.15
USH	Tierra Del Fuego, Ushuaia	Argentina	-54.9	-68.5	191	-5.87	-3.1	0.17	100%	263	0.17
PSA	Palmer Station	Antartica	-64.9	-64.0	191	2.28	1.2	0.24	100%	262	0.24
SYO	Syowa Station	Antartica	-69.0	39.6	218	18.5	8.5	0.89	91%	239	0.81
HBA	Hailey Station	UK	-75.6	-26.2	184	0.43	0.2	0.00	89%	233	0.00
SPO	South Pole	Antartica	-90.0	-24.8	181	-6.39	-3.5	0.17	92%	242	0.16
In-situ											
SUM	Summit	Greenland	72.6	-38.5	1250	67.2	5.4	0.96	90%	235	0.60
HPB	Hohenpeissenberg	Germany	47.8	11.0	1480	17.00	1.1	0.16	100%	262	0.4
RIG	Rigi	Switzerland	47.1	8.5	1490	33.80	2.3	0.53	100%	262	0.53
JFJ	Jungfraujoch	Switzerland	46.3	7.6	1160	71.8	6.2	0.36	60%	157	0.22
CVO	Cape Verde		15.1	-23.6	801	44.7	5.6	0.96	100%	263	0.96

Comments   1: Incomplete Coverage

Table S1 Footnotes:

1 Total number of samples, counting each sample from paired sampling individually.

2 Number of sampling dates that were retained after applying all data filters.

3 End of 2011 mixing ratio after removal of harmonic components of the data fit.

4 Result of Mann-Kendall test using a significance value of $\alpha = 0.01$. Non-significant rate of change results are labeled in italics and in parenthesis.

5 R2 result of a linear fit to the trend curve, sampled at times of retained whole air sampling dates.

Table S2. Site information, propane data statistics, number of considered sampling days after removal of outliers, and rate of change results.

Propane

Site Three Letter Code	Name, State	Country	Lat	Long	End of 2011 Mean Mixing Ratio (pmol mol^{-1})	Trend (pmol mol^{-1} year^{-1})	Trend (%)	R^2	2009.5-2014.5 Coverage	Total points	R2* Coverage	Comments
Global VOC Network Flasks												
ALT	Alert, Nunavut	Canada	82.5	-62.5	465	15.5	3.3	0.60	100%	262	0.60	
ZEP	Ny-Alesund, Svalbard	Norway	78.9	11.9	492	-0.30	-0.1	0.00	100%	262	0.00	
SUM	Summit	Greenland	72.6	-38.5	417	23.6	5.7	0.85	100%	263	0.85	
TIK	Tiksi	Russia	71.6	128.9	578	101	17.4	0.77	58%	152	0.44	
BRW	Barrow, Alaska	United States	71.3	-156.6	437	1.24	0.3	0.01	100%	263	0.01	
PAL	Pallas-Sammaltunturi	Finland	68.0	24.1	520	16.8	3.2	0.62	100%	263	0.62	
ICE	Storhofdi, Vestmannaeyjar	Iceland	63.3	-20.3	400	149	37.3	0.63	100%	263	0.63	
BAL	Baltic Sea	Poland	55.4	17.2		-44.0		0.91	40%	104	0.36	1
CBA	Cold Bay, Alaska	United States	55.2	-162.7	415	7.56	1.8	0.47	100%	262	0.47	
LLB	Lac La Biche, Alberta	Canada	55.0	-112.5	1080	-39.3	-3.6	0.04	73%	192	0.03	
MHD	Mace Head, County Galway	Ireland	53.3	-9.9	347	16.5	4.8	0.55	100%	263	0.55	
SHM	Shemya Island, Alaska	United States	52.7	174.1	446	17.4	3.9	0.62	100%	263	0.62	
OXK	Ochsenkopf	Germany	50.0	11.8	426	0.29	0.1	0.00	100%	263	0.00	
HPB	Hohenpeissenberg	Germany	47.8	11.0	512	-6.30	-1.2	0.08	100%	262	0.08	

268

LEF	Park Falls, Wisconsin	United States	45.9	-90.3	704	92.2	13.1	0.68	100%	262	0.68	
BSC	Black Sea, Constanta	Romania	44.2	28.7	8000	-20700	-258.8	0.57	50%	131	0.28	
THD	Trinidad Head, California	United States	41.1	-124.2	361	-6.39	-1.8	0.19	100%	262	0.19	
UTA	Wendover, Utah	United States	39.9	-113.7	352	1.26	0.4	0.02	100%	263	0.02	
AZR	Terceira Island, Azores	Portugal	38.8	-27.4	274	36.8	13.4	0.53	100%	262	0.53	
SGP	Southern Great Plains, Oklahoma	United States	36.8	-97.5	4570	480	10.5	0.88	100%	262	0.88	
TAP	Tae-ahn Peninsula	Korea	36.7	126.1	937	6.80	0.7	0.02	100%	263	0.02	
BMW	Tudor Hill	Bermuda	32.3	-64.9	419	95.1	22.7	0.55	82%	216	0.46	
IZO	Tenerife, Canary Islands	Spain	28.3	-16.5	162	-6.41	-4.0	0.33	100%	262	0.33	
MID	Sand Island, Midway	United States	28.2	-177.4	214	-1.21	-0.6	0.01	100%	263	0.01	
KEY	Key Biscayne, Florida	United States	25.7	-80.2	453	52.8	11.7	0.47	100%	262	0.47	
ASK	Assekrem	Algeria	23.2	5.4	200	17.3	8.6	0.73	100%	263	0.73	
KUM	Cape Kumakahi, Hawaii	United States	19.5	-154.8	135	0.13	0.1	0.00	100%	263	0.00	
MLO	Mauna Loa, Hawaii	United States	19.5	-155.6	76.0	3.79	5.0	0.48	100%	262	0.48	
MEX	High Altitude Global Climate Observation Center	Mexico	19.0	-97.3	336	-6.17	-1.8	0.01	100%	263	0.01	
GMI	Mariana Islands	Guam	13.4	144.8	82.6	-0.47	-0.6	0.01	100%	263	0.01	
MKN	Mount Kenya	Kenya	-0.1	37.3		0.08		0.00	40%	104	0.00	1
BKT	Bukit Kototabang	Indonesia	-0.2	100.3	12.9	32.5	251.2	0.16	100%	263	0.16	
SEY	Mahe Island	Seychelles	-4.7	55.2	45.6	0.91	2.0	0.07	100%	263	0.07	
NAT	Maxaranguape	Brazil	-5.5	-35.3	30.2	3.17	10.5	0.01	76%	199	0.01	

ASC	Ascension Island	United Kingdom	-7.9	-14.4	116	5.03	4.4	0.07	100%	262	0.07	
SMO	Tutulia	Samoa	-14.2	-170.6	16.7	1.11	6.6	0.22	100%	262	0.22	
EIC	Easter Island	Chile	-27.2	-109.5		-32.5		0.02	100%	263	0.02	2
CGO	Cape Grim, Tasmania	Australia	-40.7	144.7	40.9	0.15	0.4	0.00	100%	262	0.00	
CRZ	Crozet Island	France	-46.5	51.9	29.0	0.79	2.7	0.06	94%	245	0.06	
USH	Tierra Del Fuego, Ushuaia	Argentina	-54.9	-68.5	25.5	-1.73	-6.8	0.03	100%	263	0.03	
PSA	Palmer Station	Antartica	-64.9	-64.0	28.2	0.79	2.8	0.23	100%	262	0.23	
SYO	Syowa Station	Antartica	-69.0	39.6	25.3	1.54	6.1	0.45	91%	239	0.41	
HBA	Hailey Station	UK	-75.6	-26.2	26.0	0.13	0.5	0.12	89%	233	0.10	
SPO	South Pole	Antartica	-90.0	-24.8	27.9	-1.37	-4.9	0.15	92%	242	0.13	

						HATS						
AMT	Argyle, Maine	United States	45.0	-68.7	680	54.8	8.1	0.84	100%	262	0.84	
MBO	Mt. Bachelor Observatory	United States	44.0	-121.7	310.0333	8.51	2.7	0.05	54%	143	0.05	
WBI	West Branch, IA	United States	41.7	-91.4	1050	30.2	2.9	0.07	100%	262	0.07	
MVY	Martha's Vineyard	United States	41.3	-70.5		-82.2		0.61	33%	88	0.20	1
LEW	Lewisberg, PA	United States	40.9	-76.9		5940		0.50	22%	58	0.11	1
NWR	Niwot Ridge, CO	United States	40.1	-105.6		-31.6		0.08	44%	263	0.04	1
INX	Indianapolis Flux Exp.	United States	39.6	-86.4	1620	603	37.2	0.51	75%	196	0.38	
WGC	Walnut Grove, CA	United States	38.3	-121.5	738	-16.5	-2.2	0.12	100%	263	0.12	
STR	Sutro Tower, CA	United States	37.8	-122.5	491	-31.6	-6.4	0.68	100%	263	0.68	

MWO	Mt. Wilson Observatory	United States	34.2	-118.1		-173		0.70	84%	219	0.59	2
SCT	Beech Island, SC	United States	33.4	-81.8	795	25.2	3.2	0.18	100%	262	0.18	
WKT	Moody, TX	United States	31.3	-97.3	2352	286	12.2	0.87	100%	263	0.87	
					In-situ							
SUM	Summit	Greenland	72.6	-38.5	355	29.4	8.3	0.85	90%	235	0.54	
HPB	Hohenpeissenberg	Germany	47.8	11.0	502	0.81	0.2	0.00	100%	262	0.06	
RIG	Rigi	Switzerland	47.1	8.5	530	4.86	0.9	0.07	100%	262	0.07	
JFJ	Jungfraujoch	Switzerland	46.3	7.6	310	38.2	12.3	0.51	60%	157	0.14	
CVO	Cape Verde		15.1	-23.6	143	4.46	3.1	0.25	100%	263	0.25	

Comments: 1 Incomplete coverage, 2 Poor fitting or site influenced by local contamination

Table S2 Footnotes:

1 Total number of samples, counting each sample from paired sampling individually.

2 Number of sampling dates that were retained after applying all data filters.

3 End of 2011 mixing ratio after removal of harmonic components of the data fit.

4 Result of Mann-Kendall test using a significance value of $\alpha = 0.01$. Non-significant rate of change results are labeled in italics and in parenthesis.

5 R^2 result of a linear fit to the trend curve, sampled at times of retained whole air sampling dates.

Table S3. 2009.5 – 2014.5 ethane rate of changes calculated from the data in Table S1 with sites grouped by geographical region.

| | | Ethane Trend % Per Year | | | |
| | | | | Mean | |
Region	N	Mean[1]	Median[2]	Mean[3]	Median[4]
0-30° N	9	4.1	3.5		
30-60° N	16	2.9	2.3	3.6	2.9
60-90° N	7	3.9	3.0		

| | | Ethane Trend % Per Year | | | |
| | | | | Mean | |
Region	N	Mean[1]	Median[2]	Mean[3]	Median[4]
0-90° E	8	2.0	2.7		
90-180° E	4	4.0	2.9	3.5	2.9
0-90° W	9	4.7	4.3		
90-180° W	11	3.2	1.7		

| | | Ethane Trend % Per Year | | | |
| | | | | Mean | |
Region	N	Mean[1]	Median[2]	Mean[3]	Median[4]
Arctic	7	3.9	3.0		
North Atlantic	3	4.6	4.5		
North Pacific	6	1.9	1.9		
North America	7	5.1	4.8	4.3	4.2
Europe	5	1.3	2.1		
Asia	2	5.7	5.7		
North Africa	1	7.4	7.4		

Table S3 Footnotes:

1 Mean value of trend results of all sites within the specified geographical region.

2 Mean value of trend results of all sites within the specified geographical region.

3 Mean value of the listed regional average trends.

4 Median value of the listed regional average trends

Table S4. Year 2007 inventory ethane emission estimates for selected regions based on doubled HTAP2 anthropogenic inventory, MEGANv2.1 and FINNv1.5.

Region/Sector	2007 Emissions (Tg yr^{-1})
Globe – all	17.56
Globe – BB	2.22
Globe – MEGAN	0.37
N. America	1.55
Europe	2.07
E. Asia	2.13
C. America	0.45
N. Africa	2.81
S. Asia	3.45
SH	2.54

Table S5. Methane/ethane mass ratio from data collected near oil and natural gas sources regions in the USA.

Source Region	Methane/Ethane Mass Ratio	Reference
Texas/Oklahoma	3.3	Katzenstein et al., 2003[1]
Uintah Basin, UT	8.4	Helmig et al., 2014
Pennsylvania	14	Kang et al., 2014[2]
Haynesville, LA + TX	14	Peischl et al., 2015a[3]
Upper Green River Basin, WY	11	Field et al., 2015
Barnett Shale, TX	4.2 - 33	Smith et al., 2015[4]
9 Regions Central/Western US	1.7 - 15	Peischl et al., 2015b[5]
Mean Ratio: [6]	*11*	
Median Ratio: [7]	*10*	
Standard Deviation: [8]	*4.9*	
*0.5 * (Max - Min):* [9]	*7.6*	

[*Field et al.*, 2015; *Helmig. et al.*, 2014b; *Kang et al.*, 2014; *Katzenstein et al.*, 2003; *Peischl et al.*, 2015a; *Peischl et al.*, 2015b; *Smith et al.*, 2015]

Table S5 Footnotes:

1 Derived from data in their Table 2, after subtraction of estimated methane and ethane background levels.

2 Derived from their Figure 3A.

3 Data from Haynesville. Data from three other oil and natural gas regions were not included here as they showed lower ethane and me- thane enhancements, likely due to weaker dominance of oil and gas sources and influence from other, more diverse emission sources.

4 Lower and upper bounds of data in their Fig. 4a.

5 Lower and upper bounds of preliminary data from nine emission regions.

6,7 Mean and Median value of the listed studies, incorporating the mean values of the ranges reported in [*Peischl et al.*, 2015b; *Smith et al.*, 2015].

8 Standard Deviation of the listed studies, incorporating the mean values of the ranges reported in [*Peischl et al.*, 2015b; *Smith et al.*, 2015].

9 Half the range of listed slope values, including the mean values of the ranges reported in [*Peischl et al.*, 2015b; *Smith et al.*, 2015].

Table S6. Estimation of mass emission ratios of NMHC > C2 relative to ethane, based on published data from oil and gas regions.

	E_{NMHC}/E_{ethane}				
	DJB[1]	BAO[2]	Marcellus[3]	Marcellus[4]	Uintah[5]
Ethane	1.000	1.000	1.000	1.000	1.000
Propane	1.467	1.131	0.679	0.469	0.711
i-Butane	0.348	0.331	0.121	0.103	0.186
n-Butane	0.889	0.773	0.296	0.177	0.272
i-Pentane	0.312	0.288	0.082	0.094	0.158
n-Pentane	0.312	0.322	0.106	0.081	0.122
n-Hexane	0.100	0.090			0.083
n-Heptane	0.033	0.030			
n-Octane	0.012				
n-Nonane	0.003				
n-Decane	0.002				
Neopentane	0.002				
2,3-Dimethylbutane	0.005				
2,2-Dimethylbutane	0.004				
2-Methylpentane	0.080				
3-Methylpentane	0.043				
2,4-Dimethylpentane	0.004				
2,3-Dimethylpentane	0.004				
2-Methylhexane	0.006				
2,2,4-Trimethylpentane	0.008				
2-Methylheptane	0.007				
3-Methylheptane	0.005				
Cyclopentane	0.018				
Methylcyclopentane	0.026	0.104			
Cyclohexane	0.026	0.024			
Methylcyclohexane	0.031	0.026			
Benzene	0.016	0.022	0.009	0.021	0.024
Toluene	0.026	0.026			0.031
Estimate of unaccounted NMHC (%)	5	10	15	15	10
$\Sigma E_{NMHC > C2}/E_{ethane}$	4.0	3.6	1.6	1.2	1.8
Mean $\Sigma E_{NMHC > C2}/E_{ethane}$			2.5		
Median $\Sigma E_{NMHC > C2}/E_{ethane}$			1.8		

Table S6 Footnotes:

1 Derived from [*Swarthout. et al.*, 2013], using observations with transport from the northeast wind sector at the Boulder Atmospheric Observatory, which is associated to transport from the Denver Julesburg Basin.

2 Derived from [*Gilman et al.*, 2013], using the mean ambient observations in all data from the Boulder Atmospheric Observatory on the SW edge of the Denver Julesburg Basin.

3 Derived from [*Swarthout. et al.*, 2015], using data from the Hickory site, a residential area surrounded by oil and natural gas development in the Marcellus Shale.

4 Derived from [*Swarthout. et al.*, 2015], using data from nighttime samples near wells in the Marcellus Shale.

5 Derived from [*Helmig. et al.*, 2014b], using data from the Horsepool site which is centrally located in the Unitah Basin oil and natural gas area.
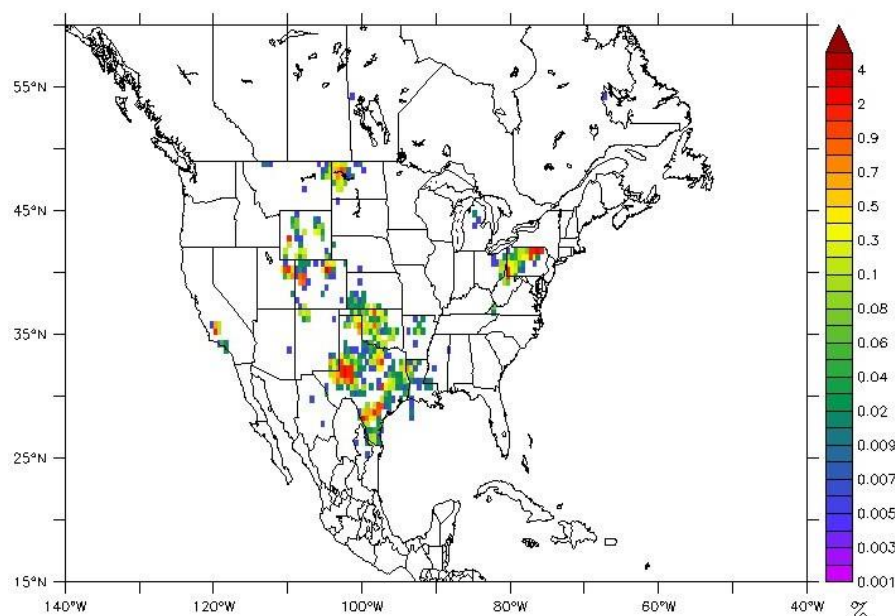
Figure S1. Model ozone sensitivity study. Geographical distribution of the NMHC emissions increase applied in the ozone modeling. The color bar on the right shows the regional relative emission increase as a fraction of the total.

Changes in Atmospheric Butanes and Pentanes and their Isomeric Ratios in the Continental United States

Sam Rossabi[1] , and Detlev Helmig[1,*]

[1]Institute of Arctic and Alpine Research, University of Colorado, Boulder, Colorado, 80303, USA

*Corresponding author: Detlev Helmig (Detlev.Helmig@colorado.edu)
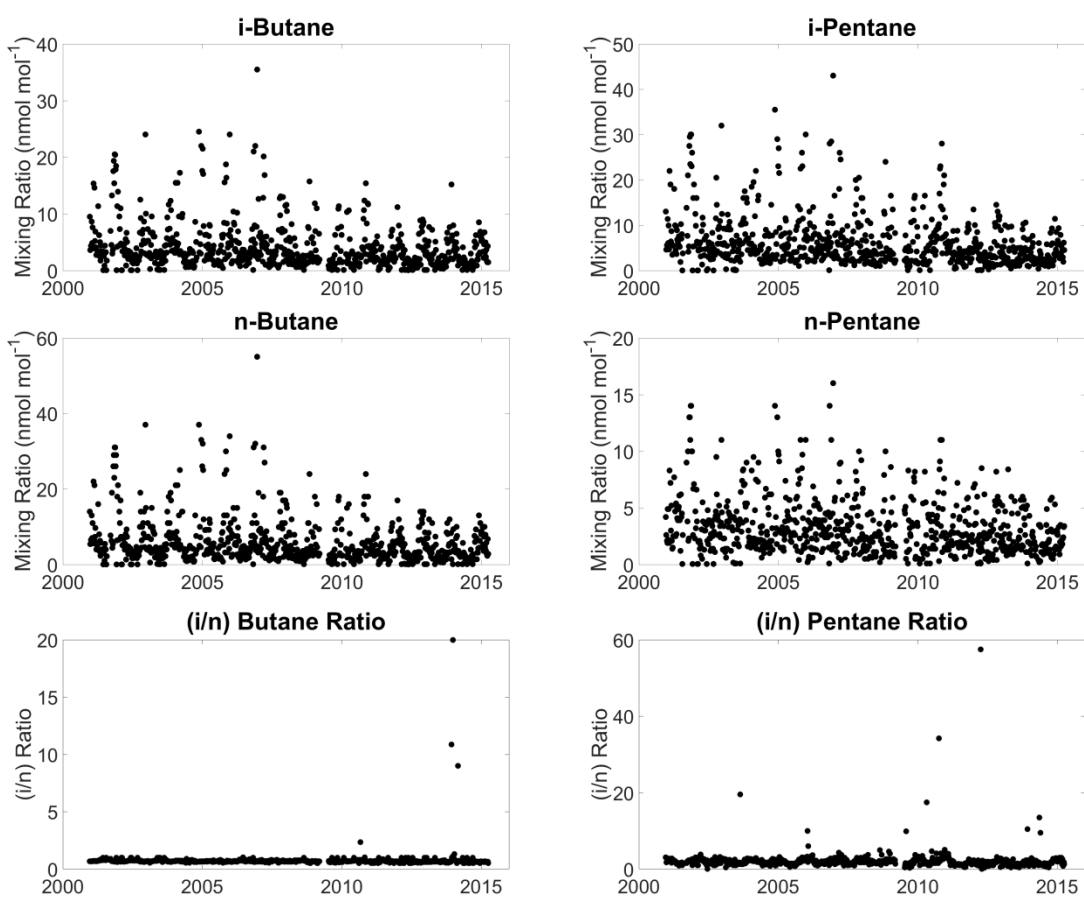
Figure S1a. Butane and pentane isomer mixing ratios and isomeric ratio data at Atlanta South De Kalb before applying any filtering.
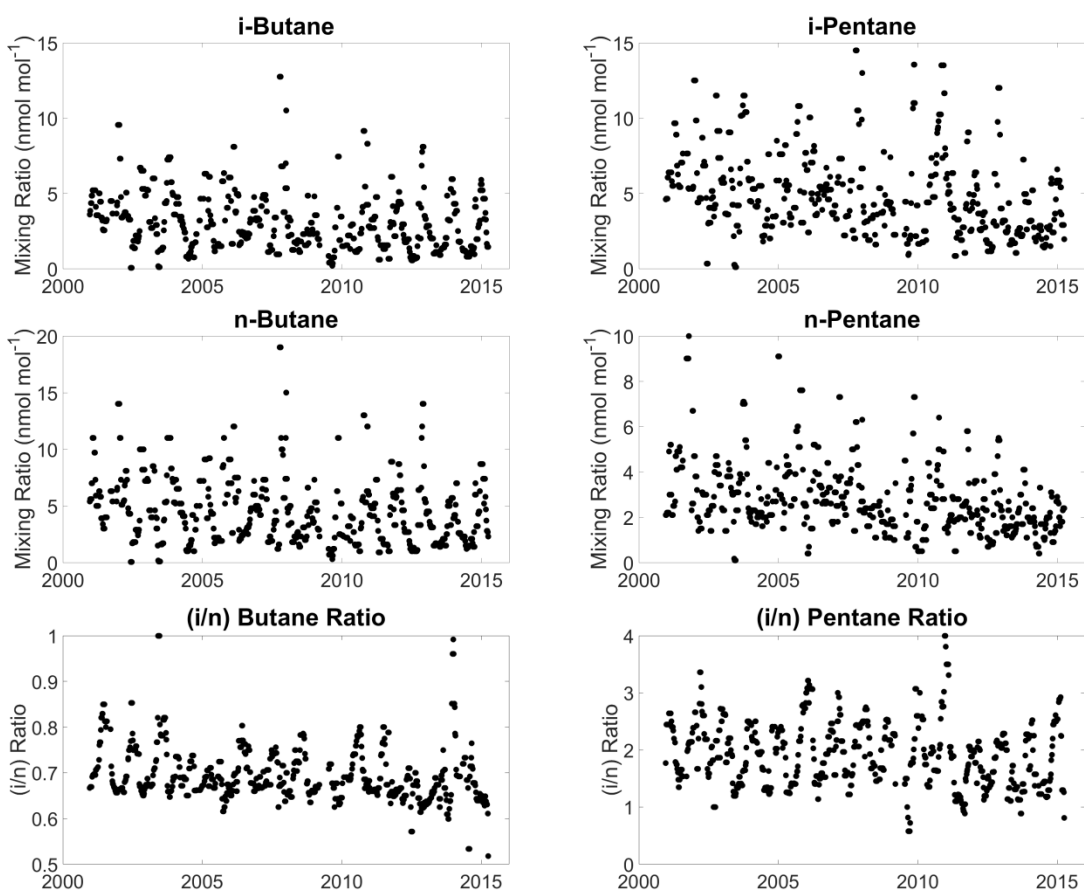
Figure S1b. Butane and pentane isomer mixing ratios and isomeric ratio data at Atlanta South De Kalb after applying the filtering as detailed in the main manuscript text.

Supplement Text STx1

Statistical Power

Statistical power is a measure of the probability that a trend test will reject the null hypothesis when it is false. A good example from the data studied in this work is the two Atlanta sites. The Atlanta - SDK site has a few statistically significant trends for compounds and ratios while the Tucker site does not have any. It is possible that the Tucker site measures different air parcels than the SDK site and does not have any statistically significant trends. However, the slope behavior is identical at these two sites, indicating some similarity of air measured. It is possible that the lack of data at Tucker impedes the Mann-Kendall test from finding statistically significant trends. Sites not directly east of, or at least ~200 miles away from a shale play to its west do not have statistically significant pentane isomeric ratio trends.
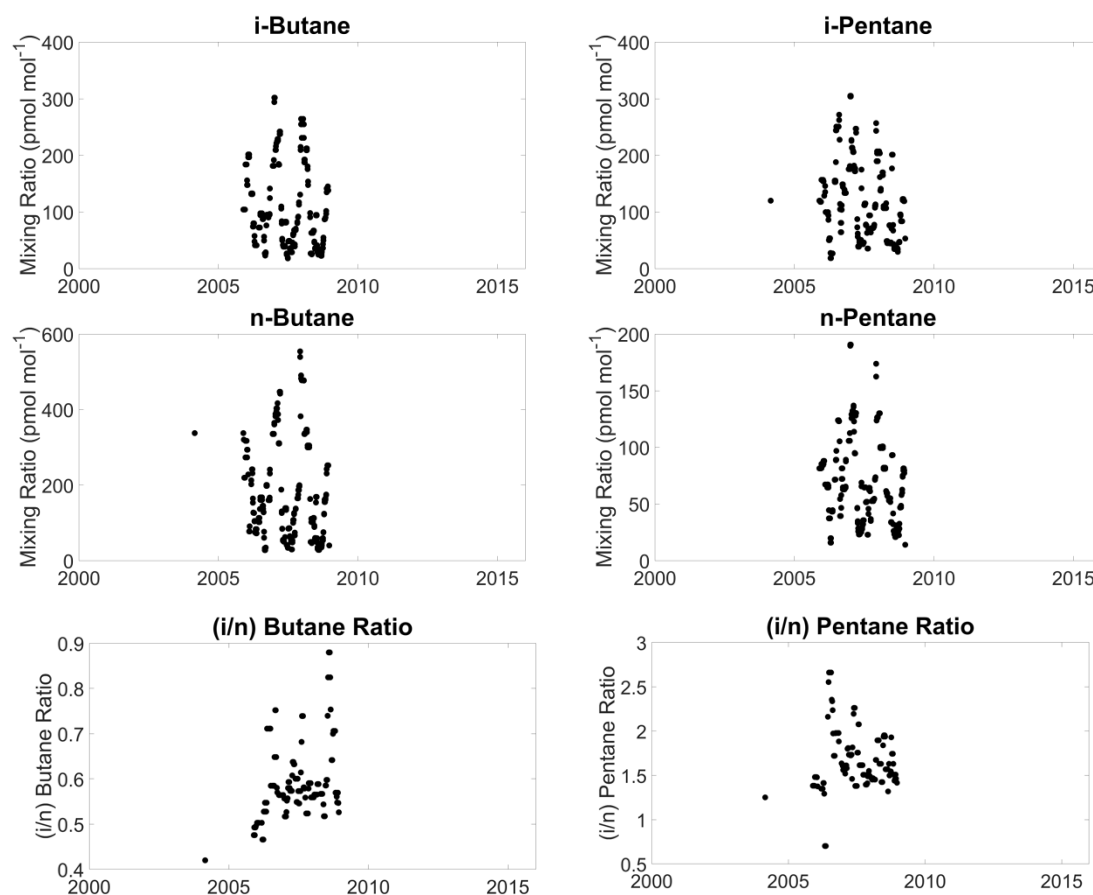
Figure S2a. Butane and pentane isomer mixing ratios and isomeric ratio data at the Argyle site.
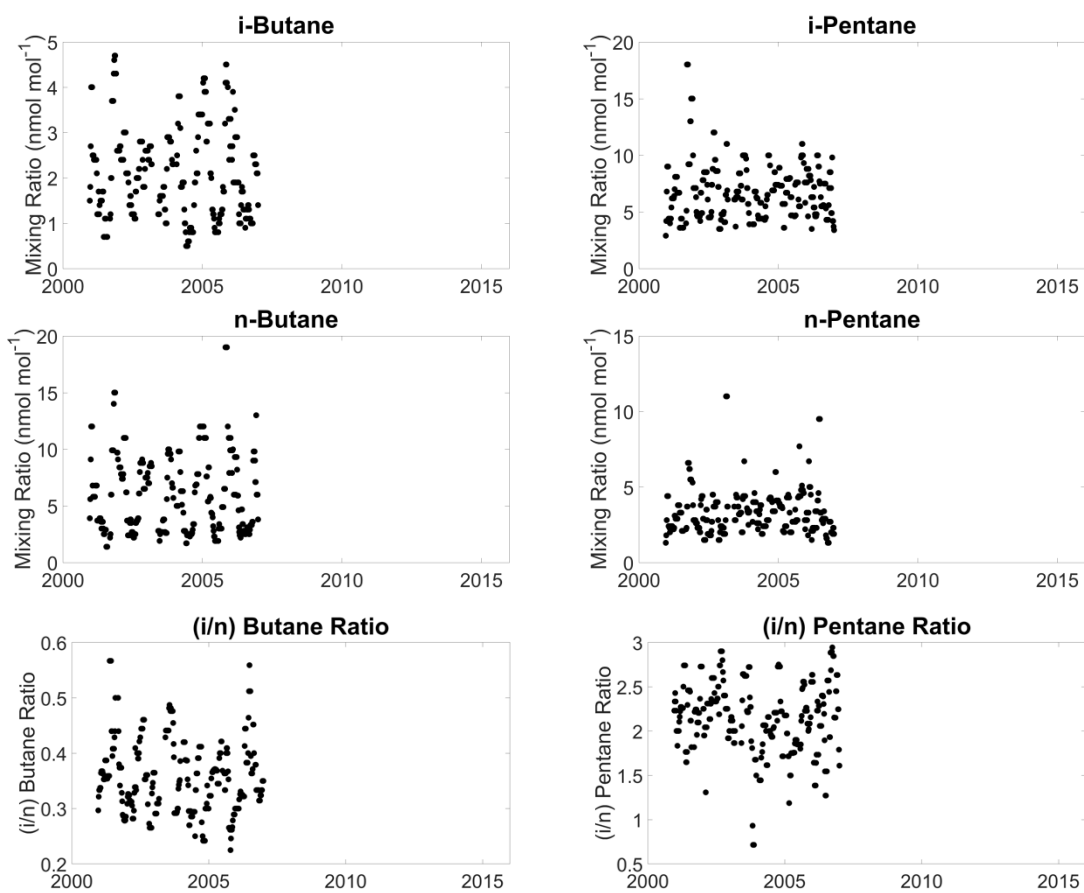
Figure S2b. Butane and pentane isomer mixing ratios and isomeric ratio data at the Atlanta – Tucker site.
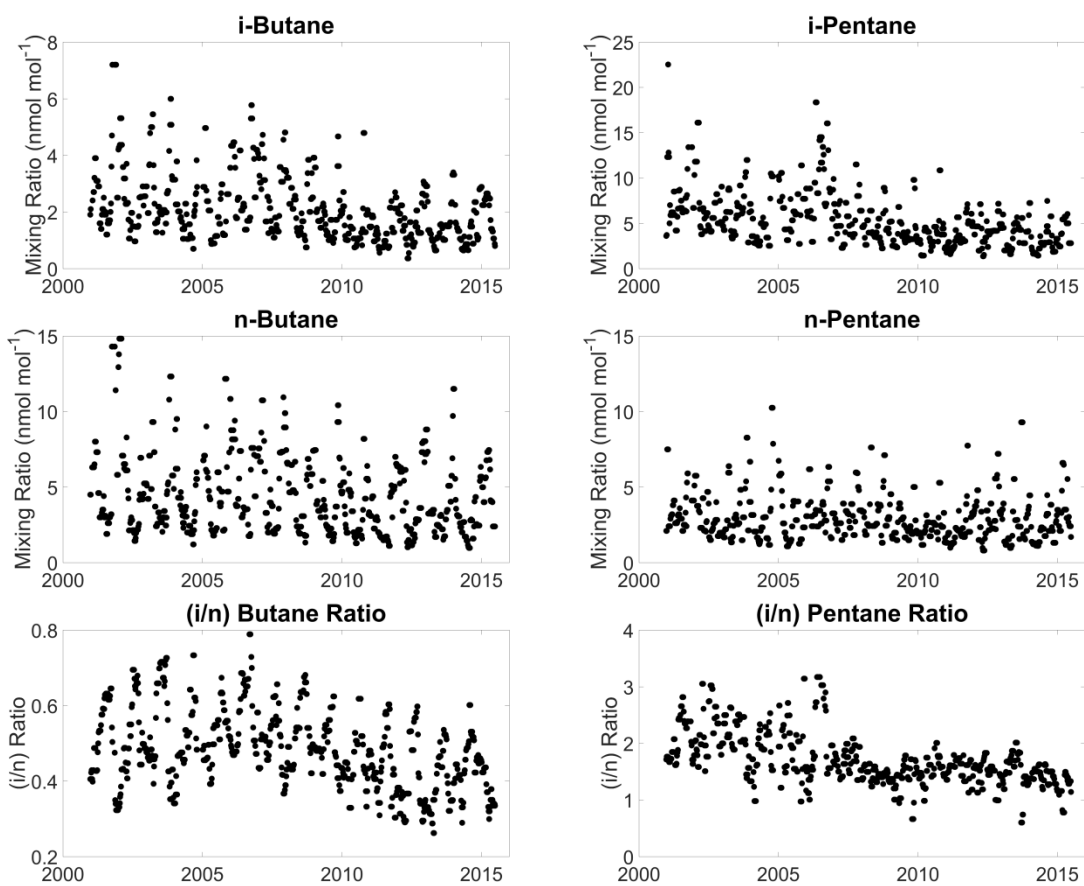
Figure S2c. Butane and pentane isomer mixing ratios and isomeric ratio data at the Baltimore site.
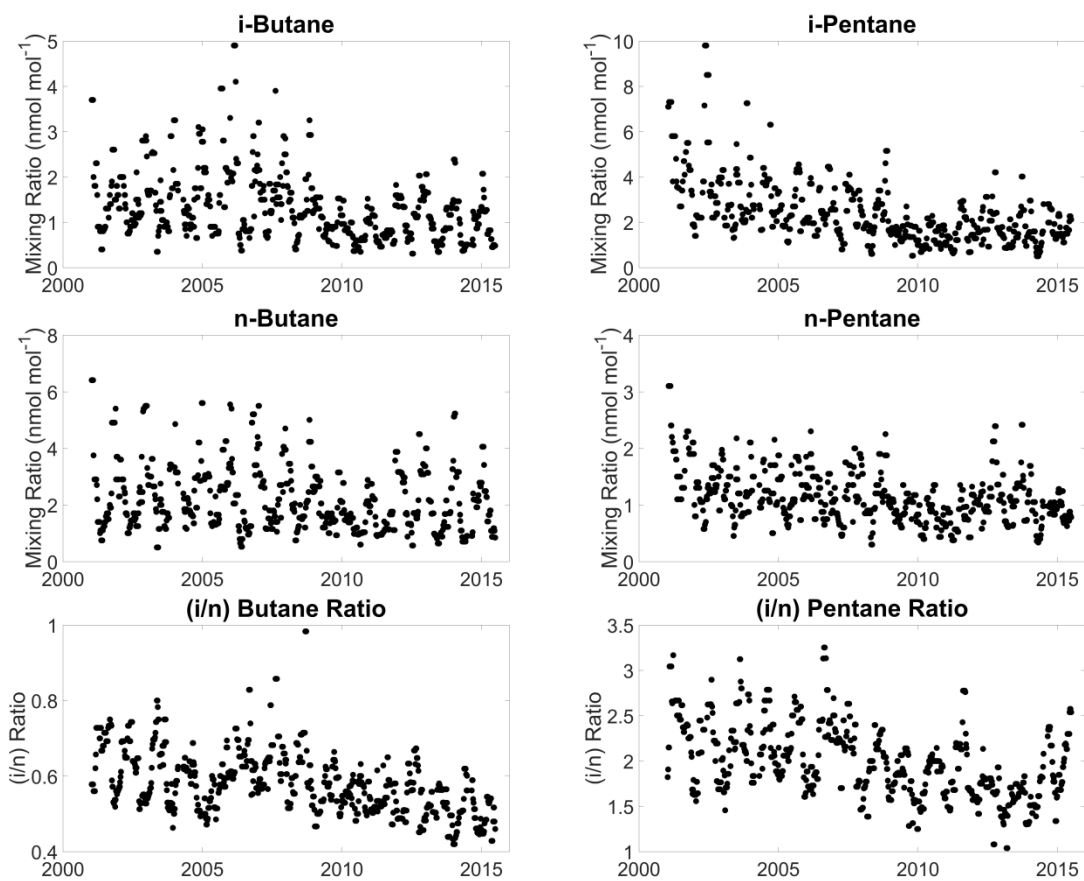
Figure S2d. Butane and pentane isomer mixing ratios and isomeric ratio data at the Boston site.
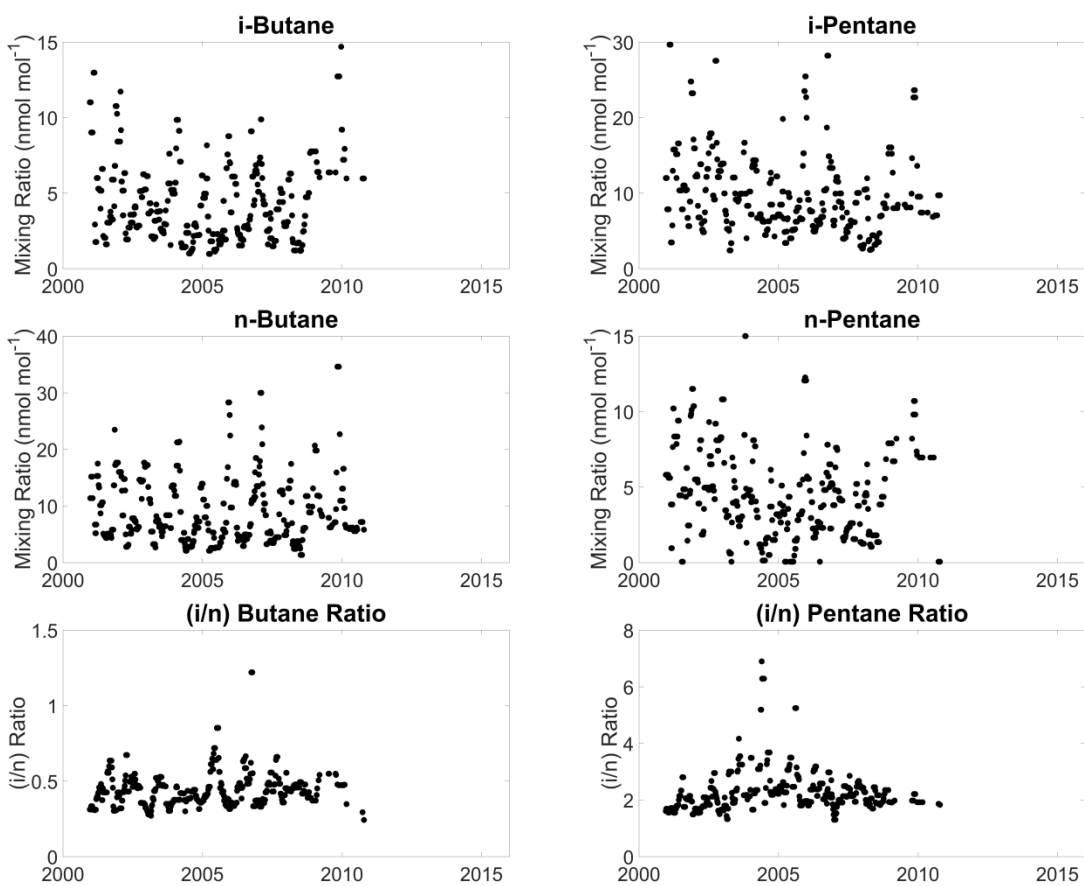
Figure S2e. Butane and pentane isomer mixing ratios and isomeric ratio data at the El Paso site.
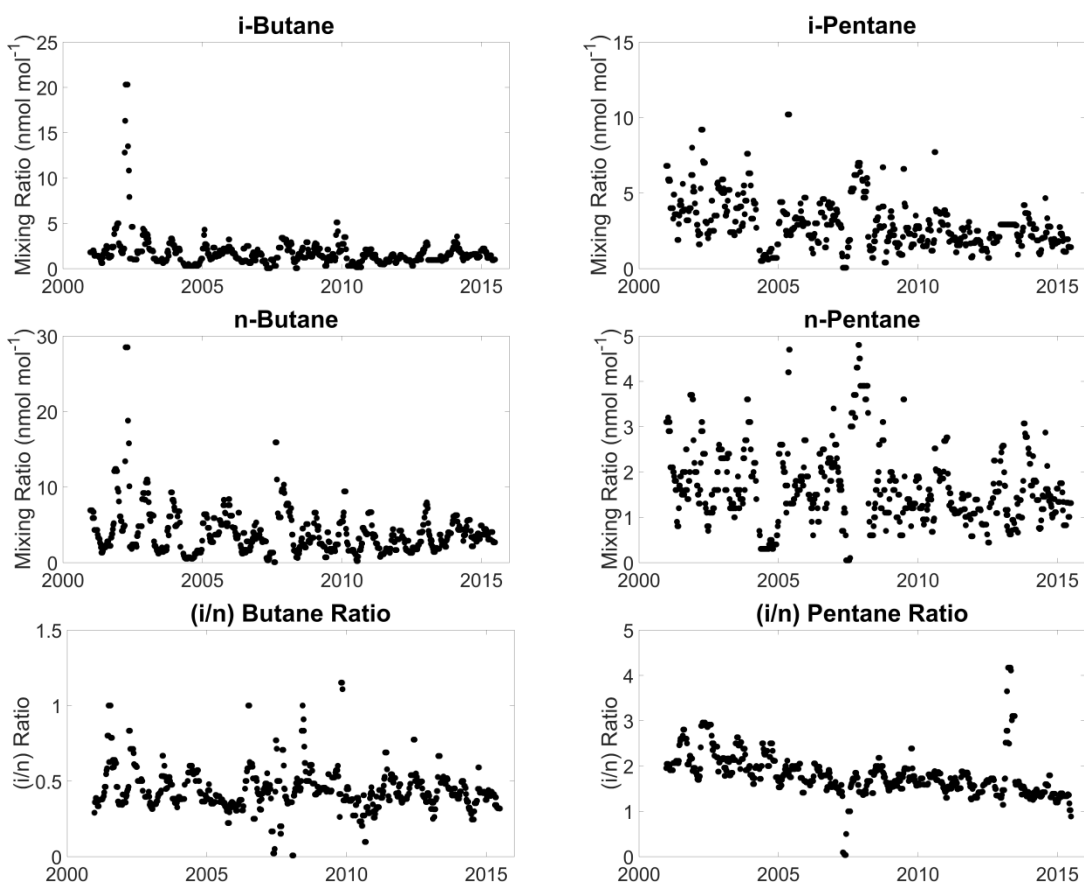
Figure S2f. Butane and pentane isomer mixing ratios and isomeric ratio data at the Gary site.
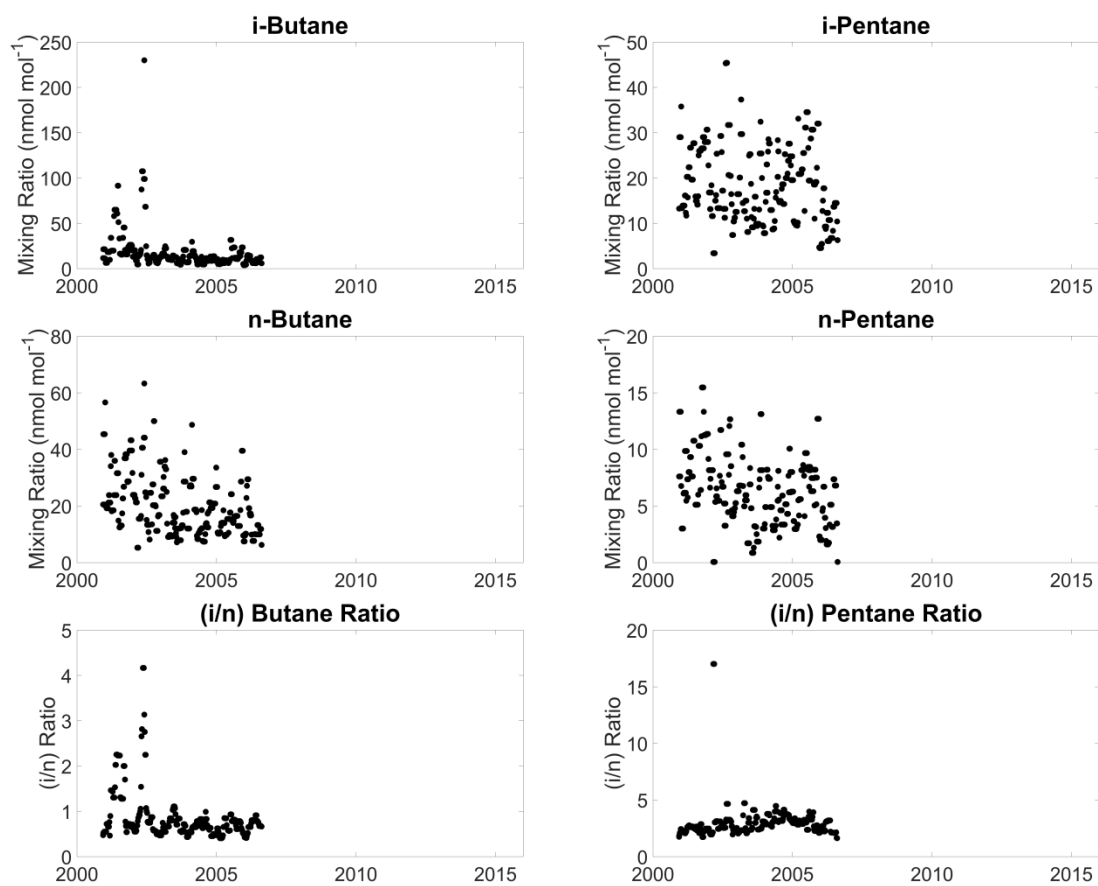
Figure S2g. Butane and pentane isomer mixing ratios and isomeric ratio data at the Houston site.
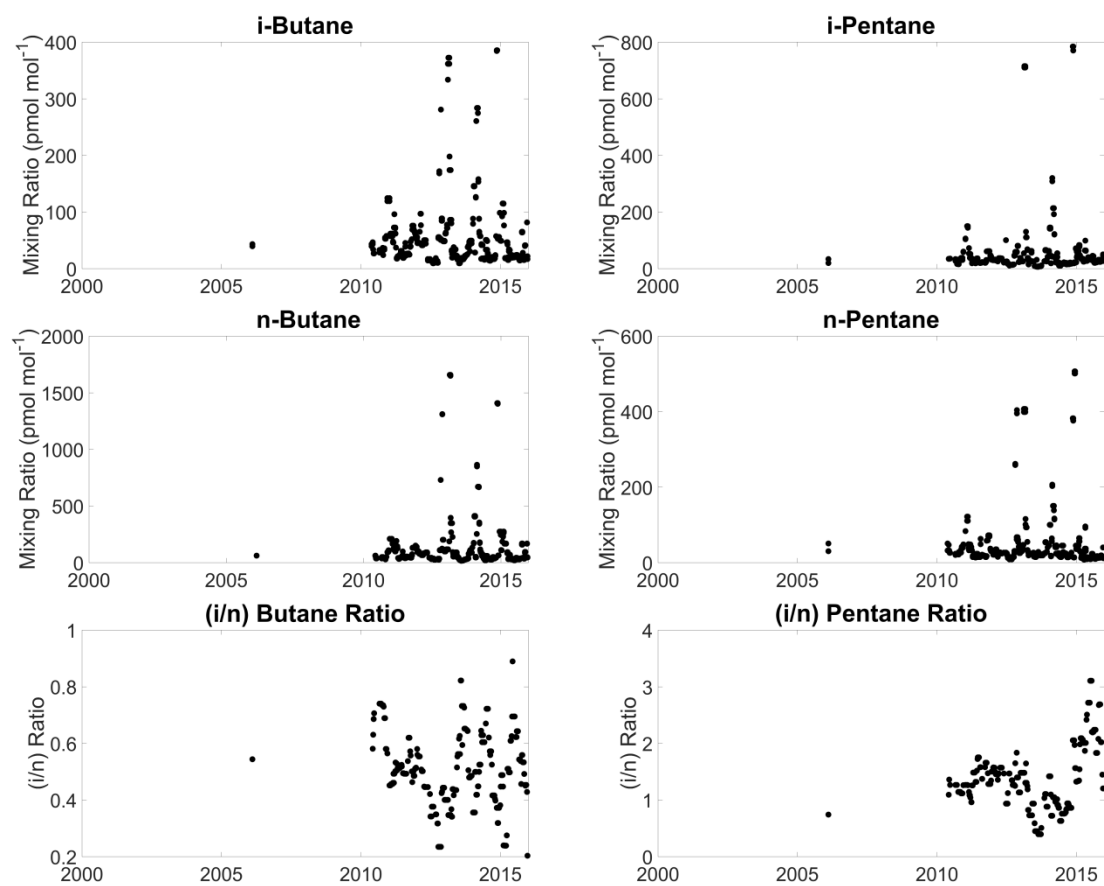
Figure S2h. Butane and pentane isomer mixing ratios and isomeric ratio data at the Key Biscayne site.
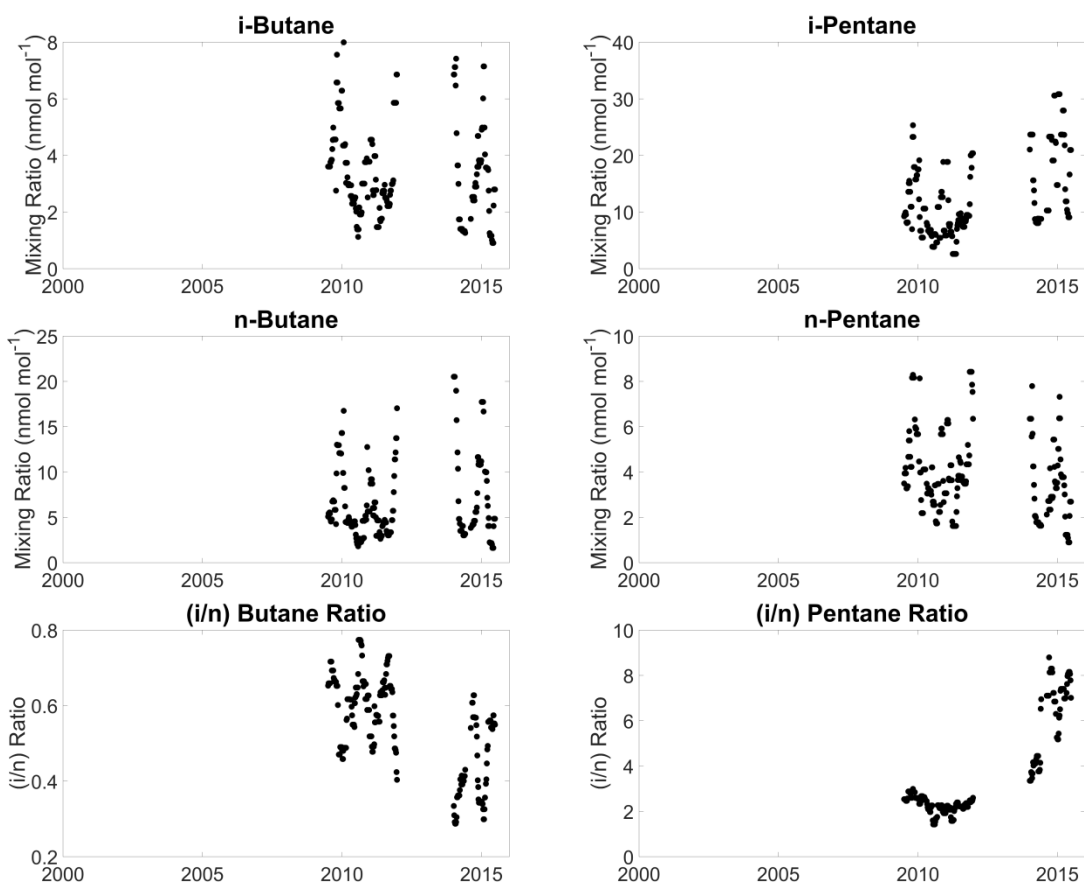
Figure S2i. Butane and pentane isomer mixing ratios and isomeric ratio data at the Los Angeles site.
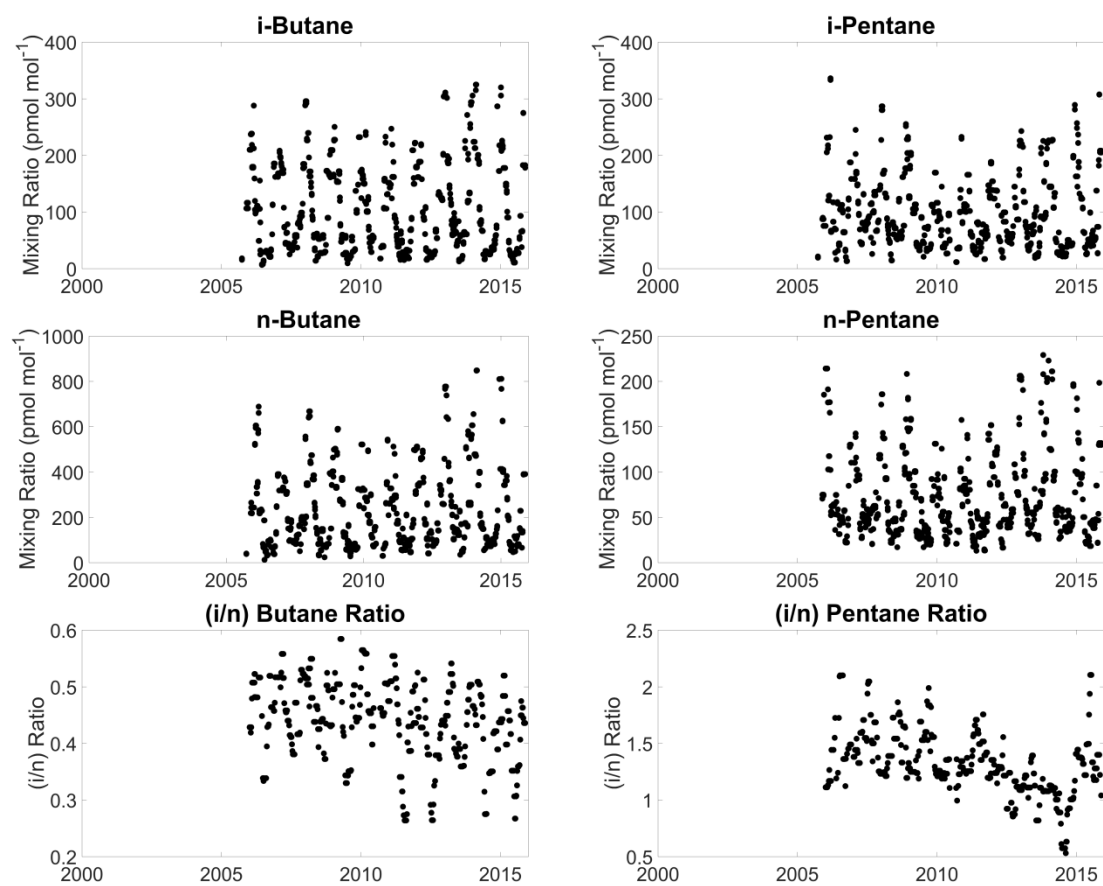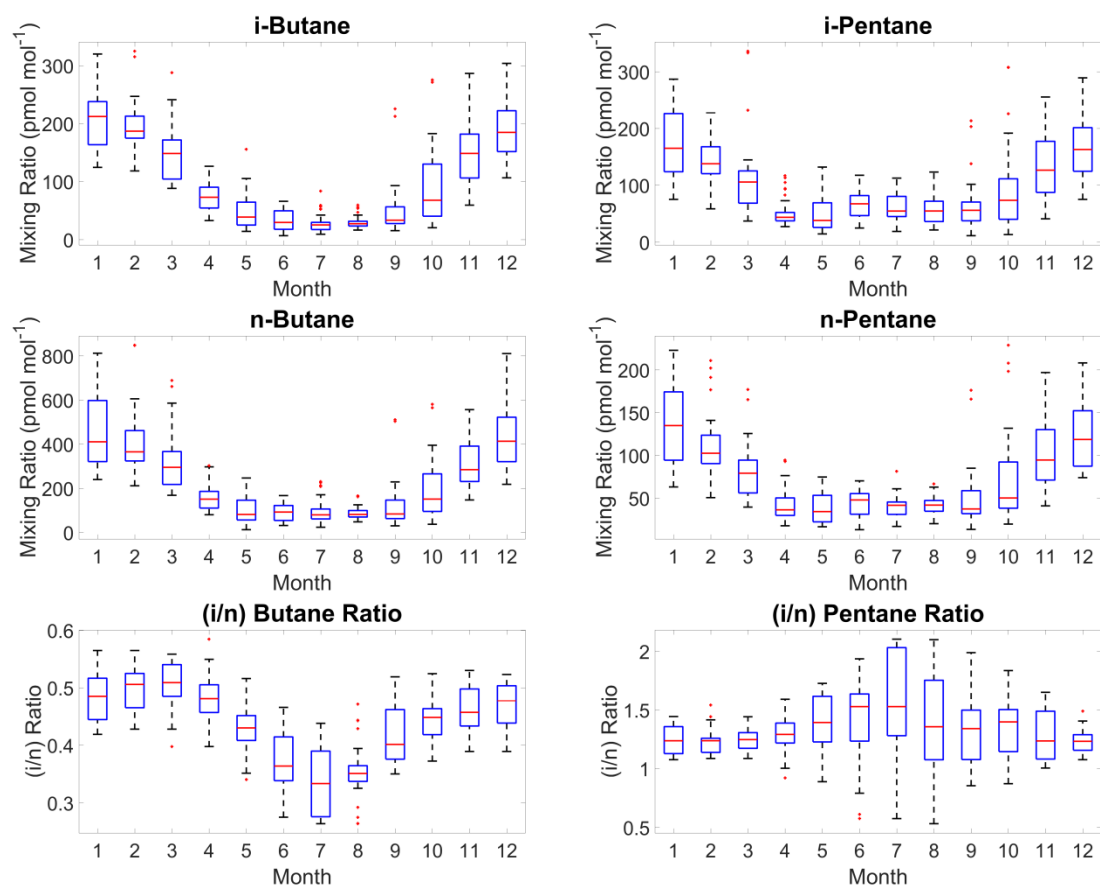
Figure S2j. Butane and pentane isomer mixing ratios and isomeric ratio data at the Park Falls site.
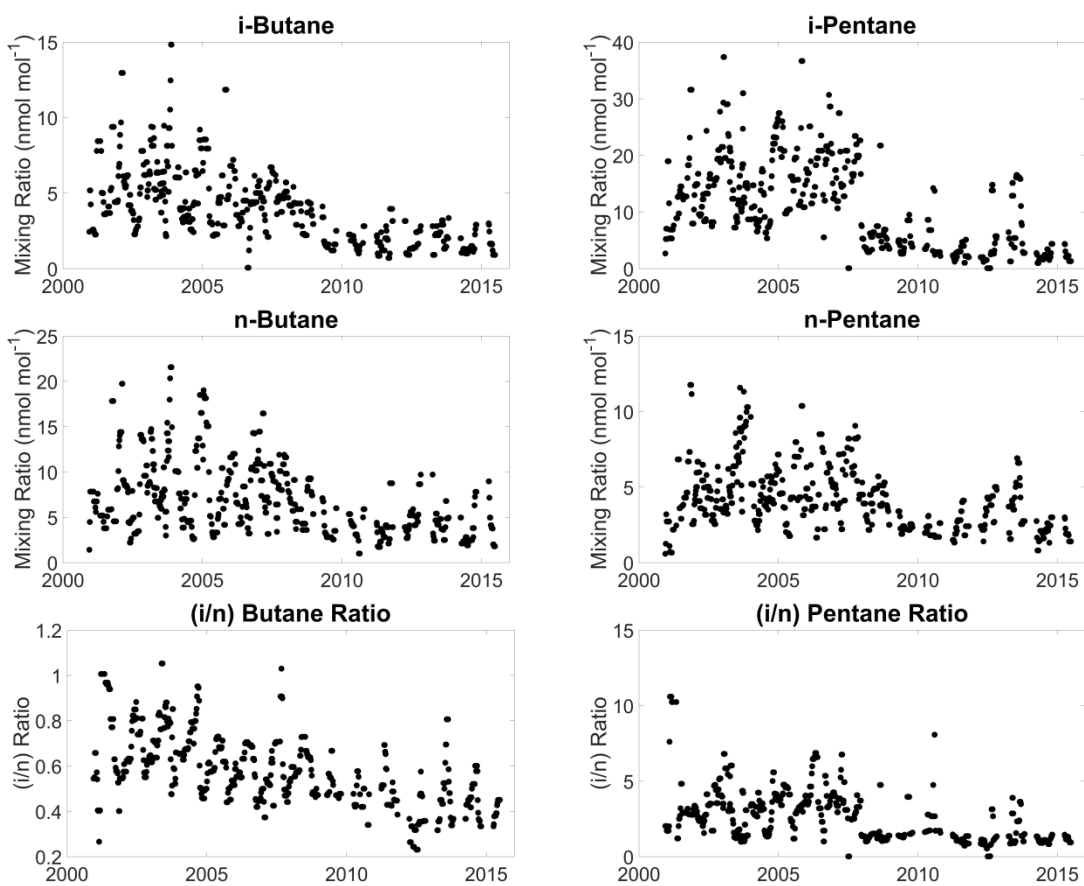
Figure S2k. Butane and pentane isomer mixing ratios and isomeric ratio data at the Philadelphia site.
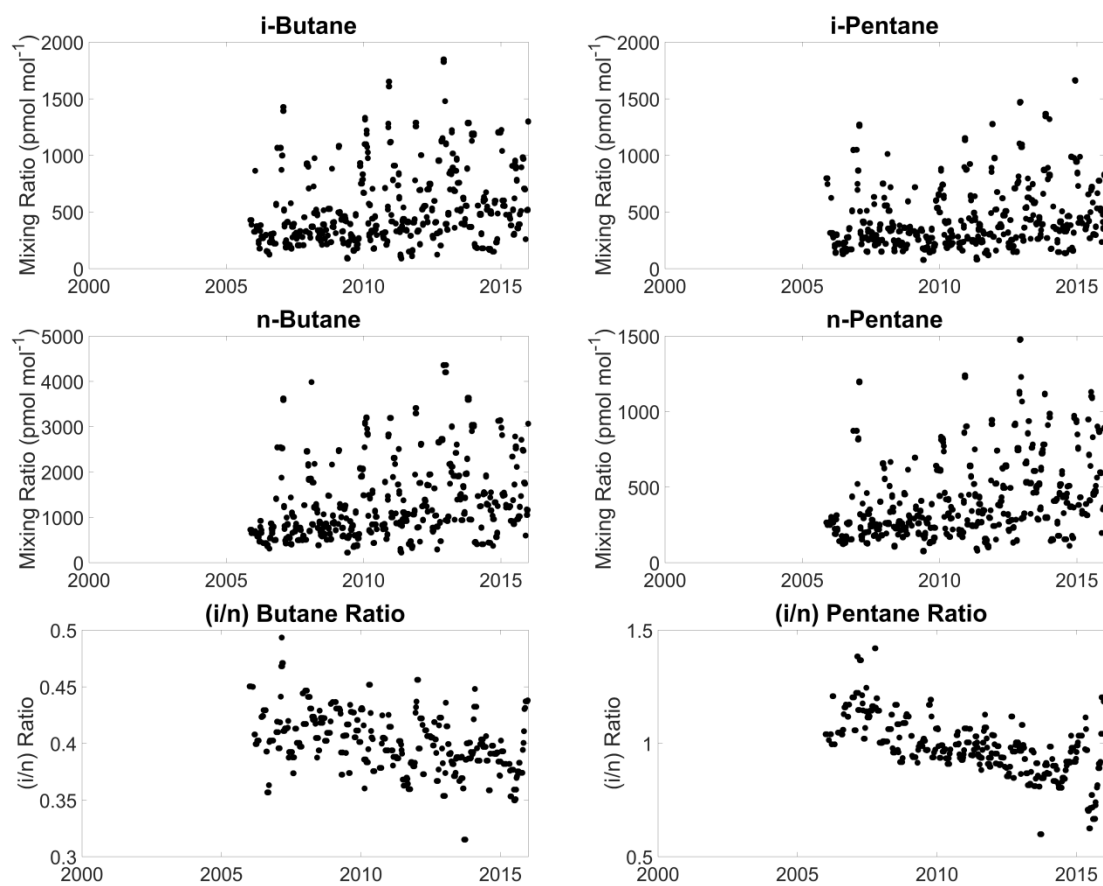
Figure S2l. Butane and pentane isomer mixing ratios and isomeric ratio data at the Southern Great Plains site.
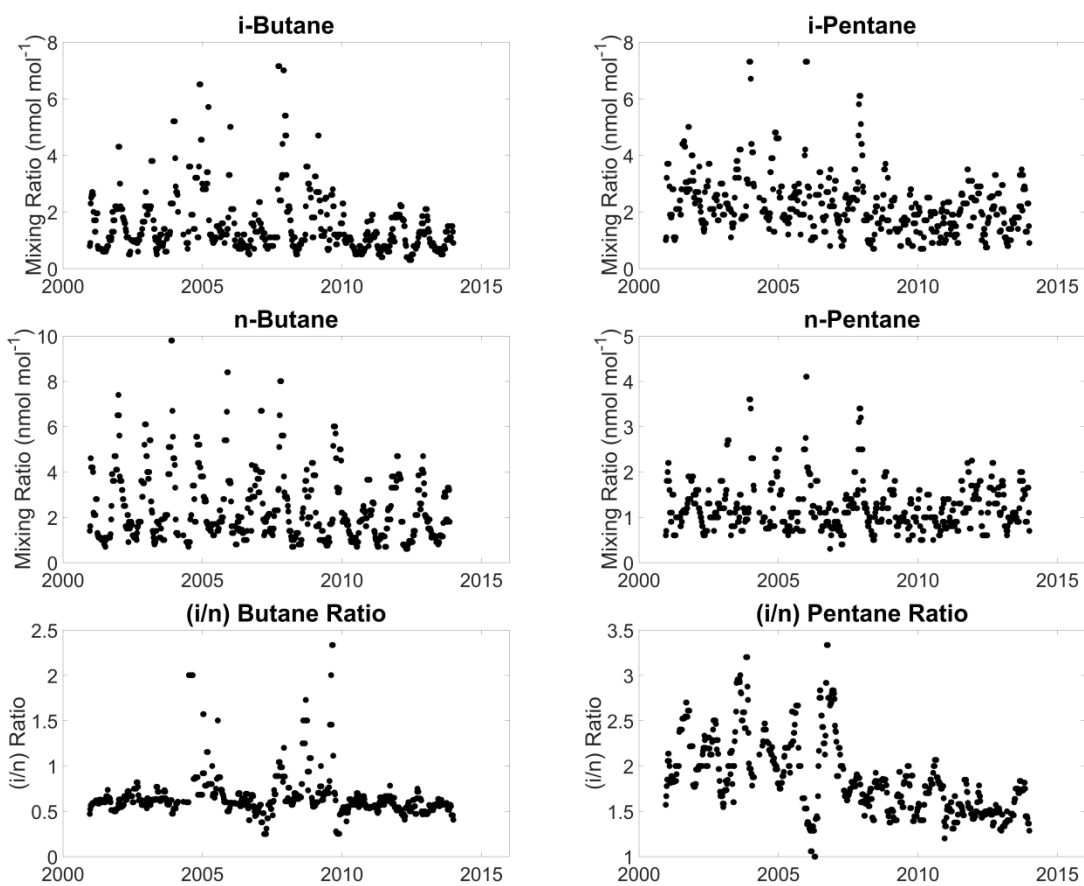
Figure S2m. Butane and pentane isomer mixing ratios and isomeric ratio data at the Springfield site.
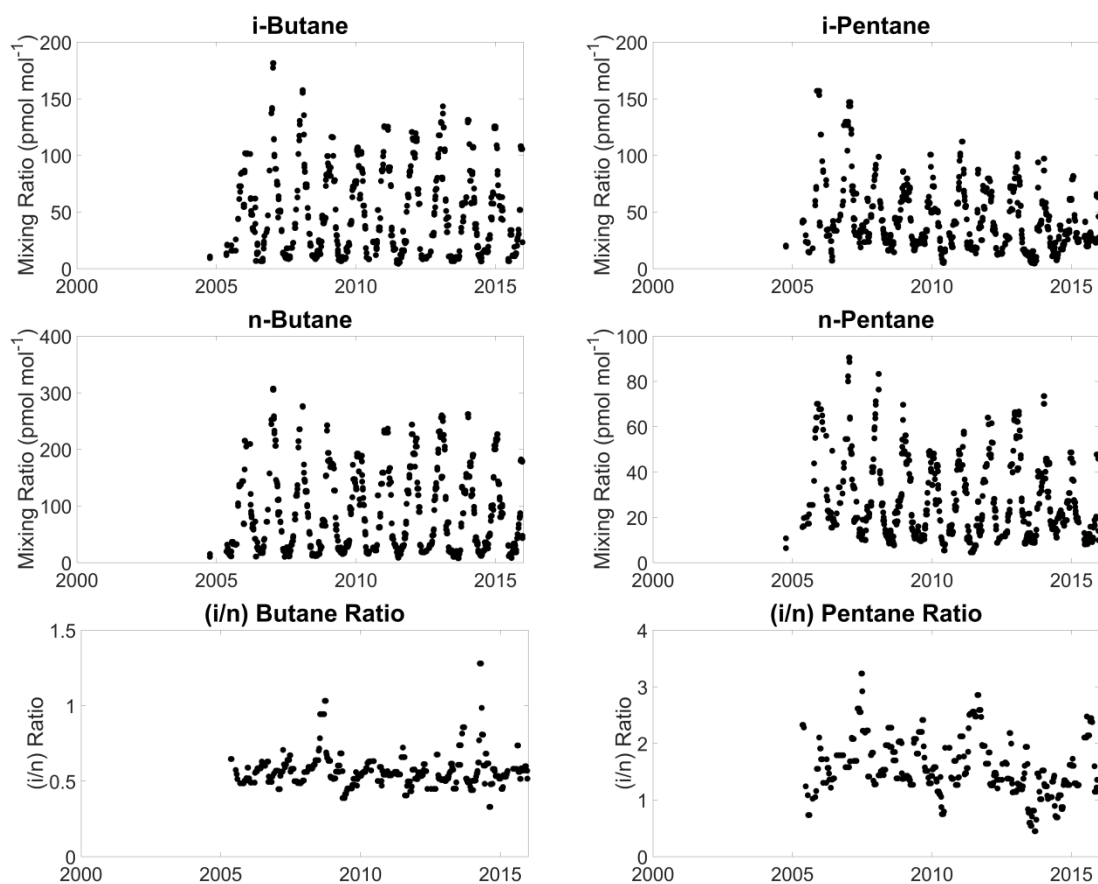
Figure S2n. Butane and pentane isomer mixing ratios and isomeric ratio data at the Trinidad Head site.
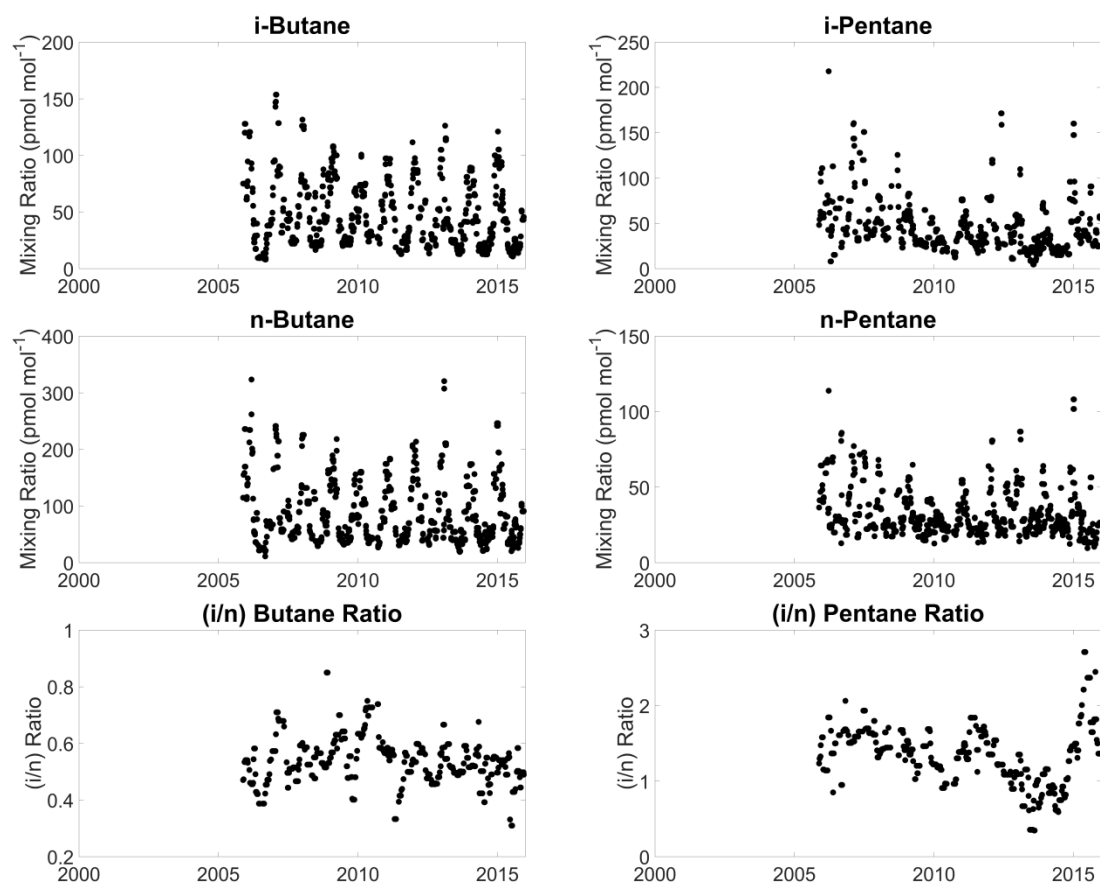
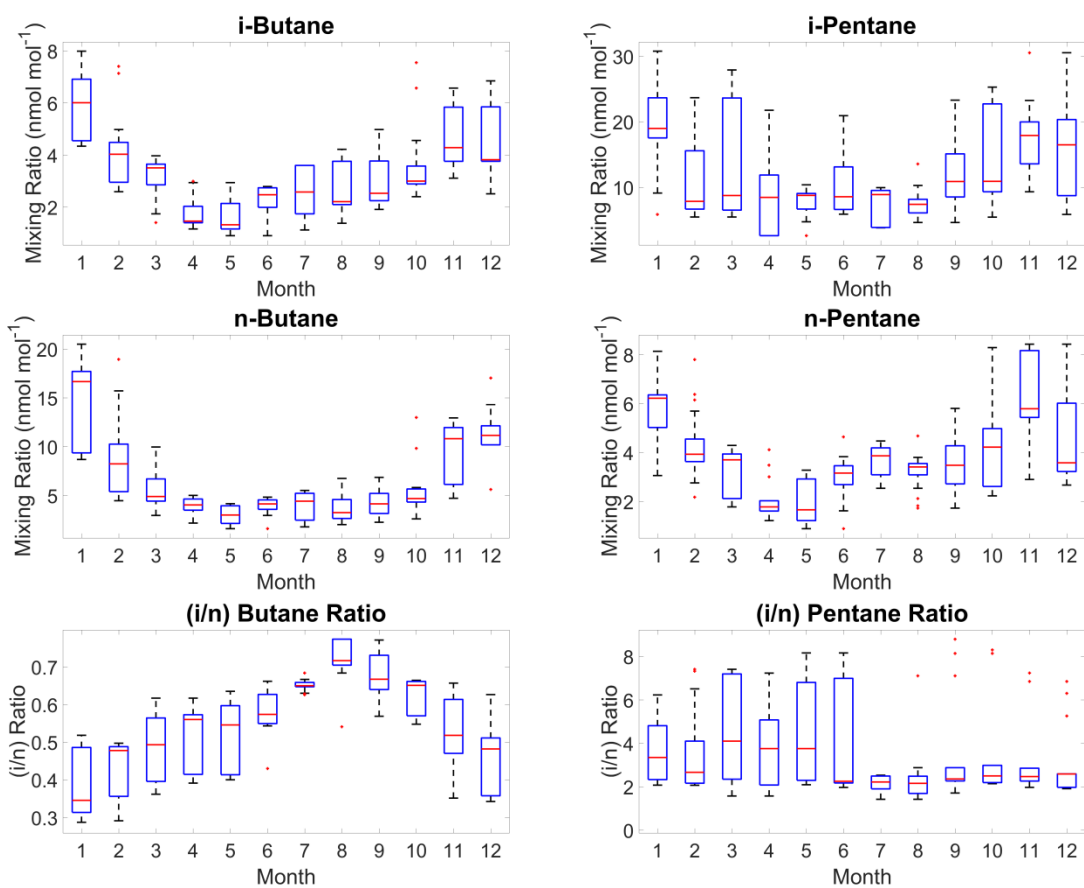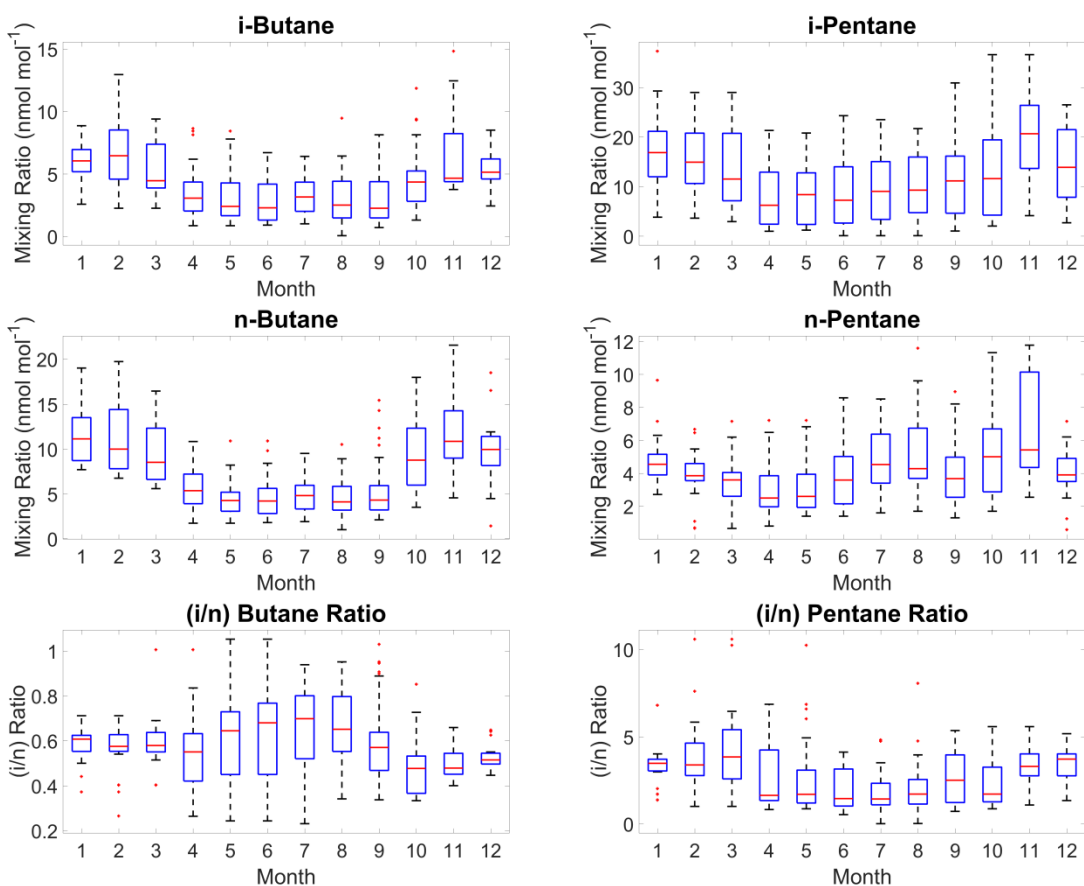Figure S2o. Butane and pentane isomer mixing ratios and isomeric ratio data at the Wendover site.
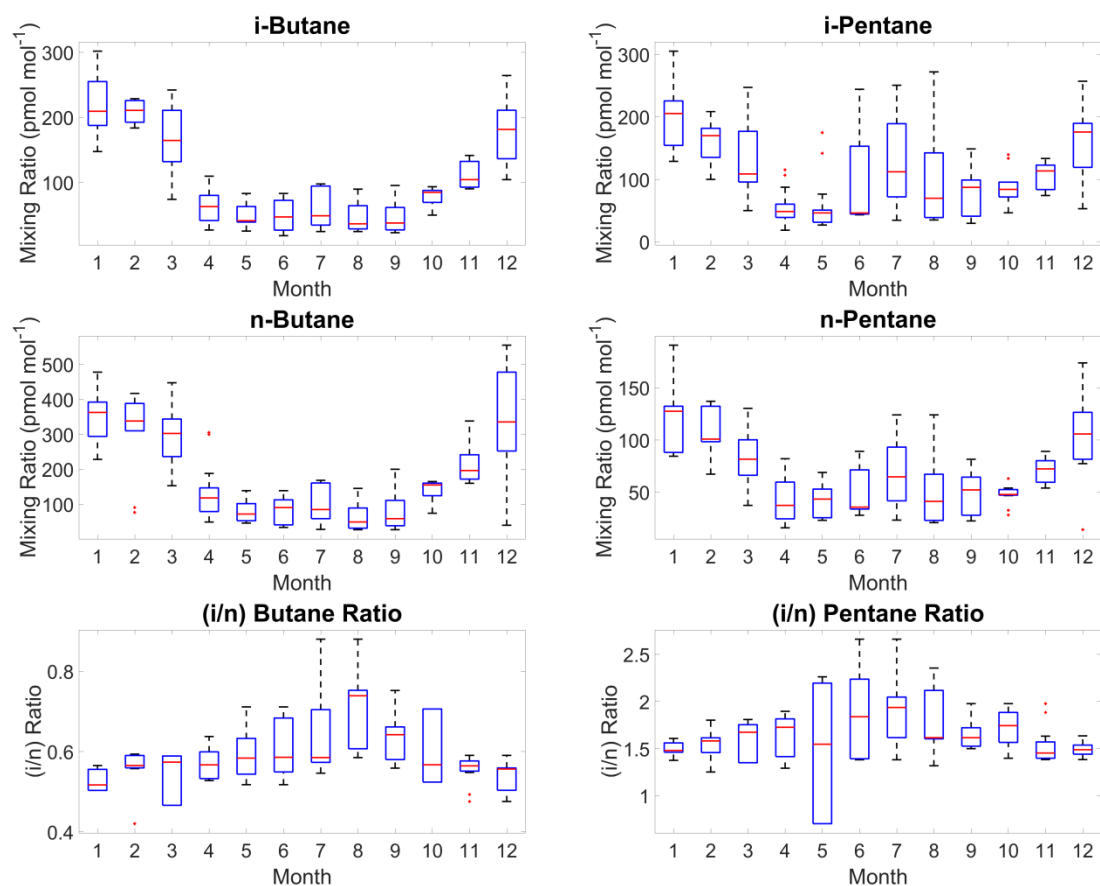
Figure S3a. Butane and pentane isomer seasonal cycles and isomeric ratio seasonal cycles at the Argyle site.
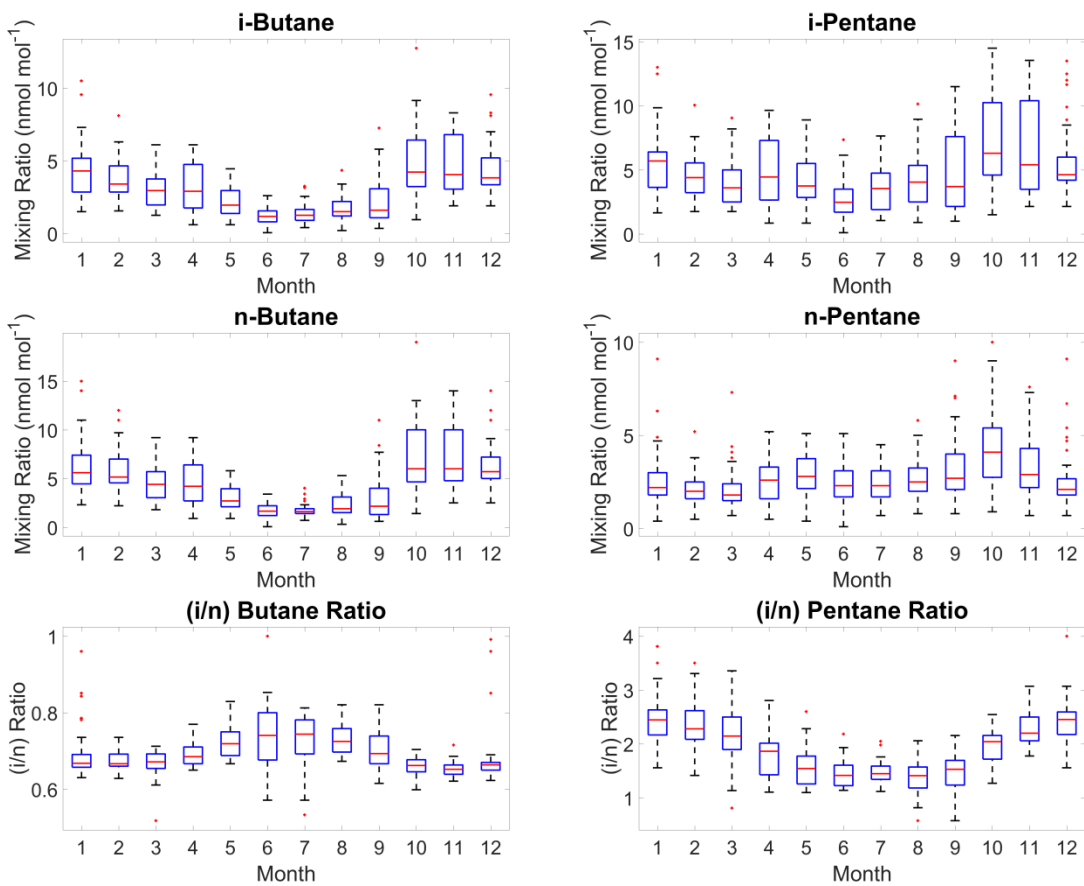
Figure S3b. Butane and pentane isomer seasonal cycles and isomeric ratio seasonal cycles at the Atlanta – S. De Kalb site.
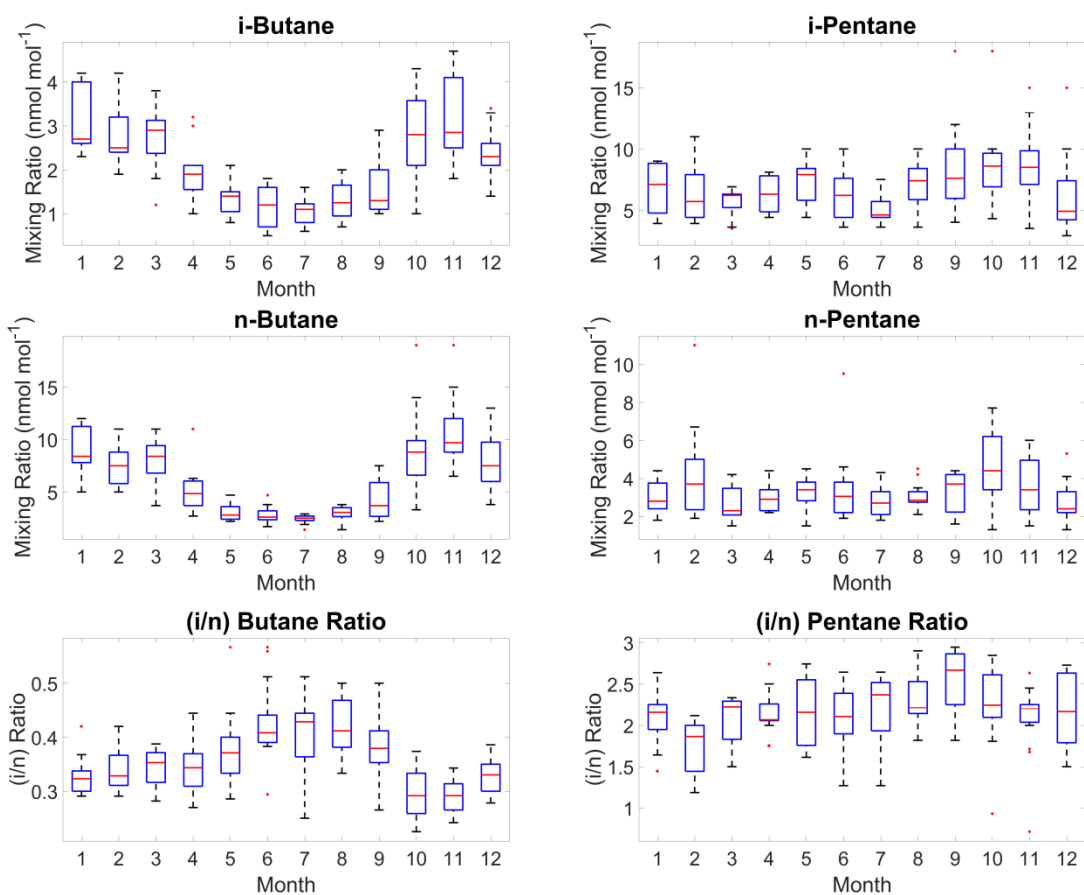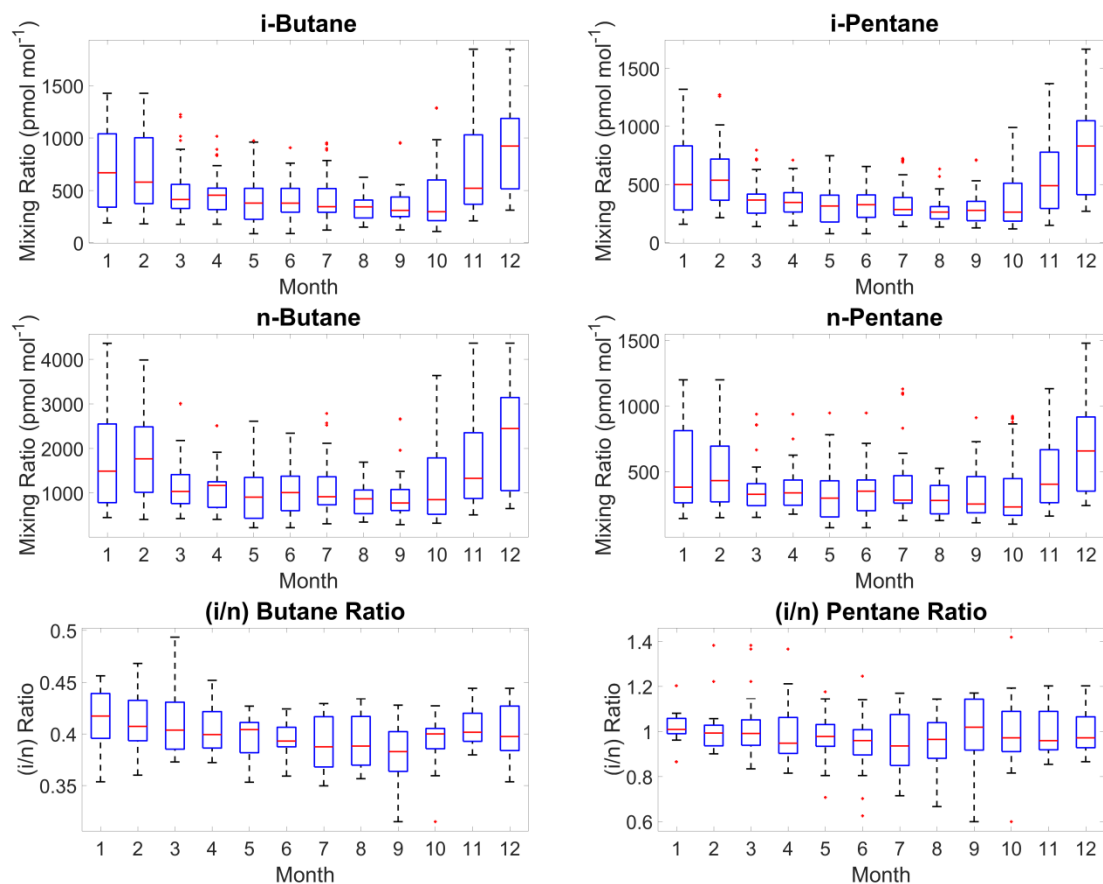
Figure S3c. Butane and pentane isomer seasonal cycles and isomeric ratio seasonal cycles at the Atlanta – Tucker site.
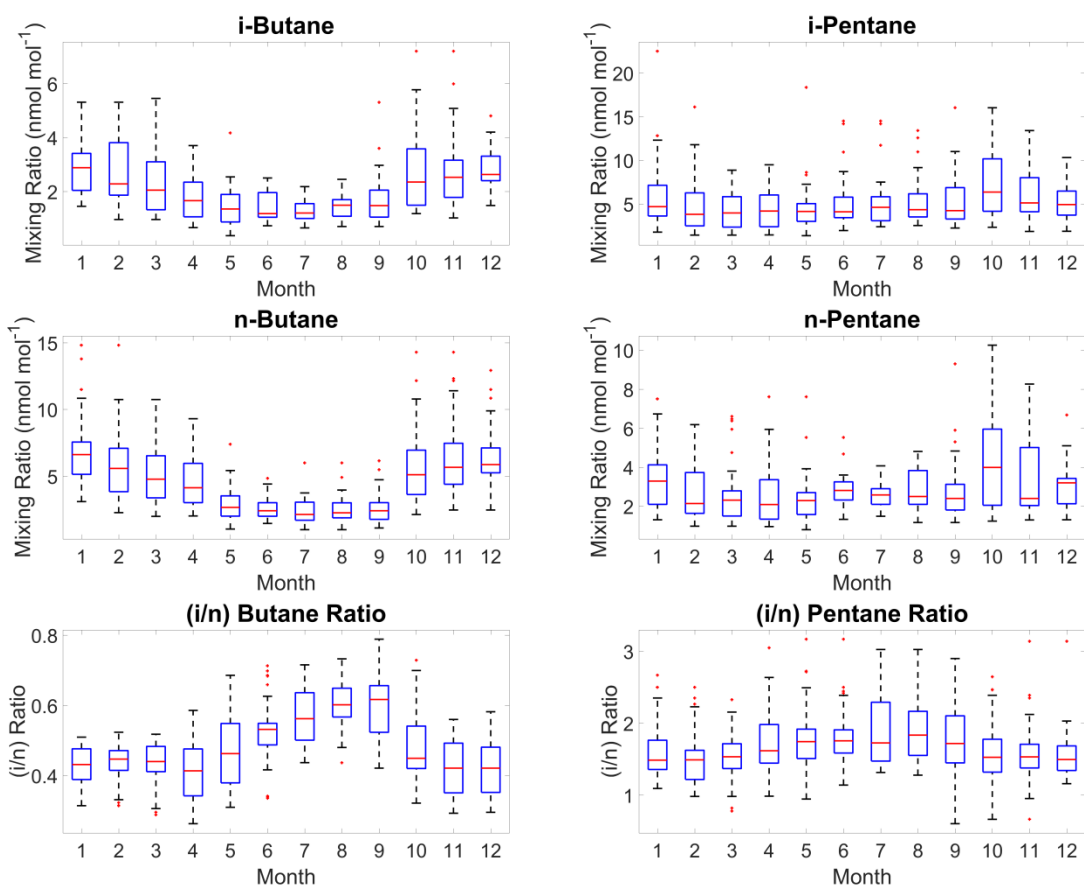
Figure S3d. Butane and pentane isomer seasonal cycles and isomeric ratio seasonal cycles at the Baltimore site.
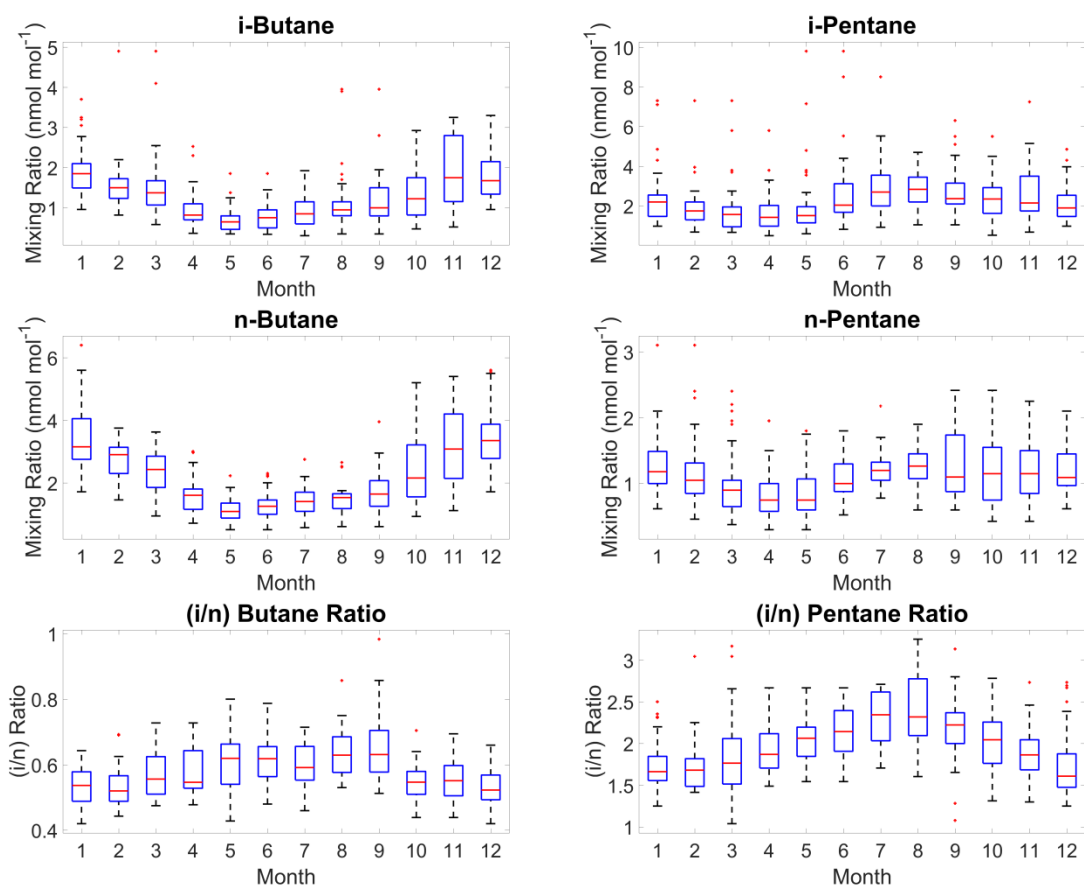
Figure S3e. Butane and pentane isomer seasonal cycles and isomeric ratio seasonal cycles at the Boston site.
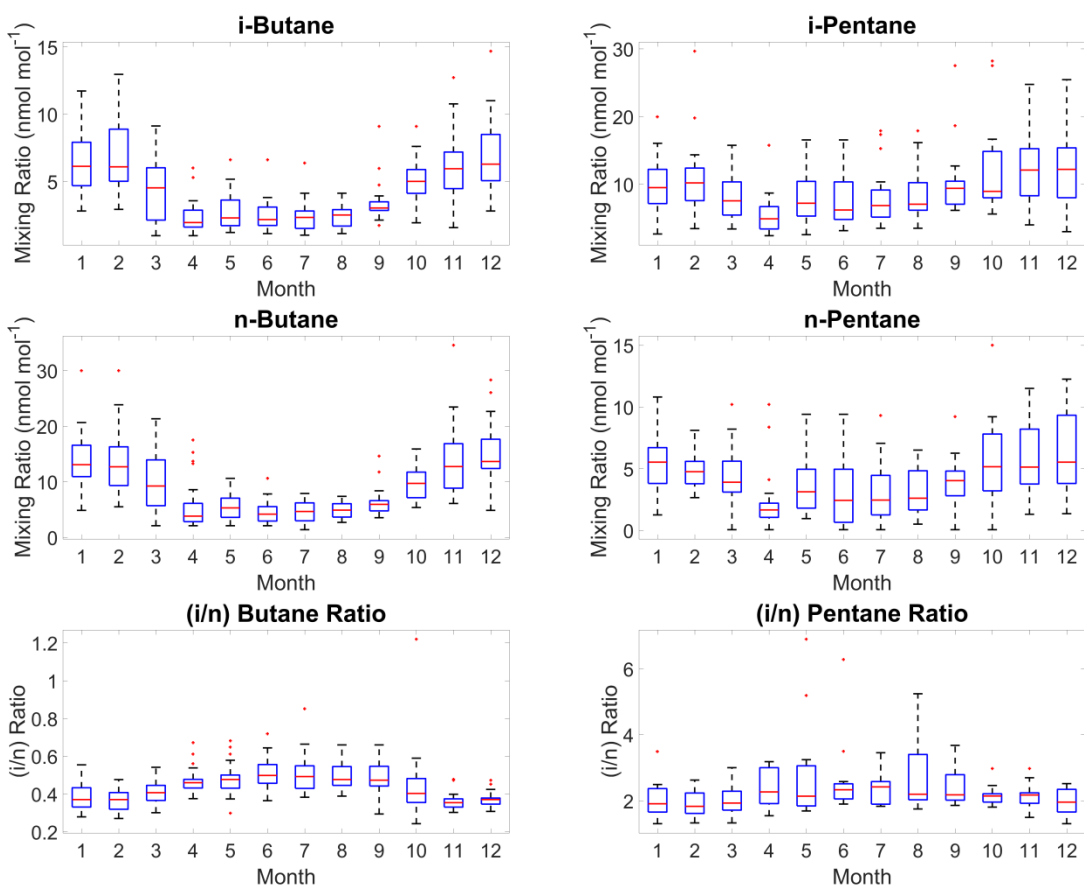
Figure S3f. Butane and pentane isomer seasonal cycles and isomeric ratio seasonal cycles at the El Paso site.
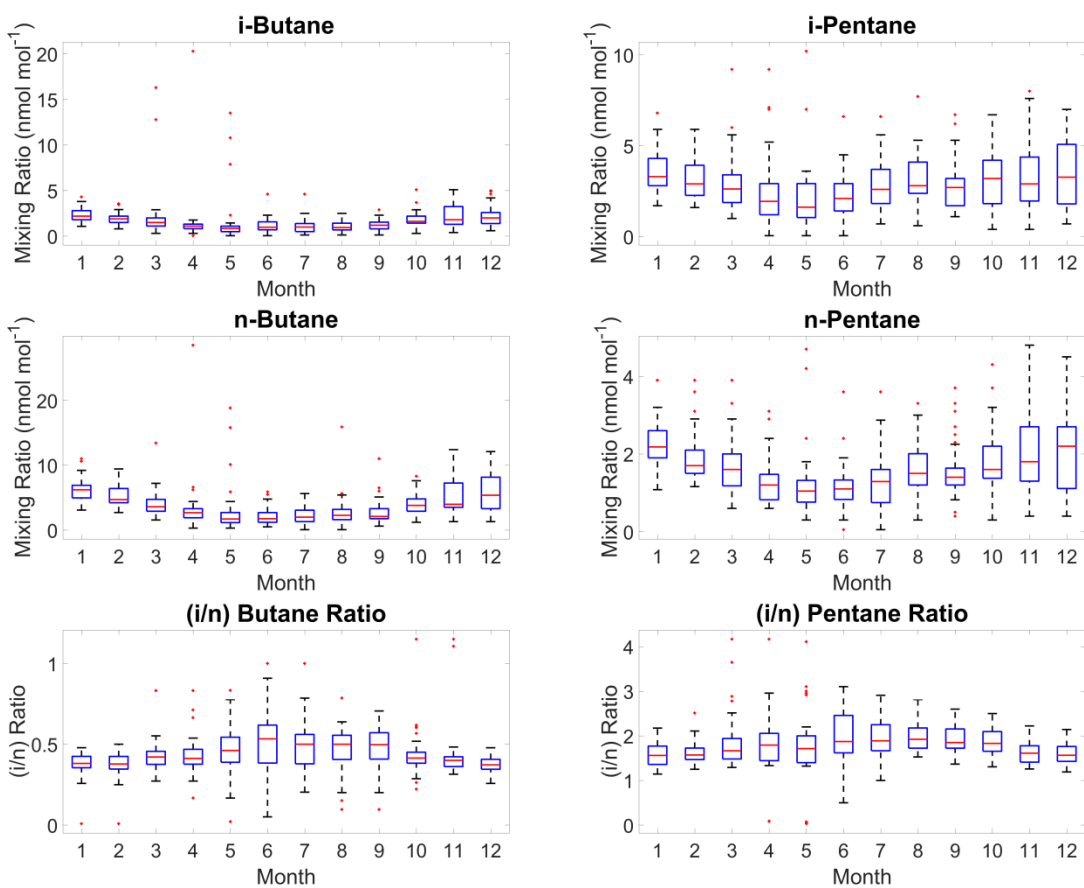
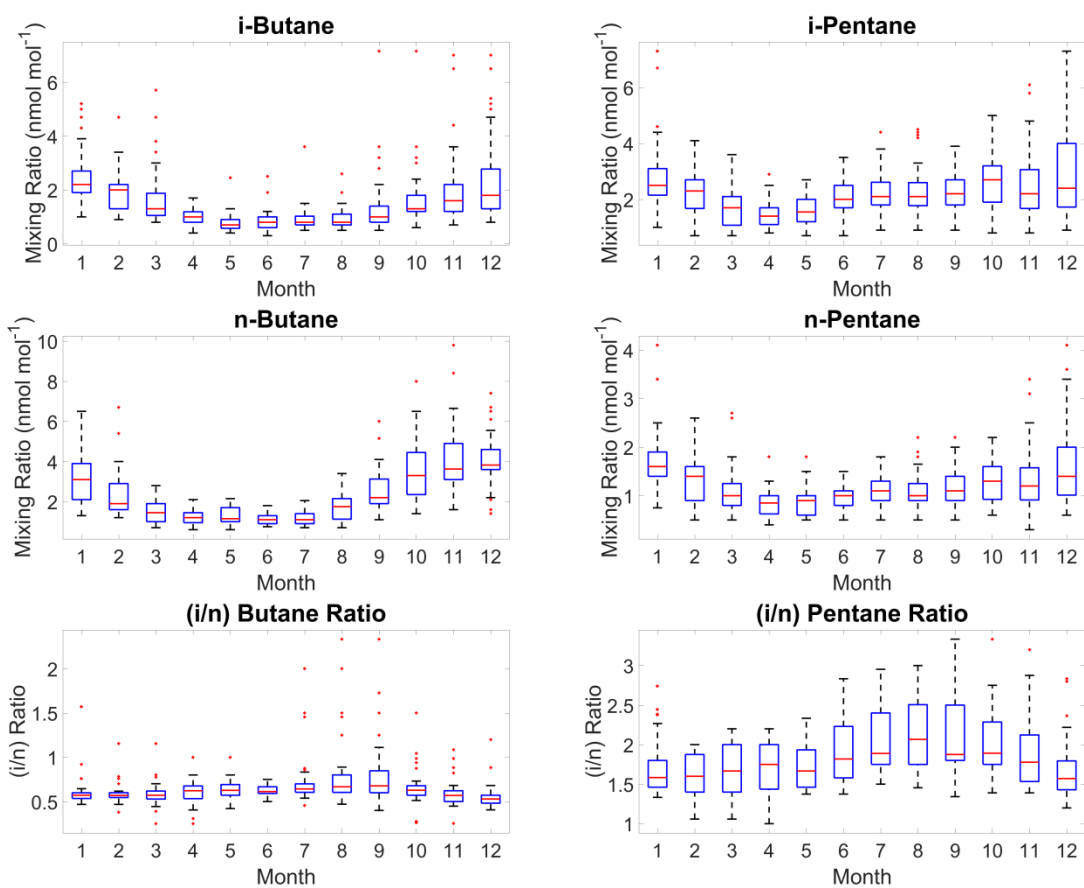Figure S3g. Butane and pentane isomer seasonal cycles and isomeric ratio seasonal cycles at the Gary site.
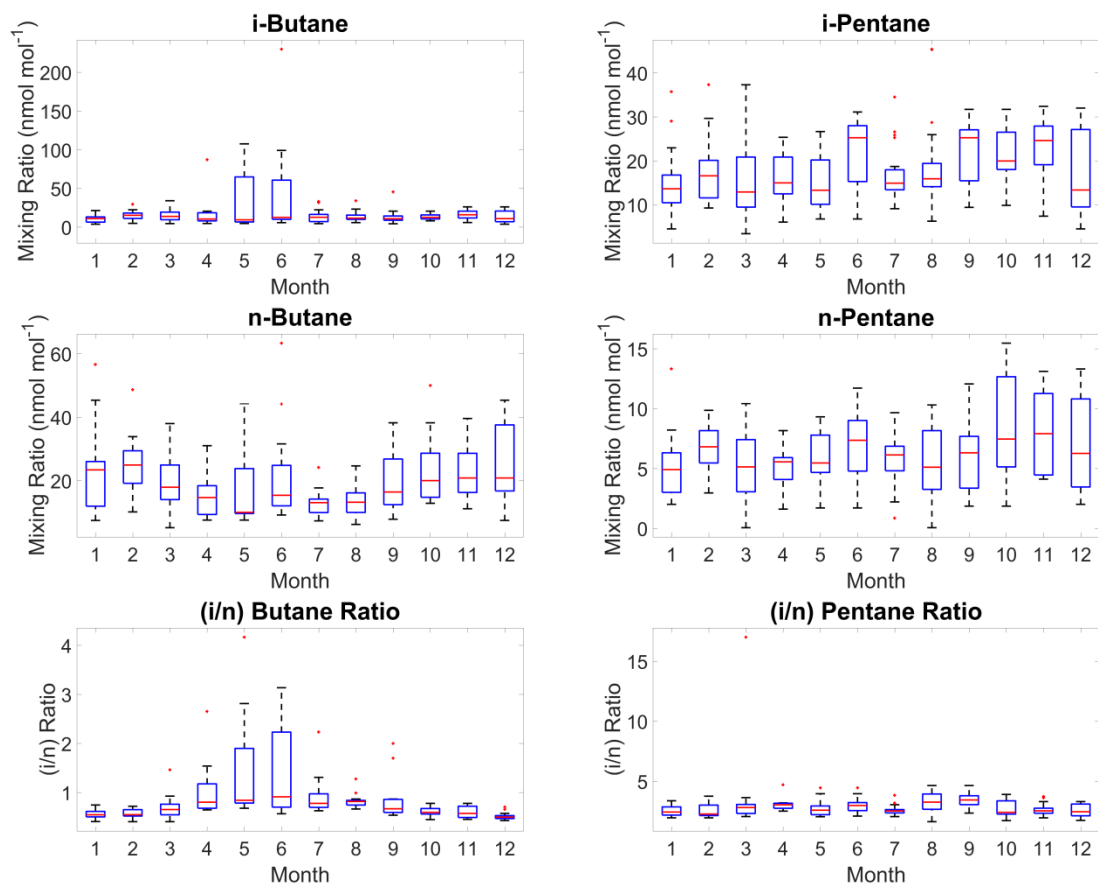
Figure S3h. Butane and pentane isomer seasonal cycles and isomeric ratio seasonal cycles at the Houston site.
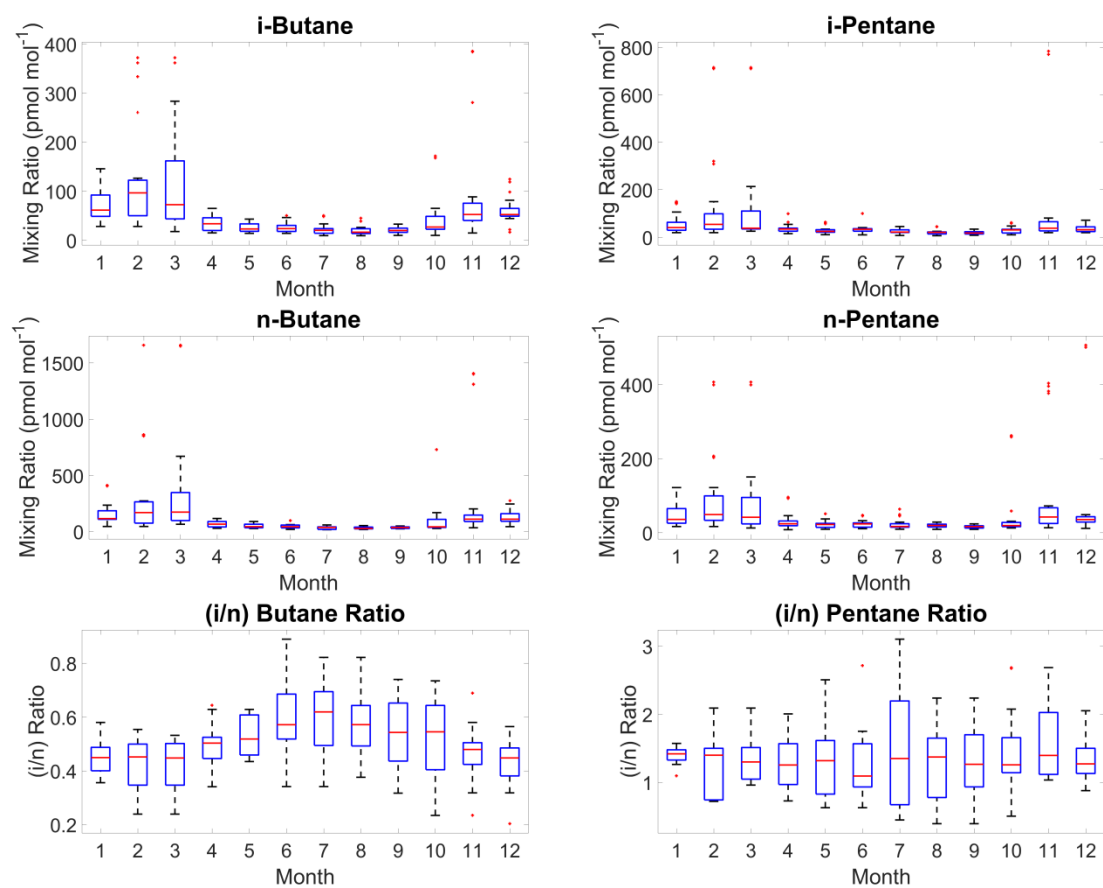
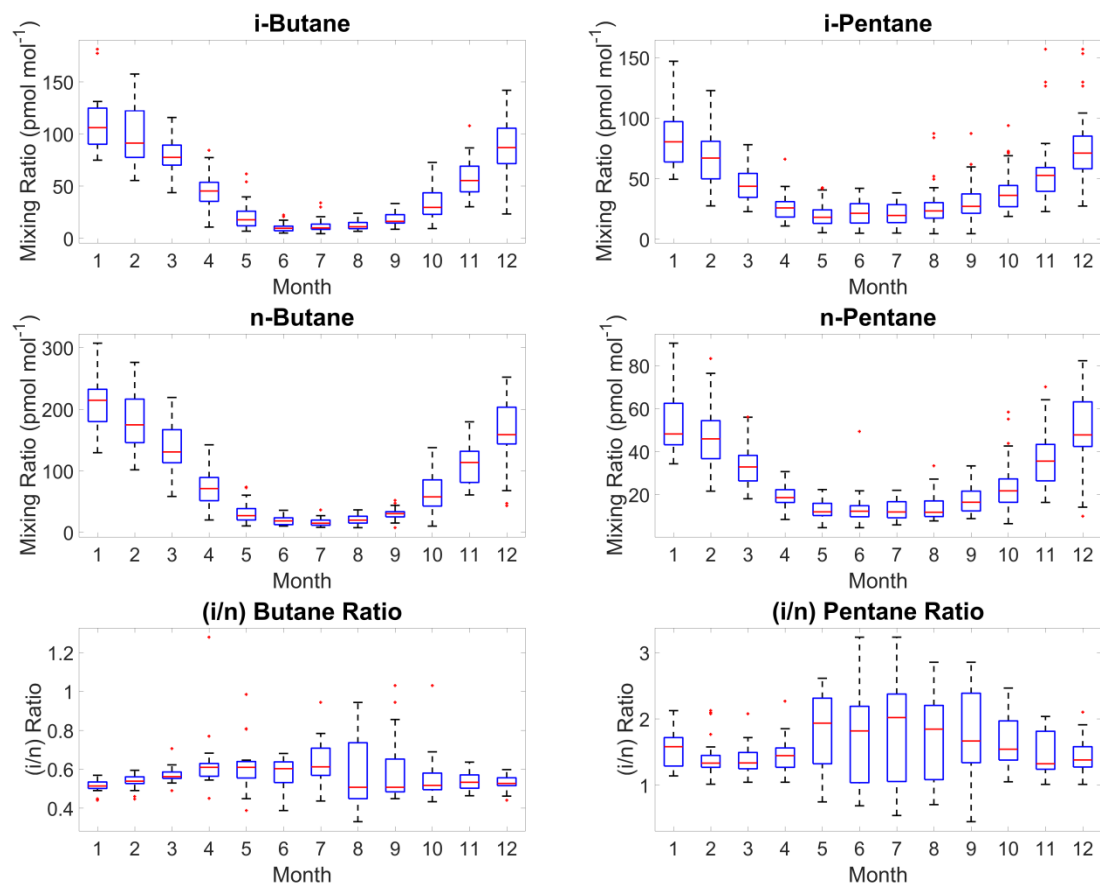Figure S3i. Butane and pentane isomer seasonal cycles and isomeric ratio seasonal cycles at the Key Biscayne site.

Figure S3j. Butane and pentane isomer seasonal cycles and isomeric ratio seasonal cycles at the Park Falls site.

Figure S3k. Butane and pentane isomer seasonal cycles and isomeric ratio seasonal cycles at the Los Angeles site.

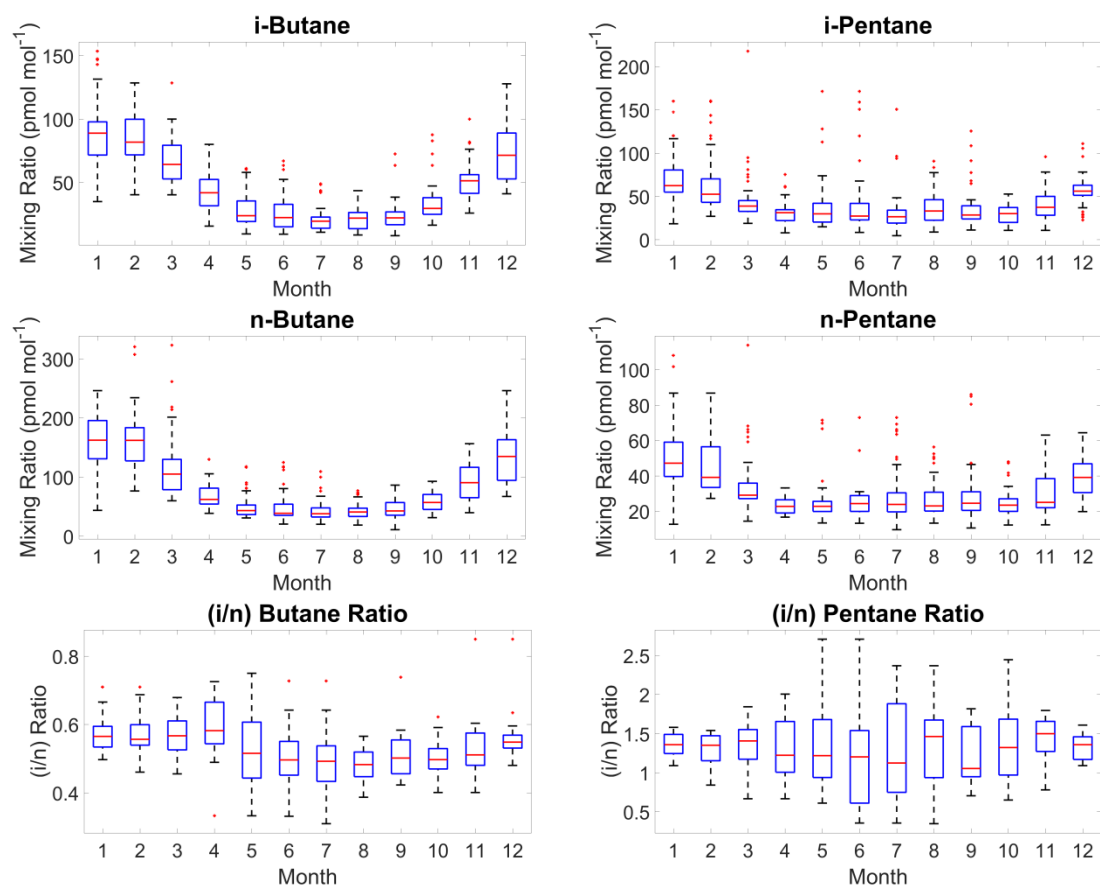Figure S3l. Butane and pentane isomer seasonal cycles and isomeric ratio seasonal cycles at the Philadelphia site.

Figure S3m. Butane and pentane isomer seasonal cycles and isomeric ratio seasonal cycles at the S. Great Plains site.

Figure S3n. Butane and pentane isomer seasonal cycles and isomeric ratio seasonal cycles at the Springfield site.

Figure S3o. Butane and pentane isomer seasonal cycles and isomeric ratio seasonal cycles at the Trinidad Head site.

Figure S3p. Butane and pentane isomer seasonal cycles and isomeric ratio seasonal cycles at the Wendover site.

Site	Confidence Interval of Trend Slopes at 95% (Low - High)											
	i-Butane		n-Butane		i-Pentane		n-Pentane		(i/n) Butane Ratio		(i/n) Pentane Ratio	
Atlanta, GA (SDK)	-0.184	-0.046	-0.243	-0.086	-0.285	-0.064	-0.189	-0.018	-0.005	0.000	-0.049	-0.003
Atlanta, GA (TKR)	-0.100	0.198	-0.551	0.400	-0.167	1.068	-0.170	0.526	-0.023	0.015	-0.094	0.025
Baltimore, MD	-0.102	0.001	-0.164	0.034	-0.325	-0.007	-0.056	0.059	-0.015	0.000	-0.067	-0.022
Boston, MA	-0.091	-0.013	-0.101	-0.006	-0.227	-0.083	-0.070	-0.016	-0.017	-0.009	-0.068	-0.025
El Paso, TX	-0.721	0.523	-0.532	0.201	-1.010	-0.031	-0.575	0.355	0.002	0.018	-0.083	0.096
Gary, IN	-0.084	0.019	-0.296	0.084	-0.246	-0.111	-0.100	-0.013	-0.005	0.007	-0.069	-0.032
Houston, TX	*	*	*	*	*	*	*	*	*	*	*	*
Los Angeles, CA	*	*	*	*	*	*	*	*	*	*	*	*
Philadelphia, PA	-0.409	-0.150	-0.512	-0.029	-1.333	-0.197	-0.275	0.014	-0.026	-0.012	-0.231	-0.041
Springfield, MA	-0.081	0.034	-0.061	0.015	-0.140	-0.004	-0.025	0.030	-0.017	0.007	-0.104	-0.048
Argyle, ME	*	*	*	*	*	*	*	*	*	*	*	*
Key Biscayne, FL	-0.00569	0.00312	-0.0111	0.00596	-0.00315	0.00101	-0.00367	0.000478	-6.91E-05	2.81E-05	-1.37E-04	2.03E-04
Park Falls, WI	-0.00963	-0.000209	-0.0150	0.00330	-0.00657	-0.00124	-0.00415	0.000875	-1.04E-05	-3.81E-06	-1.03E-04	1.09E-06
SGP, OK	0.0165	0.0579	0.0668	0.211	-0.00311	0.0412	0.0150	0.0559	-6.59E-06	-2.49E-07	-3.23E-05	-1.31E-05
Trinidad Head, CA	-0.00100	0.00447	-0.000395	0.00985	-0.00261	0.000790	-0.000948	0.000835	-1.07E-05	7.40E-06	-9.65E-05	5.45E-05
Wendover, UT	-0.00458	0.0000605	-0.00954	-0.000503	-0.00655	-0.00187	-0.00360	-0.000253	-9.49E-06	7.92E-06	-1.03E-04	3.08E-05

Supplement Table ST1. Displays confidence intervals at 95% for the slopes of all compounds and ratios at all sites. Each compound or ratio has two columns, the left column is the lower end of the confidence interval, the right column is the upper end of the confidence interval. The asterisk (*) is in place of values at sites where there was not enough data coverage to generate a confidence interval.
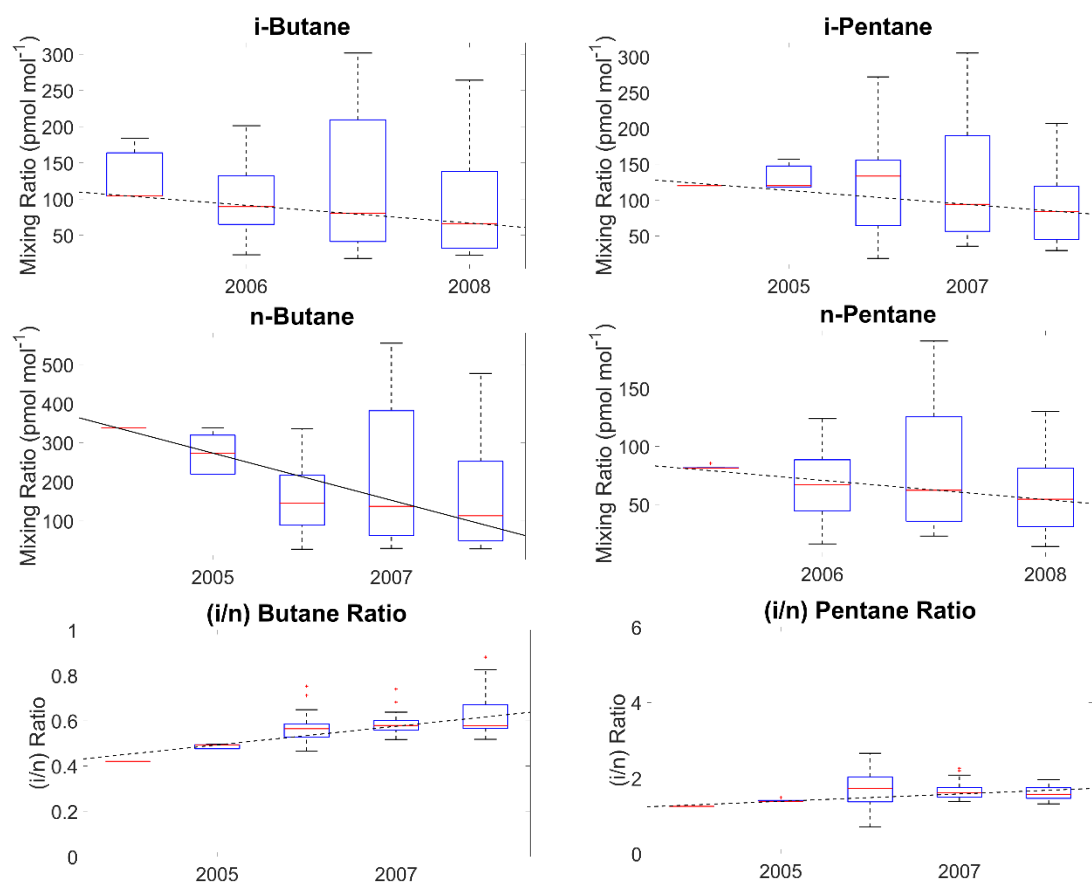
Figure S4a. Butane and pentane isomer annual boxplots and isomeric ratio annual boxplots at the Argyle site.
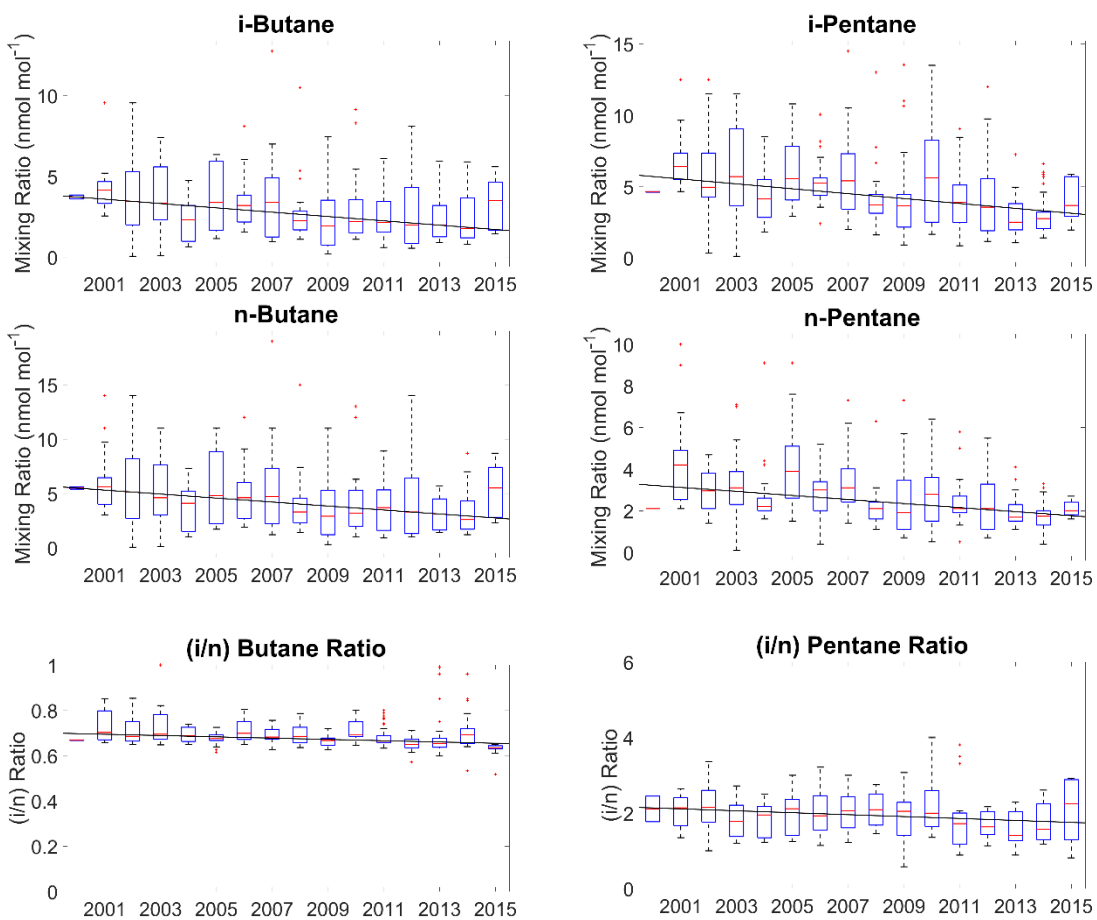
Figure S4b. Butane and pentane isomer annual boxplots and isomeric ratio annual boxplots at the Atlanta – S. De Kalb site.
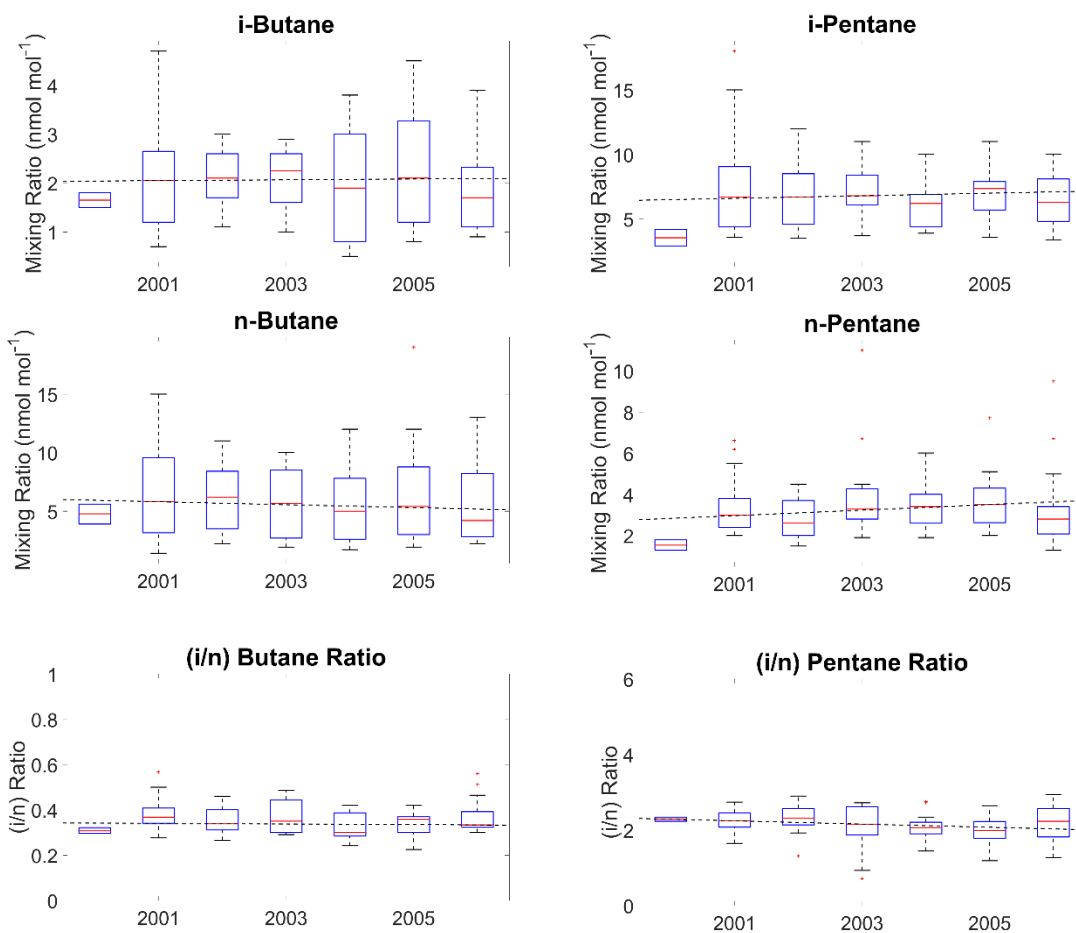
Figure S4c. Butane and pentane isomer annual boxplots and isomeric ratio annual boxplots at the Atlanta – Tucker sites.
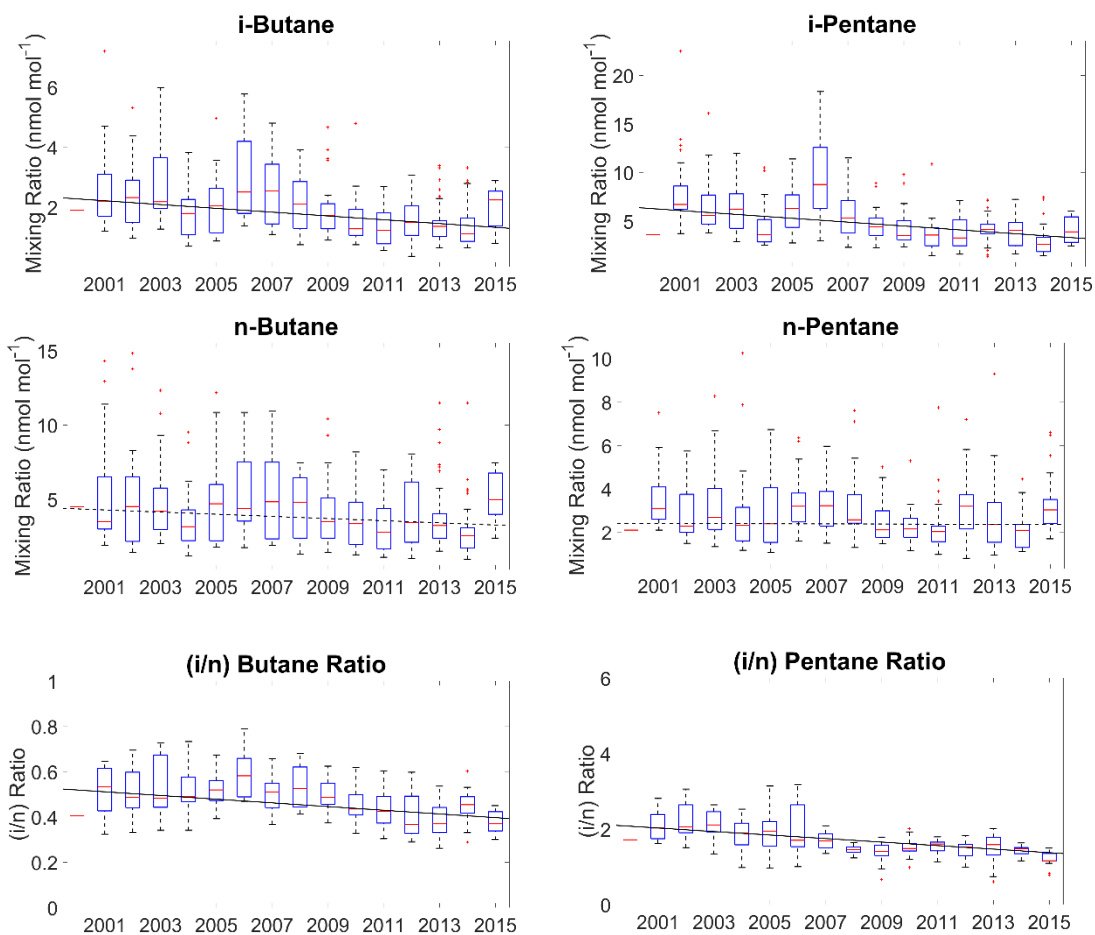
Figure S4d. Butane and pentane isomer annual boxplots and isomeric ratio annual boxplots at the Baltimore site.
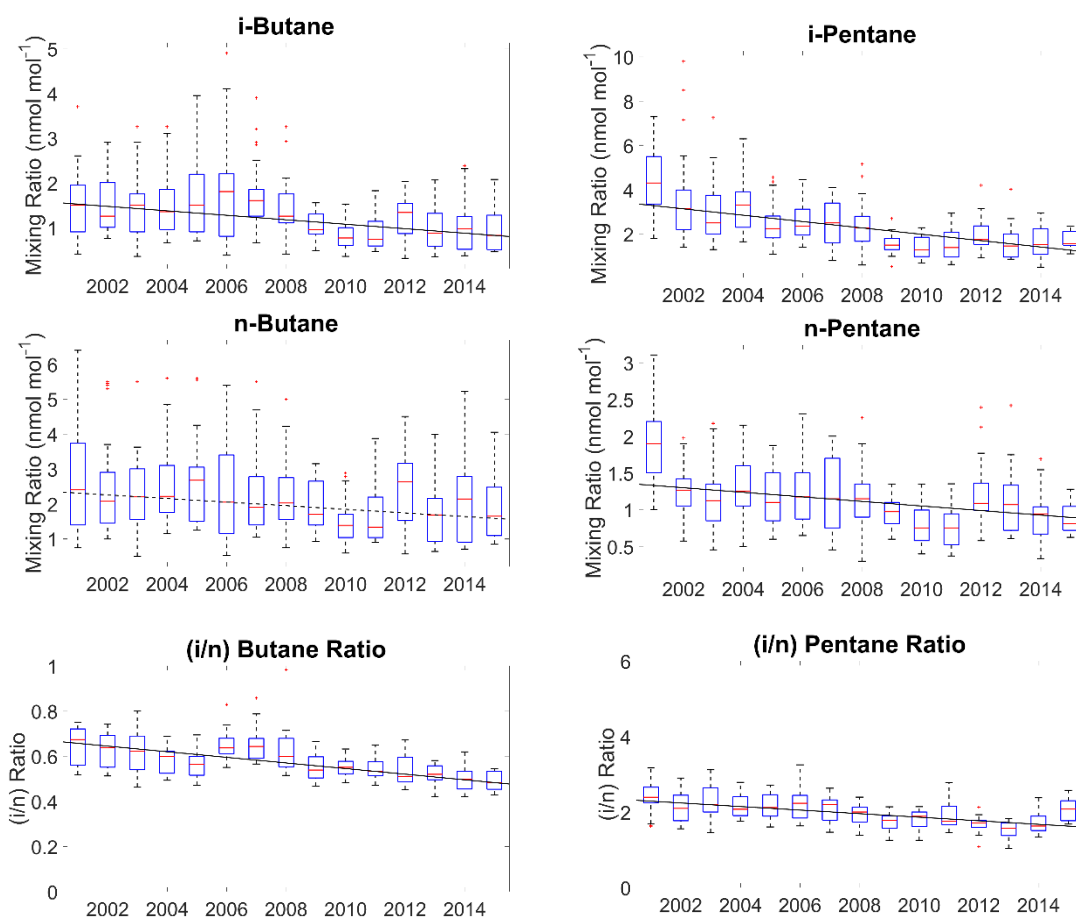
Figure S4e. Butane and pentane isomer annual boxplots and isomeric ratio annual boxplots at the Boston sites.
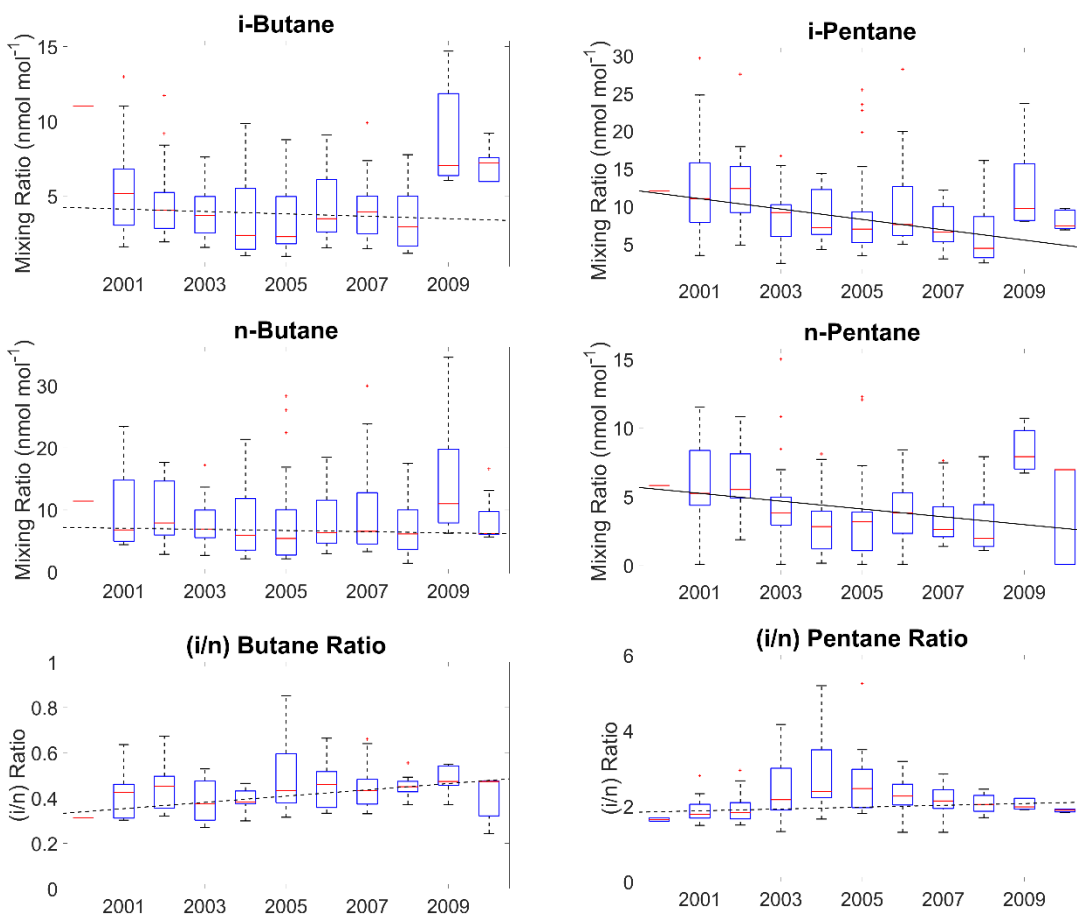
Figure S4f. Butane and pentane isomer annual boxplots and isomeric ratio annual boxplots at the El Paso site.
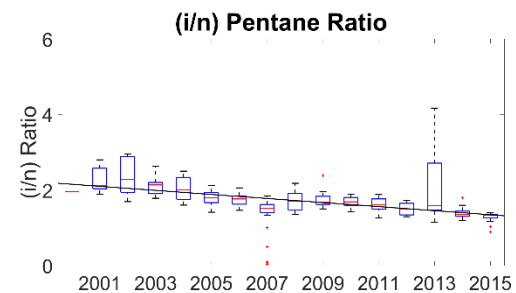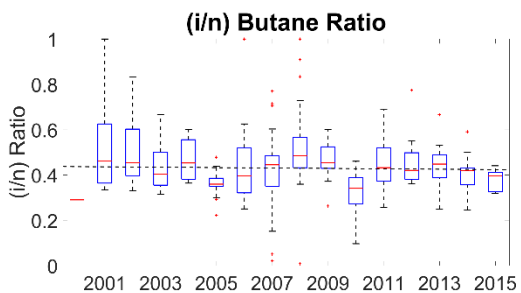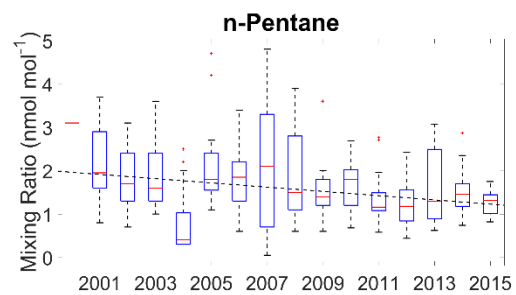
315

Figure S4g. Butane and pentane isomer annual boxplots and isomeric ratio annual boxplots at the Gary site.

Figure S4h. Butane and pentane isomer annual boxplots and isomeric ratio annual boxplots at the Houston site.

Figure S4i. Butane and pentane isomer annual boxplots and isomeric ratio annual boxplots at the Key Biscayne site.

Figure S4j. Butane and pentane isomer annual boxplots and isomeric ratio annual boxplots at the Park Falls site.

319

Figure S4k. Butane and pentane isomer annual boxplots and isomeric ratio annual boxplots at the Los Angeles site.

Figure S4l. Butane and pentane isomer annual boxplots and isomeric ratio annual boxplots at the Philadelphia site.

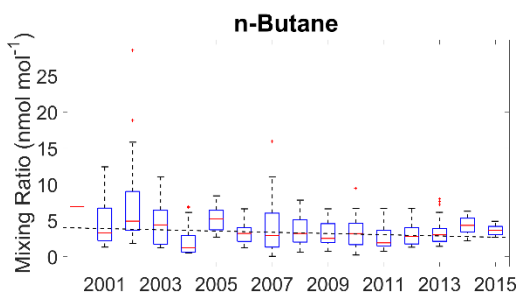Figure S4m. Butane and pentane isomer annual boxplots and isomeric ratio annual boxplots at the Southern Great Plains site.
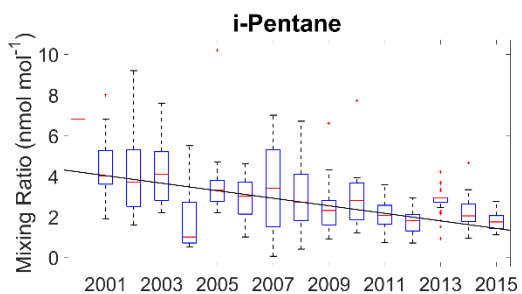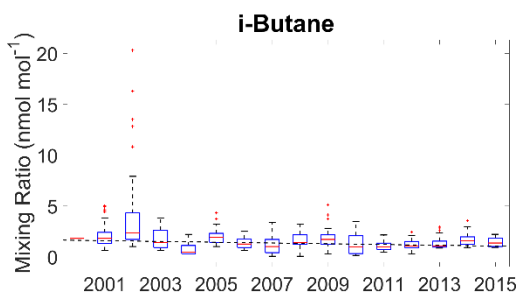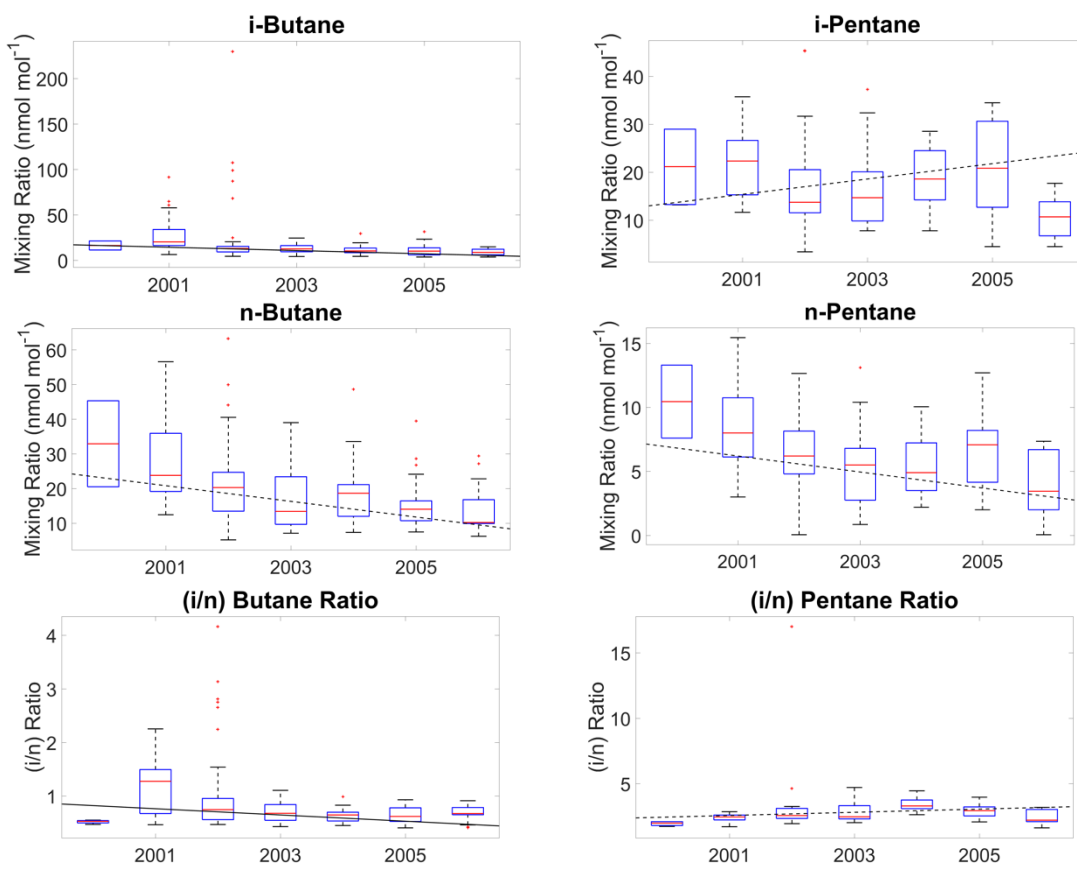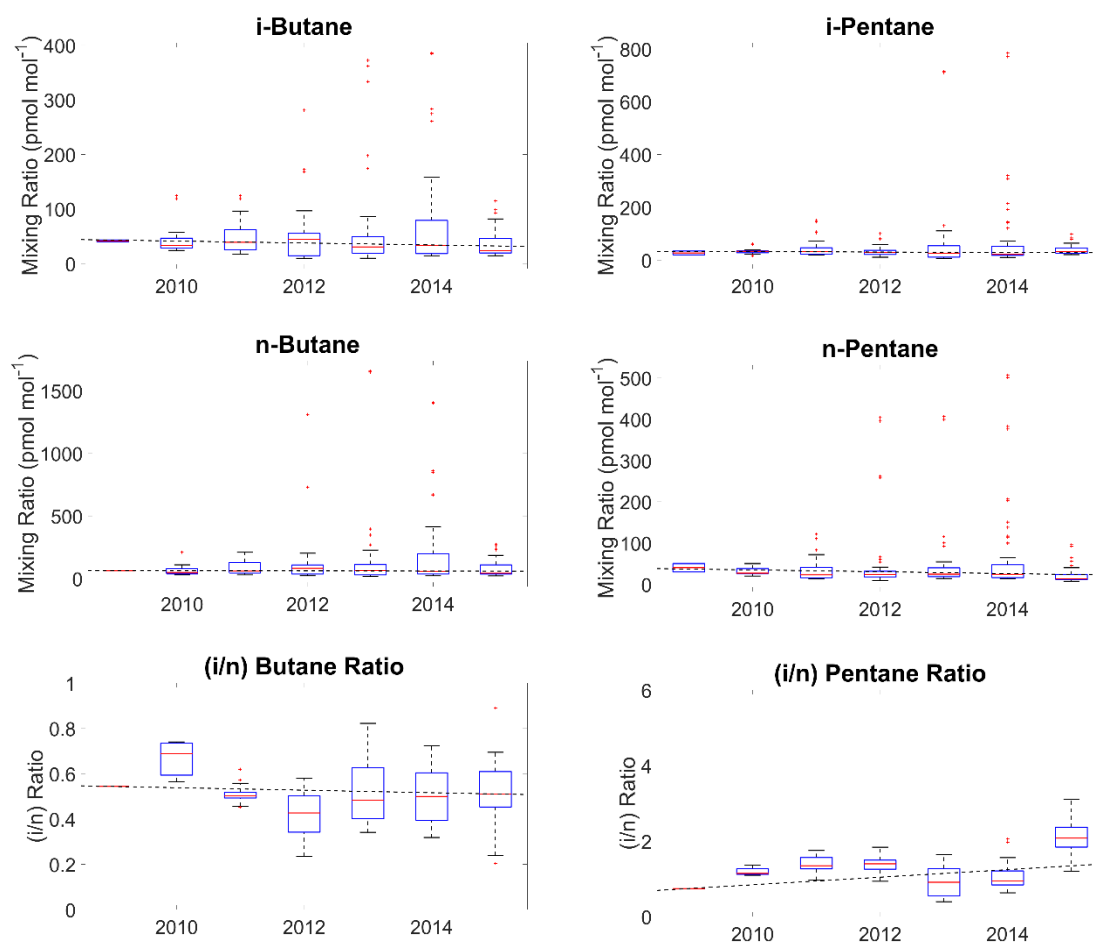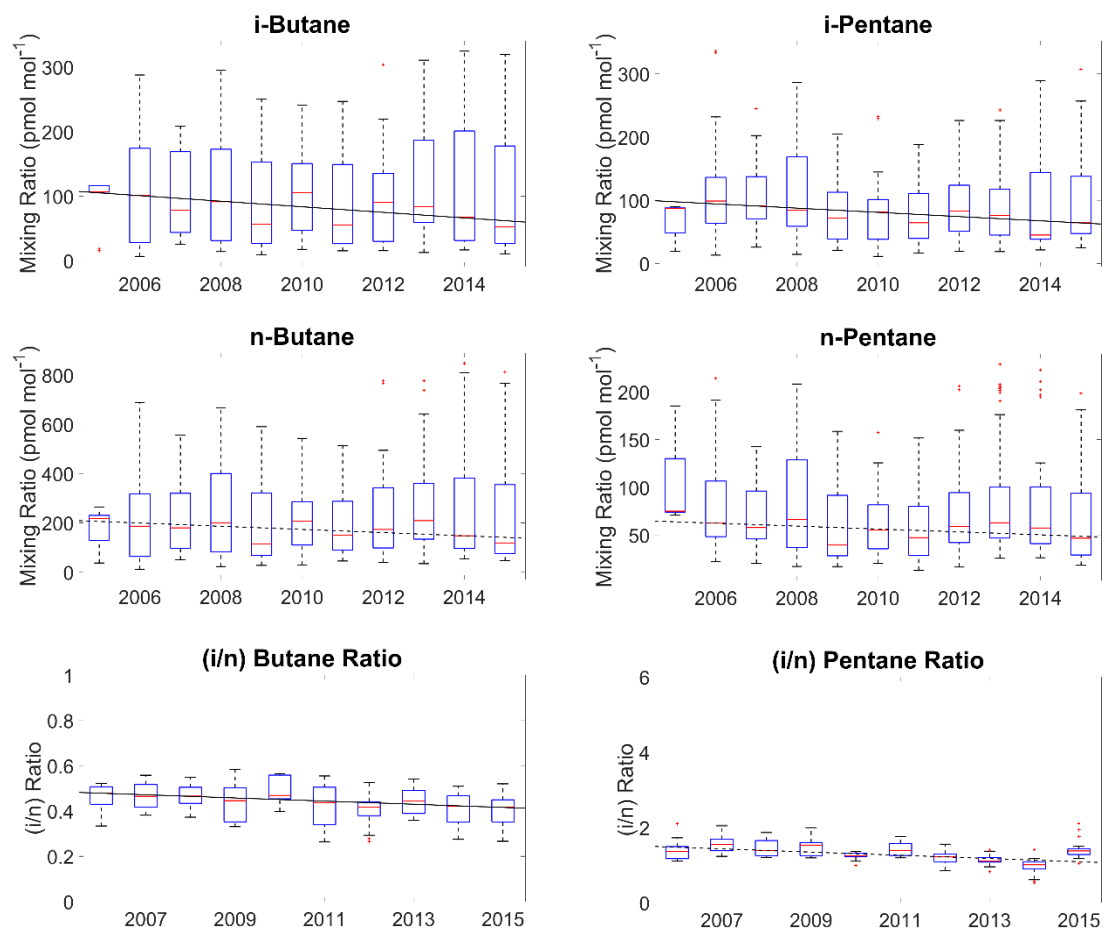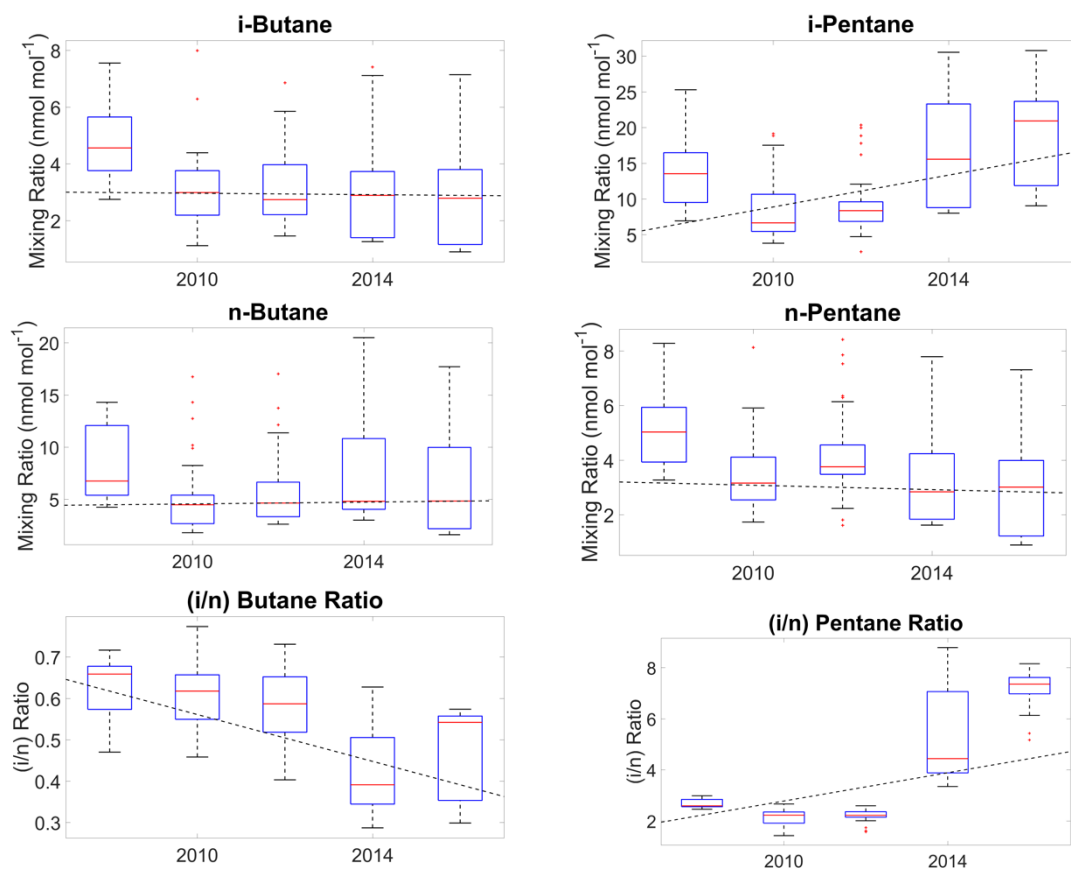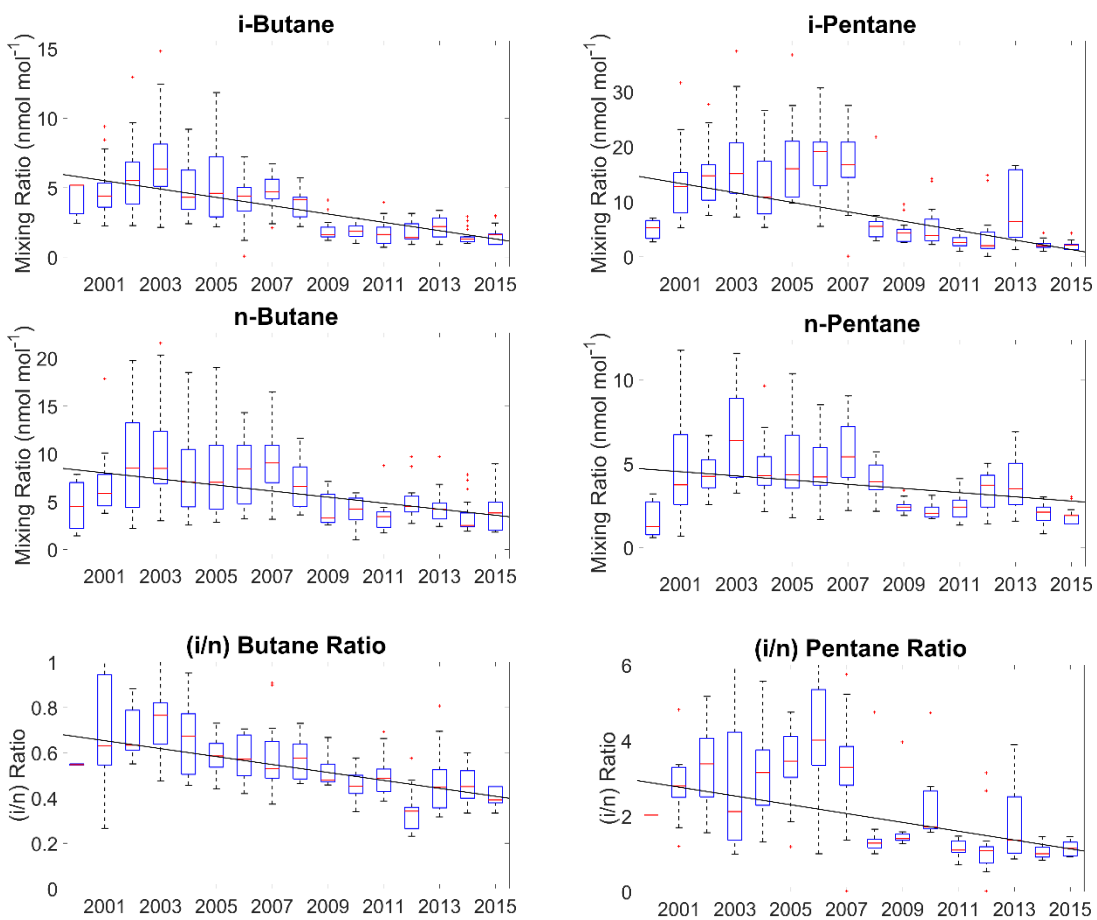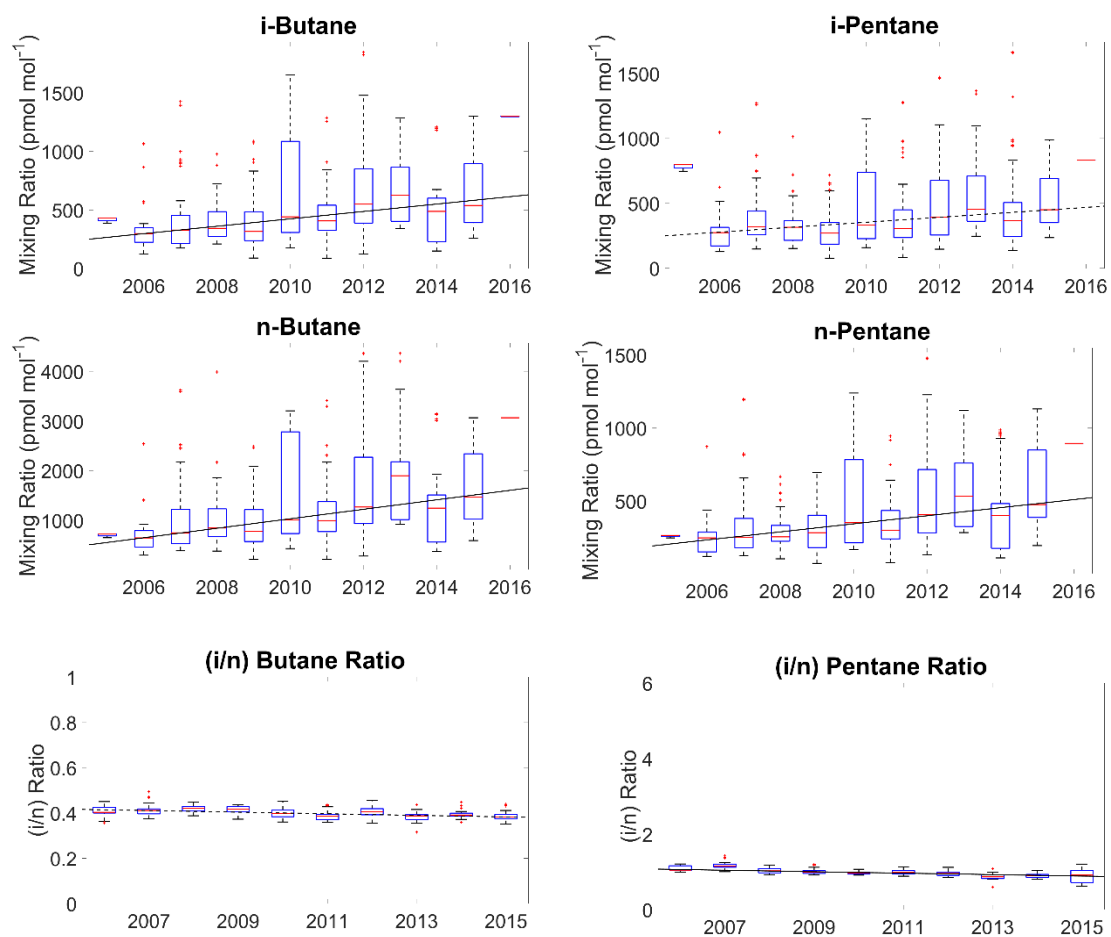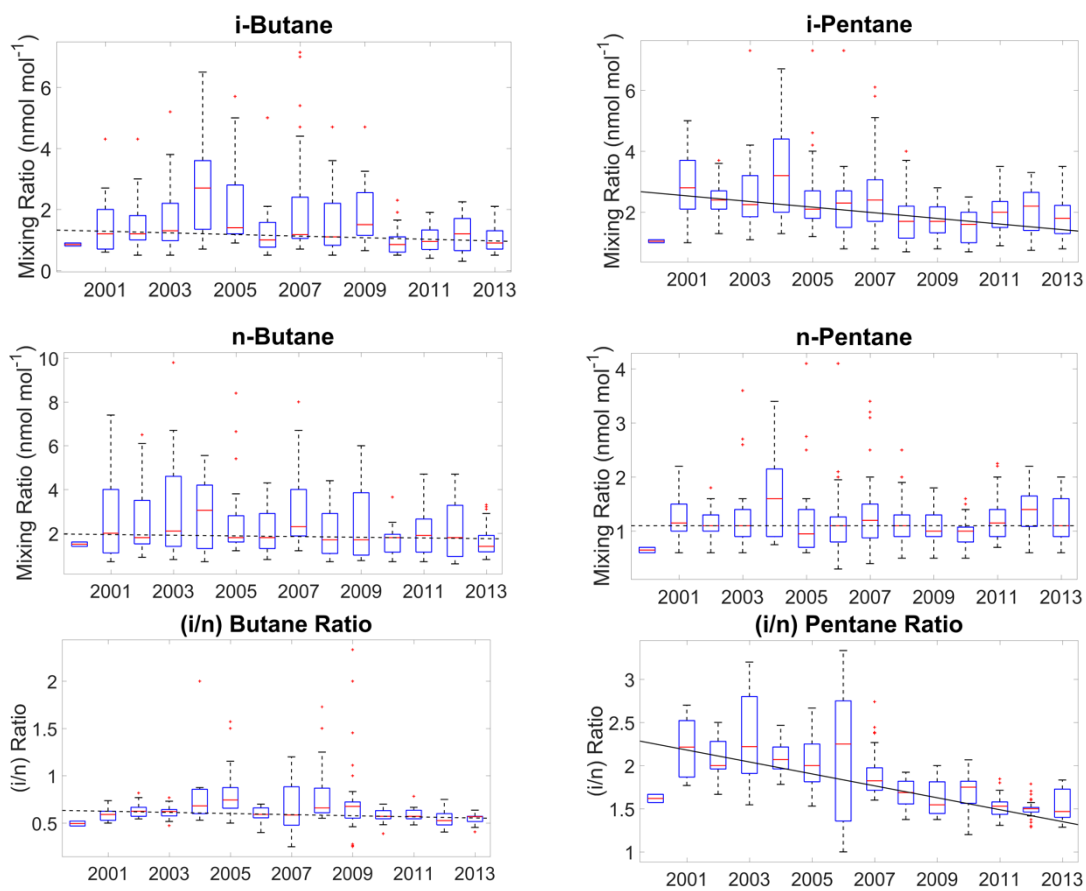
Figure S4n. Butane and pentane isomer annual boxplots and isomeric ratio annual boxplots at the Springfield site.
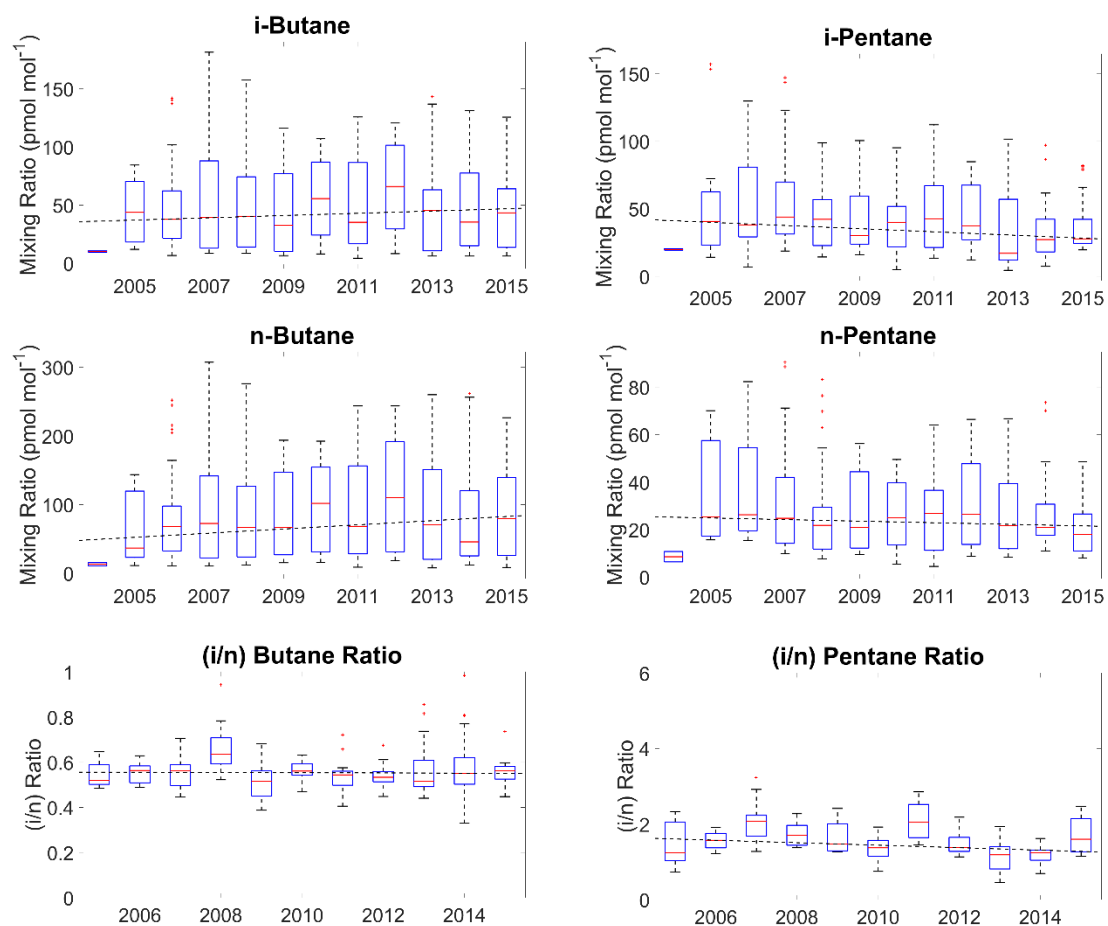
Figure S4o. Butane and pentane isomer annual boxplots and isomeric ratio annual boxplots at the Trinidad Head site.
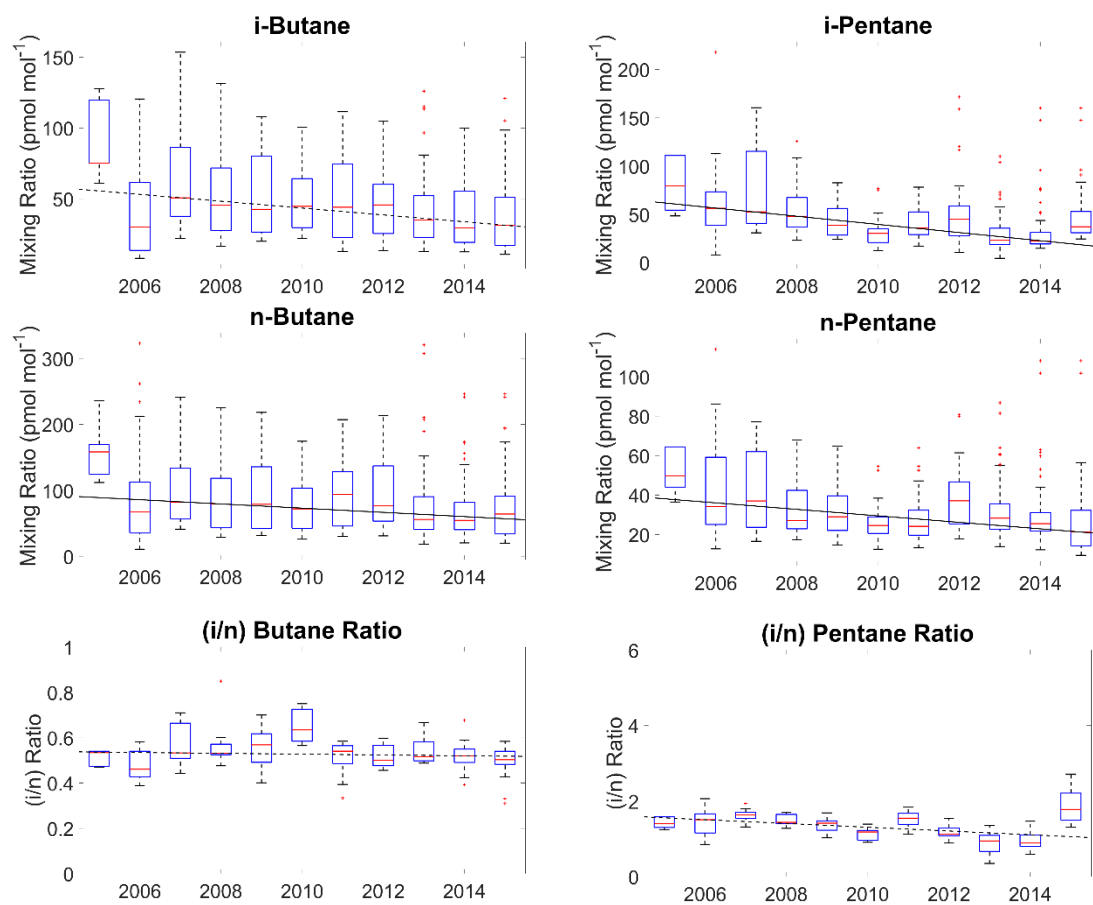
Figure S4p. Butane and pentane isomer annual boxplots and isomeric ratio annual boxplots at the Wendover site.

Table ST2. Published mean butane and pentane isomeric ratios in emissions from a variety of sources.

Location	Source	(i/n) Butane ratio	(i/n) Pentane Ratio	Reference
La Porte, Houston	Industrial, mobile sources, petrochemical	1.03	3.36	Jobson et al 2004
Washburn Tunnel, Houston	Mobile Sources	0.18	3.25	Jobson et al 2004
Vehicle Emission Studies, Houston	Mobile Sources	0.19	2.97	Jobson et al 2004
LA Basin, CA	Dry NG from pipeline	1.00	1.57	Peischl 2013
LA Basin, CA	Local NG	0.37	1.09	Peischl 2013
LA Basin, CA	LPG/Propane	6.50		Peischl 2013
LA Basin, CA	Evaporated Gasoline	0.16	2.92	Peischl 2013
LA Basin, CA	Mobile Sources	0.13	3.90	Peischl 2013
Uintah Basin, Utah	O&NG wells	0.68	1.29	Helmig 2014
Marcellus Region, Pennslyvannia - Near wells (>45 wells within 10 km)	O&NG wells	0.58	1.16	Swarthout 2015
Marcellus Region, Pennslyvannia - Far from wells (<20 wells within 10 km)	O&NG wells	0.44	1.29	Swarthout 2015
Marcellus Region, Pennslyvannia - Hickory (294 wells within 10 km)	O&NG wells	0.41	0.78	Swarthout 2015
Marcellus Region, Pennslyvannia - Raccoon Creek SP (1 well in 10 km)	Mobile sources/ O&NG wells	0.54	1.27	Swarthout 2015
Boulder, CO	Mobile sources/ O&NG wells	0.43	0.98	Swarthout 2013
Boulder, CO	Mobile sources/ O&NG wells		0.94	Petron 2012
Boulder, CO	Mobile/O&NG wells	0.40	0.91	Gilman 2013
Boulder, CO	Mobile sources/ O&NG wells		0.88	LaFranchi 2013
Savanna and Grassland	Biomass Burning	0.32	2.20	Andrae and Merlet 2001
Tropical Forest	Biomass Burning	0.37	0.57	Andrae and Merlet 2001
Extratropical Forest	Biomass Burning	0.32	0.43 - 0.52	Andrae and Merlet 2001
Biofuel Burning	Biomass Burning	0.08 - 1.66	1.14	Andrae and Merlet 2001
Charcoal Burning	Biomass Burning	0.06 - 0.5	0.70	Andrae and Merlet 2001

Figure S5. Map showing the location of the SGP monitoring station (red dot) and surrounding O&NG wells. The purple circle is a 10 mile radius centered on the SGP monitoring station.
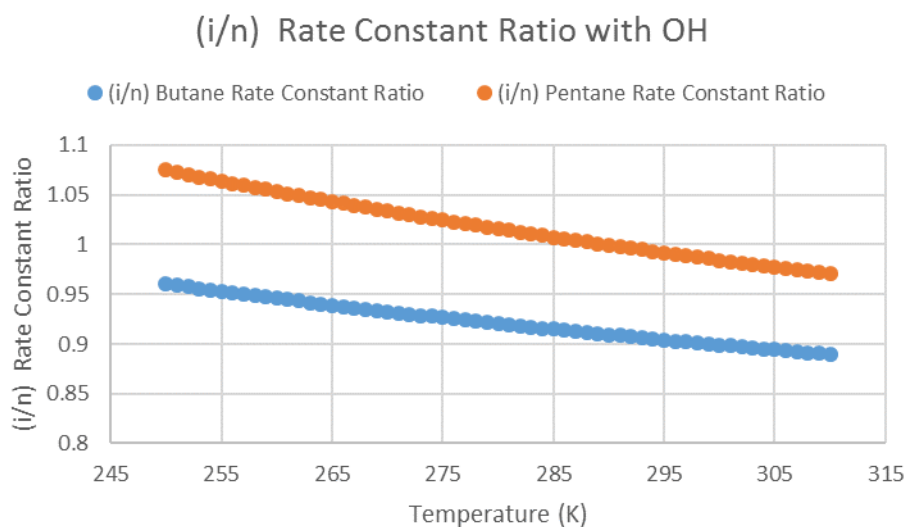
Figure S6. Ratio of the (*i/n*) OH reaction rate constant as a function of temperature. The difference in temperature dependence alone will cause a 5% seasonal cycle in (i/n) atmospheric butane ratio values at seasonally constant emissions. Reaction rate constants were calculated using data from [*Atkinson*, 2003] (butanes) and [*Wilson et al.*, 2006] (pentanes).

Supplemental Material:

Chapter 4

Volatile Organic Compounds in the Northern Colorado Front Range

Samuel Rossabi[1], Jacques Hueber[1], Reed Terrell[1], Katie Smith[1], Wei Wang[1], and Detlev Helmig[1,*]

[1]Institute of Arctic and Alpine Research, University of Colorado, Boulder, CO 80309, USA

*Corresponding author: Detlev Helmig (detlev.helmig@colorado.edu)
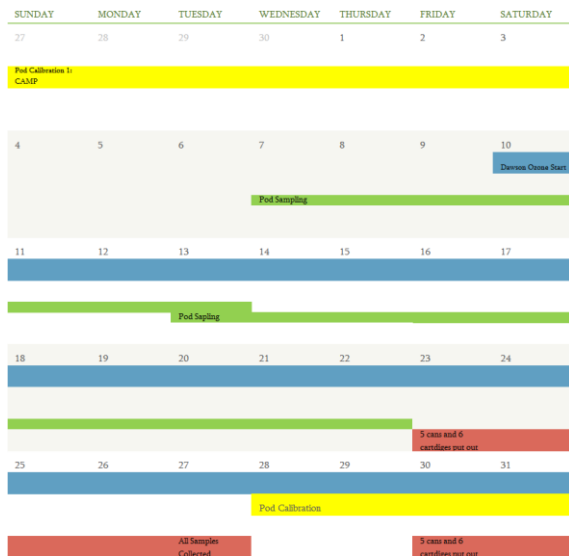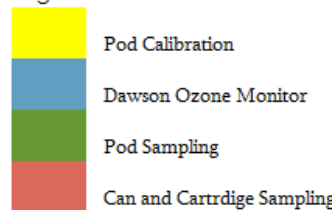
Figure S1. Sampling schedule at Boulder County Public Health campaign sites.
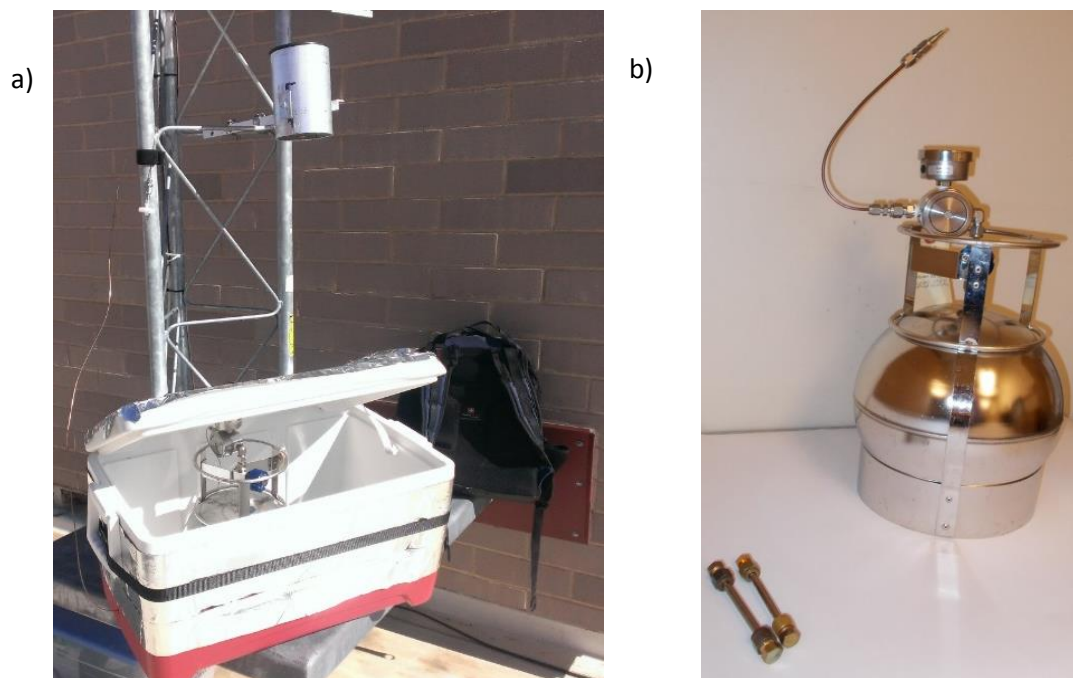
Figure S2. a) Typically field set up during the Boulder County Public Health study. b) Comparison of the size of adsorbent cartridges and canisters. The canister is shown with the passive flow controlling device installed.

Table ST1. Butane and Pentane isomeric ratio reference data.

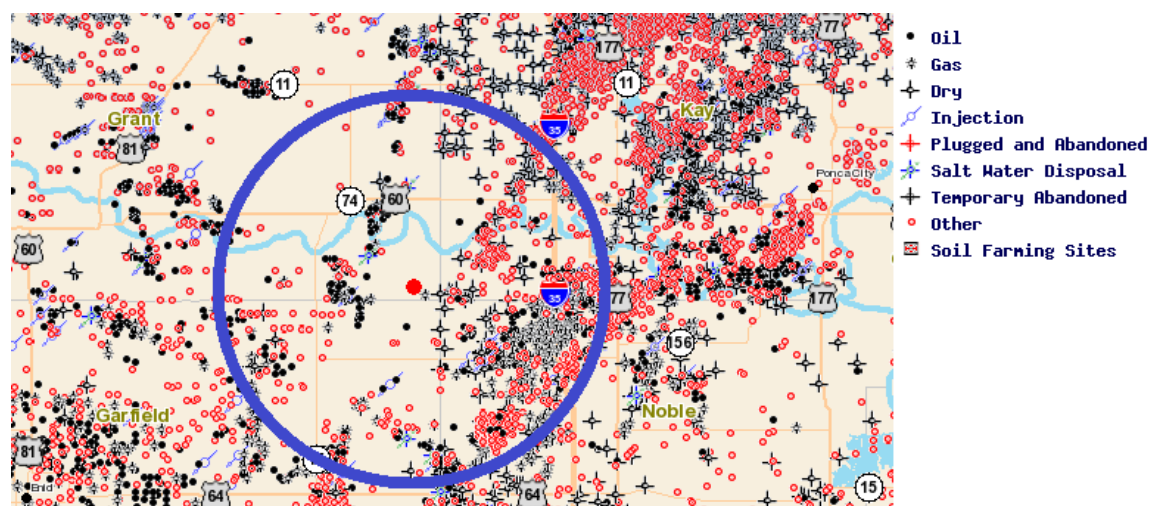| Location	Source	(i/n) Butane ratio	(i/n) Pentane Ratio	Reference
La Porte, Houston	Industrial, mobile sources, petrochemical	1.03	3.36	Jobson et al 2004
Washburn Tunnel, Houston	Mobile Sources	0.18	3.25	Jobson et al 2004
Vehicle Emission Studies, Houston	Mobile Sources	0.19	2.97	Jobson et al 2004
LA Basin, CA	Dry NG from pipeline	1.00	1.57	Peischl 2013
LA Basin, CA	Local NG	0.37	1.09	Peischl 2013
LA Basin, CA	LPG/Propane	6.50		Peischl 2013
LA Basin, CA	Evaporated Gasoline	0.16	2.92	Peischl 2013
LA Basin, CA	Mobile Sources	0.13	3.90	Peischl 2013
Uintah Basin, Utah	O&NG wells	0.68	1.29	Helmig 2014
Marcellus Region, Pennslyvannia - Near wells (>45 wells within 10 km)	O&NG wells	0.58	1.16	Swarthout 2015
Marcellus Region, Pennslyvannia - Far from wells (<20 wells within 10 km)	O&NG wells	0.44	1.29	Swarthout 2015
Marcellus Region, Pennslyvannia - Hickory (294 wells within 10 km)	O&NG wells	0.41	0.78	Swarthout 2015
Marcellus Region, Pennslyvannia - Raccoon Creek SP (1 well in 10 km)	Mobile sources/ O&NG wells	0.54	1.27	Swarthout 2015
Boulder, CO	Mobile sources/ O&NG wells	0.43	0.98	Swarthout 2013
Boulder, CO	Mobile sources/ O&NG wells		0.94	Petron 2012
Boulder, CO	Mobile/O&NG wells	0.40	0.91	Gilman 2013
Boulder, CO	Mobile sources/ O&NG wells		0.88	LaFranchi 2013
Savanna and Grassland	Biomass Burning	0.32	2.20	Andrae and Merlet 2001
Tropical Forest	Biomass Burning	0.37	0.57	Andrae and Merlet 2001
Extratropical Forest	Biomass Burning	0.32	0.43 - 0.52	Andrae and Merlet 2001
Biofuel Burning	Biomass Burning	0.08 - 1.66	1.14	Andrae and Merlet 2001
Charcoal Burning	Biomass Burning	0.06 - 0.5	0.70	Andrae and Merlet 2001

Figure S3. VOC as measured by canisters on elevation gradient on 6 sampling days during the campaign. Sites are displayed on the x-axis in order of decreasing elevation. Y-axis exhibits mixing ratios and are consistent across all plots.

Figure S4. Diurnal cycles collected by PFP samplers at elevation gradient sites.

Supplemental Material:

Chapter 5

Evaluation of Solid Adsorbent Cartridges for Diffusive Sampling of Atmospheric Oil and Natural Gas Hydrocarbons

Samuel Rossabi[1], Joshua Fuchs[1,2], Kate R. Smith[1,3], Jens Fangmeyer[1,2], Jacques Hueber[1], Detlev Helmig[1,*]

[1]Institute of Arctic and Alpine Research, University of Colorado-Boulder, Boulder, CO, 80303, USA

[2]Institute of Inorganic and Analytical Chemistry, University of Muenster, Muenster, DE
[3]Department of Chemistry, University of York, Heslington, York, UK

*Corresponding Author: Detlev Helmig (detlev.helmig@colorado.edu)

Table ST1. Components, abundances, and tolerances of standard mixtures used to calibrate the GC/MS. Four multicomponent standards were used: a) Apel-Riemer multicomponent standard, b) National Physical Laboratory multicomponent standard, c) National Institute of Standards and Technology monoterpene standard, and d) Apel-Reimer oxygenated VOC standard

(a) Apel-Riemer Environmental, Inc. multicomponent standard, Broomfield, CO, USA, prepared Summer 2014

Component	Mole fraction (nmol mol^{-1})	Tolerance (%)
Ethene	4.93	5
Acetlyene	5.73	5
Ethane	9.72	5
Propene	1.89	5
Propane	9.16	5
Propyne	4.53	5
i-Butane	4.07	5
i-Butene	2.72	5
1-Butene	2.12	5
1,3-Butadiene	1.99	5
Butane	7.84	5
t-2-Butene	0.94	5
c-2-Butene	1.99	5
1,2-Butadiene	4.79	5
i-Pentane	5.97	5
1-Pentene	0.97	5
2-Methyl-butene	0.99	5

Pentane	7.09	5
Isoprene	3.88	5
t-2-Pentene	0.77	5
c-2-Pentene	1.86	5
2-Methyl-2-butene	0.81	5
2,2-Dimethylbutane	1.86	5
Cyclopentene	0.79	5
Cyclopentane	0.97	5
2,3-Dimethylbutane	1.46	5
2-Methylpentane	0.80	5
3-Methylpentane	0.99	5
2-Methyl-1-pentene	0.75	5
Hexane	2.50	5
t-2-Hexene	0.41	5
c-2-Hexene	0.78	5
Methylcyclopentane	0.79	5
2,4-Dimethylpentane	0.79	5
Benzene	1.62	5
Cylcohexane	0.44	5
2-Methylhexane	0.81	5
2,3-Dimethylpentane	0.37	5
Cyclohexene	0.73	5
3-Methylhexane	0.74	5
1-Heptene	1.91	5
Heptane	3.55	5
Methylcyclohexane	0.82	5
2,3,4-Trimethylpentane	0.40	5
Toluene	2.26	5
2-Methylheptane	0.41	5
4-Methylheptane	0.98	5
3-Methylheptane	0.77	5
Octane	0.41	5
Ethylbenzene	0.70	5
m-Xylene	1.10	5
p-Xylene	0.36	5
Styrene	0.35	5
o-Xylene	0.38	5

(b) National Physical Laboratory multicomponent standard, London, UK, prepared December 16, 2015

Component	Mole fraction (nmol mol^{-1})	Tolerance ($\pm$ nmol mol^{-1})

Ethane	4.06	0.08
Ethene	3.91	0.08
Propane	4.09	0.08
Propene	4.02	0.08
2-Methylpropane	4.20	0.11
Butane	3.98	0.08
Ethyne	4.13	0.21
t-But-2-ene	3.97	0.08
But-1-ene	3.98	0.08
c-But-2-ene	4.02	0.08
2-Methylbutane	4.05	0.08
Pentane	4.05	0.08
1,3-butadiene	3.97	0.08
t-Pent-2-ene	3.97	0.08
Pent-1-ene	3.98	0.08
2-Methylpentane	4.06	0.08
Hexane	3.99	0.08
Isoprene	4.03	0.09
Heptane	4.02	0.08
Benzene	4.00	0.08
2,2,4-Trimethylpentane	3.99	0.08
Octane	4.03	0.08
Toluene	4.00	0.10
Ethylbenzene	4.00	0.10
m-Xylene + p-Xylene	8.04	0.21
o-Xylene	4.00	0.10
1,3,5-Trimethylbenzene	4.01	0.11
1,2,4-Trimethylbenzene	4.03	0.11
1,2,3-Trimethylbenzene	4.04	0.11

(c) Apel-Riemer Environmental, Inc. oxygenated VOC standard, Broomfield, CO, USA, prepared April 2010

Component	Mole fraction (nmol mol^{-1})	Tolerance (%)
Methanol	540	5
Acetone	538	5
Methyl Vinyl Ketone	506	5
Methacrolein	542	5
Isoprene	519	5

(d) VOC-BTEX working standard, mixing ratios (M.R.) range from 374 ppb to 1182 ppb. This standard was dynamically diluted with zero air (both standard and zero air flow controlled by MFC) to 1 ppb and 12 ppb for bag uptake experiments.

Components	M.R. (ppb)
Ethane	1182
Propane	1187
n-Butane	1080
n-Propane	900
n-Hexane	714
Benzene	709
Toluene	374
Ethylbenzene	500
m&p-Xylene	1000
o-Xylene	500
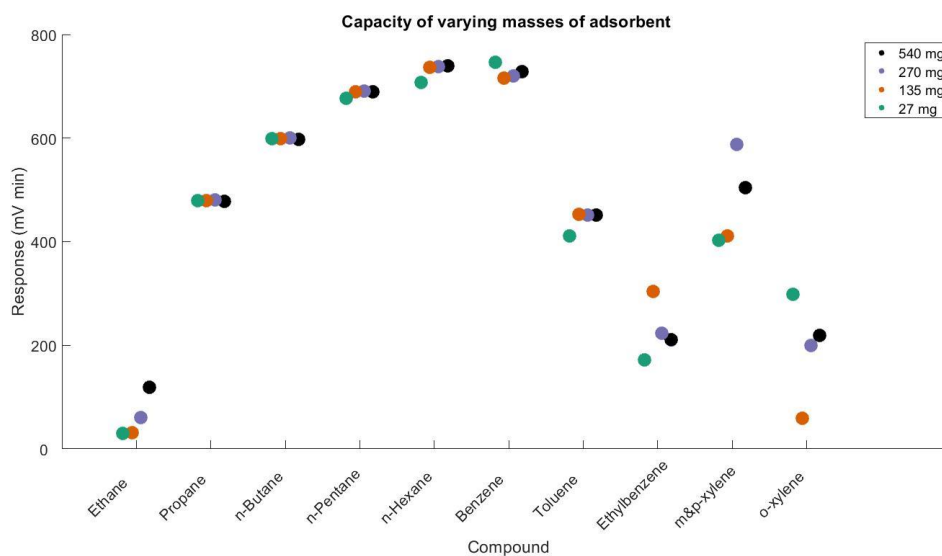
Figure S1. Sampling performance of varying masses of adsorbent loaded with 2L of a 12 nmol mol^{-1} standard.

Table ST2. Location information for field campaign sites

Site Name	Lat.	Lon.

Rose Litman Lab	40° 0' 48"	105° 15' 11" W
SEEC	40° 0' 35"	105° 14' 31" W
Stephen Day Park	40° 10' 57"	105° 3' 49" W
Lafayette Fire Department	40° 0' 6" N	105° 5' 40" W
Boulder County Public Health	40° 2' 14" N	105° 16' 53" W
Dawson School	40° 3' 50" N	105° 6' 37" W
St. Luke's Church	40° 1' 56" N	105° 3' 24" W

Table ST3. Temperature and relative humidity data for the field campaigns.

Month	Year	Avg. Temp (°C)	High Temp (°C)	Low Temp (°C)	Avg. RH (%)	High RH (%)	Low RH (%)
June	2014	18	34	6	51	100	10
July	2014	21	37	13	56	100	11
August	2014	20	33	11	53	100	13
November	2014	3	23	-19	51	100	8
November	2016	8	27	-7	44	100	9

Figure S2. Typical field sampling set up. The adsorbent cartridge is in the inverted coffee can. The canister is in a cooler box.

Table ST4. Mean peak areas (n=3), standard deviations, and relative standard deviations of compounds collected by cartridges with varying adsorbent bed masses.

Compound	Mean Peak Area (mV min)	Std. Dev.	RSD
Ethane	6.59	2.5	39%
Propane	41.6	0.6	1.4%
n-Butane	52.2	0.4	0.7%
n-Pentane	60.7	0.6	0.9%
n-Hexane	68.4	0.5	0.8%
Benzene	91.2	5.5	6.0%
Toluene	47.3	1.2	2.6%
Ethylbenzene	22.8	0.4	1.8%
m&p-Xylene	52.3	2.0	3.9%
o-Xylene	31.7	1.3	4.2%

$$J = -D\frac{\partial c}{\partial x}$$

$$J = \frac{m}{A\,t}$$

$$\frac{m}{A\,t} = -D\,\frac{\partial c}{\partial x}$$

$$m = \frac{DA}{x}\,ct$$

Figure S3. Shows the manipulation of Fick's Law of Diffusion so that it can be used to predict the mass loaded on an adsorbent bed, where m=mass loaded, D=diffusion constant, A=area of sampler opening, c=concentration, t=time, J=flux. The final equation assumes that the adsorbent bed is a perfect sink of the target compound, which allows the $\partial c/\partial x$ term to be simplified to the ambient concentration of the target compound, c, divided by x, where x is the distance from sampler opening to the adsorbent bed.
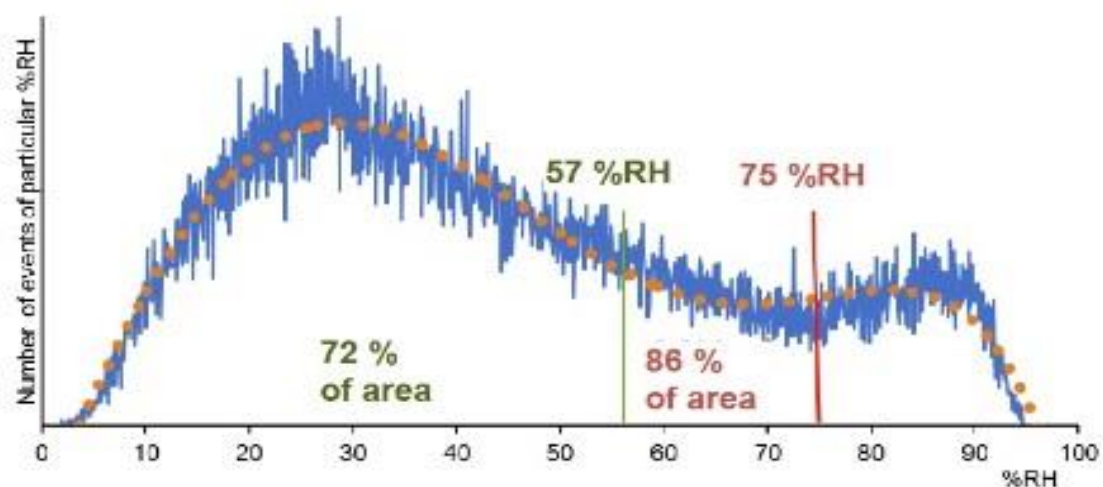
Figure S4. Probability distribution of %RH levels at David Skaggs Research Center in Boulder, Co. These humidity data were collected every half hour from 2001 – 2015 by the National Oceanic and Atmospheric Administration at the David Skaggs Research Center in Boulder, Colorado. This figure displays the number of measurements of each relative humidity value throughout this period.

Table ST5. Comparison of mixing ratios from canister samples during summer and winter 2014, and 2016 field campaigns.

Compound	Summer 2014		Winter 2014		2016	
	Avg. Mixing Ratio (ppb)	Std. Dev.	Avg. Mixing Ratio (ppb)	Std. Dev.	Avg. Mixing Ratio (ppb)	Std. Dev.
Ethane	15.1	7.95	16.6	8.09	12.4	5.32

Propane	7.46	4.76	6.87	3.87	1.74	0.67
Propene	8.01	12.20	1.08	0.32	1.13	0.30
i-Butane	2.63	1.67	1.57	0.59	1.13	0.39
n-Butane	3.43	2.62	3.65	1.79	1.73	0.68
i-Pentane	1.63	0.98	1.35	0.53	0.79	0.27
n-Pentane	1.30	0.86	1.03	0.46	0.56	0.19
n-Hexane	1.15	0.88	0.87	0.42	1.25	0.71
Benzene	11.4	6.69	3.52	1.66	0.32	0.08
Toluene	0.76	0.87	0.84	0.42	0.57	0.22
o-Xylene	0.05	0.03	0.13	0.06	1.03	0.36

Supplemental Material:

Chapter 6

Volatile organic compound emissions from soil following wetting events

Sam Rossabi[1,2], Mallory Choudoir[1], Detlev Helmig[2], Jacques Hueber[2], Noah Fierer[1,3*]

[1]Cooperative Institute for Research in Environmental Sciences, University of Colorado- Boulder, Boulder, CO, 80309, USA
[2]Institute of Arctic and Alpine Research, University of Colorado-Boulder, Boulder, CO, 80303, USA
[3]Department of Ecology and Evolutionary Biology, University of Colorado-Boulder, Boulder, CO 80309

*Corresponding Author: Noah Fierer (noah.fierer@colorado.edu)

Figure S1. Photos of the dynamic flux chamber system. (a) Flux chambers from above. (b) The system from the side and shows the chambers in the manifold. (c) and (d) A chamber with a jar for soil and 50 mL of standing water to keep the humidity higher. Note that the soil in the photo was not used in this experiment, has not been homogenized or sieved, and only used to demonstrate the soil sampling set up.

Dynamic Flux Chamber System Plumbing diagram
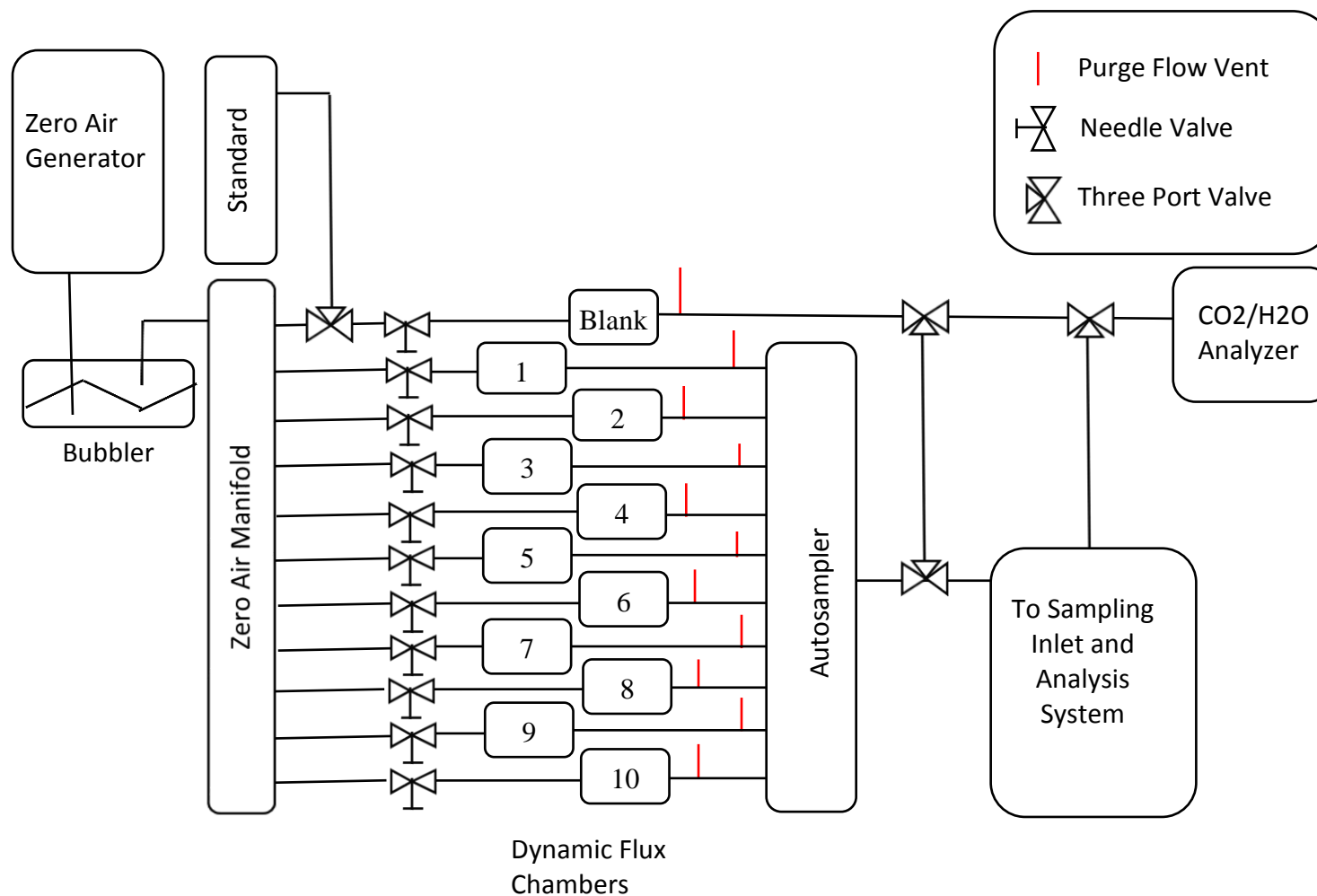
Figure S2. Diagram dynamic flux chamber system. The inlet system is shown in less detail, but is available in S1. Leaf litter jars are numbered, the first jar was used for all experiments. The vents following the Leaf Litter Jars were joined in an exhaust manifold. Diagramming this is distracting and makes it difficult to clearly see the soil sampling manifold, so this is represented by short vents.

Inlet System Plumbing diagram
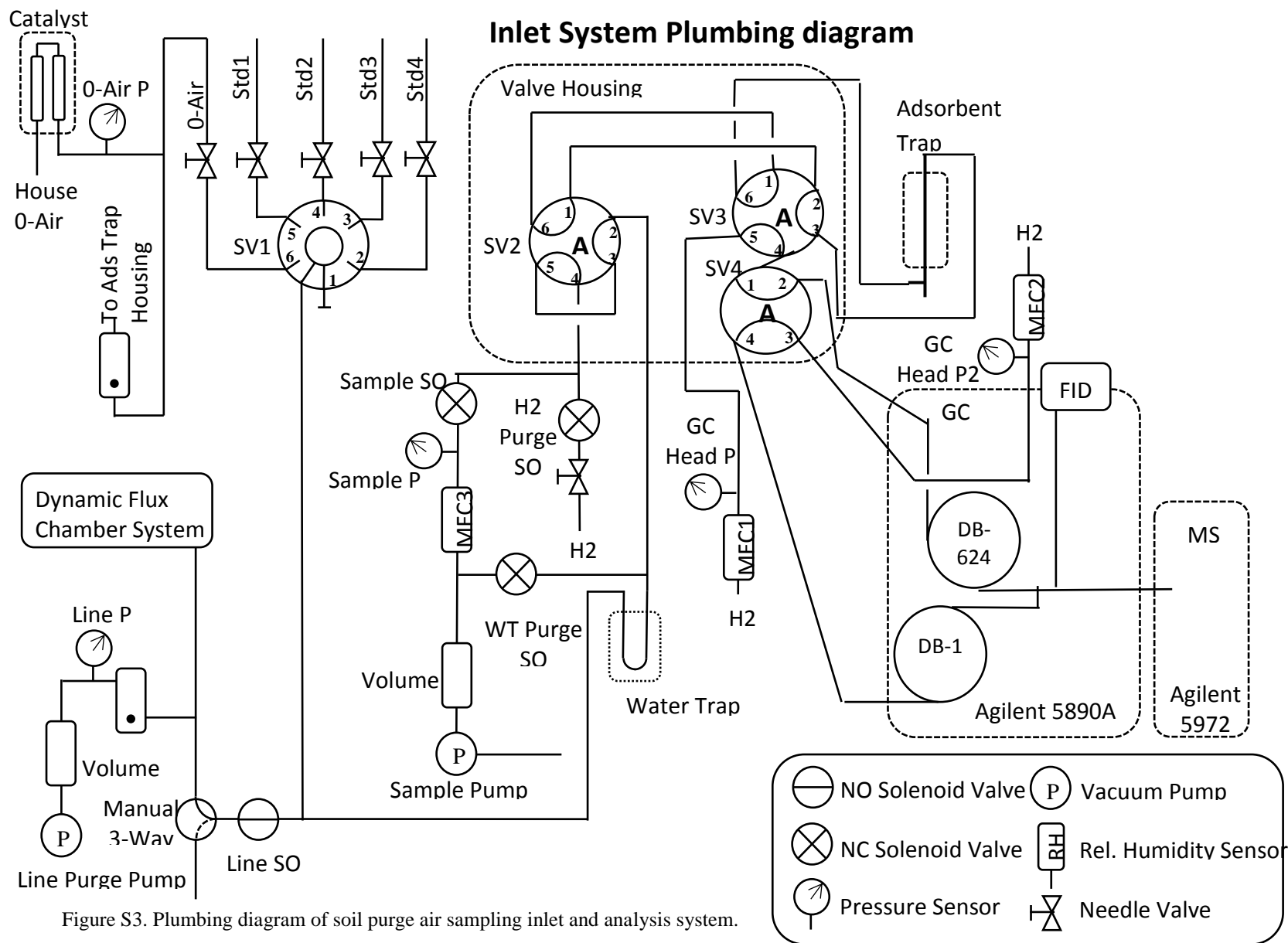
Figure S3. Plumbing diagram of soil purge air sampling inlet and analysis system.
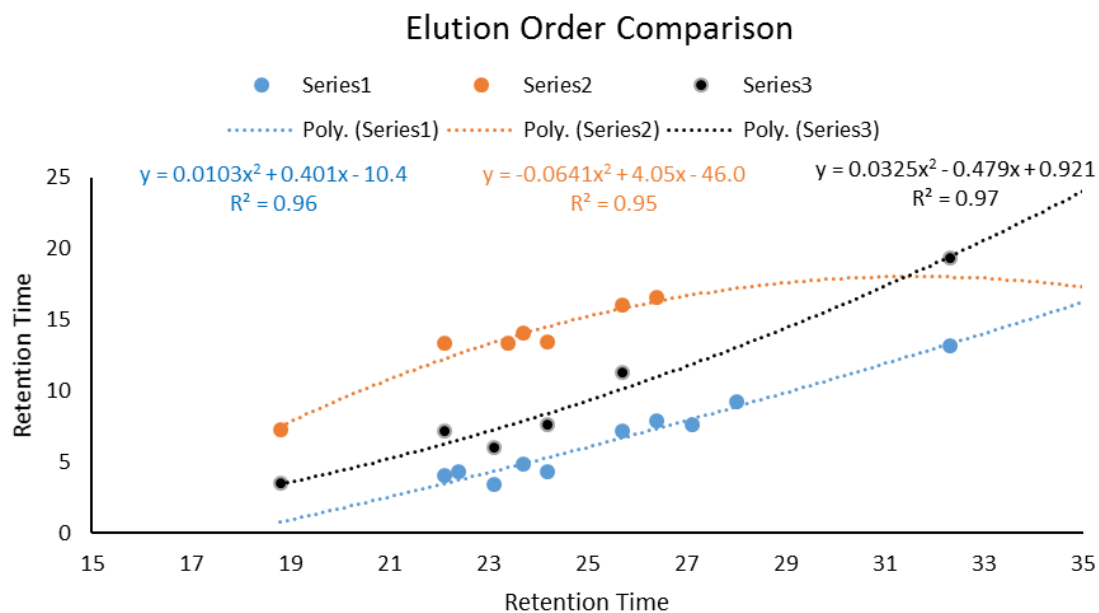
Figure S4. Elution order comparison of MS-identified compounds (x-axis) with elution orders from Agilent (blue) [*Agilent*, 2014], the NACHTT campaign (orange) [*Brown et al.*, 2013], and the Air Toxics project (black) [*Apel et al.*, 1998]. Elution correlations were fit with a 2nd order polynomial fit. Equations for these fits and corresponding R^2 values are displayed in the figure. Compounds for which elution order data were available are listed in Table ST3.
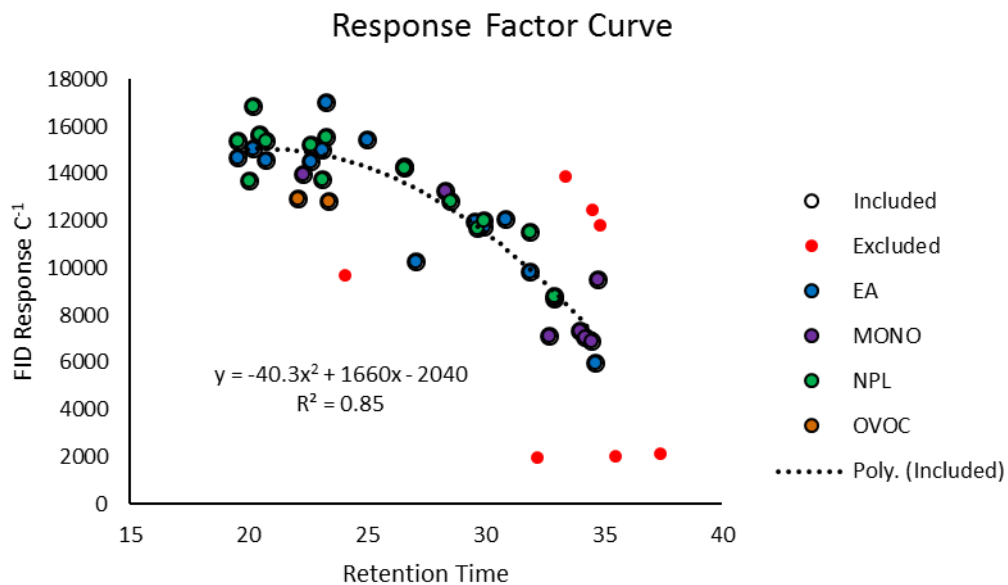
Figure S5. Response factor calibration curve used to assign response factors to compounds not present in our standards or unidentifiable compounds. The abbreviations in the legend correspond to the standards shown in Table ST1. EA = Apel-Riemer multicomponent standard, MONO = NIST monoterpene standard, NPL = National Physical Laboratory Multicomponent Standard, OVOC = Apel-Riemer oxygenated VOC standard.
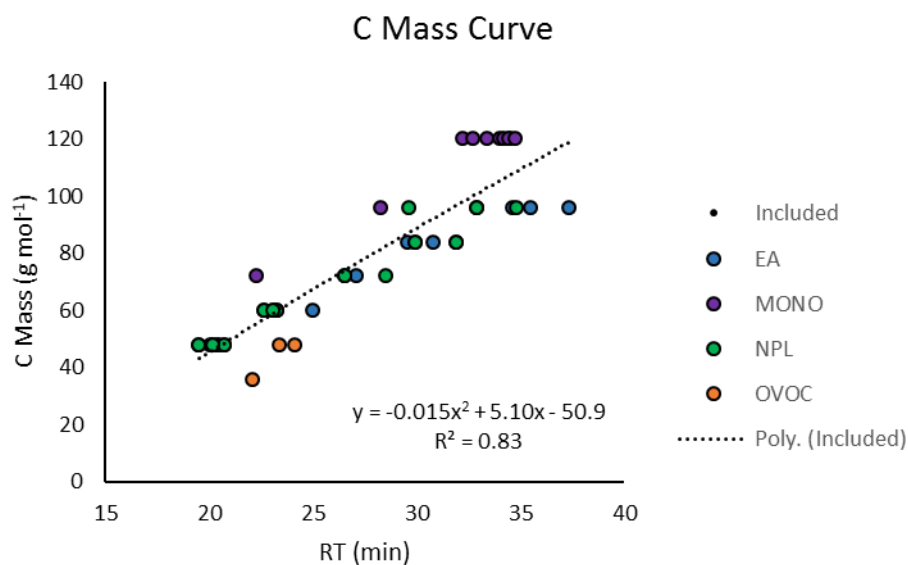
Figure S6. 2nd order polynomial fit of the C mass present in standard components versus their retention times. Retention times of unknown components were input in the curve equation to estimate the mass of carbon present in the compound. Abbreviations in the standard column are 'EA' for Apel-Riemer Multicomponent Standard, 'NPL' for National Physical Laboratory multicomponent standard, 'MONO' for NIST Monoterpene standard, 'OVOC' for NIST oxygenated VOC standard.
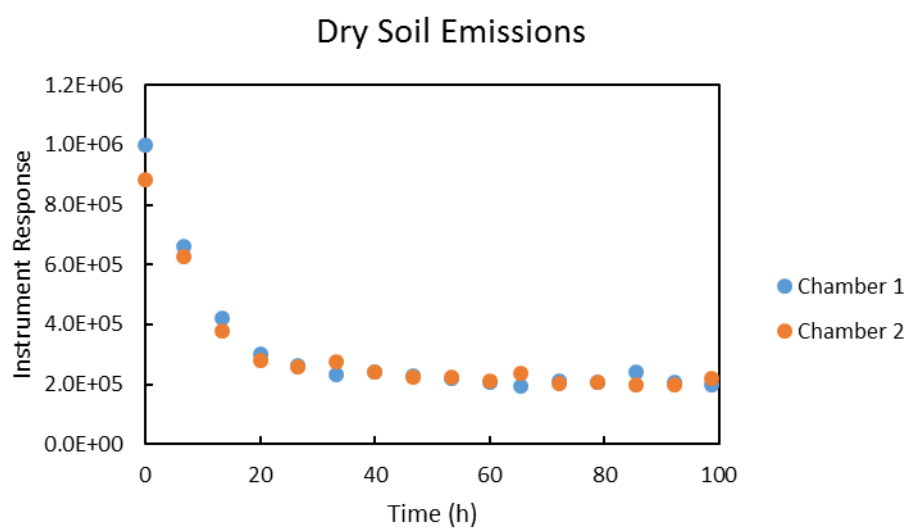
Figure S7. Emissions from dry soil samples (S1 soil, additional samples not used in rewetting experiment) in two different dynamic flux chambers over the course of 100 hours. Emissions were measured by total FID response.
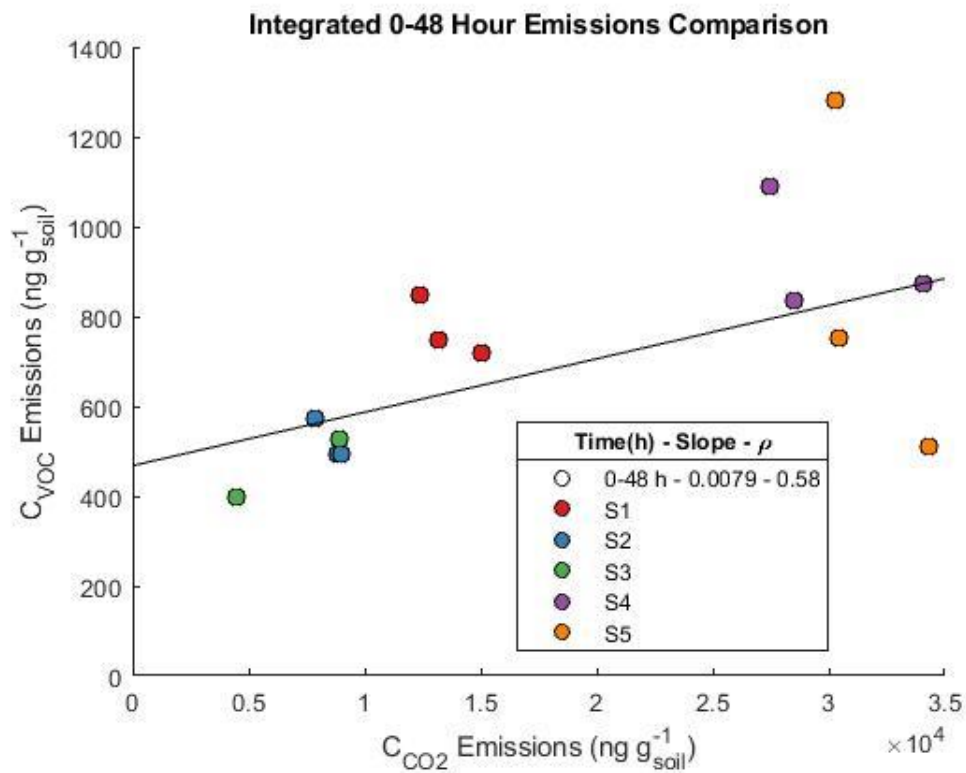
Figure S8. Integrated C_{VOC} emissions (y-axis) versus integrated C_{CO2} emissions (x-axis) for the duration of the 48 hour experiment. Note the difference in scale between CO_2 and VOC emissions. The linear regression shows the correlation between CO_2 and VOC emissions, and the Spearman ρ value is reported in the legend. The P-value is < 0.001. One S3 soil sample was excluded due to lost samples.
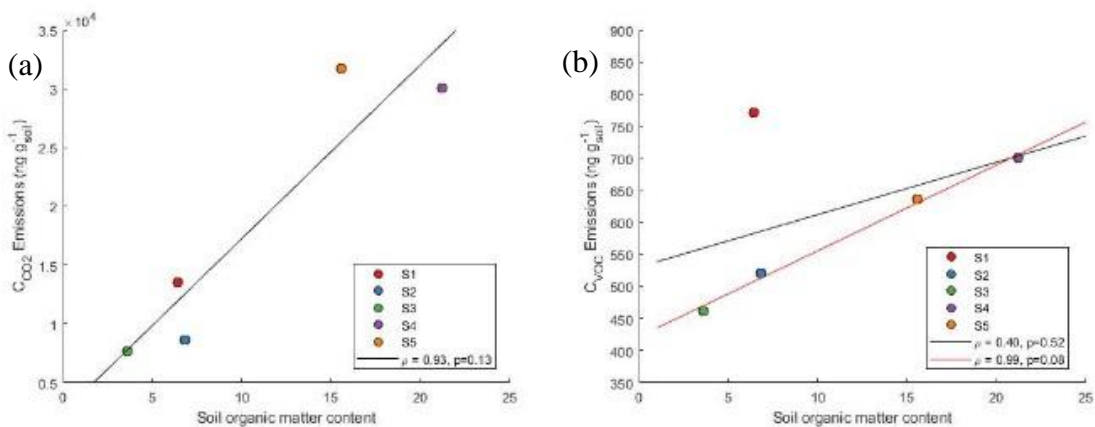
Figure S9. (a) C_{CO2} and (b) C_{VOC} emissions as a function of soil organic matter content. Each point represents a soil type, which is an average of the three replicates. Spearman correlations and p-values are given in the legend. The red line in (b) and the corresponding legend entry represent the correlation of VOC flux and soil organic matter content with S1 excluded.

Table ST1. Components, abundances, and tolerances of standard mixtures used to calibrate the GC/MS. Four multicomponent standards were used: a) Apel-Riemer multicomponent standard, b) National Physical Laboratory multicomponent standard, c) National Institute of Standards and Technology monoterpene standard, and d) Apel-Reimer oxygenated VOC standard.

(a) Apel-Riemer Environmental, Inc. multicomponent standard, Broomfield, CO, USA, prepared Summer 2014

Component	Mole fraction (nmol mol^{-1})	Tolerance (%)
Ethene	4.93	5
Acetlyene	5.73	5
Ethane	9.72	5
Propene	1.89	5
Propane	9.16	5
Propyne	4.53	5
i-Butane	4.07	5
i-Butene	2.72	5
1-Butene	2.12	5
1,3-Butadiene	1.99	5
Butane	7.84	5
t-2-Butene	0.94	5
c-2-Butene	1.99	5
1,2-Butadiene	4.79	5
i-Pentane	5.97	5
1-Pentene	0.97	5
2-Methyl-butene	0.99	5
Pentane	7.09	5
Isoprene	3.88	5
t-2-Pentene	0.77	5
c-2-Pentene	1.86	5
2-Methyl-2-butene	0.81	5
2,2-Dimethylbutane	1.86	5
Cyclopentene	0.79	5
Cyclopentane	0.97	5
2,3-Dimethylbutane	1.46	5
2-Methylpentane	0.80	5
3-Methylpentane	0.99	5
2-Methyl-1-pentene	0.75	5
Hexane	2.50	5
t-2-Hexene	0.41	5
c-2-Hexene	0.78	5
Methylcyclopentane	0.79	5
2,4-Dimethylpentane	0.79	5
Benzene	1.62	5
Cylcohexane	0.44	5
2-Methylhexane	0.81	5
2,3-Dimethylpentane	0.37	5
Cyclohexene	0.73	5
3-Methylhexane	0.74	5
1-Heptene	1.91	5
Heptane	3.55	5
Methylcyclohexane	0.82	5
2,3,4-Trimethylpentane	0.40	5
Toluene	2.26	5
2-Methylheptane	0.41	5
4-Methylheptane	0.98	5
3-Methylheptane	0.77	5
Octane	0.41	5
Ethylbenzene	0.70	5
m-Xylene	1.10	5
p-Xylene	0.36	5
Styrene	0.35	5
o-Xylene	0.38	5

(b) National Physical Laboratory multicomponent standard, London, UK, prepared December 16, 2015

Component	Mole fraction (nmol mol^{-1})	Tolerance (± nmol mol^{-1})
Ethane	4.06	0.08
Ethene	3.91	0.08
Propane	4.09	0.08
Propene	4.02	0.08
2-Methylpropane	4.20	0.11
Butane	3.98	0.08
Ethyne	4.13	0.21
t-But-2-ene	3.97	0.08
But-1-ene	3.98	0.08
c-But-2-ene	4.02	0.08
2-Methylbutane	4.05	0.08
Pentane	4.05	0.08
1,3-butadiene	3.97	0.08
t-Pent-2-ene	3.97	0.08
Pent-1-ene	3.98	0.08
2-Methylpentane	4.06	0.08
Hexane	3.99	0.08
Isoprene	4.03	0.09
Heptane	4.02	0.08
Benzene	4.00	0.08
2,2,4-Trimethylpentane	3.99	0.08
Octane	4.03	0.08
Toluene	4.00	0.10
Ethylbenzene	4.00	0.10
m-Xylene + p-Xylene	8.04	0.21
o-Xylene	4.00	0.10
1,3,5-Trimethylbenzene	4.01	0.11
1,2,4-Trimethylbenzene	4.03	0.11
1,2,3-Trimethylbenzene	4.04	0.11

(c) National Institutes of Standards and Technology monoterpene standard, Gaithersburg, MD, USA, prepared May 31, 2016

Component	Mole fraction (nmol mol^{-1})	Tolerance (± nmol mol^{-1})
n-Hexane	2.034	0.088
n-Octane	2.073	0.061
α-Pinene	2.078	0.074
3-Carene	2.028	0.088
R-Limonene	2.436	0.294
1,8-Cineole	2.053	0.162
β-Pinene	2.094	0.048
α-Terpinene	1.864	0.123
Camphene	1.882	0.050
p-Cymene	2.243	0.050

(d) Apel-Riemer Environmental, Inc. oxygenated VOC standard, Broomfield, CO, USA, prepared April 2010

Component	Mole fraction (nmol mol^{-1})	Tolerance (%)
Methanol	540	5
Acetone	538	5
Methyl Vinyl Ketone	506	5
Methacrolein	542	5
Isoprene	519	5

Table ST2. Mass Spectra of peak identifications that were not confirmed by standards and are considered 'tentative'. The left two columns give the peak retention time and the masses and relative abundances of the top five fragments in the mass spectra. The remaining columns show the top 3 matches given by the NIST spectral library. The compound name, top five fragments in the reference spectra, and library match percentage are shown. Matches are separated by dotted lines arranged by decreasing match confidence from left to right.

RT	Peak Mass (Rel. Ab.)	Best Match	Peak Mass (Rel. Ab.)	Library Match %	Next Match	Peak Mass (Rel. Ab.)	Library Match %	Next Match	Peak Mass (Rel. Ab.)	Library Match %
18.8	85(99.9), 60(83.2), 32(32.4), 87(27.9), 50(12.2)	Dichlorodifluoro methane	85(99.9), 87(31.2), 50(16.2), 31(12.4), 35(8.7)	73.7	Rubidium salt acetic acid	85(99.9), 87(39.8), 44(9.3), 43(4.0), 45(3.0)	19.1	Silicon tetrafluoride	85(99.9), 86(4.8), 87(3.2), 47(2.5), 33(1.2)	3.1
19.5	44(99.9), 29(47.4), 28(26.5), 43(17.3), 32(10.4)	Ethylene Oxide	29(99.9), 44(78.5), 15(55.0), 43(23.2), 14(20.9)	19.4	Hydroxyurea	44(99.9), 43(15.2), 42(5.0), 76 (4.6), 59(3.4)	71.0	Formic acid	44(99.9), 28(91.4), 43(67.6), 29(63.8), 15(30.6)	4.1
22.4	45(99.9), 43(24.6), 27(11.8), 29(7.6), 41(4.6)	Isopropyl alcohol	45(99.9), 43(19.1), 27(16.8), 29(12.5), 19(9.9)	62.2	Isopropyl lactate	45(99.9), 43(52.6), 41(13.0), 27(9.8), 89(4.6)	10.2	1,2-Propanediol	45(99.9), 43(15.4), 31(7.0), 44(6.0), 29(5.7)	6.6
23.4	59(99.9), 62(57.7), 47(45.3), 31(32.3), 45(29.1)	Dimethyl sulfide	47(99.9), 62(82.8), 45(62.0), 46(42.7), 35(34.8)	60.2	Dimethylphosphine	46(99.9), 62(78.6), 45(53.3), 59(25.3), 47(23.3)	26.1	Borane-methyl sulfide complex	62(99.9), 47(79.7), 61(37.9), 45(35.8), 46(30.2)	13.5
23.7	49(99.9), 84(66.8), 86(48.8), 28(26.3), 50(21.1)	Methylene chloride	49(99.9), 84(63.6), 86(39.3), 51(31.3), 47(13.9)	96.6	Dichloroacetaldehyde	49(99.9), 48(74.6), 84(64.8), 86(43.3), 51(35.5)	15.6	Trichloro-methane-D	84(99.9), 86(68.6), 47(17.5), 49(13.8), 88(11.0)	6.37
24.1	61(99.9), 46(51.1), 45(7.2), 44(4.6), 79(3.8)	Nitromethane	30(99.9), 61(53.5), 15(51.6), 46(35.5), 14(8.3)	87.7	N-methoxy-methanamine	46(99.9), 61(89.6), 28(65.8), 30(19.7), 60(16.2)	11.7	N,N',O-trimethyl-hydroxyurea	61(99.9), 46(61.0), 58(57.6), 60(18.2), 28(15.3)	0.5
24.2	76(99.9), 44(11.2), 32(10.2), 38 (8.3), 78 (5.2)	Carbon disulfide	76(99.9), 44(16.3), 32(14.2), 78(7.5), 38(4.7)	98.0	2-Butynedinitrile	76(99.9), 38(27.9), 12(17.2), 50(16.5), 62(10.0)	0.98	N-(dithiocarboxy)-N-methyl-glycine	44(99.9), 76(75.1), 42(25.1), 78(9.1), 40(7.8)	0.7
25.0	75(99.9), 45(13.9), 44(9.2), 47(8.6), 76(1.8)	Trimethyl silanol	75(99.9), 45(17.2), 47(14.1), 76(6.4), 77(4.3)	37.8	Trimethoxymethane	75(99.9), 31(34.3), 47(33.5), 15(15.8), 29(11.1)	27.4	Glycine	30(99.9), 28(20.7), 75(5.9), 45(3.2), 44(2.6)	18.8
25.7	43(99.9), 72(28.4), 32(10.6), 44(4.1), 42(3.9)	2-Butanone	43(99.9), 72(25.0), 29(17.0), 27(8.0), 57(8.0)	90.6	Methyl glyoxal	43(99.9), 15(26.4), 29(20.3), 45(15.1), 42(7.8)	6.6	N,N'-ethylenebis(N-nitro)-acetamide	43(99.9), 72(2.8), 46(2.5), 39(1.8), 55(1.5)	5.8

26.1	56(99.9), 41(66.9), 55(41.8), 44(22.1), 69(18.1)	2-Methyl-1-pentene	56(99.9), 41(79.7), 55(42.7), 39(39.5), 69(36.3)	50.6	Ethylcyclobutane	56(99.9), 41(69.1), 39(31.1), 55(30.8), 28(27.9)	13.9	Cyclohexane	56(99.9), 84(70.5), 41(67.6), 55(34.1), 42(31.0)	7.7
26.4	43(99.9), 71(67.6), 59(33.9), 28(21.5), 27(19.3)	2-Methyl-3-buten-2-ol	71(99.9), 43(81.0), 59(33.3), 41(31.9), 27(23.3)	62.2	4-methyl-2,3-Pentanedione	43(99.9), 41(18.7), 71(14.1), 27(12.7), 28(7.2)	20.2	1-Hydroxy-3-methyl-2-butanone	43(99.9), 71(51.6), 41(28.5), 28(18.6), 27(17.9)	4.4
26.5	57(99.9), 43(95.0), 41(91.5), 56(45.5), 29(28.2)	2-azido-2,3,3-trimethyl-butane	57(99.9), 41(42.0), 56(40.0), 43(25.0), 42(15.0)	52.4	N-methoxycarbonyloxy-1,1-dimethylethylamine	57(99.9), 43(71.2), 56(70.0), 44(41.2), 41(35.2)	29.0	2,2,4-trimethyl-Pentane	57(99.9), 41(30.9), 56(28.3), 43(23.8), 29(15.8)	5.4
27.1	42(99.9), 41(60.9), 72(42.1), 71(36.5), 44(19.8)	Tetrahydrofuran	42(99.9), 41(43.7), 72(38.2), 71(33.8), 43(15.5)	90.2	Ethyl oxirane	42(99.9), 41(92.6), 27(39.1), 72(34.0), 29(30.3)	7.3	4-ethyl-1,3-dioxolane	42(99.9), 71(50.9), 41(49.6), 27(29.4), 29(28.9)	2
27.5	59(99.9), 32(62.8), 73(37.5), 41(31.4), 58(20.9)	2-Methyl-pentan-3-ol	59(99.9), 73(47.3), 31(23.6), 55(19.2), 41(18.4)	70.5	2-methoxy-butane	59(99.9), 29(35.0), 27(19.1), 41(17.5), 15(16.3)	40.9	Trimethyl silane	59(99.9), 73(55.5), 43(17.5), 58(16.0), 45(9.4)	13.0
28.0	43(99.9), 41(14.7), 86(14.1), 28(8.0), 32(7.9)	3-Methyl-2-butanone	43(99.9), 86(21.1), 41(15.2), 27(7.9), 71(6.0)	86.0	2-Pentanone	43(99.9), 86(19.9), 41(11.2), 58(8.9), 71(8.6)	7.3	2,3-Butanedione	43(99.9), 15(33.9), 86(11.1), 14(10.5) 42(7.2)	4.8
29.7	57(99.9), 32(93.2), 41(59.9), 44(56.5), 43(39.5)	3,3-Dimethyl-2-butanone	57(99.9), 41(49.2), 43(29.2), 29(27.2), 100(20.1)	90.0	di-tert-Butyl dicarbonate	57(99.9), 41(18.6), 43(8.8), 59(8.2), 56(6.5)	45	2,5-di-tert-butyl-3,4-bis(trifluoromethyl)-thiolane-3,4-dicarbonitrile	57(99.9), 41(21.0), 40(9.9), 39(5.9), 58(4.4)	21.8
32.3	44(99.9), 28(70.6), 41(62.2), 43(60.7), 56(53.9)	Hexanal	44(99.9), 56(77.3), 41(69.4), 43(62.3), 27(52.9)	64.9	Homoserine	56(99.9), 43(84.7), 28(72.7), 57(61.8), 42(61.3)	12.8	α-Amino-γ-butyrolactone	43(99.9), 57(77.6), 28(54.1), 56(53.8), 42(39.5)	7.7
33.4	54(99.9), 67(66.7), 41(47.8), 110(28.6), 39(27.3)	1,3-Octadiene	54(99.9), 67(83.6), 41(57.0), 110(43.8), 39(43.0)	31.0	Norbornadieone	67(99.9), 54(58.9), 110(44.2), 41(33.8), 39(28.8)	26.5	2,3-Diazabicyclo[2.2.2]oct-2-ene	54(99.9), 41(91.8), 67(81.1), 39(54.7), 27(44.8)	6.44
38.5	57(99.9), 97(83.8), 44(30.8), 83(20.3), 69(18.4)	2,2,4,6,6-pentamethyl-3-Heptene	57(99.9), 97(94.4), 41(48.3), 69(29.4), 55(28.0)	37.1	2,4,4-Trimethyl-1-pentanol, trifluoroacetate	57(99.9), 97(33.2), 55(28.8), 41(27.9), 69(18.3)	27.7	Isobutyl ester cyclohexylmethyl-sulfurous acid	97(99.9), 55(59.1), 57(38.2), 41(24.6), 83(18.0)	10.1

Table ST3. Proposed compound identifications and comparisons to Agilent [*Agilent*, 2014], NACHTT [*Brown et al.*, 2013], and Air Toxics program [*Apel et al.*, 1998] elution order reference data. Because of the agreement between compound identifications and reference elution orders, identifications of compounds present in one of these references are considered confirmed. An 'x' is placed in the Tentative ID column for any compounds that are not supported by elution order data from any of these references. Our identifications of these compounds should be regarded as tentative because they are based only on the best match from the NIST Spectral Library (Table ST2).

Compound	RT (min)	Reference RT (min)			Tentative ID
		Agilent	NACHTT	Air Toxics	
Dichlorodifluoromethane	18.8		7.28	3.47	
Ethylene oxide	19.5				x
2-Butene	19.9				x
Acetone	22.1	4.05	13.36	7.19	
Isopropyl Alcohol	22.4	4.27			
Pentane	23.1	3.37		6.03	
Dimethyl Sulfide	23.4		13.33		
Methylene chloride	23.7	4.8	14.06		
Nitromethane	24.1				x
Carbon Disulfide	24.2	4.27	13.44	7.57	
Trimethylsilanol	25				x
2-Butanone	25.7	7.19	16.01	11.26	
2-Methyl-1-pentene	26.1				x
2-Methyl-3-buten-2-ol	26.4	7.91	16.54		
2-Azido-2,3,3-trimethyl-butane	26.5				x
Tetrahydrofuran	27.1	7.64			
2-Methyl-3-pentanol	27.5				x
3-Methyl-2-butanone	28	9.21			
3,3-Dimethyl-2-butanone	29.7				x
Hexanal	32.3	13.14		19.32	
1,3-Octadiene	33.4				x
2,2,4,6,6-Pentamethyl-3-heptene	38.5				x

Table ST4. Standard components used to build response factor calibration curve. Abbreviations in the standard column are 'EA' for Apel-Riemer Multicomponent Standard, 'NPL' for National Physical Laboratory multicomponent standard, 'MONO' for NIST Monoterpene standard, 'OVOC' for NIST oxygenated VOC standard. Retention times (RT) and effective carbon numbers [Scanlon, 1985] are listed. Italicized compounds were excluded from the final calibration curve because their residuals were greater than three standard deviations from the curve.

Compound	Standard	RT	Average Response (Counts ppb^{-1} L^{-1})	Effective Carbon Number	Response per carbon (Counts ppb^{-1} L^{-1} ECN^{-1})
2-Butene	EA	20.4	60800	3.9	15600
2-Butene	EA	20.7	56900	3.9	14600
1-Pentene	EA	22.6	71100	4.9	14500
2-Methyl 1,3-butadiene	EA	23.3	83400	4.9	17000
1-Hexene	EA	27.1	60600	5.9	10300
1-Heptene	EA	29.5	82600	6.9	12000
Isobutane	EA	19.5	58900	4.0	14700
n-Butane	EA	20.2	60300	4.0	15100
n-Pentane	EA	23.1	75200	5.0	15000
Cyclopentane	EA	25.0	77200	5.0	15400
Hexane	EA	26.6	85700	6.0	14300
n-Heptane	EA	29.9	82100	7.0	11700
Methylcyclohexane	EA	30.8	84700	7.0	12100
n-Octane	EA	32.9	69800	8.0	8720
Toluene	EA	31.9	69100	7.0	9880
Ethylbenzene	EA	34.6	48100	8.0	6010
m,p-Xylene	*EA*	*35.5*	*16300*	*8.0*	2040
o-Xylene	*EA*	*37.4*	*17200*	*8.0*	2150
n-Hexane	MONO	22.3	83900	6.0	14000
n-Octane	MONO	28.3	106000	8.0	13300
α-Pinene	*MONO*	*32.2*	*19500*	*9.9*	1970
Camphene	MONO	32.7	70800	9.9	7150
β-Pinene	*MONO*	*33.4*	*137000*	*9.9*	13900
3-Carene	MONO	34.0	72600	9.9	7340
α-Terpinene	MONO	34.2	69300	9.8	7070
Limonene	MONO	34.4	67800	9.8	6920
p-Cymene	*MONO*	*34.5*	*121000*	*9.7*	12500
1,8-Cineole	MONO	34.7	85800	9.0	9530
1-Butene	NPL	19.9	53500	3.9	13700
2-Butene	NPL	20.4	61200	3.9	15700
2-Butene	NPL	20.7	60000	3.9	15400
1-Pentene	NPL	22.6	74700	4.9	15200

2-Pentene	NPL	23.3	76300	4.9	15600
Isobutane	NPL	19.5	61700	4.0	15400
n-Butane	NPL	20.2	67500	4.0	16900
n-Pentane	NPL	23.1	68900	5.0	13800
n-Hexane	NPL	26.6	85400	6.0	14200
2,2,4-Trimethylpentane	NPL	29.6	93500	8.0	11700
n-Heptane	NPL	29.9	84200	7.0	12000
n-Octane	NPL	32.9	70700	8.0	8840
Benzene	NPL	28.5	77000	6.0	12800
Toluene	NPL	31.9	80900	7.0	11600
Ethylbenzene	*NPL*	*34.8*	94400	*8.0*	11800
Acetone	OVOC	22.1	25900	2.0	12900
Methacrolein	OVOC	23.4	37200	2.9	12800
Methylvinylketone	*OVOC*	*24.1*	28100	*2.9*	9700

Supplemental Material:

Chapter 7

A phylogenetic and functional perspective on volatile organic compound production by Actinobacteria

Mallory Choudoir[1], Sam Rossabi[1,2], Matthew Gebert[1], Detlev Helmig[2], and Noah Fierer*[1,3]

[1]Cooperative Institute for Research in Environmental Sciences, University of Colorado-Boulder, Boulder, CO, USA;
[2]Institute of Arctic and Alpine Research, University of Colorado-Boulder, Boulder, CO, USA;
[3]Department of Ecology and Evolutionary Biology, University of Colorado-Boulder, Boulder, CO USA

***Corresponding Author: Noah Fierer Noah.Fierer@colorado.edu

Table S1. Table reports strain name, taxonomic classification, culture collection, isolation information, and NCBI accession numbers (when available) for the 48 actinobacterial strains used in this study. 16S rRNA gene sequences are located in the supplementary data fasta file named Actinobacteria_16S_sequences.fa. The 24 strains used for the pseudomonad growth assay are indicated with asterisks. Originating culture collections include the Agricultural Research Service (NRRL) culture collection (https://nrrl.ncaur.usda.gov/) (Peoria, IL, USA), Fierer Lab culture collection (University of Colorado Boulder, Boulder, CO, USA), and Buckley Lab culture collection (Cornell University, Ithaca, NY, USA). See Table S2 for media recipes. Fierer Lab strains were isolated from surface soils (0–5 cm) sampled from a sub-alpine forest in Boulder Country (Boulder, CO, USA) and from airborne dust sample from glass bead traps installed at the Boulder Atmospheric Observatory (BAO) research tower (Erie, CO, USA) for two weeks during June 2016. Buckley Lab strains were isolated from grassland soils across the United States (see Andam *et al.*, 2016 and Choudoir *et al.*, 2016).

Strain	Family	Genus	Species	Culture Collection	Isolation Media	Source	NCBI Accession
B16927*	*Streptomycetaceae*	*Streptomyces*	*atratus*	ARS NRRL	unknown	unknown	NR_043490
B2000*	*Streptomycetaceae*	*Streptomyces*	*anulats*	ARS NRRL	unknown	unknown	NR_043489
B2682*	*Streptomycetaceae*	*Streptomyces*	*griesus*	ARS NRRL	unknown	unknown	SAMN05558834
B2690*	*Streptomycetaceae*	*Streptomyces*	*bikiniensis*	ARS NRRL	unknown	unknown	SAMN02645389
B2808*	*Streptomycetaceae*	*Streptomyces*	*aureus*	ARS NRRL	unknown	unknown	SAMN04002963
CLCC1251	*Nocardioidaceae*	*Kribella*		Fierer Lab	RM	sub-alpine forest soil	
CLCC1393*	*Nocardiaceae*	*Rhodococcus*		Fierer Lab	RM	sub-alpine forest soil	
CLCC1488	*Pseudonocardiaceae*	*Amycolatopsis*		Fierer Lab	RM	sub-alpine forest soil	
CLCC371A	*Nocardioidaceae*	*Nocardioides*		Fierer Lab	RM	sub-alpine forest soil	
CLCC460	*Pseudonocardiaceae*	*Amycolatopsis*		Fierer Lab	RM	sub-alpine forest soil	
CLCC501	*Mycobacteriaceae*	*Mycobacterium*		Fierer Lab	RM	sub-alpine forest soil	
CLCC567*	*Microbacteriaceae*	*Clavibacter*	*michiganensis*	Fierer Lab	RM	sub-alpine forest soil	
CLCC686	*Streptomycetaceae*			Fierer Lab	RM	sub-alpine forest soil	

360

CLCC811	*Streptomycetaceae*	*Streptomyces*		Fierer Lab	RM	sub-alpine forest soil	
CLCC866	*Actinosynnemataceae*	*Kibdelosporangium*		Fierer Lab	RM	sub-alpine forest soil	
FLCC167	*Microbacteriaceae*	*Clavibacter*	*michiganensis*	Fierer Lab	CN Gellan	airborne dust	
FLCC191*	*Micrococcaceae*	*Microbispora*		Fierer Lab	CN Gellan	airborne dust	
FLCC204	*Promicromonosporaceae*	*Promicromonospora*		Fierer Lab	CN Gellan	airborne dust	
FLCC211	*Micrococcaceae*	*Kocuria*		Fierer Lab	CN Gellan	airborne dust	
FLCC251*	*Mycobacteriaceae*	*Mycobacterium*		Fierer Lab	CN Gellan	airborne dust	
FLCC270*	*Mycobacteriaceae*	*Mycobacterium*		Fierer Lab	CN Gellan	airborne dust	
FLCC291*	*Promicromonosporaceae*	*Promicromonospora*		Fierer Lab	CN Gellan	airborne dust	
FLCC336	*Microbacteriaceae*	*Rathayibacter*	*caricis*	Fierer Lab	CN Gellan	airborne dust	
FLCC365	*Micromonosporaceae*			Fierer Lab	CN Gellan	airborne dust	
FLCC378	*Nocardiaceae*	*Rhodococcus*		Fierer Lab	CN Gellan	airborne dust	
FLCC382	*Micrococcaceae*			Fierer Lab	CN Gellan	airborne dust	
FLCC400	*Nocardioidaceae*	*Aeromicrobium*		Fierer Lab	CN Gellan	airborne dust	
FLCC424	*Microbacteriaceae*	*Frigoribacterium*		Fierer Lab	CN Gellan	airborne dust	
FLCC425	*Williamsiaceae*	*Williamsia*		Fierer Lab	CN Gellan	airborne dust	
FLCC45*	*Nocardiaceae*	*Rhodococcus*		Fierer Lab	CN Gellan	airborne dust	
FLCC483*	*Brevibacteriaceae*	*Brevibacterium*		Fierer Lab	ISP2	airborne dust	
FLCC487	*Dietziaceae*	*Dietzia*		Fierer Lab	ISP2	airborne dust	
FLCC517*	*Micrococcaceae*	*Kocuria*		Fierer Lab	ISP2	airborne dust	
FLCC536*	*Microbacteriaceae*	*Curtobacterium*		Fierer Lab	ISP2	airborne dust	
FLCC572*	*Dietziaceae*	*Dietzia*		Fierer Lab	ISP2	airborne dust	
FLCC580	*Corynebacteriaceae*	*Corynebacterium*		Fierer Lab	ISP2	airborne dust	
FLCC594*	*Streptomycetaceae*	*Streptomyces*		Fierer Lab	ISP2	airborne dust	
FLCC627*	*Micrococcaceae*	*Citricoccus*		Fierer Lab	ISP2	airborne dust	

FLCC649	*Micrococcaceae*	*Citricoccus*	*alkalitolerans*	Fierer Lab	ISP2	airborne dust	
FLCC662	*Brevibacteriaceae*	*Brevibacterium*		Fierer Lab	ISP2	airborne dust	
FLCC663*	*Dietziaceae*	*Dietzia*		Fierer Lab	ISP2	airborne dust	
FLCC678	*Brevibacteriaceae*	*Brevibacterium*		Fierer Lab	ISP2	airborne dust	
FLCC682*	*Microbacteriaceae*	*Agrococcus*	*jenensis*	Fierer Lab	ISP2	airborne dust	
FLCC712*	*Microbacteriaceae*			Fierer Lab	ISP2	airborne dust	
ms115*	*Streptomycetaceae*	*Streptomyces*	*griesus*	Buckley Lab	GA	grassland soil	SAMN07606150
or3*	*Streptomycetaceae*	*Streptomyces*	*griesus*	Buckley Lab	GA	grassland soil	SAMN07606152
t99*	*Streptomycetaceae*	*Streptomyces*	*griesus*	Buckley Lab	GA	grassland soil	SAMN07606163
wa1063	*Streptomycetaceae*	*Streptomyces*	*griesus*	Buckley Lab	GA	grassland soil	SAMN07606165

Table S2. Table reports media recipes for actinobacterial strain isolation, volatile organic compound (VOC) surveys, and pseudomonad growth assays.

CN Gellan (Gavrish *et al.* 2008)

Casamino acids	1	g
Nutrient broth (Difco)	1	g
Gellan gum	12	g
H2O	1000	mL

Autoclave

Glycerol Arginine (GA) (El-Nakeeb and Lechevalier 1963)

Glycerol	12.5	g
Arginine	1	g
NaCl	1	g
K2HPO4	1	g
MgSO4 7H2O	0.5	g
Fe2(SO4)3 6H2O	0.01	g
CuSO4 5H2O	0.001	g
ZnSO4 7H2O	0.001	g
MnSO4 H2O	0.001	g
Agar	15	g
H2O	1000	mL

Adjust pH to 8.7, autoclave

ISP2 (Shirling and Gottlieb 1966)

Yeast extract	4	g
Malt extract	10	g
Dextrose	4	g

Arginine*	2.5	g
Agar	20	g
H20	1000	mL

Autoclave

*Arginine was added to this recipe to stimulate sporulation

King's B *Pseudomonas* Media (King *et al.* 1954)

Peptone	20	g
Glycerol	10	g
K2HPO4	1.5	g
Agar	15	g
H20	1000	mL

Adjust pH to 7.2 , autoclave, adjust to 1 M MgSO4

Robin's Media (RM)

Salts		
2-(N-morpholino)ethanesulfonic acid	1.95	g
MgSO4	0.02	g
CaCl2	0.03	g
Amino Acids		
Serine	0.03	g
Glycine	0.01	g
Homosysteine	0.03	g
Isoleucine	0.03	g
Valine	0.03	g
Leucine	0.03	g
Arginine	0.04	g

Histidine	0.04	g
Tryptophan	0.05	g
Phenylalanine	0.04	g
Tyrsoine	0.05	g

Carbon Source

Malt extract	1	g
Agar	7.5	g
H2O	1000	mL

Adjust pH to 5.0, autoclave

After autoclaving, add:

Ammonium phosphate solution	1	mL
Selenite-tungstate solution	1	mL
Vitamin solution 1	1	mL
Vitamin solution 2	3	mL
Trace element soution SL-10 + Lanthinum	1	mL

Table S3. We identified a total of 126 volatile organic compounds (VOCs) produced by 48 actinobacterial strains. Table reports the presence (1) or absence (0) of distinct VOCs ordered by retention index and rentention time (min) for each strain grown on glycerol arginine (GA) and ISP2 media. Rows with 'NA' indicate the 18 and 2 strains that did not grow glycerol arginine (GA) and ISP2 media, respectively. Total VOCs are the number of compounds identified as distinct peaks in FID chromatograms. Columns highlighted in grey denote peaks identified by their mass spectra (Table S4). Asterisks indicate compounds detected in the ISP2 media blanks but not the GA media blanks, and these compounds could represent sterile media emissions.

(Table S3 is available in the supplemental file Supplement-Chapter7-TableS3_voc_table.xlsx)
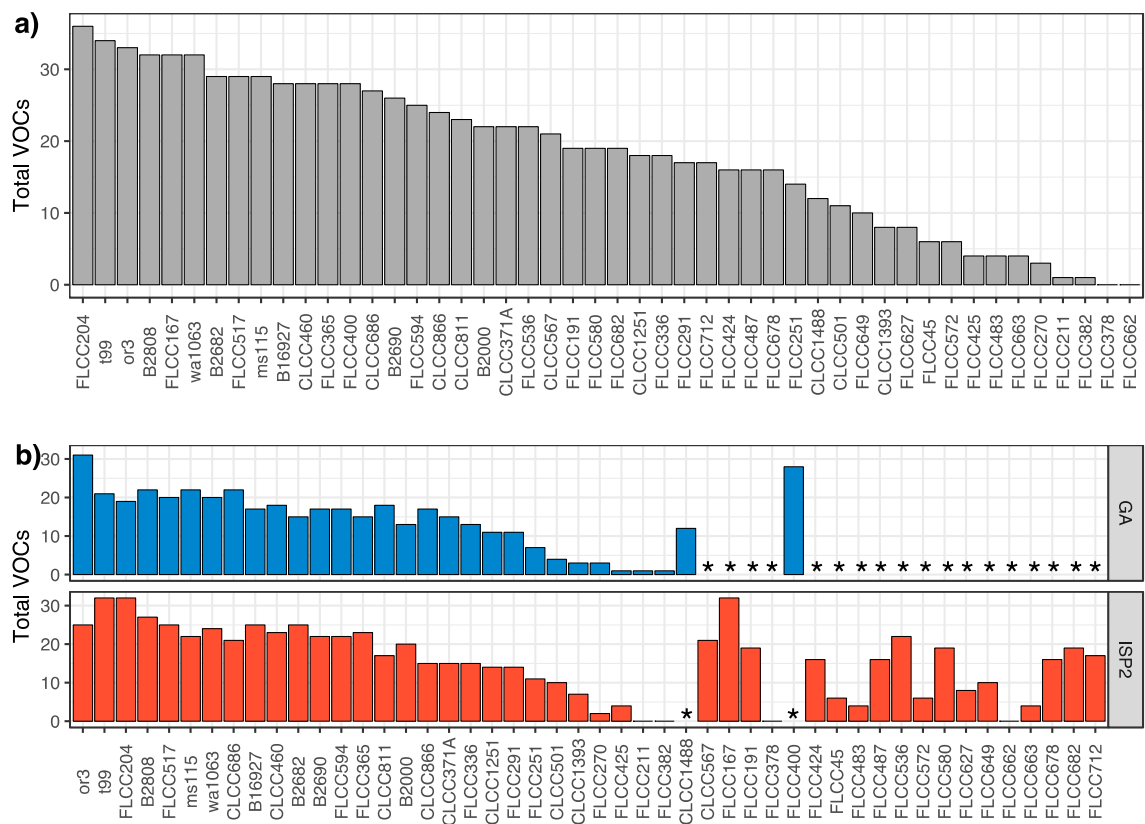
Figure S1. The number of VOCs produced varied between actinobacterial strains. Bars show the total number of distinct VOCs detected (S1a) and the total number of distinct VOCs detected on glycerol arginine (GA) and ISP2 media (S1b) for each strain. Strains unable to grow on GA or ISP2 media are marked with asterisks (S1b).
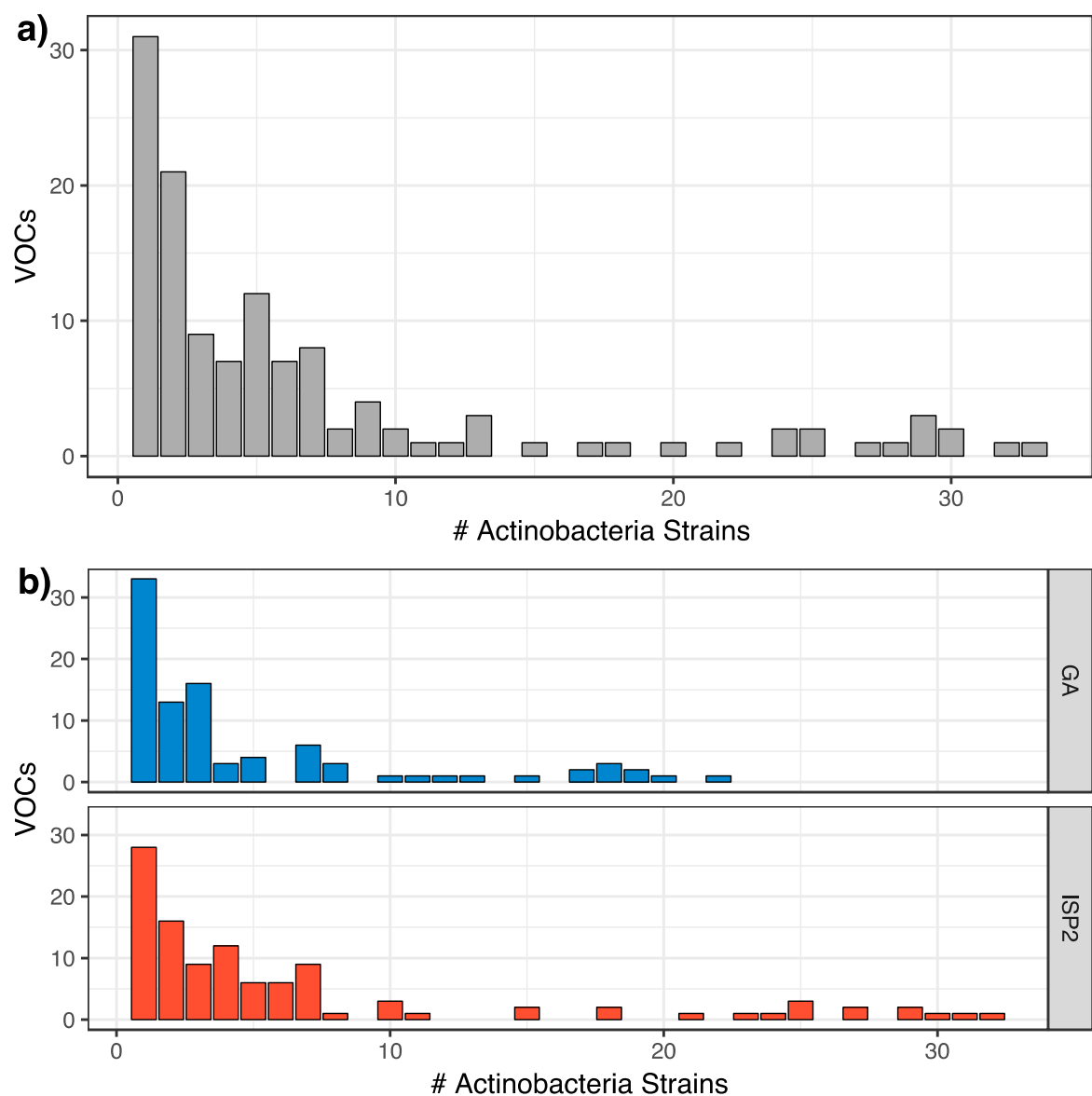
Figure S2. Most volatile organic compounds (VOCs) were produced by few actinobacterial strains, and few VOCs were produced by many strains. The histogram depicts the frequency distribution of distinct VOCs produced by actinobacterial strains (2a) and of VOCs produced on glycerol arginine (GA) and ISP2 media (2b). Strains that did not grow on a given media type and strains that produced no detectable VOCs were removed.
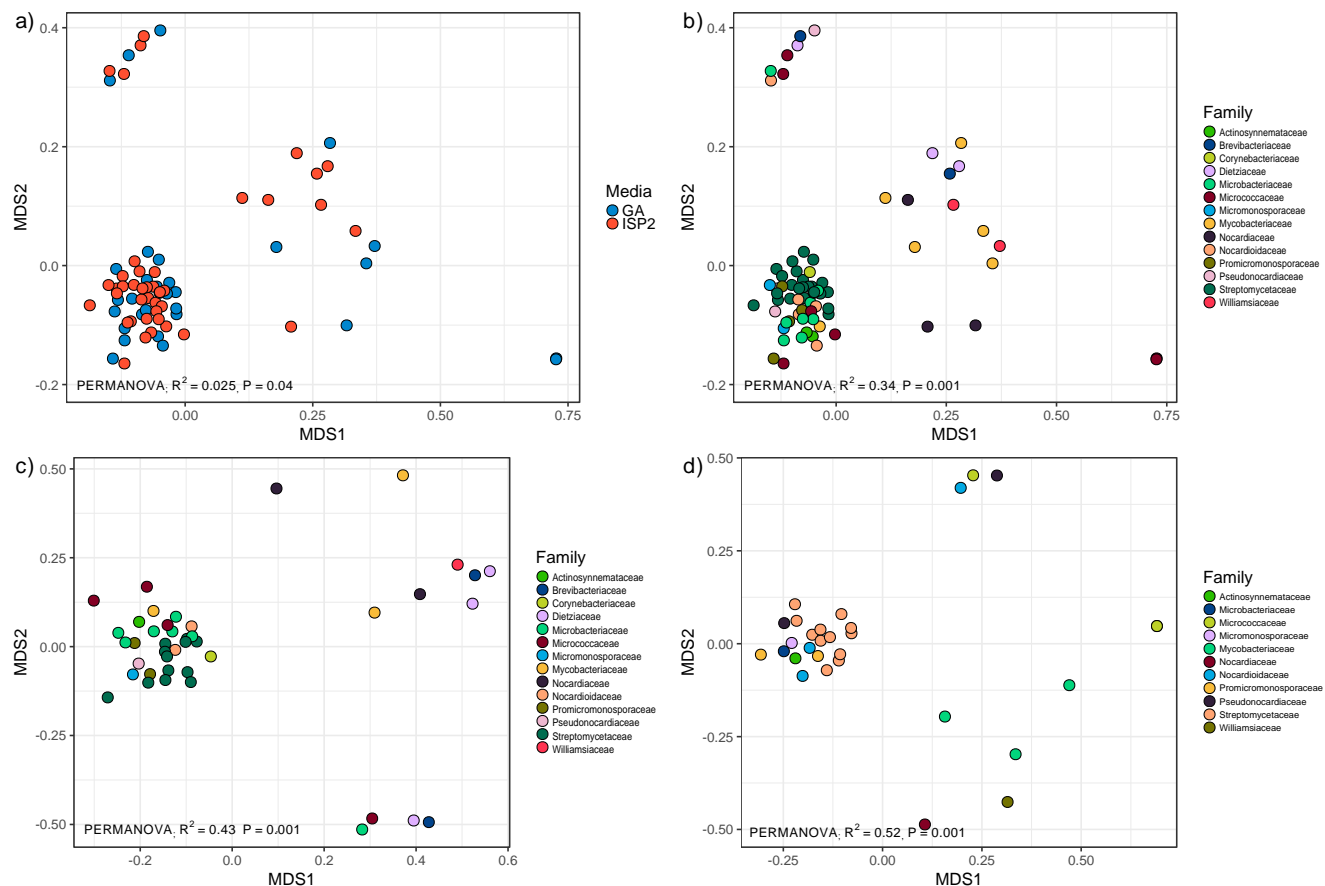
Figure S3. Non-metric multidimensional scaling (NMDS) illustrates the differentiation of actinobacterial volatile organic compound (VOC) emission profiles. Each point depicts the Jaccard distances between VOC profiles of strains grown on glycerol arginine (GA) and ISP2 media (S3a-b) and on GA (S3c) and ISP2 media alone (S3d). Strains that did not grow on a given media type and strains that produced no detectable VOCs were removed to minimize distance in the matrix. Points are colored to reflect the variation explained by media type (S3a) and by taxonomic assignment at the family level (S3b-d) according to the legend.
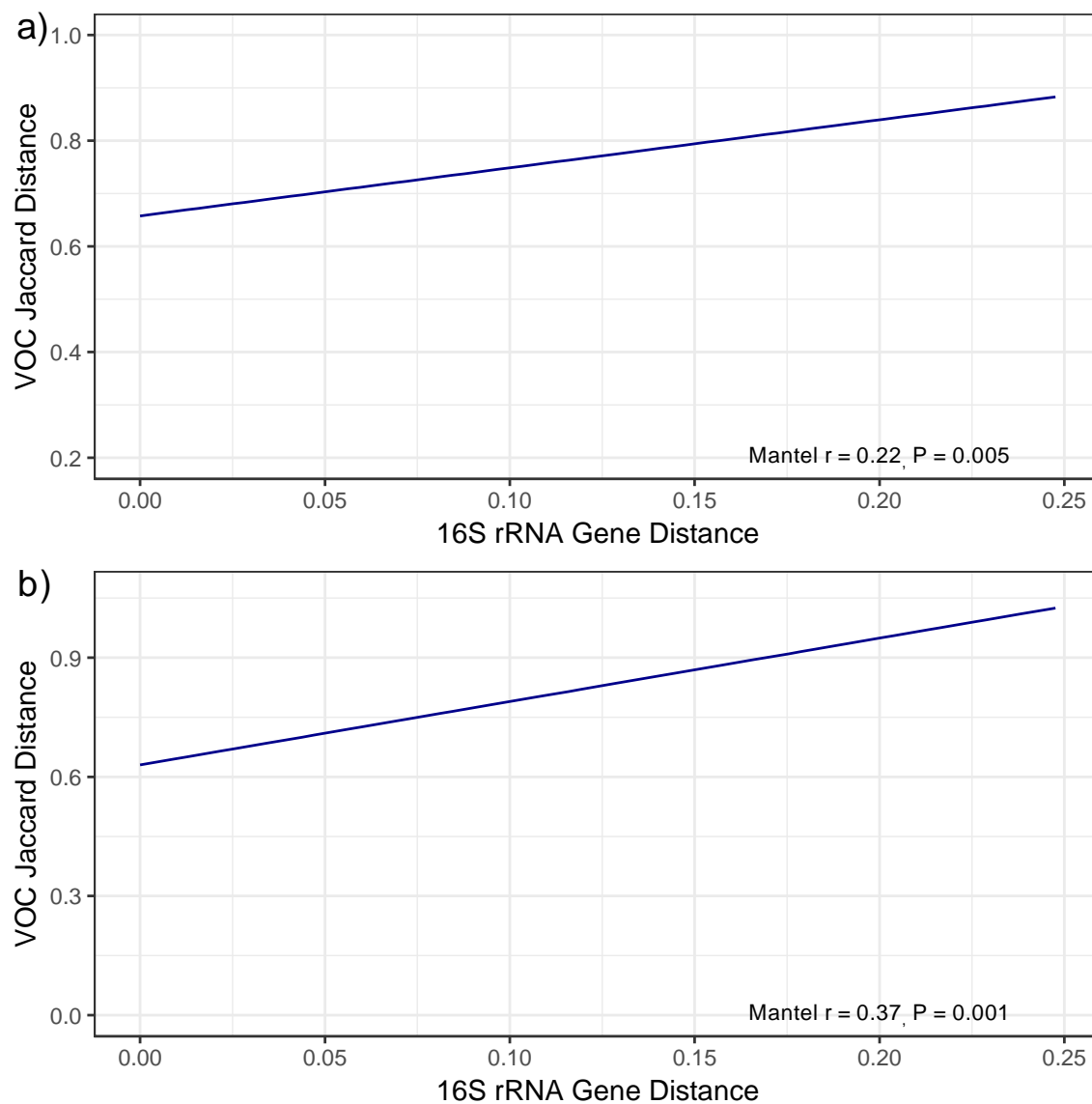
a)

b)

Figure S4. Actinobacterial VOC profiles were more different with increasing genetic distance. Each point depicts the pairwise comparisons between VOC profile Jaccard dissimilarities and 16S rRNA gene nucleotide distances for compounds detected on ISP2 (S4a) and glycerol arginine (GA) media (S4b). Strains that did not grow on a given media type and strains that produced no detectable VOCs were removed to minimize distance in the matrix. Blue lines depict the linear regression with gray shading indicating 95% confidence intervals.
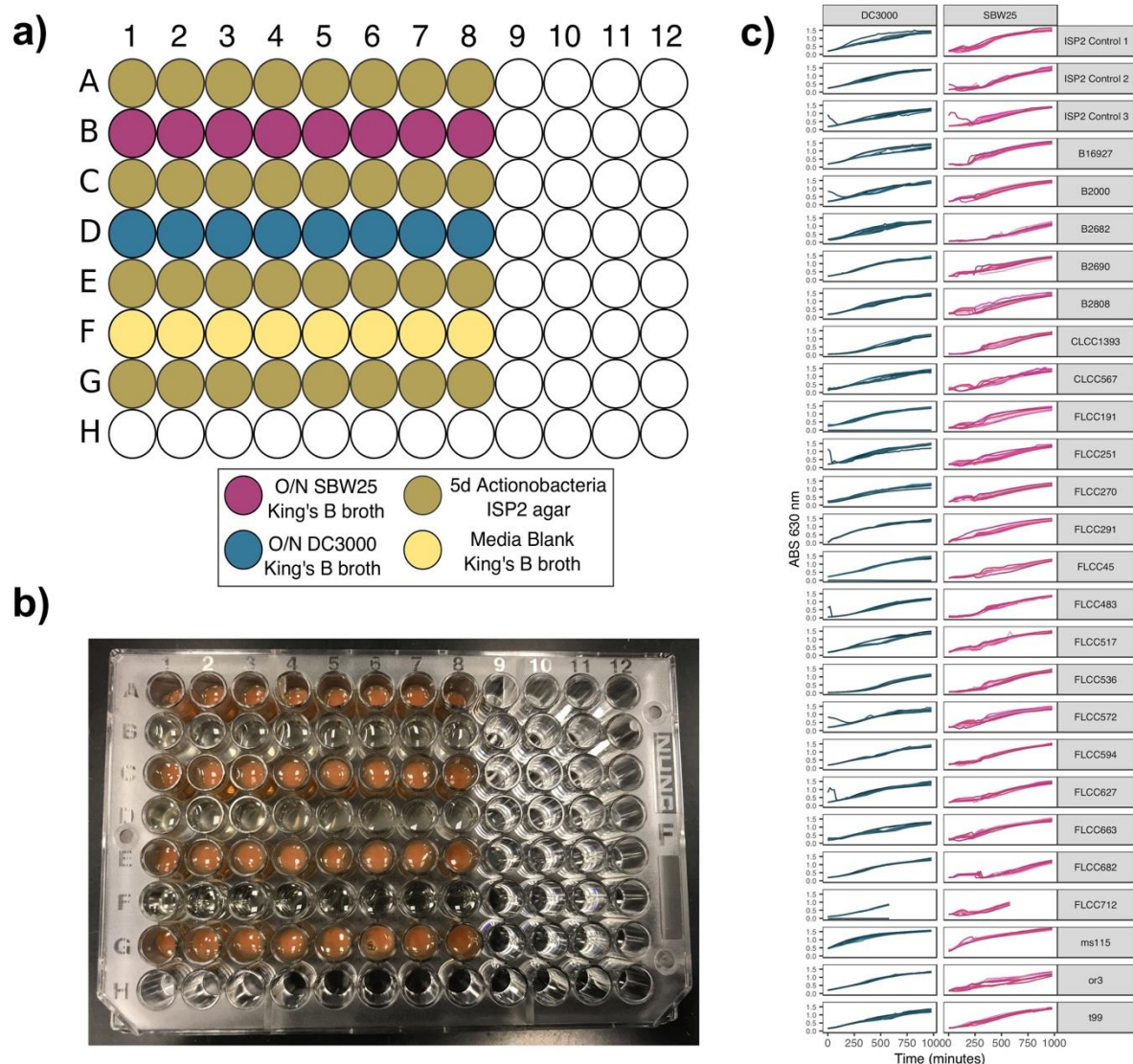
Figure S5. Non-pathogenic *Pseudomonas fluoresens* SBW25 (SBW25) and pathogenic *Pseudomonas syringae* pv. tomato DC3000 (DC3000) were exposed to VOCs produced by actinobacterial strains throughout exponential growth (see Materials and Methods). Briefly, actinobacterial cell suspensions were plated onto ISP2 agar on alternating rows of a 96-well culture plate and incubated for 5 d at 30 ˚C (S5a). Overnight (O/N) cultures of pseudomonad test strains were diluted into fresh King's B media (OD 600 nm = 0.05) and transferred into culture plates (S5a). Thus, the O/N pseudomonad cultures shared a headspace with 5 d actinobacterial strain cultures, allowing mVOCs to diffuse across the plate (S5b). The culture plate was incubated at 24 ˚C with shaking on the plate reader. Absorbance at 630 nm was measured every 20 min for a total of 980 min, and the absorbance values of media blanks were subtracted from each measurement (S5c).

Table S4. Chemical identity of MS-verified VOCs. Of the 126 distinct volatile organic compounds (VOCs) detected, we were able to identify the chemical structures of 28 compounds from their mass spectra. For each compound, the retention time (min), retention index, compound identity, the mass spectra (m/z relative abundance), the mass

spectra for the top match from the NIST mass spectral search program, and the percent library match are reported. To note, two identified compounds co-eluted at the same retention time of 31.1 min, 3-methyl-2-pentanone and dimethyldisulfide. Asterisks indicate compounds detected in the ISP2 media blanks but not the GA media blanks, and these compounds could represent sterile media emissions.

Retention Time (min)	Retention Index	Compound ID	Peak Mass Spectrum	Best Match Mass Spectrum	% Library match
19.6		Methanol	31 (999), 32 (760), 30 (60), 44 (57), 41 (6)	31 (999), 32 (743), 29 (445), 15 (123), 30 (64)	89.2
20.4	406.9	Methanethiol	47 (999), 48 (888), 45 (351), 41 (21), 37 (20)	47 (999), 48 (899), 45 (474), 46 (115), 15 (96)	94.6
20.7	417.2	Trimethylamine	58 (999), 59 (483), 42 (284), 30 (144), 57 (61)	58 (999), 59 (466), 42 (351), 30 (134), 43 (81)	83.7
20.9	424.1	Ethanol	31 (999), 45 (665), 44 (591), 46 (296), 43 (113)	31 (999), 45 (572), 46 (245), 27 (176), 29 (119)	76.3
21.6	448.3	Acetonitrile*	41 (999), 40 (519), 32 (316), 39 (101), 38 (42)	41 (999), 40 (455), 39 (132), 14 (87), 38 (59)	79.6
22.4	475.9	Isopropyl alcohol	45 (999), 43 (177), 44 (86), 42 (20), 41 (20)	45 (999), 43 (142), 27 (93), 41 (62), 29 (53)	6.87
23.4	508.6	2-Methyl-2-propanol	59 (999), 31 (206), 41 (159), 43 (61), 39 (45)	59 (999), 31 (377), 41 (257), 43 (167), 39 (111)	79.6
23.5	511.4	Acetic acid methyl ester	43 (999), 74 (283), 59 (107), 42 (102), 44 (25)	43 (999), 74 (214), 15 (150), 42 (79), 59 (64)	85.8
24.1	528.6	Nitromethane	61 (999), 46 (515), 30 (456), 32 (326), 44 (238)	30 (999), 61 (570), 15 (480), 46 (370), 29 (110)	91.4
24.2	531.4	Carbon disulfide	76 (999), 32 (269), 44 (101), 78 (64), 53 (50)	76 (999), 44 (163), 32 (142), 78 (75), 38 (47)	98.6
25.4	565.7	Acetic acid ethenyl ester	43 (999), 86 (94), 44 (89), 32 (67), 42 (34)	43 (999), 15 (110), 27 (67), 86 (65), 42 (63)	82.0

26.1	585.7	2-Butanol	45 (999), 59 (218), 43 (200), 44 (133), 31 (125)	45 (999), 59 (225), 31 (142), 41 (112), 43 (101)	70.4
27.0	603.0	2-Methyl-1-propanol	43 (999), 41 (681), 42 (638), 33 (569), 39 (231)	43 (999), 33 (679), 41 (679), 42 (679), 31 (572)	91.7
28.0	642.4	3-Methyl-2-butanone	43 (999), 86 (163), 41 (130), 39 (64), 44 (29)	43 (999), 86 (211), 41 (152), 27 (79), 71 (60)	63.4
28.1	645.5	1-Butanol	56 (999), 41 (678), 43 (581), 42 (327), 55 (198)	31 (999), 56 (992), 41 (918), 43 (827), 42 (548)	62.8
28.8	666.7	2-Pentanone	43 (999), 86 (163), 41 (101), 42 (67), 39 (61)	43 (999), 86 (197), 41 (138), 58 (98), 71 (97)	81.8
28.9	669.7	2,3-Pentanedione	43 (999), 57 (444), 100 (216), 42 (52), 44 (49)	43 (999), 29 (608), 57 (328), 27 (258), 15 (143)	85.3
29.1	675.8	3-Pentanone	57 (999), 86 (241), 32 (133), 44 (103)	57 (999), 29 (593), 86 (211), 27 (123), 28 (42)	95.4
29.3	681.8	3-Hydroxy-2-butanone	45 (999), 43 (587), 42 (64), 88 (63), 44 (34)	45 (999), 43 (533), 27 (69), 88 (64), 29 (58)	48.7
29.7	693.9	Acetic acid propyl ester	43 (999), 61 (285), 44 (94), 42 (84), 41 (35)	43 (999), 61 (226), 73 (99), 42 (78), 41 (55)	61.5
30.1	706.7	Butanoic acid methyl ester	43 (999), 74 (928), 71 (469), 59 (124), 41 (103)	43 (999), 74 (871), 71 (654), 41 (381), 59 (311)	64.2
30.3	713.3	Pyrazine*	80 (999), 53 (382), 52 (136), 40 (54), 51 (54)	80 (999), 53 (452), 26 (422), 52 (103), 51 (70)	85.1
30.4	716.7	3-Methyl-1-butanol	55 (999), 42 (772), 70 (674), 43 (631), 41 (578)	55 (999), 42 (870), 70 (696), 43 (689), 41 (598)	64.9
30.6	723.3	2-Methyl-1-butanol	57 (999), 56 (865), 41 (813), 70 (416), 55 (248)	41 (999), 57 (779), 56 (728), 29 (640), 31 (388)	62.8

31.1	740.0	3-Methyl-2-pentanone	43 (999), 57 (311), 41 (249), 72 (199), 56 (133)	43 (999), 29 (337), 57 (274), 41 (262), 72 (171)	82.7
31.1	740.0	Dimethyldisulfide	94 (999), 79 (489), 45 (451), 43 (324), 46 (271)	94 (999), 79 (570), 45 (478), 46 (250), 47 (193)	91.0
31.7	760.0	2,3-Hexanedione	43 (999), 71 (160), 41 (142), 44 (52), 114 (17)	43 (999), 41 (214), 71 (199), 27 (92), 114 (67)	62.5
31.9	766.7	3-Hexanone	43 (999), 57 (945), 71 (649), 100 (316), 41 (219)	43 (999), 57 (848), 71 (539), 29 (529), 100 (285)	82.0
32.0	770.0	Cyclopentanone	55 (999), 28 (370), 41 (340), 84 (250), 42 (240)	55 (999), 28 (500), 84 (420), 41 (377), 56 (289)	88.4